UNIVERSITÄT DES SAARLANDES

Synthesis and Structural Investigation of Softenable Polysilsesquioxanes and Their Applications

Dissertation

zur Erlangung des Grades

des Doktors der Naturwissenschaften

der Naturwissenschaftlich-Technischen Fakultät

der Universität des Saarlandes

von

Svenja Pohl

Saarbrücken, 2025

Tag des Kolloquiums:	29.01.2026
Dekan:	Prof. Dr.-Ing. Dirk Bähre
Berichterstatter:	Prof. Dr. Guido Kickelbick
	Prof. Dr.-Ing. Markus Gallei
Vorsitz:	Prof. Dr. Marc Schneider
Akademischer Mitarbeiter:	Dr. Andreas Rammo

Die vorliegende Arbeit wurde in der Zeit von August 2020 bis Oktober 2025 im Fachbereich Anorganische Festkörperchemie bei Prof. Dr. Guido Kickelbick an der Universität des Saarlandes angefertigt.

Publikationsliste

Wissenschaftliche Veröffentlichungen als Erstautorin:

Pohl, S.; Janka, O.; Füglein, E.; Kickelbick, G. Thermoplastic Silsesquioxane Hybrid Polymers with a Local Ladder-Type Structure. *Macromolecules* **2021**, *54*, 3873-3885.
DOI: https://doi.org/10.1021/acs.macromol.1c00310.

Pohl, S.; Kickelbick, G. Influence of alkyl groups on the formation of softenable polysilsesquioxanes. *J. Sol-Gel Sci. Technol.* **2023**, 107, 329-3446.
DOI: https://doi.org/10.1007/s10971-023-06126-6.

Pohl, S.; Gallei, M.; Kickelbick, G. Impact of Size and Substitution Isomerism in Polycyclic Aromatic-Substituted Trialkoxysilanes on the Formation of Softenable Polysilsesquioxanes. *Macromolecules* **2025**, *58*, 1298-1313.
DOI: https://doi.org/10.1021/acs.macromol.4c02737.

Pohl, S.; Steinbrück, N.; Pachnicz, M. P.; Kickelbick, G. Melt, mix, and glow: emulsion-based fabrication of polyphenylsilsesquioxane microspheres with embedded hydrophobic fluorophores. *Mater. Adv.* **2025**.
DOI: https://doi.org/10.1039/d5ma00849b

Wissenschaftliche Veröffentlichungen aus Kooperationen

Della Latta, E.; Sabatini, F.; Micheletti, C.; Carlotti, M.; Martini, F.; Nardelli, F.; Battisti, A.; Degano, I.; Geppi, M.; Pucci, A.; Pohl, S.; Kickelbick, G. Performant flexible luminescent solar concentrators of phenylpolysiloxanes crosslinked with perylene bisimide fluorophores. *Polym. Chem.* **2023**, *14*, 1602-1612.
DOI: http://dx.doi.org/10.1039/D2PY01428A.

Willian, T. P.; Pohl, S.; Bruch, D.; Rizzello, G.; Motzki, P.; Kickelbick, G.; Seelecke, S. Effects of Solvents on the Material Properties of Screen-Printed Electrodes and a Polydimethylsiloxane Dielectric for Dielectric Elastomer Transducers. *Adv. Eng. Mater.* **2024**, *26*, 2301736. DOI: https://doi.org/10.1002/adem.202301736.

Gießelmann, E. C. J.; Engel, S.; Pohl, S.; Briesenick, M.; Rüthing, L. P.; Kloos, C.; Koldemir, A.; Schumacher, L.; Wiethölter, J.; Schmedt auf der Günne, J.; Kickelbick, G.; Janka, O. Rapid Synthesis of a Green Emitting Phosphor by Sulfidation of Intermetallic $EuAl_2$ and its Use in a Hybrid Material. *Chem. Mater.* **2024**, 7, 97-108.
DOI: https://doi.org/10.1021/acs.chemmater.4c02093.

Danksagung

Ich möchte allen danken, die mich während meiner Promotion unterstützt, beraten und begleitet haben.

Mein besonderer Dank gilt Prof. Dr. Guido Kickelbick, der mir die Bearbeitung eines spannenden und hochaktuellen Forschungsthemas ermöglicht hat. Darüber hinaus erhielt ich durch ihn die Gelegenheit, an vielen weiteren Projekten mitzuwirken und wertvolle Erfahrungen zu sammeln, die meinen Blick weit über den universitären Tellerrand hinaus erweitert haben. Ich danke ihm für die wissenschaftlichen Anregungen, die stete Unterstützung und das mir entgegengebrachte Vertrauen.

Prof. Markus Gallei danke ich für die wissenschaftliche Begleitung und die Übernahme der Zweitkorrektur.

Dem gesamten aktuellen und ehemaligen Arbeitskreis Kickelbick, sowie dem Arbeitskreis Schäfer möchte ich für das stets angenehme Arbeitsklima, die Hilfe bei den alltäglichen Herausforderungen im Labor und die vielen lustigen Kaffee- und Kuchentreffen in der Küche danken. Es war mir eine Freude, so viele tolle Menschen kennenzulernen.

Mein besonderer Dank gilt Max, meinem langjährigen Labor- und Büropartner, für unzählige gemeinsame Stunden, unsere fachlichen wie auch nicht-fachlichen Diskussionen und die großartige Zusammenarbeit.

Tobias, Anna, Oliver, Stefan und Elias danke ich für die vielen XRD-Messungen, Elias und Michael Zimmer für die Festkörper-NMR-Messungen, Blandine Boßmann für die GPC-Analysen, Viktoria Kiefer für die Bestimmung der Quantenausbeute und Fluoreszenzlebensdauer und Lucas und Kimia für die Hilfe bei der TGA und IR, insbesondere dann, wenn die Geräte mal wieder nicht so wollten wie wir.
Mathilde danke ich für die schöne gemeinsame Zeit im Labor, für die Motivation und den Zuspruch zu meiner Arbeit.
Oliver danke ich für sein offenes Ohr und die stete Hilfsbereitschaft.

Ein herzliches Dankeschön auch an Stefan, Sylvia, Britta und Susanne, ohne deren Engagement vieles an der Universität nicht funktionieren würde.

Bedanken möchte ich mich auch bei den Kooperationspartnern der Arbeitskreise Gallei und Seelecke, insbesondere bei Anna und Tobias. Die Zusammenarbeit mit euch war sehr

bereichernd und hat mir spannende Einblicke in andere Forschungsbereiche ermöglicht. Ebenso danke ich den Projektpartnern des Projektes Optosilicon, die mich zwei Jahre begleitet haben und mir Einblicke in die Industrie eröffneten, inklusive der Gelegenheit, Hamburg und Nürnberg zu entdecken.

Mein Dank gilt auch den ehemaligen und neuen Laboranten, die mit ihrer Unterstützung den Laboralltag stets reibungslos gemacht haben.

Nils danke ich besonders herzlich. Er hat mein Interesse an diesem Thema geweckt und mich jederzeit unterstützt. Ohne dich würde es diese Arbeit nicht geben.

Ein großes Dankeschön gilt auch meinen Studienkollegen und Freunden, alt wie neu, auf die ich mich in und außerhalb der Uni stets verlassen konnte. Mit euch habe ich viele unvergessliche Momente erlebt, und die schwierigen Phasen ließen sich durch euch so viel besser meistern. Ohne unsere Kochabende, Kaffeetreffen (auch wenn es fast immer die gleiche Location war, Simon) und unzählige Stunden in der Boulderhalle wären die letzten Jahre nicht halb so schön gewesen.

Mein größter Dank gilt jedoch meiner Familie, allen voran meinen Eltern, meiner Schwester und Kevin. Ihr habt mir stets Rückhalt gegeben und ohne euch wäre all das nicht möglich gewesen.

Kurzzusammenfassung

Melting Gele sind silsesquioxanbasierte Hybridmaterialien, die bei moderaten Temperaturen reversibel erweichen und bei weiterer Erwärmung irreversibel aushärten. In Kombination mit Transparenz und thermischer Stabilität eröffnet dieses Verhalten neue Perspektiven für optische Anwendungen.

Ziel dieser Arbeit war es, die strukturellen Voraussetzungen für das Melting-Gel-Verhalten zu identifizieren und auf neue Systeme zu übertragen. Aufbauend auf einem phenylsubstituierten Referenzsystem wurden Silsesquioxane mit unterschiedlichen aliphatischen und polyzyklisch-aromatischen Substituenten synthetisiert und hinsichtlich ihrer Netzwerkstruktur und thermischen Eigenschaften untersucht.

Ein intermediärer Vernetzungsgrad, amorphe leiterartige Segmente und eine kontrollierte Zahl freier Hydroxygruppen erwiesen sich als entscheidend für das thermoplastische und duroplastische Verhalten. Während Naphthylsubstituenten die Bildung neuer Melting-Gel-Systeme ermöglichten, führten lineare *n*-Alkylgruppen nicht zu den gewünschten Eigenschaften.

Darüber hinaus wurde die Eignung der Materialien als Matrix für die Verkapselung hydrophober Farbstoffe demonstriert. Am Beispiel perylenbasierter Systeme konnten fluoreszierende Mikropartikel über eine Schmelz-Emulsions-Synthese hergestellt werden.

Die Arbeit liefert damit grundlegende Einblicke in die Struktur–Eigenschafts-Beziehungen von Melting Gelen und zeigt neue Wege zur Entwicklung funktionaler Hybridmaterialien mit regulierbaren Eigenschaften.

Abstract

Melting gels are silsesquioxane-based hybrid materials that soften reversibly at moderate temperatures and cure irreversibly upon further heating. Combined with high transparency and thermal stability, this behavior offers new opportunities for optical applications.

The aim of this work was to identify the structural prerequisites for the melting gel behavior and to extend the concept to new systems. Building on a phenyl-substituted reference system, silsesquioxanes with various aliphatic and polycyclic aromatic substituents were synthesized and studied with respect to their network structure and thermal properties.

An intermediate crosslinking density, amorphous ladder-like segments, and a controlled number of free hydroxyl groups were found to be crucial for the thermoplastic–thermosetting characteristics. While naphthyl substituents enabled the formation of new melting gel systems, linear *n*-alkyl groups did not yield the desired properties.

In addition, the suitability of these materials as matrices for encapsulating hydrophobic dyes was demonstrated. Using perylene-based systems, fluorescent microparticles were successfully prepared via a melt-emulsion process.

This study provides fundamental insights into the structure–property relationships of melting gels and highlights new strategies for designing functional hybrid materials with tunable properties.

Table of Content

List of Abbreviations

Abbreviation	Meaning
AAS	Atomic Absorption Spectrometry
ATR	Attenuated Total Reflectance
$Cr(acac)_3$	Chromium(III) acetylacetonate
DC	Degree of Condensation
DDSQ	Double-Decker Silsesquioxane
DLS	Dynamic Light Scattering
DMDES	Dimethyldiethoxysilane
DPhDES	Diphenyldiethoxysilane
DSC	Differential Scanning Calorimetry
Et	Ethyl
FTIR	Fourier Transform Infrared Spectroscopy
FWHM	Full Width at Half Maximum
GC	Gas Chromatography
GMM	Gel-Melting Method
ITO	Indium Tin Oxide
LC	Liquid Chromatography
LED	Light Emitting Diode
LG305	Lumogen® F Red 305
LPPSQ	Ladder Polyphenylsilsesquioxane
LPSQ	Ladder Polysilsesquioxane
MALDI	Matrix-Assisted Laser Desorption/Ionization
MALS	Multi-Angle Light Scattering
Me	Methyl
M_n	Number-Average Molar Mass
MS	Mass Spectrometry
MTEG	Methyltriethoxygermane
MTES	Methyltriethoxysilane

M_w	Weight-Average Molar Mass
NMR	Nuclear Magnetic Resonance Spectroscopy
OH / OR	Hydroxy / Alkoxy Groups
PDMS	Polydimethylsiloxane
Ph	Phenyl
PhTMS	Phenyltrimethoxysilane
POSS	Polyhedral Oligomeric Silsesquioxanes
PXRD	Powder X-ray Diffraction
RB	Rhodamine B
RHT	Rapid Heat Treatment
RI	Refractive Index
SAM	Self-Assembled Monolayer
SAXS	Small-Angle X-ray Scattering
SCM	Sol Concentration Method
SEC	Size Exclusion Chromatography
SEM	Scanning Electron Microscope
SQ	Silsesquioxane
TEM	Transmission Electron Microscopy
TEOS	Tetraethoxysilane
T_{95}	Temperature at 5% Mass Loss
T_{con}	Consolidation Temperature
T_g	Glass Transition Temperature
TGA	Thermogravimetric Analysis
TMOS	Tetramethoxysilane
ToF	Time of Flight
VTES	Vinyltriethoxysilane
XPS	X-ray Photoelectron Spectroscopy
XRD	X-ray Diffraction
Đ	Dispersity (Polydispersity Index)

1 Introduction

The development of new types of materials that can be processed efficiently while simultaneously meeting high functional requirements is a central challenge in modern materials science. Especially in microelectronics and optoelectronics, for example, in the encapsulation of light-emitting diode (LEDs) components, materials are required that offer thermal stability, high transparency, tailorable refractive index (RI) and processability at moderate temperatures. Traditional materials such as low-melting-point sealing glasses, which have been used for this purpose, are typically purely inorganic glasses based on mixtures of various metal oxides, such as boron oxide, bismuth oxide, lead oxide, and modifiers including alkali and alkaline earth metal oxides.[1] These materials require processing temperatures below those of conventional silicate glass. However, typical melting temperatures between 300 and 600 °C are still too high for many sensitive electronic components, resulting in limitations for industrial applications.[2]
Inorganic-organic hybrid materials combine the transparency and hardness of inorganic glasses with the processability and functionality of organic polymers.[3] Materials that embody this principle are so-called melting gels. These are siloxane-based hybrid materials that can be processed at moderate temperatures (≈ 110 °C) before being irreversibly crosslinked into robust hybrid glasses through controlled thermal treatment (130–200 °C).[4] This makes them particularly suitable for applications in temperature-sensitive optical systems.
The simplest melting gel system is based on a polysilsesquioxane with phenyl groups as organic substituents and is produced via the polycondensation of phenyltrialkoxysilane as the only monomer used.[5] Hydrolysis and condensation occur in parallel and are kinetically controlled. Because of the large number of possible reaction pathways, each with distinct kinetics, the process is highly complex and strongly dependent on the specific reaction conditions.[6] A deep understanding of both the underlying reaction mechanisms and the resulting network structure is essential for the targeted adjustment of the final hybrid material properties.
A variety of analytical methods, such as ^{29}Si nuclear magnetic resonance (NMR) spectroscopy, Fourier transform infrared spectroscopy (FTIR), thermal analysis methods, or powder X-ray diffraction (PXRD), enable the structural characterization of such systems. The insights gained can be transferred to systems with more complex formulations or different precursors, thereby contributing to the systematic expansion of the melting gel family and broadening their potential applications.

2 Theoretical Background

2.1 Hybrid Materials

Inorganic-organic hybrid materials represent one of the most rapidly growing classes of materials today. In view of increasing demands for modern materials, such as sustainability, energy efficiency, miniaturization, environmental compatibility, recyclability, and durability, they are gaining significance in both academic research and industrial applications. This trend is also reflected in the steadily rising number of scientific publications, patents, reviews, and books addressing various aspects of hybrid materials.[3, 7-14]

Hybrid materials are generally defined as the combination of inorganic and organic components at the molecular level.[10] Their properties are not solely the sum of the individual components, but are significantly influenced by the characteristics of the inner interfaces. These structural and chemical features can lead to synergistic effects, resulting in improved performance or entirely new properties.[15] Depending on the nature of the interface, hybrid materials are commonly categorized into two classes: class I, in which organic and inorganic components interact via weak forces (e.g., van der Waals interactions, hydrogen bonds, or electrostatic forces), and class II, in which the components are connected by covalent or iono-covalent bonds.[7]

The idea of combining organic and inorganic components is not a modern invention. Nature has long employed this principle to produce complex hybrid materials through biomineralization, such as shells, bones, and teeth composed of biopolymers (e.g., chitin, collagen, polysaccharides) and inorganic phases (e.g., calcium carbonate, silica, iron oxides). These structures are hierarchically organized nanocomposites whose mechanical stability, porosity, and optical properties have been optimized by evolution.[16-20]

Early human-made hybrid materials also demonstrate this principle. Prehistoric cave paintings were made using paints composed of inorganic components (e.g., Fe_2O_3, aluminosilicates), combined with organic binders such as fats or proteins.[21] Other clay-organics were found in cosmetics and medicine.[22] In ancient times, various cultures developed materials such as Maya Blue, a pigment made from the natural dye indigo and the clay mineral palygorskite, which is known for its exceptional chemical stability,[23] or lime mortars modified with sticky rice soup (providing starch, particularly amylopectin), which display remarkable durability.[24]

A systematic scientific understanding of such materials began to emerge only in the 18th and 19th centuries. Researchers such as J. B. van Helmont, J. J. Berzelius, C. Friedel, and J. M. Crafts, or F. S. Kipping, contributed significantly to the development of silane and siloxane chemistry.[11] Due to their versatile chemical properties, especially their ability to form flexible, stable Si–O–Si backbones, siloxanes soon became key building blocks in the design of hybrid materials. In particular, the early investigations of J. J. Ebelmann into the hydrolysis and condensation of alkoxysilanes in 1846 are now considered to have laid the chemical foundations for what would later become the sol–gel process.[25]

In the 20th century, particularly from the 1970s onwards, the production of inorganic-organic hybrid materials gained increasing importance due to the concept of the so-called "chimie douce".[26, 27] These approaches make it possible to produce complex, crosslinked materials with a controlled microstructure under mild conditions. Among the most prominent techniques enabled by this development is the sol–gel process, which has become a cornerstone of modern hybrid material science. The wet-chemical process, in which metal or half-metal alkoxides are converted into an inorganic or hybrid network through controlled hydrolysis and condensation, allows the direct integration of functionalized organic groups into the resulting network, leading to inorganic-organic materials with high structural control and functionality.[28] Initially, the sol–gel process was primarily used for the production of ceramics and glasses.[29, 30] Over time, however, its potential in other fields became increasingly evident. Today, it serves as a fundamental technique for the development of various advanced hybrid materials, including nanomaterials, coatings, and functional composites.[31-33]

2.2 Sol–Gel Synthesis

The sol–gel process is a standard method for producing materials with an oxide-based structure, such as glasses and ceramics. In a wet chemical process, molecular precursors, usually metal or half-metal alkoxides, are hydrolyzed and condensed. As the name suggests, kinetically controlled reactions result in the formation of sols and gels.[28]

First, a colloidal solution of particles or macromolecules is formed. Their size is in the lower nanometer range and corresponds to a nanoparticulate dispersion. The sols then aggregate to form a solid, porous three-dimensional network whose pores are filled with liquid. This stage is defined as a gel, with the transition between sol and gel referred to as gelation. Structural changes continue to occur during ageing, depending on temperature, pH, or solvent. In the final

stage, the solvent is removed through drying. Depending on the desired material properties, a subsequent high-temperature densification step may be applied to reduce porosity and achieve densities comparable to fused silica.[34]

Depending on the type of drying (evaporation induced by heating or reduced pressure, or supercritical drying), whether a densification step is applied, and the processing method (coating, gelling, precipitation, spinning), the morphology of the final product can be influenced, resulting in a variety of controlled materials such as coatings and thin films, monoliths, xerogels, aerogels, powders and fibers (Figure 1).[31, 35]

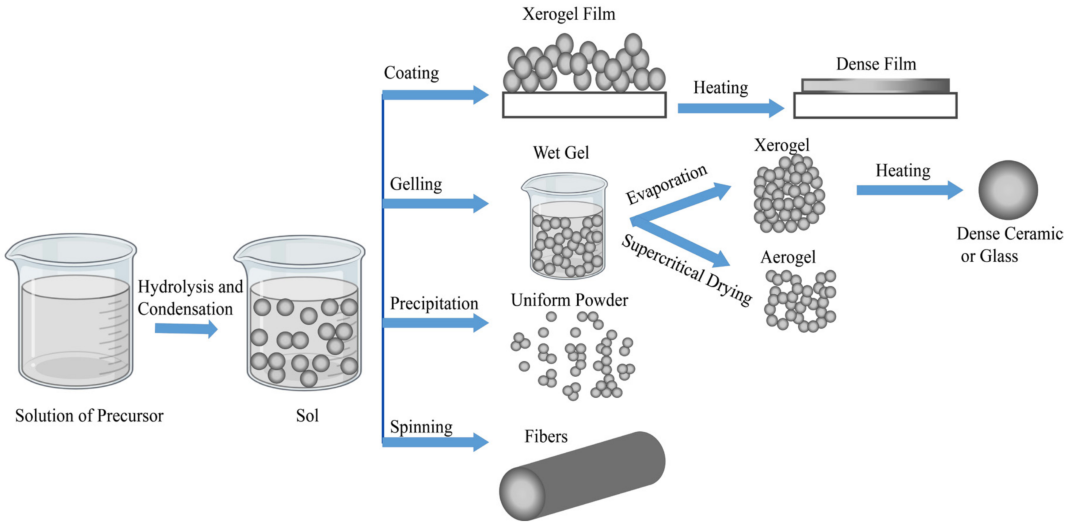

Figure 1: Different sol–gel process steps to control the final morphology of the product. Reproduced from Aboualigaledari, N.; Rahmani, M. A review on the synthesis of the TiO_2-based photocatalyst for the environmental purification. *J. Compos. Compd.* **2021**, *3*, 25–42. Licensed under CC-BY 4.0.[36]

The advantages of the sol–gel process lie in the almost unlimited combination of different building blocks, which can be used like in a LEGO® system, for example, to adjust surface properties or porosity. Furthermore, precise control of shaping and the production of nanoscale structures is possible. Mixing at the molecular level also leads to high-purity, homogeneous products. The greatest advantage lies in the low temperatures and mild chemical reaction conditions. These not only ensure resource-friendly handling but also enable the use and integration of organic molecules, making the sol–gel process particularly valuable in hybrid materials science.[31, 37]

The disadvantages are high cost of the precursors and the risk of material shrinkage, which can lead to stresses and cracks or even the collapse of the pores during the drying process.[37] While the reaction sounds simple and does not require much equipment, the processes behind it are highly complex and depend on a variety of external factors and reaction conditions that must

be precisely controlled, which often makes the transfer of the synthesis to industrial processes challenging.[34]

2.2.1 Hydrolysis and Condensation of Silica-Based Materials

The most important reactions within the sol–gel process are the hydrolysis and polycondensation of metal alkoxide precursors. In the case of silicon-based sol–gel materials, the most used precursors are tetramethoxysilane (TMOS) or tetraethoxysilane (TEOS). In the first step, the Si–OR groups (R = alkyl group, mostly methyl (Me) or ethyl (Et)) react with water and undergo hydrolysis, leading to the formation of Si–OH groups. In the second step, condensation occurs either between Si–OH functionalities or between Si–OH and Si–OR, accompanied by the elimination of water or alcohol (Figure 2).

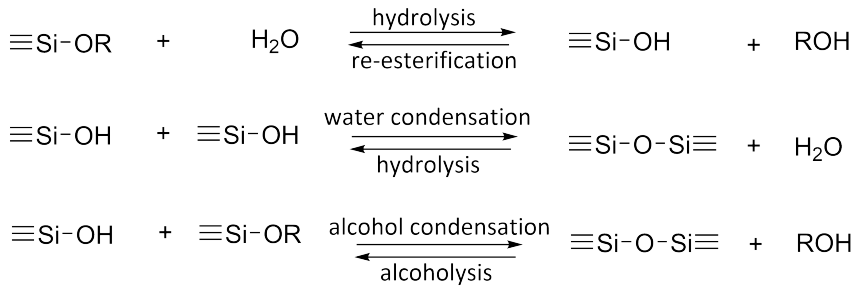

Figure 2: General hydrolysis and condensation reaction of silica precursors.

While most metal alkoxides (e.g. M = Ti, Zr, Ce) react spontaneously with water due to their lower electronegativity difference between the metal and oxygen atoms, silicon alkoxides require a catalyst to initiate and accelerate the reaction.[30] The mechanisms and resulting products differ depending on whether the catalysis is acidic or basic.[38]

In acid-catalyzed reactions (Figure 3), hydrolysis involves the protonation of the oxygen atom in the Si–OR group, while condensation proceeds via protonation of a Si–OH group. Protonation enhances the leaving-group ability and reduces the electron density on the silicon atom, thereby increasing its electrophilicity and facilitating nucleophilic attack by water or another Si–OH group. The resulting transition state is stabilized by a positive charge on the silicon, which is enhanced by electron-donating neighboring substituents in the order Si–O–Si < Si–OH < Si–OR < Si–R′ (R′ = organic group or H). Terminal alkoxy groups provide the highest electron density, rendering the silicon center more susceptible to hydrolysis and condensation. As hydrolysis or crosslinking progresses, the electron density at the silicon atom decreases, reducing the reaction rate. Acid catalysis thus typically favors the formation of linear or weakly crosslinked structures.[39]

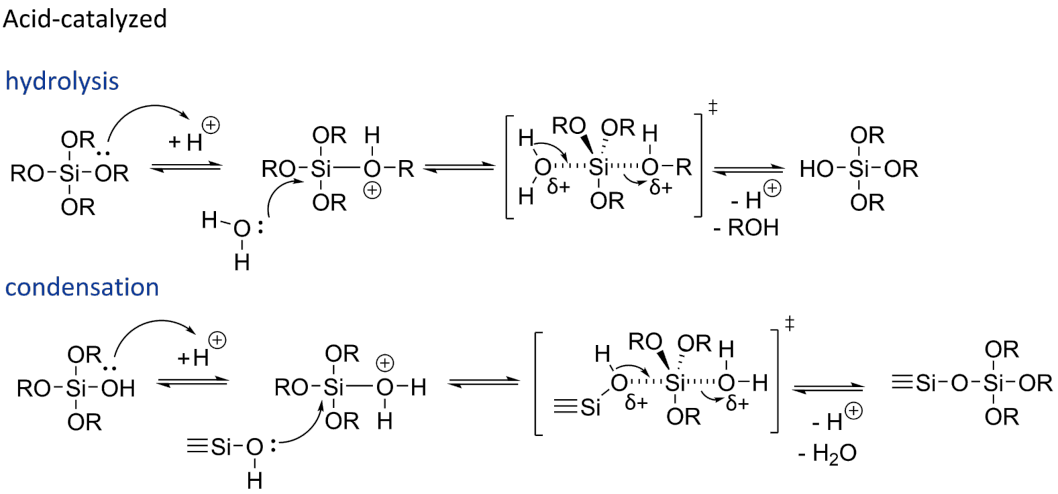

Figure 3: Mechanism of acid-catalyzed hydrolysis and condensation reactions of tetraalkoxysilanes.

In contrast, base-catalyzed reactions (Figure 4) proceed via nucleophilic attack by hydroxide ions (OH^-) or silanolate ions ($Si–O^-$) at the silicon center. This leads to the formation of a pentacoordinated intermediate, followed by the elimination of a hydroxide or alkoxide group. Unlike in acid catalysis, the reactivity increases as the electron density at the silicon atom decreases. As a result, condensation preferentially occurs at already crosslinked silicon centers, promoting the formation of highly branched, three-dimensional networks.[39]

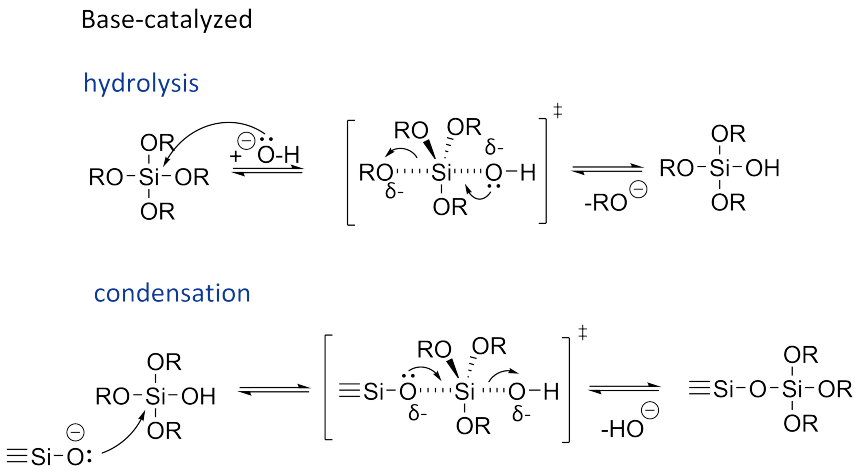

Figure 4: Mechanism of base-catalyzed hydrolysis and condensation reactions of tetraalkoxysilanes.

Hydrolysis and condensation are kinetically controlled reactions and usually take place in parallel or compete with each other. Numerous intermediate species with varying reactivities are formed during the process, making the overall reaction pathway highly complex.[40]

By adjusting the reaction parameters, the ratio of hydrolysis to condensation can be influenced to some extent, and thus the structure and properties of the final material can be tailored accordingly. The most important parameters affecting these reactions, such as the type and

concentration of the precursor, the solvent, the water-to-alkoxysilane ratio, temperature, and pH value, will be discussed in more detail in Chapter 2.4.2.

2.3 Inorganic-Organic Silica Hybrid Materials

A considerable advantage of the mild reaction conditions in the sol–gel process is the possibility of introducing organic groups into the inorganic network. This is not feasible in conventional glass production. Soda-lime silicate glass is traditionally produced by melting sodium and calcium carbonate with quartz at temperatures above 1000 °C. Under such conditions, organic compounds would simply decompose.[37] In contrast, the gentle conditions of the sol–gel process preserve the organic components, significantly expanding the range of possible materials, properties, and applications.[41]

There are two general approaches to combining organic and inorganic components, depending on the nature of their interaction. In one case, organic species such as dye molecules, polymers, or drugs are embedded within the silica network, interacting via weak chemical bonds (class I hybrid materials).[42, 43] The second approach uses alkoxysilane precursors in which the organic group is covalently bonded to silicon (class II hybrid materials).[44-46] In contrast to Si–O–C bonds, which are prone to hydrolysis and further condensation, Si–C bonds are stable under polycondensation conditions, allowing straightforward incorporation into the silica network.

One, two, or three organic groups can be introduced, and the resulting silane species are categorized as mono- (M), di- (D), tri- (T), or tetra-functional (Q) units (Figure 5), depending on how many oxygen atoms are bonded.[47] Each silicon unit is further assigned an index *m* (e.g., T^m), indicating the number of oxygen atoms connected to neighboring silicon atoms via oxygen bridges.[48] This index reflects the degree of crosslinking within the material.

While tetraalkoxysilanes lead to the formation of silica (SiO_2), organotrialkoxysilanes form oligo- or polysilsesquioxanes ($R'SiO_{3/2}$). In contrast, diorganodialkoxysilanes ($R'_2SiO_{2/2}$) do not form networks but rather siloxane chains, as found in silicones, and triorganoalkoxysilanes ($R'_3SiO_{1/2}$) act only as terminal groups. As a result, the crosslinking density of the inorganic network decreases with each additional organic substituent. Therefore, mixtures of Q and T units are often used in the sol–gel process to retain the high crosslinking density and typical properties of the inorganic network, while also expanding its functionality, for example, by adjusting polarity or enabling further functionalization.[49, 50]

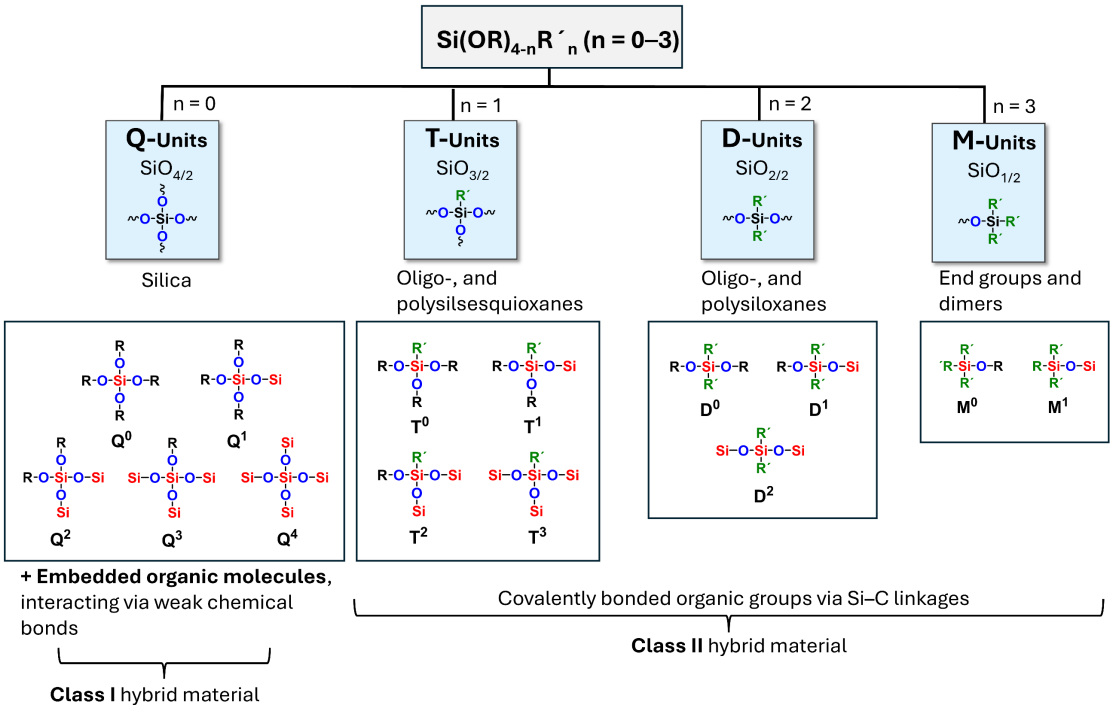

Figure 5: Unit structures for silica (Q^m units), silsesquioxanes (T^m units), siloxane chains (D^m units), and end groups (M^m units). The index *m* (e.g., Q^0–Q^4) indicates the number of Si–O–Si bridges and thus the degree of condensation (DC). R´ = H or organic group; R = H or alkoxy group. Classification into class I and class II hybrid materials according to the nature of the inorganic–organic interaction.

2.4 Silsesquioxanes

The term *silsesquioxane* (SQ) is derived from the components *sil* (silicon), *sesqui* (one and a half), *ox* (oxygen), and *ane* (hydrocarbon group).[51] It refers to the characteristic silicon-to-oxygen ratio of 1:1.5 and the presence of an organic substituent or a hydrogen atom at the silicon center, according to the general formula $R´SiO_{3/2}$.[52] Each silicon atom is surrounded by three oxygen atoms, hence these units are also referred to as T-units.

The chemistry of silsesquioxanes began in the early 20th century with the work of F. S. Kipping, who was able to synthesize a variety of organo- and chlorosilanes using the Grignard reaction.[53] This development continued with the independent invention of an industrial process by R. Müller and E. G. Rochow in 1940, which enabled the large-scale synthesis of methylchlorosilanes. J. F. Hyde at Corning Glass Works recognized the potential of these precursors for the development of silicone resins for high-temperature electrical insulation, which were primarily based on silsesquioxanes. These advancements eventually led to the

founding of Dow Corning in 1943 and the commercial production of silicones, which sparked a growing interest in silsesquioxane chemistry.[11, 54]

Silsesquioxanes can exist as oligomeric species with discrete structures composed of a limited number of tetrahedral units. Examples include fully condensed closed cages (commonly referred to as polyhedral oligomeric silsesquioxanes, POSS), open cages, double-decker cages, small ladders, or irregular oligomers. They can also occur as polymeric species, forming high-molecular-weight ladder polysilsesquioxanes (LPSQ), lamellar sheets, or random networks (Figure 6).[55] Depending on whether they appear in oligomeric or polymeric form, and on the degree of structural order, their properties and applications vary significantly. In the literature, most attention is focused on cage and ladder structures due to their regular, recurring structural motifs and their interesting physicochemical properties. In the absence of well-controlled reaction conditions, silsesquioxane structures tend to form irregularly, incorporating a mixture of structural motifs along with defects such as uncondensed alkoxy and hydroxy groups.

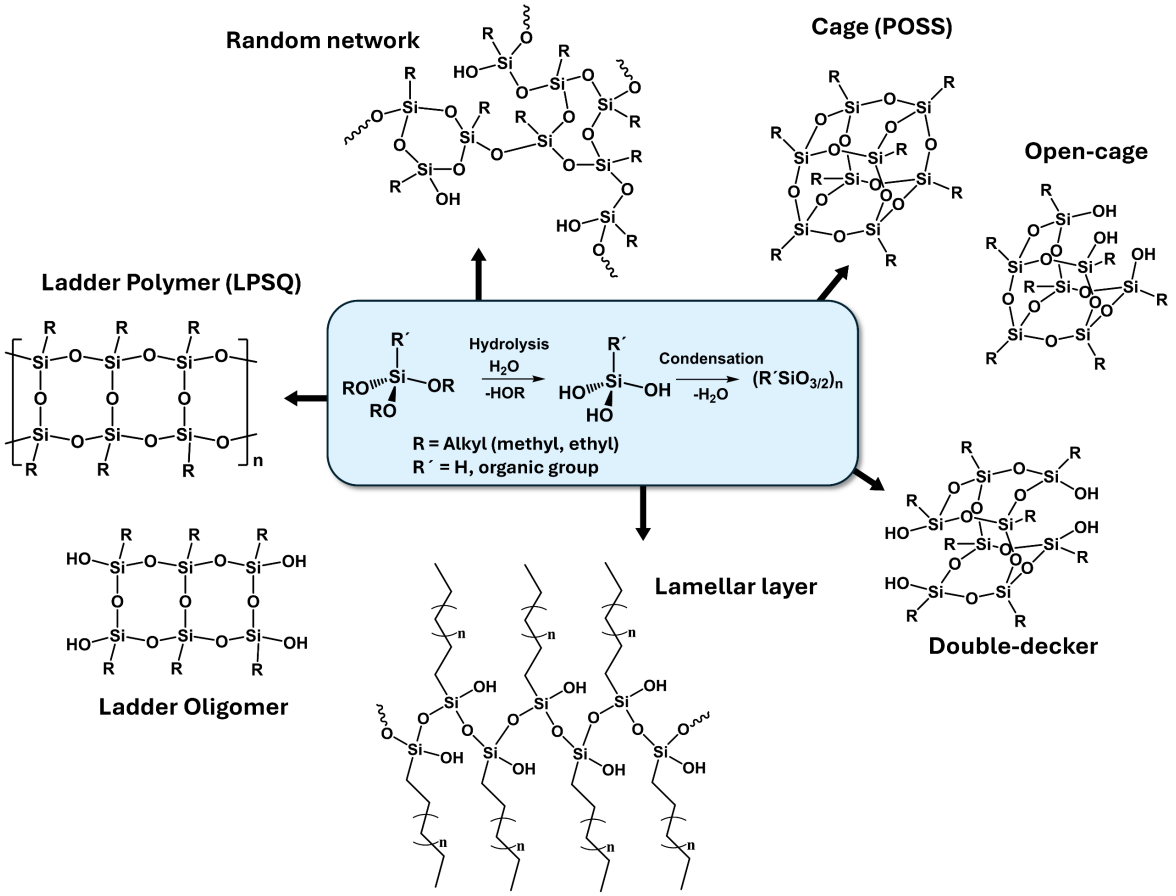

Figure 6: Structural types of silsesquioxanes, including cage, ladder, lamellar, and random network structures.

2.4.1 Structure Types

2.4.1.1 Polyhedral oligomeric silsesquioxanes (POSS)

The first fully condensed and isolable POSS was reported by Scott in 1946.[56]. This was followed in 1965 by Brown and Vogt, who published the first partially condensed cage framework.[57] Another example of a POSS cage variation is the double-decker motif, described by Yoshida et al. in 2003.[58]

Owing to their hybrid nature, well-defined architecture, and the variety of functional groups enabling unique material properties, research has since focused on isolating new cage systems with varying sizes and substitution patterns.

Fully condensed cages can be represented by the general formula $(R'SiO_{3/2})_n$ (T_n), where *n* is an even number ≥ 6. These three-dimensional, nanoscale structures typically range from 1 to 3 nm in diameter, making them among the smallest silica-based nanoparticles.[59] The most well-known structure is the T_8 cage,[60] although T_6,[61] T_{10}, T_{12},[62] T_{14},[63] and T_{18}[64] have also been isolated, and even larger cages have been detected in product mixtures.[65] Depending on the size, different isomeric forms may occur, each with varying stabilities.[66]

The fundamental synthetic route for cage-like silsesquioxanes involves hydrolysis and condensation of trifunctional organosilanes $R'SiX_3$ (X = Cl or alkoxy). The process usually yields a mixture of open and closed cage structures of different sizes, which must be separated afterward.[64, 65] Non-functionalized organic derivatives are commonly used as strengtheners in polymer blends. When physically mixed into a matrix, they can improve mechanical or thermal stability or be used to modify viscosity.[67, 68] Alternatively, functionalized organic groups can be incorporated to enable covalent bonding within polymer systems or to allow for further molecular derivatization. Vinyl-substituted cages, for example, can be introduced via hydrosilylation and act as crosslinkers.[69]

POSS can also be synthesized directly in open forms (e.g., $R_7Si_7O_9(OH)_3$) or be reopened under acidic or basic conditions, which allows for further functionalization through corner capping.[70, 71] Depending on the number of reactive corners, mono-functionalized derivatives can serve as end-groups,[72] while multifunctionalized variants can be used as chain extenders[73] or crosslinking agents in polymers (Figure 7).[74] Common reactive corner groups include hydride, halide, hydroxyl, amino, epoxy, acrylate, styrene, and ester functionalities.[75, 76]

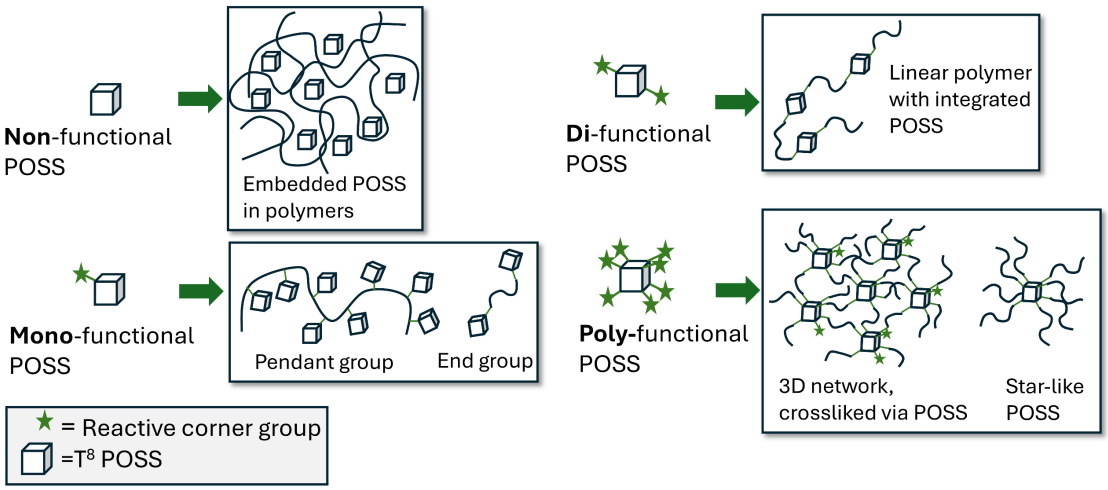

Figure 7: Schematic representation of POSS with different numbers of reactive corners integrated into a polymer matrix: non-functional POSS is physically embedded, mono-functional POSS acts as pendant or end group, di-functional POSS is incorporated as a linear chain segment, and poly-functional POSS serves as crosslinking point or star-like structure.

The unique properties of these nanostructures derive directly from their defined, three-dimensional cage geometry and their hybrid composition. The inorganic core imparts high thermal, mechanical, and oxidative stability.[77, 78] Through the targeted selection of organic substituents at the cage corners, polarity, reactivity, and compatibility with various organic or inorganic environments can be finely tuned.[79, 80] This enables the modification of interfaces, the control of self-assembly behavior, or the adjustment of rheological properties in composite systems.[79, 81-83] Incorporation into polymers affects local molecular interactions and segmental mobility, which can, for instance, lead to changes in the glass transition temperature (T_g).[84]
A known drawback of POSS is its tendency to aggregate or crystallize.[85] It often exhibits poor solubility in solvents or matrices, leading to phase separation. Its use in polymer systems is therefore typically limited to low concentrations and requires precise tailoring of the organic substituents to the matrix in order to ensure homogeneous dispersion.[85]
Applications are primarily found in polymer composites,[86] biomedical fields (e.g., as drug carrier[87] or biomaterials[88]), sensors,[89-91] catalysis,[92] and coatings.[93, 94]

2.4.1.2 Ladder polysilsesquioxanes (LPSQ)

The first ladder-type silsesquioxane structure was proposed by Brown et al. in 1965.[95] Using KOH-catalyzed equilibration polymerization of phenyltrichlorosilane, they synthesized a high-molecular-weight, soluble polyphenylsilsesquioxane. Based on X-ray diffraction (XRD) and

FTIR analysis, Brown proposed a ladder-like architecture with a double-stranded cis-syndiotactic conformation.[96, 97] In 1971, Frye and Klosowski revised this assumption. They attributed the formation of structural defects to the instability of phenyltrisilanol intermediates and concluded that the product did not exhibit a perfect ladder configuration. Instead, they suggested that the structure consisted mainly of randomly connected polycyclic cages.[98] Further progress in the 1980s came from Shklover et al., who successfully synthesized bicyclic ladder-type silsesquioxanes of the form $Me_6Ph_2Si_6O_7$, significantly advancing the development of well-defined ladder polysilsesquioxanes.[99]

Although Brown's proposed ladder structure was not universally accepted, these early findings laid the groundwork for more targeted synthetic strategies aiming at structurally defined, defect-minimized ladder systems with high molecular weights, which remain a central focus in LPSQ research.

Ladder structures are ordered, one-dimensional networks, typically composed of double-stranded Si–O–Si chains with cyclic linkages acting as ladder rungs.[100]

The general synthetic strategy for ladder-type silsesquioxanes relies on hydrolysis and condensation reactions but may vary in terms of the precursors used and the reaction conditions applied. One established approach involves the use of cyclic silanol derivatives, particularly cyclotetrasiloxanetetraol, as molecular building blocks for ladder construction. Unno et al. reported the synthesis of such cyclic precursors and their subsequent conversion into oligomeric ladder siloxanes with structures ranging from bicyclic to nonacyclic frameworks.[101, 102] This methodology has also proven suitable for the preparation of well-defined ladder polymers (Figure 8a).[103-106] Another strategy involves self-organization of precursors, where the organic side groups act as structure-directing elements. These assemble via hydrogen bonding (Figure 8b),[107] π–π interactions,[108, 109] or ionic interactions (Figure 8c),[110] followed by dehydration-driven condensation. A particularly simple approach was demonstrated by Choi and Lee et al., who used a K_2CO_3-catalyzed one-pot sol–gel reaction. In this process, either cage or ladder structures were formed depending on the precursor concentration (Figure 8d).[111, 112]

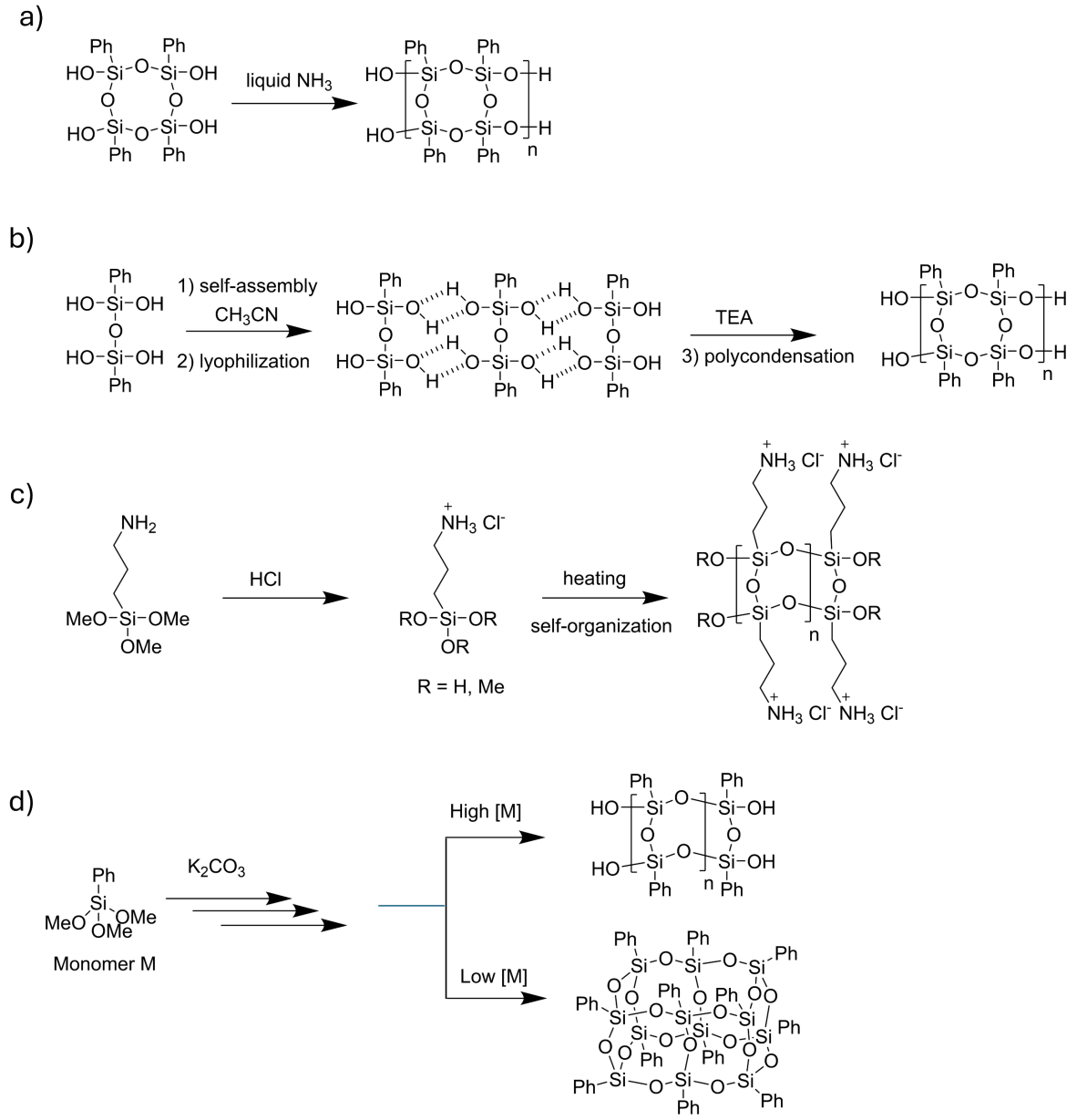

Figure 8: Different strategies for the synthesis of LPSQ: a) condensation of cyclotetrasiloxanetetraol in liquid ammonia,[106] b) self-assembly via hydrogen-bonding, lyophilization and polycondensation,[109] c) self-organization using 3-aminopropyltrimethoxysilane as the starting material,[110, 113] d) one-pot synthesis from phenyltrimethoxysilane at high precursor concentration.[111]

Due to their inorganic backbone and rigid double-stranded architecture, ladder silsesquioxanes exhibit high chemical and thermal robustness,[114] oxidative resistance,[115] and mechanical stability,[116, 117] all comparable to POSS. Their covalently bound organic groups improve solubility in organic solvents and polymers, allowing for good processability and the formation of homogeneous, transparent phases.[118, 119] Functional groups can also be introduced to

modulate polarity,[120] or to enable properties such as self-healing.[121] Porosity is influenced by the steric demand of the organic substituents, as their size determines the spacing between polymer chains.[122, 123]

These properties make ladder-type polysilsesquioxanes attractive for use in protective coatings,[123-125] in gate dielectrics,[126] in electrochemical devices,[127] in gas separation membranes,[128] or as LED encapsulation materials.[129]

A key distinction from POSS lies in the polymeric nature of LPSQ, which allows them to form continuous films or free-standing bodies.[111] While POSS often serves as an additive, ladder-type silsesquioxanes can function as independent structural materials.

However, the major drawback of such well-defined structural motifs is the complexity of their synthesis. Side reactions of silanol intermediates, such as cyclization,[130] and uncontrolled inter- or intramolecular condensation can easily introduce structural defects, ultimately affecting material performance.[131]

2.4.1.3 Random-branched silsesquioxanes

In the absence of strict control over reaction conditions, the hydrolysis and condensation of organotrialkoxysilanes typically result in the formation of irregular, randomly branched polysilsesquioxane networks. These non-crystalline structures lack a uniform, defined architecture and often exhibit a high density of structural defects, particularly in the form of uncondensed silanol and alkoxy groups.[132, 133]

Random networks tend to be insoluble,[134] display a broad molar mass distribution, and generally exhibit lower average molecular weights compared to defined LPSQ.[133]

Free silanol groups can negatively affect key material properties, as they are highly hydrophilic, promoting water absorption, which can cause swelling, optical property changes (e.g. RI variation), and thermal expansion of the absorbed water, potentially leading to crack formation under thermal cycling.[135] Furthermore, Si–OH groups can undergo further condensation during or after film formation, potentially leading to undesirable structural shrinkage and cracking.[136]

Mixing the silanol-rich silsesquioxanes in polymer matrices can cause self-aggregation and poor dispersion in the matrix, and can adversely affect storage stability or thermal performance.[137]

To overcome these undesirable effects, residual silanol groups are often capped post-synthetically using reagents such as trimethylchlorosilane,[138, 139] or hexamethyldisilazane,[140, 141] or thermally driven to further condense into siloxane bridges.[136] This post-treatment improves network stability and reduces moisture sensitivity.[135]

Compared to well-defined structures like POSS or LPSQ, random networks generally exhibit poorer solubility, lower mechanical and thermal stability, and less reproducibility in processing and properties.[132, 133] For this reason, full hydrolysis and subsequent condensation are often targeted in synthesis of silsesquioxanes.

However, a partially condensed network may also be desirable in certain applications. The presence of residual silanol or alkoxy groups can result in a less crosslinked and thus more flexible material.[133] Si–OR groups can act as internal lubricants, increasing free volume and facilitating chain mobility or serve as intermediates for post-functionalization.[142, 143] The low network density is advantageous in producing soft or liquid polysilsesquioxanes.[144] Finally, the presence of silanol groups offers opportunities for thermal crosslinking in the solid state, [145-149] leading to network reorganization and solidification without the need for external curing agents.[150]

The synthesis of both ladder and cage-type silsesquioxanes typically starts from trifunctional silane precursors. The final structure, as well as the extent of defects it contains, is strongly influenced by the reaction conditions. The choice of precursor, the catalyst used, and the precursor concentration all determine whether the resulting silsesquioxanes are polymeric or oligomeric, form ladders, cages, or a mixture thereof and exhibit low or high degrees of crosslinking.[39] Choi et al. demonstrated that even the concentration of phenyltrimethoxysilane (PhTMS) alone can direct the outcome of a base-catalyzed hydrolysis and condensation reaction. At higher PhTMS concentrations, ladder-like polymers formed, whereas at lower concentrations, the product shifted toward T_{12} cages.[111]

A clear understanding of how individual parameters affect hydrolysis and condensation, and how these influence the resulting network architecture, is therefore essential for the design of silsesquioxane-based materials.

2.4.2 Influence of Reaction Conditions on Structural Formation

2.4.2.1 pH value and catalyst

The reaction mechanisms of hydrolysis and condensation differ significantly depending on whether an acidic or basic catalyst is used. These mechanisms have already been discussed in detail in Chapter 2.2.1. The rates of hydrolysis and condensation, as well as the resulting structures, show a strong dependence on pH and catalyst type.[151, 152] Hydrolysis is at its minimum rate around pH 7 and increases rapidly with decreasing pH (Figure 9).

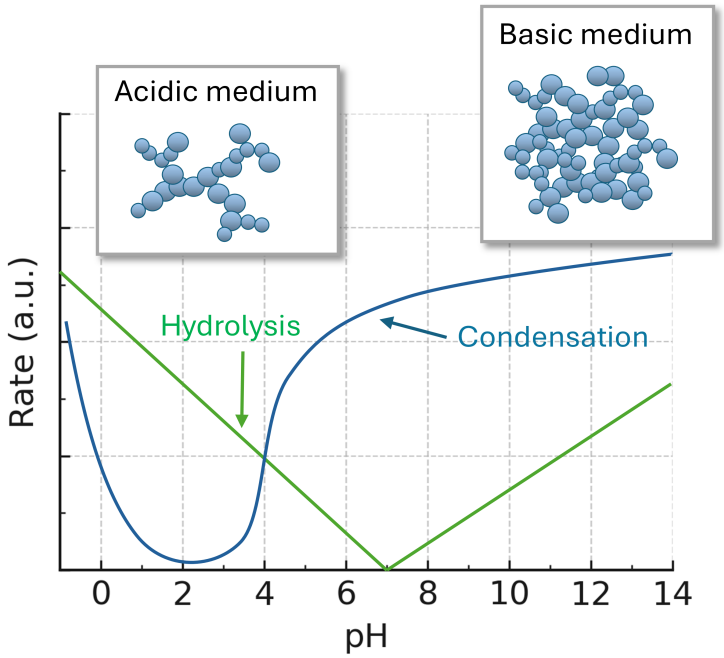

Figure 9: Effect of pH on hydrolysis and condensation kinetics of tetraalkoxysilanes, showing general trends in structural development in an acidic and basic medium. Adapted from Fricke, J.; Emmerling, A. Aerogels – Preparation, properties, applications. In Chemistry, Spectroscopy and Applications of Sol–gel Glasses; Reisfeld, R.; Jørgensen, C. K. (Eds.); Springer, Berlin, Heidelberg, **1992**; pp 37–87. Copyright 1992 Springer Nature.[153] Adaptation as presented in Linhares, T.; de Amorim, M. T. P.; Durães, L., *J. Mater. Chem. A* **2019**, 7, 22768–22802.[154]

At pH values below 5, hydrolysis becomes the dominant reaction, while condensation becomes the rate-limiting step. This results in the formation of monomers and small oligomers bearing reactive Si–OH groups. At around pH 2–4, the condensation rate reaches its minimum. When the pH increases above 5, the condensation rate rises significantly, and hydrolysis becomes the rate-limiting step. In this regime, species containing hydroxyl groups condense rapidly.[155]

Under basic conditions, small, highly branched colloidal particles with porous structures are preferentially formed.[156] The Stöber process, one of the most widely used methods for synthesizing monodisperse, spherical silica nanoparticles, typically involves the hydrolysis and condensation of alkoxysilanes under basic conditions, using ammonia in an alcoholic medium.[157]

In contrast, acidic conditions tend to favor the formation of linear and weakly crosslinked structures. Due to the reduced condensation rate, residual Si–OH groups often remain.[156, 158] The resulting amorphous materials are typically transparent and exhibit low porosity, making them suitable for preparing films or freestanding monoliths.[159-161]

Beyond these macroscopic properties, the choice of catalyst also plays a key role in directing the formation of discrete structural motifs such as cages or ladder-like architectures.[151] Hydrochloric acid (HCl) is one of the most frequently used catalysts, particularly because it is released during the hydrolysis of chlorosilane precursors.[162-164] However, many other organic and inorganic acids and bases are employed in the polycondensation of alkoxysilanes, such as phosphoric acid,[165] hydrofluoric acid,[166] nitric acid (HNO_3),[144] acetic acid,[167] sulfonic acids,[168, 169] ammonia,[106] potassium carbonate (K_2CO_3),[116] sodium hydroxide,[170] or trimethylamine.[171]

Well-defined cage-like and ladder-type structures can be synthesized under both acidic and basic conditions.[60] Kaneko et al. demonstrated that, under otherwise identical conditions, 3-aminopropyltrimethoxysilane formed ladders in the presence of HCl and HNO_3, while trifluoromethanesulfonic acid led to the formation of cages.[172] The group of Bassindale established the use of tetrabutylammonium fluoride as a catalyst for transforming alkoxysilanes into T_8-POSS in the presence of water.[173] For the one-pot synthesis of LPSQ, K_2CO_3 has proven to be an effective catalyst.[111, 123]

2.4.2.2 Solvent

Since most alkoxysilane precursors are not soluble in water, a solvent is typically added to obtain a homogeneous reaction mixture and to control the precursor concentration. However, the choice of solvent also affects the kinetics of hydrolysis and condensation as well as the formation of the resulting silsesquioxane structures. Solvent properties such as viscosity, polarity, and protic or aprotic character influence the reaction.[174]

Polarity is particularly important for ensuring precursor solubility in the reaction medium, while the ability to donate a labile proton influences the stability of hydroxyl and hydronium ions, the solvation of transition states, and thus the activation energy of the reaction.[175-177] Depending on

whether the reaction is performed under acidic or basic conditions, H^+ or OH^- ions catalyze hydrolysis and condensation (see mechanism in Figure 3 and 4). Solvent molecules capable of interacting with or binding these catalytic species can reduce their activity. Protic solvents enhance hydrolysis and condensation under acidic conditions, but in basic media they tend to stabilize hydroxide ions, thereby hindering condensation.[178]

Viscosity and steric hindrance also play a role in influencing reaction rates.[179] In general, an increase in viscosity or steric hindrance leads to a reduction in hydrolysis rates.[178, 180]

Solvents not only affect the mechanism of the sol–gel process but can also stabilize defined structural motifs by forming hydrogen bonds with oligomeric silanols. These interactions can either suppress further condensation or direct it toward specific configurations. For instance, Władyczyn and John demonstrated that a double-decker silsesquioxane ($DDSQ(OH)_4$) preferentially formed in protic solvents like isopropanol, whereas aprotic solvents such as THF favored the formation of $POSS(OH)_3$. This difference was attributed to the ability of $POSS(OH)_3$ to form intermolecular dimers, whereas the $DDSQ(OH)_4$ was stabilized by hydrogen bonding, favoring linear associations.[181]

Among solvents, alcohols are the most widely used, particularly in the Stöber process, where they are employed in nearly all reactions.[182] It must be noted that, besides hydrolysis, esterification can occur as a competing reverse reaction.[183] To avoid undesired transesterification or alkoxy group exchange, the alcohol typically matches the alkoxy group of the precursor (e.g., methanol for methoxysilanes).[184]

Finally, the sol–gel process can also proceed without any added solvent. Although most alkoxides are water-insoluble, the alcohol formed as a by-product during hydrolysis can accumulate at the interface between the water and alkoxysilane phases and contribute to mixing. This allows the reaction to proceed homogeneously even without the addition of an external solvent.[144, 185, 186]

2.4.2.3 Temperature

The polymerization of alkoxysilanes follows the Arrhenius equation: an increase in temperature leads to higher reaction rates for both hydrolysis and condensation.[187-189]

Depending on the pH, temperature can be used to selectively adjust the relative rates of these two reactions. Under acidic conditions, condensation can be almost completely suppressed at low temperatures, enabling the isolation of silanols such as phenylsilanetriol.[190] Zhang et al. exploited this effect by inducing the self-assembly of 1,3-diphenyl-tetrahydroxydisiloxane into

an ordered ladder superstructure, which was fixed into a solid film by lyophilization. Subsequent condensation under a triethylamine atmosphere yielded a well-ordered condensed ladder structure (Figure 8b).[109] If molecular pre-organization occurs prior to condensation, for example through hydrogen bonding between silanol monomers, this arrangement can also be maintained by thermally induced condensation, leading to the formation of supramolecularly ordered networks.[189]

Higher temperatures promote intermolecular reactions, resulting in the earlier formation of crosslinked structures and colloids and in an overall higher degree of condensation (DC).[191, 192] Under these conditions, hydrolysis and condensation occur simultaneously and at high rates, often resulting in disordered networks.

2.4.2.4 Water-to-alkoxysilane ratio

The addition of water is essential for the hydrolysis of alkoxysilane precursors. Theoretical studies by Kudo and Gordon demonstrated that even a single water molecule can reduce the energy barriers for both hydrolysis and the subsequent condensation to linear siloxanes or cyclosiloxanes close to 0 kcal·mol^{-1}. Water acts as a proton-transfer catalyst and stabilizes the transition state through hydrogen bonding, allowing the reactions to proceed essentially barrier-free in aqueous solution.[175-177]

The amount of water strongly influences the formation of oligomers, cyclization, molar mass, and its distribution.[112, 168, 193, 194]

The molar ratio of water to alkoxysilane (r) determines the hydrolysis kinetics. Theoretically, complete hydrolysis of an organotrialkoxysilane requires three moles of water per mole of silane, corresponding to the number of alkoxy groups. In practical systems, however, a smaller amount of water can be sufficient because the condensation of two silanol groups releases an additional water molecule. According to the literature, the complete condensation of M-, D-, T-, and Q-units requires 0.5, 1, 1.5, and 2 equivalents of water, respectively.[6]

In the case of silsesquioxanes, a low water content often results in incomplete hydrolysis, leading to linear or only slightly crosslinked structures with residual alkoxy groups (Figure 10a).[161, 162] Under these conditions, alcohol condensation is often favored over the classical water condensation.[6] Increasing the water content promotes hydrolysis, and with higher water levels, the conversion of alkoxysilanes to silanol groups proceeds more rapidly and more completely.[195] At the same time, intramolecular cyclization is favored over linear chain

extension.[161, 162] Furthermore, an increase in the average molecular weight is typically observed with increasing water content (Figure 10b).[112, 194]

For the production of POSS or ladder structures, moderate to high water content (≥ 3 equivalents) are typically required.[111] However, an excessive amount of water can inhibit hydrolysis, for example, due to the solubility of certain alkoxysilanes in water or changes in the acidity of the medium.[196]

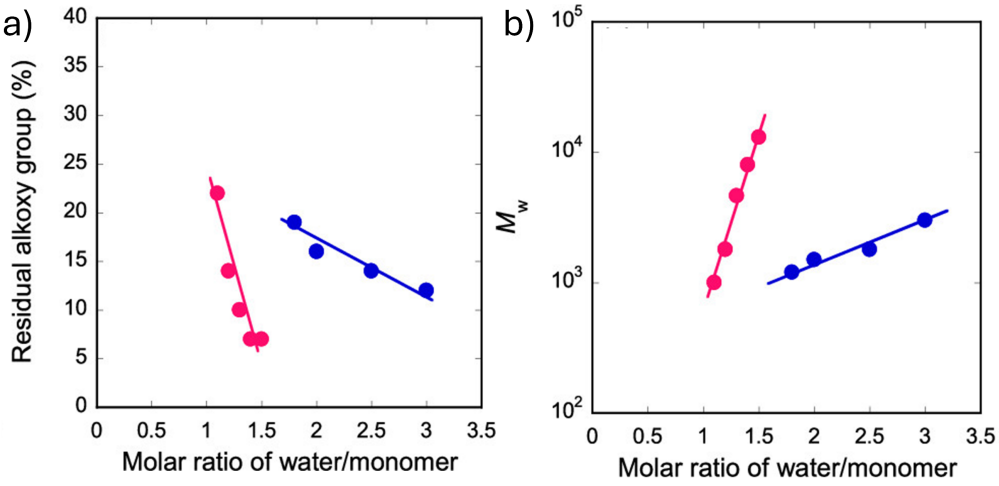

Figure 10: Effect of the water-to-monomer molar ratio on (a) the residual alkoxy group content (b) the weight-average molecular mass (M_w) in polymethylsilsesquioxanes obtained from methyltrimethoxysilane (pink symbols) and methyltriisobutoxysilane (blue symbols). Adapted with permission from Hamada, T.; Goto, T.; Takase, S.; Okada, K.; Uedono, A.; Ohshita, J. Structure–Thermal Property Relationships of Polysilsesquioxanes for Thermal Insulation Materials. ACS *Appl. Polym. Mater.*, **2022**, 4, 2851-2859. Copyright 2022 American Chemical Society.[197]

2.4.2.5 Precursor

The type of precursor, defined by its organic substituent *R´* and three leaving groups (X = OR, Cl) attached to the silicon atom, is the key factor controlling solubility, reaction kinetics, structural formation, and the properties of the final material. Electronic and steric effects of these groups influence hydrolysis and condensation rates. The polarity of both the organic substituent and the leaving group affects solubility and impacts reaction equilibria and precipitation.[198]

Leaving group (-X)

The hydrolysis of the Si–X group is a prerequisite for the subsequent polycondensation of silsesquioxanes. The steric demand of the leaving group plays a decisive role: the larger and

more branched the alkoxy substituent, the slower the hydrolysis proceeds (Figure 10).[199, 200] Methoxy groups are considered the most reactive leaving groups after chloro substituents. However, their high reactivity often leads to the formation of less ordered, three-dimensional networks.[201] In contrast, isopropoxysilanes undergo only incomplete hydrolysis and require much harsher conditions (higher temperatures and larger amounts of water).[202] Ethoxy substituted precursor often provide a useful compromise between the rapid but less ordered reaction of methoxy groups and the slow, incomplete reaction of bulky OR groups.[195] They allow for better control over the progress of hydrolysis and condensation, enabling stepwise reactions that can yield more ordered structures, as is particularly desirable in the synthesis of POSS.[58]

These differences in reaction kinetics can be deliberately exploited to tailor the structure and properties of the final material. For example, Naik et al. prepared self-assembled monolayers (SAMs) from octadecyltrialkoxysilanes in which the surface arrangement, layer thickness, and contact angles varied depending on the leaving group (trichloro-, trimethoxy-, or triethoxy group) due to differences in hydrolysis rates.[203] Hamada et al. studied the influence of residual ethoxy and isobutoxy groups on the insulating properties of polymethylsilsesquioxane films, finding that thermal diffusivity increased with the proportion of unhydrolyzed alkoxy groups, with the bulky isobutoxy group yielding lower thermal diffusivity than the ethoxy group.[197] Jitianu et al. demonstrated that the T_g of polyphenylsilsesquioxanes depends on the precursor alkoxy substituent. Polysilsesquioxanes derived from PhTMS had a T_g of 41.6 °C, compared to 33.1 °C for those from phenyltriethoxysilane.[150]

Although the alkoxy group has no functional role in the final material, its reactivity strongly influences hydrolysis and condensation kinetics. Incomplete conversion can leave residual groups behind, which act as structural defects and, in turn, affect the material properties.[197]

Organic group (R´)

In contrast to the leaving group, the organic substituent (Si–R′) remains intact during hydrolysis and condensation and persisting in the final material, determining its hybrid properties.[204] The electronic, steric, and polar/apolar characteristics of R′ significantly influence reaction kinetics and structural formation.

From the mechanisms of hydrolysis and condensation (Figure 3 and 4), it is evident that the electronic effects of the organic substituent affect the reaction kinetics. Under acidic catalysis, electron-donating substituents increase the electron density at the silicon atom, stabilizing the positively charged transition state and thereby accelerating hydrolysis relative to condensation.

Conversely, electron-withdrawing substituents have the opposite effect, promoting condensation. Under basic conditions, this effect is reversed, as the negatively charged transition state is stabilized by electron-withdrawing groups.[39]

The organic substituent can also directly participate in hydrolysis. Methacryloyloxymethylsilanes exhibit exceptionally high hydrolysis and condensation rates due to intramolecular activation of the silicon atom by the electronic influence of the ester group.[158] Likewise, amino-containing trialkoxysilanes display high hydrolysis rates because the amino group can form hydrogen bonds with a neighboring ethoxy or water molecule, thereby stabilizing the hydrolysis transition state, or act as a base itself.[205] As a result, aminoalkoxysilanes can react even in neutral media (pH = 7) without a catalyst.[171]

Jitianu et al. determined via gas chromatography-mass spectrometry (GC-MS), ^{29}Si NMR, and IR spectroscopy a reactivity order of alkoxides under acid conditions: TEOS < vinyltriethoxysilane (VTES) < methyltriethoxysilane (MTES) in the early stages of the hydrolysis–polycondensation process, which is in good agreement with mechanistic considerations.[204]

Steric effects also play a decisive role, often competing with or overriding the electronic effects. Generally, the larger and bulkier the substituent, the lower the hydrolysis and condensation rates. The steric hindrance of long or branched alkyl chains can even outweigh the rate-enhancing inductive effect of electron-donating alkyl groups.[206]

For example, the bulky tert-butyl group in the corresponding trialkoxysilane strongly inhibits condensation, so that even after several months in an acidic or basic medium, only the corresponding trisilanol and small oligomers are formed, without further network formation.[134] This shows that OH groups can remain stable; their potential for spontaneous self-condensation or formation of hydrogen bonds depends on the size of the organic group. Bulky substituents allow the isolation of low-molecular-weight silanol-containing oligomers,[181, 207] or fully hydrolyzed organotrisilanols.[208, 209] Examples include phenyl-,[147, 190] cyclohexyl-,[210] and tert-butyl-trisilanol.[211]

Silanol-rich oligomers formed in the initial stages of hydrolysis and condensation can undergo either intra- or intermolecular condensation and rearrange to yield various silsesquioxane architectures. Kim et al. investigated substituent effects on the microstructure formation of polyalkylsilsesquioxanes using matrix-assisted laser desorption/ionization coupled to time-of-flight mass spectrometry (MALDI-ToF MS) and found that large, extended organic substituents, such as propyl and isobutyl, preferentially undergo intramolecular condensation,

leading to partially open or perfect cage structures. This behavior was attributed to the steric and hydrophobic effects of the substituents on the configuration of the initial oligomers, which control the rate of intramolecular cyclization over chain-extending condensation reactions.[212] In contrast, small organic substituents, such as methyl, favor intermolecular condensation, producing random networks or ladder-like structures.[213, 214] Park et al. further showed via FTIR spectroscopy that phenyl- and isobutyl-containing polysilsesquioxanes tend to form cage-like structures compared to methyl-substituted analogues.[215]

As alkyl chain length increases, hydrophobic interactions between the organic groups become more pronounced, promoting self-organization into regular, highly ordered structures. Trifunctional silane monomers with C_{16} or C_{18} alkyl chains hydrolyze to form amphiphilic molecules, where hydrophobic interactions drive the formation of monolayers or lamellar structures.[148, 216]

2.4.2.6 Precursor concentration

The hydrolysis of alkoxysilanes is generally described as a first-order or pseudo-first-order reaction.[112, 217, 218] This means that increasing the alkoxysilane concentration leads to a higher hydrolysis rate.[112, 219] Furthermore, the initial silane concentration also affects the molecular weight as well as the type of structures formed.[111, 112]

Lee et al. showed that the weight-averaged molecular weight (M_w) of the obtained LPSQ increased with increasing PhTMS concentration but decreased once the precursor concentration exceeded 13.3 mol·L^{-1} (Figure 11). They attributed the initial increase to the enhanced hydrolysis rate, which produces a larger number of hydrolyzed species that can further condense. Beyond a certain concentration, the reaction mixture becomes supersaturated, which causes lower-molecular-weight intermediates to precipitate, thereby reducing the overall molar mass.[112] The same group further demonstrated that, depending on the precursor concentration, either ladder structures (high concentrations) or cages (low concentration) can be obtained (Figure 8, d).[111] This finding was later reproduced by other researchers. Using *in situ* IR spectroscopy coupled with ^{29}Si NMR, size exclusion chromatography (SEC), and MALDI-ToF MS, they demonstrated that at high PhTMS concentrations (≥ 1.5 mol·L^{-1}) LPSQ precipitates, whereas at lower concentrations (0.5 mol·L^{-1}) short-chain LPSQ fragments undergoes chain scission and rearrangement to form POSS.[220]

Reactions carried out in neat or highly concentrated solutions favor intermolecular interactions and thus the formation of silsesquioxane polymers, including random and ladder structures. In

contrast, condensation under diluted conditions occurs predominantly intramolecularly, favoring the formation of POSS.[221, 222]

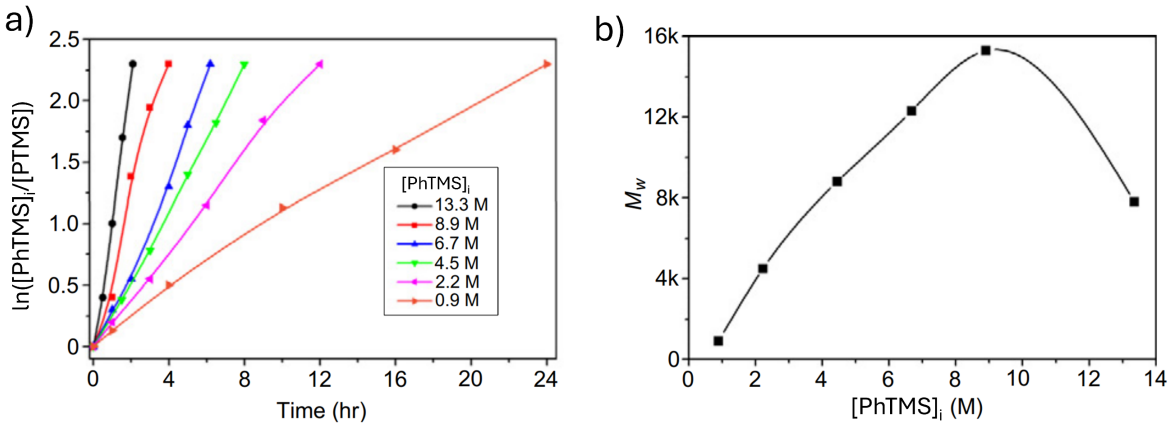

Figure 11: (a) First-order kinetic plots for the hydrolysis of phenyltrimethoxysilane (PhTMS) at various initial PhTMS concentrations ($[PhTMS]_i$) with $[H_2O]_i$ = 30 mol·L^{-1} at 25 °C, showing $\ln([PhTMS]_i/[PhTMS])$ versus reaction time. (b) M_w of the obtained LPSQ as a function of $[PhTMS]_i$. Adapted with permission from Lee, A. S.; Choi, S.-S.; Baek, K.-Y.; Hwang, S. S., Hydrolysis kinetics of a sol–gel equilibrium yielding ladder-like polysilsesquioxanes. *Inorg. Chem. Commun.***2016**, 73, 7–11, Copyright 2016 Elsevier.[112]

2.4.3 Characterization Methods

Different molecular structures of silsesquioxanes result in distinct physical and chemical properties, thereby also influencing their fields of application. A precise understanding of the structure is therefore essential: Do the compounds exhibit cage-like or ladder-like architectures? What is the degree of crosslinking? Are defects such as unreacted hydroxy or methoxy groups present?

To answer these questions, comprehensive characterization is required. In most cases, the use of a single analytical technique is insufficient. Because of the structural complexity of silsesquioxanes, a combination of complementary methods is necessary. Each technique provides specific insights, and only the concerted use of these methods enables a comprehensive understanding of the material's structure.

Over the years, various techniques have been established for the structural analysis of silsesquioxanes.[6, 198, 223, 224] The most important include FTIR and Raman spectroscopy, NMR spectroscopy, XRD, fluorescence and UV/Vis spectroscopy, molar mass determination, and

thermal analysis methods such as thermogravimetric analysis (TGA) and differential scanning calorimetry (DSC).

This chapter presents and discusses these key analytical techniques, focusing on their relevance and informative value for the characterization of different silsesquioxane structures.

2.4.3.1 NMR spectroscopy

The most commonly used nuclei for the characterization of siloxanes and silsesquioxanes are ^{1}H, ^{13}C and ^{29}Si NMR.[225] These techniques provide complementary information that together offers a comprehensive picture of the structure. Depending on the solubility of the samples and the type of information sought, both solution-state and solid-state NMR spectroscopy are commonly applied.

^{13}C and ^{1}H NMR spectroscopy are primarily employed to identify the organic substituents. They can be used to demonstrate that the organic groups are incorporated unchanged into the Si–O–Si network and to verify whether unreacted alkoxy groups are present. By integrating the characteristic proton signals of the alkoxy groups in the ^{1}H NMR spectrum, the degree of hydrolysis can be quantified. This parameter reflects how many alkoxy substituents have reacted, but it does not directly correspond to the number of silanol groups formed, since these may either remain as Si–OH functionalities or undergo subsequent condensation to Si–O–Si linkages.

A direct determination of the OH groups by ^{1}H NMR spectroscopy is challenging. Hydroxyl protons typically produce broad, poorly integrated signals, due to rapid exchange within the sample, particularly with other exchangeable protons such as additional –OH or –NH functionalities.[226] In addition, hydrogen bonding or chemical exchange with the NMR solvent can shift or even suppress these signals, meaning that their observability strongly depends on the solvent used.[227] Therefore, the quantification of OH groups via the ^{1}H NMR is only possible to a limited extent, particularly for polymers with a strongly varying chemical environment.

The most important tool for identifying the silsesquioxane species is ^{29}Si NMR spectroscopy. In addition to ^{1}H NMR spectroscopy, it provides detailed information about the substitution pattern of the silicon atoms and the DC. Both the number of Si–O–Si bonds and the number of organic substituents per silicon center can be derived from the chemical shift ($\delta(^{29}Si)$). The $\delta(^{29}Si)$ value shifts downfield as the number of organic groups on the silicon atom decreases. The chemical shift typically follows the trend: M > D > T > Q functionalized silicon centers.[225] Within a given functionality, each additional Si–O–Si bond leads to a further downfield shift

($T^0 > T^1 > T^2 > T^3$).[228] The hydrolysis of an alkoxy group can also be detected by a downfield shift of the corresponding Si signal by ~ 1–2 ppm (e.g., $T^2_{OR} > T^2_{OH}$) (Figure 12).[204, 229] A change of the alkoxy substituent from for example ethoxy to methoxy is also visible by a downfield shift ($\delta((^{29}Si)PhSi(OEt)_3) = -58.6$ ppm vs. $(\delta(^{29}Si)PhSi(OMe)_3 = -55.4$ ppm solution NMR with neat monomer). However, the influence of the alkoxy group becomes negligible with increasing condensation degree and a higher number of hydrolyzed groups.[134]

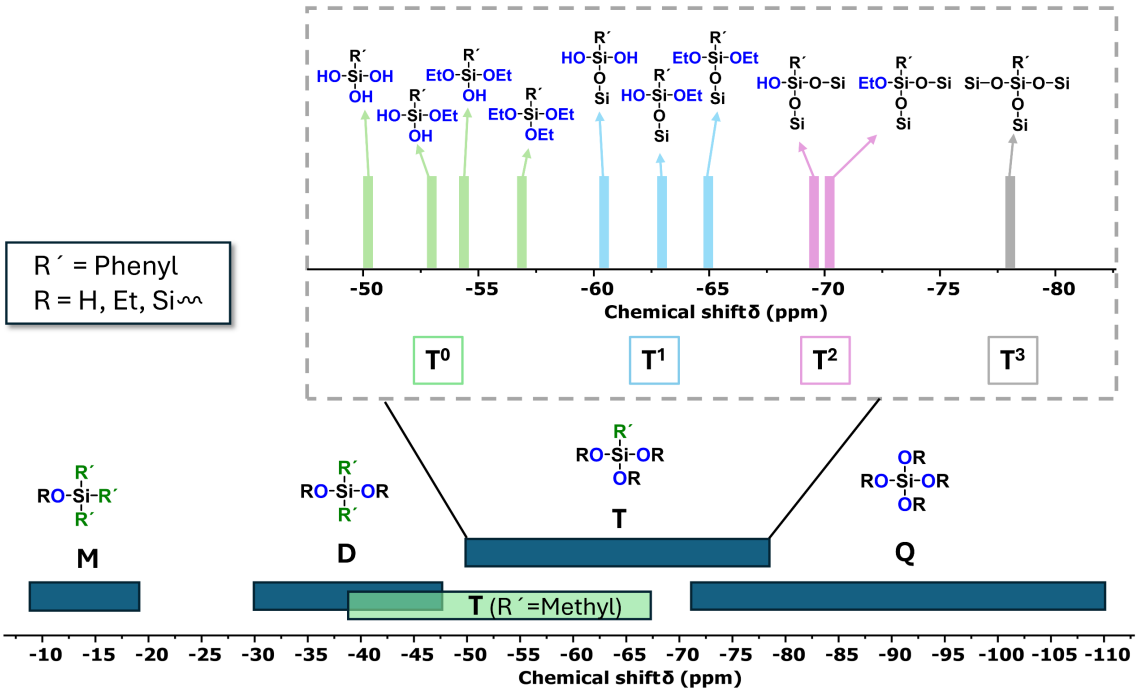

Figure 12: Chemical shifts of different silicon species (M, D, T, and Q units) with phenyl substituents (R´). Particular emphasis is placed on T units as the fundamental building blocks of polysilsesquioxanes, showing chemical shifts for T^0–T^3 and distinguishing between OH- and OEt-terminated groups. The values shown for the T units are based on ^{29}Si MAS NMR and may vary in solution.[229] For comparison, chemical shifts of methyl-functionalized T units are also included.

The type of organic substituents bound to silicon also significantly influences the chemical shift of the ^{29}Si NMR signal. For example, replacing a methyl group with a phenyl group leads to an upfield shift of the signal by approximately 15 ppm.[134] A comprehensive overview of the chemical shifts of hydrolyzed and condensed alkoxysilanes with various organic substituents can be found in the review by Sato et al..[223] While the absolute values are strongly solvent dependent, the trends described above are consistent irrespective of the solvent.

In addition to routine 1D measurements, 2D NMR experiments such as heteronuclear single quantum coherence (HSQC) or heteronuclear multiple bond correlation (HMBC) spectroscopy

enable correlations between protons, carbons, and silicon centers. This makes it possible to assign organic substituents to specific T units in silsesquioxanes and to follow hydrolysis and condensation processes more directly, for example by monitoring the disappearance of alkoxy groups and the emergence of silanol or siloxane linkages.[230] The advantages of 2D NMR become even more apparent in complex systems, such as mixtures of silsesquioxanes with different comonomers or combinations of silsesquioxanes and siloxanes.[142, 231, 232] In these cases, the technique allows substituents to be traced back to their corresponding M-, D-, or T-type silicon species, thereby providing detailed insight into the evolving network structure and precursor reactivity.

For further silsesquioxane characterization, the proportions of the various T^n species can be determined quantitatively or semi-quantitatively by deconvolution and integration of the ^{29}Si NMR spectra. The DC can then be calculated from these proportions using the following formula (1):[233]

$$DC[\%] = \frac{T^3[\%] \cdot 3 + T^2[\%] \cdot 2 + T^1[\%]}{3} \quad (1)$$

It must be taken into account that quantitative ^{29}Si NMR spectroscopy presents inherent challenges. These arise from the low natural abundance of the ^{29}Si isotope (4.7%), its long relaxation times, and the comparatively small gyromagnetic ratio.[234] These factors result in low signal sensitivity, making it difficult to obtain high-quality spectra and to perform precise quantitative analysis. To improve quantifiability by reducing the relaxation time, liquid-state NMR spectra can be recorded in the presence of a paramagnetic relaxation agent, such as chromium(III) acetylacetonate ($Cr(acac)_3$).[235, 236] In the solid state, it is recommended to acquire ^{29}Si NMR spectra using single-pulse experiments (SP-MAS). Cross-polarization measurements (CP-MAS) are less suitable because the signal intensity strongly depends on the number and distance of neighboring protons.[237, 238] As a result, the population ratios of the individual silicon species are often not accurately represented. However, if large amounts of protons are present, for example, due to uniformly distributed organic substituents in T units, these deviations between different T species are minimized, allowing trends in the DC to be reliably detected via CP measurements.[239]

Based on the DC and the amount of remaining alkoxy groups, which can be determined from the ^{1}H NMR spectra, the amount of OH groups can be calculated using formula (2).[144]

$$OH[\%]=100 – DC[\%] - OMe[\%] \quad (2)$$

The full width at half maximum (FWHM) of the T-peaks can be used to analyze the structural organization of the material. Polymers often exhibit variations in their chemical structure or tacticity, which result in slightly different chemical environments along the polymer backbone. These differences cause small shifts in the chemical resonance, leading to broad peaks composed of numerous closely spaced, unresolved signals. The more uniform and regular the structure, the sharper and more defined the peaks appear in the spectrum. A narrow FWHM of the T^3 peak is therefore indicative of a high degree of regularity in ladder-type architectures.[108, 141, 240, 241]

In contrast, precursors or cages typically exhibit single, well-defined peaks that are clearly distinguishable from the broader signals of ladder-like or random networks.[111] The chemical shift and the number of peaks observed depend on the size of the cage, the organic substituents, and the number of possible isomers, which together allow precise structural identification.[60, 64]

NMR spectroscopy is one of the most powerful tools for the structural characterization of silsesquioxanes. It provides detailed information on the type and number of T units present, the degree of crosslinking, and the presence of structural defects within the network. It also enables initial insights into the degree of structural order.

The chemical shift of defined POSS compounds serves as a reliable indicator of purity and allows their identification. However, in the case of polymeric materials with ladder-type or random architectures, additional analytical techniques are required to achieve a comprehensive understanding of the structure.

2.4.3.2 IR spectroscopy

Infrared spectroscopy can be used to analyze both the substituents and the network structure of silsesquioxanes. Brown et al. already described IR spectroscopy as a “perhaps most valuable” method for determining the structural arrangement of the silsesquioxane network, since the skeletal vibrations of the polysiloxane framework are strongly infrared-active and respond sensitively to structural changes.[96] The region between 1000–1200 cm^{-1} is particularly important for detecting Si–O–Si stretching vibrations (Figure 13a). Silsesquioxanes with ladder, cage, partial cage, or random structures exhibit characteristic absorption bands in this range, which are widely used in the literature for structural classification.[223]

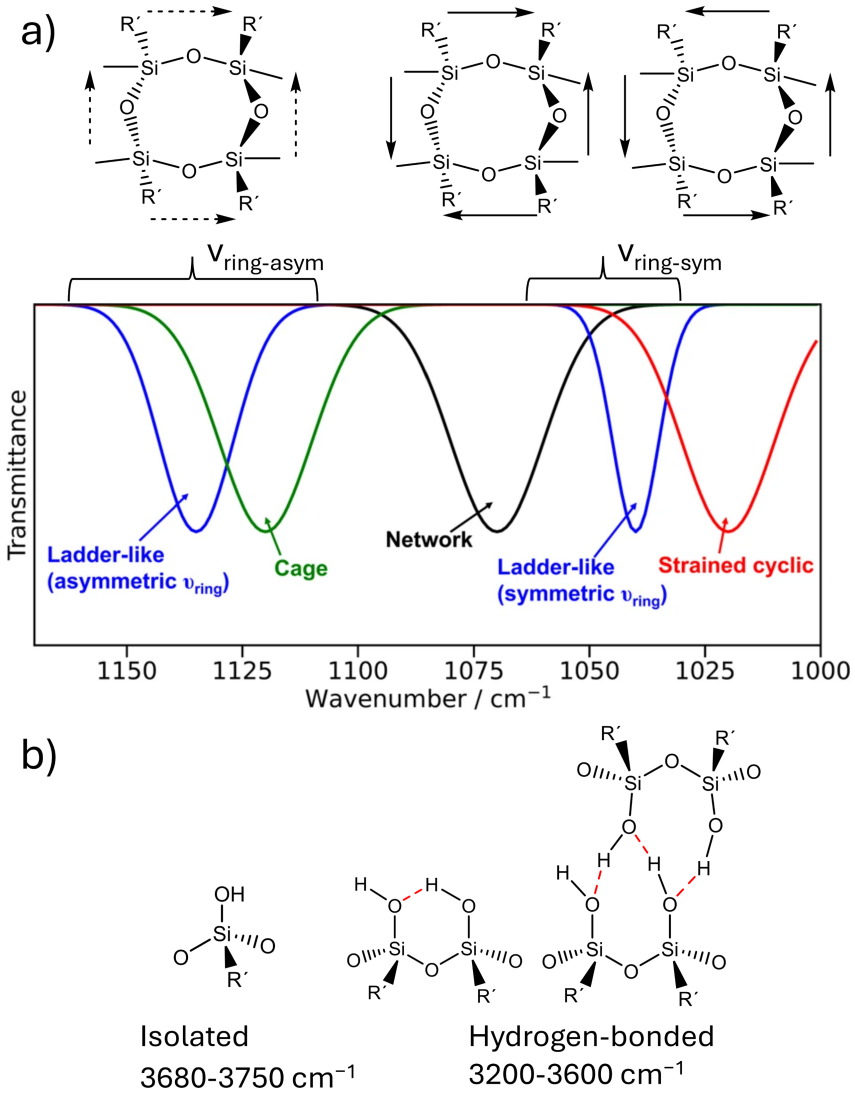

Figure 13: a) IR band maxima of various silsesquioxane structures, including ladders, cages, networks, and small cycles. Reproduced with permission from Sato, Y.; Hayami, R.; Gunji, T. Characterization of NMR, IR, and Raman spectra for siloxanes and silsesquioxanes: a mini review. *J. Sol-Gel Sci. Technol.* **2022**, 104, 36–52. Copyright 2022 Springer Nature.[223] Illustration of the $\nu_{ring\text{-}asym}$ and $\nu_{ring\text{-}sym}$ vibrational modes of $(SiO)_4$ units, indicated by arrows. Adapted with permission from Park, E. S.; Ro, H. W.; Nguyen, C. V.; Jaffe, R. L.; Yoon, D. Y. Infrared Spectroscopy Study of Microstructures of Poly(silsesquioxane)s. *Chem. Mater.* **2008**, *20*, 1548-1554. Copyright 2008 American Chemical Society.[215] b) Structures of isolated and different hydrogen-bonded silanols with their corresponding IR absorption ranges.

Park et al. combined theoretical and experimental IR studies to determine the microstructure of variously substituted polysilsesquioxanes. They analyzed the $(Si–O)_4$ ring as a subunit of the siloxane framework and its characteristic vibrational modes. Each Si–O–Si edge contributes an asymmetric stretching vibration that can combine into symmetric ($\nu_{ring\text{-}sym}$) or asymmetric

($\nu_{ring\text{-}asym}$) modes relative to the ring center. When the oxygen atoms on opposite sides of the ring are displaced in parallel, the $\nu_{ring\text{-}asym}$ vibration appears at around 1150 cm^{-1}. In contrast, antiparallel displacement leads to the $\nu_{ring\text{-}sym}$ vibration at 1050–1100 cm^{-1} (Figure 13a). The latter is IR-inactive in highly symmetric cages with $(Si–O)_{2n}$ rings (e.g., T_8), as no change in the dipole moment occurs. In open cages or ladder structures, however, this mode becomes IR-active and is visible in the spectrum.[215]

Consequently, fully condensed cage structures described in the literature typically exhibit a single, well-defined Si–O–Si stretching band at higher wavenumbers (around 1120 cm^{-1}).[242-244] Ladder structures, on the other hand, display lower symmetry, which is reflected in the presence of two bands at approximately 1100–1150 cm^{-1} and 1050–1100 cm^{-1}; the intensity of the $\nu_{ring\text{-}sym}$ band increases relative to the $\nu_{ring\text{-}asym}$ band as symmetry decreases.[106, 111, 139, 215, 245]

The Si–O–Si network in linear, crosslinked or cyclic units typically shows absorption near 1075 cm^{-1},[246, 247] while strained cyclic siloxanes exhibit a band at lower wavenumbers, around 1020 cm^{-1}.[247, 248]

The position of the Si–O–Si stretching vibrations is primarily determined by the network structure, though the nature of the organic substituent also has a minor influence due to electronic effects.[249, 250] As a result, both structure and substituents can cause slight shifts in the wavenumber of the Si–O–Si band, which accounts for variations reported in the literature. For defined structures, such as fully condensed POSS cages or small ladder structures, IR spectra serve as characteristic fingerprints. However, mixed structures are common, leading to broad, overlapping Si–O–Si bands that make precise identification of individual structural motifs difficult.[251]

In addition to the Si–O–Si backbone vibrations, organic groups and reactive substituents display characteristic bands that aid structural analysis. The bands of hydroxyl and alkoxy groups provide valuable information on reaction progress and kinetics,[230, 252] as well as on whether unreacted groups remain in the material. The OH stretching band in the region of 3000–3800 cm^{-1} is of particular interest, as the detection of OH groups via NMR is often challenging. In IR spectroscopy, the position of this band offers insights into the bonding environment of the OH groups, since it is influenced by hydrogen bonding. Isolated silanols typically absorb at 3680–3750 cm^{-1} and hydrogen-bonded silanols between 3200 and 3600 cm^{-1} (Figure 13b).[253]

The vibrations of organic substituents provide further structural information. Different organic groups show characteristic IR bands, which can be used to assess whether they remain intact or have undergone changes such as oxidation or thermal degradation.[254, 255]

In silsesquioxanes with long *n*-alkyl chains, C–H stretching vibrations, particularly the symmetric (d^+) and asymmetric (d^-) modes of $–CH_2–$ and $–CH_3$ groups between 2800 and 3000 cm^{-1}, allow conclusions about the chain conformation and packing order. Comparison of peak position and FWHM with highly crystalline trans-*n*-alkanes provides information on conformational order.[216, 256] In amorphous samples or solutions, these bands shift to higher wavenumbers, indicating increased gauche defects and reduced packing order (Figure 14).[257]

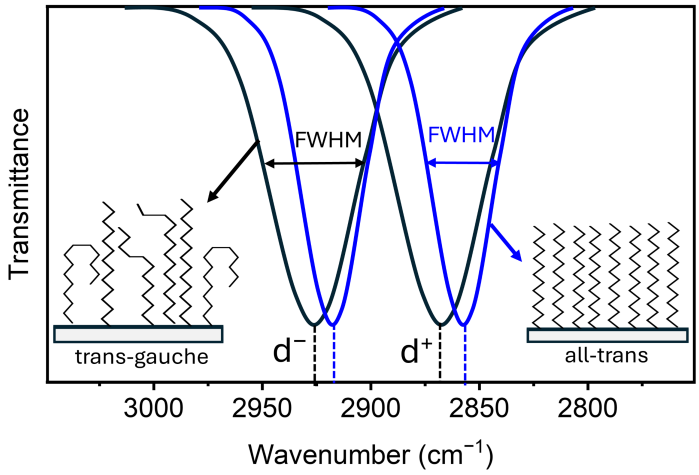

Figure 14: IR band maxima of *n*-alkylsilsesquioxanes for the methylene ($-CH_2-$) symmetric (d^+) and antisymmetric (d^-) stretching vibrations. Increasing gauche defects (decreasing conformational/ packing order) shift both bands to higher wavenumbers and increase FWHM.

IR spectroscopy is thus an important complement to NMR analysis, offering more detailed insights into the siloxane structure and the presence of OH groups. Furthermore, attenuated total reflectance (ATR) FTIR spectroscopy enables the analysis of insoluble samples with minimal effort and preparation. However, band overlap, including contributions from by-products such as water or alcohol, can complicate precise structural assignments.

2.4.3.3 Raman spectroscopy

Raman spectroscopy serves as a complementary technique to IR spectroscopy. It allows the detection of vibrational modes that are inactive in IR spectra. A key principle in this context is the mutual exclusion rule, which applies strictly to idealized molecules with a center of inversion symmetry: vibrational modes that are IR-active are Raman-inactive, and vice versa. IR activity requires a change in the dipole moment during the vibration, whereas Raman activity requires a change in the molecular polarizability. Consequently, symmetric vibrations with

respect to the center of symmetry are Raman-active, while asymmetric vibrations are IR-active.[258]

Thus, the symmetric vibration of $(Si–O)_{2n}$ ring subunits in highly symmetrical POSS can only be observed in the Raman spectrum. These vibrations typically appear between ~ 400–600 cm^{-1}, depending on the ring size, and are slightly shifted by the nature of the organic substituents.[259]

Marcolli and Calzaferri developed a formula to estimate the position of ring-breathing vibrations based on ring size: larger rings appear at lower frequencies, while smaller rings occur at higher frequencies.[260] Six-membered rings are typically observed near 600 cm^{-1}, eight-membered rings near 480 cm^{-1}, and ten-membered rings near 400 cm^{-1} (Figure 15).[259]

Analogous to IR spectroscopy, hydrolysis can also be monitored by Raman spectroscopy, as the Si–O deformation mode shifts to higher frequencies with an increasing number of hydrolyzed groups Thus, it is possible to distinguish between $PhSi(OMe)_3$ (656 cm^{-1}), $PhSi(OMe)_2$**OH** (668 cm^{-1}), $PhSi(OMe)$**$(OH)_2$** (682 cm^{-1}) and $PhSi$**$(OH)_3$** (690 cm^{-1}) (Figure 15).[230]

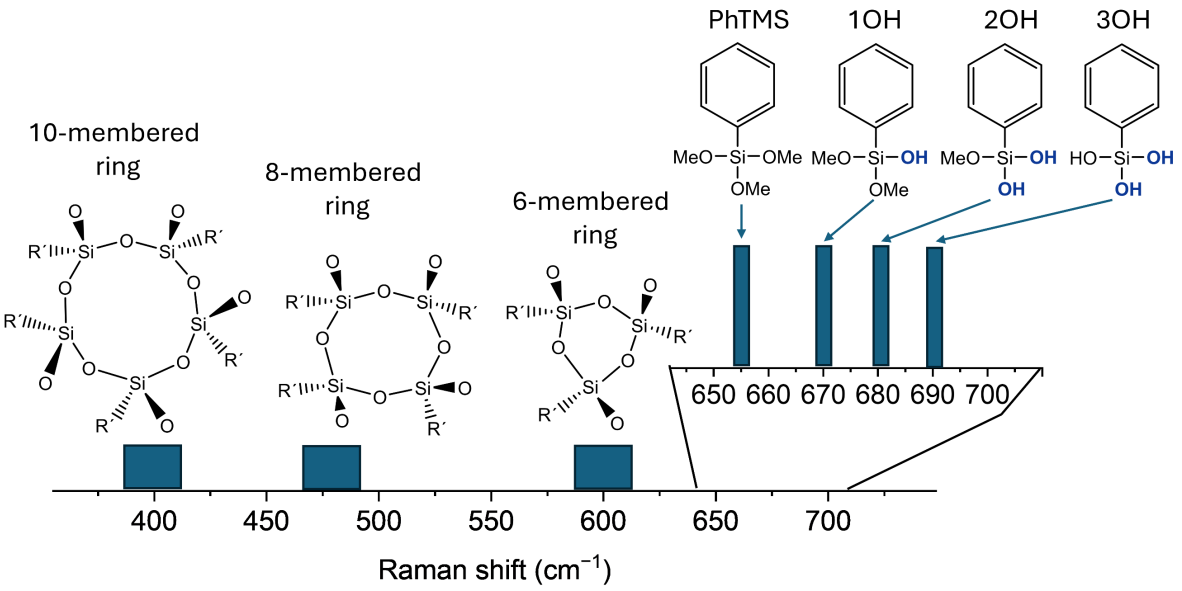

Figure 15: Positions of the symmetric vibrations of six-, eight-, and ten-membered silsesquioxane rings, as well as the Si–O deformation mode shift of partially and fully hydrolyzed PhTMS in the Raman spectrum.

Raman spectroscopy provides complementary structural information that cannot be obtained from IR spectroscopy alone. In addition, it allows hydrolysis processes to be monitored in detail, particularly during the early stages of the reaction, by distinguishing between monohydrolyzed, dihydrolyzed, and trihydrolyzed trialkoxysilanes.

2.4.3.4 Powder X-ray diffraction (PXRD)

Silsesquioxanes can exhibit amorphous, semicrystalline, or crystalline structures, depending on their molecular architecture. PXRD is a suitable technique to distinguish between these structural states and can further provide insight into mesophases or supramolecular organization in partially ordered systems.[261]

The diffraction pattern of a silsesquioxane is mainly determined by the topology of the inorganic siloxane network and the degree of structural order. While the type and size of the organic substituents influence the packing and organization of the material, the dominant diffraction peaks primarily originate from the silicon atoms and their arrangement within the network, since the scattering contribution of the organic groups is weak.

Amorphous silica exhibits only short-range order due to the random connectivity of its SiO_4 tetrahedra, with significant variation in Si–O–Si bond angles. In PXRD, it is characterized by a broad, diffuse scattering region in the 2θ range 10–35° (d_2), which is attributed to the average distance between neighboring silicon atoms connected through oxygen bridges.[262, 263] This distance remains largely constant and is independent of the specific chemical composition.[264]

The incorporation of organic groups into the silica network can enhance long-range structural ordering, which manifests in PXRD as an additional, sharper diffraction peak at lower scattering angles (d_1).[262, 265]

An early example of PXRD being used to support structural assignments in silsesquioxanes is found in the work by Brown et al. and Adrianov et al., who were among the first to describe a ladder-like polyphenylsilsesquioxane.[100, 266] Brown et al. reported two characteristic reflections at $d_1 \approx 12.5$ Å and $d_2 \approx 5.0$ Å,[100] which have since been used as a structural fingerprint for ladder-type silsesquioxanes. The first low-angle reflection d_1 is associated with lateral packing of the parallel double-stranded siloxane backbones and is commonly interpreted as the intermolecular chain-to-chain distance, or the width of the ladder. The second reflection d_2 corresponds to the thickness of a single siloxane strand (Figure 16b).[139, 141, 240] The position of the d_1 reflection is highly sensitive to structural modifications. Larger organic substituents with greater van der Waals volume or longer alkyl chains generally increase the chain spacing, resulting in a shift of the d_1 reflection to lower 2θ angles (larger distances).[116, 267] Conversely, backbone defects, such as OH or OR groups, can lead to tighter packing, shifting d_1 to higher 2θ angles (lower distances).[268]

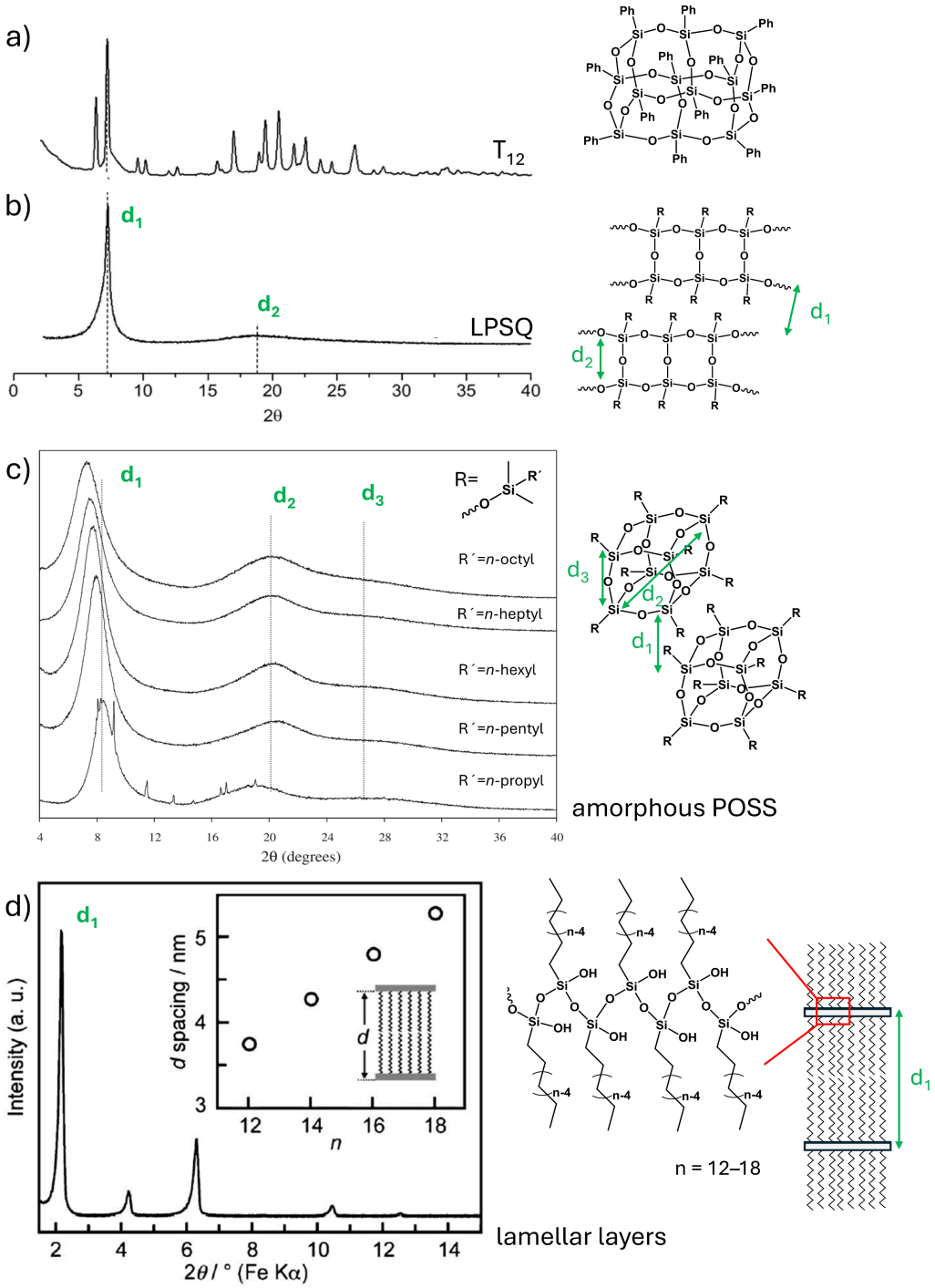

Figure 16: PXRD patterns of various silsesquioxane structures with characteristic *d*-spacing: a) crystalline T_{12}-Ph POSS. b) Ladder-type polyphenylsilsesquioxane. PXRD patterns in figures a and b adapted with permission from Choi, S.-S.; Lee, A. S.; Hwang, S. S.; Baek, K.-Y. Structural Control of Fully Condensed Polysilsesquioxanes: Ladderlike vs Cage Structured Polyphenylsilsesquioxanes. *Macromolecules* **2015**, *48*, 6063–6070. Copyright 2015 American Chemical Society.[111] c) Oktakis(alkyldimethylsiloxy)octasilsesquioxane, $R'_8Q_8M_8$, with R´ = *n*-octyl, *n*-heptyl, *n*-hexyl, *n*-pentyl, *n*-propyl. PXRD patterns adapted with permission from Perrin, F. X.; Nguyen, T. B. V.; Margaillan, A. Linear and branched alkyl substituted octakis(dimethylsiloxy)octasilsesquioxanes:

WAXS and thermal properties. *Eur. Polym. J.* **2011**, 47, 1370-1382. Copyright 2011 Elsevier.[269] d) Lamellar layered *n*-alkylsilsesquioxane (n = 18); the inset shows the d_1 spacing as a function of alkyl chain length. PXRD pattern adapted from Shimojima, A. Design of nanohybrid and nanoporous materials through self-assembly of organosilane molecules, *J. Ceram. Soc. Jpn.* **2008**, 116, 278–283. Licensed under CC-BY 4.0.[270] Structural illustrations were added by the author.

The FWHM of the d_1 peak provides insight into the average size of the ordered domains. In addition, the intensity ratio of d_1 to d_2 ($R = I(d_1)/I(d_2)$) is frequently used as an indicator of structural order.[132] A smaller FWHM or a larger R value indicates higher structural order and fewer defects. In the literature, this order is often equated with the relative fraction of ladder motifs within the structure.[132, 137, 268] In contrast to d_1, the d_2 reflection is relatively insensitive to structural variation. Both its position and intensity remain nearly constant upon changes in the organic substituents or the backbone structure.[116, 268]

Many POSS crystallize in well-ordered lattices, leading to sharp and well-defined diffraction peaks.[111, 271] These patterns are easily distinguishable from those of amorphous or partially ordered silsesquioxane networks (Figure 16a). However, not all POSS structures are crystalline. Amorphous variants often show PXRD patterns resembling those of ladder-type silsesquioxanes, which complicates structural assignment. Amorphous POSS typically display three broad reflections that occur in the same scattering angle range as those characteristic of ladder structures (Figure 16c).[269, 272-274] The first (d_1) is associated with the average intermolecular distance between POSS cages and is influenced by the size and flexibility of the organic substituents, which act as spacers. The second and third reflections (d_2 and d_3) are commonly assigned to internal structural dimensions, such as the body diagonal of the cage and the distance between opposite Si_4O_4 faces.[269] Open-cage POSS frequently exhibit two broad peaks, comparable to those observed in ladder-like systems.[275, 276] Likewise, linear oligo- and polysiloxanes derived from dialkoxysilane precursors can produce similar two-peak patterns, with d_1 reflecting the average distance between neighboring polymer chains.[189, 277]

As a result, PXRD alone is often insufficient to unambiguously assign structural motifs. Additional characterization techniques are essential to support the structural interpretation and to distinguish between ladder-type, cage-like, and random network architectures.

In addition to ordering phenomena originating from the inorganic siloxane network, the organic substituents themselves can contribute significantly to the structural organization of polysilsesquioxanes. This is particularly relevant for long alkyl chains, which may undergo self-assembly or partial crystallization. Studies have shown that chains of C_{12} and longer are

particularly prone to forming lamellar arrangements, where the alkyl groups pack in ordered domains (Figure 16d).[216, 278-280] This ordering gives rise to characteristic low-angle reflections in PXRD patterns, indicative of regular interlayer spacing governed by van der Waals interactions. The d-spacing typically increases with chain length, but factors such as gauche conformations, chain entanglement, or partial disorder can reduce the periodicity.[278, 279] The degree of alkyl chain crystallinity strongly influences the overall structural state and may either enhance or disrupt long-range order within the material. Thermal treatment can trigger rearrangements, including phase transitions into semicrystalline or more disordered states, depending on chain length and the degree of network condensation.[278, 281] As a result, diffraction features in such hybrid materials may reflect a combination of backbone structure and alkyl chain packing.

While PXRD is not usually the first method considered for silsesquioxane characterization, it is a valuable tool for identifying structural features such as crystallinity, lamellar order, or periodic domain packing. However, as it reflects only the average structural information, PXRD alone is often insufficient to fully resolve complex silsesquioxane architectures.

2.4.3.5 Size exclusion chromatography (SEC)

While spectroscopic methods such as NMR or FTIR primarily provide structural and functional information at the molecular level, chromatographic techniques enable the separation of individual species in the reaction medium based on physical properties such as volatility or molecular size. This allows for a detailed analysis of molar mass distribution, oligomer formation, and polydispersity.

Various chromatographic methods can be applied to separate silsesquioxane species, including gas chromatography (GC),[282] liquid chromatography (LC),[194] and SEC.

SEC is one of the most commonly used methods for determining molar mass averages and molar mass distributions of oligo- and polysiloxanes as well as silsesquioxanes. It can be applied over a wide molar mass range, typically covering a range from ~ 200 to 1,000,000 $g \cdot mol^{-1}$.[6]

SEC separates molecules according to their hydrodynamic volume in solution. Larger molecules elute earlier because they penetrate less into the pores of the stationary phase.[283]

Detection is typically carried out using RI or UV detectors, or in combination with multi-angle light scattering (MALS), which enables the determination of absolute molecular mass independently of calibration standards. Nevertheless, many studies still rely on calibrations with

standards such as polystyrene. This approach introduces systematic uncertainties, as the hydrodynamic behavior of polystyrene often does not reflect that of the silicon-containing species under investigation.[168, 284]

Furthermore, it is important to note that SEC alone does not provide structural information on the eluted fractions. Identification of the separated species therefore requires complementary characterization techniques such as NMR or mass spectrometry (MS).[168, 285, 286]

However, trends in molar masses and indirect conclusions about molecular architecture can be drawn from the SEC trace.

Discrete cage-like silsesquioxanes often yield sharp, narrowly distributed peaks with low polydispersity indices (Đ ~ 1.0–1.1) (Figure 17a).[111, 284] In contrast, linear or ladder-like oligomers typically result in broad and often asymmetric peaks, indicating a greater diversity in structure and molar mass distribution (Figure 17b).[105, 106, 141] Ladder-type polyphenylsilsesquioxanes, for instance, have been reported with number-average molar masses (M_n) up to M_n = 238,100 g·mol^{-1} (M_w = 540,400 g·mol^{-1}, Đ = 2.3).[287]

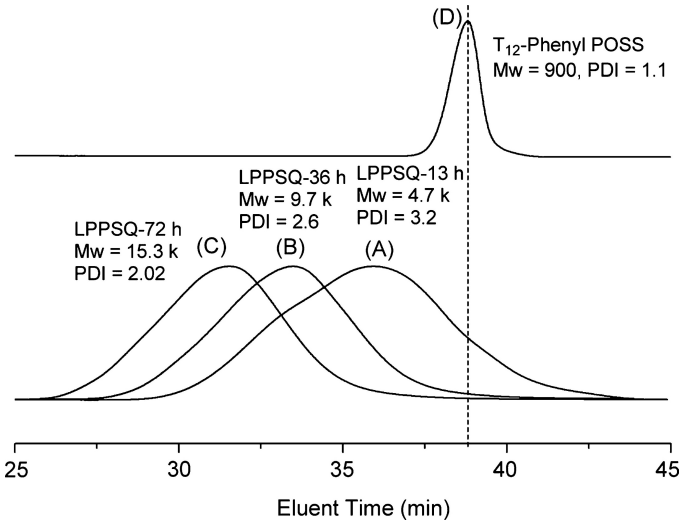

Figure 17: SEC curves of (a) T_{12}-phenyl-POSS and (b) phenyl-LPSQ (LPPSQ) at different reaction times ranging from 13 to 72 h. Reproduced with permission from Choi, S.-S.; Lee, A. S.; Hwang, S. S.; Baek, K.-Y. Structural Control of Fully Condensed Polysilsesquioxanes: Ladderlike vs Cage Structured Polyphenylsilsesquioxanes. *Macromolecules* **2015**, *48*, 6063–6070. Copyright 2015 American Chemical Society.[111]

Time-resolved SEC measurements can be used to monitor polymerization processes and to follow shifts in molecular weight distributions during the reaction..[166, 168] Moreover, the influence of various synthesis parameters, such as catalyst type or reaction temperature, on the product distribution can be assessed directly from SEC data.[166, 288]

In summary, SEC is a key analytical tool in polymer science, particularly for the determination of molar mass distributions and polydispersity. In the field of silsesquioxanes, and especially in ladder structure research, it serves to evaluate the success of synthetic strategies aimed at producing high molar mass polymers. Synthetic parameters can be systematically studied to assess their impact on molecular mass distribution.
Nonetheless, SEC cannot be applied to highly crosslinked or insoluble samples, as these cannot be dissolved and chromatographically separated.

2.4.3.6 MALDI-ToF MS

Mass spectrometry is based on the ionization of a sample, followed by the separation and detection of the resulting ions according to their mass-to-charge-ratio (m/z). For polyorganosilsesquioxanes, matrix assisted laser desorption/ionization (MALDI) has proven to be a particularly suitable ionization method, as it is a soft ionization technique. This means that molecules remain largely intact and undergo minimal fragmentation. In MALDI, the sample is irradiated together with a light absorbing matrix. The laser energy is transferred from the matrix to the analyte molecule, leading to its desorption and ionization into the gas phase. The resulting ions are typically singly charged, which significantly simplifies the interpretation of the mass spectra.[289] However, the method is less suitable for compounds with low molar masses (below ~ 1000 g·mol^{-1}), as matrix peaks dominate in this region.[290]
When combined with a time-of-flight (ToF) detector, which determines the mass based on the ions' flight time, MALDI-ToF MS enables fast and high resolution analysis over a wide mass range.[291] This technique is increasingly used for the structural characterization of siloxanes and silsesquioxanes, as it allows the direct detection of cage structures, hydrolysis and condensation products, as well as polymeric species.[285, 292-295]
In the spectrum, oligomers and polymers typically appear as clusters, whose positions reflect the number of Si units and can be assigned to specific structural motifs. Well defined cages such as T_8 or T_{12} yield sharp, distinct peaks corresponding to their exact molecular mass (Figure 18a),[296-298] while ladder-type polymers form multiple clusters separated by regular mass intervals corresponding to the mass of a repeating unit (Figure 18b).[139]

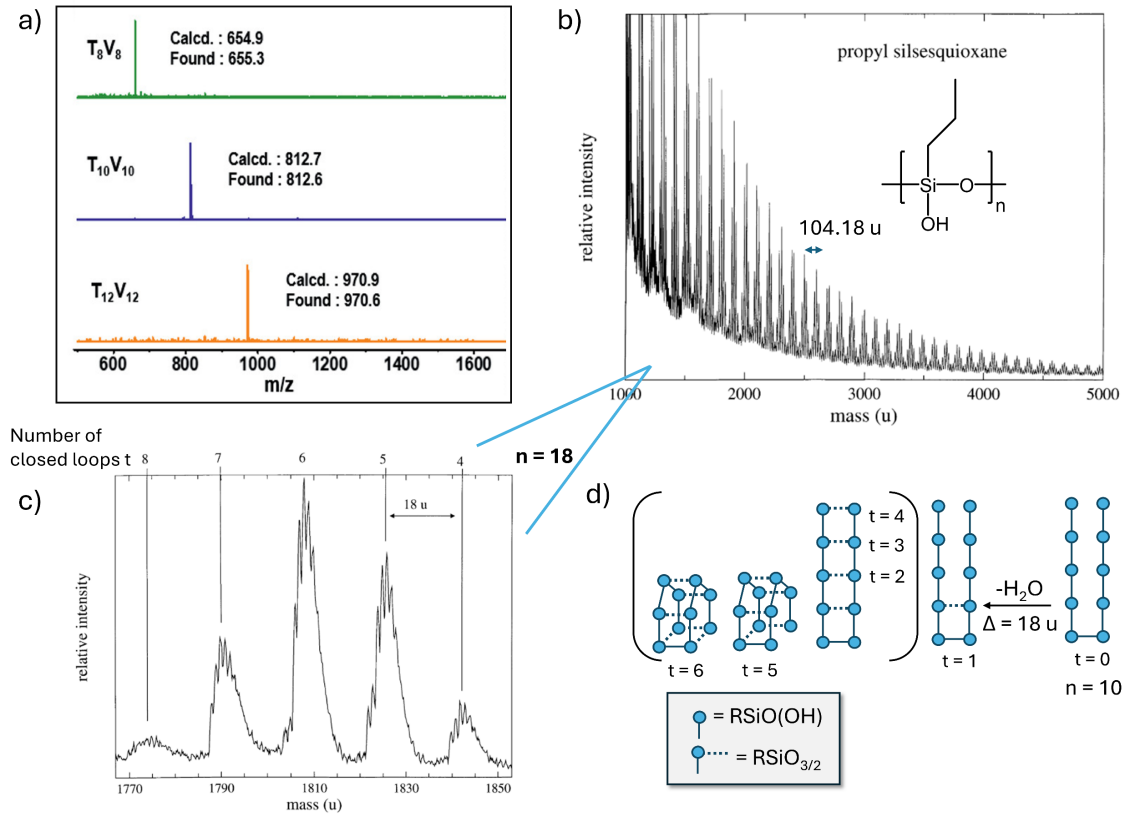

Figure 18: a) MALDI-ToF mass spectra of vinyl-functionalized T_8, T_{10}, and T_{12} POSS (peaks correspond to $[M \cdot Na]^+$). Reproduced with permission from Zhou, D.-L.; Li, J.-H.; Guo, Q.-Y.; Lin, X.; Zhang, Q.; Chen, F.; Han, D.; Fu, Q. Polyhedral Oligomeric Silsesquioxanes Based Ultralow-k Materials: The Effect of Cage Size. *Adv. Funct. Mater.* **2021**, 31, 2102074. Copyright 2021 Wiley-VCH GmbH.[299] b) MALDI-ToF mass spectrum of *n*-propylsilsesquioxane. The mass differences between clusters correspond to the mass of one repeating unit [R´SiO_2H]. c) Zoom-in on a single major cluster (from the spectrum in b)) containing peaks corresponding to 18 repeating units. The peak-to-peak distance of 18 u is indicative of intramolecular water loss and loop (*t*) formation. Figure b) is adapted and figure c) is reprinted with permission from Wallace, W. E.; Guttman, C. M.; Antonucci, J. M. Polymeric silsesquioxanes: degree-of-intramolecular-condensation measured by mass spectrometry. *Polymer* **2000**, 41, 2219-2226. Copyright 2000 Elsevier.[290] d) Possible structures that can form within an oligosilsesquioxane containing 10 repeating units (*n*) through intramolecular condensation reactions accompanied by water elimination. Theoretically, up to six loops can be generated using the formula $t = ½(n + 1)$ for *n* even, and $t = ½(n - 1) + 1$ for *n* odd.[290]

Moreover, substituents such as organic side groups, OH, or OR groups can be identified based on precise mass differences. This allows the distinction between open, partially condensed, and closed structures within product mixtures of varying composition.[293, 294]

Within individual clusters, mass differences of 18 g·mol^{-1} are frequently observed and correspond to the loss of water (Figure 18c). These signals indicate intramolecular condensation reactions, specifically the formation of Si–O–Si loops (*t*) within a molecule (Figure 18d). Using simple arithmetic analysis, the number and distribution of intramolecular ring closures per oligomer can be determined. These insights provide valuable information about the molecular topology, revealing whether an oligomer is branched-linear, ladder like, polyhedral, or a hybrid of these forms.[290, 295]

MALDI-ToF MS thus provides direct access to the molecular composition and structural diversity of silsesquioxane-based systems. It is particularly effective for verifying the formation of well-defined cage structures. However, the interpretation of polysilsesquioxanes with broad molar mass distributions and structural heterogeneity can be challenging due to the complexity and overlap of mass spectral signals.

2.4.3.7 Differential scanning calorimetry (DSC)

DSC is a widely used method for investigating the thermal properties of polymers, making glass transition, melting points, and degradation events visible. Most polysilsesquioxanes are amorphous and exhibit a T_g, which provides information on the chemical composition, architecture of the polymer network, and intermolecular interactions.

The T_g is determined by segmental mobility, which depends strongly on crosslinking density.[300] Defects such as non-condensed groups or the incorporation of dialkoxysilanes into the silsesquioxane network increase free volume and lower T_g, while increasing crosslinking density reduces chain mobility and raises T_g.[231, 301, 302]

Ladder-type polysilsesquioxanes show no or significantly higher T_g compared to linear polymers or random networks, due to the rigidity of their double-chain structure.[141, 241, 303, 304]

Other factors influencing the T_g include hydrogen bonding, which acts as intermolecular "bridges" that increase the material's rigidity and restrict segmental mobility.[305] The nature of the organic substituents also plays an important role.[306] Aromatic groups are rigid and provide significant steric hindrance, resulting in a higher T_g. In contrast, the presence of spacers between the silica backbone and the aromatic group (e.g., benzyl, phenethyl) increases mobility and lowers the T_g.[307]

Silsesquioxanes with long *n*-alkyl substituents (e.g. C_{14}, C_{16}, C_{18}) exhibit a melting signal in DSC, which originates from the phase transition due to trans–gauche transformations of the alkyl chains, as they shift from an ordered to a disordered state.[281, 308]

POSS compounds can exhibit either a melting point or a T_g, depending on their substitution pattern and cage size. They may form crystalline solids or behave like amorphous polymers.[55, 309-312] Due to high thermal stability or volatility, POSS often do not show classical DSC transitions in the accessible temperature range.[242, 313]

DSC analysis can therefore be effectively used to detect crystalline phases and phase transitions. However, the detection of a T_g does not necessarily exclude the presence of POSS, as these compounds can also exist in an amorphous form. Observing the T_g is particularly useful for analyzing changes in polymer architecture, for example as a result of temperature exposure. Good solubility of the material, together with the absence of phase transitions (glass transition, melting, or crystallization), is often an indication of an ordered ladder structure.[111, 141]

2.4.3.8 Thermogravimetric analysis (TGA)

Polysilsesquioxanes are known for their high thermal stability, primarily due to the high bond dissociation energy of the Si–O bond (108 kcal·mol^{-1}).[314] This value significantly exceeds that of C–C (85.2 kcal·mol^{-1}) and C–O bonds (82.6 kcal·mol^{-1}).[315] The high degree of crosslinking of the T-units further enhances stability by limiting rearrangement reactions and chain scission, which are more commonly observed in linear polysiloxanes.[316, 255]

The thermal behavior of silsesquioxanes is strongly influenced by their molecular architecture (cage vs. ladder structure), the type of organic substituents, molar mass, and DC.[101, 111, 136, 242, 254] In general, two major degradation pathways can be distinguished: volatilization of low-molecular species and the formation of ceramic residues through thermally induced rearrangements and oxidation processes.[317] The specific mechanisms are complex and significantly affected by the atmosphere, whether inert or oxidative.[242]

Under inert conditions, fully condensed alkyl-substituted cage compounds (e.g. $R_8Si_8O_{12}$) often show pronounced sublimation or evaporation behavior. The temperature at which volatilization occurs increases with the size of the alkyl chain and overall molecular mass. Propyl cages volatilize at 150–200 °C, whereas octyl-substituted cages remain stable up to > 300 °C. In such cases, mass loss can exceed 80%, reflecting the high volatility of these discrete molecules.[317]

In contrast, partially condensed systems such as $R_8Si_8O_{11}(OH)_2$ may undergo concurrent condensation during heating, leading to a significantly higher residual mass.[318]

Incorporation of POSS into a polymer largely suppresses sublimation, as the cages are covalently bound in the network.[318] Degradation occurs primarily through cleavage of Si–C or C–C bonds in the organic substituents, followed by redistribution reactions forming thermally stable SiOC ceramics.[242, 319]

In oxidative environments, thermal behavior changes due to the strong influence of oxygen. Although evaporation or sublimation still occurs, it competes with oxidation of the organic moieties. This leads to subsequent fragmentation through classical radical pathways and ultimately results in the formation of a silica phase.[242] The significantly reduced loss of volatile silsesquioxane species is reflected in the increased ceramic residue.[317]

Short ladder silsesquioxanes, such as isopropyl-substituted tricyclic to heptacyclic oligomers, also sublime under nitrogen. However, their sublimation temperatures are significantly higher than those of cage structures with the same number of silicon atoms (for instance, 2-propyl-tricyclic ladder $T_{subl.} \approx 390$ °C vs. 2-propyl-T_8 POSS $T_{subl.} \approx 282$ °C).[101] As the chain length and molar mass increase, volatility decreases. In high-molecular-weight ladder polymers, sublimation is no longer observed. Instead, these materials exhibit decomposition at much higher temperatures (e.g., methyl-substituted ladder polymer with a temperature at 5% mass loss (T_{95}) above 400 °C)[101], typically involving the degradation of the organic side chains followed by crosslinking of the siloxane backbone.[320]

Phenyl substitution significantly increases thermal stability under both inert and oxidative conditions.[255, 321] Decomposition temperatures well above 400 °C have been reported.[106, 141, 322]

As observed with alkyl-substituted systems, phenyl-substituted ladders exhibit higher thermal stability than their cage-based counterparts. The T_{95} value is approximately 60 °C higher in phenyl ladders compared to T_{12}-phenyl POSS (Figure 19).[111]

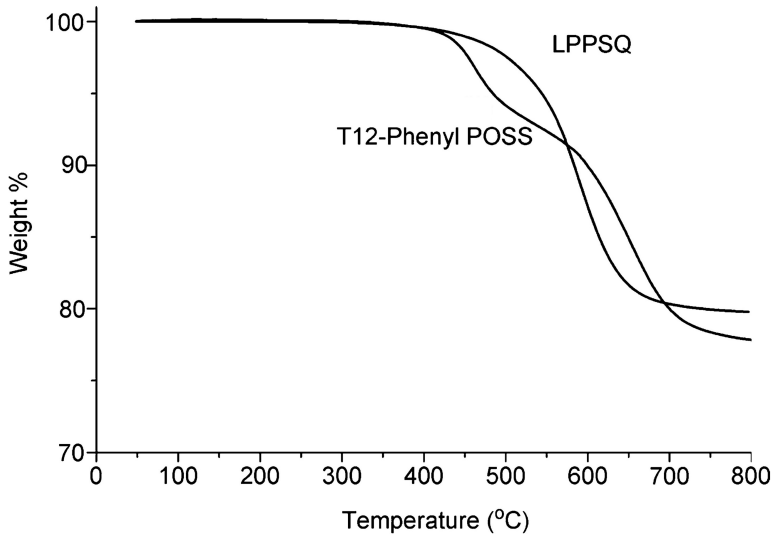

Figure 19: TGA under N_2 for phenyl containing ladder polymer (LPPSQ) and T_{12}-phenyl POSS, reproduced with permission from Choi, S.-S.; Lee, A. S.; Hwang, S. S.; Baek, K.-Y. Structural Control of Fully Condensed Polysilsesquioxanes: Ladderlike vs Cage Structured Polyphenylsilsesquioxanes *Macromolecules* **2015**, *48*, 6063–6070. Copyright 2015 American Chemical Society.[111]

In general, an initial mass loss below 250 °C in TGA is typically attributed to ongoing condensation reactions releasing water or alcohol, indicating a partially condensed network.[136] In this temperature range, volatilization of low-molecular-weight oligomers may also occur.[254] In fully condensed materials, thermal degradation begins thereafter, typically above 400 °C in the case of phenyl-substituted systems. POSS may undergo partial sublimation; alternatively, similar to ladder-type materials, they can degrade via side-chain cleavage accompanied by rearrangement into a dense network (Figure 20).
Under inert conditions, the resulting residue consists of a mixture of SiOC-type species, whereas in oxidative atmospheres, the residue is predominantly silica.[323]

The shape of the TGA curve, including onset temperature, step profile, and percentage of final residue, provides insight into thermal stability as well as information on the condensation state, the underlying structure, and the stability of the organic substituents. Coupled techniques such as TGA-FTIR or TGA-MS allow identification of the gaseous degradation products and thus significantly enhance the interpretability of the thermal analysis.[254, 324]

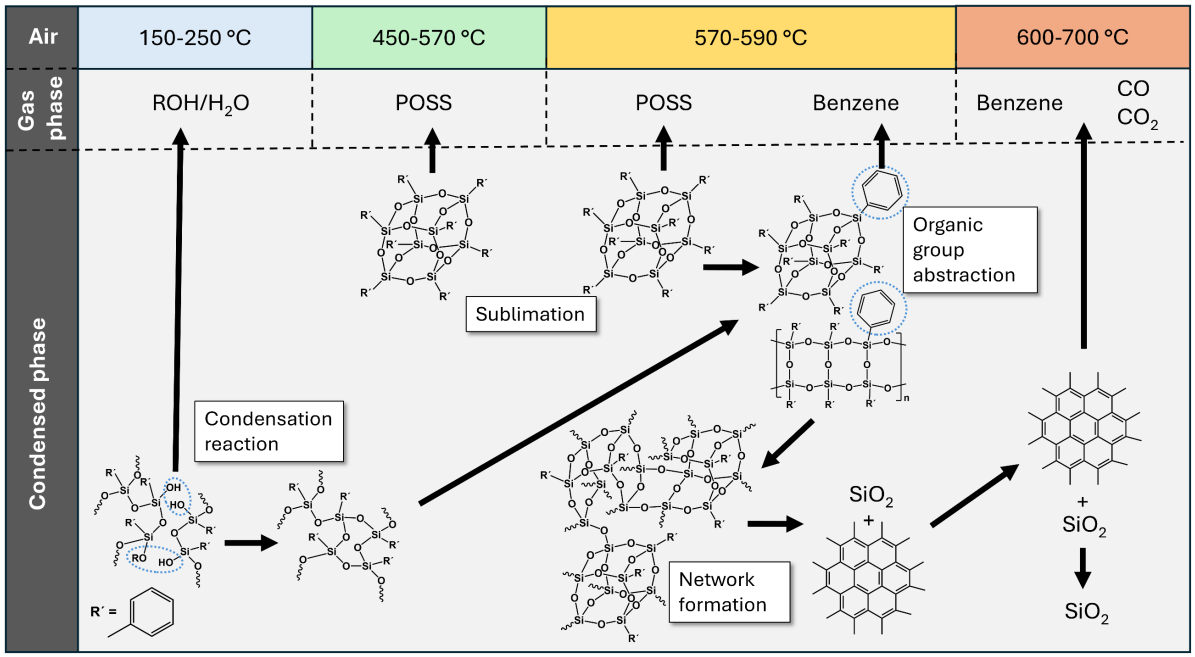

Figure 20: Mechanism of phenyl group functionalized silsesquioxane degradation of different structures under air. Scheme based on the work of Zhang, D.; Yang, R.; Qin, Z.; Zhang, W. Study on the thermal behaviors of polyhedral oligomeric octaphenylsilsesquioxane (OPS). *J. Therm. Anal. Calorim.* **2023**, *148*, 2345-2355.[323]

2.4.3.9 Fluorescence spectroscopy

Fluorescence spectroscopy is a well-established method for investigating the photophysical properties of aromatic polymers. While the siloxane backbone itself is non-fluorescent, aromatic substituents such as phenyl, naphthyl, or other polycyclic groups can act as fluorophores. Their emission is highly sensitive to the molecular environment, making them useful probes for deriving structural information about the surrounding polymer network.

A notable phenomenon in such systems is the formation of excited dimers, which arises from π–π interactions between closely spaced aromatic units. These so-called excimers are non-covalent complexes that exist only in the excited state, typically involving an excited molecule (A*) and a ground-state counterpart (A) (Figure 21a).[325] They are commonly observed in polycyclic aromatic hydrocarbons such as pyrene, naphthalene, and perylene.[326-328] This behavior also extends to polymers containing these aromatic units, where both inter- and intramolecular interactions give rise to characteristic emission features.[329-331]

The photophysical behavior of aromatic polymers has been extensively investigated by fluorescence spectroscopy, with polystyrene serving as a prototypical model system.[329, 332, 333]

Two main types of fluorescence emission have been reported for polystyrene: monomer emission from individual phenyl groups around 285 nm, and a broader, red-shifted band in the 320–340 nm region, attributed to excimer formation.[334]

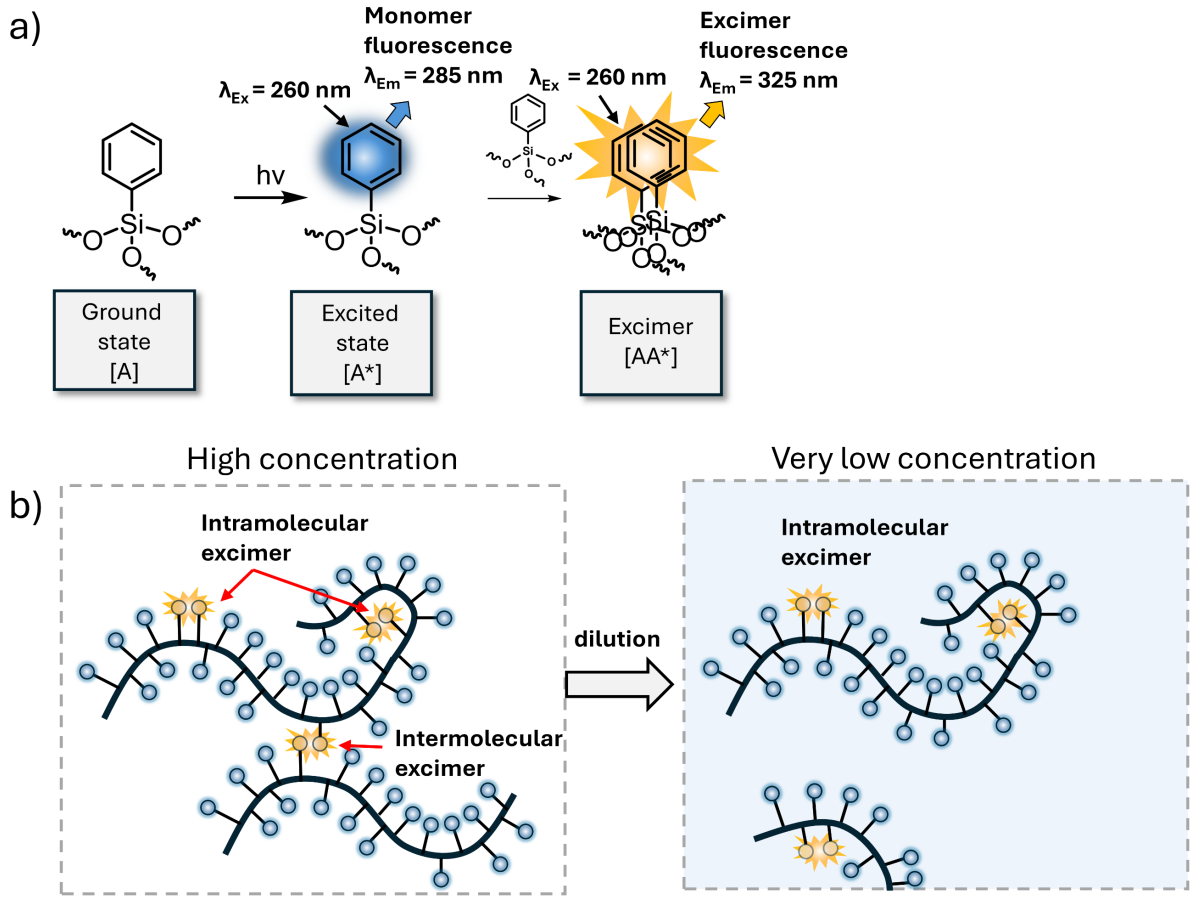

Figure 21: a) Formation of an excimer in polyphenylsilsesquioxanes with the corresponding excitation wavelength (λ_{Ex}) and the resulting emission wavelength (λ_{Em}) of the monomer and excimer emission. A ground-state monomer [A] combines with an excited-state monomer [A*] to form an excimer [AA*]. b) Formation of intramolecular and intermolecular excimers within a polymer chain at high and low polymer concentrations in solution.

Intramolecular excimer formation requires specific structural preconditions. These were studied by Hirayama, who investigated diphenyl and triphenyl alkanes for their ability to form intramolecular excimers. He discovered that phenyl groups separated by three carbon atoms along an alkyl chain exhibited excimer fluorescence. Based on this, he formulated the so-called "n = 3 rule," which requires a parallel sandwich-like arrangement with an interchromophoric separation of ~ 3 Å.[335]

Of particular interest is the excimer-to-monomer intensity ratio (I_E/I_M). Analyzing how this ratio changes with concentration enables the distinction between interactions occurring within a

single polymer chain and those involving multiple chains (Figure 21b).[299] If I_E/I_M remains constant upon further dilution, it indicates that the excimers are formed intramolecularly, since intermolecular interaction become less probable at low concentrations.[336]
Liu et al. used fluorescence spectroscopy to investigate the molecular conformation of ladder-like polyphenylsilsesquioxanes. Intramolecular excimer emission was observed, and molecular modeling confirmed that this interaction is geometrically feasible only in a cis-isotactic configuration.[331] Ladder-type silsesquioxanes show pronounced intramolecular excimer fluorescence due to the rigid, double-stranded polymer backbone, which facilitates efficient interaction between chromophores.[108, 337] An increased intensity of excimer emission correlates with a higher degree of structural organization in the ladder-type framework.[268, 338]
In contrast, POSS exhibit significantly weaker excimer bands. The spatial distribution of chromophores around the 3D core leads to less ordered interactions and reduced excimer formation.[337]

Consequently, once chromophores are incorporated within the silsesquioxane network, fluorescence spectroscopy becomes a powerful tool for visualizing π–π interactions along the chains and for characterizing molecular architectures.

Numerous additional analytical or theoretical methods have been employed in the literature to study reaction kinetics and structural properties, including X-ray photoelectron spectroscopy (XPS), small-angle X-ray scattering (SAXS), transmission electron microscopy (TEM), atomic absorption spectrometry (AAS), dynamic light scattering (DLS), rheology, and others.[142, 339-344] These techniques are not discussed in detail here, as they are either not applied in this work or only of marginal relevance and are therefore beyond the scope of this thesis.

2.4.4 Polysilsesquioxane-Based Particles as Host Matrices

The sol–gel process can be employed to synthesize nano- and microparticles with controlled sizes and morphologies. A classical example is the well-known Stöber method, developed in 1968, which enables the synthesis of monodisperse colloidal silica particles through base-catalyzed hydrolysis and condensation of TEOS.[157]
Silica nanoparticles are widely used as fillers in polymer-based nanocomposites.[345] However, a major drawback of pure silica particles is their tendency to agglomerate, which often compromises mechanical stability and optical properties of the polymer matrix.[346, 347] Surface functionalization has been shown to improve compatibility between the silica filler and the

organic polymer matrix, thereby promoting a more homogeneous particle dispersion.[348, 349] This can be achieved either by post-synthetic modification of surface OH groups with silane coupling agents (e.g. 3-aminopropyltriethoxysilane),[350] by co-condensation of organotrialkoxysilanes with TEOS,[351] or through direct synthesis from pure organotrialkoxysilanes (Figure 22).[352] The last approach yields the highest organic content.

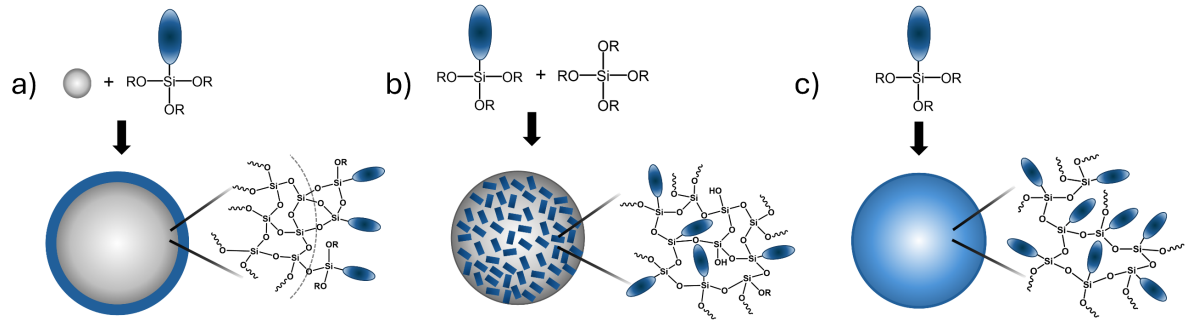

Figure 22: Strategies for the synthesis of organically functionalized particles: a) surface post-functionalization of silica particles, b) co-condensation of tri- and tetraalkoxysilanes, and c) preparation of polysilsesquioxane particles.

The synthesis of polysilsesquioxane particles is typically carried out in aqueous or mixed solvent systems via base- or combined acid–base catalyzed hydrolysis and condensation. This can be performed either emulsion based in the presence of surfactants,[353, 354] or under additive-free conditions.[355, 356] The substituents strongly influence hydrolysis and condensation kinetics, thereby determining particle size and DC.[352] Reported particle sizes range from the nanometer to the micrometer scale, depending on the chosen precursors and reaction conditions.[354] The DC usually remains below 90%, with small substituents such as methyl yielding higher values (~ 89%) compared to sterically demanding groups such as phenyl (~ 80%).[357] As a result, several groups reported softening of phenyl-modified polysilsesquioxane particles at elevated temperatures, resulting in a loss of spherical morphology.[307, 357-359] While this behavior may initially appear disadvantageous, it can also be exploited in specific contexts, as discussed in more detail in the next chapter on melting gels (Chapter 2.5).

In the literature, polysilsesquioxane particles have mainly been studied with respect to particle size, morphology, dispersity and DC, whereas internal structural motifs have been less frequently addressed. Dong et al. synthesized hollow spheres from MTMS, PhTMS, VTMS and trifluoropropylTMS and characterized them by ^{29}Si NMR, XRD and FTIR, concluding that the materials consisted of a mixture of incomplete cages, ladder-like, and network structures.[360] In contrast, Wang et al. described polyphenylsilsesquioxane particles explicitly as ladder-type

frameworks, based on ^{29}Si NMR, XRD and IR spectroscopy.[241] Overall, reports suggest that polysilsesquioxane particles can exhibit different structural motifs depending on synthesis conditions and substituents, but systematic and comprehensive analyses remain scarce.

Silica and silsesquioxane micro- and nanoparticles are also widely employed as hosts for dyes or drug molecules.[361-364] Encapsulation offers protection from external influences such as light and humidity, prevents dye aggregation, or allows controlled release under defined conditions.[363, 365, 366]

Generally, incorporation strategies can be divided into covalent and non-covalent approaches (Figure 23). Covalent strategies involve the incorporation of functionalized dyes, for example trialkoxysilane-modified perylene derivatives, into the silica network, thereby preventing dye leaching (Figure 23a).[367, 368] Non-covalent strategies rely on weak physical interactions such as electrostatic attraction. Chen et al. prepared organosilica nanoparticles containing intrinsic secondary amines, which enabled the binding of either anionic or cationic dyes depending on the surface charge of the particles.[369] Lu et al. integrated Rhodamine B (RB) into poly(3-mercaptopropylsilsesquioxane) microspheres, where Si–OH groups of the matrix interacted electrostatically with the dye ($SiO^{-}\cdots RB^{+}$) (Figure 23b).[370]

While ionic species can be readily incorporated due to their affinity for the hydrophilic silica matrix, hydrophobic molecules are more challenging. Phenyl-modified polysilsesquioxane matrices have proven particularly advantageous, as their hydrophobic and aromatic domains facilitate entrapment of organic dyes. The phenyl substituents can engage in π–π interactions with aromatic guest molecules, which promotes retention within the matrix and reduces dye leaching (Figure 24c). In addition, the matrix provides a protective environment that limits photobleaching and minimizes dye self-quenching, thereby preserving the photophysical properties of the embedded chromophores.[365, 371] However, the amount of dye incorporated is strongly dependent on the organic content of the network which complicates control over dye loading.

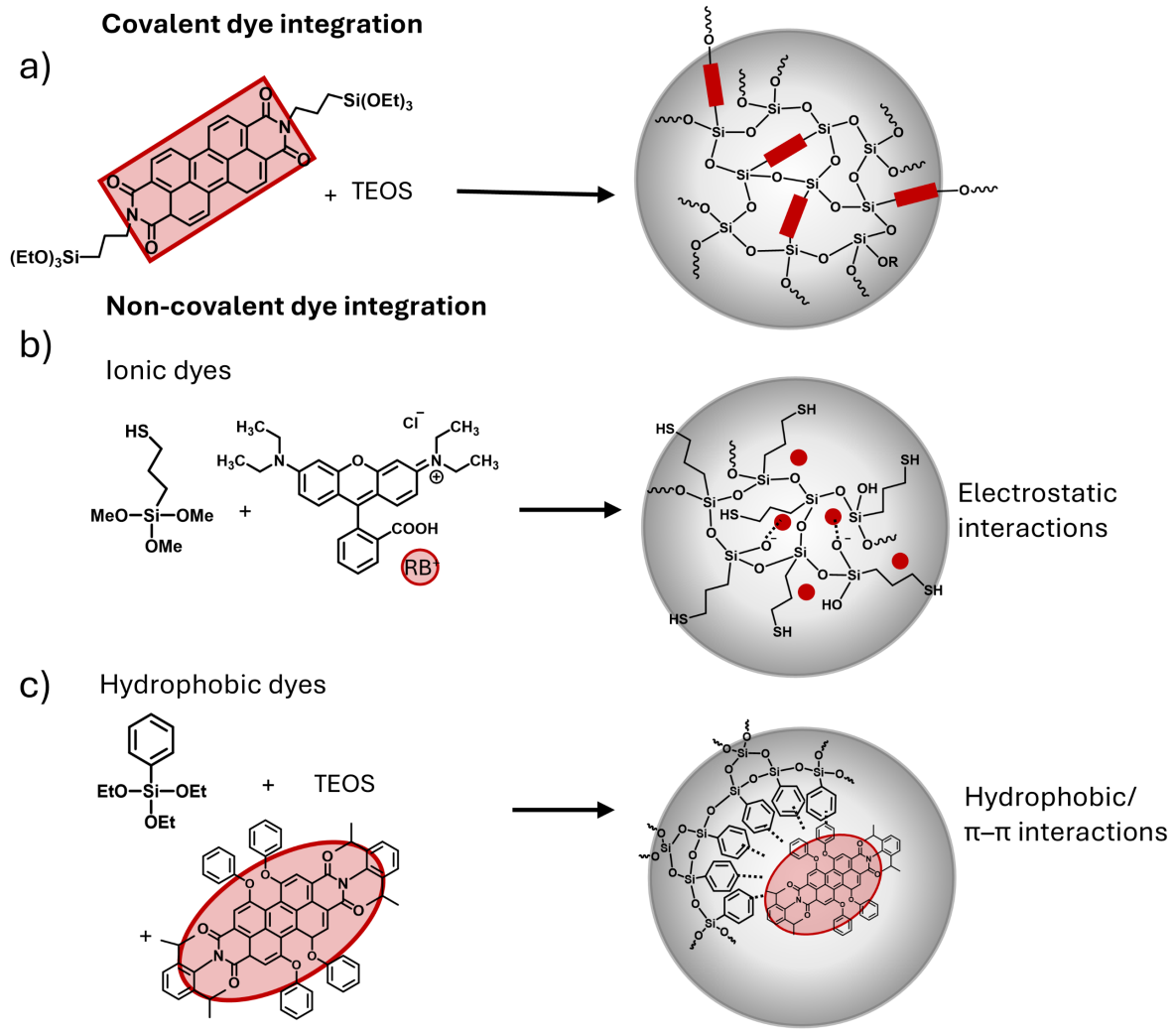

Figure 23: Covalent and non-covalent encapsulation of dyes in polysilsesquioxane particles: a) covalent incorporation of trialkoxysilane-modified perylene in a silica matrix;[372] b) physical embedding of Rhodamine B (RB) in poly(3-mercaptopropylsilsesquioxane) via electrostatic interactions with the negatively charged matrix;[370] c) embedding of Lumogen Red in phenylsilsesquioxane-silica core-shell particles, stabilized by π–π and hydrophobic interactions with phenyl groups.[365]

2.5 Melting Gel

Melting gels are silsesquioxane-based inorganic–organic hybrid materials that, due to the covalent bonding between their organic components and the inorganic Si–O–Si network, are classified as class II hybrid materials. They possess the ability to liquefy upon heating to a temperature T_l ($T_l > T_g$, T_l typically around 110 °C) and to solidify again upon cooling below T_g. This process is reversible and can be repeated over many cycles without loss of their softening capacity. When the gels are heated to the consolidation temperature T_{con} ($T_{con} > T_l$),

the degree of crosslinking in the siloxane network increases until the material loses its thermoreversibility and transitions into a permanently solid state (Figure 24).[4, 373] The gels are synthesized by mixing organically substituted alkoxysilane precursors, which are hydrolyzed and condensed via a sol–gel-like process under acidic or combined acidic/basic catalysis. Silsesquioxanes containing exclusively phenyl groups were the first system in which thermoreversible properties were studied in detail.[358]

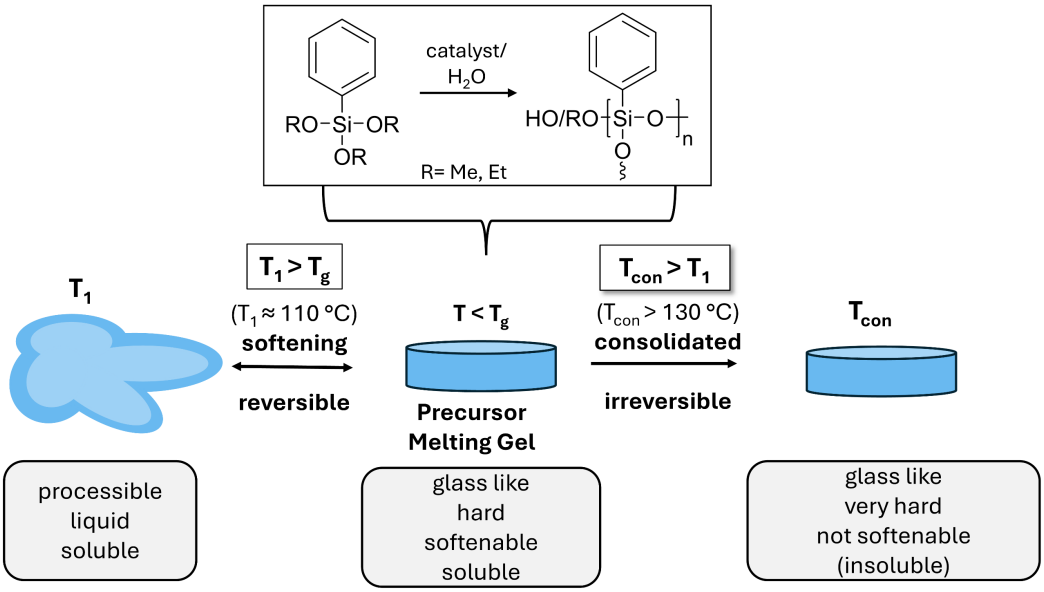

Figure 24: Schematic representation of the formation of a phenylsilsesquioxane melting gel showing temperature-dependent thermoplastic and thermosetting behavior and its appearance at different temperatures. The values for T_g and T_{con} given in parentheses refer to phenylsilsesquioxane melting gels but may vary depending on the organic substituents.

The following chapter traces the progression from these early examples of polyphenylsilsesquioxanes to purpose-designed functional materials synthesized from multiple precursors. It examines reported systems, their key properties, the structural origins of these properties, and the applications that have already been explored.

2.5.1 History and Development of Different Melting Gel Systems

The origin of melting gels stems from the distinct thermal behavior of certain polysilsesquioxane resins, characterized by a T_g above room temperature that renders them both flowable and processable. In 1987, Hurwitz et al. reported on the use of phenyl, methyl and propylsilsesquioxanes as well as their copolymers as melt-processable precursor polymers for the fabrication of ceramic materials. They exploited the melt flow of these materials to spin

fibers, which were subsequently pyrolyzed under inert conditions.[374, 375] Around the same time other groups investigated the thermoplastic behavior of aryl-substituted polysilsesquioxanes and of copolymers composed of phenylsilsesquioxane and diphenylsiloxane units, employed as more easily processable ceramic precursors.[376, 377]

Matsuda et al. were the first to systematically apply the thermoplastic properties of polysilsesquioxanes for the preparation of transparent films. They deposited phenyl and benzylsilsesquioxane particles onto indium tin oxide (ITO)-coated glass substrates by electrophoretic sol–gel deposition, and the resulting layers were melted above their T_g. Melting induced densification of the layers, leading to a reduction in thickness and an improvement in transparency (Figure 25a).[358]

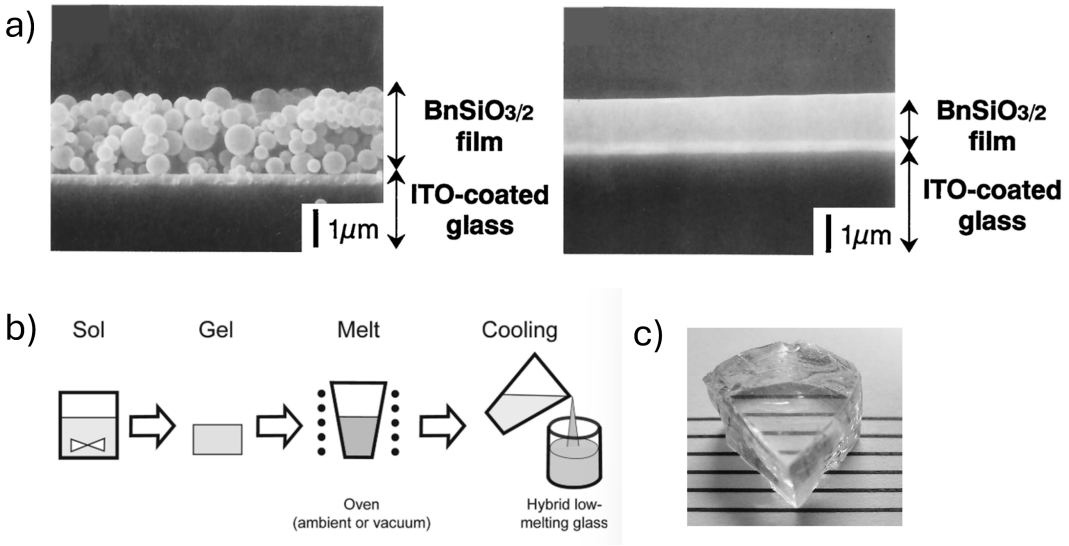

Figure 25: a) Scanning electron microscope (SEM) images of benzylsilsesquioxane particles deposited onto ITO-coated glass substrates by electrophoretic sol–gel deposition, shown before (left) and after (right) heat treatment at 100 °C for 2 h. Reproduced with permission from Matsuda, A.; Sasaki, T.; Hasegawa, K.; Tatsumisago, M.; Minami, T. Thermal Softening Behavior and Application to Transparent Thick Films of Polybenzylsilsesquioxane Particles Prepared by the Sol–Gel Process. *J. Am. Ceram. Soc.* **2001**, *84* (4), 775–780. Copyright 2001 John Wiley & Sons, Inc.[378] b) Schematic representation of the gel–melting method. c) Photograph of a $PhSiO_{3/2}$ glass piece synthesized by the gel–melting method. Figures b) and c) are reproduced with permission from Masai, H.; Takahashi, M.; Tokuda, Y.; Yoko, T. "Gel-melting method for preparation of organically modified siloxane low-melting glasses." *J. Mater. Res.* **2005**, *20*, 1234–1241. Copyright 2005 Springer Nature.[5]

While phenylsilsesquioxane underwent further crosslinking during isothermal treatment above T_1 and exhibited irreversible curing, polybenzylsilsesquioxane particles retained their thermoplastic character even after heat exposure. The authors attributed these differences to

variations in the degree of polymerization and to distinct molar mass distributions around the softening temperature.[358, 378] The balance between thermoplastic and thermoset behavior could be deliberately adjusted by the choice of solvent and by varying the monomer concentration during synthesis.[301, 359]

Masai et al. recognized the potential of the thermal softening properties of polysilsesquioxanes for the development of lead-free low melting glasses with the aim of providing alternatives to the commonly used lead-containing glasses. They developed the so-called gel-melting method (GMM) (Figure 25b,c), in which phenyltriethoxysilane (PhTES) and diphenyldiethoxysilane (DPhDES) or MTES and dimethyldiethoxysilane (DMDES) were first hydrolyzed under acidic catalysis and subsequently condensed using ammonia. In this way, they obtained polysilsesquioxane-polysiloxane networks with low softening points.[5] The synthesis was extended through subsequent treatment of the gels with NaOH in Et_2O in order to complete the polycondensation reaction.[379] Using ^{29}Si NMR and SEC it was shown that the binary systems consist of three-dimensionally crosslinked networks with organic groups, while at the same time exhibiting high chemical and thermal stability. By varying the monomer ratios they obtained materials with varying stability against thermal curing and loss of reflow properties.[5]

The characteristic rheological behavior of softenable polysilsesquioxanes was attributed to temperature-dependent changes in the free volume of the material. Flowability arises from weakly crosslinked and only slightly entangled molecules whose mobility is influenced by the number of bridging oxygen atoms as well as by the organic groups. These organic groups control the molar mass and act as network terminators.[340, 380]

Further investigations focused on the influence of reaction parameters such as acid concentration, water content, and temperature on hydrolysis and condensation.[229] In addition, the activation energy for viscous flow was determined to be 180–200 kJ per mol of monomer which is comparable to the activation energy of alkali silicate glasses.[381] The influence of terminating reagents such as trimethylsilyl or vinyldimethylsilyl groups was also examined.[137] These studies focused in particular on softenable phenyl-modified silsesquioxanes.

In addition to GMM, in which the gel is first formed and subsequently transferred into the molten state by heating, Kuniyoshi et al. developed the sol concentration method (SCM). In this approach the monomers are hydrolyzed and condensed using HCl or acetic acid as catalyst. The sol is then concentrated by heating above the softening temperature, resulting in the direct formation of the glass melt without the need for a gelation step. The authors cited reduced shrinkage, prevention of cracking, and higher transmission as advantages of SCM.[382] A

subsequent rapid heat treatment (RHT) was also applied, in which the material was held briefly just below the decomposition temperature of the organic groups. This treatment led to the almost complete elimination of residual OH groups.[135, 383]

Jitianu, Klein and co-workers further advanced the concept of softenable hybrid glasses and introduced the term *melting gels* for this class of materials. The designation derives from the previously used expression “melting”, which had already been frequently used in the literature in connection with these materials.[5, 150]

More accurately, the term melting is not entirely correct, since melting gels are amorphous materials and do not exhibit a classical melting point in the thermodynamic sense. Instead, they undergo a continuous transition from a solid to a viscoelastic state characterized by a T_g. In this regime parts of the network undergo relaxation-induced structural rearrangements without a classical phase transition taking place. The term melting gel therefore refers less to an actual melting process and more to the intended application of these materials as substitutes for conventional low-melting-temperature glasses.

They developed various multicomponent melting gel systems based on phenyl- or methyl-containing di- and trialkoxysilanes.[373] SAXS measurements demonstrated that tri- and dialkoxysilane components are homogeneously mixed and do not undergo phase separation.[142] They also synthesized ternary systems by adding TEOS or TMOS to the binary mixtures.[384, 385] Their work focused in particular on the investigation of thermal stability, the relationship between structure, T_g, and consolidation temperature, as well as the resulting application potential.[150, 201, 386-388]

In addition to methyl and phenyl groups, longer chain alkyl groups have also been investigated in softenable polysilsesquioxanes. Macan et al. analyzed the softening behavior of particles synthesized from aryl- and alkyltrialkoxysilane precursors through acid- and base-catalyzed hydrolysis and condensation reactions. Biphasic silsesquioxanes derived from phenyl and methyl, ethyl, propyl, or octyl substituents exhibited a glass transition whose temperature decreased with increasing chain length. The glass transitions were not reversible, as the materials underwent further condensation and permanent crosslinking once the transition was exceeded. At the same time, longer alkyl chains led to lower thermal stability.[389, 390] Alkyl groups larger than butyl additionally tended to crystallize as a result of self-assembly.[307]

Seto et al. employed a cosolvent-free acid-catalyzed hydrolytic polycondensation to synthesize thermoplastic poly(Ph co R′SQ) (R = ethyl, propyl, vinyl) systems. The incorporation of the alkyl substituents effectively suppressed cracking during the preparation of transparent

pellets.[391] The same group also succeeded in synthesizing silsesquioxanes with melting gel properties from cyclohexyltrimethoxysilane. Due to the steric hindrance imposed by the organic groups, these materials exhibited increased resistance to thermal crosslinking, described as thermoset resistance.[163]

A similar behavior was observed by Briesenick et al. who combined phenyltrimethoxysilane with dialkoxysilanes containing polycyclic aromatic groups such as naphthyl and phenanthrenyl in order to produce high RI films. Owing to the steric demand of these bulky substituents the materials remained softenable even after thermal treatment at 200 °C.[232]

Another approach was pursued by Steinbrück et al., in which an alkoxy terminated polydimethylsiloxane (PDMS) was incorporated into a system together with PhTMS, MTMS and DMDMS. The integration of the siloxane chain resulted in elastic samples after curing, referred to as *elasto-melting gels*. Material properties such as the T_g and the RI of the consolidated samples could be tuned by varying the monomer composition.[231]

Klein and Jitianu reported in a review on previously unpublished work in which about one percent of the silicon was replaced by germanium through the incorporation of methyltriethoxygermane (MTEG). This slight modification of the composition resulted in a significant reduction in T_g (–18.8 °C to –25.9 °C) and a decrease in consolidation temperature (150 °C to 120 °C).[4]

Table 1 summarizes the melting gel systems developed to date, classified according to their composition into single, binary, ternary and multicomponent systems. Only those systems were considered if they either exhibit a T_g above room temperature or can be thermally consolidated to yield a solid at room temperature. Materials such as phenethylsilsesquioxane were not considered. This compound exhibits a T_g below room temperature and cannot be converted into a solid even after thermal treatment at 200 °C.[377] This distinction was made with regard to potential applications such as low melting sealing glasses, for which the presence of a solid glass is essential.

Table 1: Reported melting gel systems categorized by organic substituents. The systems are distinguished by the number of monomers used and classified as mono-, di-, tri-, or multi-component systems. The number of organic substituents indicates whether the material consists of T, D or M, units. Q units are incorporated via TEOS or TMOS. Reported T_g and T_{con} are listed; these values may vary between studies depending on composition and synthesis method. Materials that did not cure are designated as thermoset resistant, with the temperature given in parentheses at which no curing was observed. Explicitly stated properties, as well as investigated applications reported in the references, are included.

Organic group	T_g [°C]	T_{con}	Special properties/applications
Mono-component			
Phenyl[a]	33–59,[5, 150, 163, 382, 392, 393] 125,[137] 160[390]	≥ 130 °C (24 h)[150]	High thermal stability (T^{95} = 510 °C),[393] host for hydrophobic dyes,[394] filler for thermal and fire resistance,[392] micropatterning[395]
Benzyl	35[307, 378]	Thermoset resistance (300 °C, 2 h)[378]	High refractive index (RI = 1.62)[358], micropatterning[378]
Cyclohexyl	33[163]	Thermoset resistance (200 °C, 6 h)[163]	Adhesive to glass, metals, several polymers, deep UV transparency (up to 220 nm)[163]
1-Naphthyl[a]	50[396]	Thermoset resistance (200 °C, 24 h)[396]	High thermal stability (T^{95} = 465 °C), high refractive index (RI = 1.615), fluorescence[396]
2-Naphthyl[a]	41[396]	200 °C (24 h) [396]	High thermal stability (T^{95} = 400 °C), high refractive index (RI = 1.61), fluorescence[396]
Di-component			
Phenyl + Diphenyl	0–34,[150] 86–91[376]	130–180 °C (24 h),[150] thermoset resistance ($70PhSiO_{3/2}$–$30Ph_2SiO_{1/1}$, 200 °C, 1200 h)[5]	High thermal stability (T^{95} = 440 °C),[376] High refractive index (RI = 1.58),[135] ultra low saturated water absorption (< 0.1 mass%),[135] hydrophobic coating (contact angle = 96°),[150]
Phenyl + Dimethyl	−61–6[373, 387]	150–205 °C (24 h)[373, 387]	Hydrophobic coating (contact angel = 102°),[387] host for $EuAl_2S_4$[397]
Methyl + Dimethyl	−57–0[373, 398, 399]	135–170 °C[201, 373]	Very low porosity,[142] adhesive to metal,[400] good UV stability,[401] LED encapsulation material,[401] hydrophobic coating (contact angle = 109°),[201] hermetic protective coatings,[398] corrosion protection,[400, 402] low-k dielectrics,[386] host for gold nanoparticles[403]

Ethyl + Diethyl	−91–−34[404]	122–153 °C[404]	Corrosion protection[404]
Phenyl + Cyclohexyl	~ 35–45[163]	[b]	
Phenyl + Cyclopentyl	~ 15–40[163]	[b]	
Phenyl + Methyl	~60–85,[391] 200, 380[389]	[b]	
Phenyl + Ethyl	~ 10–50,[163, 391] 160, 170[389]	Thermoset resistance (140 °C, 24 h)[391]	Suppress crack formation, adhesive to bond glass plates[391]
Phenyl + Propyl	~ −20–45,[163, 391]	[b]	Suppress crack formation,[391] fiber-spinning[375]
Phenyl + Pentyl	145[389]	[b]	
Phenyl + Octyl	< RT–150,[389, 390]	[b]	
Phenyl + Vinyl	~ 35–65[391]	[b]	Suppress crack formation[391]
Cyclohexyl + Methyl	~ 40–70[163]	200 °C (6 h) [163]	
Cyclohexyl + Ethyl	~ 25–40[163]	Thermoset resistance (200 °C, 6 h)[163]	Suppress crack formation, adhesive to glass, metals, several polymers, deep UV transparency (up to 220 nm)[163]
Tri-component			
Phenyl + Dimethylvinyl (end group) + Trimethyl (end group)	4–45[137]	[b]	
Ph + Diphenyl + TEOS or TMOS	20–59[385]	165–218 °C[385]	Surface patterning for water harvesting[405]
Ph + TEOS + Trimethyl (end group)	130–150[c406]	[b]	High hydrophobicity (contact angle 113°), additive in pressure-sensitive adhesive formulations[406]
Ph + Phenyl-1(2)-Naphthyl or Phenyl-Phenanthrenyl + Diphenyl or Dimethyl	−5–22[232]	Thermoset resistance (200 °C, 72 h)[232]	High refractive index (RI = 1.62), high thermal stability (T^{95} = 470 °C),**[232]** host for $EuAl_2S_4$[397]
Multi-component			
Phenyl + Methyl + Dimethyl + PDMS	<< RT[231]	150–200 °C[231]	Elastic, LED encapsulation material**[231]**

[a]Systems are part of this thesis.

[b]No specific information about T_{cons} was provided.

[c]softeing point (> T_g)

2.5.2 Properties and Applications of Melting Gels

Melting gels were originally developed as an alternative to conventional low melting sealing glasses, whose processing temperatures are too high for many microelectronic applications, particularly in electronic packaging.[401] Owing to their structural versatility and the wide range of tunable properties associated with it, additional fields of application have since emerged (Figure 26).

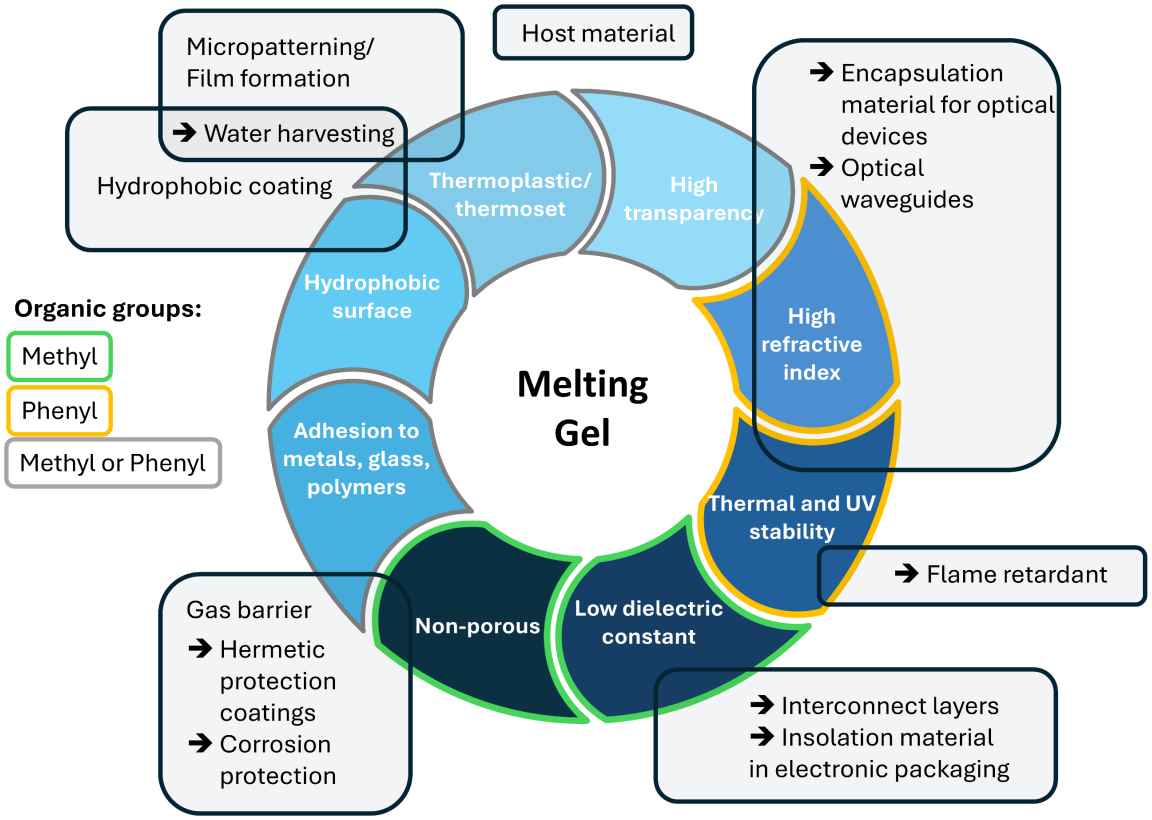

Figure 26: Melting gel properties and corresponding application examples. The properties primarily refer to phenyl- or methyl-functionalized melting gels.

The key characteristic of melting gels is their reversible thermoplastic behavior above the T_g, which, depending on composition and degree of crosslinking can extend over a broad temperature range (Figure 27).[4] This behavior is attributed to the predominantly linear structure of the network, which in the unconsolidated state exhibits high segmental mobility. The T_g is directly related to physical properties such as viscosity, dielectric constant, and mechanical strength, and reflects the degree of crosslinking within the silsesquioxane network.[150] Through careful selection of the monomers this parameter can be controlled: dialkoxysilanes reduce the network density and thus lower the T_g, while trialkoxysilanes increase T_g by introducing additional crosslinking points.[387, 398]

When the material is thermally treated above a critical temperature, T_{con}, residual silanol groups condense, leading to the formation of a three-dimensionally crosslinked network. This process is irreversible, yielding a material that can no longer be deformed thermoplastically.[201, 359, 407] The exact value of the consolidation temperature strongly depends on the type and ratio of siloxane precursors employed. A high proportion of T units, for example from PhTES, lowers T_{con}, whereas the incorporation of D units, such as DMDES, leads to higher consolidation temperatures (Figure 27).[150, 201, 387]

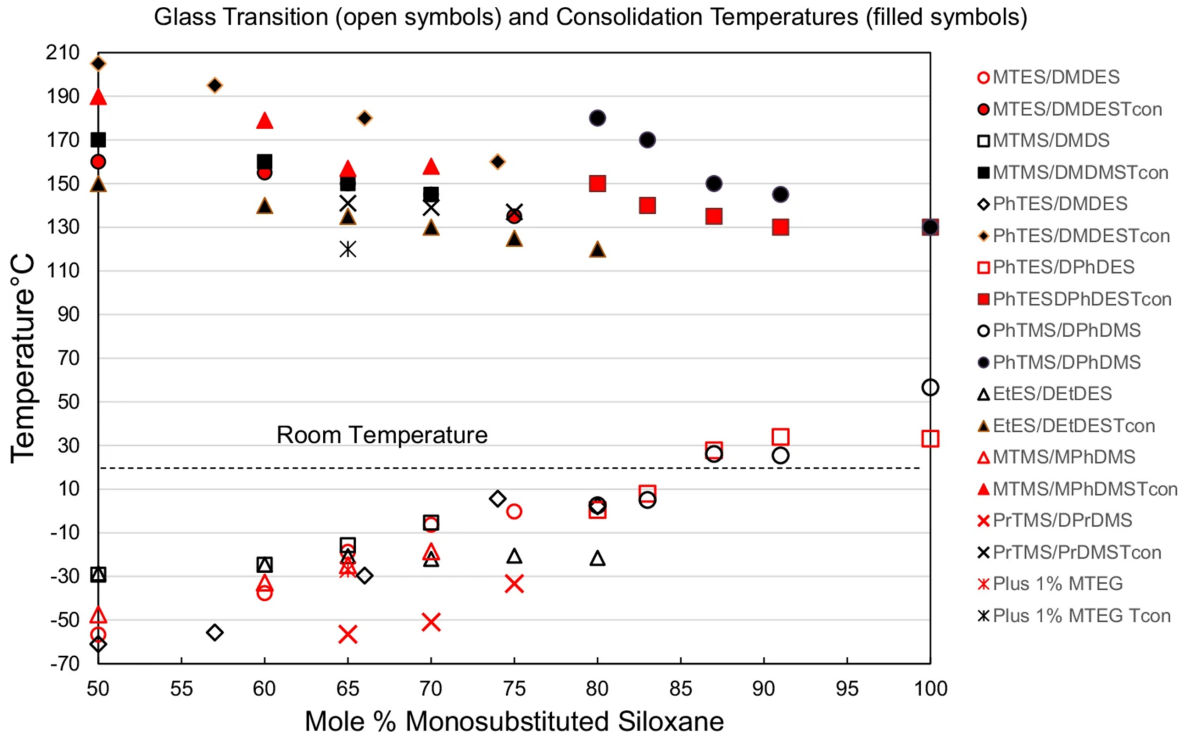

Figure 27: T_g and T_{con} of various melting gel systems composed of T and D units with methyl, phenyl, ethyl, and propyl substituents, plotted against the mol% of T units. Reproduced from Klein, L. C.; Jitianu, A. Hybrid organic-inorganic gels that are melting gels. *J. Sol-Gel Sci. Technol.* **2025**, *113*, 30–38, under CC BY 4.0.[388]

Not all systems referred to the melting gel family, however, undergo such irreversible curing. Compositions with a high content of sterically demanding groups such as cyclohexyl,[163] benzyl,[377] naphthyl, and phenanthrenyl[232] substituents remain permanently thermoplastic.

The precise composition of a melting gel therefore defines its processing window ($T_g < T_l < T_{con}$), which can be tailored to the intended application. This window is critical for processes such as molding, casting, and precise surface patterning. Takahashi et al. employed phenyl

modified silsesquioxane particles to fabricate micropatterns on ITO-coated substrates.[395] Klein et al. structured melting gel surfaces for water harvesting by condensation from humid air.[405]

Melting gels exhibit excellent film-forming properties. Thin and thick layers can be applied by casting, electrospraying, or electrochemical deposition.[201, 388, 404] The viscosity of the solution enables precise control of the film thickness. Surface-near organic groups such as phenyl or methyl result in contact angles greater than 90°, which makes these materials suitable for hydrophobic coatings.[150, 201]

Structural analyses by SAXS and BET demonstrate that especially methyl-modified gels contain almost no micro- or nanopores, since organic groups fill voids within the network.[142, 385] As a result, these materials exhibit high barrier properties against atmospheric gases, suggesting applications as hermetic protective coatings in microelectronics,[201, 398] and for corrosion protection of AISI 304 steel or magnesium alloys.[400, 402, 404] The residual Si–OH groups in incompletely consolidated materials further promote adhesion to glass or metallic substrates through M–O–Si bond formation.[163]

Optically, melting gels are highly transparent. Layers of phenyl modified polysilsesquioxanes reach transmission values of up to 94% in the visible spectral range.[378, 382, 408, 409] At the same time, they exhibit good UV stability, which makes them attractive as encapsulation materials for high power thermally stable UV LEDs.[401] The optical band gap depends on the type of organic substituent. Phenyl groups typically absorb around 284 nm due to π–π* transitions,[409] whereas alkyl modified systems such as those derived from cyclohexyltrimethoxysilane remain transparent into the deep UV region, which is particularly relevant for optical components, for example in UV disinfection.[163]

The thermal stability of these materials is especially pronounced in aromatically substituted systems. For phenyl-containing gels a 5% mass loss was only observed at 410–440 °C.[376] This also makes melting gels promising as flame retardant additives for polymer composites. Either the glass alone or in combination with clay acts as a flame retardant in epoxy resins by forming a glassy layer with high thermal stability.[392] In contrast, the incorporation of alkyl groups decreases thermal stability, with further reductions observed as the alkyl chain length increases.[307, 389]

Another advantage arises from the dielectric and optical properties of melting gels. Aromatically substituted systems exhibit high refractive indices due to the polarizability of the π electrons, with values up to RI = 1.57 for phenyl and RI = 1.62 for benzyl groups.[232, 358] The RI can be further tuned by adjusting the monomer ratios, for example by substituting $Ph_2SiO_{2/2}$

with $PhSiO_{3/2}$.[409] These comparatively high refractive indices in the field of polymer-based materials make melting gels attractive for applications such as LED encapsulation or optical waveguides.[308]

In contrast, methyl substituted gels with a high content of dimethylsiloxane exhibit low dielectric constants ($k \approx 3.3$ at 1 kHz), since direct Si–C bonds are less polarizable than Si–O–Si linkages. They are therefore suitable as low-k dielectrics in interconnect layers or as insulating materials in electronic packaging.[373, 386]

In addition, melting gels provide interesting opportunities as host materials for functional nanoparticles or ternary sulfides. For instance, gold nanoparticles could be embedded in the gel without affecting either their plasmonic properties or the softenability of the gel.[403] Magnetic particles such as magnetite and hematite were also successfully incorporated, paving the way for applications such as magnetically controllable inks and inkjet printing under microgravity conditions.[388] Furthermore, aryl group-functionalized melting gel matrices allow the embedding of $EuAl_2S_4$ powder, providing moisture protection and simultaneously acting as an intrinsic filter for the UV excitation of the Eu^{2+} cations.[397]

Finally, unconsolidated gels display remarkable storage stability. When sealed in airtight containers, they retain their thermoplastic properties for more than one year.[4]

Over time, the synthesis of melting gels has become increasingly diverse and complex. The pursuit of broader material properties has led to the incorporation of a wide range of organoalkoxysilanes, each introducing additional functionalities to the system. In particular, in the present era where energy efficiency and green chemistry are of central importance, further advancement of this class of advanced materials is essential to tailor their properties to current technological challenges.

3 Motivation and Task Definition

Melting gels are inorganic–organic hybrid materials whose properties arise from the combination of an inorganic siloxane network with organic substituents. By varying the monomer structure (type and number of organic groups), the ratio of mono-, di- and trialkoxysilanes, and the degree of crosslinking, their thermal, optical and mechanical properties can be tailored in a modular way. This versatility makes melting gels a promising platform for the design of functional materials in a wide range of applications.

To systematically exploit this potential, a detailed understanding of the structural foundations is required, in particular with respect to reversible thermoplastic behavior and irreversible consolidation.

The simplest and most extensively studied melting gel system is the polyphenylsilsesquioxane. Despite numerous investigations, a comprehensive, multi-method characterization that correlates structural motifs with the observed melting behavior is still lacking. In particular, the role of specific network units such as cages, ladder motifs or cyclic structures has not yet been systematically addressed in this context.

The aim of this work was therefore to investigate the structural prerequisites for melting gel behavior using different polysilsesquioxanes as model systems. The focus was placed on understanding how the type of organic substituent, the degree of crosslinking and the molecular architecture influence the thermal properties.

The thesis is structured into four main parts:

1. **Structural analysis of polyphenylsilsesquioxane as a melting gel model system**

   The established polyphenylsilsesquioxane was selected as a reference system for the melting gel family and was comprehensively characterized using IR, Raman, NMR, UV–Vis, fluorescence spectroscopy, TGA, DSC, PXRD and SEC. The objective was to clarify how structural motifs, the degree of crosslinking, and defects in the form of non-crosslinked OH or OR groups influence the thermal response of the material. A particular focus was placed on correlating these structural features with the unique properties that distinguish melting gels.

2. Influence of aliphatic alkyl substituents on melting gel properties

Since polysilsesquioxane melting gels with purely *n*-alkyl substituents have not been reported in the literature, the goal was to investigate how *n*-alkyl groups affect key properties such as T_g and consolidation behavior. A series of *n*-alkyltrimethoxysilanes with chain lengths from C_1 to C_{18} was studied. The resulting polysilsesquioxanes were analyzed before and after thermal treatment at 300 °C and compared to the phenyl-based melting gel regarding thermoplastic and thermoset behavior. The influence of chain length on crystallization tendencies, crosslinking behavior and thermal transitions was systematically evaluated and correlated with the molecular structure.

3. Influence of polycyclic aromatic groups on melting gel properties

To expand the structural spectrum of melting gels, polycyclic aromatic substituents such as 1-naphthyl, 2-naphthyl and 9-phenanthrenyl were introduced. In addition to examining the impact of isomerism and the size of the aromatic system on thermoplastic and thermoset behavior, particular attention was given to fluorescence introduced via the extended π-electron systems.

4. Utilization of thermoplastic properties of melting gels for the fabrication of fluorescent microparticles

Finally, the reversible softening of the phenyl melting gel was exploited to fabricate fluorescent microparticles. Due to the hydrophobic nature of the gel, hydrophobic perylene dyes could be easily incorporated during the gelation stage of synthesis. By means of a newly developed melt-emulsion strategy followed by base-catalyzed curing, spherical fluorescent microparticles were obtained. In addition to fluorescence properties, the effect of the base on the structure of the particles was also investigated in detail.

4 Results and Discussion

In this chapter, four publications related to the topic of the thesis are presented. The contributions of the respective authors are specified for each publication, accompanied by a brief summary. The associated supporting information can be found in Chapter 7. All results presented have been published in peer-reviewed scientific journals.

4.1 Thermoplastic Silsesquioxane Hybrid Polymers with a Local Ladder-Type Structure

Published as an article:

Svenja Pohl, Oliver Janka, Ekkehard Füglein, Guido Kickelbick, *Macromolecules* **2021**, *54* (8), 3873-3885. DOI: 10.1021/acs.macromol.1c00310.

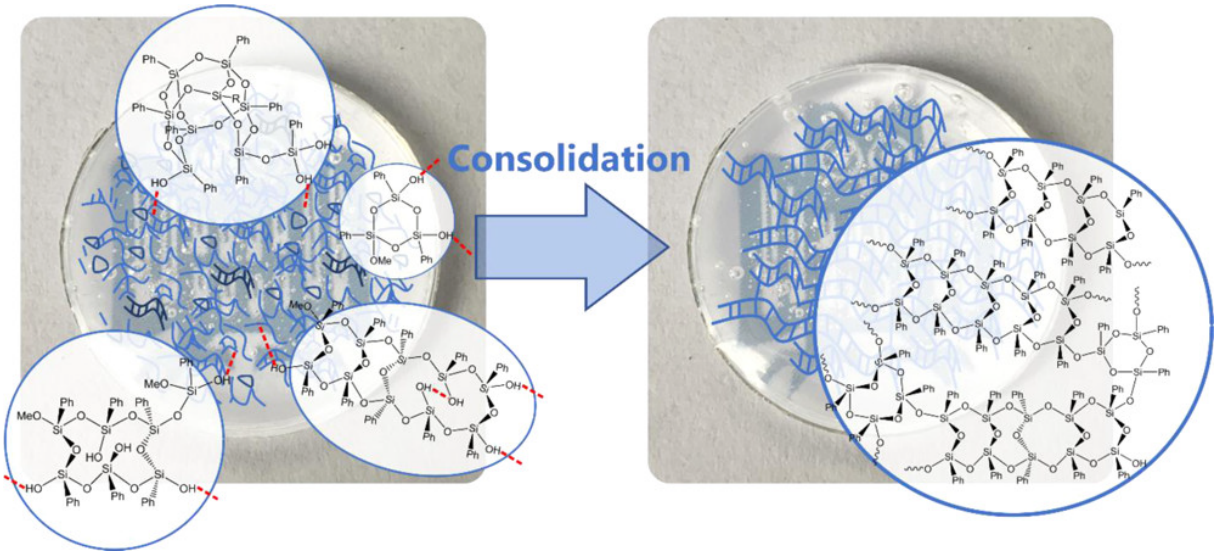

The supporting information is provided in Chapter 7 and is available online at: *https://doi.org/10.1021/acs.macromol.1c00310*.

The author's contribution to this work amounts to 75% (40% of the results were obtained during the author's master's thesis and 35% during the PhD studies).

Detailed statement of the individual contributions of the author and co-authors:

Svenja Pohl wrote the complete draft of this manuscript that was acknowledged by all named authors. She performed the synthesis and characterization of the melting gels and was primarily responsible for the interpretation of the key data and results. The foundational research was carried out as part of her Master's thesis,[410] including the synthesis of the melting gels and the acquisition and evaluation of NMR, FTIR, Raman, DSC, PXRD, TGA, fluorescence, and UV-Vis data. Additional experiments, such as TG-FTIR analyses, SEC and temperature-dependent PXRD measurements, were performed during her PhD studies, along with the preparation of the manuscript. Oliver Janka supported the PXRD and temperature-dependent measurements

and contributed to data interpretation. Ekkehard Füglein carried out the TG-FTIR measurements and provided guidance in the interpretation of the results. Prof. Dr. Guido Kickelbick initiated and supervised the project, contributed to scientific discussions, and revised the manuscript to its final version.

Melting gels are characterized by their temperature-dependent thermoplastic and thermosetting behavior. Their tunable rheological and thermal properties allow precise control over material shaping and processing, which has led to increasing interest in novel functionalities and application fields. However, the structural origins of their thermal transitions remain only partially understood. A deeper insight into the underlying network motifs could significantly expand the scope of melting gel formulations and enable the design of materials with tailored properties.

The publication titled *"Thermoplastic Silsesquioxane Hybrid Polymers with a Local Ladder-Type Structure"* addresses this gap through a comprehensive structure–property analysis of a model system based exclusively on $PhSiO_{3/2}$ units. Owing to its simplicity and well-defined composition, polyphenylsilsesquioxane serves as a prototypical reference material for elucidating key principles underlying melting gel behavior.

The synthesis involved solvent-free, acid-catalyzed hydrolysis and condensation of phenyltrimethoxysilane. The resulting material was characterized using NMR, IR, Raman, and fluorescence spectroscopy, thermal methods (TGA, DSC), temperature-dependent PXRD, and SEC. In addition, time-resolved IR and Raman spectroscopy were employed to monitor the hydrolysis and condensation processes during gel formation.

The combined results revealed a partially crosslinked structure with defects in the form of residual methoxy and hydroxy groups. This low crosslinking allows segmental chain mobility and explains the reversible softening behavior at higher temperatures. IR and fluorescence spectroscopy showed that hydrogen bonding and π–π interactions within the precursor gel contribute to its structural stability and result in a T_g above room temperature. PXRD data indicate the presence of ladder-like motifs within the silsesquioxane network. However, the structure also contains a high number of defects, such as cage-like units, small rings, and randomly distributed elements. The reversible softening up to 110 °C was confirmed by DSC and repeated temperature-cycled PXRD measurements, showing no significant structural transformation over multiple heating cycles.

Upon thermal consolidation at 200 °C, remaining silanol groups undergo further condensation, increasing the crosslinking density and reducing molecular mobility. This transition leads to a permanently rigid, thermoset-like material that no longer softens. Additionally, structural reorganization during consolidation leads to a higher proportion of ordered ladder-like segments while reducing structural defects.

This study offers a comprehensive structural characterization of a melting gel system and identifies key network motifs that govern the characteristic thermal transitions. The insights gained serve as a structural foundation for understanding and tailoring melting gel behavior in related hybrid materials.

Macromolecules

pubs.acs.org/Macromolecules Article

Thermoplastic Silsesquioxane Hybrid Polymers with a Local Ladder-Type Structure

Svenja Pohl, Oliver Janka, Ekkehard Füglein, and Guido Kickelbick*

Cite This: *Macromolecules* 2021, 54, 3873–3885 Read Online

ACCESS | Metrics & More | Article Recommendations | Supporting Information

ABSTRACT: Organosilsesquioxane hybrid materials are an important class of functional materials due to their tailorable functions and high thermal and optical stability. Recently, several studies showed that phenyl-substituted trialkoxysilanes can be converted into reversibly melting gels by applying hydrolysis and condensation reactions. We studied the underlying mechanisms of their formation and the final structure in detail by a combination of various spectroscopic techniques, thermal analysis, size exclusion chromatography, and X-ray diffraction. Our investigations reveal that local ladder-type silsesquioxanes with a defect-rich structure are formed in a first hydrolysis and condensation step. The partial presence of stable −OH and methoxy groups attached to the aryl-substituted silicon atoms in the ladderlike polymer explains their thermoplastic behavior. Heating above a particular consolidation temperature leads to further condensation reactions of the residual groups as well as a structural reorientation of the ladder-type polymers. The final materials are hard and cross-linked hybrid glasses with thermal stability higher than 400 °C and high optical transparency.

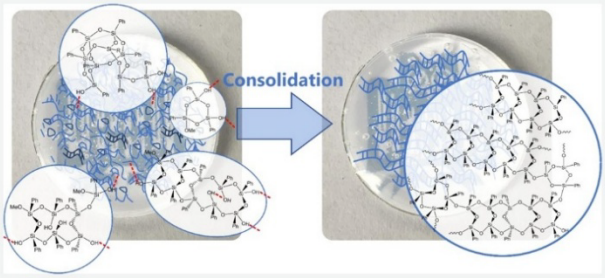

INTRODUCTION

Silsesquioxanes are known for decades; especially, cage compounds have attracted a lot of attention in the 20th century.[1,2] Derivatives of these compounds are partially condensed cages[3] and ladderlike silsesquioxanes.[4] Since the first structural characterizations, the field of silsesquioxanes has greatly expanded and the molecules are used as building blocks for inorganic−organic hybrid materials in a wide range of areas, such as pharmacy or aerospace.[5−8] Their outstanding optical properties make them ideal materials for optoelectronic applications, such as LED encapsulants.[9] Structures of silsesquioxanes can vary from open or closed cagelike oligosilsesquioxanes consisting of discrete structures formed from a limited number of tetrahedral units to polymeric species with a defined ladder structure or random networks (Figure 1).[10]

Oligo- or polysilsesquioxanes are commonly synthesized by polycondensation reactions based on the sol−gel process. Hydrolysis of monosilanes with the general structure $RSiX_3$ (R = organic group, X = Cl, OMe, OEt, etc.) under acidic or basic conditions forms the corresponding silanol species. In a second step, the reactive groups condense with other silanols or alkoxysilanes with elimination of water and alcohol to form organosilsesquioxanes of different structures.[11−13] The structural motifs created are strongly dependent on the choice of the precursor and the prevailing synthesis conditions.[14−16] In recent years, it has been shown that organoalkoxysilanes can produce so-called melting gels under very specific reaction conditions in acid- or base-catalyzed hydrolysis and condensation reactions.[17,18] Melting gels are inorganic−organic hybrid materials that can soften when heated to a specific temperature T_1 and harden again when cooled to room temperature. The softening of the material was described as melting. It is not melting in a thermodynamic sense but describes the property of flowing due to incomplete cross-linking. This reversible process is in strong contrast to all other observations on sol−gel-derived materials, which form thermally stable cross-linked resins. When the gels are heated to the so-called consolidation temperature T_2 ($T_2 > T_1$), the material permanently hardens and can no longer be melted. The result is described as a hybrid glass.[19−21]

A softening behavior of polysilsesquioxane particles was initially observed by Matsuda et al.[22−24] Later on, Masai et al. developed binary gels of phenyl- and methyl-containing di- and trialkoxysilanes. Using the so-called "gel-melting method", the researchers obtained organically modified siloxanes with low softening points.[17] Klein et al. also developed various one-, two-, and three-component melting gels containing phenyl and methyl substituents as organic groups.[18,19,25] Their focus was mainly on the investigation of thermal stability, the relationship

Received: February 9, 2021
Revised: March 12, 2021
Published: April 14, 2021

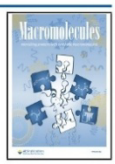

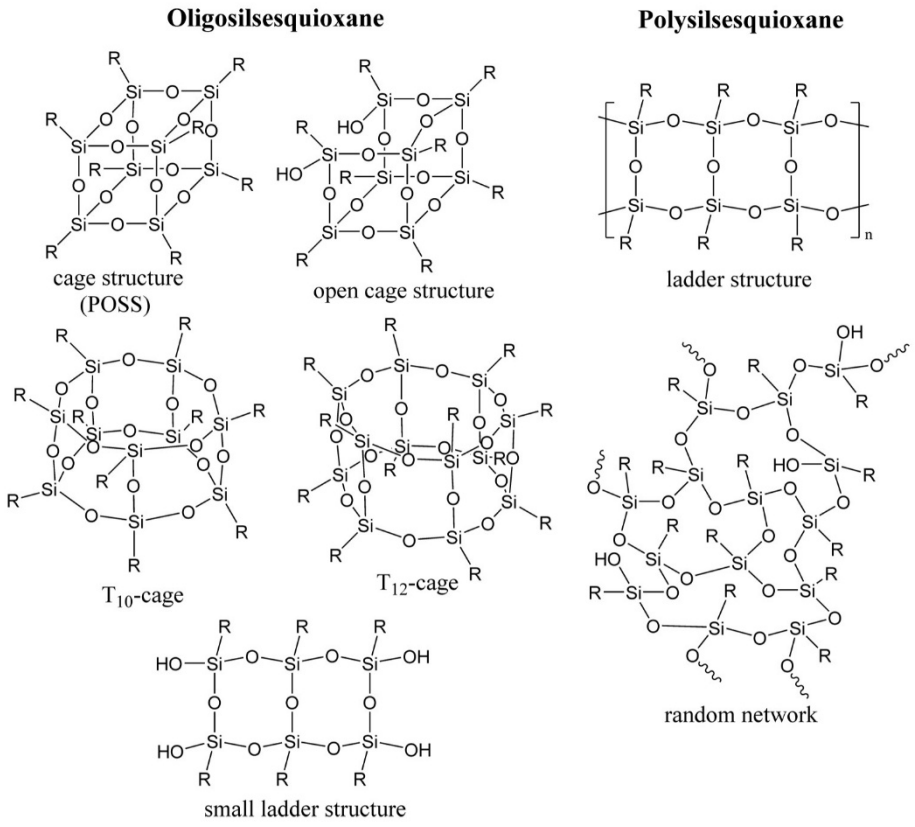

Figure 1. Possible oligo- and polysilsesquioxane structures.

between structure, glass transition temperature (T_g), and consolidation temperature (T_{con}), and the development of possible applications.[26,27] Previously, we showed that the concept can be applied for optoelectronic materials and can be expanded to an elastomer-like behavior.[9] However, none of these previous studies has investigated in detail the mechanism of the unusual behavior of these materials.

The goal of our study is to provide a detailed explanation of the structure evolution and the mechanism of melting gel formation. For a simplification of the investigation, we applied only phenyltrimethoxysilane as a precursor. All structures were investigated for both the nonconsolidated and consolidated materials applying NMR, IR, Raman, and fluorescence spectroscopy, DSC, TG, and XRD analyses. Time-dependent IR and Raman measurements were carried out to investigate the kinetics of the hydrolysis and condensation reaction. DSC and XRD measurements were used to demonstrate the reversibility of the melting process. As proof of concept, we expanded the studies to a naphthyl-containing polysilsesquioxane with melting gel-like properties.

EXPERIMENTAL SECTION

Materials. Phenyltrimethoxysilane (97%), 1-bromnaphthaline (97%), and tetramethoxysilane (98%) were all purchased from abcr (Germany), hydrochloric acid was provided by Bernd Kraft GmbH (Germany), and magnesium chips were obtained from Fisher Scientific GmbH (Germany). All chemicals were used as received. Hydrochloric acid was diluted to pH 2.5 with demineralized water.

Instrumentation. Fourier transform infrared spectra (FT-IR) were recorded in attenuated total reflectance mode on a Vertex 70 spectrometer (Bruker Optics, Ettlingen, Germany) from 400 to 4500 cm^{-1} with a resolution of 4 cm^{-1} and 10 scans.

UV−vis transmission measurements were performed in aluminum frames (8 × 2 mm^2) on a Lambda 750 instrument (PerkinElmer Inc., Shelton, USA) equipped with a 100 mm integration sphere from 250 to 600 nm with a 4 nm increment and a 0.2 s integration time.

Solution NMR spectra were recorded on an Avance III 300 MHz spectrometer and an Avance III HD 400 MHz spectrometer (Bruker, Billerica, USA) with 300.13/400.13 MHz for ^{1}H NMR spectra, 75.47/100.61 MHz for ^{13}C NMR spectra, and 59.63/79.49 MHz for ^{29}Si NMR spectra. All NMR samples were prepared in chloroform-*d* ($CDCl_3$). ^{29}Si NMR spectra of the dissolved polymers were analyzed after subtraction of a blank spectrum. Solid-state CP-MAS NMR spectra were recorded on an Avance III HD—Ascend 400WB spectrometer (Bruker, Billerica, USA) using 4 mm inner diameter ZrO_2 rotors with a 13 kHz rotation frequency. The resonance frequencies were 100.65 MHz for ^{13}C and 79.53 MHz for ^{29}Si NMR spectra.

Thermogravimetric measurements (TG) were carried out applying a TGA/DSC STARe System 1 (Mettler-Toledo, Schwerzenbach, Switzerland) at a heating rate of 10 K min^{-1} between 25 and 800 °C using an oxygen gas flow of 40 mL min^{-1}.

TG-FT-IR measurements were performed using a PERSEUS TG 209 F1 Libra (NETZSCH-Gerätebau GmbH, Selb, Germany and Bruker Optics, Ettlingen, Germany). The measurements were carried out at a 20 K min^{-1} heating rate in the temperature range between 25 and 1000 °C under synthetic air flow (40 mL min^{-1}, N_2/O_2 75:25%).

Differential scanning calorimetry (DSC) was performed with a DSC 204 F1 Phoenix calorimeter (NETZSCH-Gerätebau GmbH, Selb, Germany) using aluminum crucibles with pierced lids under nitrogen flow (100 mL min^{-1}) applying a heating rate of 10 K min^{-1} from −40 to 400 °C. The value of the glass transition temperature (T_g) was taken by determining the inflection point of the glass event.

Fluorescence spectroscopy was performed applying a FluoroMax 4 spectrofluorometer (Horiba Scientific, Kyoto, Japan) with an excitation wavelength of 260 nm.

https://doi.org/10.1021/acs.macromol.1c00310
Macromolecules 2021, 54, 3873−3885

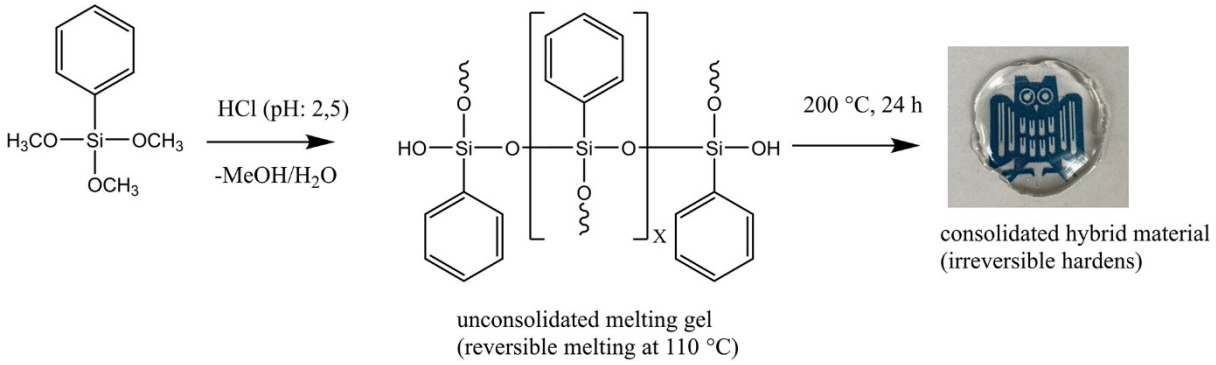

Figure 2. Melting gel synthesis via hydrolysis and condensation of phenyltrialkoxysilanes.

Size exclusion chromatography (SEC) was performed with a PSS SECcurity[2] system composed of a 1260 IsoPump-G7110B (Agilent Technologies, Santa Clara, CA), a 1260 VW-detector G7162A at 270 nm (Agilent Technologies), and a 1260 RI detector G7114A at 30 °C (Agilent Technologies), with THF as the mobile phase (flow rate 1 mL min^{-1}) on an SDV column set (SDV 103, SDV 105, SDV 106) from PSS (Polymer Standard Service, Mainz, Germany). Calibration was carried out using PS standards (from PSS). SEC measurements with DMF (1 g L^{-1} LiBr) as the mobile phase (flow rate 1 mL min^{-1}) were obtained with a Waters system composed of a 515 HPLC Pump, a 2487 UV detector at 260 nm, and a 2410 RI detector at 40 °C on a GRAM column set (GRAM 30, GRAM 1000, GRAM 1000) from PSS (Polymer Standard Service, Mainz, Germany) at 60 °C. Calibration was carried out using PMMA standards.

Powder X-ray diffraction (PXRD) patterns of the pulverized samples were recorded at room temperature on a D8-A25-Advance diffractometer (Bruker AXS, Karlsruhe, Germany) in Bragg−Brentano θ−θ geometry (goniometer radius 280 mm) with Cu Kα radiation (λ = 154.0596 pm). A 12 μm Ni foil working as a K_β filter and a variable divergence slit were mounted at the primary beam side. A Lynxeye detector with 192 channels and a variable slit diaphragm in front of it was used at the secondary beam side. Experiments were carried out in a 2θ range of 3−40° with a step size of 0.013° and a total scan time of 1 h. The recorded data was evaluated using TOPAS 5.0 (Bruker AXS, Karlsruhe, Germany) software,[28] with the observed reflections being treated via single-line fits. Powder X-ray diffraction patterns at elevated temperatures were recorded on the same diffractometer using an XRK 900 reactor chamber (Anton Paar GmbH, Graz, Austria). The samples were investigated in air in the temperature range of 30−110 °C at heating rates of 10 K min^{-1}. Again, a 12 μm Ni foil working as a K_β filter and a variable divergence slit were mounted at the primary beam side. The secondary beam side was equipped with a Lynxeye detector and a variable slit diaphragm. Diffraction patterns were recorded between 3 and 40° 2θ. The thermal expansion of the reaction chamber and the sample holder was determined using elemental Si (NIST Standard Reference Material 640f). The obtained data was refined in TOPAS 5.0 software,[28] keeping the lattice parameter of Si fixed while refining the height displacement. This was conducted for different temperatures and a linear regression was performed. For the subsequent measurements, the z-height was modified by the previously determined values depending on the temperature used. Prior to the investigation, the gel was molded into a stainless-steel sample holder so that the upper surface was in plane with the edges of the holder. To account for a potential expansion of the polysilsesquioxanes during heating, one sample was mixed with SiO_2 and measured at 30, 80, and 110 °C (SI Figure S14). From these measurements, the zero shift was determined by linear regression, which was subsequently used to correct the 2θ angles of the peak positions (SI Figure S15).

Monomer Preparation. The trialkoxysilane was synthesized according to a modified literature procedure.[29]

1-Naphthyltrimethoxysilane (1-NpSi(OMe)$_3$). Magnesium chips (3.70 g, 0.152 mol, 1.5 equiv), tetramethoxysilane (46.35 g, 0.304 mol, 3 equiv), and abs. THF (160 mL) were stirred in a three-necked round-bottom flask at 30 °C under an argon atmosphere. 1-Bromnaphthaline (20.72, 0.100 mol, 1 equiv) was added dropwise over a period of 20 min at 30 °C with a dropping funnel. The reaction mixture was heated to 50 °C for 1 h, then the temperature was increased further to 75 °C for 1 h, and finally allowed to cool to room temperature overnight. Magnesium and THF were removed from the reaction mixture by filtration and concentration. Afterward, 250 mL of n-hexane was added to the residue, boiled for 10 min under reflux conditions, and filtered after cooling to room temperature. The procedure was repeated a second time using 125 mL of n-hexane. The solvent of the combined filtrates was removed, and the product was distilled (2 × 10^{-2} mbar, 140 °C), resulting in a transparent liquid (19.32 g, 78%).

^{1}H NMR (300 MHz, $CDCl_3$): δ = 8.32−8.29 (m, 1H, 1-Np), 7.99−7.94 (m, 2H, 1-Np), 7.89−7.86 (m, 1H, 1-Np), 7.59−7.48 (m, 3H, 1-Np), 3.68 (s, 9H, OMe) ppm.

^{13}C NMR (75 MHz, $CDCl_3$): δ = 50.93 (O−CH_3), 125.11, 125.85, 126.73, 127.75, 128.39, 128.83, 131.50, 133.40, 136.31, 137.13 (1-Np) ppm.

^{29}Si NMR (60 MHz, $CDCl_3$): δ = −54.71 ppm.

Gel Preparation. The melting gel was synthesized according to a modified literature procedure.[18]

Polyphenylsilsesquioxane Melting Gel (PhMG) and Poly-1-Naphthylsilsesquioxane Melting Gel (1-NpMG). Here, we only describe the procedure for the preparation of PhMG; the 1-NpMG was prepared accordingly. One equivalent phenyltrimethoxysilane and 1.5 equiv hydrochloric acid (pH = 2.5) were stirred in a closed vial at 45 °C for 8 h. Afterward, the mixture was stirred with the lid removed until gelation was completed (25 °C, 18 h). The vial was transferred into a compartment drier to remove water and methanol in two steps. First, the material was heated at 70 °C for 24 h and afterward at 110 °C for an additional 24 h. The transparent polymer was allowed to cool to room temperature to obtain a solid hybrid glass material. The precursor melting gel ($PhMG_{prec}$) softens reversibly at $T_1 \approx$ 110 °C and consolidates (hardens irreversibly) by thermal treatment at $T_2 \approx$ 200 °C for 24 h to obtain a transparent solid glasslike material ($PhMG_{cons}$). To handle the precursor gel, it was melted in a preheated 110 °C oven for 10 min. After processing, it was cooled to room temperature by removing it from the oven.

■ RESULTS AND DISCUSSION

As described in the Experimental Section, phenyltrimethoxysilane can be polymerized to receive a nonconsolidated melting gel that is reversibly meltable up to 110 °C and soluble in solvents like acetone, chloroform, or THF. The hydrolysis and condensation process can be visually monitored by homogenization of the initial two-phase mixture in the first few minutes and subsequently increasing viscosity. Temper-

https://doi.org/10.1021/acs.macromol.1c00310
Macromolecules 2021, 54, 3873−3885

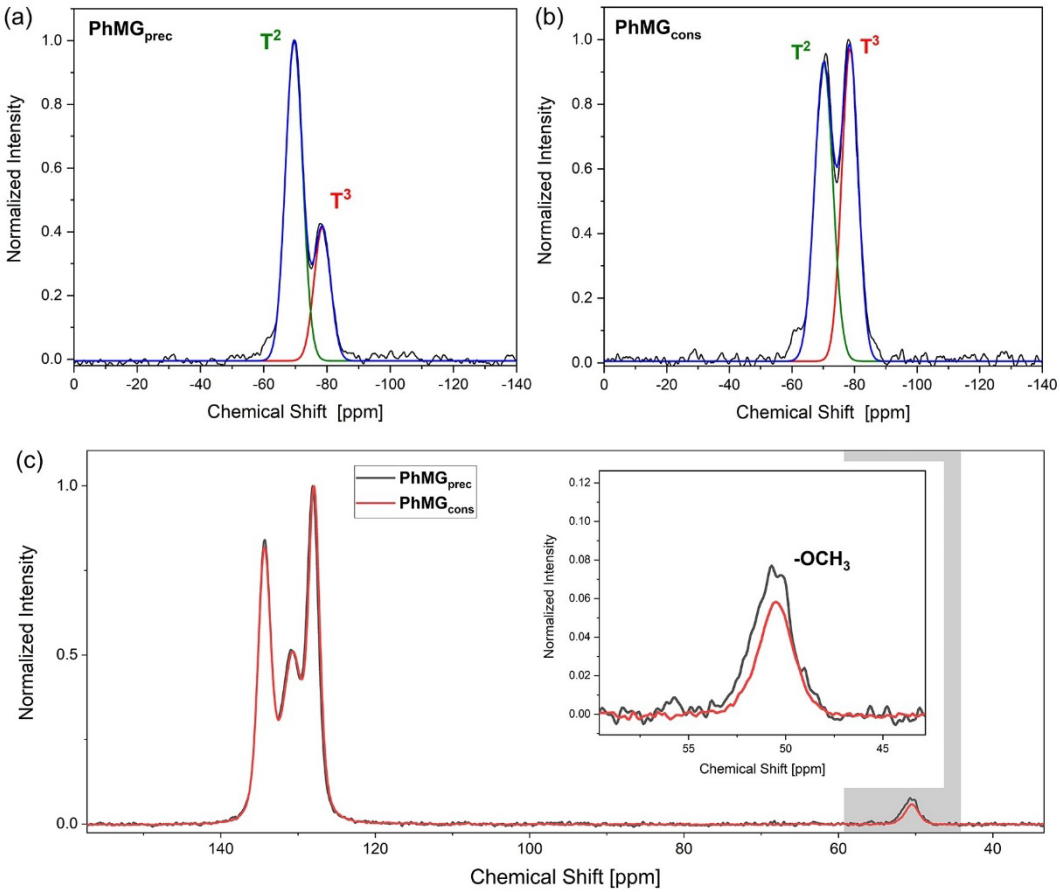

Figure 3. (a) ^{29}Si CP-MAS NMR spectra of the nonconsolidated gel fitted by a Gaussian function, (b) ^{29}Si CP-MAS NMR spectra of the consolidated gel fitted by a Gaussian function, and (c) ^{13}C CP-MAS NMR spectra of the consolidated and nonconsolidated gels.

ature treatment at 110 °C leads to the removal of condensation byproducts such as water and methanol and further cross-linking. As 110 °C is the highest temperature used in synthesis, the melting gel is softened at this temperature for processing and reversibility testing. Above 200 °C, without the addition of any further catalysts, an irreversible consolidation forming a transparent, solid, insoluble glasslike material takes place (Figure 2).

NMR Spectroscopy. ^{13}C and ^{29}Si CP-MAS NMR spectroscopy was applied to investigate the molecular structure of the prepared nonconsolidated and consolidated gels, to generate an overview of the cross-linked groups, and to determine the degree of condensation (DC). By means of ^{1}H NMR, the number of remaining methoxy groups of the nonconsolidated gel was quantified, which provided information about the degree of hydrolysis of the monomer. By combining the information from the NMR techniques, the composition of the PhMG$_{prec}$ can be calculated, with respect to the percentage of −OH, −OMe, and Si−O−Si- groups. Furthermore, the consolidation step can be demonstrated by changing the cross-linking units.

Solid-state ^{13}C NMR spectra (Figure 3c) show intense peaks from the phenyl groups in the region of 128−135 ppm and weak signals from residual alkoxy groups at 50 ppm in the nonconsolidated and consolidated melting gels. By integrating the visible peaks in the ^{1}H NMR, the number of remaining methoxy groups in the polymer can be determined (SI Figure S5). Approximately 10% of the −OMe groups remain in the precursor gel. Due to the insolubility of the consolidated gel, no quantitative information about the number of −OMe groups in the consolidated state can be obtained. However, the comparison of the area of the visible peaks in the ^{13}C CP-MAS NMR indicates that the number of −OMe groups is lower after consolidation (Figure 3c).[30] ^{29}Si CP-MAS NMR spectra (Figure 3a,b) of the polymers show two peaks in the range of −74 to −66 and −80 to −77 ppm that can be assigned to T^2 and T^3 species.[9] The lack of T^0 signals shows a complete integration of the precursor trialkoxysilane in condensed species. The presence of T^2 signals indicates the existence of −OH or −OMe groups in the gel because not all trialkoxysilane groups are fully condensed to T^3 species. Liquid NMR spectra of the nonconsolidated sample confirm the results of the CP-MAS NMR spectroscopy (SI Figures S6 and S7). Fitting and integration of the T^2 and T^3 signals by a Gaussian function allow the calculation of the T unit ratio and thus the degree of condensation according to the following equation[31]

$$\mathrm{DC}\ [\%] = \frac{\mathrm{T}^3\ [\%]\cdot 3 + \mathrm{T}^2\ [\%]\cdot 2}{3}$$

Using the proportion of the cross-linked Si atoms (DC) and the remaining methoxy groups of the nonconsolidated gel, obtained from the integration of the ^{1}H NMR, the percentage

https://doi.org/10.1021/acs.macromol.1c00310
Macromolecules 2021, 54, 3873−3885

of hydroxy groups can be calculated applying the following formula[32]

$$OH\ [\%] = 100\% - DC\ [\%] - OMe\ [\%]$$

Table 1 shows that the consolidation process of the precursor gel leads to a higher degree of condensation. Temperature

Table 1. Ratio of Condensation Products T^2 and T^3, Degree of Condensation, and Ratio of −OMe and −OH Groups

	T^2 [%]	T^3 [%]	DC [%]	OMe [%]	OH [%]
$PhMG_{prec}$	71	29	76	10	14
$PhMG_{cons}$	51	49	83	<10	

treatment results in further condensation of −OH and −OMe groups. Flexible T^2 chains transform into a rigid network formed by T^3 species, which is the reason for the irreversible hardening of the previously meltable gel.[17] However, $PhMG_{cons}$ does not show a complete cross-linking, which can be due to the following two facts: (i) the bulkiness of the phenyl groups and (ii) the electronic structure of the phenyl substituent, which is known to stabilize the formation of silanol groups.[31,33,34]

FT-IR/Raman Spectroscopy. FT-IR and Raman spectroscopy was used to identify the functional groups and to monitor the progress of the hydrolysis and condensation reaction (Figure 4a). The presence of phenyl groups in the FT-IR spectra was identified by the presence of absorption peaks at 3074 and 3052 cm^{-1} ($\nu_{asym}(CH)_{Ar}$, $\nu_{sym}(CH)_{Ar}$), 1593 cm^{-1} ($\nu(C-H)_{Ar}$), 1427 cm^{-1} ($\nu(C-C)_{Ar}$), 1027, 994 cm^{-1} (C_6H_6 ring deformation), 1126 cm^{-1} ($\nu(Si-C)_{Ar}$), and 734, 692 cm^{-1} ($\delta(C-H)_{Ar}$).[19,35] The organic group remains unaffected by the hydrolysis and condensation reaction and the thermal treatment. The presence and intensity of other vibrations depend on the progress of the synthesis. The precursor gel showed the vibrations of the Si−OH groups at 950 cm^{-1}; it served as evidence for hydrolyzed groups.[36] The vibrations of the hydroxy groups, found between 3700 and 3000 cm^{-1}, are dependent on the environment.[37] A distinction can be made between H-bonded (3500−3150 cm^{-1}) and isolated (3620 cm^{-1}) groups (Figure 4b). Since water and methanol were not present in the polymer after the gel synthesis, it can be assumed that the visible peaks are not overlapping with the vibrations of the byproducts and can be assigned solely to the vibrations of the melting gel. After the consolidation, only the vibration of the isolated hydroxyl groups existed. It can be concluded that the −OH groups, which previously interacted via H bonds, were condensed and only the isolated groups remain in the gel. This result suggests that the interacting groups are important for the stabilization of the nonconsolidated melting gel structure and the melting behavior of the gel. Vibrations of the methoxy groups (1190 cm^{-1}) disappeared almost completely in both melting gel stages, indicating the completion of the hydrolysis reaction.[36] The condensation reaction is reflected in the presence of the Si−O−Si band between 1000 and 1150 cm^{-1} (Figure 4c).[38] The broad complex band shows the presence of different silsesquioxane species. Silsesquioxanes show absorption at 1050 cm^{-1} ($\nu_{ring\text{-}sym}$) that can be assigned to low-symmetry structures, like random networks. More symmetrical species, like ladder structures or open cages, show an additional absorption at 1150 cm^{-1} ($\nu_{ring\text{-}asym}$).[39] Small tricycles are visible at 1018 cm^{-1}.[40] The consolidation process led to a more cross-linked structure and an increase in absorption at 1100 cm^{-1}. This suggests an increase in symmetric structural units like ladder structures.

Raman spectroscopy confirmed the FT-IR results (Figure 5a). The reduction of the intensity of the $-OCH_3$ vibrations by 1103, 654, and 477 cm^{-1} served as proof of the hydrolysis reaction.[36] New bands present at 198 and 582 cm^{-1} could be assigned to condensed siloxane species.[35,41] The spectra of the nonconsolidated and consolidated melting gels showed no significant difference (Figure S13).

Raman and IR measurements confirm the NMR results and suggest a partially cross-linked silsesquioxane. In addition to the −OMe groups visible in the NMR spectra, the IR measurements show the remaining −OH groups interacting via H bonds in the nonconsolidated gel. The defect-rich structure determines the thermoplastic properties. Consolidation of the gel leads to a further condensation of the interacting groups and a transformation of the silsesquioxane structure, resulting in a rigid hybrid glass.

Time-Dependent IR and Raman Spectroscopy. IR and Raman spectra were measured at different times for a better

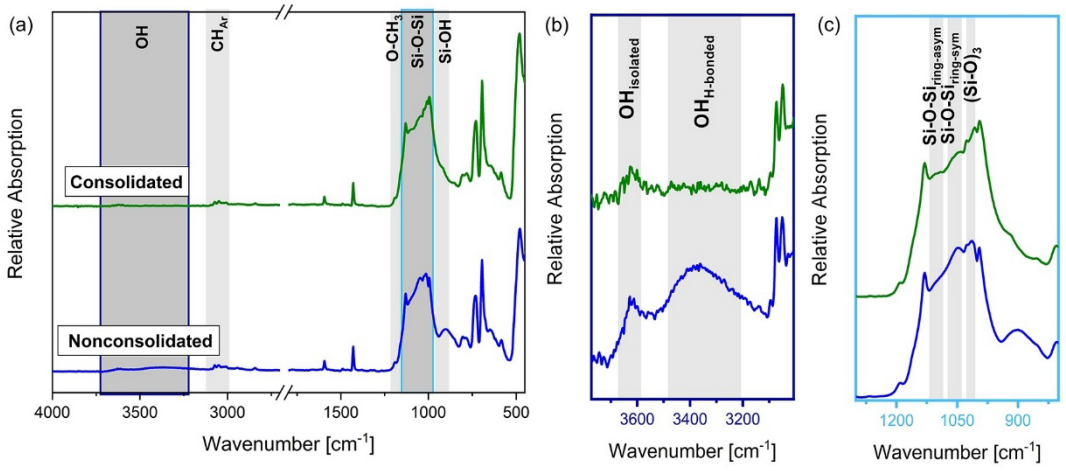

Figure 4. FT-IR spectra of the nonconsolidated (blue) and consolidated (green) phenyl-silsesquioxane melting gels: (a) complete spectra, (b) detailed view of the vibrations of isolated and associated hydroxy groups, and (c) detailed view of the Si−O−Si vibrations.

https://doi.org/10.1021/acs.macromol.1c00310
Macromolecules 2021, 54, 3873−3885

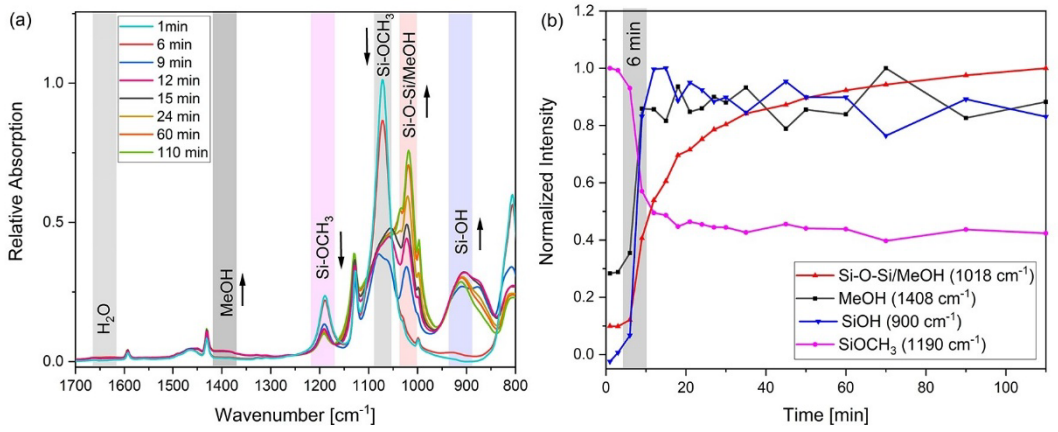

Figure 5. (a) Time-dependent FT-IR spectra from the hydrolysis and condensation of phenyltrimethoxysilane at selected time intervals and (b) graphical representation of the important time-dependent intensity vibrational modes during the hydrolysis and condensation reaction of phenyltrimethoxysilane.

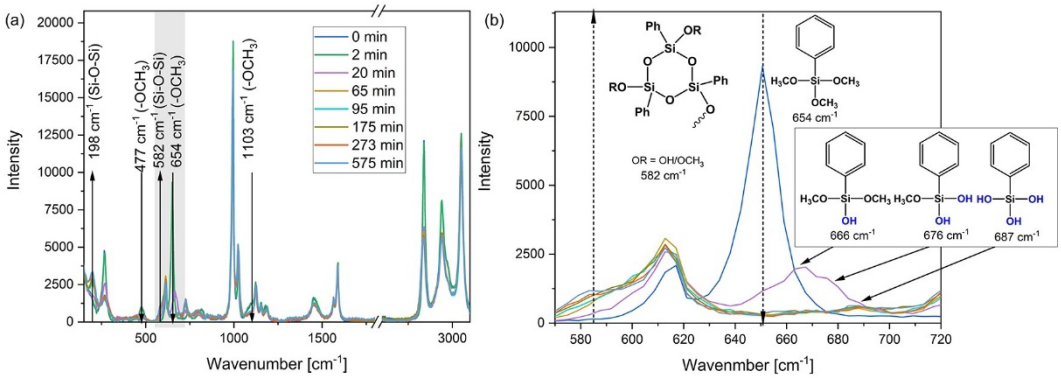

Figure 6. Time-dependent Raman spectra from the hydrolysis and condensation of phenyltrimethoxysilane at selected time intervals: (a) complete spectrum from 150 to 3100 cm^{-1} and (b) magnified area from 570 to 720 cm^{-1}.

understanding of the process of hydrolysis and condensation within the melting gel synthesis. In contrast to NMR spectroscopy, the −OH groups in the gel are directly visible and can be included in the studies. The measurements were started with the addition of hydrochloric acid to phenyltrimethoxysilane. At distinct time intervals, samples were withdrawn from the reaction vial, and IR and Raman spectra were recorded (selected time intervals, Figure 6a; all recorded spectra are shown in Supporting Information Figure S12). IR spectroscopy allows the monitoring of the formed byproducts methanol (1408 cm^{-1}) and water (1639 cm^{-1}) as well as the hydrolysis and condensation of the educts and the products Si−OMe (1190 cm^{-1}), Si−OH (900 cm^{-1}), and Si−O−Si (1150−1000 cm^{-1}).[36] The range of the Si−O−Si vibration was difficult to quantify because of the overlap of different silsesquioxane species with methanol and methoxy groups. At this stage of the reaction, we focused on the absorption of the tricycles at 1018 cm^{-1} as this is the band that undergoes the greatest transformation. Figure 5b shows a significant change of all bands in intensity from the sixth minute. The intensity of the Si−OMe peak decreased and that of the Si−OH peak and the MeOH peak increased. This process represents the hydrolysis reaction: −OMe groups were replaced by −OH groups and methanol was formed. The reaction occurred abruptly and was indicated by homogenization of the solution. Water was not used in an equimolar amount. Therefore, it was immediately consumed in the reaction and limited the initial hydrolysis reaction. As soon as the first groups were hydrolyzed, the condensation reaction started, visibly by an increase in the band at 1018 cm^{-1}. Since the methanol peak at 1408 cm^{-1} showed no significant change after the initial hydrolysis, but the band at 1018 cm^{-1} continued to rise, this increasing peak could be attributed to the formation of Si−O−Si bonds. In the same way as methanol, the intensity of −OH and $-OCH_3$ vibrations developed toward a plateau after the hydrolysis. Also, the peak of Si−O−Si vibrations flattened out at a later stage. An equilibrium was established between the different siloxane species.

Raman spectroscopy offers the possibility to observe the intermediate hydrolyzed monomer species in the range from 640 to 700 cm^{-1} (Figure 6b).[36] During hydrolysis, the vibration of the $PhSi(OMe)_3$ monomer shifted to a higher frequency with increasing number of hydrolyzed groups. Since the hydrolysis in the melting gel synthesis was extremely fast, the monomer peak at 654 cm^{-1} disappeared instantly when the two-phase reaction solution became homogeneous. The vibration bands of the hydrolyzed phenyltrimethoxysilane at 666 (1 OH), 676 (2 OH), and 687 cm^{-1} (3 OH) were not present for an extended time, which leads to the conclusion that a fast condensation occurred. At the same time, new bands at 198 and 582 cm^{-1} emerged and could be assigned to the formation of siloxane species. The vibration at a higher

https://doi.org/10.1021/acs.macromol.1c00310
Macromolecules 2021, 54, 3873−3885

frequency (582 cm^{-1}) is attributed to cyclotrisiloxanes.[19,41−43] Hence, the Raman results confirm the IR measurements.

The first step of the melting gel synthesis consists of an initial hydrolysis reaction in which the water is completely consumed. Due to the almost simultaneous condensation reaction, small, condensed siloxane species like cyclotrisiloxanes are formed. These were partially hydrolyzed and stabilized by the methanol formed.[44] IR bands between 1050 and 1150 cm^{-1}, which indicate a cross-linked structure, were not visible up to this point. Only the following gelation step and the temperature treatment at 110 °C led to further condensation reactions and a cross-linking takes place, as revealed in the FT-IR spectrum (Figure 4).

From all NMR, IR, and Raman spectra, mainly the hydrolysis and condensation reactions can be followed. In the literature, it is suggested that the condensation of trisilanols leads to linear, cyclic, and final polycyclic or polyhedral silsesquioxanes,[3,4,45] which is underlined by our results. However, interpretation of the final structure is quite vague, given the spectroscopic data. If ladder structures are established during the hydrolysis and condensation steps, this should lead to variations in structural observations, which can be detected by XRD and fluorescence spectroscopy due to the formation of regular intra- and intermolecular distances as well as the interactions arising between the aromatic groups.

Powder X-ray Diffraction (PXRD). The XRD patterns of our samples show two diffraction maxima, which are described to be characteristic of a ladderlike structure.[12,46−49] The first reflection at lower angles is associated with the chain-to-chain distance (d_1) between the siloxane backbones and correlates with the packing density of the network.[15,50] The second reflection is related to the average thickness of the double-stranded siloxane backbone (d_2) (Figure 7, Table 2). Both samples reveal similar d_2 values (0.45 nm), which is a known phenomenon in ladderlike structures.[15,51,52] The chain-to-chain distance d_1 shows a shift to lower 2θ values within the consolidation process. As shown before, d_1 also depends on the bulkiness and the steric demand of the organic groups as well as the defect concentration in the form of unreacted −OH and −OMe groups.[15,53] The precursor gel has a flexible structure due to the non-cross-linked and defect-rich architecture and the increased T^2 content. Therefore, the siloxane chains can arrange themselves quite close to each other, which leads to a lower chain-to-chain distance (0.83 nm). The consolidation process results in a higher degree of condensation and a more rigid structure. The restricted chain mobility and the bulky aromatic groups lead to a larger chain-to-chain distance (1.15 nm) and a lower packing density close to the values described in the literature for ladderlike polyphenylsilsesquioxanes.[48,52] It becomes clear that the condensation process does not only occur intramolecularly in the ladder-type structure but also intermolecularly. A thermal-induced exclusively intramolecular cross-linking would lead to a more perfect ladder-type polymer structure, which still can be molten or softened, like a polymer chain. Only an intermolecular process at the consolidation temperature can lead to a cross-linked nonmeltable hybrid glass.

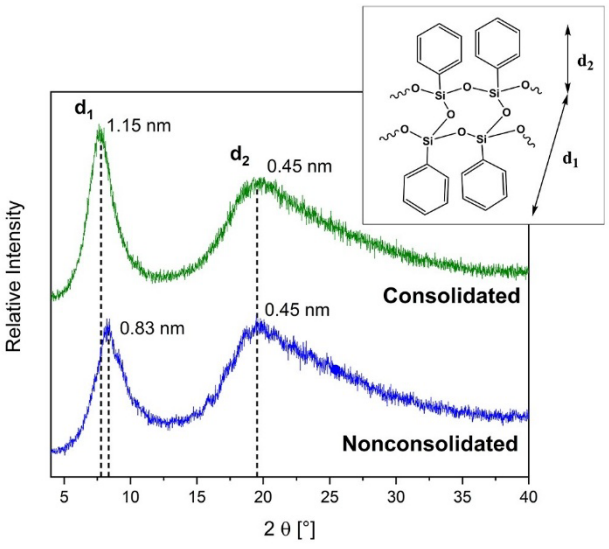

Figure 7. PXRD pattern of nonconsolidated $PhMG_{prec}$ (blue line) and consolidated $PhMG_{cons}$ (green line).

Table 2. Comparison of the Theoretically Calculated d_1 and d_2 Values for the Cis-Isotactic and Cis-Syndiotactic Configurations of a Polyphenylsilsesquioxane Ladder Structure with the Measured Values of the Prepared PhMG and Determined R Values

	theoretical calculations from Liu et al.[59]		measured values from XRD analysis	
	cis-isotactic [nm]	cis-syndiotactic [nm]	nonconsolidated gel [nm]	consolidated gel [nm]
d_1	1.18	0.8	0.83	1.15
d_2	0.49	0.62	0.45	0.45
R			0.98	1.15

The ratio of the intensity of the d_1 and d_2 values ($R = I(d_1/d_2)$) reflects the structural regularity of the ladderlike structure.[54] R becomes smaller when the defect concentration increases and the percentage of ladderlike segments in the material decreases. Table 2 shows the increasing R value caused by the consolidation process and an increase in the ladder structure parts. The PXRD measurements show that ladderlike silsesquioxane units are present in the gel, which are further increased after the consolidation process by a reorientation of the siloxane chains and an inter- and intramolecular condensation of unreacted −OMe and −OH groups.

The PXRD analysis offers an insight into the structure of the material. For this reason, the method was used to observe the reversibility of the $PhMG_{prec}$. A previously melted and cooled sample was heated *in situ* to 110 °C several times and then cooled again to 30 °C. XRD measurements were carried out at defined temperatures over a period of 2 h. To verify that the visible changes are intrinsic to the sample and not caused by thermal expansion/contraction of the measurement setup, a reference sample was measured (see the Experimental Section and the Supporting Information, Figures S14 and S15). All reported data have been corrected for the results of this calibration. An *in situ* observation of the consolidation process at 200 °C could not be carried out, as no meaningful results were generated due to the formation of bubbles in the sample during the measurement.

By comparison of the d_1, d_2, and R values (Figure 8a,b), a statement about structural changes in the gel can be made. First, it is noticeable that all values strongly fluctuate with applied temperature changes. An increase in temperature leads

https://doi.org/10.1021/acs.macromol.1c00310
Macromolecules 2021, 54, 3873−3885

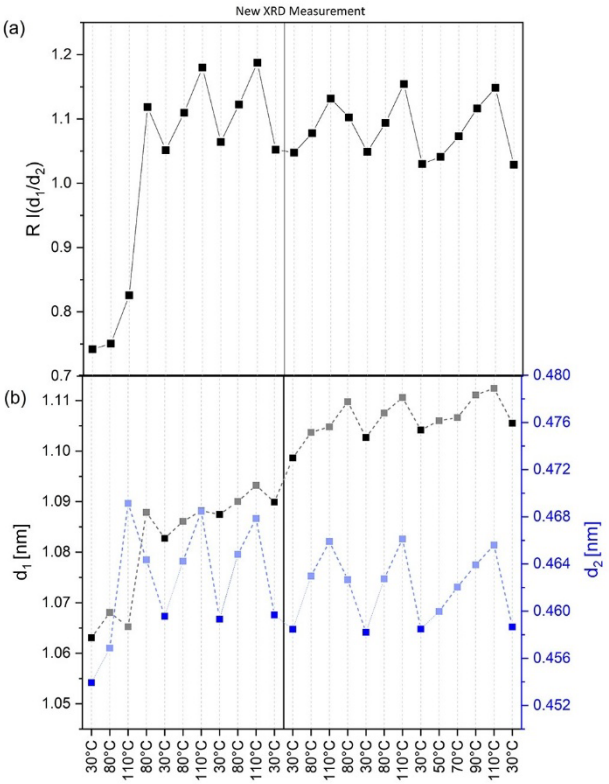

Figure 8. Evolution of the (a) R value and (b) d_1 and d_2 values of nonconsolidated $PhMG_{prec}$ determined from PXRD data measured at different temperatures. The break after three cycles is marked by a vertical line; at this stage, the sample was melted under standard conditions.

to a stronger oscillation of the atoms and subsequently to increased interatomic atomic distances. To compare the different cycles, we focused only on the measurements at 30 °C. Interestingly, cycle 1 differed from the other cycles by a strong increase in all values. This suggests that the slow and controlled heating and cooling processes and the long measuring times, which differ from the standard procedure, led to a rearrangement of the individual structural elements and further condensation reactions. After the third cycle, the measurement was stopped, and the gel was melted outside the reaction chamber using the standard melting conditions to check if the sample returned to the initial state before cycle 1 due to the abrupt heating and cooling. However, there is no reduction of the d and R values back to the starting point. Therefore, it can be concluded that the system irreversibly changed due to the *in situ* heating conditions. The d_2 and R values demonstrated no more change in cycles 4−6. The constant R value indicated that no further condensation of −OH and −OMe groups occurred and the degree of cross-linking remained the same over the next cycles. In contrast, the d_1 value showed a small increase with each heating cycle. If we assume that the d value depends on the defect concentration and the steric effect of the phenyl groups, and a change in the cross-linking can be excluded by the constant R value, it can be concluded that the increasing chain distance must be a consequence of the rearrangement of the organic groups and a change in tacticity after every cycle.

In summary, the degree of cross-linking and the number of defects remained constant and therefore a reversible melting process can be assumed under defined heating and cooling conditions. Therefore, the melting gel can be used as a thermoplastic polymer.

Fluorescence Spectroscopy. The photophysical properties of aromatic polymers are extensively investigated in the literature by fluorescence spectroscopy. Polystyrene and derivatives thereof are the preferred materials in the application of this method.[55−57] However, tacticity studies can also be carried out on ladderlike polyphenylsilsesquioxanes by fluorescence spectroscopy.[58,59] The emission spectrum of the precursor melting gel, dissolved in CH_2Cl_2, showed two emission bands of 285 and 325 nm (Figure 9a). The first one could be assigned to a single monomeric phenyl group and the second one to excimer fluorescence of an excited complex of two phenyl groups.[59−61] The presence of intramolecular excimer fluorescence depends on the spacial arrangement of the phenyl rings. Their evidence allows conclusions about the steric structure of the substituted ladder. By varying the gel concentration, the fluorescence emission intensities at 290 nm (I_M) and 325 nm (I_E) remained constant in the range of 0.74−5.35 wt % (I_M/I_E = const.) (Figure 9b). Furthermore, no shift of the bands could be detected in the spectrum in the same concentration range. Both properties described here are typical for intramolecular excimer formation.[59,62]

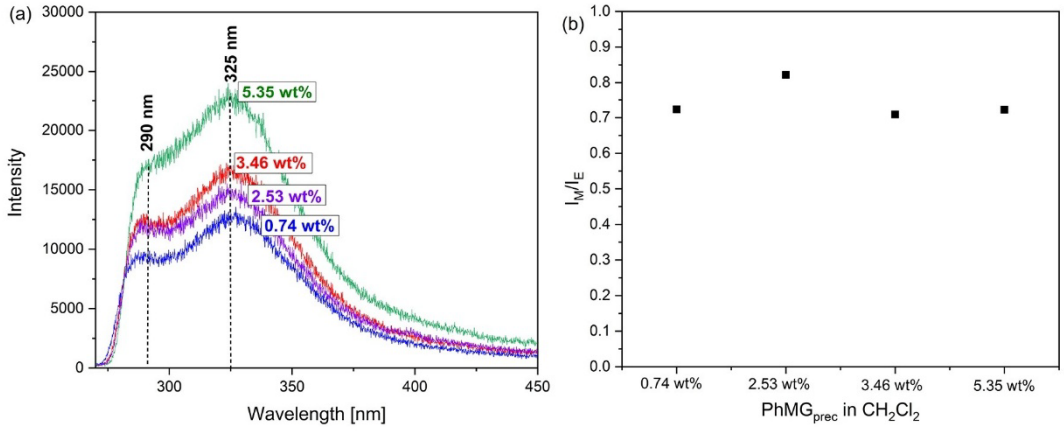

Figure 9. (a) Fluorescence spectra and (b) I_M/I_E of $PhMG_{prec}$ in CH_2Cl_2 at different concentrations.

https://doi.org/10.1021/acs.macromol.1c00310
Macromolecules 2021, 54, 3873−3885

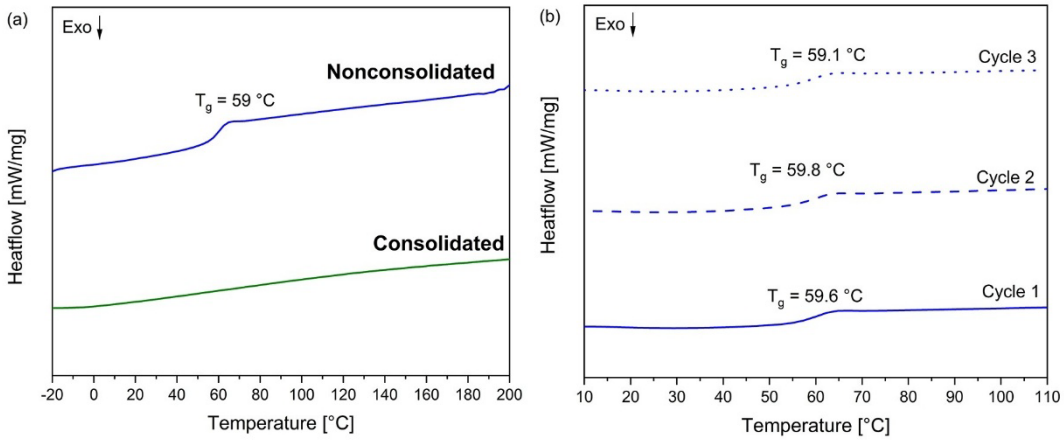

Figure 10. (a) DSC analysis of $PhMG_{prec}$ (blue line) and $PhMG_{cons}$ (green line) and (b) DSC analysis of $PhMG_{prec}$, reversibility tests.

Ladderlike polyphenylsilsesquioxanes have two types of conformations: cis-syndiotactic and cis-isotactic. Huang et al. report that intramolecular excimer fluorescence is only possible in the cis-isotactic configuration. A high emission at 270 nm indicated a sterically irregular structure with syndiotactic units and defects in the form of non-cross-linked groups.[53,58] This suggested that the precursor melting gel contained a ladderlike structure with a cis-isotactic conformation. However, the rather strong monomer band at 270 nm indicated a defect-rich structure. The comparison of the d_1 and d_2 values determined by PXRD of the prepared melting gels with calculated values of Liu et al. for a cis-isotactic and a cis-syndiotactic conformation of ladderlike polyphenylsilsesquioxanes confirmed this result (Table 2).[59] The chain-to-chain distance of the precursor melting gel is located between the calculated conformations.

Fluorescence measurements of the consolidated melting gel in CH_2Cl_2 were not possible because of the insolubility of the material. The values obtained by PXRD measurements, which are almost identical to those of the cis-isotactic structure, and the higher degree of condensation indicate a ladder structure with a cis-isotactic structure with fewer defects than in the precursor gel. In summary, the fluorescence measurements complement the previously performed XRD studies and confirm that defects, as well as units with other tacticity, will be fixed and rearranged by the consolidation process. It can be assumed that the $\pi-\pi$ stacking plays an important role in the structure formation and contributes to stabilization of the melting gel structure.

Size Exclusion Chromatography. SEC measurements of two separately synthesized $PhMG_{prec}$ samples were performed in DMF (PMMA standard) and THF (polystyrene standard) and were detected with RI and UV detectors (SEC results can be found in the Supporting Information, Figure S16). The prepared samples displayed only minor deviations in the measured values, which shows the very good reproducibility of the materials under the given synthetic conditions. Both RI and UV detectors were able to detect the polymer equally well, imaging almost the same SEC profile. The data obtained in the different eluents differ significantly. In DMF, a weight-average molecular weight (M_w) of 1416 (RI) was measured with a molecular weight distribution (M_w/M_n) of 1.534. In THF, M_w increased to 3451 and showed a broad distribution, with an M_w/M_n of 2.354. The increased polydispersity index in THF can be explained by interactions of the non-cross-linked hydroxy and methoxy groups with the eluent and an associated broadening of the SEC profile. Similar low molecular weights in the range of 300−7000 were also reported in the literature for softenable polyphenylsilsesquioxanes.[23,63] Ladder structures synthesized via base-catalyzed polycondensation show significantly higher values.[46] In general, the standards used for the calibration of the SEC system are more suitable for the characterization of flexible single-chain polymers. However, the melting gel consists of a cross-linked structure. Therefore, the absolute molecular weights must be interpreted with caution. However, the results show the presence of relatively short-chain polymer structures with hydrogen bond-forming groups that could be reproducibly synthesized.

Thermal Analysis. *Differential Scanning Calorimetry (DSC).* DSC was used to determine the glass transition temperature (T_g) and to analyze the cross-linking behavior of the precursor gel and the consolidated material. An increase in T_g indicates an increase in rigidity and cross-linking.[9,64] The DSC curve of the precursor gel showed a T_g of ≈ 60 °C (Figure 10a). This value is higher than that of melting gels prepared from di- and trialkoxyilanes in the literature,[9,18] but lower than that of ladder-type polyphenylsilsesquioxanes,[12,59,65] and shows that there were still some defects in the form of unlinked groups. The application of temperatures higher than the melting temperature of 110 °C led to further condensation reactions of the methoxy and hydroxy groups. The consolidation process resulted in additional cross-linking, with the consequence that no T_g was visible anymore. As the reversible softening of the samples is directly related to cross-linking, reversibility can be demonstrated by DSC. Within three heating cycles to 110 °C, there was no change in the T_g of the precursor gel (Figure 10b). No further condensation occurred, and the polymer remained meltable. This agrees well with the XRD reversibility studies.

TG-FT-IR. To characterize the thermal stability and to observe the consolidation process, both the precursor gel and the consolidated gel were heated to 800 °C under an oxygen atmosphere. The temperature at which 5% of the mass is lost (T_{95}) was determined to be 400 °C for the precursor gel and 510 °C for the consolidated gel. The difference between the T_{95} values could be observed by the first mass loss at 236 °C, which occurred only in the precursor gel (Figure 11). In agreement, the consolidated gel showed a higher residual mass

https://doi.org/10.1021/acs.macromol.1c00310
Macromolecules 2021, 54, 3873−3885

than the precursor gel. In general, the melting gel presented an extremely high thermal stability.

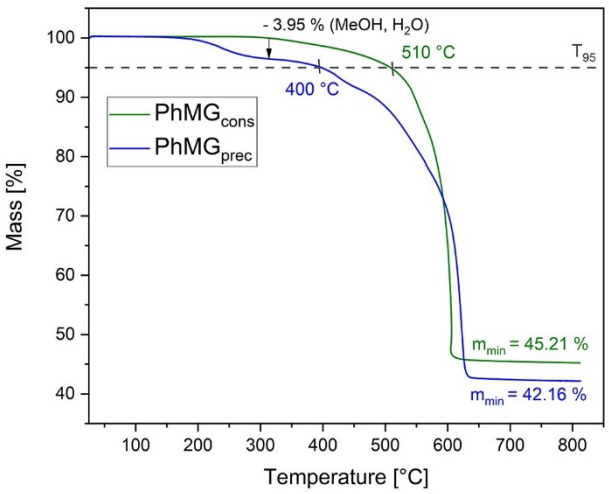

Figure 11. Thermogravimetric results of the nonconsolidated $PhMG_{prec}$ (blue line) and the consolidated $PhMG_{cons}$ (green line) (10 K min^{-1}, O_2).

TG-FT-IR measurements of $PhMG_{prec}$ were carried out in a synthetic air atmosphere to identify the released gases during the first mass loss step and further decomposition products (Figure 12a). The thermogravimetric results showed that the degradation temperature shifted to higher values compared to Figure 11, due to increased heating rates and lower oxygen content. The first mass loss can be attributed to the elimination of water and methanol (Figure 12b). The unreacted −OH and −OMe groups present in the precursor gel condense, resulting in increased cross-linking. Since the consolidated gel did not show this mass loss step, it can be assumed that it exhibited the highest possible degree of cross-linking. At higher temperatures, cleavage of the Si−phenyl bond and proton abstraction took place, forming benzene. The proton abstraction and dehydrogenation reaction led to a condensation of the aromatic structures, resulting in further cross-linking.[66−68] The free carbon was oxidized during thermal treatment in air, and CO_2 and CO were detected (Figure 12b). The white residual mass of 43.76% remaining in the crucible can be attributed to SiO_2, formed by the full decomposition of the melting gel.

Studies on Polycyclic Aromatic Compounds (1-NpMG). To prove the generality of the obtained results for aryl-substituted melting gels, we repeated selected experiments with 1-naphthyltrimethoxysilane as the monomer. 1-NpMG was produced applying the same procedure as that for PhMG. The only observed difference between the two polymers was the time it takes to homogenize the starting solution. 1-$NpSi(OMe)_3$ took about 15 times longer than $PhSi(OMe)_3$, which could be attributed to the bulkier naphthyl groups and resulting slower hydrolysis. The final gel was a glasslike, transparent material that reversibly softened at 110 °C (1-$NpMG_{prec}$). However, complete curing could not be established by a heat treatment at 200 °C for 24 h (1-$NpMG_T$). The increased bulkiness of the naphthyl group led to a significantly lower degree of condensation of 55% for the 1-NpMG and 67% after thermal treatment (1-$NpMG_T$).[31] The high number of nonconnected groups ensured that the gel could still be melted. Furthermore, the XRD patterns showed a chain-to-chain distance (d_1) of 12.0 Å after thermal treatment, which was larger than the d_1 value of the $PhMG_{cons}$. The rigid naphthyl group provided larger distances between ladder structures, resulting in a decreased packing density.[15] The thermally treated material is less transparent and yellowish because the high degree of aromaticity preferentially absorbed shorter-wavelength light and the sample appeared yellow (Figure 13).[15] The corresponding NMR, DSC, XRD, TG, and FT-IR measurements can be found in the Supporting Information (SI Figures S17−S29 and Tables S2 and S3). The produced softenable transparent gel shows that the melting gel synthesis can be transferred to further trimethoxysilane precursors. It is also possible to use bulkier residues than phenyl groups to synthesize thermoplastic-like materials with a partial ladder structure. The size of the organic group influences the cross-linking and the softening and consolidation of the polymer.

■ CONCLUSIONS

The molecular structure and the melting gel formation mechanism of nonconsolidated and consolidated phenylsilsesquioxane melting gels were investigated. The model system showed a partially cross-linked structure with some defects originating from unlinked methoxy and hydroxy

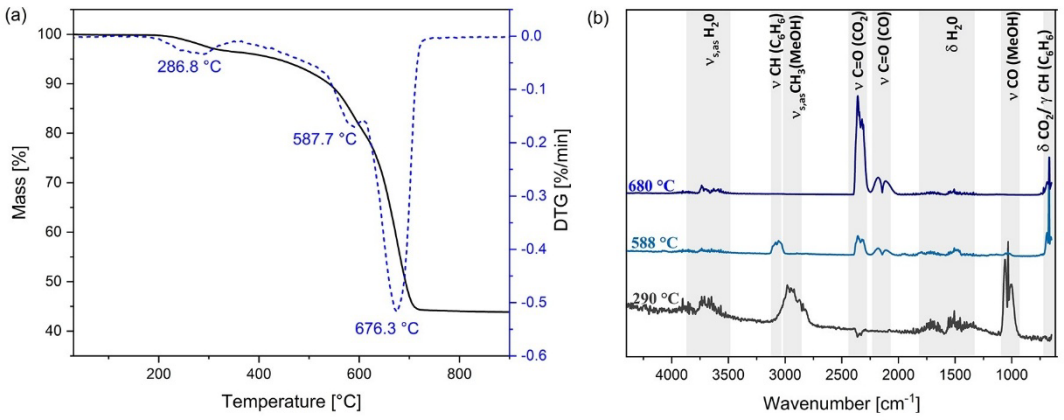

Figure 12. (a) TG of $PhMG_{prec}$ (20 K min^{-1}, synthetic air) and (b) FT-IR spectra of the released gases at 290, 588, and 680 °C of $PhMG_{prec}$.

https://doi.org/10.1021/acs.macromol.1c00310
Macromolecules 2021, 54, 3873−3885

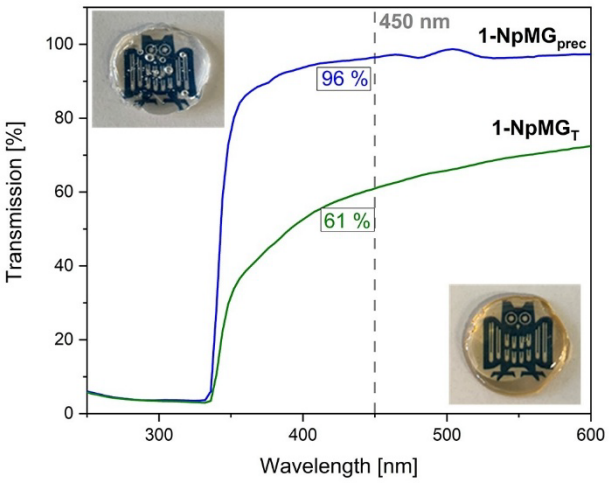

Figure 13. UV−vis spectrum and pictures of 1-NpMG$_{prec}$ and 1-NpMG$_T$.

groups. We suppose that the defects were responsible for the reversible melting of the precursor gel at temperatures above 110 °C, while hydrogen bonds and $\pi-\pi$ interactions stabilize the network. Thermal treatment at the consolidation temperature leads to further cross-linking and irreversible curing (Figure 14). PXRD revealed local ladder structures with a cis-isotactic structure in both melting gel states; fluorescence measurements underlined this structural picture by observing excimer fluorescence unique to this structural arrangement.The consolidated material exhibited a higher percentage of the ladder structure with fewer defects in the form of unreacted groups and cis-syndiotactic units. In addition, the IR spectrum showed roughly defined siloxane structures in addition to the ladder structure, which could be cycles or cages involved in a random network. Finally, DSC and temperature-dependent PXRD studies proved the reversibility of the melting process at 110 °C under defined heating conditions. As proof of concept, a transparent reversible meltable polynaphthylsilsesquioxane has also been prepared. The bulky naphthyl groups lead to a less cross-linked structure, preventing complete curing. It could be shown that these larger aromatic groups lead to a melting gel-like processable transparent gel. This work shows that even under nonrigorously controlled conditions, ladderlike silsesquioxane polymers with a thermoplastic behavior can be obtained. From the current standpoint, this process seems to be universal for aromatic trialkoxysilanes. Due to the unique optical and thermal properties of the resulting materials and their potential consolidating step, which creates nonmeltable hybrid glasses, this material class opens new routes for applications in various fields.

■ ASSOCIATED CONTENT

Supporting Information

The Supporting Information is available free of charge at https://pubs.acs.org/doi/10.1021/acs.macromol.1c00310.

Spectroscopic and SEC data of the prepared polymers and results from XRD measurements and thermal analysis data (PDF)

■ AUTHOR INFORMATION

Corresponding Author

Guido Kickelbick − *Inorganic Solid-State Chemistry, Saarland University, 66123 Saarbrücken, Germany;* orcid.org/0000-0001-6813-9269; Email: guido.kickelbick@uni-saarland.de

Authors

Svenja Pohl − *Inorganic Solid-State Chemistry, Saarland University, 66123 Saarbrücken, Germany*

Oliver Janka − *Inorganic Solid-State Chemistry, Saarland University, 66123 Saarbrücken, Germany;* orcid.org/0000-0002-9480-3888

Ekkehard Füglein − *NETZSCH-Gerätebau GmbH, 95100 Selb, Germany*

Complete contact information is available at: https://pubs.acs.org/10.1021/acs.macromol.1c00310

Notes

The authors declare no competing financial interest.

■ ACKNOWLEDGMENTS

Instrumentation and technical assistance for this work were provided by the Service Center X-ray Diffraction, with financial support from Saarland University and the German Science Foundation (project number INST 256/349-1). We thank Blandine Bossmann and Frank Hartmann for recording and

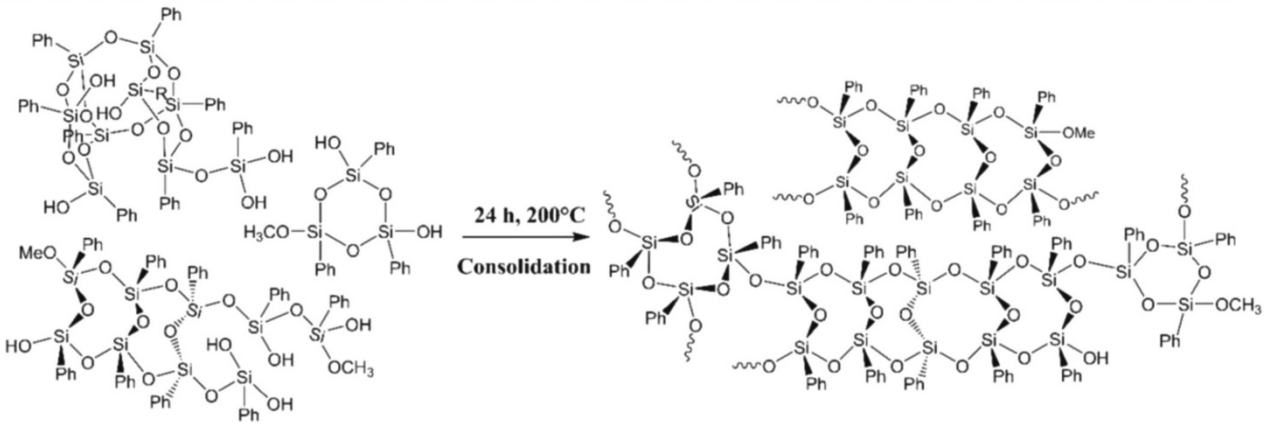

Figure 14. Postulated melting gel structure and consolidation process.

https://doi.org/10.1021/acs.macromol.1c00310
Macromolecules 2021, 54, 3873−3885

analyzing the size exclusion chromatograms, Dr. Michael Zimmer for the CP-MAS NMR measurements, and Prof. Markus Gallei at Saarland University for helpful discussions.

REFERENCES

(1) Baney, R. H.; Itoh, M.; Sakakibara, A.; Suzuki, T. Silsesquioxanes. *Chem. Rev.* **1995**, *95*, 1409−1430.
(2) Scott, D. W. Thermal Rearrangement of Branched-Chain Methylpolysiloxanes. *J. Am. Chem. Soc.* **1946**, *68*, 356−358.
(3) Brown, J. F.; Vogt, L. H. The Polycondensation of Cyclohexylsilanetriol. *J. Am. Chem. Soc.* **1965**, *87*, 4313−4317.
(4) Brown, J. F. The Polycondensation of Phenylsilanetriol. *J. Am. Chem. Soc.* **1965**, *87*, 4317−4324.
(5) Croissant, J.; Maynadier, M.; Mongin, O.; Hugues, V.; Blanchard-Desce, M.; Chaix, A.; Cattoën, X.; Wong Chi Man, M.; Gallud, A.; Gary-Bobo, M.; Garcia, M.; Raehm, L.; Durand, J.-O. Enhanced Two-Photon Fluorescence Imaging and Therapy of Cancer Cells via Gold@Bridged Silsesquioxane Nanoparticles. *Small* **2015**, *11*, 295−299.
(6) Niemczyk, A.; Dziubek, K.; Sacher-Majewska, B.; Czaja, K.; Czech-Polak, J.; Oliwa, R.; Lenża, J.; Szolyga, M. Thermal Stability and Flame Retardancy of Polypropylene Composites Containing Siloxane-Silsesquioxane Resins. *Polymers* **2018**, *10*, No. 1019.
(7) Chan, K. L.; Sonar, P.; Sellinger, A. Cubic Silsesquioxanes for Use in Solution Processable Organic Light Emitting Diodes (OLED). *J. Mater. Chem.* **2009**, *19*, 9103−9120.
(8) Gilman, J. W.; Schlitzer, D. S.; Lichtenhan, J. D. Low Earth Orbit Resistant Siloxane Copolymers. *J. Appl. Polym. Sci.* **1996**, *60*, 591−596.
(9) Steinbrück, N.; Pohl, S.; Kickelbick, G. Platinum Free Thermally Curable Siloxanes for Optoelectronic Application − Synthesis and Properties. *RSC Adv.* **2019**, *9*, 2205−2216.
(10) Pescarmona, P. P.; Maschmeyer, T. Oligomeric Silsesquioxanes: Synthesis, Characterization and Selected Applications. *Aust. J. Chem.* **2001**, *54*, 583−596.
(11) Harrison, P. G. Silicate Cages: Precursors to New Materials. *J. Organomet. Chem.* **1997**, *542*, 141−183.
(12) Yu-zhong, F.; Sheng-li, Q.; Jing-jing, L.; Zhan-peng, W.; Xiaoping, Y.; Ri-guang, J.; De-zhen, W. Preparation and Characterization of Ordered Ladder Like Polyphenylsilsesquioxane via Two-Step Sol-Gel Method. *Chem. Res. Chin. Univ.* **2011**, *27*, 516−519.
(13) Kuniyoshi, M.; Takahashi, M.; Tokuda, Y.; Yoko, T. Hydrolysis and Polycondensation of Acid-Catalyzed Phenyltriethoxysilane (PhTES). *J. Sol-Gel Sci. Technol.* **2006**, *39*, 175−183.
(14) Ro, H. W.; Soles, C. L. Silsesquioxanes in Nanoscale Patterning Applications. *Mater. Today* **2011**, *14*, 20−33.
(15) Hwang, S. O.; Lee, A. S.; Lee, J. Y.; Park, S.-H.; Jung, K. I.; Jung, H. W.; Lee, J.-H. Mechanical Properties of Ladder-like Polysilsesquioxane-Based Hard Coating Films Containing Different Organic Functional Groups. *Prog. Org. Coat.* **2018**, *121*, 105−111.
(16) Ahmed, N.; Fan, H.; Dubois, P.; Zhang, X.; Fahad, S.; Aziz, T.; Wan, J. Nano-Engineering and Micromolecular Science of Polysilsesquioxane Materials and Their Emerging Applications. *J. Mater. Chem. A* **2019**, *7*, 21577−21604.
(17) Masai, H.; Takahashi, M.; Tokuda, Y.; Yoko, T. Gel-Melting Method for Preparation of Organically Modified Siloxane Low-Melting Glasses. *J. Mater. Res.* **2005**, *20*, 1234−1241.
(18) Jitianu, A.; Amatucci, G.; Klein, L. C. Phenyl-Substituted Siloxane Hybrid Gels That Soften Below 140 °C. *J. Am. Ceram. Soc.* **2009**, *92*, 36−40.
(19) Jitianu, A.; Gonzalez, G.; Klein, L. C. Hybrid Sol-Gel Glasses with Glass-Transition Temperatures Below Room Temperature. *J. Am. Ceram. Soc.* **2015**, *98*, 3673−3679.
(20) Klein, L. C.; Jitianu, A. Organic-Inorganic Hybrid Melting Gels. *J. Sol-Gel Sci. Technol.* **2010**, *55*, 86−93.
(21) Klein, L. C.; McClarren, B.; Jitianu, A. Silica-Containing Hybrid Nanocomposite "Melting Gels. *Mater. Sci. Forum* **2014**, *783*−*786*, 1432−1437.
(22) Katagiri, K.; Hasegawa, K.; Matsuda, A.; Tatsumisago, M.; Minami, T. Preparation of Transparent Thick Films by Electrophoretic Sol − Gel Deposition Using Phenyltriethoxysilane-Derived Particles. *J. Am. Ceram. Soc.* **1998**, *81*, 2501−2503.
(23) Matsuda, A.; Sasaki, T.; Hasegawa, K.; Tatsumisago, M.; Minami, T. Thermal Softening Behavior of Poly-(Phenylsilsesquioxane) and Poly (Benzylsilsesquioxane) Particles. *J. Ceram. Soc. Jpn.* **2000**, *108*, 830−835.
(24) Matsuda, A.; Sasaki, T.; Hasegawa, K.; Tatsumisago, M.; Minami, T. Thermal Softening Behavior and Application to Transparent Thick Films of Poly(Benzylsilsesquioxane) Particles Prepared by the Sol-Gel Process. *J. Am. Ceram. Soc.* **2001**, *84*, 775−780.
(25) Klein, L. C.; Al-Marzoki, K.; Jitianu, A.; Rodriguez, G. Effect of Tetraethoxysilane (TEOS) on Melting Gel Behavior. *J. Am. Ceram. Soc.* **2020**, *103*, 4140−4149.
(26) Jitianu, A.; Lammers, K.; Arbuckle-Kiel, G. A.; Klein, L. C. Thermal Analysis of Organically Modified Siloxane Melting Gels. *J. Therm. Anal. Calorim.* **2012**, *107*, 1039−1045.
(27) Klein, L. C.; Kallontzi, S.; Fabris, L.; Jitianu, A.; Ryan, C.; Aparicio, M.; Lei, L.; Singer, J. P. Applications of Melting Gels. *J. Sol-Gel Sci. Technol.* **2019**, *89*, 66−77.
(28) Bruker AXS (2011): TOPAS V5: General profile and structure analysis software for powder diffraction data. - Bruker AXS, Karlsruhe, Germany.
(29) Wei, H.; Bichen, P.; Xin, Y.; Youxue, Y.; Ying, Z.; Xiaojuan, Z. Preparation Method of Naphthyl Alkoxysilane. CN Patent CN104788488A, July 22, 2015.
(30) Faz Cano, A.; Mermut, A. R.; Ortiz, R.; Benke, M. B.; Chatson, B. 13C CP/MAS-NMR Spectra of Organic Matter as Influenced by Vegetation, Climate, and Soil Characteristics in Soils from Murcia, Spain. *Can. J. Soil Sci.* **2002**, *82*, 403−411.
(31) Odenwald, C.; Kickelbick, G. Additive-Free Continuous Synthesis of Silica and ORMOSIL Micro- and Nanoparticles Applying a Microjet Reactor. *J. Sol-Gel Sci. Technol.* **2019**, *89*, 343−353.
(32) Sakuragi, A.; Igarashi, Y.; Kajihara, K.; Kanamura, K. Synthesis of Silanol-Rich Long-Life Polysilsesquioxane Liquids by Cosolvent-Free Hydrolytic Polycondensation of Organotrimethoxysilanes Followed by Aging. *Dalton Trans.* **2016**, *45*, 3151−3157.
(33) Loy, D. A. Sol-Gel Processing of Hybrid Organic-Inorganic Materials Based on Polysilsesquioxanes. In *Hybrid Materials*; Kickelbick, G., Ed.; Wiley-VCH: Weinheim, 2007; p 233.
(34) Kawahara, K.; Tachibana, H.; Hagiwara, Y.; Kuroda, K. A Spherosilicate Oligomer with Eight Stable Silanol Groups as a Building Block of Hybrid Materials. *New J. Chem.* **2012**, *36*, 1210−1217.
(35) Li, Y.-S.; Wang, Y.; Ceesay, S. Vibrational Spectra of Phenyltriethoxysilane, Phenyltrimethoxysilane and Their Sol-Gels. *Spectrochim. Acta, Part A* **2009**, *71*, 1819−1824.
(36) Chen, X.; Eldred, D.; Liu, J.; Chiang, H.; Wang, X.; Rickard, M. A.; Tu, S.; Cui, L.; LaBeaume, P.; Skinner, K. Simultaneous In Situ Monitoring of Trimethoxysilane Hydrolysis Reactions Using Raman, Infrared, and Nuclear Magnetic Resonance (NMR) Spectroscopy Aided by Chemometrics and Ab Initio Calculations. *Appl. Spectrosc.* **2018**, *72*, 1404−1415.
(37) Hu, N.; Rao, Y.; Sun, S.; Hou, L.; Wu, P.; Fan, S.; Ye, B. Structural Evolution of Silica Gel and Silsesquioxane Using Thermal Curing. *Appl. Spectrosc.* **2016**, *70*, 1328−1338.
(38) Brown, J. F. Double Chain Polymers and Nonrandom Crosslinking. *J. Polym. Sci., Part C: Polym. Symp.* **2007**, *1*, 83−97.
(39) Park, E. S.; Ro, H. W.; Nguyen, C. V.; Jaffe, R. L.; Yoon, D. Y. Infrared Spectroscopy Study of Microstructures of Poly-(Silsesquioxane)S. *Chem. Mater.* **2008**, *20*, 1548−1554.
(40) Young, C. W.; Servais, P. C.; Currie, C. C.; Hunter, M. J. Organosilicon Polymers. IV. Infrared Studies on Cyclic Disubstituted Siloxanes. *J. Am. Chem. Soc.* **1948**, *70*, 3758−3764.
(41) Pakjamsai, C.; Kobayashi, N.; Koyano, M.; Sasaki, S.; Kawakami, Y. Characterization of the Benzene-Insoluble Fraction of the Hydrolyzate of Phenyltrimethoxysilanes in the Presence of

https://doi.org/10.1021/acs.macromol.1c00310
Macromolecules 2021, 54, 3873−3885

Benzyltrimethylammonium Hydroxide. *J. Polym. Sci., Part A: Polym. Chem.* **2004**, *42*, 4587−4597.
(42) Kim, J.-S.; Yang, S.; Bae, B.-S. Thermally Stable Transparent Sol-Gel Based Siloxane Hybrid Material With High Refractive Index For Light Emitting Diode (LED) Encapsulation. *Chem. Mater.* **2010**, *22*, 3549−3555.
(43) Jitianu, A.; Cadars, S.; Zhang, F.; Rodriguez, G.; Picard, Q.; Aparicio, M.; Mosa, J.; Klein, L. C. ^{29}Si NMR and SAXS Investigation of the Hybrid Organic-Inorganic Glasses Obtained by Consolidation of the Melting Gels. *Dalton Trans.* **2017**, *46*, 3729−3741.
(44) Kudo, T.; Gordon, M. S. Theoretical Studies of the Mechanism for the Synthesis of Silsesquioxanes. 2. Cyclosiloxanes (D3 and D4). *J. Phys. Chem. A* **2000**, *104*, 4058−4063.
(45) Sprung, M. M.; Guenther, F. O. The Partial Hydrolysis of Methyltriethoxysilane. *J. Am. Chem. Soc.* **1955**, *77*, 3990−3996.
(46) Choi, S.-S.; Lee, A. S.; Hwang, S. S.; Baek, K.-Y. Structural Control of Fully Condensed Polysilsesquioxanes: Ladderlike vs Cage Structured Polyphenylsilsesquioxanes. *Macromolecules* **2015**, *48*, 6063−6070.
(47) Zhang, W.; Wang, X.; Wu, Y.; Qi, Z.; Yang, R. Preparation and Characterization of Organic-Inorganic Hybrid Macrocyclic Compounds: Cyclic Ladder-like Polyphenylsilsesquioxanes. *Inorg. Chem.* **2018**, *57*, 3883−3892.
(48) Anisimov, A. A.; Polshchikova, N. V.; Vysochinskaya, Y. S.; Zader, P. A.; Nikiforova, G. G.; Peregudov, A. S.; Buzin, M. I.; Shchegolikhina, O. I.; Muzafarov, A. M. Condensation of All-Cis-Tetraphenylcyclotetrasiloxanetetraol in Ammonia: New Method for Preparation of Ladder-like Polyphenylsilsesquioxanes. *Mendeleev Commun.* **2019**, *29*, 421−423.
(49) Lee, E.-C.; Kimura, Y. Structural Regularity of Poly(Phenylsilsesquioxane) Prepared from the Low Molecular Weight Hydrolysates of Trichlorophenylsilane. *Polym. J.* **1998**, *30*, 234−242.
(50) Kang, W. R.; Lee, A. S.; Park, S.; Park, S. H.; Baek, K.-Y.; Lee, K. B.; Lee, S.-H.; Lee, J.-H.; Hwang, S. S.; Lee, J. S. Free-Standing, Polysilsesquioxane-Based Inorganic/Organic Hybrid Membranes for Gas Separations. *J. Membr. Sci.* **2015**, *475*, 384−394.
(51) Jo, Y. Y.; Lee, A. S.; Baek, K. Y.; Lee, H.; Hwang, S. S. Thermally Reversible Self-Healing Polysilsesquioxane Structure-Property Relationships Based on Diels-Alder Chemistry. *Polymer* **2017**, *108*, 58−65.
(52) Zhang, Z.-X.; Hao, J.; Xie, P.; Zhang, X.; Han, C. C.; Zhang, R. A Well-Defined Ladder Polyphenylsilsesquioxane (Ph-LPSQ) Synthesized via a New Three-Step Approach: Monomer Self-Organization-Lyophilization - Surface-Confined Polycondensation. *Chem. Mater.* **2008**, *20*, 1322−1330.
(53) Xinsheng, Z.; Lianghe, S.; Chaoran, H. More on the Structures of Polyphenylsilsesquioxanes. *Chin. J. Polym. Sci.* **1987**, *5*, 353−358.
(54) Liu, F.; Zeng, X.; Lai, X.; Li, H. Synthesis and Characterization of Polyphenylsilsesquioxane Terminated with Methyl and Vinyl Groups Low-Melting Glass. *J. Adhes. Sci. Technol.* **2017**, *31*, 2399−2409.
(55) Yanari, S. S.; Bovey, F. A.; Lumry, R. Fluorescence of Styrene Homopolymers and Copolymers. *Nature* **1963**, *200*, 242−244.
(56) De Sainte Claire, P. Molecular Simulation of Excimer Fluorescence in Polystyrene and Poly(Vinylcarbazole). *J. Phys. Chem. B* **2006**, *110*, 7334−7343.
(57) Kuo, A. Fluorescence Resulting from π-Stacking in Polystyrene Solutions. *CheM* **2011**, *1*, 80−86.
(58) Chaoran, H.; Guangzhi, X.; Xinsheng, Z.; Lianghe, S. Studies on the Excimer Fluorescence and the Steric Tacticity of Polyphenylsilsesquioxanes. *Chin. J. Polym. Sci.* **1987**, 347−352.
(59) Liu, C.; Liu, Y.; Shen, Z.; Xie, P.; Zhang, R.; Yang, J.; Bai, F. Study of the Steric Tacticity of Novel Soluble Ladderlike Poly(Phenylsilsesquioxane) Prepared by Stepwise Coupling Polymerization. *Macromol. Chem. Phys.* **2001**, *202*, 1581−1585.
(60) Yang, J.; Bai, F.; Liu, C.; Liu, Y.; Xie, P.; Zhang, R. Temperature Dependence of the Fluorescence Spectra of Ladderlike Polyphenylsilsesquioxane and Ladderlike 1,4- Phenylene-Bridged Polyvinylsiloxane. *Chin. J. Polym. Sci.* **2002**, *20*, 15−23.
(61) Chakraborty, D. K.; Kurian, J.; Trumbo, D.; Harwood, H. J.; Kennedy, J. P.; Mattice, W. L. Electronic vs. Steric Effects of Substituents on the Intramolecular Excimer Fluorescence from Dilute Solutions of Halogen-substituted Polystyrenes. *Makromol. Chem.* **1993**, *194*, 329−338.
(62) Zhang, X.; Xie, P.; Shen, Z.; Jiang, J.; Zhu, C.; Li, H.; Zhang, T.; Han, C. C.; Wan, L.; Yan, S.; Zhang, R. Confined Synthesis of a Cis-Isotactic Ladder Polysilsesquioxane by Using a π-Stacking and H-Bonding Superstructure. *Angew. Chem., Int. Ed.* **2006**, *45*, 3112−3116.
(63) Yu, D.; Kleemeier, M.; Wu, G. M.; Schartel, B.; Liu, W. Q.; Hartwig, A. A Low Melting Organic-Inorganic Glass and Its Effect on Flame Retardancy of Clay/Epoxy Composites. *Polymer* **2011**, *52*, 2120−2131.
(64) Deng, K.; Zhang, T.; Zhang, X.; Zhang, A.; Xie, P.; Zhang, R. A Concerted H-Bonding Self-Assembly-Based Approach to Ladder Poly(Silsesquioxane). *Macromol. Chem. Phys.* **2006**, *207*, 404−411.
(65) Wang, X.; Li, J.; Wu, L. Preparation of Poly(Phenylsilsesquioxane) (PPSQ) Particles with Ladder Structure and the Thermal Stability of PP/PPSQ Composites. *Polym. Adv. Technol.* **2011**, *22*, 2151−2156.
(66) Xinsheng, Z.; Lianghe, S.; Shuqing, L.; Yizhen, L. Thermal Stability and Kinetics of Decomposition of Polyphenylsilsesquioxanes and Some Related Polymers. *Polym. Degrad. Stab.* **1988**, *20*, 157−172.
(67) Fina, A.; Tabuani, D.; Carniato, F.; Frache, A.; Boccaleri, E.; Camino, G. Polyhedral Oligomeric Silsesquioxanes (POSS) Thermal Degradation. *Thermochim. Acta* **2006**, *440*, 36−42.
(68) Zhou, W.; Yang, H.; Guo, X.; Lu, J. Thermal Degradation Behaviors of Some Branched and Linear Polysiloxanes. *Polym. Degrad. Stab.* **2006**, *91*, 1471−1475.

■ NOTE ADDED AFTER ASAP PUBLICATION

This paper was published on April 14, 2021, with an incorrect unit of measurement listed in Table 2. The corrected version was reposted on April 14, 2021.

https://doi.org/10.1021/acs.macromol.1c00310
Macromolecules 2021, 54, 3873−3885

4.2 Influence of alkyl groups on the formation of softenable polysilsesquioxanes

Published as an article:

Svenja Pohl, Guido Kickelbick, *J. Sol-Gel Sci. Technol.* ***2023****, 107, 329–346. DOI: 10.1007/s10971-023-06126-6.*

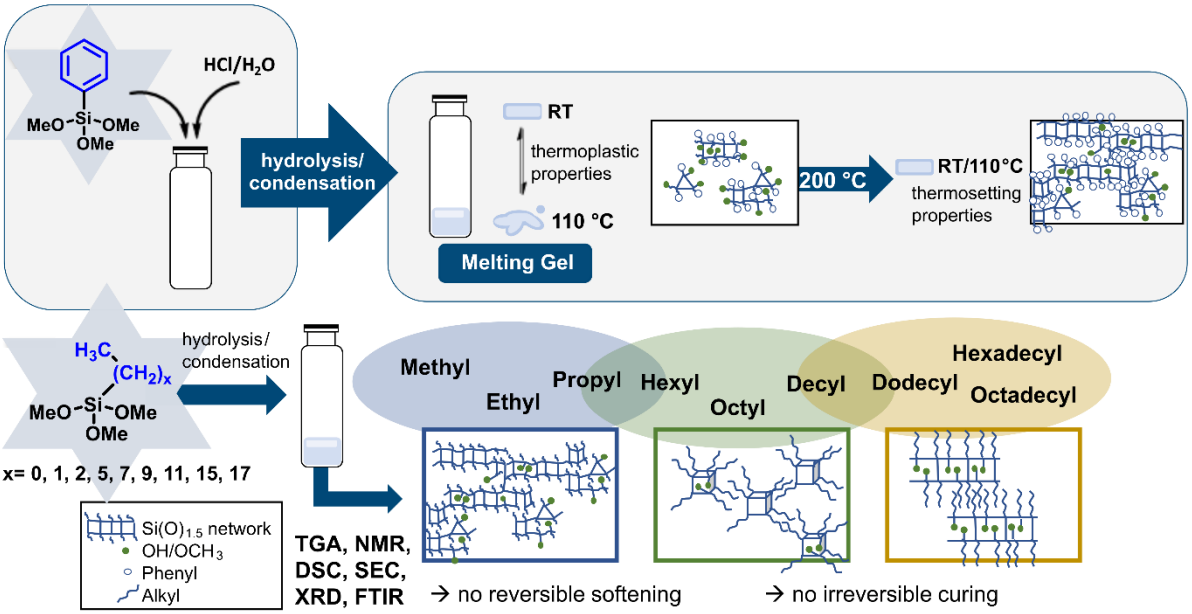

The supporting information is provided in Chapter 7 and is available online at: *https://doi.org/10.1007/s10971-023-06126-6*.

The author's contribution to this work amounts to 85%.

Detailed statement of the individual contributions of the author and co-authors:

Svenja Pohl prepared the complete draft of the manuscript, which was reviewed and approved by all co-authors. She performed the synthesis and characterization of the polysilsesquioxanes and was responsible for the interpretation of the results. Prof. Dr. Guido Kickelbick gave the input to this project, provided scientific guidance and supervision, and revised the manuscript to its final version.

In the preceding chapter, it was demonstrated that polyphenylsilsesquioxanes can form transparent, glass-like materials, which exhibit thermoplastic softening above their T_g and irreversible curing at higher temperatures. This so-called "melting gel" behavior has so far been observed predominantly in silsesquioxanes with aromatic substituents, but not in systems bearing only linear *n*-alkyl groups.

The publication *"Influence of alkyl groups on the formation of softenable polysilsesquioxanes"* systematically investigates whether alkyl-substituted systems can exhibit melting gel behavior and how the length of the alkyl chain affects the resulting silsesquioxane structure. For this purpose, various *n*-alkyltrimethoxysilanes with chain lengths ranging from C_1 to C_{18} were reacted under acid-catalyzed, solvent-free conditions analogous to the synthesis of the phenyl substituted melting gel. The resulting polyalkylsilsesquioxanes were comprehensively characterized with respect to their structure and thermal properties using NMR, FTIR, TGA, DSC, SEC, and PXRD.

The results reveal a pronounced chain-length-dependent structural evolution. Short-chain derivatives (C_1–C_3) form densely cross-linked, glassy solids that promote extensive intermolecular condensation and rigid network formation, thereby suppressing thermoplastic behavior. Medium-chain systems (C_6, C_8) yield viscous resins that favor intramolecular reactions. Despite their relatively high degree of condensation, these materials lack a continuous network structure and instead consist of isolated, locally cross-linked domains, which prevent irreversible curing. In the case of long-chain substituents (C_{10}, C_{12}, C_{16}, C_{18}), hydrophobic interactions and self-assembly lead to lamellarly ordered materials exhibiting distinct crystalline phase transitions.

Unlike phenyl substituents, *n*-alkyltrialkoxysilanes alone were found to be unsuitable for the preparation of melting gel-type polysilsesquioxanes. The presence of moderately bulky substituents is required to stabilize residual hydroxyl and alkoxy groups and to balance intermolecular condensation, thereby preventing premature network formation. In addition, suppressing molecular ordering that promotes crystallinity is essential for obtaining glassy, softenable materials.

Overall, this study therefore provides further insights into the structural requirements for the development of thermoplastic-thermosetting properties and highlights the critical role of aromatic substituents in stabilizing reactive groups in such hybrid systems.

Journal of Sol-Gel Science and Technology (2023) 107:329–346
https://doi.org/10.1007/s10971-023-06126-6

ORIGINAL PAPER: SOL-GEL, HYBRIDS AND SOLUTION CHEMISTRIES

Influence of alkyl groups on the formation of softenable polysilsesquioxanes

Svenja Pohl[1] · Guido Kickelbick[1]

Received: 29 November 2022 / Accepted: 28 April 2023 / Published online: 25 May 2023

Abstract

Polysilsesquioxanes (PSQ) containing phenyl groups as substituents on the silicon atom can form transparent, hard and glassy materials at room temperature, which reversibly soften when heated above the glass transition temperature. Further increase in temperature leads to irreversible curing. With this property, polyphenylsilsesquioxanes can be assigned to the so-called melting gels. In contrast to the aromatic systems, polysilsesquioxanes with alkyl groups belonging to this class of materials are not known. To identify structural differences between aryl and alkyl systems, polyalkylsilsesquioxanes (RPSQs with R = methyl, ethyl, propyl, hexyl, octyl, decyl, dodecyl, hexadecyl, and octadecyl) were synthesised by a solvent-free, acid-catalysed hydrolysis and condensation reaction of alkyltrimethoxysilanes followed by thermal treatment at 300 °C under N_2 atmosphere. The influence of the alkyl chain length on the structure built and the thermally initiated further condensation reactions were investigated via NMR, FTIR, TGA, DSC, SEC, and XRD. Depending on the alkyl chain length, the formation of highly crosslinked, insoluble systems (Me-PrPSQ), low molecular weight oligosilsesquioxanes in the form of cages (Hex-DecPSQ) to semicrystalline, lamellar layers (Dodec-OctadecPSQ) were detected. A low degree of condensation, inhibition of self-assembly and preferentially intermolecular condensation reactions were found to be crucial factors in the melting gel formation.

Graphical Abstract

So called melting gels are usually prepared by acid-catalysed hydrolysis and condensation of aromatic trialkoxysilanes. The final materials show a thermoplastic and a thermoset temperature regime based on the stabilisation of silanol groups in the material. In this study we transferred the typical synthetic conditions to alkyltrialkoxysilanes with different alkyl chain lengths and obtained completely changed structures of the synthesised polyalkylsilsesquioxanes compared to their aromatic counterparts. Depending on the chain length, densely cross-linked solids, viscous gels with cage-like structure and waxes with a lamellar composition were formed. Moreover, missing stabilisation of the OH groups and self-assembly phenomena, which favour the cage and semicrystalline layer formation were detected in the resulting materials, which leads to the loss of the typical melting gel properties.

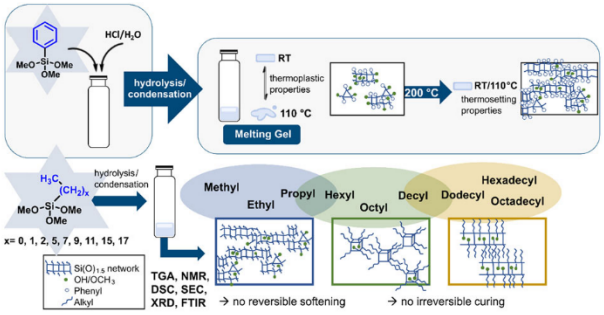

Supplementary information The online version contains supplementary material available at https://doi.org/10.1007/s10971-023-06126-6.

✉ Guido Kickelbick
guido.kickelbick@uni-saarland.de

[1] Saarland University, Inorganic Solid-State Chemistry, Campus, Building C4.1, 66123 Saarbrücken, Germany

330 Journal of Sol-Gel Science and Technology (2023) 107:329–346

Keywords Melting gel · Polysilsesquioxane · Polycondensation · Alkyl groups · Self-assembly

Highlights

- Synthesis of polyalkylsilsesquioxanes $(RSiO_{1.5})_n$ (R = methyl, ethyl, propyl, hexyl, octyl, decyl, dodecyl, hexadecyl, octadecyl) via an acid-catalysed solvent-free hydrolysis and condensation reaction.
- Comparison of the structure-property relationship of alkyl groups containing polysilsesquioxanes with a polyphenylsilsesquioxane in terms of temperature dependant thermoplastic and thermosetting behaviour.
- Depending on the length of the alkyl chain, solid materials with a dense network structure (C_1–C_4), viscous liquids with cage-like motifs (C_6, C_8, C_{10}), and waxy materials with lamellar layered structures (C_{10}, C_{12}, C_{16}, C_{18}) were formed.
- The presence of groups in trialkoxysilanes that inhibit self-assembly and lower the degree of condensation due to steric hindrance is an essential factor in the softening properties of polysilsesquioxanes.

1 Introduction

Polysilsesquioxanes (PSQ) with the general formula $(RSiO_{1.5})_n$ consist of an inorganic Si-O-Si backbone and various organic groups. Due to their hybrid character, silsesquioxanes offer a broad range of properties, such as excellent heat stability and flame retardancy, resistance to environmental conditions, an ultra-low dielectric constant, good mechanical properties, and biocompatibility [1–6]. The synthesis is typically carried out by an acid- or base-catalysed hydrolysis and condensation reaction from organotrialkoxy- or organotrichlorosilanes. Depending on the synthesis conditions, such as temperature, monomer concentration, water content or pH value and the properties of the organic substituent, silsesquioxanes with different structures are formed [7–9]. Ladder-like structures, open and closed cage structures of different sizes or random networks are the best-known structural motifs [10].

The so-called melting gel is a unique material that either contains silsesquioxane structural features or consists entirely of them. The term melting is used incorrectly when referring to these materials known from the literature, as it is not a crystalline material. Instead, it is used to describe the softening of the material, i.e., the glass transition. The term "melting gel" was first used in connection with organically substituted, melting siloxane-based inorganic glasses and has come to be used to describe the materials [11, 12]. The compounds are usually prepared from di- and trialkoxysilanes with methyl and phenyl groups via an acid- and/or base-catalysed hydrolysis and condensation reaction [11]. They form transparent, glass-like materials at room temperature that can be reversibly softened at about 110 °C. If the temperature is further increased, irreversible hardening can be observed.

In particular, Klein et al. produced materials with different glass transition temperatures (T_g) and consolidation temperatures by varying the ratio of di- and trialkoxysilanes, as well as by changing the organic group or introducing tetraalkoxysilanes [13, 14]. The hybrid character and the variable composition according to a modular system lead to various promising properties, such as high transparency, high thermal stability, an adjustable high refractive index, low gas permeability, and low water absorption [15–18]. Due to the thermoplastic and thermosetting behaviour, processability via spin coating or injection moulding is possible. The group of Klein et al. investigated the softenable material in a variety of applications, such as anticorrosive coatings, imprinted lithography, electrospray deposition or in the field of water harvesting [19, 20]. In recent studies, our group focused on a detailed structure description of a softenable polyphenylsilsesquioxane, synthesised via a one-step acid-catalysed, solvent-free sol-gel reaction of phenyltrimethoxysilane [18]. We identified a low crosslinked structure with random parts and ladder-like domains. The oligomeric units interacted via π-π-interactions of the aromatic groups, as well as via hydrogen bonds of non-bridged OH and OCH_3 groups. Increasing the temperature up to 200 °C led to further condensation reactions and a highly crosslinked material. It was suggested that the hydroxy and methoxy groups, stabilised by aromatic groups that are difficult to accommodate in the network, contributed to the reversible softening and subsequent irreversible curing. The material is mainly characterised by a T_g, which shifts to higher temperatures through further condensation reactions and disappears entirely in the consolidated state [11].

So far, the temperature-dependent thermoplastic and thermosetting behaviour has been observed mainly in systems containing trialkoxysilanes substituted by aromatic groups, as well as in mixtures with methyltri- and dimethyldimethoxysilanes [16, 19, 21]. Melting gels with long chain alkyl groups have not been described to our knowledge. Consequently, we wanted to investigate the reason for this lack of thermosoftening and why aromatic substituents seem to play an essential role in this class of materials. We were particularly interested in the differences in the structure of the final material, depending on the chain length of the alkyl group.

Previous investigations on the hydrolysis and condensation behaviour of alkyltrialkoxysilanes and

alkyltrichlorosilanes mainly focused on octadecyl and hexadecyl groups due to their self-assembling properties to form ordered lamellar layers [22–28]. Detailed structural studies on the influence of chain length on the degree of order of lamellar layer structures as well as the packing order and conformational order of alkyl chains were performed by Shimojima et al. [29] (C_{12}–C_{18}) as well as Ni et al. (C_8–C_{18}) [30]. Low molecular mass products were observed for shorter-chain PSQs starting from ethyl as organic group, building cage structures and cyclic oligosilsesquioxanes with increasing chain length [31–33]. A systematic study of the polycondensation of alkyl- and aryltriethoxy- and trimethoxysilanes with a particular focus on gelation properties was performed by Loy et al. [34] Strong inhibition of gelation by phase separation of oligomeric and polymeric silsesquioxanes was shown. Similar to our studies, Kajihara et al. synthesised from ethyl-, propyl-, and butyltrimethoxysilanes stable, viscous liquids with an increased proportion of OH groups at room temperature and investigated the further crosslinking at higher temperatures [35]. Takahashi et al. concentrated their studies on the influence of substituents in polyorganosilsesquioxane particles on glass transition phenomena. They were able to show that materials with shorter alkyl groups (≤C_4), as well as aromatic compounds, exhibit a T_g, while longer chains (C_5, C_8) tend to crystallise [36].

Most previous works focused on synthesising preferably crosslinked polymers and the self-assembly of the hydrolysed long-chain alkyltrihydroxysilanes in the material. Little attention was paid to defect-rich, incompletely hydrolysed systems and their properties. In addition, there is no systematic structural study on the polycondensation of organotrialkoxysilanes starting from small methyl substituents to octadecyl alkyl chains and their thermal initiated structural changes. In the present study, polysilsesquioxanes were prepared from alkyltrimethoxysilanes with methyl, ethyl, propyl, hexyl, octyl, decyl, dodecyl, hexadecyl, and octadecyl groups by a solvent-free, acid-catalysed hydrolysis and condensation reaction in bulk. The structure of the partially hard and glassy to highly viscous and transparent silsesquioxanes, as well as samples thermally treated at 300 °C under a nitrogen atmosphere, were investigated by FTIR, liquid and solid-state NMR, DSC, XRD, TGA, and SEC. The influence of the length of the alkyl chain on the structure and the stabilisation of non-crosslinked OH and OMe groups in the materials were analysed. Furthermore, the effect of high temperature on the rearrangement of the system was considered. The results were compared with a softenable polyphenylsilsesquioxane that had previously been investigated in detail [18], to determine the effect of replacing the aromatic groups with alkyl groups on the structure-property relationships of the resulting materials.

2 Experimental

2.1 Materials

Methyltrimethoxysilane (C_1TMS, 97%), n-octyltrimethoxysilane (C_8TMS, 97%), n-dodecyltrimethoxysilane (C_{12}TMS, 95%), and tetramethylsilane (TMS, 99.9%), were obtained from *abcr* (Karlsruhe, Germany). Ethyltrimethoxysilane (C_2TMS, 97%), n-hexyltrimethoxysilane (C_6TMS, 97%), n-hexadecyltrimethoxysilane (C_{16}TMS, 92%), and octadecyltrimethoxysilane (C_{18}TMS, 92%) were received from Gelest (Morrisville, USA). n-Propyltrimethoxysilane (C_3TMS, >98.0%) and decyltrimethoxysilane (C_{10}TMS, > 97.0%) were ordered from TCI (Portland, USA) and chromium (III) acetylacetonate ($Cr(acac)_3$, 98%) from bldpharm (Shanghai, China). All chemicals were used without further purification and the reactions were performed under ambient atmosphere.

2.2 Instrumentation

Fourier transform infrared spectra (FTIR) were recorded in total reflectance mode on a Vertex 70 spectrometer (Bruker Optics, Ettlingen, Germany) from 450–4500 cm^{-1} with a resolution of 4 cm^{-1} and 16 scans. Low temperature FTIR measurements were carried out from 2600–3200 cm^{-1} with a resolution of 2 cm^{-1} and 32 scans. The samples were cooled below the phase transition using a container cooled with liquid nitrogen.

Solution NMR spectra were recorded on an Avance III 300 MHz spectrometer and an Avance III HD 400 MHz spectrometer (Bruker, Billerica, USA) with 300.13/400.13 MHz for ^{1}H NMR spectra and 59.63/79.49 MHz for ^{29}Si NMR spectra. All NMR samples were prepared in chloroform-d ($CDCl_3$). Quantitative ^{29}Si NMR measurements were performed in deuterated chloroform containing v/v1%TMS as internal standard and $Cr(acac)_3$ as relaxation agent (10^{-2} mol L^{-1}). ^{1}H NMR spectra were analysed with MestReNova; [37] ^{29}Si NMR spectra were evaluated with OriginPro [38] using a Gaussian function.

Solid-state SPE-MAS NMR spectra were recorded on an Avance III HD – Ascend 400WB spectrometer (Bruker, Billerica, USA) using 4 mm inner diameter ZrO_2 rotors with 13 kHz rotation frequency. The resonance frequencies were 79.53 MHz for ^{29}Si NMR spectra and 100.65 MHz for ^{13}C NMR spectra. Adamantane was used for ^{13}C NMR and octakis(trimethylsiloxy)silsesquioxane for ^{29}Si NMR as external standard. The spectra were analysed and integrated with OriginPro [38] using a Gaussian function.

Thermogravimetric measurements (TG) were carried out using a TGA/DSC Stare System 1 (Mettler-Toledo, Greifensee, Switzerland) applying a heating rate of 10 K min^{-1} between 30 and 1000 °C using an oxygen or nitrogen gas flow of 40 ml min^{-1}.

TG-FTIR measurements were performed on a TG F1 Iris (NETZSCH-Gerätebau GmbH, Selb, Germany). Samples were heated at 10 K/min from RT to 1000 °C under nitrogen atmosphere (40 ml/min). The evolving gases were transferred through a heated line (200 °C) to a Bruker Vertex 70 spectrometer, mentioned above. The FT-IR spectra were recorded with 32 scans, a resolution of 4 cm^{-1} and in a range of 4500 to 550 cm^{-1}.

Differential scanning calorimetry (DSC) was performed with a DSC 204 F1 Phoenix calorimeter (NETZSCH-Gerätebau GmbH, Selb, Germany) using aluminium crucibles with pierced lids under nitrogen atmosphere (100 mL min^{-1}) applying a heating and cooling rate of 10 K min^{-1} from −130/−120 to 110 °C with an isothermal step for 10 min at 110 °C for the viscous PSQs. Solid PSQs were heated from 0 to 200 °C. Three cycles were run in each measurement.

Size exclusions chromatography (SEC) measurements were performed in toluene with a Waters 515 pump (Waters, Milford, Massachusetts) applying two PSS SDV 1000 Å and a PSS SDV 100000 Å column from PSS (Polymer Standard Service, Mainz, Germany) using a flowrate of 1 ml min^{-1} and a RI-Shodex-101 detector (Showa Denko KK, Tokyo, Japan). Calibration was carried out using polystyrene standards (from PSS). For data acquisition and evaluation of the measurements, PSS WinGPC® UniChrom [39] was used.

Powder X-ray diffraction (PXRD) patterns of the pulverised or viscous samples were recorded at room temperature on a D8-A25-Advance diffractometer (Bruker AXS, Karlsruhe, Germany) in Bragg-Brentano θ-θ-geometry (goniometer radius 280 mm) with Cu K_α-radiation (λ = 154.0596 pm). A 12 µm Ni foil working as K_β filter and a variable divergence slit were mounted at the primary beam side. A Lynxeye detector with 192 channels and a variable slit diaphragm in front of it was used at the secondary beam side. Experiments were carried out in a 2θ range of 3–40° with a step size of 0.013° and a total scan time of 1 h.

Low temperature powder X-ray diffraction (LT-PXRD) patterns were recorded on the same diffractometer using a TTK600 (Anton Paar GmbH, Graz, Austria) low-temperature chamber. The samples were dropped onto the sample holder lined with Teflon tape (XRD of the sample holder with and without Teflon in Supplementary Fig. S1). The samples were investigated in vacuum in the temperature range of 5 to −180 °C with cooling rates of 20–50 K min^{-1}, respectively. A 12 µm Ni foil working as K_β filter and a variable divergence slit were mounted at the primary beam side. The secondary beam side was equipped with a LYNXEYE detector (192 channels). Diffraction patterns were recorded between 3 and 40° 2θ with a step size of 0.013° and a total scan time of 2 h with 30 min precool time for each temperature. The thermal contraction of the reaction chamber and sample holder was determined using elemental Si (NIST Standard reference material 640 f, $a = 5.4311(1)$ nm). The obtained data were refined using the Bruker TOPAS 5.0 software package [40], keeping the lattice parameter of Si fixed while refining the height displacement. This was conducted for different temperatures from which a linear regression was determined (Supplementary Fig. S2). For the subsequent measurements, the z-height was modified in the software package by the previously determined values as a function of the temperature used. All recorded data was evaluated using the Bruker TOPAS 5.0 software [40],with the observed reflections being treated via single-line fits.

2.3 Preparation

The polyalkylsilsesquioxanes were synthesised according to a modified literature procedure for melting gels [18]. The alkyltrimethoxysilane (RTMS) (1.5 g, 1 eq) was stirred with aqueous HCl solution in a closed 20 ml headspace vial at 45 °C for 8 h or 7 days. The silane/water ratio was 1.5 or 3 and the pH value was adjusted to 2.5 (exact synthesis parameters for different $AlkylSi(OMe)_3$ are described in Table 1). Afterwards, the sample was stirred open at room temperature for 18 h. To remove by-products of the sol-gel reaction, such as water and methanol, the samples were placed in a compartment dryer at 70 °C and 110 °C for 24 h each. For further consolidation, samples were thermally treated at 300 °C under nitrogen atmosphere for 1 h. Additional measurements were carried out with the polyalkylsilsesquioxanes (RPSQ) and the thermally treated polyalkylsilsesquioxane ($RPSQ_T$) cooled down to RT.

3 Results and discussion

The synthesis procedure used in this work is based on the preparation of a softenable polyphenylsilsesquioxane via solvent-free acid-catalysed hydrolysis and condensation reaction, described elsewhere (Fig. 1a) [18]. Maintaining the conditions of this standard synthesis, the influence of the alkyl groups on the behaviour during synthesis and on the properties and structure of the final product should be directly comparable to the behaviour of a polyphenylsilsesquioxane as a model system for temperature-dependant reversible softenable and irreversible curable melting gel systems.

In the first synthesis step, stirring of the trialkoxysilanes with 1.5 equivalents of water and acid at 45 °C, the phenyltrimethoxysilane showed a homogenisation of the 2-phase mixture of an organic and aqueous component after approximately 10 min. In this step, hydrolysis and partial condensation occur with the simultaneous formation of

Table 1 Alkyltrimethoxysilanes used, synthesis conditions and properties of PSQs in comparison with a polyphenylsilsesquioxane, investigated elsewhere [18]

$RSi(OCH_3)_3$	Sample name	Ratio water[a]/silane	Stirring time at 45 °C [d][b]	Appearance after synthesis	Change in viscosity at 110 °C	Curable at 200 °C[c]
PhenylTMS	PhPSQ	1.5	0.33	Hard, transparent, glass like	yes	yes
MethylTMS	MePSQ	1.5	0.33	Hard, transparent, glass like	no	[d]
EthylTMS	EtPSQ	1.5	0.33	Hard, transparent, glass like	no	[d]
PropylTMS	PrPSQ	1.5	0.33	Hard, transparent, glass like	no	[d]
HexylTMS	HexPSQ	1.5	1	Viscous, transparent, liquid	no	no
OctylTMS	OctPSQ	3	7	Viscous, transparent, liquid	no	no
DecylTMS	DecPSQ	3	7	Viscous, transparent, liquid	no	no
DodecylTMS	DodecPSQ	3	7	Viscous, transparent, liquid	no	no
HexadecylTMS	HexadecPSQ	6	7	White, waxy	yes, transparent liquid	no
OctadecylTMS	OctadecPSQ	3	7	White, waxy	yes, transparent liquid	no

[a]Aqueous acid with pH 2.5

[b]In a closed headspace vial. The following synthesis steps, 18 h stirring at RT, 24 h 70 °C, 24 h 110 °C in an open headspace vial are the same for all samples

[c]Test with spatula. Does not deform by pressure on the specimen at 200 °C

[d]Already cured after the synthesis

methanol. Methanol serves as a solvent for the present partially hydrolysed dimers and small cycles. The alkyltrimethoxysilanes with methyl, ethyl, propyl, and hexyl groups showed similar behaviour, with homogenisation of the two-phase mixture taking different times depending on the alkyl chain. The longer the alkyl chain, the longer the homogenisation takes. Methyltrimethoxysilane displayed homogenisation after a few seconds, while hexyltrimethoxysilane changed to a one-phase solution after one day. Octyl-, decyl-, dodecyl-, hexadecyl-, and octadecyltrimethoxysilane showed no homogenisation within the applied 8 h of stirring time. Only when 3 equivalents of water and an extended stirring time of 7 days were used, a change within the reaction mixture was observed for the long-chain derivatives. Thus, C_8-, C_{10}-, and C_{12}TMS formed a cloudy gel phase, while C_{18}TMS was present as a white, waxy compound. C_{16}TMS needed 6 eq of water to change into a white, waxy material. Subsequently, all products were stirred in open vessels for 18 h at RT, and then the by-products methanol and water were removed by a treatment in the compartment dryer for 24 h at 70 and 110 °C each. Except for the HexadecPSQ and OctadecPSQ, all polysilsesquioxanes were homogeneous and transparent after the synthesis (Fig. 1b). Me-, Et-, and PrPSQ were hard, glassy and insoluble in common solvents and showed no change in the viscosity at 110 °C. In comparison, Hex-, Oct-, Dec-, and DodecPSQ, were highly viscous liquids. The HexadecPSQ, and OctadecPSQ featured a waxy, white form that reversibly transformed into a transparent liquid upon heating (Fig. 1c). The synthesis parameters and the appearance of the materials obtained, compared with the known PhPSQ, are shown in Table 1.

HexadecPSQ and OctadecPSQ differ optically from the shorter-chain materials by their waxy and white consistency and phase transformation at elevated temperatures. It is known that long-chain trimethoxysilanes can form lamellar layers due to the surfactant-like behaviour of the hydrolysed alkyltrialkoxysilanes [29]. An order-disorder process of the alkyl chains can explain the reversible phase transition from liquid to solid. NMR and FTIR- measurements showed a low degree of hydrolysis and condensation in the samples prepared here, with a remaining number of methoxy groups >67% (Supplementary Figs. S3 and S4) and a significant monomer peak in the ^{29}Si NMR (Supplementary Fig. S5). In consequence, the polycondensation of the long-chain TMS is difficult under the conditions presented here. For this reason, we decided to limit our structural characterisation to the shorter chain PSQs (C_1–C_{12}).

Visually, it was established that none of the present products from C_1- to C_{12}PSQ showed comparable properties to a PhPSQ, such as a transparent, hard and glass-like appearance with a reversible softening at 110 °C as well as irreversible curing at 200 °C. Nevertheless, the different

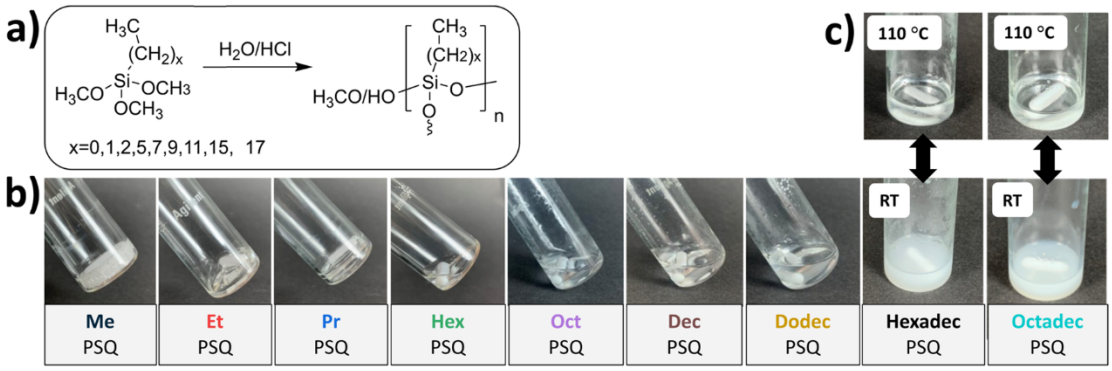

Fig. 1 **a** General equation for the acid catalysed hydrolysis and condensation reaction of the AlkylPSQ, **b** pictures of AlkylPSQs after synthesis at RT, **c** pictures of HexadecPSQ and OctadecPSQ at 110 °C

behaviour during synthesis indicated a significant influence of the chain length on the hydrolysis and condensation reaction and therefore on the resulting materials structure. Structural differences of the Me-, Et-, Pr-, Hex-, Oct-, Dec-, and DodecPSQ, as well as the influence of thermal treatment, were analysed using various spectroscopic and thermal methods, as well as PXRD measurements at different temperatures, in comparison with a softenable polyphenylsilsesquioxane [18].

3.1 Characterisation

3.1.1 TGA and TG-FTIR

Polysilsesquioxanes are generally known to be thermally very stable. Polyphenylsilsesquioxane in particular, is characterised by temperature stability up to about 500 °C under inert and under oxygen atmospheres [41, 42]. Alkylsilsesquioxanes, on the other hand, decompose earlier, with stability depending on the organic group, the structure, and the atmosphere where the samples are treated. Polyoctahedral silsesquioxanes (POSS) with propyl to octadecyl groups, for example, showed evaporation under N_2 atmosphere in a one-step process directly from the molten state, with the onset of weight loss shifting to higher temperatures with increasing alkyl chain length (T_8C_3 at 166 °C, T_8C_{10} at 353 °C) [43]. The alkyl chains can form volatile components by Si-C as well as by C-C chain cleavage [44]. Redistribution of volatile cycles and polycyclic oligomers is also possible [45]. In contrast, oxidation and partial crosslinking of the material occurs under oxygen atmosphere, which leads to the observation that the total weight loss is lower than under nitrogen atmosphere [46].

This tendency can also be detected in the thermal decomposition of the synthesised AlkylPSQs. The total weight loss under O_2 atmosphere increases with increasing chain length (Fig. 2a, exact values in Supplementary Table S1). Under inert atmosphere, the total weight loss is larger but shows no dependence on chain length, indicating differences in the crosslinking and the amount of volatile silsesquioxane components evaporated during the heat treatment.

The temperature, where 95 % of the sample is still present (T_{95}), can be considered as a parameter for the thermal stability (Fig. 2b, exact values in Supplementary Table S1). In the oxygen atmosphere, the value is lower than in a N_2 atmosphere, as the onset of decomposition is at lower temperatures [46]. Compared to POSS systems, the materials prepared here are not fully crosslinked, resulting in an effect of residual OH and OMe groups on stability.

It is known that further condensation reactions of the non-crosslinked units can occur [22, 47, 48]. The softenable polyphenylsilsesquioxane, for example, showed the loss of methanol and water at 236 °C. After the consolidation, this step was no longer detectable [18]. An initial mass loss between 150 and 300 °C is also visible for the AlkylPSQs, which affects the T_{95} value. The samples treated under O_2 show a strong overlap of the condensation step with the decomposition step of the organic chains (TGA curves are shown in Supplementary Fig. S6). Under N_2 atmosphere, however, a mass loss could be detected in the Et-, Pr-, Hex-, and DodecPSQ, which can be assigned to condensation reactions (inset, Fig. 2c). The condensation stage indicates the presence of stable OH and OMe groups in the material, which react only at high temperatures [49]. Oct- and DecPSQ, on the other hand, show only a single decomposition step at around 500 °C. The absence of further mass losses suggests a high degree of condensation and a low number of non-crosslinked groups.

The decomposition of MePSQ has been considered in detail in the literature [50]. The three stages, also visible here, were assigned to the loss of ethanol and oligosilsesquioxanes, methane and oligosilsesquioxanes, and methane, water, and hydrogen. Furthermore, the incorporation of carbon into the network was observed.

Journal of Sol-Gel Science and Technology (2023) 107:329–346

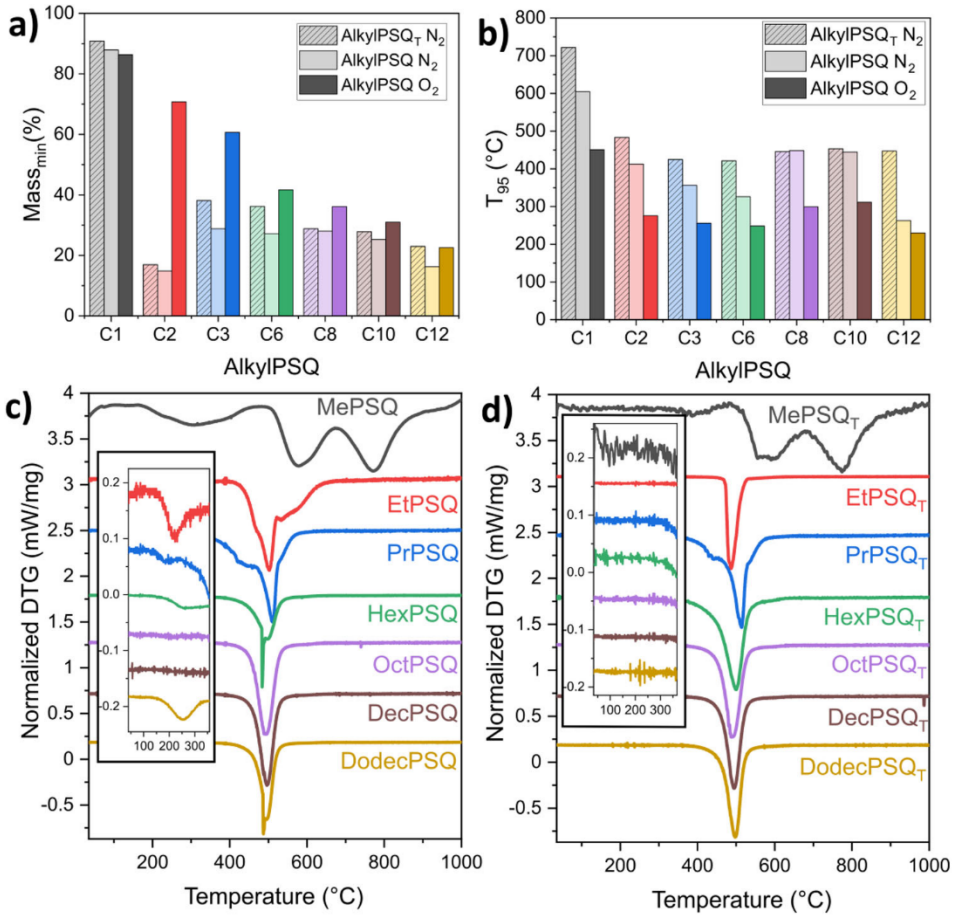

Fig. 2 **a** Residual masses and **b** T_{95} values, determined by TGA-measurements of AlkylPSQ under N_2 and O_2 atmosphere and AlkylPSQ$_T$ under N_2 atmosphere, **c** DTG of the TGA measurements of the AlkylPSQ under N_2 atmosphere, **d** DTG of the TGA measurements of the AlkylPSQ$_T$ under N_2 atmosphere

Since the TG curves of the other PSQs are significantly different from that of the MePSQ, the decomposition gases were investigated via TG-FTIR (Supplementary Figs. S7 and S8). Unfortunately, neither methanol nor water could be detected within the first decomposition stage. The amount is expected to be too small to be visible in the FTIR spectrum. The loss of oligosilsesquioxanes within this stage can also not be ruled out. Decomposition by partial loss of organic substituents at around 500 °C is detectable in all PSQs. The loss of oligosilsesquioxanes is also possible since an absorption could be detected in the region of the Si-O-Si band. Furthermore, subsequent incorporation of the remaining organics into a SiO_xC_y network can be expected [47].

As it is demonstrated that the thermally initiated condensation step takes place up to 300 °C, all samples were treated at 300 °C for 60 min under N_2 atmosphere. The aim was to force the stable OH groups to undergo further condensation reactions, comparable with the consolidation behaviour that is known for the melting gel family. After thermal treatment, the materials remained transparent, and no discolouration was detected. This suggests that no decomposition of the organic groups or incorporation of carbon into the network occurs up to this temperature. In the TG curve, the first mass loss disappeared in all samples and a single decomposition step at about 500 °C was observed (Fig. 2d). Consequently, all PSQs show a comparable high T_{95} value around 480 °C (Fig. 2b). Furthermore, the residual mass is higher compared to the thermally untreated samples because it is now independent of non-reacted groups and is determined by the decomposition of the network and the mass of the organic group. As a result, it shows a dependence on chain length from C_3 to C_{12}PSQ and becomes larger the longer the alkyl chain (Fig. 2a).

In summary, Me-, Et-, Pr-, Hex-, and DodecPSQ contain stabilised OH and OMe groups that can thermally react. Oct- and DecPSQ already exhibit a highly condensed structure after synthesis. Thus, the decomposition is determined by the degradation of the alkyl groups as the main mass loss step. After thermal treatment at 300 °C, all PSQs show almost identical decomposition in one degradation step and high thermal stability under inert atmosphere, suggesting that highly condensed materials are present. A detailed determination of the structures present and the influence of thermal condensation on the structure will be investigated in the following sections.

3.1.2 DSC

DSC measurements of all materials were performed to visualise possible phase transformations and T_g. The phenyl-containing PSQ showed a T_g at about 60 °C, which reflected the amorphous structure as well as the softening of the material [18]. The T_g depends on the mobility of the polymer chains and therefore on the substituent and the degree of crosslinking [51, 52]. Further condensation reactions and complete curing of the PhPSQ could be demonstrated by the complete disappearance of the T_g. The solid samples with methyl, ethyl, and propyl groups were measured from 30 to 200 °C to investigate softening in this temperature range (Fig. 3a). No significant change in heat flow was detected in the Me- and PrPSQ, and reversible softening, can be excluded. A T_g is visible in EtPSQ at 35 °C. This can be attributed to increased mobility due to a large number of non-crosslinked groups, as already seen in the TGA, based on the first decomposition step. However, the softening is weak, so the material retains its original shape at higher temperatures. Processing the softened material, similar to the PhPSQ, was not possible.

The prepared polysilsesquioxanes with chains between C_6 and C_{12} exist as viscous liquids at room temperature, therefore low-temperature measurements down to −130 °C were performed. Oct- and HexPSQ showed a glass transition at −77 and −97 °C, respectively. No crystallisation can be observed, which also indicates an amorphous structure. In contrast, DecPSQ and DodecPSQ showed a distinct endothermic signal at 5 °C (Fig. 3b) and −20 °C (Fig. 3c) that remains constant over three cycles with an isothermal treatment at 110 °C for 10 min at every cycle. This behaviour has already been observed for poly(di-*n*-alkylsiloxane) with alkyl chains of C_7 to C_{10} [53], as well as for polyalkylsilsesquioxanes with dodecyl, hexadecyl, and octadecyl groups [22, 24, 54]. The endothermic signal is assigned to lamellar layers, where the transition from solid to liquid is thermally induced by a trans-gauche transformation of the long-chain alkyl groups, which leads to a disordered structure [54].

After thermal treatment, the signals of Hex-, Dec-, and DodecPSQ shift to higher temperatures (Fig. 3d). As the T_g depends on the crosslinking of the polymers, the increase in the T_g of C_6PSQ can be attributed to an increased degree of condensation due to the thermal treatment. However, OctPSQ showed no condensation step in the thermal analysis, indicating that no significant crosslinking was thermally initiated, which explains the missing change of the DSC signal.

Since it is described in the literature that the endothermic signal in Dec- and DodecPSQ is generated by the crystallisation of the alkyl chains, it depends mainly on their arrangement and less on the crosslinking of the Si-O-Si backbone. The shift to higher temperatures and the simultaneously more defined signals indicate increased order and regularity in the alkyl chains [55].

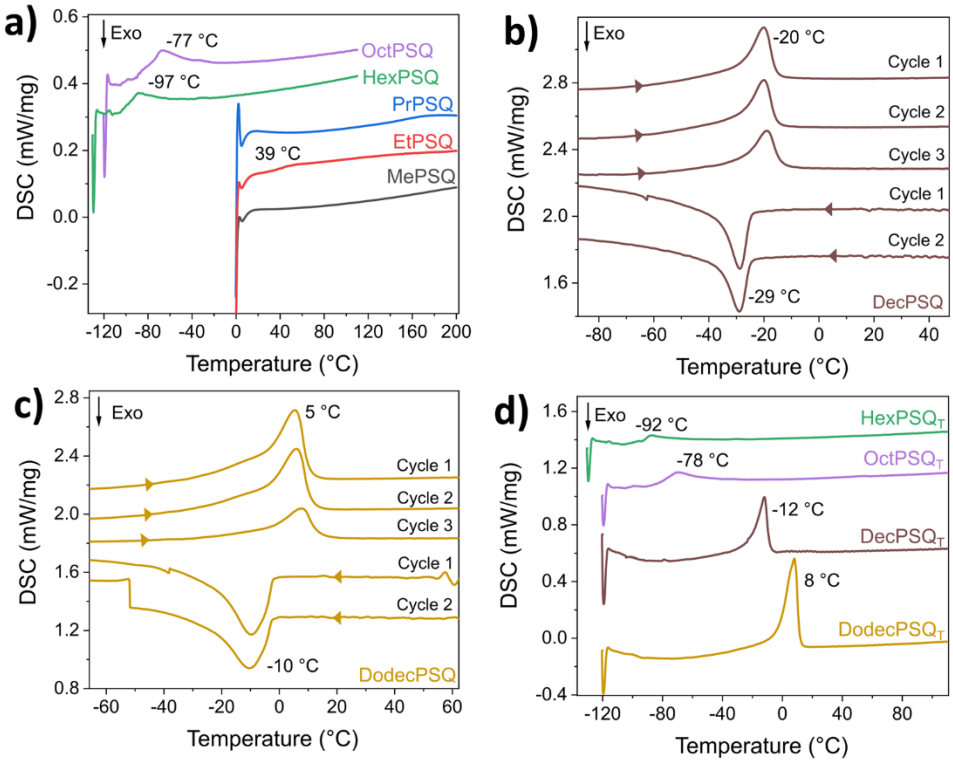

Fig. 3 DSC measurements **a** second cycle after heating to 110 °C of Oct- and HexPSQ, in the region −120 to 110 °C and Me-, Et-, and PrPSQ in the region 0 to 200 °C, **b** and **c** heating and cooling cycle, measured between −120 to 110 °C with isothermal treatment for 10 min at 110 °C with focus on endo- and exothermic signals of DecPSQ and DodecPSQ, **d** second cycle after heating to 110 °C of Oct-, Dec-, and DodecPSQ$_T$, in the region −120 to 110 °C and HexPSQ$_T$ in the region −130 to 110 °C

In general, DSC measurements reveal a clear dependence of the structure on the length of the alkyl chains. While Me-, Et-, and PrPSQ are present in a dense amorphous network, showing little mobility, the long-chain C_6 and C_8 derivatives lead to increased mobility with a resulting low T_g. Decyl and dodecyl groups, on the other hand, result in a phase transition by cooling to a semi-crystalline material, suggesting a structure with lamellar layers and an increased alkyl chain order by temperature treatment.

3.1.3 FTIR spectroscopy

FTIR spectroscopy can be used to identify groups that are part of the hydrolysis and condensation process. These include the methoxy groups, which can be detected in the monomer at 2839 cm^{-1}, 1191 cm^{-1}, and 1082 cm^{-1} [56]. In particular, the PSQs with shorter alkyl groups (methyl, ethyl, and propyl) show a significant decrease in the absorption at 1191 cm^{-1}, indicating nearly complete hydrolysis of the alkoxy groups (Fig. 4c). The bending mode of the CH_2 groups attached to the Si reveals a red-shift with longer alkyl chain length (1271 cm^{-1} for MePSQ and 1191 cm^{-1} for HexPSQ) and overlaps with the vibration of the OCH_3 group at 1191 cm^{-1} [35]. Therefore, in C_6-, C_8-, and C_{10}PSQ, the disappearance of the absorption at 2839 cm^{-1} demonstrates the reaction of the monomer (Fig. 5). DodecPSQ still presents a peak at 1082 cm^{-1}, indicating that in comparison with the other materials, an increased number of OMe groups or monomers is still present.

Bands arising from hydrolysed and non-crosslinked OH groups can be located between 3000 and 3700 cm^{-1}, as well as at 893 cm^{-1} (Fig. 4a, c). The absorption band of the νOH in silanols can be divided into different regions depending on the interaction of the OH group [57, 58]. Between 3550–3200 cm^{-1}, strongly hydrogen-bonded OH-groups with a short distance between these bonds are visible (OH_{ass}). At about 3630 cm^{-1}, vicinal hydrogen bonded silanols are found (OH_{vic}) and isolated as well as geminal hydroxy groups are further shifted to higher wavenumber. Noticeably, the strongly interacting groups are significantly more represented in the C_1-, C_2-, and C_3PSQs. It is assumed that the different siloxane species are located closer together due to the smaller groups, resulting in the formation of H-bridges that interact intra- and intermolecularly over shorter distances. The longer hydrophobic alkyl chain in Hex-, Oct-, Dec-, and DodecPSQ ensure separation of the different silsesquioxane species, whereby a blue shift of the νOH band becomes visible by the absorption of vicinal interacted silanols. After thermal treatment at 300 °C, absorption of the silanols was no longer visible, indicating a further condensation reaction and confirming the TGA measurements. Further crosslinking can also be shown in Oct- and DecPSQ, although this was first excluded in the TGA. However, these reactions are assumed to occur primarily via condensation of OH groups, visible in the FTIR spectra. This leads to a lower mass loss compared to condensation between OH and OMe groups.

The Si-O-Si region in the FTIR spectra is often used in the literature to identify defined moieties, such as ladder structures, cycles, or cages. Ladders are detected by two defined peaks at 1020 cm^{-1} and 1115 cm^{-1}, which can be assigned to the vibrational mode of the $(Si\text{-}O)_4$ cycles. The

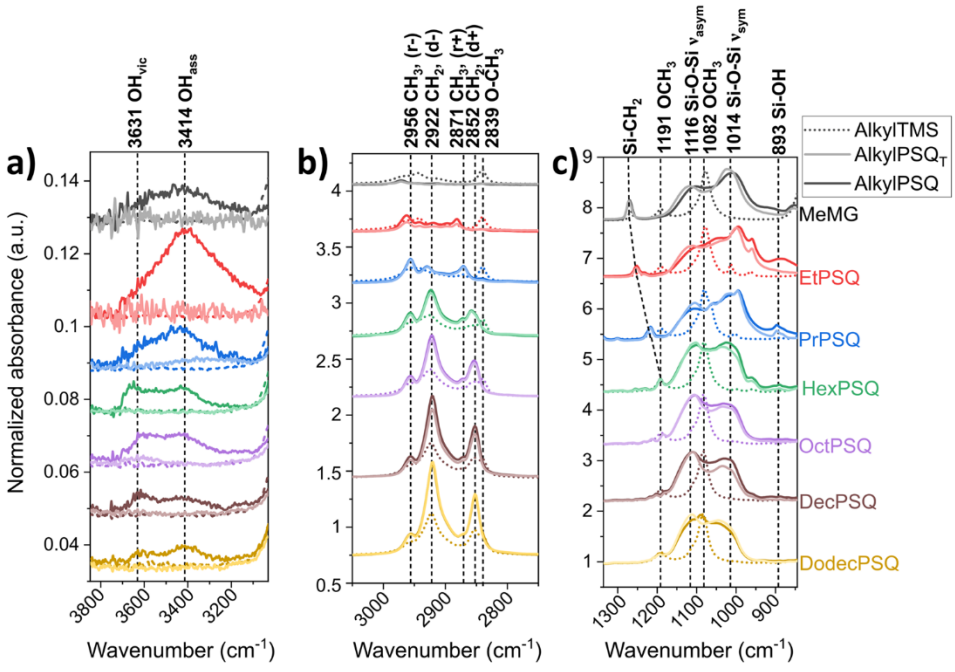

Fig. 4 FTIR spectra of polyalkylPSQ, dotted line = monomer, solid, dark line = AlkylPSQ, solid, bright line = thermally treated AlkylPSQ, **a** OH-region, **b** C-H-region and **c** Si-O-Si region

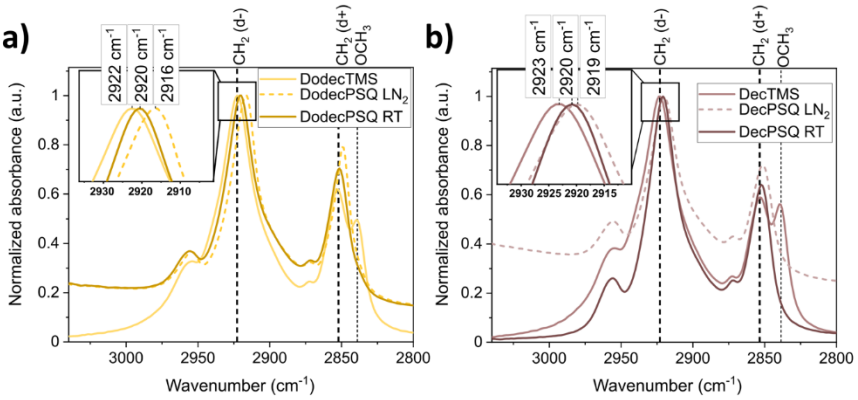

Fig. 5 FTIR spectra of the CH-region between 2800 und 3040 cm^{-1} of the monomer, AlkylTMS, AlkylPSQ and liquid N_2 cooled AlkylPSQ with **a** decyl and **b** dodecyl groups

symmetric stretching vibration at 1020 cm^{-1} is characteristic of a two-dimensional linear structure of ladders, while the antisymmetric stretching vibration at 1115 cm^{-1} is associated with a three-dimensional structure of cages [59, 60]. These two signals are particularly prominent in the Me-, Hex-, Oct-, Dec-, and DodecPSQ, indicating a ladder-like structure. It is noticeable that with increasing chain length, the peak at 1116 cm^{-1} becomes more prominent, which suggests an increase in cage-like units. It can be assumed that more extended hydrophobic groups favour intramolecular condensation reactions over intermolecular ones, explaining the formation of a larger number of three-dimensional structural units [33]. After the thermal treatment, there is also an increase in the intensity of the $\nu_{ring\text{-}asym}$ at 1116 cm^{-1} in comparison with the $\nu_{ring\text{-}sym}$ at lower wavenumbers. It indicates an increase in cage-like oligosilsesquioxanes (Fig. 4c). Furthermore, a disappearance of the OMe band at 1082 cm^{-1} is observed in the DodecPSQ, showing that methoxy groups, in addition to OH groups are further condensed by the thermal treatment.

Long-chain trimethoxysilanes are known to show surfactant-like behaviour, leading to highly ordered lamellar layers in which the alkyl groups are in an all-trans zig-zag conformation. Based on the methylene vibrations, the crystalline trans conformation can be distinguished from the amorphous parts with a certain gauche character [25]. The positions of the symmetric CH_2 and CH_3 stretching vibrations (d+, r+) and anti-symmetric CH_2 and CH_3 stretching vibrations (d−, r−) can be correlated with the conformational order of the alkyl chains [22]. In amorphous samples or solution, the peaks are shifted to higher wavenumbers because more gauche defects are present, leading to higher vibrational energies.

Considering the symmetric CH_2 stretching vibrations (d−), Dec- and DodecPSQ show a slight shift of 3 cm^{-1} and 2 cm^{-1}, respectively (Fig. 5a, b), to lower wavenumber, indicating an ordering of the alkyl chains relative to the monomer due to polycondensation. Compared to literature values of all-trans alkyl chains (d+: 2846–2850 cm^{-1}, d−: 2915–2918 cm^{-1}) [61], the change in band position is very small, suggesting a large disorder with many gauche defects in the chain.

However, DSC measurements showed a phase transition at low temperatures for Dec- and DodecPSQ. It was described that an order-disorder transition of the alkyl chains in the lamellar PSQs takes place. To verify this hypothesis, a low-temperature IR spectrum of the two samples was measured below the phase transition temperature. In the spectrum, an increase in the background is apparent, due to condensed water using liquid nitrogen. However, this does not affect the position of the peaks. In particular, the DodecPSQ shows a substantial shift to smaller wavenumber (2916 cm^{-1}, Fig. 5a), indicating an increasing population of chains in trans conformation. The shift in the DecPSQ (2919 cm^{-1}, Fig. 5a) is much smaller, suggesting the presence of gauche defects below the phase transition due to a lower self-assembly ability, which strongly impacts the packing and conformation of the alkyl chains [30]. The thermally treated samples show the same behaviour with the shifts to lower wavenumber with increased order (Supplementary Fig. S9). This suggests an intact order of the alkyl chain conformation even after thermal treatment, as already shown in the DSC measurements.

FTIR spectroscopy demonstrated the successful synthesis of crosslinked AlkylPSQ. Absorption between 3000 cm^{-1} and 3700 cm^{-1} showed non-crosslinked interacting OH groups in all samples. The measurements generally reveal different structural motifs depending on the chain length. Et- and PrPSQ, for example, have a broad Si-O-Si profile with few defined bands, comparable to PhPSQ. This indicates a primarily random structure with many different structural units, including ladders and cages. With a longer alkyl chain, intramolecular condensation reactions are favoured over intermolecular ones, forming cyclic and cage-like motifs. The longer the chain, the more hydrophobic interactions of the alkyl chains play a role and influence the order and packing of the alkyl chains. Below the phase

transition, an order of the alkyl groups in Dec-, and DodecPSQ can be shown, indicating a lamellar structure. Thermal condensation led to further condensation of non-crosslinked OH and OMe groups, as well as an increase in cage-like structural motifs. The order of the alkyl chains does not seem to be affected.

3.1.4 NMR spectroscopy

Further information on the structure of the resulting polysilsesquioxanes was obtained via ^{1}H, ^{29}Si, and ^{13}C NMR spectroscopy. To allow quantification, liquid NMR spectra were conducted in the presence of the relaxation agent $Cr(acac)_3$ [62, 63], and solid-state NMR spectra were measured in a single pulse experiment [25]. Thus, the areas of the ^{29}Si and ^{13}C NMR signals are proportional to the fraction of the assigned compound. Me-, Et-, and PrPSQ were not soluble in the conventional solvents and were analysed via MAS-NMR (^{13}C-MAS NMR is shown in Supplementary Fig. S10).

In all ^{1}H NMR spectra of the soluble AlkylPSQ and the thermally treated samples the CH_3-, -CH_2-, and CH_2-Si signals could be observed in the correct ratio (Supplementary Figs. S11 and S12), indicating no decomposition of the alkyl chains by thermal treatment [35].

Furthermore, residues of OCH_3 groups in the range of 3.5 ppm were detected, and the content in the sample was determined by integration (Table 2). This value gives an idea of how well the hydrolysis worked and how large the defect density of non-reacted groups is in the material. Me-, Et-, Pr-, and HexPSQ show values between 2.3 and 9.4%. Oct- and DecPSQ present almost no OMe groups, and DodecPSQ exhibits the highest value with 15.3 %. It is known that a higher proportion of H_2O leads to a higher hydrolysis rate, whereas groups with larger steric hindrance decrease hydrolysis [64, 65]. Me- and EtPSQ demonstrate almost complete hydrolysis of the monomer. From propyl to hexyl group, the number of remaining non-crosslinked groups increases, while longer-chain trimethoxysilanes ($> C_6$) synthesised with 1.5 eq. of water showed no reaction within the synthesis conditions used here. By increasing the amount of water to 3 eq., complete hydrolysis of Oct- and DecPSQ is obtained, whereas the formation of silanols in DodecPSQ decreases significantly. A high number of monomers can be detected in Hexadec- and OctadecPSQ. A clear influence of the amount of water and the alkyl group length on the number of remaining methoxy groups can be detected. It is expected that hydrophobic interactions of the alkyl groups rather than steric hindrance play a role in the polycondensation of samples ≥C_3PSQ [32].

After thermal treatment, a significant reduction of the OCH_3 groups can be observed (Table 2) in all samples, confirming the assumption that the first mass loss in the TGA represents, besides the reaction of two hydroxy groups, the condensation of hydroxy and methoxy groups.

Table 2 Percentages of residual OCH_3, T-units and degree of condensation of the AlkylPSQ, obtained from ^{1}H, ^{29}Si, and ^{13}C NMR in comparison with a PhPSQ [18]

Sample	T^0 [%]	T^1 [%]	T^2 [%]	T^3 [%]	Residual OCH_3 groups [%]	DC [%]
PhPSQ [18]	/	/	71	29	10	76
$PhPSQ_T$ [18]	/	/	51	49	<10	83
MePSQ[a]	/	/	30	70	2.3	90
$MePSQ_T$	/	/	23	77	1	92
EtPSQ[a]	/	/	56	44	2.7	81
$EtPSQ_T$	/	/	45	55	2	85
PrPSQ[a]	/	5	40	55	4	84
$PrPSQ_T$	/		20	80	3	93
HexPSQ	/	10	24	66	9.4	85
$HexPSQ_T$	/	/	11	89	<1	97
OctPSQ	/	/	22	78	<1	93
$OctPSQ_T$	/	/	20	80	/	93
DecPSQ	/	/	21	79	2.0	93
$DecPSQ_T$	/	/	13	87	/	95
DodecPSQ	5	14	21	60	15.3	78
$DodecPSQ_T$	/	6	30	64	5.0	86

[a]Measured by SP-MAS NMR

The influence of chain length on crosslinking is visible in the ^{29}Si NMRs. The spectra show various signals with different chemical shifts, depending on the number of siloxane bonds (Fig. 6a). As only trialkoxysilanes were used, only T^n units in the range between −41 ppm and −69 ppm are visible, with n = number of siloxane bonds. Besides the assignment of the T-units, it is possible to determine the percentage of crosslinking units and the degree of condensation ($DC = (T^1 + T^2 \cdot 2 + T^3 \cdot 3)/3$) by integrating the area of the peaks. Apart from the DodecylPSQ, none of the samples show signals of the monomer (T^0), indicating a complete integration of all alkyltrimethoxysilanes. Depending on the chain length and the amount of water used, the percentages of T units change. Me- and EtPSQ show only T^2 and T^3 units, while Pr- and HexPSQ exhibit further dimers (T^1). Oct and DecPSQ demonstrate the highest crosslinking with a degree of condensation (DC) of about 93% compared to all other PSQs. DodecPSQ, on the other hand, contains residual monomer in addition to T^1, T^2, and T^3 units, which also explains the high amount of OMe groups and the distinct band at 1083 cm^{-1} in the FTIR spectra. In general, it was found that the higher water content and the longer stirring time resulted in increased condensation.

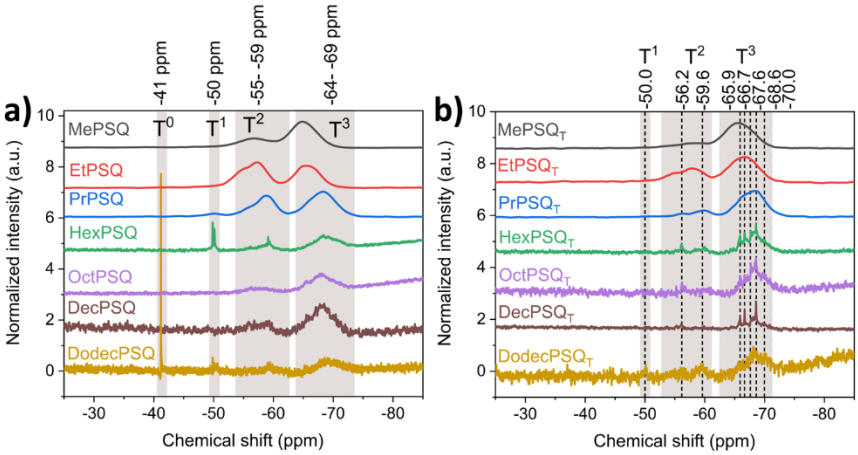

Fig. 6 ^{29}Si NMR spectra **a** AlkylPSQ **b** AlkylPSQ$_T$ with assignment of T-units, Me-, Et-, and PrPSQ was measured by ^{29}Si MAS NMR, Hex-, Oct-, Dec-, and DodecPSQ was measured by liquid ^{29}Si NMR with a relaxation agent

Furthermore, in the series of 1.5 eq. water and 3 eq. water, a higher number of T^1 units and even monomers were detectable with longer alkyl chain length. However, this tendency cannot be transferred to the number of crosslinked T^3 and the degree of condensation. In general, especially the longer-chain PSQ C_6, C_8, and C_{10} show a comparatively high proportion of T^3 units, while Et-, PrPSQ and also the PhPSQ have a balanced ratio of chain-like (T^2) and crosslinking (T^3) silsesquioxane groups. The high number of T^3 units, while at the same time, low crosslinked T^1 units are also present, indicates that hydrolysis or condensation of already hydrolysed systems is preferred. Due to the hydrolysis of trialkoxysilanes, monomers with longer alkyl chains form amphiphilic molecules that tend to aggregate. The longer the chain, the more easily the aggregates form and condensation occurs [23]. The silanols of methyl-, ethyl-, and propyltrimethoxysilane are instead distributed homogeneously and disordered, which leads to a lower degree of condensation, a higher number of chain-like units, and thus a more extensive network.

Thermal treatment significantly increases the degree of condensation. The monomer signal in the DodecPSQ, as well as the T^1 signals in the Pr- and HexPSQ disappeared and the number of crosslinked T^3 units increased (Fig. 6b). This confirms again, the thermally initiated condensation reactions. Furthermore, it is noticeable that after thermal treatment, defined signals are formed mainly in the T^3 region of the ^{29}Si NMR of Hex-, Oct-, and DecPSQ. It is known that there is a competition between intermolecular condensation and intramolecular cyclisation in the formation of polysilsesquioxanes. The tendency to cage formation increases with increasing size of the organic groups [31, 33]. Intramolecular condensation reactions are preferred due to surfactant-like behaviour, whereby the hydrolysed head groups are directed inward, and the hydrophobic alkyl chains are oriented outward [32]. The defined signals indicate the building of cages and can be assigned to T_8 (−66.7 ppm), T_{10} (−68.6 ppm), T_{12} (>70 ppm) and also incomplete condensed cages [33, 66].

In DodecPSQ, no defined peaks of open and closed cages can be detected. Instead, an increase in T_2 units was observed and the degree of condensation is comparatively low with 86.1%, implying the presence of lamellar layers. Compared to the polyalkylsilsequioxanes, the PhPSQ showed low crosslinking (76%) with a high number of remaining OMe groups (10%). It is described that a high amount of stabilised unbridged groups and a low crosslinked structure are important factors for the reversible softening of the material [18].

It is concluded that methyl to propyl groups in PSQ form a dense network with only a few non-bridged stabilised groups, resulting in a solid material without visible softening. At the same time, long-chain AlkylPSQs of C_6–C_{10} show a high proportion of T^3 units, which further increased after thermal treatment. The almost complete conversion of the alkoxy groups, together with the appearance of defined signals that can be assigned to cubic systems, confirms the conclusion that primarily the long-chain PSQs undergo intramolecular condensation reactions to form cages. As the DodecPSQ has a lower crosslinking than the shorter-chain PSQs, it can be assumed that a lamellar structure is induced by the increasing hydrophobic interactions. Overall, the formation of oligosilsesquioxanes separated by the long alkyl groups and the mainly intramolecular condensation reactions are considered to be the reason for the lack of complete curing compared with the polyphenylsilsesquioxane.

3.1.5 SEC

SEC measurements in toluene were carried out to determine the molecular weight distribution of the soluble AlkylPSQ and the thermally treated soluble samples (exact values of M_w, M_n, M_z, Đ are presented in Supplementary Table S2). Since polystyrene was used as the standard and its structure

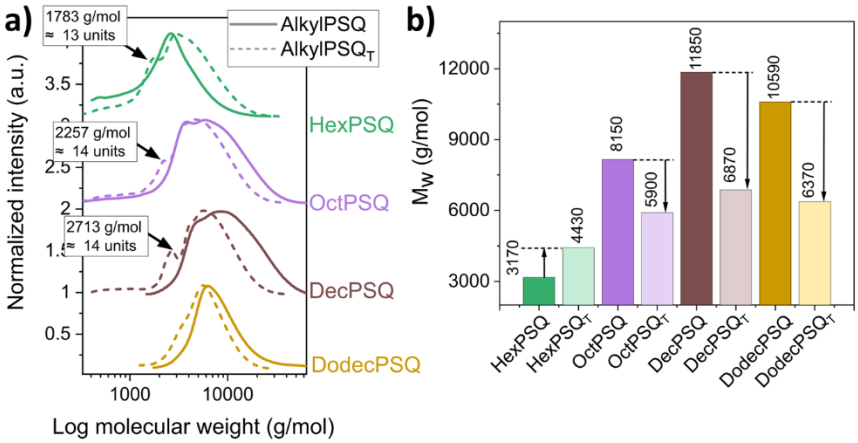

Fig. 7 **a** SEC measurements of soluble AlkylPSQ and AlkylPSQ$_T$, **b** comparison of M_n of AlkylPSQ and AlkylPSQ$_T$

is very different from the samples described here, no absolute values can be determined. Nevertheless, tendencies between the molecular weights of the individual samples could be observed. The measurements demonstrate higher molecular weights with increasing water content (Fig. 7) [67]. Thus, Oct-, Dec-, and DodecPSQ exhibit significantly larger molecular weights than HexPSQ. The degree of condensation and the high proportion of T^3 units revealed in the NMR measurements were also reflected in larger molecular weights of the longer-chain AlkylPSQs. After thermal treatment, increased molecular weight and an increased Đ-value were obtained for the HexPSQ (Fig. 7a) [35]. Surprisingly, PSQ with longer alkyl chains showed the opposite tendency and a lower and more defined molecular weight distribution was obtained. This confirms the previous observation that PSQs with long alkyl chains condense primarily intramolecularly. Also, Andianov et al. described a reduction of OH groups and a lower molecular weight during distillation of the hydrolysis products of hexyl-, heptyl-, octyl-, and iso-nonyltrichlorosilane [31]. They concluded that intramolecular condensation reactions form cage-like and cyclic systems. A defined shoulder that can be assigned to 13 and 14 $RSiO_{1.5}$ units is observed for Hex-, Oct-, and DecPSQ (Fig. 7b). Since the ^{29}Si NMR spectra showed the formation of cage structures with various sizes, it can be assumed that open or closed cages are represented here, which is in agreement with the observation of Andianov et al.. In addition to the shoulder at 1783 g/mol, HexPSQ shows an increase in molecular weight unlike the other measured PSQ$_T$s, leading to the conclusion that the intramolecular cyclization rate is almost equal to the chain elongating condensation. While the extended hydrophobic alkyl chains in Oct- and DecPSQ are expected to form mainly cubes, the unstructured SEC curve of DodecPSQ suggests that the thermally induced condensation reactions preferentially occur within the postulated lamellar layer structure and no cages were formed, as already indicated by the lack of defined peaks in the NMR spectra.

SEC measurements demonstrate the thermally induced intramolecular condensation reactions favoured by long alkyl chains to form mainly cage-like silsesquioxanes. Within the soluble materials, HexPSQ, with the shortest alkyl chain, shows intermolecular condensation reactions to form a network in addition to the formation of cage structures. In contrast, despite intramolecular condensation, no cubes can be detected in DodecPSQ with the longest chain despite intramolecular condensation, indicating a lamellar structure of partially crosslinked ladders.

3.1.6 PXRD

DSC and low-temperature FTIR measurements detected a phase transformation to an ordered structure in Dec- and DodecPSQ. Furthermore, the presence of cage structures, as well as a lamellar layered structure were postulated. To visualise the transition and clarify the structural differences from PSQs with smaller alkyl chains, PXRD measurements at room temperature (RT-PXRD) and at low temperatures (LT-PXRD) down to −180 °C were performed.

3.2 RT-PXRD

PXRD is widely used to study the structure of polysilsesquioxanes. The amorphous form of polymethylsilsesquioxane has already been analysed in detail in the literature [59, 68, 69]. The two broad reflections appearing at 8.53 Å (d_1) and 3.89 Å (d_2) are attributed to the plane-plane distance, as well as the thickness of molecular chains, and generally assigned to the occurrence of ladder structures (Fig. 8a) or a layered material [70]. It is known from the literature, the smaller the 2θ value of d_1, the less defect rich the structure. For example, uncondensed methoxy and OH groups, as well as conformational changes of the organic groups, contribute to an increased 2θ value [71]. PhPSQ also has two broad reflections with $d_1 = 8.3$ Å and

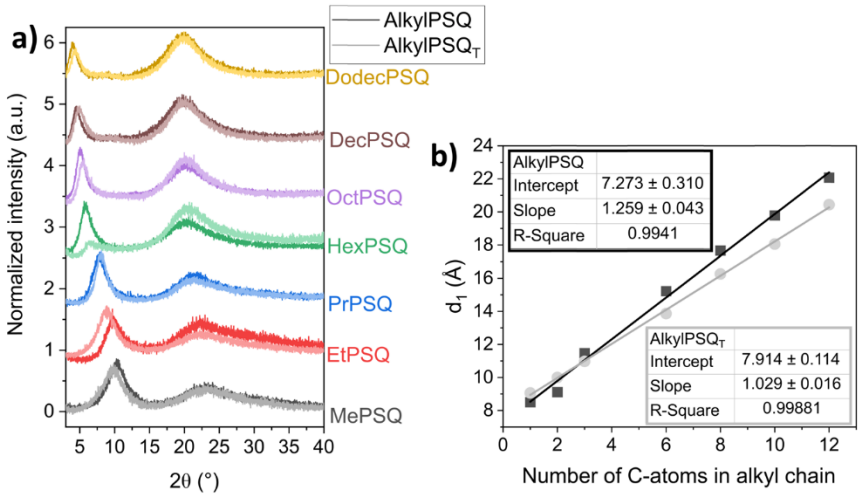

Fig. 8 **a** XRDs of AlkylPSQs, measured at RT, **b** linear fit of d_1-values against the number of C-atoms in the alkyl chain of the PSQs, dark line = AlkylPSQ, bright line = $AlkylPSQ_T$

$d_2 = 4.5$ Å. After the consolidation of this material, the d_1 value shifts to a lower angle and a chain distance of 11.5 Å can be detected, indicating further condensation reactions and reorientation to a more ordered structure containing ladder motifs [18].

All polysilsesquioxanes, synthesised here, are amorphous at room temperature and exhibit the two reflections characteristic of ladder-like systems (Fig. 8a). The d_1 value shifts with longer alkyl groups to larger chain-to-chain distances from 8.53 Å (MePSQ) to 22.07 Å (DodecPSQ). Plotting the d_1 values against chain length demonstrates a linear dependence between chain-to-chain distance and chain length with an increment value of 1.3 Å (Fig. 8b).

Shimojima et al. described an increase in basal spacing of 2.53 Å per carbon atom when considering lamellar ordered C_{12}-, C_{14}-, C_{16}-, and C_{18}PSQs [29]. This value could be assigned a value twice as large as the average C-C distance of all-trans alkyl chains. The authors concluded a bimolecular layered structure with alkyl chains perpendicular to the layer.

The value obtained here is much lower, suggesting a high gauche content and an entanglement of the longer alkyl chains in agreement with the FTIR measurements at room temperature [53]. It has already been shown that thermal treatment leads to further condensation, which should significantly lower the defect concentration in the form of non-condensed groups. It is expected that the distance between the chains, analogous to the phenyl-containing material, will increase and generally a higher order will result [72]. Et- and MePSQ confirm this statement by showing a shift of the 2θ value (d_1) to smaller angles after further condensation. However, all other PSQs demonstrate the opposite tendency, and a lower plane-to-plane distance is observed. The plot of the chain lengths against the d_1 value simultaneously shows a smaller slope and yields an incremental value of 1.03 Å (Fig. 8b).

The average distance of the main chains of Me-, Et-, and also Ph- containing PSQs are largely independent of the conformation within the organic group. Only defects in the Si-O-Si chain and the arrangement of the backbone into a cis-syndiotactic or cis-isotactic conformation contribute to the change of intermolecular distances [71, 73]. Consequently, condensation reactions alone influence the arrangement of the Si-O-Si network, forming of a wide-ranging and less defective network. In contrast, the final structure and ordering in PSQs with long-chain alkyl groups strongly depend on the alkyl chains conformation. It is assumed that the alkyl chains can adopt random arrangements due to thermally increased mobility, which reduces the steric hindrance and allows condensation reactions that were not possible before [29]. Thus, the structure favoured by the hydrophobic groups can become more disordered by a thermal treatment. A reorientation of the system and preferentially intramolecular condensation reactions take place, and the formation of cycles and cubes leads to a change of the chain-chain distance to smaller distances, destroying the layered structure. This reorientation has already been described in the literature after the thermal treatment of a octadecylsilsesquioxane, where a significant increase in T^3 signals and the formation of an amorphous material was observed after heating up to 100 °C [29]. It was explained as the formation of random orientations of the interlayer alkyl chains at higher temperatures resulting in further condensation reactions leading to an irreversible rearrangement into a more disordered system. However, the conformation of the alkyl chains was less affected by the thermal treatment [61], explaining why the DSC measurements showed an endothermic transition of the Dec- and DodecPSQ synthesised here, even after thermal treatment. Also, the FTIR measurements indicated no change in the alkyl conformation after curing.

In general, all PSQs have a highly disordered amorphous structure, with a ladder-like or layer-like composition of the silsesquioxane units. The average chain-to-chain distance is mainly influenced by the length of the alkyl chains, which are in a disordered state at room temperature. Furthermore, the crosslinking, as well as the hydrophobic interactions between the alkyl chains and the resulting structures, also play a role. Therefore, further crosslinking in Me- and EtPSQ leads to a more ordered structure, while the thermal treatment reduces the lamellar structuring properties of the alkyl chains in the longer-chain PSQs. Random condensation reactions can take place, leading to a more disordered structure. This influence becomes more prominent the longer the alkyl chain and the stronger the hydrophobic interactions.

3.3 LT-PXRD

Using DSC and low-temperature FTIR measurements, a phase transition was detected in Dec- and DodecPSQ, implying a crystalline structure. To visualise the structural change upon cooling, the two PSQs in comparison with OctPSQ, cooled below the phase transition or T_g were investigated by LT-PXRD (Fig. 9). Due to the surface tension of the gels, there may be height differences between the samples within the preparation of the XRDs, resulting in a slight shift of the reflections. The exact values must be interpreted with caution.

Dec- and DodecPSQ show a significant narrowing and a small shift of the d_2 value, while at the same time, the d_1 value disappears completely in all investigated PSQs (Fig. 9a, b). The appearance of the defined reflection at 20.73 Å and 20.54 Å reflects a phase rearrangement to a semi-crystalline material, as already expected from DSC. It can be assigned to the alkyl chain packing within the layers, which crystallizes into an all-trans conformation at low temperatures [22]. The significantly broader d_2 reflection in DecPSQ and the amorph structure in OctPSQ (Fig. 9c) indicate a higher gauche content with shorter alkyl chain length [53]. Furthermore, sharp and defined reflections in the small angle region have been described in the literature for crystalline polyalkylsilsesquioxanes with 12–18 carbon atoms. The basal spacing and the associated higher order diffraction, were assigned to the repeating distances of the lamellar layers [29]. For Dec- and DodecPSQ two weak and broadened signals can be identified in the small angle region instead of the more intense d_1 value, indicating the destruction of the order in the Si-O-Si backbone after the phase transition. Crystallisation of the alkyl groups is described as the driving force by which arrangement into a lamellar structure occurs [33]. The structural arrangement changes the distance of the siloxane backbone, causing the complete disappearance of the amorphous d_1 signal. The semicrystalline behaviour described here is preferred for lamellar materials, which lose their long-range order by further condensation [24, 29]. It can be assumed that the hydrophobic interactions of the alkyl chains, in combination with the synthesis conditions, are not sufficient to generate a highly ordered system.

In general, the low-temperature measurements show that the phase transition of Dec- and DodecPSQ is mainly caused by the crystallisation of the alkyl chains. This leads to a rearrangement of the Si-O-Si backbone into a more disordered lamellar structure. The lack of order, despite long-chain hydrophobic chains, can be attributed to the high degree of condensation, which results in a collapse of the lamellar arrangement.

4 Conclusion

In a solvent-free acid-catalysed hydrolysis and condensation reaction of phenyltrimethoxysilanes, glass-like, transparent, reversibly softenable and irreversibly curable at high temperatures systems so-called melting gels can be synthesized. The synthesis of a known polyphenylsilsesquioxane melting

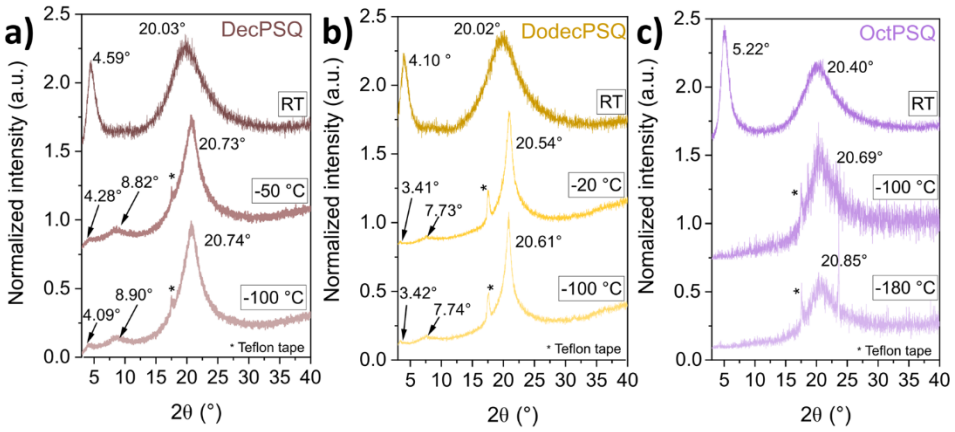

Fig. 9 PXRD measurements of **a** DecPSQ, **b** DodecPSQ, and **c** OctPSQ at different temperatures

gel was transferred to the preparation of polyalkylsilsesquioxanes with methyl, ethyl, propyl, hexyl, octyl, decyl, dodecyl, hexadecyl, and octadecyl groups. Short-chain trimethoxysilanes (Me-Pr) showed a glassy and transparent appearance but no softening ability. On the other hand, long-chain PSQs (Hex-Dodec) were highly viscous at RT and indicated no significant increase in viscosity even after thermal treatment at 300 °C. Hexadec- and OctadecPSQs were white and waxy and formed reversibly transparent viscous liquids with increasing temperature. In both cases, high monomer content and low crosslinking were observed. The goal was to determine the structural difference of the various AlkylPSQs, even after a temperature treatment at 300 °C, compared with a softenable, phenyl groups containing material using spectroscopic, chromatographic, and thermal methods.

Overall, the role of the organic group in structure formation was shown to be crucial. Important factors include the steric hindrance and the increasing hydrophobic interactions with longer alkyl chains. Hydrolysis and condensation involve competition between the random condensation reaction and the self-assembling hydrophobic properties also observed in surfactants. There is an equilibrium between inter- and intramolecular condensation reactions, which depends on the size of the organic group.

Methyl, ethyl, and propyl groups exhibited mainly intramolecular condensations to an extended silsesquioxane network with a wide variety of silsesquioxane units due to the short chains with low steric hindrance and low hydrophobic interaction. The immediate change to a dense structure was the reason for the missing visible softening and solubility. In contrast, hydrophobic interactions as well as increased steric hindrance of long-chain alkyl groups (C_6, C_8) led to aggregation during synthesis revealing preferential intramolecular condensation reactions to form cage-like structural motifs and an overall high degree of condensation. This reaction was particularly favoured by thermally induced condensation reactions.

When the alkyl chain length was further increased (C_{10}, C_{12}, C_{16}, C_{18}), the self-assembling hydrophobic interactions resulted in the formation of lamellar layers. Dec- and DodecPSQ showed a phase transition upon lowering the temperature to −20 and 5 °C, while longer-chain AlkylPSQs (C_{16}, C_{18}) were already present in a waxy state at RT, demonstrating the formation of a semicrystalline material. It was shown that the transition was mainly favoured by the crystallisation of the alkyl chains. In contrast to the other materials obtained, the T_g characteristic of softenable polysilsesquioxanes could not be detected.

The results described lead to the conclusion that the choice of the organic group is crucial, to obtain a material that can be assigned to the melting gel family. Substituents that prefer self-assembly into cage structures or lamellar layers should be avoided. At the same time, substituents that exhibit increasing steric hindrance and form an incompletely cross-linked structure with stabilised residual OH and alkoxy groups are required.

Overall, the influence of alkyl chains of different lengths on the structure formation could be shown using different characterisation methods. As a result, the main characteristics that an organic group must have in order to produce a softenable material with temperature dependant thermosetting properties were established.

Acknowledgements Instrumentation and technical assistance for this work were provided by the Service Center X-ray Diffraction, with financial support from Saarland University and the German Science Foundation (project number INST 256/349-1). We thank Blandine Boßmann for recording and analysing the SEC measurements, Elias Gießelmann for SPE-MAS NMR measurements, and Dr. Oliver Janka for the support in the collection of low temperature PXRD diffraction data.

Author contributions Conceptualisation: SP and GK; Methodology: SP; Formal analysis and investigation: SP; Writing - original draft preparation: SP; Writing - review and editing: GK; Funding acquisition: GK; Resources: GK; Supervision: GK.

Funding Open Access funding enabled and organized by Projekt DEAL.

Compliance with ethical standards

Conflict of interest The authors declare no competing interests.

Publisher's note Springer Nature remains neutral with regard to jurisdictional claims in published maps and institutional affiliations.

References

1. Niemczyk A, Dziubek K, Sacher-Majewska B, Czaja K, Czech-Polak J, Oliwa R, Lenża J, Szołyga M (2018) Thermal stability and flame retardancy of polypropylene composites containing siloxane-silsesquioxane resins. Polymers 10(9):1019
2. Croissant JG, Fatieiev Y, Khashab NM (2017) Degradability and clearance of silicon, organosilica, silsesquioxane, silica mixed oxide, and mesoporous silica nanoparticles. Adv Mater 29(9):1604634
3. Hamada T, Sugimoto T, Maeda T, Katsura D, Mineoi S, Ohshita J (2022) Robust and transparent antifogging polysilsesquioxane film containing a hydroxy group. Langmuir 38(18):5829–5837

4. Lim Y, Park Y-S, Kang Y, Jang DY, Kim JH, Kim J-J, Sellinger A, Yoon DY (2011) Hole injection/transport materials derived from heck and sol−gel chemistry for application in solution-processed organic electronic devices. J Am Chem Soc 133(5):1375–1382
5. Su RQ, Müller TE, Procházka J, Lercher JA (2002) A new type of low-ϰ dielectric films based on polysilsesquioxanes. Adv Mater 14(19):1369–1373
6. Vadarevu H, Juneja R, Lyles Z, Vivero-Escoto JL (2021) Light-activated protoporphyrin IX-based polysilsesquioxane nanoparticles induce ferroptosis in melanoma cells. Nanomaterials 11(9):2324
7. Pescarmona PP, Maschmeyer T (2002) Oligomeric silsesquioxanes: synthesis, characterization and selected applications. Aust J Chem 54(10):583–596
8. Choi S-S, Lee AS, Hwang SS, Baek K-Y (2015) Structural control of fully condensed polysilsesquioxanes: ladderlike vs cage structured polyphenylsilsesquioxanes. Macromolecules 48:6063–6070
9. Ahmed N, Fan H, Dubois P, Zhang X, Fahad S, Aziz T, Wan J (2019) Nano-engineering and micromolecular science of polysilsesquioxane materials and their emerging applications. J Mater Chem A 7:21577–21604
10. Baney RH, Itoh M, Sakakibara A, Suzuki T (1995) Silsesquioxanes. Chem Rev 95:1409–1430
11. Masai H, Takahashi M, Tokuda Y, Yoko T (2005) Gel-melting method for preparation of organically modified siloxane low-melting glasses. J Mater Res 20:1234–1241
12. Yu D, Kleemeier M, Wu GM, Schartel B, Liu WQ, Hartwig A (2011) A low melting organic-inorganic glass and its effect on flame retardancy of clay/epoxy composites. Polymer 52:2120–2131
13. Klein LC, Al-Marzoki K, Jitianu A (2017) Phase separation in melting gels. Phys Chem Glasses Eur J Glass Sci Technol B 58(4):142–149
14. Klein LC, McClarren B, Jitianu A (2014) Silica-containing hybrid nanocomposite "melting gels". Mater Sci Forum 783-786:1432–1437
15. Jitianu A, Doyle J, Amatucci G, Klein LC (2008) Methyl-modified melting gels for hermetic barrier coatings. Proceedings MS&T 2008 enabling surface coating systems: multifunctional coatings, Pittsburgh, PA, pp 2171–2182
16. Briesenick M, Gallei M, Kickelbick G (2022) High-refractive-index polysiloxanes containing naphthyl and phenanthrenyl groups and their thermally cross-linked resins. Macromolecules 55(11):4675–4691
17. Kuniyoshi M, Takahashi M, Tokuda Y, Yoko T (2006) OH-free phenyl modified siloxane low-melting glasses with ultra low saturated water -absorption. J Ceram Soc Jpn 114(7):660–664
18. Pohl S, Janka O, Füglein E, Kickelbick G (2021) Thermoplastic silsesquioxane hybrid polymers with a local ladder-type structure. Macromolecules 54(8):3873–3885
19. Klein LC, Kallontzi S, Fabris L, Jitianu A, Ryan C, Aparicio M, Lei L, Singer JP (2019) Applications of melting gels. J Sol Gel Sci Technol 89:66–77
20. Jenkins S, Sciarrone E, Klein LC (2022) Texturing melting gels for water harvesting. J Sol Gel Sci Technol 101(1):37–45
21. Macan J, Tadanaga K, Tatsumisago M (2010) Influence of copolymerization with alkyltrialkoxysilanes on condensation and thermal behaviour of poly(phenylsilsesquioxane) particles. J Sol Gel Sci Technol 53(1):31–37
22. Parikh AN, Schivley MA, Koo E, Seshadri K, Aurentz D, Mueller K, Allara DL (1997) n-Alkylsiloxanes: from single monolayers to layered crystals. the formation of crystalline polymers from the hydrolysis of n-octadecyltrichlorosilane. J Am Chem Soc 119(13):3135–3143
23. Shen SK, Hu DD (2007) Fluorescent probe as reporter on the local structure and dynamics in hydrolysis-condensation process of organotrialkoxysilanes. J Phys Chem B 111:7963–7971
24. De Prado LASA, Torriani IL, Yoshida IVP (2010) Poly(n-alkylsilsesquioxane)s: synthesis, characterization, and modification with poly(dimethylsiloxane). J Polym Sci Part A Polym Chem 48:1220–1229
25. Chemtob A, Ni L, Croutxé-Barghorn C, Demarest A, Brendlé J, Vidal L, Rigolet S (2011) Self-organized poly(n-octadecylsilsesquioxane) films via sol–gel photopolymerization. Langmuir 27(20):12621–12629
26. Ni LL, Rigolet S, Chemtob A, Croutxe-Barghorn C, Brendle J, Vidal L (2013) Head-to-head and head-to-tail multilayer n-alkylsilsesquioxane films. C R Chim 16(10):897–905
27. Ke Q, Li G, Liu Y, He T, Li X-M (2010) Formation of superhydrophobic polymerized n-octadecylsiloxane nanosheets. Langmuir 26(5):3579–3584
28. Bourlinos AB, Chowdhury SR, Jiang DD, An Y-U, Zhang Q, Archer LA, Giannelis EP (2005) Layered organosilicate nanoparticles with liquidlike behavior. Small 1(1):80–82
29. Shimojima A, Sugahara Y, Kuroda K (1997) Inorganic-organic layered materials derived via the hydrolysis and polycondensation of trialkoxy(alkyl)silanes. Bull Chem Soc Jpn 70:2847–2853
30. Ni L, Chemtob A, Croutxé-Barghorn C, Brendlé J, Vidal L, Rigolet S (2012) Photoinduced synthesis and ordering of lamellar n-alkylsiloxane films. J Mater Chem 22(2):643–652
31. Andrianov KA, Izmaylov BA (1967) Hydrolytic polycondensation of higher alkyltrichlorosilanes. J Organomet Chem 8(3):435–441
32. Kim HJ, Lee JK, Kim JB, Park ES, Park SJ, Yoo DY, Yoon DY (2001) Substituent effects on microstructure and polymerization of polyalkylsilsesquioxanes. J Am Chem Soc 123:12121–12122
33. Matějka L, Dukh O, Hlavatá D, Meissner B, Brus J (2001) Cyclization and self-organization in polymerization of trialkoxysilanes. Macromolecules 34(20):6904–6914
34. Loy DA, Baugher BM, Baugher CR, Schneider DA, Rahimian K (2000) Substituent Effects on the Sol-Gel Chemistry of Organotrialkoxysilanes. Chem Mater 12:3624–3632
35. Kajihara K, Seto R, Kanamura K, Onodera Y, Kohara S (2019) Structure, microscopic ordering, and viscous properties of amorphous poly(n-alkylsilsesquioxane) liquids and solids synthesized by cosolvent-free hydrolytic polycondensation of n-Alkyltrimethoxysilanes. Phys Status Solidi A 216(3):1800475
36. Takahashi K, Tadanaga K, Hayashi A, Tatsumisago M (2011) Substituent effects on the glass transition phenomena of polyorganosilsesquioxane particles prepared by two-step acid–base catalyzed sol–gel process. J Ceram Soc Jpn 119(1387):173–179
37. MestReNova (2020), v14.2.0-26256, Mestrelab Research, S.L., Santiago de Compostela, Spain, https://mestrelab.com
38. Origin(Pro) (2020b), OriginLab Corporation, Northampton, MA, USA, https://www.originlab.com
39. PSS WinGPC® UniChrom 8.31 (2018), Polymer Standard Service, Mainz, Germany, https://www.pss-polymer.com
40. Topas 5 (2014), Bruker AXS, Karlsruhe, Germany, https://www.bruker.com
41. Anisimov AA, Polshchikova NV, Vysochinskaya YS, Zader PA, Nikiforova GG, Peregudov AS, Buzin MI, Shchegolikhina OI, Muzafarov AM (2019) Condensation of all-cis-tetraphenylcyclotetrasiloxanetetraol in ammonia: new method for preparation of ladder-like polyphenylsilsesquioxanes. Mendeleev Commun 29:421–423
42. Kowalewska A, Nowacka M, Makowski T (2015) Macroporous materials by self-assembly of linear oligo(phenylsilsesquioxanes). Express Polym Lett 9(11):984–1000
43. El Aziz Y, Bassindale AR, Taylor PG, Stephenson RA, Hursthouse MB, Harrington RW, Clegg W (2013) X-ray crystal structures, packing behavior, and thermal stability studies of a homologous series of n -alkyl-substituted polyhedral oligomeric silsesquioxanes. Macromolecules 46:988–1001

44. Fina A, Tabuani D, Carniato F, Frache A, Boccaleri E, Camino G (2006) Polyhedral oligomeric silsesquioxanes (POSS) thermal degradation. Thermochim Acta 440:36–42
45. Mutin PH (2002) Role of redistribution reactions in the polymer route to silicon–carbon–oxygen ceramics. J Am Ceram Soc 85(5):1185–1189
46. Bolln C, Tsuchida A, Frey H, Mülhaupt R (1997) Thermal properties of the homologous series of 8-fold alkyl-substituted octasilsesquioxanes. Chem Mater 9(6):1475–1479
47. Mantz RA, Jones PF, Chaffee KP, Lichtenhan JD, Gilman JW, Ismail IMK, Burmeister MJ (1996) Thermolysis of polyhedral oligomeric silsesquioxane (POSS) macromers and POSS−siloxane copolymers. Chem Mater 8(6):1250–1259
48. Schneider O (1988) Thermoanalytical investigations on curing and decomposition of methyl silicone resin. Thermochim Acta 134:269–274
49. Kurumada K-I, Ashraf KM, Matsumoto S (2014) Effects of heat treatment on various properties of organic–inorganic hybrid silica derived from phenyltriethoxysilane. Mater Chem Phys 144(1):132–138
50. Haußmann M, Reznik B, Bockhorn H, Denev JA (2011) Thermal degradation of polymethylsilsesquioxane and microstructure of the derived glasses. J Anal Appl Pyrolysis 91(1):224–231
51. Stutz H, Illers K-H, Mertes J (1990) A generalized theory for the glass transition temperature of crosslinked and uncrosslinked polymers. J Polym Sci Part B Polym 28(9):1483–1498
52. Allcock HR, Connolly MS, Sisko JT, Al-Shali S (1988) Effects of organic side group structures on the properties of poly(organophosphazenes). Macromolecules 21(2):323–334
53. Turetskii A, Out GJJ, Klok H-A, Möller M (1995) Structural transformations in poly(di-n-alkylsiloxane)s with alkyl side groups containing 7 to 10 carbon atoms. Polymer 36(6):1303–1308
54. Fujii K, Fujita T, Iyi N, Kodama H, Kitamura K, Yamagishi A (2003) Synthesis of 2-dimensional inorganic/organic hybrid polymers: Novel meltable layered alkylsiloxanes. J Mater Sci Lett 22(20):1459–1461
55. Perera HJ, Latifi R, Blum FD (2019) Development of structure in hexadecyltrimethoxysilane adsorbed on silica. J Phys Chem C 123(31):19005–19012
56. Wallace WE, Guttman CM, Antonucci JM (2000) Polymeric silsesquioxanes: degree-of-intramolecular-condensation measured by mass spectrometry. Polymer 41(6):2219–2226
57. Sato Y, Hayami R, Gunji T (2022) Characterization of NMR, IR, and Raman spectra for siloxanes and silsesquioxanes: a mini review. J Sol Gel Sci Technol 104(1):36–52
58. Warring SL, Beattie DA, McQuillan AJ (2016) Surficial siloxane-to-silanol interconversion during room-temperature hydration/dehydration of amorphous silica films observed by ATR-IR and TIR-Raman Spectroscopy. Langmuir 32(6):1568–1576
59. Baatti A, Erchiqui F, Bébin P, Godard F, Bussières D (2017) A two-step Sol-Gel method to synthesize a ladder polymethylsilsesquioxane nanoparticles. Adv Powder Technol 28(3):1038–1046
60. Park ES, Ro HW, Nguyen CV, Jaffe RL, Yoon DY (2008) Infrared spectroscopy study of microstructures of poly(silsesquioxane)s. Chem Mater 20:1548–1554
61. Wang R, Baran G, Wunder SL (2000) Packing and thermal stability of polyoctadecylsiloxane compared with octadecylsilane monolayers. Langmuir 16(15):6298–6305
62. Echeverría JC, Moriones P, Arzamendi G, Garrido JJ, Gil MJ, Cornejo A, Martínez-Merino V (2018) Kinetics of the acid-catalyzed hydrolysis of tetraethoxysilane (TEOS) by 29Si NMR spectroscopy and mathematical modeling. J Sol Gel Sci Technol 86:316–328
63. Xu X, Wu C, Zhang B, Dong H (2013) Preparation, structure characterization, and thermal performance of phenyl-modified MQ silicone resins. J Appl Polym Sci 128(6):4189–4200
64. Lee AS, Choi S-S, Baek K-Y, Hwang SS (2016) Hydrolysis kinetics of a sol-gel equilibrium yielding ladder-like polysilsesquioxanes. Inorg Chem Commun 73:7–11
65. Ni L, Moreau N, Chemtob A, Croutxé-Barghorn C (2012) Organic–inorganic tandem route to polymer nanocomposites: kinetic products versus thermodynamic products. J Sol Gel Sci Technol 64(2):500–509
66. Rikowski E, Marsmann HC (1997) Cage-rearrangement of silsesquioxanes. Polyhedron 16(19):3357–3361
67. Hamada T, Goto T, Takase S, Okada K, Uedono A, Ohshita J (2022) Structure–thermal property relationships of polysilsesquioxanes for thermal insulation materials. ACS Appl Polym Mater 4(4):2851–2859
68. Wang J, Xin Z (2012) Synthesis and characterization of polymethylsilsesquioxane microspheres by the two-step sol-gel method. e-Polymers 12:046
69. Meng G, Li Y, Wang Z, Pan C, Gao W, Cheng Y (2021) Preparation and characterization of narrow size distribution PMSQ microspheres for high-frequency electronic packaging. Materials 14(15):4233
70. Papkov VL, Gerasimov MV, Buzin M, Il'ina MN, Kazaryan LG (1996) The structure of ordered phases in polydiphenylsiloxane. Polym Sci A 38:1097–1102
71. Xinsheng Z, Lianghe S, Chaoran H (1987) More on the structures of polyphenylsilsesquioxanes. Chin J Polym Sci 5:353–358
72. Prado LASDA, Radovanovic E, Pastore HO, Yoshida IVP, Torriani IL (2000) Poly(phenylsilsesquioxane)s: structural and morphological characterization. J Polym Sci Part A Polym Chem 38(9):1580–1589
73. Liu C, Liu Y, Shen Z, Xie P, Zhang R, Yang J, Bai F (2001) Study of the steric tacticity of novel soluble ladderlike poly (phenylsilsesquioxane) prepared by stepwise coupling polymerization. Macromol Chem Phys 202:1581–1585

4.3 Impact of Size and Substitution Isomerism in Polycyclic Aromatic-Substituted Trialkoxysilanes on the Formation of Softenable Polysilsesquioxanes

Published as an article:

Svenja Pohl, Markus Gallei, Guido Kickelbick, *Macromolecules* ***2025***, *58 (3), 1298-1313. DOI: 10.1021/acs.macromol.4c02737*.

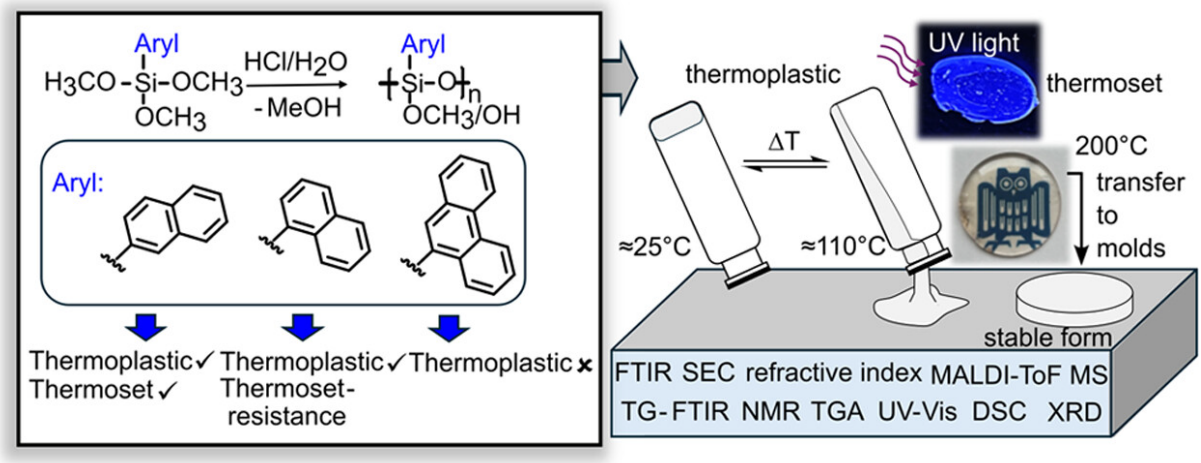

The supporting information is provided in Chapter 7 and is available online at: *https://doi.org/10.1021/acs.macromol.4c02737*.

The author's contribution to this work amounts to 80%.

Detailed statement of the individual contributions of the author and co-authors:

Svenja Pohl prepared the complete draft of the manuscript, which was reviewed and approved by all co-authors. She performed the synthesis and characterization of the polysilsesquioxanes and was responsible for the interpretation of the results. Prof. Dr.-Ing. Markus Gallei facilitated access to SEC and MALDI-ToF MS measurements, supported data interpretation, and contributed to the final revision of the manuscript. Prof. Dr. Guido Kickelbick gave the input to this project, provided scientific guidance and supervision, and revised the manuscript to its final version.

Previous studies have shown that aromatic groups play a central role in the formation of melting gel behavior. While phenyl substituents have proven to be highly suitable for producing thermoplastically deformable materials that subsequently cure irreversibly, *n*-alkyl groups are far less effective in this regard. Based on this observation, the question arises as to how polycyclic aromatic substituents, particularly their molecular size and substitution pattern, influence the structure and processing behavior of silsesquioxanes. Although naphthyl and phenanthrenyl groups have already been studied in copolymeric polysiloxane systems, where they demonstrated melting gel-like behavior, such investigations have so far been lacking for pure silsesquioxane systems.

The publication *"Impact of Size and Substitution Isomerism in Polycyclic Aromatic-Substituted Trialkoxysilanes on the Formation of Softenable Polysilsesquioxanes"* systematically explores the influence of both the size of the aromatic system and the substitution pattern in silsesquioxanes. For this purpose, 1-naphthyl-, 2-naphthyl-, and 9-phenanthrenyltrimethoxysilanes were polymerized under acid-catalyzed, solvent-free conditions. The resulting materials were comprehensively characterized with respect to their structural and thermal properties using NMR, FTIR, MALDI-ToF MS, SEC, fluorescence spectroscopy, and PXRD.

The study demonstrates that the nature of the organic substituent has a decisive influence on the resulting network structure as well as on the thermoplastic and thermosetting behavior. Both 1-naphthyl- and 2-naphthyl-substituted polysilsesquioxanes form transparent, glass-like materials with a high RI of approximately 1.61, characteristic fluorescence, and high thermal stability up to about 460 °C. While both materials can be reversibly softened, only the 2-naphthyl-derived polymer undergoes irreversible curing at 200 °C, similar to classical phenyl-based melting gels. In contrast, the 1-naphthyl-based material remains softenable even after thermal treatment. This behavior arises from structural effects of the substitution isomerism: the sterically more demanding 1-naphthyl group reduces the overall degree of condensation and stabilizes residual methoxy and silanol groups, thereby hindering the formation of an extended cross-linked network and preserving flow behavior.

A further enlargement of the aromatic system to the 9-phenanthrenyl substituent results in predominantly intramolecular condensation reactions, leading to isolated, cage-like silsesquioxane structures. The combination of extended aromaticity and restricted segmental mobility yields a rigid, brittle solid that exhibits neither flowability nor processability.

The results demonstrate that an increase in aromatic ring size can, in principle, promote melting gel-like behavior; however, excessive steric congestion and molecular rigidity ultimately hinder processability.

Overall, the study deepens the understanding of the structural prerequisites for the formation of softenable polysilsesquioxanes and demonstrates that the network architecture can be deliberately tailored by varying the polycyclic aromatic substituent. This strategy broadens the portfolio of functional silsesquioxanes exhibiting enhanced optical and thermal properties.

Macromolecules

pubs.acs.org/Macromolecules
Article

Impact of Size and Substitution Isomerism in Polycyclic Aromatic-Substituted Trialkoxysilanes on the Formation of Softenable Polysilsesquioxanes

Svenja Pohl, Markus Gallei, and Guido Kickelbick*

Cite This: Macromolecules 2025, 58, 1298−1313

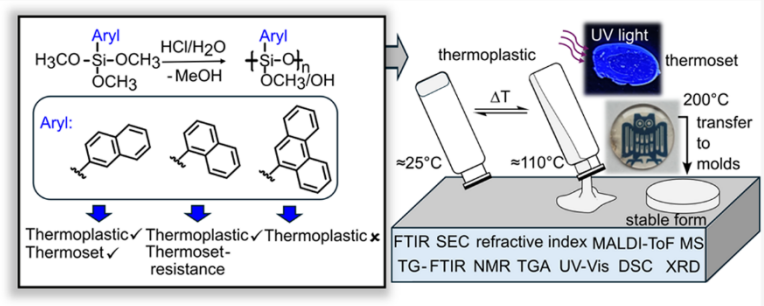

ABSTRACT: Polyphenylsilsesquioxanes are known to form glassy materials that can reversibly soften when heated above their glass transition temperature, with irreversible curing occurring upon a further temperature increase. In this study, the effects of the size and isomerism of polycyclic aromatic groups on the synthesis and structure of polysilsesquioxanes are investigated, with a focus on their thermoplastic and thermoset properties. Polysilsesquioxanes were synthesized by acid-catalyzed polycondensation using 1-naphthyl, 2-naphthyl, and 9-phenanthrenyltrimethoxysilanes. Characterization techniques, including spectroscopy, thermal analysis, mass determination, and powder X-ray diffraction, showed that steric hindrance by the aromatic groups significantly affects the degree of condensation, the formation of OH groups, and the nature of intra- or intermolecular condensation. Bulky phenanthrenyl groups hinder chain mobility and prevent detectable flow behavior, while 1- and 2-naphthyl groups enable the formation of thermoplastic materials with reversible softening. Notably, 2-naphthylsilsesquioxane undergoes irreversible curing at 200 °C, whereas 1-naphthylsilsesquioxane resists this transition. The incorporation of both polycyclic substituents not only preserves the characteristic thermoplastic behavior of melting gels but also introduces additional properties, such as fluorescence, a high thermal stability up to 460 °C and a high refractive index of 1.61, enhancing the potential of these materials for optical applications.

INTRODUCTION

Polysilsesquioxanes $(RSiO_{1.5})_n$ exhibit an inorganic−organic hybrid composition consisting of an inorganic Si−O−Si backbone in which each Si atom is covalently bonded to three oxygen atoms and one organic substituent. This combination of functions imparts versatile properties to this class of compounds, including excellent heat stability, flame retardancy, resistance to environmental influences, ultralow dielectric constant, favorable mechanical properties, or biocompatibility.[1−4] Synthesis typically involves acid- or base-catalyzed hydrolysis and condensation reactions with organotrialkoxy- or organotrichlorosilanes.[5] The resulting structure varies depending on synthesis conditions such as temperature, monomer concentration, water content, pH value, and organic substituent nature, leading to ladder-like structures, open and closed cages, or random networks.[6,7]

A special material containing polyorganosilsesquioxanes was described from Masai et al. to provide an alternative to lead-containing low-melting glasses.[8] The ability to exhibit a defined glass transition temperature (T_g),[9−11] above which the polysilsesquioxane shows reflow behavior, i.e., it becomes flowable and moldable, has been used to produce transparent, hard, and glass-like thermoplastics. Although the materials did not show melting in the conventional sense and feature an amorphous structure, the term "melting gel" was established. Melting gels are produced from trialkoxysilanes or from a mixture of di- and trialkoxysilane, mostly with methyl and/or phenyl groups as organic substituents.[12] Most of them are hard and glass-like at room temperature and can be reversibly

Received: November 6, 2024
Revised: January 6, 2025
Accepted: January 20, 2025
Published: February 3, 2025

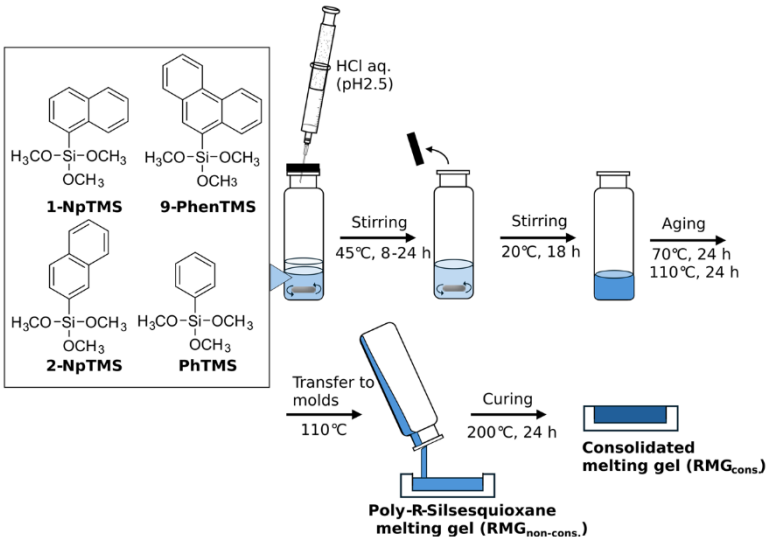

Figure 1. Scheme of the melting gel synthesis and structure of used trimethoxysilanes (TMS) with different aromatic substituents.

softened at around 110 °C. In this softened state, the material shows good processability similar to thermoplastics. At a consolidation temperature of ≥130 °C, melting gels cure irreversibly, and the resulting transparent, glassy material is neither softenable nor soluble. By varying the composition and type of monomers, the T_g, the viscosity, the consolidation temperature, and the refractive index can be adjusted.[13−16] These properties, as well as high thermal stability,[17] hydrophobic surface,[18,19] low gas permeability,[20] and transparency in a wide wavelength range,[15,21] make the materials interesting as hermetic barrier,[20] anticorrosive coatings,[22] for imprinted lithography,[23] in the field of water harvesting,[24] and for optoelectronic applications.[25,26]

When considering a softenable phenylsilsesquioxane as a model system for melting gels, the precursor gel is primarily composed of smaller oligomeric units, arranged in a random structure with partially ladder-like domains.[27] Stable OH and alkoxy groups (OR) interacting via H-bridges, as well as intra- and intermolecular $\pi-\pi$-interactions of the phenyl groups, result in the extraordinary hardness, as well as the thermoplastic properties up to 110 °C. An increase in temperature results in condensation reactions of the interacting OH and OR groups and a reorientation of the structure to an increased number of ladder-like domains and a highly cross-linked material. Due to the high degree of cross-linking, no further softening of the material is possible.

Depending on the organic substituent, organotrialkoxysilanes show differences in their tendency to condense to softenable polysilsesquioxanes. *N*-alkyl chains as organic groups lead, according to the chain length, to highly cross-linked, insoluble solids, viscous oils, and even semicrystalline layered structures.[28] Only together with a comonomer like phenyl or methyltrialkoxysilane, *n*-alkyl substituents result in glass-like thermoplastics.[20,29−31] Recently, a poly(cyclohexyl)-silsesquioxane was described to form a stiff, transparent, softenable material.[21] In contrast to the conventional melting gels, it showed resistance to thermal curing, even after 6 h at 200 °C, which the authors attribute to the large steric hindrance of the cyclohexyl groups, preventing polycondensation between remaining Si−OH groups. A thermoset resistance of up to 300 °C was also observed by the incorporation of benzyl groups in silsesquioxanes.[10,32] A further extension of the spacer between benzene and the siloxane backbone to the phenethyl group resulted in a viscous oil at room temperature.[33] The steric and electronic effects of the organic group seem to play an essential role in the formed structure and the softening and curing behavior of polysilsesquioxanes.

Since our group has previously shown that aromatic groups favor the formation of silanols[34,35] and that these seem to be a prerequisite for the formation of melting gels, we are interested in investigating the influence of the steric limits of aromatic substituents in polysilsesquioxanes and the formation of polymers with softening properties.

Aromatic compounds were mainly added to polysiloxanes in order to increase the refractive index for optoelectronic applications.[26,36−38] An influence of the type of the polycyclic group was also observed, both in the condensation tendency and in the fluorescence behavior.[26] The influence of polycyclic aromatic rings on the synthesis and structure of polysilsesquioxanes with no added comonomers has not yet been investigated in detail. We have recently shown that 1-naphthyltrimethoxysilane leads to softenable materials in a solvent-free, acid-catalyzed polycondensation reaction.[27] In the present study, we systematically investigated the influence of the isomerism and the size of the aromatic group on the hydrolysis and condensation behavior and consequently on the structure of the polysilsesquioxane as well as on resulting optical and thermal properties. Our aim is to extend the spectrum of melting gels by integrating further building blocks to add properties such as fluorescence or a high refractive index, which are associated with the incorporation of polycyclic aromatic compounds. Therefore, we condensed 1- and 2-naphthyltrimetoxysilane, as well as 9-phenanthrenyltrimethoxysilane via an acid-catalyzed polycondensation reaction analogous to a synthesis of a polyphenylsilsesquioxane melting gel (PhMG) described previously,[27] with the goal of forming aryl melting gels with polycyclic groups (Figure 1). The resulting structures were analyzed both after synthesis and after thermal treatment at 200 °C via nuclear magnetic resonance (NMR) spectroscopy, Fourier transform infrared (FTIR) spectroscopy, differential scanning calorimetry (DSC), thermogravimetric analysis (TGA), fluorescence spectroscopy, size

https://doi.org/10.1021/acs.macromol.4c02737
Macromolecules 2025, 58, 1298−1313

exclusion chromatography (SEC), matrix-assisted laser desorption/ionization time-of-flight mass spectrometry (MALDI-ToF MS), and powder X-ray diffraction (PXRD).

EXPERIMENTAL SECTION

This section provides a description of the most important syntheses only; additional details on synthesis and characterization are available in the Supporting Information (SI).

Melting Gel Synthesis. The melting gels were prepared according to a modified previously described synthesis.[27]

Naphthyl Melting Gel (NpMG). 1-Naphthyltrimethoxysilane (2-naphthyltrimethoxysilane) (2 g, 8 mmol, 1 equiv) was stirred with aqueous HCl, pH 2.5 (0.217 mL, 1.5 equiv related to H_2O) in a 20 mL sealed headspace vial at 45 °C for 8−24 h (600 rpm), until a homogenization of the two-phase mixture was visible. Afterward, the lid of the vessel was opened, and a significant increase in viscosity was observed over a stirring period of 18 h at room temperature. The byproducts, water and methanol, of the polycondensation reaction were subsequently removed by oven treatment at 70 and 110 °C for 24 h each, resulting in a transparent, glassy material at room temperature, which can be reversibly softened at 110 °C.

9-Phenanthrenyl Melting Gel (9-PhenMG). 9-Phenanthrenyltrimethoxysilane (0.3 g, 1 mmol, 1 equiv) was dissolved in acetone (2 mL) and stirred with aqueous HCl, pH 2.5 (0.168 mL, 3 equiv related to H_2O) in a 20 mL sealed headspace vial at 45 °C for 24 h (600 rpm). Afterward, the lid of the vessel was opened, and the solvent was allowed to evaporate over a stirring period of 18 h at 45 °C. The byproducts, water and methanol, of the polycondensation reaction were subsequently removed from the gel by oven treatment at 70 and 110 °C for 24 h each, resulting in a yellowish, brittle solid.

Melting Gel Consolidation. For consolidation, the precursor gels were treated on Teflon plates at 200 °C for 24 h in a compartment dryer. The rigidity of the samples was tested at 200 °C by using a spatula. The material was cured as soon as no deformation could be detected under pressure.

RESULTS AND DISCUSSION

Synthesis and Appearance of Melting Gels. A one-step acid-catalyzed method was employed to synthesize melting gels using 1-naphthyl, 2-naphthyl, and 9-phenanthrenyltrimethoxysilane (Figure 1). Liquid aryltrialkoxysilanes initially form a biphasic mixture with aqueous acid, which homogenizes through partial hydrolysis and condensation, producing methanol as a byproduct. Homogenization of $PhSi(OCH_3)_3$ as monomer was reported to occur after approximately 6 min,[27] while 1-naphthyl- and 2-naphthyltrimethoxysilane investigated in this study required significantly more time to exhibit a visible reaction. The 1-$NpSi(OCH_3)_3$ initially showed turbidity and yielded a clear liquid after about 4−6 h (the exact time is highly dependent on stirring speed and the size of the reaction vessel). In contrast, 2-$NpSi(OCH_3)_3$ precipitated a white solid within the first 2 h, becoming homogeneous after about 6−24 h. The white solid could be isolated, and 2-$NpSi(OH)_3$ was identified as an intermediate in the reaction (Figures S4−S6). Contrary 1-$NpSi(OCH_3)_3$ formed no stable, isolable silanol, suggesting that it immediately condenses after hydrolysis.

After gelation and drying at 110 °C for 24 h, both naphthyl-containing samples resulted in glass-like, hard, and transparent materials, which exhibited viscous flow at 110 °C (Figure 2). Lenses prepared with a thickness of 1.6 mm showed transmission of 86% and 88% at 450 nm (Figure S7) and a high refractive index of 1.6152 and 1.6096 at 589 nm for 1-NpMG and 2-NpMG (Figure S8), respectively, due to the large number of delocalized π-electrons and the high polarizability of the naphthyl groups.[26,36,39]

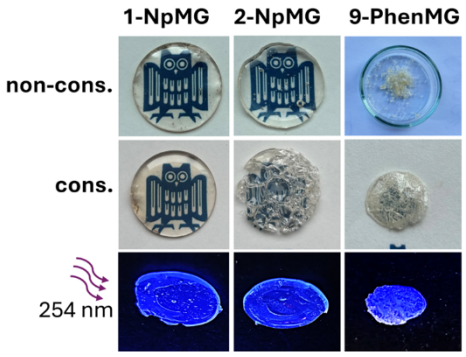

Figure 2. Images of non-consolidated and consolidated 1-NpMG, 2-NpMG, and 9-PhenMG under daylight and UV light (254 nm).

In contrast to the naphthylalkoxysilanes, the 9-phenanthrenyltrimethoxysilane is solid and was therefore dissolved in acetone as the solvent is known to successfully lead to hydrolysis of 9-phenanthrenyltriethoxysilane.[38] Under the standard conditions (1.5 equiv of H_2O, pH 2.5), no reaction of the monomer could be detected. Only by doubling the amount of water, a yellowish, hard, and brittle material was formed, indicating a successful polycondensation reaction. Softening at 110 °C could not be detected visually. As the temperature increased further, a slight flow of the resulting solid could be observed. The increase in the size of the aromatic system and the associated higher polarizability of the electrons resulted in a higher refractive index of 1.6476.

The known phenyl-containing melting gels exhibit not only thermoplastic properties at 110 °C but also thermoset behavior when treated at temperatures >130 °C. For this reason, all arylsilsesquioxanes produced were treated thermally at 200 °C for 24 h in order to induce further condensation reactions and further cross-linking. All materials exhibited a distinct yellow coloration [1-NpMG lenses showed a decrease in transmission to 64% at 450 nm (Figure S7)] after the temperature treatment.

Permanent hardening was observed in the 2-NpMG after 24 h when it was reheated to 200 °C. The absence of reflow properties was confirmed by bubbles remaining on the surface of the material, which were formed by the degassing of the byproducts, water and methanol (Figure 2). The material was also found to be insoluble in conventional solvents after curing, suggesting the formation of a macroscopic silica network.[40] The 9-PhenMG underwent permanent curing after the additional thermal treatment, but it remained soluble in conventional solvents, unlike the 2-NpMG. The 1-NpMG, on the other hand, remained soluble and remeltable, showing resistance to thermally induced curing. Although not all samples are cured completely, they are labeled as consolidated (cons.) in the following to illustrate a similar thermal treatment to the phenyl melting gel.

The different reactivities during the synthesis as well as the varying softening and curing behaviors demonstrate that the size and the isomerism of the organic group have a crucial influence on the structure and properties of polysilsesquioxanes. The different characteristics of the produced melting gels will be investigated in the following by using spectroscopic and thermogravimetric methods as well as SEC, MALDI-ToF mass spectrometry, and XRD.

https://doi.org/10.1021/acs.macromol.4c02737
Macromolecules 2025, 58, 1298−1313

Analysis of Melting Gel Softening via Glass Transition Determination. The glass-like behavior of both NpMGs and 9-PhenMG in the consolidated and non-consolidated states was analyzed using DSC. The phenyl melting gel, used as a comparison, exhibited a T_g of about 60 °C. This temperature remained constant across several heating cycles up to 110 °C, highlighting its reversible softening behavior within this range.[27] After consolidation, the T_g was no longer detectable, suggesting the formation of a three-dimensional network and the loss of reflow behavior.[8]

The T_g is directly related to the mobility of the polymer chains, which is influenced by factors such as cross-linking, the presence of hydroxy groups, and the nature of organic substituents.[41−43] As a result, T_g serves as an important indicator for assessing changes in the degree of cross-linking due to temperature-induced condensation reactions. The 1- and 2-naphthyl melting gels exhibit a T_g of around 50 and 40 °C, respectively (Figure 3), while the 9-PhenMG shows a

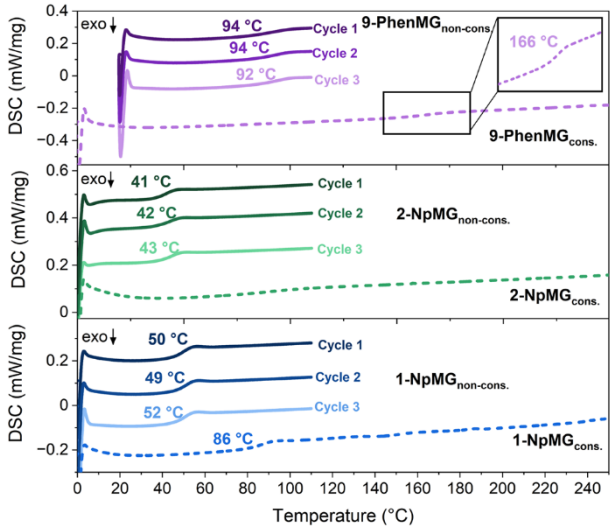

Figure 3. DSC measurement of non-consolidated and consolidated 1-Np-, 2-Np-, and 9-PhenMG, including determination of the T_g. Testing the reversible softening of the non-consolidated samples over three cycles up to 110 °C and monitoring the softening behavior of the consolidated samples in the range of 0−250 °C.

significantly higher value of 94 °C. All non-consolidated materials maintained stable glass transition temperatures across multiple heating cycles up to 110 °C, indicating that no structural changes occurred during this thermal treatment. The observed shift in softening to higher temperatures with increasing steric demand of the aromatic groups can be attributed to a reduction in intersegmental free volume, which consequently decreases chain mobility.[26,44]

However, cross-linking density also plays a crucial role. Despite having the smallest aromatic group, PhMG exhibits a T_g value higher than that of both 1- and 2-NpMG, indicating lower chain mobility due to a denser network, as highlighted in the NMR analysis.

After thermal treatment at 200 °C, the T_g increases by approximately 30 °C for 1-NpMG and 70 °C for 9-PhenMG, reflecting enhanced cross-linking. However, a complete disappearance of T_g is not observed, suggesting the absence of a macroscopic network for both samples. In 1-NpMG, it is reflected by the retention of visible flow properties after thermal treatment. 9-PhenMG shows no flow behavior despite the presence of a T_g, which is due to the larger conjugated system with increased $\pi-\pi$ interactions and greater steric hindrance, whereby the movement of the polymer chains can also be hindered above the T_g.

In contrast, 2-NpMG exhibits only a slight increase in heat flow without a defined glass transition point, suggesting the formation of a three-dimensional network similar to that of PhMG. This finding aligns with visual and tactile observations, indicating that 2-NpMG is fully thermally cured.

Structural Characterization. *NMR Spectroscopy.* ^{1}H NMR spectroscopy was employed to identify the organic substituents and to quantify the remaining nonhydrolyzed methoxy (OMe) groups, providing insights into the hydrolysis tendency of the monomer. Integration of the OMe groups relative to the aryl groups revealed that nonhydrolyzed groups remained intact in both naphthyl gels (Figures S9 and S10). The hydrolysis tendency, compared to that of PhMG, can be described in the following order: Ph > 2-Np > 1-Np, with 10, 13, and 19% remaining OMe groups (Figure 4a). Subsequent treatment at 200 °C resulted in further reduction of alkoxy groups in the naphthyl melting gels by further hydrolysis or condensation between the methoxy and hydroxy groups, visible in ^{1}H NMR and ^{13}C cross-polarization magic-angle-spinning (CP-MAS) NMR spectra (Figures S11 and 4b).

In contrast, 9-PhenMG shows almost complete hydrolysis of all methoxy groups, along with residues of acetone (Figure 4b), which can be attributed to the altered reaction conditions (higher water content, reaction in solvent). Furthermore, free phenanthrene was found via ^{1}H NMR, as evidenced by sharp peaks in the aromatic region between 8.8 and 7.0 ppm, which are unusual for condensed polysilsesquioxanes (Figures S12 and S13). Si−C bond cleavage is a known phenomenon in the polycondensation of organosilica hybrids, as reported in the literature. It has been observed during the thermal condensation of diarylsilanediols,[35,45] whereby the stability of silanols decreased with increasing size of the aromatic compound.[46] The catalyzing effect of acid or base supports the cleavage, leading to the conclusion that the low Si-Phen bond stability, the acidic environment, and the increased water content cause partial Si−C bond cleavage in 9-PhenMG.

To investigate the local silicon environment, solid-state and liquid ^{29}Si NMR spectra were collected (Figure 4c,d). Since only organotrimethoxysilanes were involved, species with one direct silicon−carbon bond (T^n) are expected. Depending on the cross-linking, the chemical shift decreases with each added O−Si segment, marked with a superscript (T^0, T^1, T^2, T^3).[47] None of the samples showed a T^0 peak, indicating the complete conversion of the monomers. Instead, T^1, T^2, and T^3 units are visible in all precursor gels in varying intensities, confirming the successful condensation reaction and highlighting variations in cross-linking density among the samples. Due to the detected Si−C bond cleavage in both the non-consolidated and consolidated 9-PhenMG, quaternary silicon (Q^n) is expected in addition to T species. However, no signal was observed in the typical Q^1-Q^4 range between 85 and 110 ppm,[48] in either liquid or solid-state NMR. This absence is attributed to a low signal-to-noise ratio combined with a low concentration of Q units.

Due to the high number of varying oligomers or polymers with different chemical environments, partially condensed silsesquioxanes often give broad, ill-defined peaks that extend over a wide ppm range.[49] For example, 1-NpMG shows

https://doi.org/10.1021/acs.macromol.4c02737
Macromolecules 2025, 58, 1298−1313

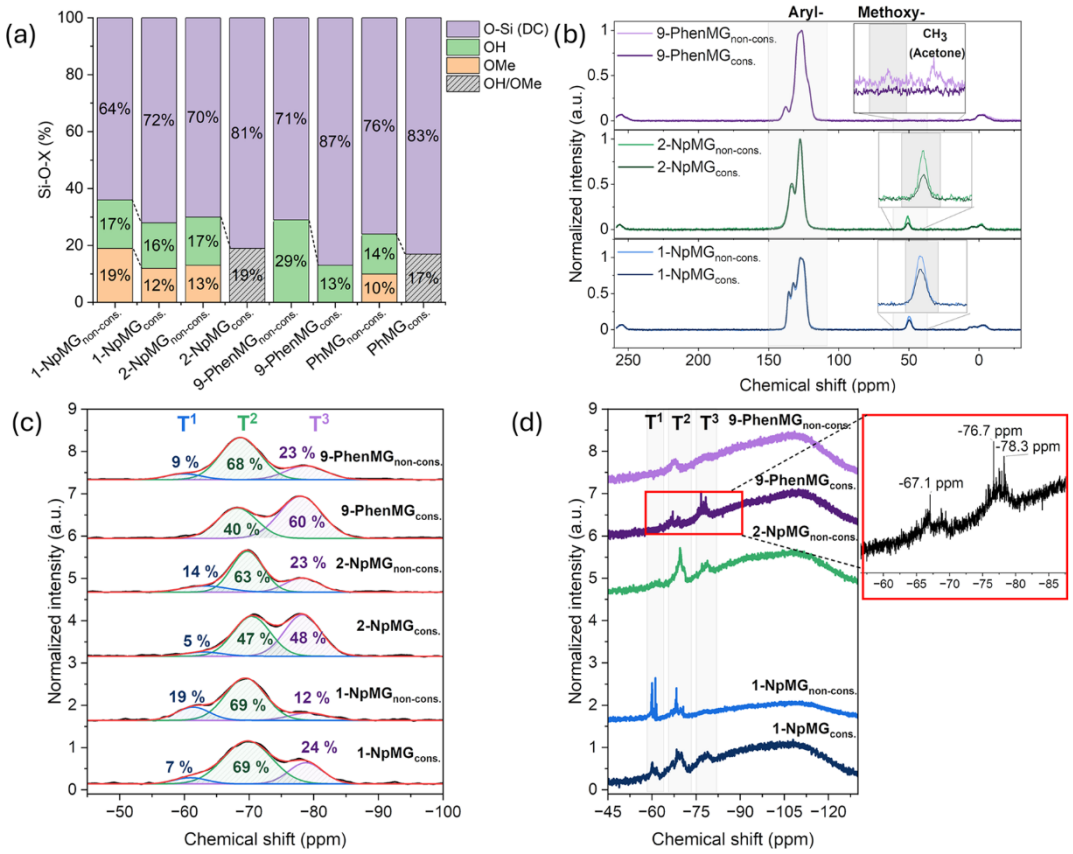

Figure 4. (a) Percentage of OH groups, OMe groups, and the degree of condensation (DC) of consolidated and non-consolidated 1-Np-, 2-Np-, 9-Phen-, and PhMG. PhMG values were taken from the literature.[27] The DC was calculated using deconvoluted ^{29}Si CP-MAS NMR according to the formula: DC (%) = (T^3 (%)·3 + T^2 (%)·2 + T^1 (%))/3. OH group percentages were derived from OMe group amounts, determined from ^{1}H NMR using the formula: OH (%) = 100 (%) − DC (%) − OMe (%), (b) ^{13}C CP-MAS NMR of consolidated and non-consolidated melting gels, with a zoom of the region of residual OMe groups, (c) ^{29}Si CP-MAS NMR of consolidated and non-consolidated melting gels, fitted with a Gaussian function, showing T^1, T^2, and T^3 percentages based on integral calculations, (d) liquid ^{29}Si NMR in $CDCl_3$ of consolidated and non-consolidated melting gels, with peak assignment for 9-PhenMG$_{cons.}$.

individual peaks in the area of T^1 and T^2 before consolidation, indicating oligomeric units in an early stage of condensation (Figure 4d).[50] Thermal treatment, which increases cross-linking and molecular mass, results in peak broadening and an increase in T^2 and T^3. 9-PhenMG, on the other hand, exhibits the opposite behavior. After consolidation, individual peaks appear in the T^2 and T^3 regions. This observation suggests that thermal treatment causes a reduction in the diversity of silsesquioxane species, leading to more ordered structures, such as cage-like forms.[51]

The amount of T^n species and the degree of condensation can be determined semiquantitatively by deconvolution and integration of the ^{29}Si CP-MAS NMR spectra (Figure S14). Since cross-polarized measurements depend on both the distance and the amount of protons, the population of individual silicon species is often not accurately represented.[52,53] Given the large number of protons in the sample due to aryl groups, one can assume that the proton density is homogeneously distributed throughout the sample. This homogeneity minimizes errors in the relative quantification of the different T species and enables reliable trends in the degree of condensation to be observed [^{29}Si SP-MAS and ^{29}Si CP-MAS NMR spectra for 2-NpMG$_{cons}$ showed very similar spectra (Figure S15)].[54]

The degree of condensation (DC) shows the same tendency as the hydrolysis rate. With increasing steric demand of the organic group, the DC decreases in the order Ph > 2-Np > 1-Np (Figure 4a). Due to the changed reaction conditions, 9-PhenMG does not follow this trend and shows a similar DC to 2-NpMG with a value of 71%. After thermal treatment, all melting gels exhibit a significant increase in T^3 species and a decrease in T^1, reflecting a marked increase in the number of cross-linked units. By subtracting the amount of bonded Si−O units (using DC value) and the amount of OMe groups obtained from the ^{1}H spectra, from the total amount of theoretically cross-linkable units, it becomes evident that OH groups remain in all samples, even after thermal treatment (Figure 4a). This persistence can be attributed to the aromatic groups, which sterically protect and hinder the remaining OH groups from participating in further thermally induced condensation reactions.

Overall, the NMR spectroscopic investigation demonstrates a significantly reduced hydrolysis and condensation tendency for 1-NpMG compared to 2-NpMG. Due to the same electronic situation, this behavior can be attributed to steric influences. Binding in the α-position results in a greater inhibition of attack by water or a Si−OH group compared to the β-position, resulting in a lower degree of condensation.

https://doi.org/10.1021/acs.macromol.4c02737
Macromolecules 2025, 58, 1298−1313

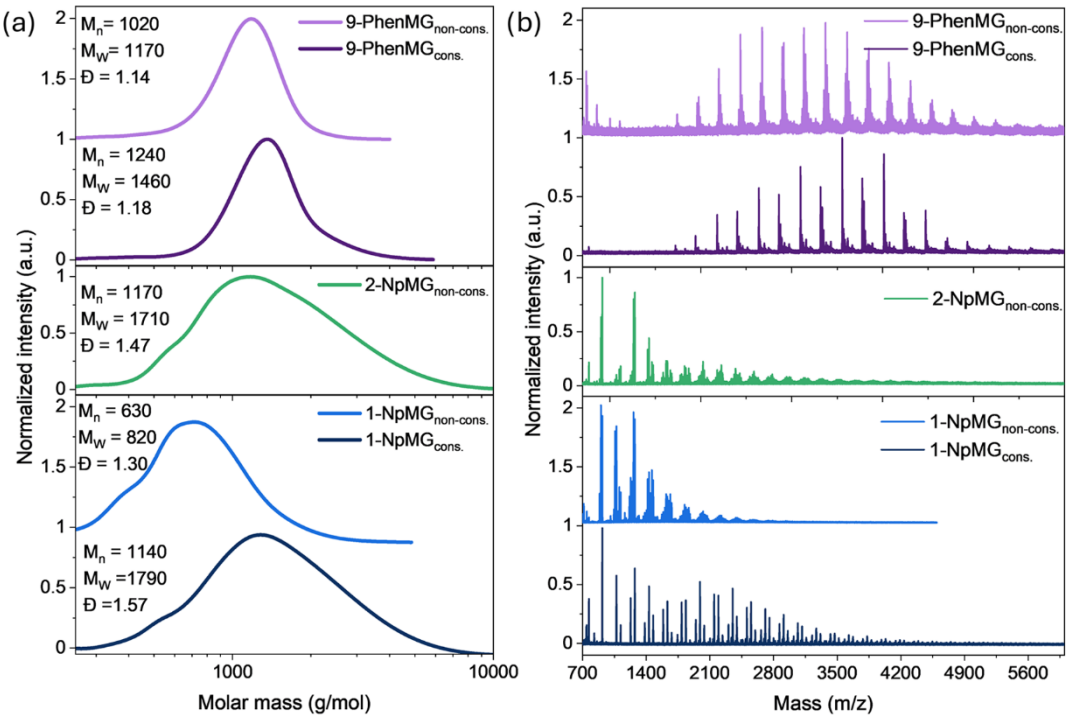

Figure 5. (a) SEC measurements (PS standard in THF) showing M_n, M_w, and $Đ$. (b) MALDI-ToF MS spectra of soluble consolidated and non-consolidated 1-Np-, 2-Np-, and 9-PhenMGs.

Despite thermal treatment, a large number of OH and methoxy groups remain stable, reflected in the retention of flow character and solubility of the 1-NpMG. The more extended 2-Np group containing molecule, which is more accessible for condensation reactions, leads to a higher degree of condensation after thermal treatment, making it more comparable with the DC of the known PhMG. In contrast, 9-PhenMG undergoes nearly complete hydrolysis of its methoxy groups due to the higher water content in the synthesis. The increased condensation tendency of the large amount of OH groups results in the highest cross-linking among all of the materials investigated. The fact that it is still soluble after consolidation as well as the formation of defined silsesquioxane species due to thermal treatment indicates mainly temperature-induced intramolecular condensation reactions.

SEC/MALDI-ToF MS. The NMR spectroscopy gives a good overview of hydrolysis and condensation tendencies, as well as the degree of cross-linking, but it does not provide information about the molecular mass of the silsesquioxane species formed. Hence, we applied SEC and MALDI-ToF MS to determine the molecular mass and polydispersity ($Đ$), as well as changes in molecular mass resulting from thermally initiated condensation reactions in all soluble samples (Figure 5). The non-consolidated 1-NpMG shows a low average molecular mass (M_w) of 820 g/mol with a small $Đ$ value of 1.30 (Figure 5a), which corresponds well to the low DC and defined peaks detected via the NMR measurements. Thermal treatment at 200 °C results in an increase in size to M_w = 1800 g/mol, along with a widening of the molar mass distribution, which is typical for intermolecular condensation reactions.[21] Nevertheless, the SEC results of the consolidated 1-NpMG remain low and are in a similar range to those of non-consolidated 2-NpMG, with a M_w = 1790 g/mol and a polydispersity of 1.47. As the molecular mass is an important parameter influencing flow behavior at temperatures above the T_g, the low M_w, even after thermal treatment, is visible in the lack of curing of the 1-NpMG.[16] Compared to the PhMG$_{non-cons.}$ with M_w = 3470 g/mol and $Đ$ = 2.41,[27] the measurements indicate a clear trend: the greater the steric hindrance (Ph < 2-Np < 1-Np), the lower the number and the weight-average molecular mass.

9-PhenMG differs from NpMGs in its low polydispersity of 1.14 and a molar mass that hardly changes during consolidation, indicating defined structural units and predominantly intramolecular condensation reactions.[55]

A more precise statement about the different silsesquioxane species formed and the type of condensation reaction can be made using MALDI-ToF MS. All melting gels give typical spectra characteristic of condensed polymers (Figure 5b).[56] Major clusters are identified and can be attributed to oligomers with a defined number of repeating units, n (Figure 6a,c). Within each n, the oligomers differ in the type and number of non-cross-linked units, forming minor clusters (Figure 6b,d). Replacing an OMe group with an OH group results in a reduction in a mass of 14 g/mol. The formation of a ring through the condensation of two OH groups or one OH and one OMe group results in mass losses of 18 and 32 g/mol, respectively. However, identifying the major clusters is challenging, particularly in naphthyl gels, as these span a wide mass range from the heaviest species (linear oligomers with only OMe groups) to the lightest species (fully cross-linked structures). Overall, the MALDI-ToF MS results align with the trend observed in SEC measurements, although the SEC results tend to slightly underestimate the mass of 9-PhenMG. This discrepancy can be attributed to the presence of the OH groups, which cause a more pronounced change in the hydrodynamic volume of 9-PhenMG compared to that of the polystyrene (PS) standards.

https://doi.org/10.1021/acs.macromol.4c02737
Macromolecules 2025, 58, 1298−1313

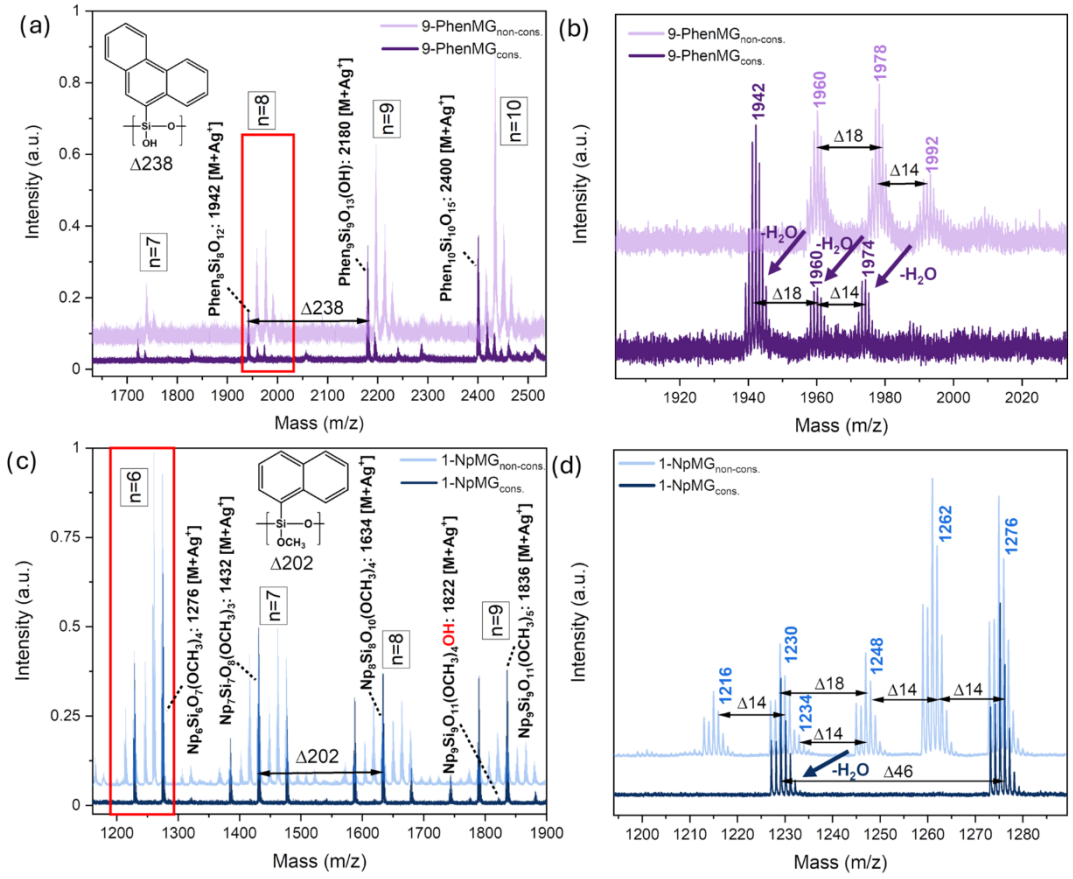

Figure 6. (a) Zoom in the full mass spectrum of the consolidated and non-consolidated 9-PhenMG, highlighting major clusters with 7−10 repeating units (n) with a spacing between them of 238 u. The highest peak is assigned to the corresponding silsesquioxane unit of 9-PhenMG$_{cons.}$, (b) single repeating unit with n = 8 of the full mass spectrum of consolidated and non-consolidated 9-PhenMG. The distance between the peaks is 18 u for intramolecular condensation with the loss of water and 14 u for OH replacement by OMe, (c) zoom in the full mass spectrum of the consolidated and non-consolidated 1-NpMG, highlighting major clusters with 6−9 repeating units with a spacing between them of 202 u. The highest peak is assigned to the corresponding silsesquioxane unit of 1-NpMG$_{cons.}$, (d) single repeating unit with n = 6 of the full mass spectrum of consolidated and non-consolidated 1-NpMG. The distance between the peaks is 18 u for intramolecular condensation with the loss of water, 14 u for OH replacement by OMe, and 46 u for the replacement of two OMe groups by an Si−O bonding.

The comparison between the non-consolidated and consolidated samples is particularly insightful, as it provides information about inter- or intramolecular condensation reactions.

Due to its high degree of hydrolysis, 9-PhenMG shows well-separated major clusters with repeating units that differ in the number of rings and OH and OMe groups (Figure 6a). The comparison of the spectra between the non-consolidated and consolidated 9-PhenMG indicates that the thermally initiated condensation reactions are predominantly intramolecular. Looking at the main cluster with 8 repeating units in detail (Figure 6b), a mass reduction of 18 g/mol is observed, corresponding to the condensation of two OH groups and thus the formation of additional cycles, remaining T^8 (1942 g/mol: $Phen_8Si_8O_{12}$ + Ag^+) as the main peak as well as T^8 with an open edge and OMe or OH groups (1960 g/mol: $Phen_8Si_8O_{11}(OH)_2$ + Ag^+, 1974 g/mol $Phen_8Si_8O_{11}(OH)(OCH_3)$ Ag^+) as the second and third peaks. After consolidation, T^8−T^{20} are detectable as the main peak, along with open variants containing stabilized hydroxy groups and a few remaining OMe groups. The well-defined peaks observed previously in the ^{29}Si NMR spectrum can thus be correlated with one or more of these cubes. However, a precise assignment of these peaks is not possible without isolating the individual components. The overall mass spectrum shows no change in the number of repeating units due to the thermally initiated condensation reactions and only a reduction in the minor cluster, which highlights the intramolecular ring formation to highly cross-linked silsesquioxanes.[57]

In comparison, both naphthyl gels exhibit a significantly more complex mass spectrum. Due to a high number of hydroxy and methoxy groups, each major cluster consists of many minor clusters, differing by 14 g/mol, reflecting variations in the ratio of OH/OMe groups (Figure 6c). However, consideration of the overall spectrum of 1-NpMG$_{cons}$ shows a clear shift toward higher molar masses after thermal treatment at 200 °C, resulting from intermolecular condensation reactions. A closer look at oligomers with n = 6 (Figure 6d), for example, reveals partially cross-linked silsesquioxanes containing only methoxy groups after consolidation. Within individual clusters, the oligomers differ by a mass delta of 46 g/mol, which corresponds to the formation of a ring by the reduction of two OMe groups (1230 g/mol: 1-$Np_6Si_6O_8(OCH_3)_2$ + Ag^+ and 1276 g/mol: 1-

https://doi.org/10.1021/acs.macromol.4c02737
Macromolecules 2025, 58, 1298−1313

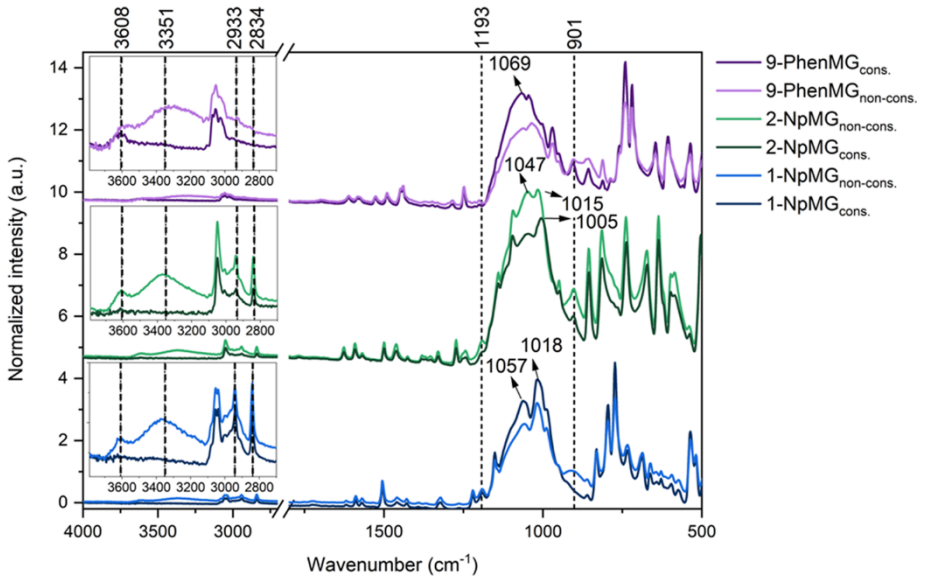

Figure 7. FTIR spectra of consolidated and non-consolidated 1-Np-, 2-Np-, and 9-PhenMGs with a zoomed view of the OH region and highlighting of key vibration peaks.

$Np_6Si_6O_7(OCH_3)_4 + Ag^+$). It can be assumed that the OH groups in the 1-NpMG are less stabilized, as oligomers with isolated hydroxyl groups are observed only from $n = 9$.

The microstructure of 2-NpMG$_{non\text{-}cons.}$ is comparable to that of 1-NpMG$_{non\text{-}cons.}$, with the distinction that oligomers can be detected in higher mass ranges. As already recognized by the increased molar mass in the SEC measurements and the higher DC in the NMR measurements, the MALDI-ToF MS results confirm the formation of larger silsesquioxane units with an increased number of repeating units. Compared to 1-NpMG and 9-PhenMG, a further reduction in the stability of the OH groups is expected, promoting a stronger tendency toward intermolecular condensation and intermolecular entanglement.

The SEC/MALDI-ToF MS measurements highlight the influence of the aromatic groups on the molar mass, OH group stabilization, and type of condensation reaction. Depending on the size of the aryl group, either inter- or intramolecular condensation reactions are favored. Phenanthrenyl, the largest moiety investigated here, forms oligomers with a size of 7−20 repeating units. Thermally initiated condensation reactions occur intramolecularly within these oligomers, resulting in a significantly higher degree of cross-linking but minimal change in molecular size. The preferred formation of both open and closed cubes is observed. 1-NpMG with 1-naphthyl as the next largest organic group exhibits not only intramolecular but also intermolecular condensation reactions. This results in an increase in the average molecular mass and a broadened molar mass distribution. In contrast to 9-PhenMG, a large number of OMe groups are present, stabilizing the oligomers with a small number of repeating units. The presence of linear polysilsesquioxanes with a few rings or a ladder-like structure can be predicted. The 2-naphthyl group has the lowest steric hindrance due to its extended structure. This leads to an increased hydrolysis rate and a stronger condensation tendency, as evidenced by the significantly higher M_w compared to 1-NpMG$_{non\text{-}cons.}$. It can be assumed that the consolidation promotes intermolecular condensation reactions, resulting in the formation of an extended network, which causes insolubility and a lack of chain mobility.

ATR-FTIR Spectroscopy. ATR-FTIR spectroscopy was used for further analysis of the silsesquioxane structure. The process of hydrolysis and condensation can be detected by examining specific vibrational bands of methoxy- and hydroxy groups.[58] All polysilsesquioxanes display a reduction in the signals from the OMe at 2834 and 2933 cm^{-1} (υCH_3), 1193 cm^{-1} (ρCH_3O), and 1069 cm^{-1} (υCO) due to the hydrolysis reaction (Figure 7).[59,60] However, the complete disappearance of these absorption bands is not observed in 1- and 2-NpMG, demonstrating the persistence of OMe groups, consistent with results from NMR measurements. Furthermore, an absorption band corresponding to OH groups is visible at 900 cm^{-1} and between 3000 and 3700 cm^{-1}. A distinction can be made between OH groups interacting via hydrogen bonding (3000−3500 cm^{-1}) and isolated OH groups (>3600 cm^{-1}).[8] Upon thermal treatment at 200 °C, the associated OH groups nearly disappear. Hydroxy groups shielded by the aromatic moiety remain visible as isolated groups in the range >3600 cm^{-1}.

Condensation reactions and resultant Si−O−Si cross-linking become apparent through absorption in the Si−O−Si vibration range between 1000 and 1150 cm^{-1}. This segment of the spectrum is particularly interesting, as it provides insights into the forming silsesquioxane network.[61,62] Both NpMGs exhibit a defined Si−O−Si vibration band focused on lower wavenumbers between 1000 and 1100 cm^{-1} with two maxima around 1040−1060 cm^{-1}, featuring the Si−O−Si network with low symmetric linear or cross-linked units, and 1015/1018 cm^{-1} representing strained cycles.[63−65]

With consolidation, only a definition of the existing peaks is observed in 1-NpMG, indicating no major change in the microstructure despite further condensation reactions.

In contrast, the FTIR spectra of 2-NpMG$_{cons}$ show a decrease in the Si−O−Si network band at 1058 cm^{-1}, while the band corresponding to the strained cycles shifts from 1018 to 1005 cm^{-1} and becomes dominant. The formation of a band in the low wavenumber range of the Si−O−Si region is also reported in the literature after the thermal condensation of silanols, such as $PhSi(OH)_3$.[66,67] During the melting gel synthesis, the partial formation of 2-NpSi(OH)$_3$ was detected.

https://doi.org/10.1021/acs.macromol.4c02737
Macromolecules 2025, 58, 1298−1313

It can be assumed that the solvent-free, thermal condensation of silanols preferentially results in the formation of cyclic structures (like $(Si-O)_6$ or cyclotrisiloxanes).[68] The absence of softening and the lack of solubility indicate that these cyclic structures are condensed, forming a dense network.

The Si−O−Si region of 9-PhenMG has no prominent peaks and is more concentrated around 1070 cm^{-1}, representing open cages of varying sizes, as detected in the MALDI-ToF MS.[69] Further intramolecular condensation reactions lead to the formation of more defined silsesquioxanes, including fully cross-linked cages. This transformation is visible in the spectrum by a narrowing of the full width at half-maximum in the Si−O−Si region.

Variances in the structure of the melting gels, influenced by the different organic groups, were detected via MALDI-ToF and manifested in the Si−O−Si vibration range. In 1-NpMG, small low-symmetry silsesquioxane structures, such as small rings, linear chains, or ladders, are found, while the 2-Np substituent appears to favor condensed cycles, as 2-naphthyltrihydroxysilane is formed as an intermediate during synthesis, dictating subsequent structure development. In contrast, cage structures of different sizes are observed in 9-PhenMG, represented by a broad band around 1070 cm^{-1}. All samples show a definition of the FTIR region after thermal condensation, indicating the formation of a more ordered silsesquioxane structure.

Powder XRD. PXRD measurements are a known method to study the structural order of polysilsesquioxanes. Ladder-like polysilsesquioxanes or layered polysiloxanes typically exhibit two broad, amorphous reflections in the diffractogram. The assignment of the first reflection (d_1) varies in the literature, attributed to the width of ladder-like structures[70−72] or interpreted as the intermolecular chain-to-chain distance in ladders or between layers or cages.[51,73,74] In both interpretations, the position of the first signal depends on the type of the organic group and the defect concentration. Bulkier and more spatially extended organic groups lead to greater separation between silsesquioxane layers, resulting in a higher d_1 value and lower packing density.[3] Defects, such as non-condensed methoxy or hydroxy groups, as well as changes in the conformation of the organic group, lead to a lower d_1 distance and a decrease in the relative intensity of the first reflection compared to the second (R value).[72,75] All three aryl melting gels display a signal corresponding to d_1 (Figure 8), indicating a layered structure. The low R value (Table 1) and broadening of the first reflection suggest a low long-range order and a structure that is rich in defects. The d_1 value of the non-consolidated gels represents the increased bulkiness and spatially extended length in the order Ph < 1-Np < 2-Np < 9-Phen, as well as the chain packing density in reverse order. Temperature-induced cross-linking becomes evident by an increase in the d_1 values, accompanied by an increase in the R value. NMR and MALDI-ToF MS results indicate still a defect-rich structure with non-condensed groups, even in the consolidated materials. Therefore, observed d_1 values are far from an ideal ordered arrangement and could potentially be significantly larger.

The R value increases in the order 1-Np < 2-Np < Ph < 9-Phen. The increase in order can be correlated with the proportion of hydrolyzed species detected by NMR spectroscopy. It has been shown that silanols thermally condense, thereby retaining the structure that predominates in the crystal.[35] The higher the proportion of OH groups, the more structuring units are present, resulting in a more uniform structure.

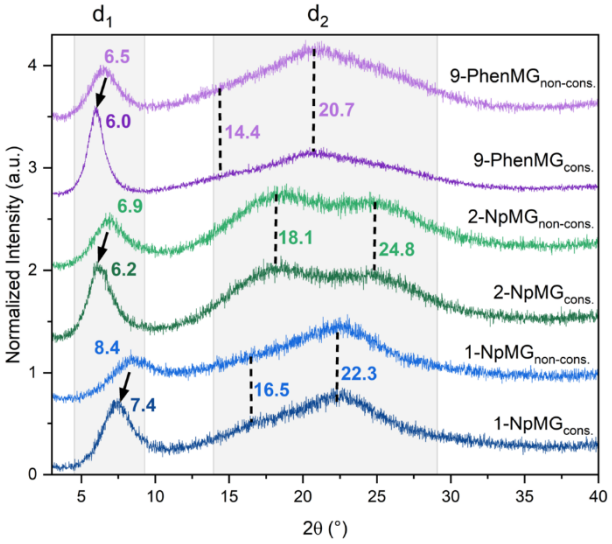

Figure 8. PXRD patterns of consolidated and non-consolidated 1-Np-, 2-Np-, and 9-PhenMG with marked positions of the d_1 and d_2 reflections.

Table 1. d_1, d_2, and R Values of Consolidated and Non-consolidated 1-Np-, 2-Np-, and 9-PhenMG Measured by PXRD[a27]

sample		maximum d_1 [nm]	maximum d_2 [nm]	R $(I(d_1)/I(d_2))$
1-NpMG	non-cons.	1.05	0.40	0.62
	cons.	1.19		0.90
2-NpMG	non-cons.	1.28	0.49	0.71
	cons.	1.42		1.01
9-PhenMG	non-cons.	1.36	0.43	0.78
	cons.	1.47		1.78
PhMG	non-cons.	0.83	0.45	0.98
	cons.	0.98		1.15

[a]Values for PhMG were taken from the literature.[27]

The amorphous part of the material is represented by a d_2. The phenyl melting gel shows an amorphous, broad signal at 0.45 nm, consistent with the literature attributing this to the average thickness of the molecular chains.[3,72,76] The value is described as independent of the organic group and the cross-linking. Unexpectedly, all melting gels exhibit two overlapping diffuse peaks in the range of d_2. The 2-NpMG display two distinct maxima at 0.49 and 0.36 nm, while 1-NpMG and 9-PhenMG show a maximum at 0.40/0.43 nm with a shoulder at 0.54/0.61 nm. As the consolidation leaves the reflections unchanged, but structural change becomes apparent via IR and NMR, it can be assumed that the position of d_2 is not directly linked to the resulting structural arrangement. The observed differences are likely influenced by the asymmetric nature of the organic group in comparison with the phenyl substituent.

XRD measurements confirm the presence of a layered structure in all of the melting gels. However, the low R value indicates a high degree of structural disorder in the non-consolidated materials due to a large amount of non-condensed hydroxy and methoxy groups. The size of the organic substituent is reflected in the d_1 parameter, which

https://doi.org/10.1021/acs.macromol.4c02737
Macromolecules 2025, 58, 1298−1313

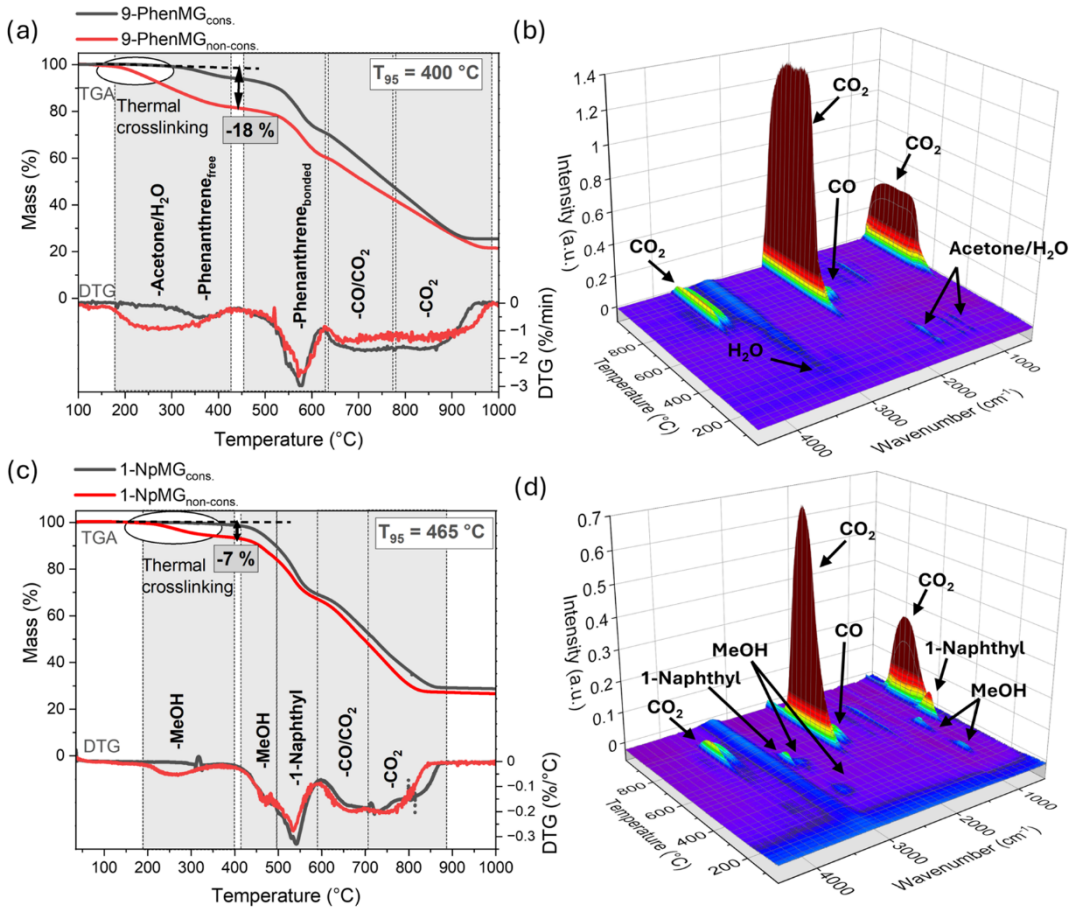

Figure 9. TG curve under air and DTG curve of the consolidated and non-consolidated melting gels, with assignment of the gases released during each decomposition stage, T^{95} value of the consolidated melting gel, and the marked mass loss in the first decomposition stage of the non-consolidated melting gel: (a) 1-NpMG and (c) 9-PhenMG. Three-dimensional (3D) graphic of the FTIR spectra of degradation products as a function of temperature, with the assignment of the detected gases: (b) 1-NpMG$_{non\text{-}cons.}$ and (d) 9-PhenMG$_{non\text{-}cons.}$.

correlates with the interlayer distance and increases from phenyl to phenanthrenyl. Thermal treatment and further cross-linking lead to structural expansion and increased ordering, consistent with FTIR results. The quantity of OH groups acting as structuring elements proves to be a crucial factor in thermally initiated condensation.

Thermal Analysis. *TGA/Thermogravimetric Analysis-Fourier Transform Infrared Spectroscopy (TG-FTIR).* Polysilsesquioxanes are known for their exceptionally high thermal stability, which is attributed to their high Si−O binding energy.[77] In addition, the cross-linking properties minimize bond cleavage and ring formation, which occurs more frequently in linear polysiloxanes during thermal decomposition.[78,79] The organic group also plays an important role in decomposition. Phenyl groups have been found to be particularly stable, both in an inert atmosphere and under air.[80] The phenyl melting gel showed a mass loss of 5% (T_{95} value) in an oxygen atmosphere at 400 °C in its non-consolidated state and at 510 °C after the consolidation, demonstrating a high thermal stability, which is typical for polyphenylsilsesquioxanes.[27] By using TG-FTIR, a 3.95% mass loss due to water and methanol was detected starting at 200 °C, which resulted from the thermally induced condensation reactions. Further decomposition, involving Si-Ph bond cleavage, proton abstraction, and oxidation of free carbon, was observed at 590 and 670 °C through the monitoring of benzene, CO_2, and CO.

The influence of the different polycyclic aromatic groups on thermal stability and decomposition under air was investigated via TGA and TGA-FTIR, analogous to the studies on PhMG. The decomposition of naphthyl and phenanthrenyl melting gels is very similar to that of the polyphenylsilsesquioxane. All samples show three defined mass losses in the range 180−380 °C; 400−650 °C; and 600−950 °C, whereby the derivative thermogravimetric (DTG) curves indicate overlapping decomposition stages in the range of the second and third mass losses for NpMGs (Figures 9a,c and S16). For the qualification of the gases produced during consolidation and further decomposition, TG-FTIR measurements were performed (Figures 9b,d and S16).

The first mass loss, starting at about 200 °C for the NpMGs, can be assigned to the reaction of OMe and OH groups, primarily forming methanol as byproduct. Water cannot be detected in the FTIR spectra of the gaseous decomposition products, possibly due to a further hydrolysis reaction of the remaining methoxy groups. After consolidation, the initial mass loss is no longer visible, and further decomposition of the materials does not start until 400 °C. This is explained by the condensation of all available and interacting OH groups, and only the addition of external agents (for example, a base as a

https://doi.org/10.1021/acs.macromol.4c02737
Macromolecules 2025, 58, 1298−1313

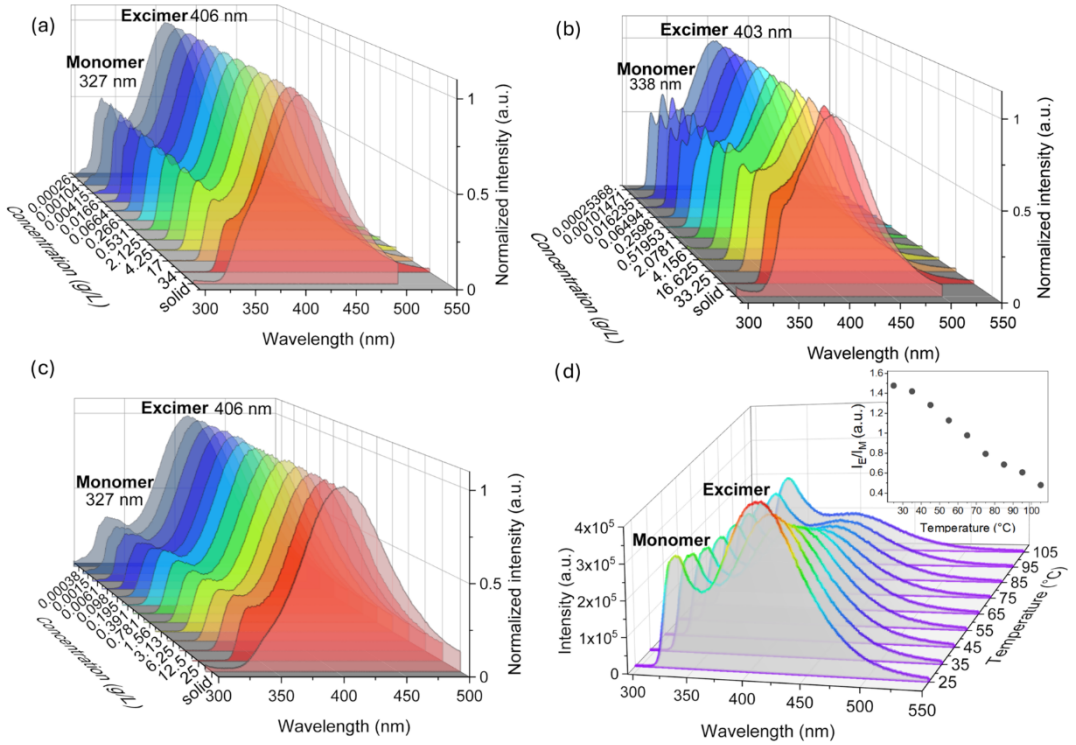

Figure 10. Concentration-dependent fluorescence spectra of (a) 1-NpMG$_{non\text{-}cons.}$, (b) 2-NpMG$_{non\text{-}cons.}$, and (c) 1-NpMG$_{cons}$ in DCM with λ_{ex} = 285 nm. (d) Temperature-dependent measurements of 1-NpMG$_{non\text{-}cons.}$ in dimethyl sulfoxide (DMSO) between 25 and 105 °C, λ_{ex} = 285 nm, c = 0.6 g/L. The inlet shows the temperature-dependency excimer-to-monomer fluorescence ratio.

catalyst) would enable further cross-linking in the cured materials. The two naphthyl groups primarily differ in the magnitude of the first step, with the 1-NpMG exhibiting a mass loss of about 1.5 times larger than that of the 2-NpMG. This difference can be explained by the lower DC of the non-consolidated 1-NpMG and an increasing number of condensation reactions, resulting in a higher loss of byproducts. However, both materials show high thermal stability, with a T_{95} of about 460 °C after temperature treatment.

The 9-PhenMG exhibits a significantly larger first degradation step of about 18%, starting earlier at 180 °C (Figure 9c). Analysis of the gaseous components reveals the presence of mainly residual solvent from the synthesis and water from condensation reactions (Figure S17). The removal of acetone at such a late stage suggests interactions between the carbonyl group and the silanols of the melting gel via hydrogen bonds.[81] However, the 18% mass loss cannot be attributed solely to the condensation byproducts and residual solvents. It is to be expected that the sublimation of free phenanthrene, detected by ^{1}H NMR, is also reflected in this stage. Since no condensation stage occurs in the consolidated material, the mass loss of around 350 °C relates to the release of the aromatic compound. Due to the high boiling point of phenanthrene, it crystallizes in the transfer line before reaching the IR detector and is therefore not visible in the IR spectra of the gaseous degradation products (^{1}H NMR spectrum of the crystals from the TGA furnace is given in Figure S18).

The second mass loss begins around 400 °C. Methanol is initially detected during this stage in the naphthyl melting gels, coming from the decomposition of OMe groups that were not reacted in the first condensation step. Overlapping with the formation of methanol, the FTIR spectrum shows an absorption of the aromatic C−H vibration. It indicates the cleavage of the Si-naphthyl bond and the detection of naphthalene.[79] The 9-PhenMG shows a mass loss at a similar temperature, which cannot be detected by FTIR. The cleavage of the Si-phenanthrenyl bond and the loss of the aromatic group are expected in this step, similar to those of the NpMGs.

Complete oxidation of the carbon results in a release of CO and CO_2 during the final degradation step, visible in all three silsesquioxanes between 600 and 950 °C.[82]

The different attachment of the naphthyl group and the size of the aromatic group do not appear to have a significant effect on thermal stability and oxidative decomposition. All materials reveal a thermal stability of ≥400 °C, with their thermal decomposition differing primarily in the number of remaining hydroxy and methoxy groups. The high thermal oxidative stability distinguishes the aromatic melting gels from the reversibly softenable silsesquioxanes with alkyl groups or alkyl spacer between the silicon and the aromatic group, as described in the literature.[28,33,83] Since 9-PhenMG contains only a very small number of OMe groups, no release of methanol can be identified. However, acetone, interacting via hydrogen bonds, and phenanthrene, cleaved by acidic polycondensation during the synthesis, can be detected. The 1-Np- and 2-NpMG differ only in the size of the condensation step, which is dependent on their degree of condensation.[28,83]

Fluorescence Analysis. Under UV light, the aromatic melting gels show pronounced fluorescence behavior (Figure 2). Fluorescence spectroscopy can be used to investigate interactions within polymers, as fluorescence is highly dependent on the environment of fluorophores. Polycyclic aromatic hydrocarbons such as pyrene, benzene, naphthalene, perylene, and their derivatives are known to show a

https://doi.org/10.1021/acs.macromol.4c02737
Macromolecules 2025, 58, 1298−1313

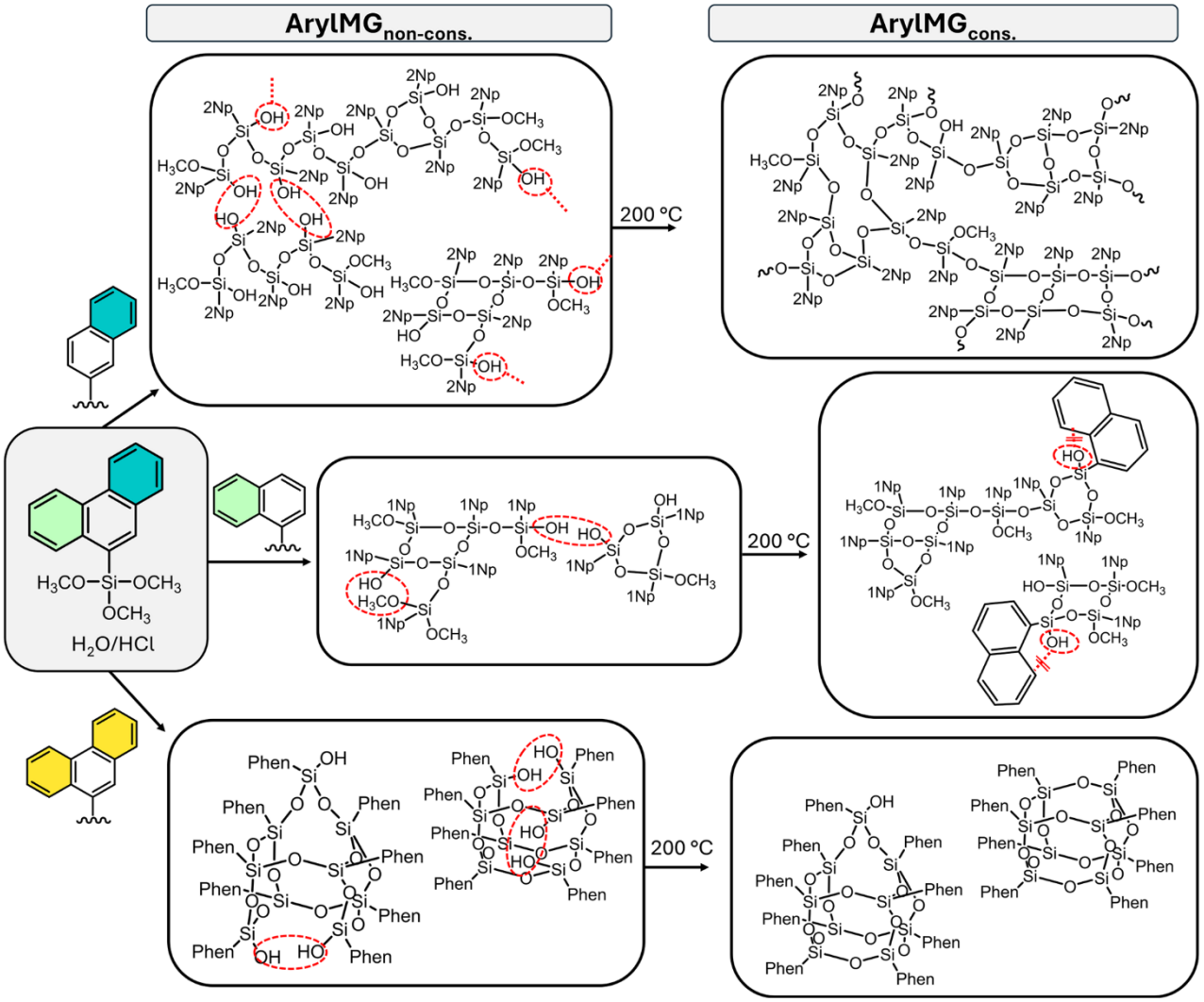

Figure 11. Schematic representation of the proposed structures of the three investigated melting gels (1-NpMG, 9-PhenMG, and 1-NapMG) in their non-consolidated and consolidated forms. The structural motifs shown are a representative selection of the units postulated in the materials and reflect the most important characteristics of the respective material state.

concentration-dependent formation of a structureless band. This band is attributed to excimers, which result from an attachment of an excited aromatic molecule with an unexcited one.[84−86] Excimer formation can also occur within oligomers and polymers, such as polystyrenes,[87] polyvinylnaphthalenes,[88] and even polyphenylsiloxanes[89] or polyphenylsilsesquioxanes,[90] provided the aromatic groups adopt a stable sandwich conformation.[91] Concentration-dependent measurements allow one to distinguish between inter- and intramolecular excimer formation. If the ratio between the monomer and excimer band in a diluted solution shows no concentration dependence, interactions within the polymer chain can be expected.[90] As PhMG is known to form inter- and intramolecular excited dimers,[27] concentration-dependent fluorescence spectra were also measured for the soluble naphthyl- and phenanthrenyl melting gels in the consolidated and non-consolidated states.

Naphthalene shows a moderately prominent excimer band at high concentrations at room temperature, which becomes more prominent in certain naphthalene derivatives, with a maximum between 392 and 408 nm.[92] Concentration-dependent fluorescence spectra of the monomers 1-Np- and 2-NpSi(OMe)$_3$ in DCM confirm this observation (Figures S19 and S20, absorption spectra in DCM of monomers and polymers see Figure S21). 1-NpSi(OMe)$_3$ shows monomer fluorescence at 329 nm with shoulders at 323 and 335 nm, while 2-NpSi(OMe)$_3$ presents three defined peaks at 323, 338, and 353 nm. A red shift is observed due to self-absorption at high concentrations. In the absence of solvent, a structureless band at 403 nm (1-NpSi(OMe)$_3$), as well as a structureless band at 390 nm (2-NpSi(OMe)$_3$), dominates the spectra, which can be assigned to the excimer band. The ratio between monomer and excimer fluorescence is strongly concentration-dependent, which is typical for intermolecular excimer fluorescence. In contrast, phenanthrene is known not to exhibit excimer fluorescence, except under exceptional environments or the use of substituted phenanthrenes.[93−95] This behavior is mirrored in the monomer 9-PhenSi(OMe)$_3$, which displays a defined monomer fluorescence with a peak maximum at 367 nm, accompanied by a spectral shift caused

https://doi.org/10.1021/acs.macromol.4c02737
Macromolecules 2025, 58, 1298−1313

by self-quenching at increased concentrations (Figure S22).[96] Unlike the naphthyl monomers, 9-PhenSi(OMe)$_3$ does not show a red-shifted, unstructured band, indicating the absence of excimer formation.

The non-consolidated melting gels containing naphthyl groups show the previously described peaks corresponding to excimer and monomer fluorescence (Figure 10a,b). The excimer band, which appears at 406 nm for 1-NpMG and at 403 nm for 2-NpMG, persists even at low concentrations <0.0026 g/L. As soon as the spectrum is no longer influenced by self-absorption, the ratio of monomer to excimer fluorescence remains constant. At this point, the oligomeric structures are fully separated by solvent, eliminating intermolecular interactions. The fluorescence detected under these conditions can be assigned to intramolecular excimer fluorescence, which suggests that the naphthyl groups, both in α and β positions, must be present in a symmetrical sandwich conformation. The same experiments were repeated with consolidated, soluble 1-NpMG (Figure 10c). A prominent, concentration-independent excimer band is also formed at 406 nm. Compared to the non-consolidated gel, the ratio of excimer to monomer fluorescence increases from I_{Ex}/I_M = 1.9 for the non-consolidated to I_{Ex}/I_M = 3.2 for the consolidated sample. It can be concluded that the additional cross-linking leads to an increased number of intramolecular excimers, suggesting a more ordered system with a lower number of defects.[97] These findings align with the XRD measurements, which also demonstrated structural ordering induced by the thermal treatment.

In contrast, 9-PhenMG exhibits no excimer band in either the non-consolidated or consolidated state (Figure S23), consistent with the known behavior of phenanthrenyl substituents, which do not form excimers.

The effect of temperature on excimer formation in 1-Np- and 2-NpMG was studied in DMSO over a range of 25−105 °C. In both melting gels, the excimer fluorescence decreases with increasing temperature, while the monomer fluorescence remains largely unaffected, leading to a reduction in the relative ratio I_{Ex}/I_{Em} (Figures 10d and S24). The temperature dependence of the excimers is a known phenomenon in the literature and can be attributed to thermal dissociation.[98,99] These findings highlight the thermally initiated changes in aromatic interactions that contribute to the observed thermoplastic behavior.

CONCLUSIONS

In this study, we investigated the influence of the aromatic group size and isomerism on the structural and thermal properties of polysilsesquioxane-based melting gels. Through acid-catalyzed polycondensation, we synthesized polysilsesquioxanes from 1-naphthyl, 2-naphthyl, and 9-phenanthrenyltrimethoxysilanes, examining their behavior in terms of reversible softening at 110 °C and irreversible curing at 200 °C, similar to known phenyl-containing melting gels.

Our structural analyses revealed that aryl group isomerism and size significantly affect molecular mass, cross-linking density, and overall structure (Figure 11). 1-NpMG forms low-mass oligomers with numerous stabilized non-cross-linked OH and OMe groups. The low degree of condensation allows reversible softening and solubility even after thermal treatment at 200 °C, making the material resistant to thermal curing. In contrast, the more linear and less bulky structure of the 2-naphthyl group facilitates cross-linking and extended network formation, resulting in a material that softens at 110 °C but transitions to a thermoset upon further heating. Meanwhile, the 9-phenanthrenyl group induced mainly intramolecular condensation due to its bulkiness, forming rigid, cage-like structures with limited flow behavior.

The incorporation of naphthyl groups into polysilsesquioxanes enables the creation of materials with high refractive indices >1.6, fluorescence, and thermoplastic properties across a wide temperature range while maintaining high thermal stability >400 °C. These characteristics distinguish them from known phenyl-based melting gels, broadening their potential applications in fields like optoelectronics.

ASSOCIATED CONTENT

Supporting Information

The Supporting Information is available free of charge at https://pubs.acs.org/doi/10.1021/acs.macromol.4c02737.

Experimental section including used materials, instrumentation, and monomer synthesis, spectroscopic data of monomers and formed intermediates during synthesis, spectroscopic data, deconvoluted ^{29}Si CP-MAS NMR spectra, RI measurements, and TG-FTIR spectra of the prepared polymers (PDF)

AUTHOR INFORMATION

Corresponding Author

Guido Kickelbick − *Inorganic Solid-State Chemistry, Saarland University, 66123 Saarbrücken, Germany; Saarene, Saarland Center for Energy Materials and Sustainability, 66123 Saarbrücken, Germany;* orcid.org/0000-0001-6813-9269; Email: guido.kickelbick@uni-saarland.de

Authors

Svenja Pohl − *Inorganic Solid-State Chemistry, Saarland University, 66123 Saarbrücken, Germany*

Markus Gallei − *Polymer Chemistry, Saarland University, 66123 Saarbrücken, Germany; Saarene, Saarland Center for Energy Materials and Sustainability, 66123 Saarbrücken, Germany;* orcid.org/0000-0002-3740-5197

Complete contact information is available at: https://pubs.acs.org/10.1021/acs.macromol.4c02737

Notes

The authors declare no competing financial interest.

Declaration of AI and AI-Assisted Technologies in the Writing Process During the preparation of this work, the authors utilized AI tools, including Deepl.com and ChatGPT to enhance the clarity of the language and to correct spelling, punctuation, and grammatical errors. After using these tools, the authors carefully reviewed and edited the content as necessary and take full responsibility for the accuracy and integrity of the publication.

ACKNOWLEDGMENTS

Instrumentation and technical assistance for this work were provided by the Service Center X-ray Diffraction, with financial support from Saarland University and the German Science Foundation (project number INST 256/349-1). The authors thank Blandine Boßmann for recording and analyzing the SEC measurements, Elias Gießelmann for MAS NMR measurements, Dr. Alexander Schießer (Department of Chemistry, Mass Spectrometry, Technische Universität Darmstadt) for the

https://doi.org/10.1021/acs.macromol.4c02737
Macromolecules 2025, 58, 1298−1313

MALDI-ToF MS measurements, and also the Deutsche Forschungsgemeinschaft (Grant INST 163/445-1 FUGG).

REFERENCES

(1) Niemczyk, A.; Dziubek, K.; Sacher-Majewska, B.; Czaja, K.; Czech-Polak, J.; Oliwa, R.; Lenża, J.; Szołyga, M. Thermal Stability and Flame Retardancy of Polypropylene Composites Containing Siloxane-Silsesquioxane Resins. *Polymers* **2018**, *10* (9), 1019.

(2) Park, S.; Jeong, H.-J.; Moon, J.-H.; Jang, E.-Y.; Jung, S.; Choi, M.; Choi, W.; Park, K.; Ahn, H.-W.; Hong, J. Polysilsesquioxane with potent resistance to intraoral stress: Functional coating material for the advanced dental materials. *Appl. Surf. Sci.* **2022**, *578*, No. 152085.

(3) Hwang, S. O.; Lee, A. S.; Lee, J. Y.; Park, S.-H.; Jung, K. I.; Jung, H. W.; Lee, J.-H. Mechanical properties of ladder-like polysilsesquioxane-based hard coating films containing different organic functional groups. *Prog. Org. Coat.* **2018**, *121*, 105−111.

(4) Xi, K.; He, H.; Xu, D.; Ge, R.; Meng, Z.; Jia, X.; Yu, X. Ultra low dielectric constant polysilsesquioxane films using $T^8(Me_4NO)_8$ as porogen. *Thin Solid Films* **2010**, *518* (17), 4768−4772.

(5) Baney, R. H.; Itoh, M.; Sakakibara, A.; Suzuki, T. Silsesquioxanes. *Chem. Rev.* **1995**, *95*, 1409−1430.

(6) Ahmed, N.; Fan, H.; Dubois, P.; Zhang, X.; Fahad, S.; Aziz, T.; Wan, J. Nano-engineering and micromolecular science of polysilsesquioxane materials and their emerging applications. *J. Mater. Chem. A* **2019**, *7*, 21577−21604.

(7) Temnikov, M. N.; Muzafarov, A. M. Polyphenylsilsesquioxanes. New structures−new properties. *RSC Adv.* **2020**, *10* (70), 43129−43152.

(8) Masai, H.; Takahashi, M.; Tokuda, Y.; Yoko, T. Gel-melting method for preparation of organically modified siloxane low-melting glasses. *J. Mater. Res.* **2005**, *20*, 1234−1241.

(9) Katagiri, K.; Hasegawa, K.; Matsuda, A.; Tatsumisago, M.; Minami, T. Preparation of Transparent Thick Films by Electrophoretic Sol−Gel Deposition Using Phenyltriethoxysilane-Derived Particles. *J. Am. Ceram. Soc.* **1998**, *81*, 2501−2503.

(10) Matsuda, A.; Sasaki, T.; Hasegawa, K.; Tatsumisago, M.; Minami, T. Thermal Softening Behavior of Poly(phenylsilsesquioxane) and Poly (benzylsilsesquioxane) Particles. *J. Ceram. Soc. Jpn.* **2000**, *108*, 830−835.

(11) Katagiri, K.; Hasegawa, K.; Matsuda, A.; Tatsumisago, M.; Minami, T. Preparation of Transparent Thick Films by Electrophoretic Sol-Gel Deposition Using Phenyltriethoxysilane-Derived Particles. *J. Am. Ceram. Soc.* **1998**, *81* (9), 2501−2503.

(12) Klein, L. C.; Jitianu, A. Organic-Inorganic hybrid melting gels. *J. Sol-Gel Sci. Technol.* **2010**, *55*, 86−93.

(13) Jitianu, A.; Amatucci, G.; Klein, L. C. Phenyl-Substituted Siloxane Hybrid Gels that Soften Below 140°C. *J. Am. Ceram. Soc.* **2009**, *92*, 36−40.

(14) Jeong, S.; Ahn, S.-J.; Moon, J. Fabrication of Patterned Inorganic−Organic Hybrid Film for the Optical Waveguide by Microfluidic Lithography. *J. Am. Ceram. Soc.* **2005**, *88* (4), 1033−1036.

(15) Menaa, B.; Takahashi, M.; Tokuda, Y.; Yoko, T. Preparation and properties of polyphenylsiloxane-based hybrid glass films obtained from a non-aqueous coating sol via a single-step dip-coating. *Opt. Mater.* **2007**, *29*, 806−813.

(16) Kakiuchida, H.; Takahashi, M.; Tokuda, Y.; Masai, H.; Kuniyoshi, M.; Yoko, T. Viscoelastic and structural properties of a phenyl-modified polysiloxane system with a three-dimensional structure. *J. Phys. Chem. B* **2006**, *110*, 7321−7327.

(17) Yu, D.; Kleemeier, M.; Wu, G. M.; Schartel, B.; Liu, W. Q.; Hartwig, A. A low melting organic-inorganic glass and its effect on flame retardancy of clay/epoxy composites. *Polymer* **2011**, *52*, 2120−2131.

(18) Jitianu, A.; Doyle, J.; Amatucci, G.; Klein, L. C. Methyl modified siloxane melting gels for hydrophobic films. *J. Sol-Gel Sci. Technol.* **2010**, *53*, 272−279.

(19) Kuniyoshi, M.; Takahashi, M.; Tokuda, Y.; Yoko, T. OH-Free Phenyl Modified Siloxane Low-Melting Glasses with Ultra Low Saturated Water-Absorption. *J. Ceram. Soc. Jpn.* **2006**, *114* (7), 660−664.

(20) Jitianu, A.; Doyle, J.; Amatucci, G.; Klein, L. C. In *Methyl-Modified Melting Gels for Hermetic Barrier Coatings*, Proceedings MS&T 2008 Enabling Surface Coating Systems: Multifunctional Coatings, Pittsburgh PA, 2008.

(21) Kajihara, K.; Suzuki, R.; Seto, R.; Itakura, H.; Ishijima, M. Poly(cyclohexylsilsesquioxane)-Based Hydrophilic Thermoset-Resistant Deep-Ultraviolet-Transparent Glasses with Low Melting Temperatures. *ACS Appl. Mater. Interfaces* **2023**, *15* (26), 31880−31887.

(22) Aparicio, M.; Jitianu, A.; Rodriguez, G.; Degnah, A.; Al-Marzoki, K.; Mosa, J.; Klein, L. C. Corrosion Protection of AISI 304 Stainless Steel with Melting Gel Coatings. *Electrochim. Acta* **2016**, *202*, 325−332.

(23) Klein, L. C.; McClarren, B.; Jitianu, A. Silica-Containing Hybrid Nanocomposite "Melting Gels. *Mater. Sci. Forum* **2014**, *783*−*786*, 1432−1437.

(24) Jenkins, S.; Sciarrone, E.; Klein, L. C. Texturing melting gels for water harvesting. *J. Sol-Gel Sci. Technol.* **2022**, *101* (1), 37−45.

(25) Steinbrück, N.; Pohl, S.; Kickelbick, G. Platinum free thermally curable siloxanes for optoelectronic application-synthesis and properties. *RSC Adv.* **2019**, *9* (4), 2205−2216.

(26) Briesenick, M.; Gallei, M.; Kickelbick, G. High-Refractive-Index Polysiloxanes Containing Naphthyl and Phenanthrenyl Groups and Their Thermally Cross-Linked Resins. *Macromolecules* **2022**, *55* (11), 4675−4691.

(27) Pohl, S.; Janka, O.; Füglein, E.; Kickelbick, G. Thermoplastic Silsesquioxane Hybrid Polymers with a Local Ladder-Type Structure. *Macromolecules* **2021**, *54* (8), 3873−3885.

(28) Pohl, S.; Kickelbick, G. Influence of alkyl groups on the formation of softenable polysilsesquioxanes. *J. Sol-Gel Sci. Technol.* **2023**, *107*, 329.

(29) Macan, J.; Tadanaga, K.; Tatsumisago, M. Influence of copolymerization with alkyltrialkoxysilanes on condensation and thermal behaviour of poly(phenylsilsesquioxane) particles. *J. Sol-Gel Sci. Technol.* **2010**, *53* (1), 31−37.

(30) Macan, J.; Tadanaga, K.; Tatsumisago, M. Softening of Octyl-modified Phenylsilsesquioxanes. *Polimeri* **2011**, *32* (3−4), 112−118.

(31) Seto, R.; Kanamura, K.; Yoshida, S.; Kajihara, K. Cosolvent-free synthesis and characterisation of poly(phenyl-co-n-alkylsilsesquioxane) and poly(phenyl-co-vinylsilsesquioxane) glasses with low melting temperatures. *Dalton Trans.* **2020**, *49* (8), 2487−2495.

(32) Matsuda, A.; Sasaki, T.; Hasegawa, K.; Tatsumisago, M.; Minami, T. Thermal Softening Behavior and Application to Transparent Thick Films of Poly(benzylsilsesquioxane) Particles Prepared by the Sol−Gel Process. *J. Am. Ceram. Soc.* **2001**, *84* (4), 775−780.

(33) Takahashi, K.; Tadanaga, K.; Hayashi, A.; Tatsumisago, M. Substituent effects on the glass transition phenomena of polyorganosilsesquioxane particles prepared by two-step acid−base catalyzed sol−gel process. *J. Ceram. Soc. Jpn.* **2011**, *119* (1387), 173−179.

(34) Kannengießer, J.-F.; Briesenick, M.; Meier, D.; Huch, V.; Morgenstern, B.; Kickelbick, G. Synthesis and Hydrogen-Bond Patterns of Aryl-Group Substituted Silanediols and -triols from Alkoxy- and Chlorosilanes. *Chem. - Eur. J.* **2021**, *27* (66), 16461−16476.

(35) Kannengießer, J.-F.; Morgenstern, B.; Janka, O.; Kickelbick, G. Oligo-Condensation Reactions of Silanediols with Conservation of Solid-State-Structural Features. *Chem. - Eur. J.* **2024**, *30* (16), No. e202303343.

(36) Meier, D.; Huch, V.; Kickelbick, G. Aryl-group substituted polysiloxanes with high-optical transmission, thermal stability, and refractive index. *J. Polym. Sci.* **2021**, *59* (20), 2265−2283.

(37) Legrand, S.; Kabir, R.; Kärkkäinen, A. New Phenanthrenyl-Substituted Hybrid Organic-Inorganic Polysiloxanes for Optoelectronic Applications. *ChemistrySelect* **2023**, *8* (5), No. e202204271.

(38) Legrand, S.; Kärkkäinen, A. Design, synthesis, characterization, and aging properties of a new end-capped three-dimensional high-

https://doi.org/10.1021/acs.macromol.4c02737
Macromolecules 2025, 58, 1298−1313

refractive index hybrid organic−inorganic polysiloxane. *J. Appl. Polym. Sci.* **2021**, *138* (21), 50467.
(39) Liu, J.-G.; Ueda, M. High refractive index polymers: fundamental research and practical applications. *J. Mater. Chem.* **2009**, *19* (47), 8907−8919.
(40) Kurumada, K.-I.; Ashraf, K. M.; Matsumoto, S. Effects of heat treatment on various properties of organic−inorganic hybrid silica derived from phenyltriethoxysilane. *Mater. Chem. Phys.* **2014**, *144* (1), 132−138.
(41) Allcock, H. R.; Connolly, M. S.; Sisko, J. T.; Al-Shali, S. Effects of organic side group structures on the properties of poly(organophosphazenes). *Macromolecules* **1988**, *21* (2), 323−334.
(42) Stutz, H.; Illers, K.-H.; Mertes, J. A generalized theory for the glass transition temperature of crosslinked and uncrosslinked polymers. *J. Polym. Sci., Part B: Polym. Phys.* **1990**, *28* (9), 1483−1498.
(43) Bandzierz, K.; Reuvekamp, L.; Dryzek, J.; Dierkes, W.; Blume, A.; Bielinski, D. Influence of Network Structure on Glass Transition Temperature of Elastomers. *Materials* **2016**, *9* (7), 607.
(44) Dvornic, P. R.; Lenz, R. W. Exactly alternating silarylene-siloxane polymers. 9. Relationships between polymer structure and glass transition temperature. *Macromolecules* **1992**, *25* (14), 3769−3778.
(45) Schott, G.; Sprung, W. D. Silanole. V. Die thermische Kondensation von Diaryl-silandiolen. *Z. Anorg. Allg. Chem.* **1964**, *333* (1−3), 76−89.
(46) Shirai, S.; Goto, Y.; Mizoshita, N.; Ohashi, M.; Tani, T.; Shimada, T.; Hyodo, S.-a.; Inagaki, S. Theoretical Studies on Si−C Bond Cleavage in Organosilane Precursors during Polycondensation to Organosilica Hybrids. *J. Phys. Chem. A* **2010**, *114* (19), 6047−6054.
(47) Kuniyoshi, M.; Takahashi, M.; Tokuda, Y.; Yoko, T. Hydrolysis and polycondensation of acid-catalyzed Phenyltriethoxysilane (PhTES). *J. Sol-Gel Sci. Technol.* **2006**, *39*, 175−183.
(48) Gunji, T.; Hayashi, Y.; Komatsubara, A.; Arimitsu, K.; Abe, Y. Preparation and properties of flexible free-standing films via polyalkoxysiloxanes by acid-catalyzed controlled hydrolytic polycondensation of tetraethoxysilane and tetramethoxysilane. *Appl. Organomet. Chem.* **2012**, *26* (1), 32−36.
(49) Bain, A. D.; Eaton, D. R.; Hamielec, A. E.; Mlekuz, M.; Sayer, B. G. Line broadening in the carbon-13 NMR spectra of crosslinked polymers. *Macromolecules* **1989**, *22* (9), 3561−3564.
(50) Borovin, E.; Callone, E.; Ribot, F.; Diré, S. Mechanism and Kinetics of Oligosilsesquioxane Growth in the In Situ Water Production Sol−Gel Route: Dependence on Water Availability. *Eur. J. Inorg. Chem.* **2016**, *2016* (13−14), 2166−2174.
(51) Choi, S.-S.; Lee, A. S.; Hwang, S. S.; Baek, K.-Y. Structural Control of Fully Condensed Polysilsesquioxanes: Ladderlike vs Cage Structured Polyphenylsilsesquioxanes. *Macromolecules* **2015**, *48*, 6063−6070.
(52) Sen, T.; Bruce, I. J. Surface engineering of nanoparticles in suspension for particle based bio-sensing. *Sci. Rep.* **2012**, *2* (1), No. 564.
(53) Cabañas, M.; Lozano, D.; Torres-Pardo, A.; Sobrino, C.; González-Calbet, J.; Arcos, D.; Vallet-Regí, M. Features of amino-propyl modified mesoporous silica nanoparticles. Implications on the active targeting capability. *Mater. Chem. Phys.* **2018**, *220*, 260−269.
(54) Shea, K. J.; Loy, D. A.; Webster, O. Arylsilsesquioxane gels and related materials. New hybrids of organic and inorganic networks. *J. Am. Chem. Soc.* **1992**, *114* (17), 6700−6710.
(55) Andrianov, K. A.; Izmaylov, B. A. Hydrolytic poly-condensation of higher alkyltrichlorosilanes. *J. Organomet. Chem.* **1967**, *8* (3), 435−441.
(56) Wallace, W. E.; Guttman, C. M.; Antonucci, J. M. Molecular structure of silsesquioxanes determined by matrix-assisted laser desorption/ionization time-of-flight mass spectrometry. *J. Am. Soc. Mass Spectrom.* **1999**, *10* (3), 224−230.
(57) Wallace, W. E.; Guttman, C. M.; Antonucci, J. M. Polymeric silsesquioxanes: degree-of-intramolecular-condensation measured by mass spectrometry. *Polymer* **2000**, *41* (6), 2219−2226.
(58) Chen, X.; Eldred, D.; Liu, J.; Chiang, H.; Wang, X.; Rickard, M. A.; Tu, S.; Cui, L.; LaBeaume, P.; Skinner, K. Simultaneous In Situ Monitoring of Trimethoxysilane Hydrolysis Reactions Using Raman, Infrared, and Nuclear Magnetic Resonance (NMR) Spectroscopy Aided by Chemometrics and Ab Initio Calculations. *Appl. Spectrosc.* **2018**, *72*, 1404−1415.
(59) Li, Y.-S.; Wang, Y.; Ceesay, S. Vibrational spectra of phenyltriethoxysilane, phenyltrimethoxysilane and their sol-gels. *Spectrochim. Acta, Part A* **2009**, *71*, 1819−1824.
(60) Newton, W. E.; Rochow, E. G. Vibrational spectra of some trialkoxysilanes. *J. Chem. Soc. A* **1970**, 2664−2668.
(61) Brown, J. F. The Polycondensation of Phenylsilanetriol. *J. Am. Chem. Soc.* **1965**, *87*, 4317−4324.
(62) Orel, B.; Ješe, R.; Vilčnik, A.; Štangar, U. L. Hydrolysis and Solvolysis of Methyltriethoxysilane Catalyzed with HCl or Trifluoroacetic Acid: IR Spectroscopic and Surface Energy Studies. *J. Sol-Gel Sci. Technol.* **2005**, *34* (3), 251−265.
(63) Tagliazucca, V.; Callone, E.; Dirè, S. Influence of synthesis conditions on the cross-link architecture of silsesquioxanes prepared by in situ water production route. *J. Sol-Gel Sci. Technol.* **2011**, *60* (3), 236−245.
(64) Unno, M.; Alias, S. B.; Saito, H.; Matsumoto, H. Synthesis of Hexasilsesquioxanes Bearing Bulky Substituents: Hexakis((1,1,2-trimethylpropyl)silsesquioxane) and Hexakis(tert-butylsilsesquioxane). *Organometallics* **1996**, *15* (9), 2413−2414.
(65) Sassi, Z.; Bureau, J. C.; Bakkali, A. Spectroscopic study of TMOS−TMSM−MMA gels: Previously identification of the networks inside the hybrid material. *Vib. Spectrosc.* **2002**, *28* (2), 299−318.
(66) Ishida, H.; Koenig, J. L. Vibrational Assignments of Organosilanetriols. II. Crystalline Phenylsilanetriol and Phenylsilanetriol-D3. *Appl. Spectrosc.* **1978**, *32* (5), 469−479.
(67) Korkin, S. D.; Buzin, M. I.; Matukhina, E. V.; Zherlitsyna, L. N.; Auner, N.; Shchegolikhina, O. I. Phenylsilanetriol-synthesis, stability, and reactivity. *J. Organomet. Chem.* **2003**, *686* (1), 313−320.
(68) Hu, N.; Rao, Y.; Sun, S.; Hou, L.; Wu, P.; Fan, S.; Ye, B. Structural Evolution of Silica Gel and Silsesquioxane Using Thermal Curing. *Appl. Spectrosc.* **2016**, *70*, 1328−1338.
(69) Ye, M.; Wu, Y.; Zhang, W.; Yang, R. Synthesis of incompletely caged silsesquioxane (T_7-POSS) compounds via a versatile three-step approach. *Res. Chem. Intermed.* **2018**, *44*, 4277−4294.
(70) Ren, Z.; Xie, P.; Jiang, S.; Yan, S.; Zhang, R. Study of the supramolecular Architecture-Directed synthesis of a Well-Defined Triple-Chain ladder polyphenylsiloxane. *Macromolecules* **2010**, *43*, 2130−2136.
(71) Yu-zhong, F.; Sheng-li, Q.; Jing-jing, L.; Zhan-peng, W.; Xiaoping, Y.; Ri-guang, J.; De-zhen, W. Preparation and Characterization of Ordered Ladder Like Polyphenylsilsesquioxane via Two-step Sol-gel Method. *Chem. Res. Chin. Univ.* **2011**, *27*, 516−519.
(72) Xinsheng, Z.; Lianghe, S.; Chaoran, H. More on the Structures of Polyphenylsilsesquioxanes. *Chin. J. Polym. Sci.* **1987**, *5*, 353−358.
(73) Kang, W. R.; Lee, A. S.; Park, S.; Park, S. H.; Baek, K.-Y.; Lee, K. B.; Lee, S.-H.; Lee, J.-H.; Hwang, S. S.; Lee, J. S. Free-standing, polysilsesquioxane-based inorganic/organic hybrid membranes for gas separations. *J. Membr. Sci.* **2015**, *475*, 384−394.
(74) Papkov, V.; Gerasimov, M. V.; Buzin, M.; Il'ina, M. N.; Kazaryan, L. G. The structure of ordered phases in polydiphenylsiloxane. *Polym. Sci., Ser. A* **1996**, *38*, 1097−1102.
(75) Liu, F.; Zeng, X.; Lai, X.; Li, H. Synthesis and characterization of polyphenylsilsesquioxane terminated with methyl and vinyl groups low-melting glass. *J. Adhes. Sci. Technol.* **2017**, *31*, 2399−2409.
(76) Shang, X.; Cao, X.; Ma, Y.; Kumaravel, J. J.; Zheng, K.; Zhang, J.; Zhang, R. Diphenylsiloxane-bridged ladder-like hydrido-polysiloxane and the derivatisation by triphenylsiloxy substitution. *Eur. Polym. J.* **2018**, *106*, 53−62.

https://doi.org/10.1021/acs.macromol.4c02737
Macromolecules 2025, 58, 1298−1313

(77) Jovanovic, J. D.; Govedarica, M. N.; Dvornic, P. R.; Popovic, I. G. The thermogravimetric analysis of some polysiloxanes. *Polym. Degrad. Stab.* **1998**, *61* (1), 87−93.
(78) Camino, G.; Lomakin, S. M.; Lageard, M. Thermal polydimethylsiloxane degradation. Part 2. The degradation mechanisms. *Polymer* **2002**, *43* (7), 2011−2015.
(79) Xinsheng, Z.; Lianghe, S.; Shuqing, L.; Yizhen, L. Thermal Stability and Kinetics of Decomposition of Polyphenylsilsesquioxanes and Some Related Polymers. *Polym. Degrad. Stab.* **1988**, *20*, 157−172.
(80) Zhou, W.; Yang, H.; Guo, X.; Lu, J. Thermal degradation behaviors of some branched and linear polysiloxanes. *Polym. Degrad. Stab.* **2006**, *91*, 1471−1475.
(81) McManus, J. C.; Harano, Y.; Low, M. J. D. Infrared study of the interactions of acetone and siliceous surfaces. *Can. J. Chem.* **1969**, *47* (14), 2545−2554.
(82) Zhang, D.; Yang, R.; Qin, Z.; Zhang, W. Study on the thermal behaviors of polyhedral oligomeric octaphenylsilsesquioxane (OPS). *J. Therm. Anal. Calorim.* **2023**, *148* (6), 2345−2355.
(83) Bolln, C.; Tsuchida, A.; Frey, H.; Mülhaupt, R. Thermal Properties of the Homologous Series of 8-fold Alkyl-Substituted Octasilsesquioxanes. *Chem. Mater.* **1997**, *9* (6), 1475−1479.
(84) Förster, T.; Kasper, K. Ein Konzentrationsumschlag der Fluoreszenz des Pyrens. *Z. Elektrochem. Ber. Bunsenges. Phys. Chem.* **1955**, *59* (10), 976−980.
(85) Stevens, B.; Hutton, E. Radiative Life-time of the Pyrene Dimer and the Possible Role of Excited Dimers in Energy Transfer Processes. *Nature* **1960**, *186* (4730), 1045−1046.
(86) Birks, J. B.; Christophorou, L. G.; Flowers, B. H. 'Excime' fluorescence. IV. Solution spectra of polycyclic hydrocarbons. *Proc. R. Soc. London, Ser. A* **1964**, *277* (1371), 571−582.
(87) Vala, M. T., Jr.; Haebig, J.; Rice, S. A. Experimental Study of Luminescence and Excitation Trapping in Vinyl Polymers, Paracyclophanes, and Related Compounds. *J. Chem. Phys.* **1965**, *43* (3), 886−897.
(88) Fox, R. B.; Price, T. R.; Cozzens, R. F.; McDonald, J. R. Photophysical Processes in Polymers. IV. Excimer Formation in Vinylaromatic Polymers and Copolymers. *J. Chem. Phys.* **1972**, *57* (1), 534−541.
(89) Salom, C.; Horta, A.; Hernandez-Fuentes, I.; Pierola, I. F. Poly(phenylsiloxanes) electronic spectra. *Macromolecules* **1987**, *20*, 696−698.
(90) Liu, C.; Liu, Y.; Shen, Z.; Xie, P.; Zhang, R.; Yang, J.; Bai, F. Study of the Steric Tacticity of Novel Soluble Ladderlike Poly(phenylsilsesquioxane) Prepared by Stepwise Coupling Polymerization. *Macromol. Chem. Phys.* **2001**, *202*, 1581−1585.
(91) Hirayama, F. Intramolecular excimer formation. I. Diphenyl and triphenyl alkanes. *J. Chem. Phys.* **1965**, *42*, 3163−3171.
(92) Aladekomo, J. B.; Birks, J. B. 'Excimer' fluorescence VII. Spectral studies of naphthalene and its derivatives. *Proc. R. Soc. London, Ser. A* **1965**, *284*, 551−565.
(93) Lewis, F. D.; Burch, E. L. Excimer fluorescence from phenanthrene-9-carboxylate derivatives. *J. Photochem. Photobiol., A* **1996**, *96* (1), 19−23.
(94) Jones, P. F.; Nicol, M. Excimer Emission of Naphthalene, Anthracene, and Phenanthrene Crystals Produced by Very High Pressures. *J. Chem. Phys.* **1968**, *48* (12), 5440−5447.
(95) Chandross, E. A.; Thomas, H. T. Excited dimer luminescence of pairs of phenanthrene molecules. *J. Am. Chem. Soc.* **1972**, *94* (7), 2421−2424.
(96) Chandross, E. A.; Longworth, J. W.; Visco, R. E. Excimer Formation and Emission via the Annihilation of Electrogenerated Aromatic Hydrocarbon Radical Cations and Anions. *J. Am. Chem. Soc.* **1965**, *87* (14), 3259−3260.
(97) Chaoran, H.; Guangzhi, X.; Xinsheng, Z.; Lianghe, S. Studies on the Excimer Fluorescence and the Steric Tacticity of Polyphenylsilsesquioxanes. *Chin. J. Polym. Sci.* **1987**, *5*, 347−352.
(98) Belova, A. S.; Kononevich, Y. N.; Sazhnikov, V. A.; Safonov, A. A.; Ionov, D. S.; Anisimov, A. A.; Shchegolikhina, O. I.; Alfimov, M. V.; Muzafarov, A. M. Solvent-controlled intramolecular excimer emission from organosilicon derivatives of naphthalene. *Tetrahedron* **2021**, *93*, No. 132287.
(99) Chandross, E. A.; Dempster, C. J. Intramolecular excimer formation and fluorescence quenching in dinaphthylalkanes. *J. Am. Chem. Soc.* **1970**, *92* (12), 3586−3593.

https://doi.org/10.1021/acs.macromol.4c02737
Macromolecules 2025, 58, 1298−1313

4.4 Melt, mix, and glow: emulsion-based fabrication of polyphenylsilsesquioxane microspheres with embedded hydrophobic fluorophores

Published as an article:

Svenja Pohl, Nils Steinbrück, Michał Piotr Pachnicz, Guido Kickelbick, M*ater. Adv.* **2025**. DOI: 10.1039/D5MA00849B.

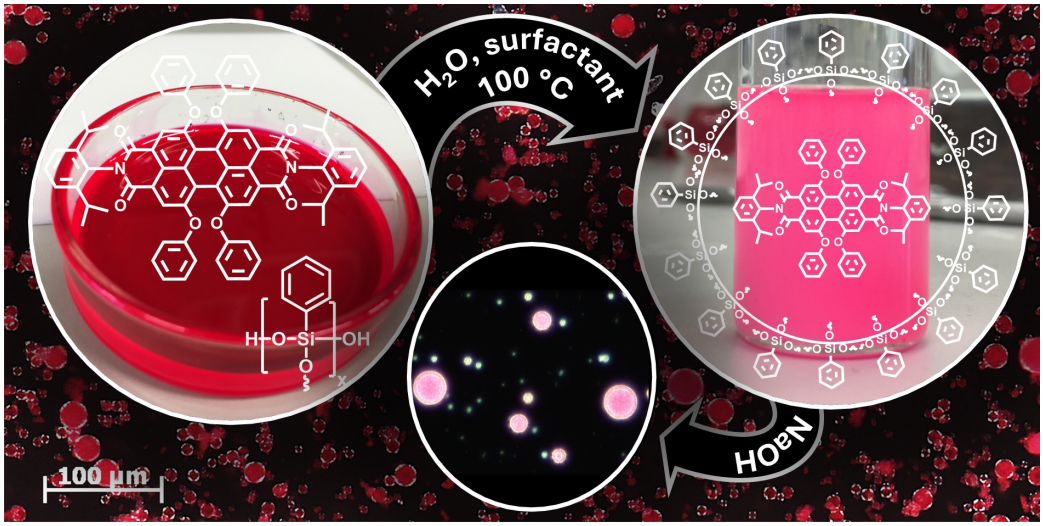

The supporting information is provided in Chapter 7 and is available online at: *https://doi.org/10.1039/D5MA00849B*.

The author's contribution to this work amounts to 40%.

Detailed statement of the individual contributions of the authors and co-authors:

Svenja Pohl and Nils Steinbrück contribute equally and wrote the complete draft of this manuscript that was acknowledged by all named authors. The topic of this article was initiated by Nils Steinbrück during his doctoral research.[411] He performed the initial characterization of the materials using TGA, IR, and NMR, and investigated the influence of stirring rate on particle size and size distribution. Nils Steinbrück conducted measurements and evaluations of the photophysical properties. Svenja Pohl extended the study by encapsulating additional dyes and incorporating them into polymethylsiloxane resins. She synthesized particles with varying concentrations of Lumogen F Red 305, examining the effect of concentration on the quantum

yield. In addition, she applied further characterization methods such as XRD and SP-MAS NMR, and TCSPC analysis, placing particular emphasis on the structural features and their changes during synthesis and thermal treatment. Michal P. Pachnicz supported the synthesis and characterization, proofread the manuscript, and contributed to the discussion of the results. Prof. Dr. Guido Kickelbick gave the input to this project, supervised and discussed it, and optimized the manuscript to its final form.

The thermoplastic processability of melting gels, combined with their compatibility with aromatic compounds, provides a promising platform for the encapsulation of functional, hydrophobic molecules. π–π interactions with the phenyl-functionalized siloxane matrix enable the straightforward incorporation of hydrophobic dyes such as Lumogen® F Red 305 by direct addition during synthesis.

The publication "*Melt, mix, and glow: emulsion-based fabrication of polyphenylsilsesquioxane microspheres with embedded hydrophobic fluorophores"*, presents a melt-emulsion approach that utilizes the softening behavior of a phenyltrimethoxysilane-derived precursor gel to generate fluorescent microspheres. The hydrophobic perylene-based dye Lumogen® F Red 305 (LG305) was successfully incorporated during the gelation step, yielding a red, fluorescent hybrid material. Emulsification in a hot, aqueous surfactant solution followed by base-catalyzed polycondensation resulted in spherical particles with a narrow size distribution. A broad range of characterization techniques, including NMR, FTIR, TGA, fluorescence spectroscopy, quantum yield and fluorescence lifetime measurements, and PXRD, was employed to investigate the photophysical behavior and structural transformations during microsphere formation.

The as-prepared particles were partially crosslinked and dispersible in polar solvents due to residual surfactant present on the surface. Subsequent thermal treatment at 200 °C achieved nearly complete crosslinking and surfactant removal, yielding solvent-resistant, hydrophobic microspheres. Despite the high crosslinking density, selective dye leaching was observed in certain organic solvents, while the dye remained stably encapsulated in polar and strongly apolar media. Spectroscopic analysis revealed a significantly increased proportion of ladder-like structural motifs compared to the original phenyl-based precursor gel.

Effective encapsulation of LG305 was achieved over a wide concentration range (220–26,000 ppm), yielding quantum efficiencies of up to 74% and a significant increase in fluorescence lifetime compared to the pure dye. Furthermore, additional hydrophobic dyes such as Oracet® FL Pink 285 and Oracet® FL Orange 240 were successfully embedded using the same strategy. This melt-emulsion approach provides a versatile route for the preparation of functional silsesquioxane-based microspheres, enabling controlled encapsulation of hydrophobic dyes across a broad concentration range. The chemical stability of the silsesquioxane matrix combined with adjustable emission characteristics make these materials suitable for applications in optoelectronics or luminescent solar concentrators.

Materials Advances

ROYAL SOCIETY OF CHEMISTRY

PAPER

View Article Online
View Journal

Cite this: DOI: 10.1039/d5ma00849b

Melt, mix, and glow: emulsion-based fabrication of polyphenylsilsesquioxane microspheres with embedded hydrophobic fluorophores

Svenja Pohl, †[a] Nils Steinbrück, †[a] Michał P. Pachnicz [a] and Guido Kickelbick *[ab]

A novel melt-emulsion strategy is presented for synthesizing polyphenylsilsesquioxane (PPSQ) microspheres embedded with hydrophobic perylene-based fluorescent dyes. The approach utilizes a low-crosslinked, thermally softenable PPSQ precursor – referred to as a "melting gel" – which incorporates polycyclic aromatic dyes such as Lumogen® F Red 305 (LG305) taking advantage of both hydrophobic compatibility and π–π interactions within the phenyl-rich matrix. Upon heating above 70 °C, the precursor forms an emulsion in boiling water containing Triton™ X-405, followed by sodium hydroxide-induced condensation to yield solid microspheres (~3 μm diameter). A subsequent thermal treatment at 200 °C enhances crosslinking, forming a condensed $PhSiO_{1.5}$ network and removing surfactant residues, thereby shifting surface polarity from hydrophilic to hydrophobic. Comprehensive characterization using NMR, FTIR, XRD, TGA, fluorescence spectroscopy, fluorescence lifetime and quantum yield analysis confirms the formation of a ladder-type silsesquioxane structure and retention of dye fluorescence. This two-step process enables efficient encapsulation of various hydrophobic dyes across a wide concentration range, offering a versatile platform for developing stable, processable luminescent materials for applications such as LED encapsulants and luminescent solar concentrators.

Received 4th August 2025,
Accepted 17th September 2025

DOI: 10.1039/d5ma00849b

rsc.li/materials-advances

Introduction

Silica- and silsesquioxane particles modified with fluorescent dyes have gained significant attention due to their versatile applications in fields such as bioimaging,[1] sensors,[2,3] light-harvesting systems[4] or light emitting diodes (LED).[5,6] Their silicon-oxide based matrix offers several advantages, including ease of surface functionalization, good biocompatibility, chemical inertness, and photochemical stability.[7–9] These properties make it an ideal host for dye molecules, providing a protective environment that minimizes both photobleaching and self-aggregation.[4,5,10] Moreover, the matrix's transparency in the visible spectrum ensures that the photophysical properties of embedded chromophores remain unaffected.[11,12]

Traditional synthesis methods for silica particles, such as the Stöber process[13] and reverse microemulsion techniques,[14] rely on sol–gel chemistry involving the acid- or base-catalyzed hydrolysis and condensation of alkoxide precursors. By employing organofunctional alkoxysilanes as precursors, organically modified silica (ORMOSIL) nanoparticles can be produced, with tunable properties based on the nature of the organics substituents attached to the monomers.[15,16] Dyes may be incorporated into these matrices either covalently or non-covalently. Covalent attachment prevents dye leaching but requires suitable functional groups on the dye that can react with the alkoxysilane precursor.[17–20] While ionic dyes are relatively easy to integrate,[21,22] nonionic, hydrophobic dyes pose a significant challenge due to their poor solubility in common solvents used in the sol–gel process like water or ethanol.

Recent efforts have explored modified Stöber processes to incorporate hydrophobic aromatic dyes into phenyl-functionalized silica particles.[4,23,24] In these cases, hydrophobic and π–π stacking interactions between the phenyl groups of the trialkoxysilane precursor and aromatic dye facilitate the physical entrapment of the fluorophores within the matrix. However, dye loading remains difficult to control and is largely dependent on the phenyl group content in the matrix.[4]

An entirely different approach for particle synthesis involves melt emulsification, a technique well-established in fields such as food technology,[25] pharmaceuticals,[26] and additive manufacturing.[27] This method utilizes thermoplastic materials that are melted and emulsified in a continuous phase with

[a] Inorganic Solid-State Chemistry, Saarland University, Campus, Building C4.1, 66123 Saarbrücken, Germany. E-mail: guido.kickelbick@uni-saarland.de
[b] Saarene, Saarland Center for Energy Materials and Sustainability, 66123 Saarbrücken, Germany
† These authors contributed equally to this work.

surfactants under shear, forming droplets that solidify upon cooling into spherical particles. Despite its versatility, this approach has not been applied to silica-based systems, primarily due to the absence of thermoplastic materials with a Si–O–Si backbone.

A promising class of materials that meets the requirements for melt-emulsion processing is the so-called melting gel – a silica-based gel that is rigid and glass-like at room temperature but softens upon heating to approximately 100 °C. Further heating above 130 °C induces irreversible thermal curing.[28,29] These materials are known for their high thermal stability,[30] low gas permeability,[31] and broad-range optical transparency.[32,33] Most melting gels are functionalized with phenyl groups, which not only contribute to their thermal and optical properties but also enable non-covalent incorporation of aromatic, hydrophobic dyes such as perylene diimides. These dyes are particularly attractive for applications in luminescent solar concentrators (LSCs) and LED technologies.[34–36]

In this study, we report the synthesis of a polyphenylsilsesquioxane (PPSQ) melting gel into which various perylene-based dyes (Lumogen® F Red 305 (LG305), Oracet® FL Pink 285, Oracet® FL Orange 240) were incorporated during synthesis. This precursor gel was used to form fluorescent microspheres *via* a modified two-step melt emulsion method. In this process, the dye containing softenable gel formed an emulsion in boiling aqueous surfactant solution, which was subsequently solidified by the addition of NaOH as a basic condensation catalyst.

The successful encapsulation of the dyes was confirmed by fluorescence spectroscopy and fluorescence lifetime analysis and the effect of Lumogen® F Red 305 concentration on quantum yield was investigated. The structure of the precursor gel, as well as structural changes occurring during particle formation, were analyzed using various spectroscopic and thermal methods, as well as powder X-ray diffraction (PXRD).

Encapsulation within the PPSQ matrix not only protects the embedded fluorophores from environmental degradation but also facilitates their integration into secondary matrices, such as elastomeric materials, for use in bulk optical applications.

Experimental

Materials

Phenyltrimethoxysilane (97%, abcr GmbH, Germany), polyoxyethylene(40)isooctylphenylether solution (Triton™ X-405, 70% in water, Sigma-Aldrich/Merck KGaA, Germany), hydrochloric acid (Bernd Kraft GmbH, Germany) and sodium hydroxide (85%, Grüssing GmbH Analytica, Germany) were used as received. The commercially available, curable OE6630 polysiloxane resin (Dow, Dow Corning Inc., USA) and the perylene dyes Lumogen® F Red 305 (LG305, BASF, Germany), Oracet® FL Orange 240 (SunChemical, Germany) and Oracet® FL Pink 285 (SunChemical, Germany) were also used as received without any further purification. The hydrochloric acid was diluted with demineralized water (pH = 2.5). Sodium hydroxide was dissolved in demineralized water (3 mol l^{-1}). NMR characterization of key reactants, melting gels, and microspheres is provided in (Fig. S1–S8).

Instrumentation

Solution nuclear magnetic resonance (NMR) spectra were recorded on an Avance III 300 MHz spectrometer and an Avance III HD 400 MHz spectrometer (Bruker, Billerica, USA) with 300.13/400.13 MHz for ^{1}H NMR spectra, 75.47/100.61 MHz for ^{13}C NMR spectra and 59.63/79.49 MHz for ^{29}Si NMR spectra. NMR samples were prepared in $CDCl_3$ and D_2O. Spectra were analyzed using MestReNova.[37] Single-pulse (SP) magic angle spinning (MAS) NMR spectra were recorded on an Avance III HD – Ascend 400WB spectrometer (Bruker, Billerica, USA) using 4 mm inner diameter ZrO_2 rotors with 13 kHz rotation frequency. The resonance frequencies were 79.53 MHz for ^{29}Si NMR spectra and 100.65 MHz for ^{13}C NMR spectra. The measurements were performed with a relaxation of 20 s. Adamantane was used for ^{13}C NMR and octakis(trimethylsiloxy)silsesquioxane for ^{29}Si NMR as external standard. Peaks of ^{29}Si CP-MAS spectra were deconvoluted and integrated with a Lorentzian-Gaussian fit using MestReNova.[37] For the visualization of sub millimeter structures an Axioskop 50 transmitted light/fluorescence microscope (Carl Zeiss Microscopy GmbH, Germany) with an AxioCam MRc (1388 × 1040 pixel) was used. The particles were counted with the help of the ImageJ software (version 1.53 k).[38] Attenuated total reflectance Fourier transform infrared (ATR-FTIR) spectra were recorded on a Vertex 70 spectrometer (Bruker Optics, Billerica, USA) in total reflectance mode from 450–4500 cm^{-1} with a resolution of 4 cm^{-1} and 16 scans. Thermogravimetric analysis-Fourier transform infrared spectroscopy (TG-FTIR) was performed using a Vertex 70 spectrometer (Bruker Optics, Ettlingen, Germany) coupled to a TG F1 Iris (NETZSCH-Gerätebau GmbH, Selb, Germany). Each FTIR spectrum was performed in the wavenumber range 550–4500 cm^{-1} and by averaging 16 scans with a spectral resolution of 4 cm^{-1}. The measurements were carried out at 20 K min^{-1} heating rate in the temperature range between 30 and 1000 °C under synthetic air flow (40 mL min^{-1}, N_2/O_2 75%/25%). Fluorescence spectroscopy of particles was performed applying a FluoroMax 4 Spectrofluorometer (Horiba Scientific, Kyoto, Japan) as solid in quartz glass tubes. Absolute photoluminescence quantum yields were measured in a Quantaurus C11347-11 integration sphere setup (Hamamatsu Photonics, Hamamatsu, Japan) with a xenon high-pressure lamp and a multichannel analyzer. Fluorescence lifetime measurements were performed on the samples in the solid state using time-correlated single-photon counting (TCSPC) under magic angle conditions. A pulsed laser (λ_{exc} = 490 nm, FemtoFiber pro TVIS, Toptica Photonics, Gräfelfing, Germany, 80 MHz) served as excitation source, passed through a 470/40 bandpass clean-up filter. For detection, a photocounting detector (PDM series, Micro Photon Devices, Bolzano, Italy), a photocounting device (Pico Harp 300, PicoQuant, Berlin, Germany), and a 685/70 bandpass filter were used. An instrumental response function (IRF) was recorded with a diluted colloidal silica solution (LUDOX TM-50, Sigma-Aldrich, St. Louis, MO, USA). Data analysis was carried out with commercial software

SymPhoTime.[39] Powder X-ray diffraction (PXRD) patterns of the pulverized samples were recorded at room temperature on a D8-A25-Advance diffractometer (Bruker-AXS, Karlsruhe, Germany) in Bragg–Brentano θ–θ-geometry (goniometer radius 280 mm) with non-monochromatic Cu K_α radiation (λ = 154.0596 pm). A 12 μm Ni foil working as K_β filter and a variable divergence slit were mounted at the primary beam side. A Lynxeye detector with 192 channels and a variable anti-scatter slit in front of it was used at the secondary beam side. Experiments were carried out in a 2θ range of 3 to 40° with a step size of 0.013° and a total scan time of 1 h. The recorded data was evaluated using the TOPAS 5.0 software.[40] UV-VIS measurements were performed on a Lambda 750 instrument (PerkinElmer Inc., Shelton, USA) equipped with a 100 mm integration sphere with a 2 nm increment and 0.2 s integration time. Transmission spectra of the composites, cured in aluminum frames, were recorded from 300 to 800 nm. Scanning electron microscope (SEM) images were obtained using a JEOL JSM-7000 F microscope (JEOL, Freising, Germany) operating at 20 kV with a working distance of 10 mm. The SEM samples were prepared by placing a small amount of the particles on a specimen stub covered with a carbon adhesive foil followed by deposition of a gold layer (JEOL JFC-1300 auto fine coater, 30 mA, 40 s) to avoid charging effects. The complex viscosity was determined applying a MCR-302 rheometer with a CTD-450 convection heating system (Anton Paar GmbH, Graz, Austria) in the oscillatory mode using parallel-plate geometry with an upper diameter of 25 mm, an amplitude of 1% and a frequency of 1 Hz. During the measurement the temperature was lowered from 100 °C to 55 °C with the rate of 2 K min^{-1}.

Preparation

Synthesis of precursor melting gel (MG). Following a reported procedure,[41] phenyltrimethoxysilane (7 g, 35.30 mmol) and aqueous hydrochloric acid (pH = 2.5, 0.95 g, 52.95 mmol, 1.5 eq.) were stirred in a sealed vial (45 °C, 8 h). The solution was transferred into a beaker (100 mL) and a certain amount of LG305 (Oracet® FL Orange 240 or Oracet® FL Pink 285) was added (5.15 mg, n(LG305) = 5.3 μmol). The mixture was stirred until gelation was completed (25 °C, 18 h), visible by a significant increase in viscosity. The beaker was transferred into a vacuum oven to interrupt reactions by removing water, hydrochloric acid and methanol in two steps (30 mbar, 70 °C, 24 h; 110 °C, 24 h). The viscous and flowable red material was cooled to room temperature to obtain the solid PPSQ precursor melting gel (4.48 g, 1150 ppm dye). The material softens reversible at temperature >70 °C. At temperatures >130 °C it consolidates irreversibly. The unconsolidated material containing the dye LG305 was denoted with MG LG305. The consolidated material (200 °C, 24 h) was denoted with $MG_{cons.}$ LG305.

For concentration-dependent quantum yield measurements, additional MGs containing 26 000 ppm, 10 600 ppm, 4350 ppm, 2450 ppm and 220 ppm of LG305 were prepared by simply adjusting the amount of dye added during synthesis. The exact sample weights and calculated dye concentrations are provided in (Table S1).

Table 1 Variation of stirring rate, stirring time and dispersion method for the synthesis of MGP LG305

Sample	Stirring rate [rpm]	Stirring time
MGP-1	500	1 h
MGP-2	500	2 h
MGP-3	800	1 h
MGP-US	500	10 min
	Only ultra-sonic (150 W)	2 min
MGP-UT	500	10 min
	10 000 (disperser)	2 min

Synthesis of melting gel microspheres (MGP). Polyoxyethylene(40)isooctylphenylether solution (90 mg, Triton™ X-405, 70 wt% in water (~0.356 mmol g^{-1})) was added to water (14 mL, 0.77 mol) and stirred at 500 rpm at 100 °C. The precursor melting gel (100 mg) was then added to the hot solution, forming an emulsion upon softening. Stirring was continued at a 800 rpm for 1 h at 100 °C. A sodium hydroxide solution (1 mL, 3 mol L^{-1}) was subsequently added to the emulsion, followed by further stirring at 500 rpm for 1 h at 100 °C. The emulsion was then cooled in an ice bath. The resulting melting gel microspheres were isolated by centrifugation, washed four times with water, and dried in a compartment drier under reduced pressure (80 °C, 5 mbar). The product obtained from MG LG305 was denoted as MGP LG305.

To investigate the influence of varying mechanical energy input on particle morphology, five experiments were conducted using different stirring procedures (Table 1), employing MG LG305 (1150 ppm). Different stirring rates and durations were tested, along with the effect of high-energy processes, by applying an ultrasonic probe (US) (150 W) and an Ultra-Turrax™ disperser (UT) (10 000 rpm) after an initial stirring at 500 rpm for 10 min at 100 °C. The specified stirring rates and durations refer to the experimental steps prior to the addition of sodium hydroxide. After the base was added, all samples were stirred at 500 rpm for 1 h at 100 °C. Particle size and distribution were determined by measuring and counting particles from microscopy images.

Post-curing. For further investigations of temperature-induced changes in structure or heat stability, the MGP LG305 microspheres were additionally heat treated in a post-curing process (200 °C, 24 h). The obtained tempered particles were denoted with MGP-T LG305.

Particle integration in polyphenylmethylsiloxane resin. MGP-T microspheres (1 wt% of MGP-T (1150 ppm dye)) were added to the polyphenylmethylsiloxane resin Dow Corning OE6630 (Dow). The two Dow components, A and B, were premixed according to the manufacturer's specifications (1/4). The particles were then incorporated into this matrix, and gas was removed under reduced pressure (4 mbar, >30 min). The degassed mixture was cast into aluminum frames (8 × 2 mm) and cured for 2 h at 150 °C.

Results and discussion

Synthesis and characterization of the dye-doped precursor

The dye-doped precursor melting gel was synthesized *via* an acid-catalyzed polycondensation reaction of phenyltrimethoxysilane,

forming partially crosslinked structures.[41,42] During the gelation step a perylene-based dye (Lumogen® F 305 Red, Oracet® FL Orange 240 or Oracet® FL Pink 285) was added (Fig. 1). At this stage, oligomeric phenylsilsesquioxane and methanol generated from hydrolysis and partial condensation are present, providing a medium in which the dye is soluble. This enables homogeneous incorporation into the network despite its insolubility in water. In the following, we will concentrate on the characterization of the material containing Lumogen® F 305 Red (MG LG305, 1150 ppm dye).

The resulting material is a rigid, transparent, red-colored solid, soluble in organic solvents and thermally softenable above 70 °C. Rheological measurements (Fig. S10) confirm its softening behavior. Upon thermal treatment above 130 °C, irreversible curing occurs, yielding MG_{cons}. LG305, which is insoluble and no longer softenable. The structural properties of both the precursor and the cured precursor, excluding the dye, have been thoroughly examined in a previous study.[41]

FTIR spectroscopy of MG LG305 reveals the expected vibration bands of the PPSQ network, including broad ν(Si–O–Si) vibrations between 1000 and 1150 cm^{-1} and phenyl group associated signals at 3080–3010 ($(C–H)_{ring}$), 1595 and 1430 cm^{-1} ($\nu(C–C)_{ring}$) and 1130 cm^{-1} ($\nu(Si–C)_{ring}$). Additional vibration bands at 3380 ($\nu(O–H)_{associated}$), 3620 ($\nu(O–H)_{isolated}$), 910 (ν(Si–OH)), 2940–2840 ($\nu(C–H(O–CH_3))$), 1090 and 806 cm^{-1} ($\nu(Si–O–CH_3)$) indicate the presence of residual hydroxy and methoxy groups (Fig. 2).[43–45]

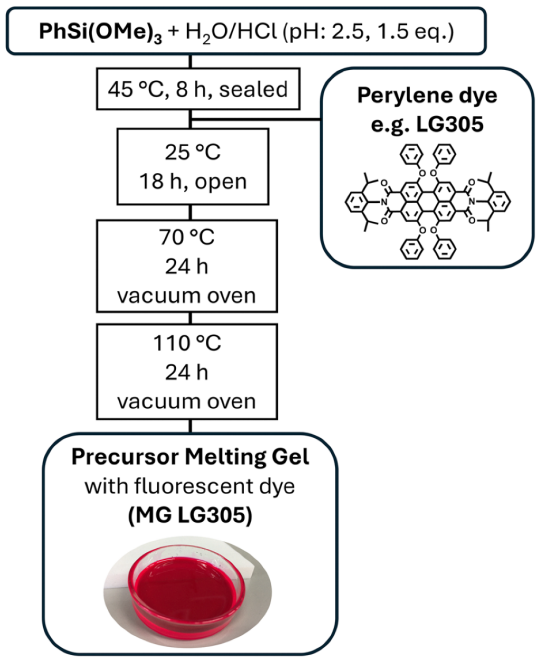

Fig. 1 Synthesis procedure for the Lumogen® F 305 Red (LG305) containing polyphenylsilsesquioxane precursor melting gel (MG LG305). The amount of monomer and dye loading can be adjusted; in this study, samples with dye concentrations between 220 and 26 000 ppm were prepared. Alternatively, other hydrophobic dyes can be incorporated using the same approach.

^{1}H and ^{13}C NMR spectra confirm the presence of phenyl and methoxy groups, with phenyl proton signals between 7.84–6.65 ppm and methoxy proton signals at 3.76–2.86 ppm. The estimated remaining methoxy group content is around 10% (Fig. S4). The corresponding carbon chemical shifts appear at 134.35–127.83 ppm (phenyl) and 50.65 ppm (OCH_3) (Fig. 3(a)). Due to the low dye concentration (1150 ppm) in the sample investigated, signals from the integrated dye are barely visible in both the IR and NMR spectra.

^{29}Si NMR spectra indicate a partially crosslinked structure, predominantly composed of T^2 (−71.6 ppm) and T^3 (−79.5 ppm) units, where T refers to a silicon atom bonded to one carbon atom and three oxygen atoms, while the superscript denotes the number of siloxane bonds (Si–O–Si) per unit. The percentage share of T^2 and T^3 is 53% and 40%, as determined by deconvolution of ^{29}Si SP-MAS NMR spectra (Fig. 3(b) and Fig. S5). The low degree of condensation (DC) of 78%, along with residual alkoxy and hydroxy groups causes flexibility of the polymer chains at elevated temperatures and explains reversible softening and solubility.[41]

Thermal treatment of the precursor at 200 °C induces further condensation of residual OH and OCH_3 groups, resulting in irreversible consolidation. This is evidenced by a TGA mass loss of 4% starting at about 200 °C. The evolved gas analysis by FTIR at these temperatures shows characteristic vibrations of the condensation by-products, methanol and water (Fig. S11). Following this consolidation step, degradation of the organic groups and the polymer network begins only at 500 °C, demonstrating the material's high thermal stability. The FTIR spectrum of the cured material shows a reduction in OH-associated bands at 3380 cm^{-1} (Fig. 2), while ^{29}Si SP-MAS NMR indicates an increase in T^3 units and a decrease in T^2 and T^1 species (Fig. 3(b)) consistent with further crosslinking. However, the presence of residual OCH_3 groups detected in ^{13}C SP-MAS NMR, along with a degree of condensation of 83%, and the persistence of isolated OH group, observed in FTIR spectra at 3620 cm^{-1}, suggest incomplete crosslinking. This partial crosslinking of phenyltrialkoxysilanes was already reported for silsesquioxane-based particles and can be explained by the bulky phenyl substituents that sterically hinder the formation of dense T^3 networks.[15,46,47] Nevertheless, the crosslinking is sufficient to eliminate chain mobility, rendering the material insoluble and thermally stable.

PXRD and FTIR spectroscopy provide more detailed insights into the structure of silsesquioxanes, which typically include cage, open-cage, and ladder structures, as well as random silsesquioxanes or mixtures thereof.[48] PXRD analysis reveals two broad amorphous peaks, indicative of ladder-like structural motifs (Fig. 4). The first reflection (d_1) corresponds to interchain distances modulated by phenyl groups, while the second (d_2) relates to Si–O–Si spacing.[49–51]

Thermal curing leads to a shift of $2\theta_{d_1}$ to lower values (larger chain-to-chain distance), an increase in the $2\theta_{d_1}/2\theta_{d_2}$ intensity ratio, as well as a sharpening of $2\theta_{d_1}$ reflection (reduction in full width at half maximum) (Table S2). These changes indicate enhanced structural order and an increase in ladder-like content in the $MG_{cons.}$ LG305.[52,53]

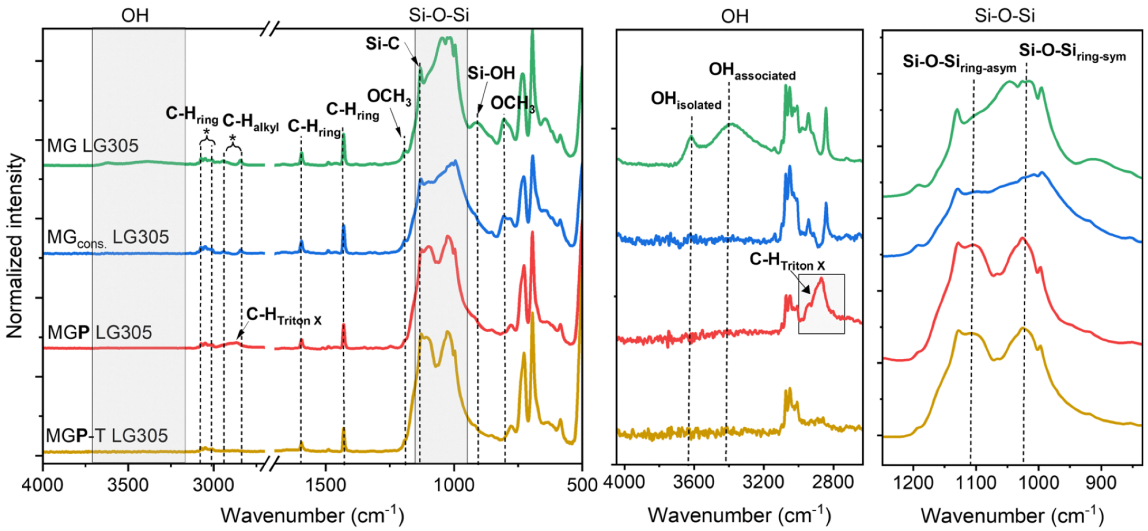

Fig. 2 FTIR spectra of MG LG305, $MG_{cons.}$ LG305, MGP LG305 and MGP-T LG305, showing the full spectrum and a magnified view of the OH-group region and the Si–O–Si vibration region with assignment of the most important vibrations.

FTIR spectra support this interpretation, showing a moderate splitting of the Si–O–Si stretching vibrations at $\nu(Si–O–Si)_{ring\text{-}asym}$ = 1106 cm^{-1} and $\nu(Si–O–Si)_{ring\text{-}sym}$ = 1023 cm^{-1}, characteristic of ladder-like architectures.[54,55] However, the intensity of $\nu(Si–O–Si)_{ring\text{-}asym}$ coming from highly symmetrical $(Si–O)_4$ ring subunits is significantly lower than that observed for phenyl ladders reported in the literature.[50,56,57] Furthermore the Si–O–Si region is quite unstructured, indicating a high number of defects caused by residual hydroxy and methoxy groups, random structural units with various silsesquioxane motifs, such as small rings or open and closed cages.[41]

Overall, the integration of LG305 does not significantly affect the hydrolysis or condensation behavior of phenyltrimethoxysilane and the final structure of the precursor gel, due to the low dye concentration. At the loading of 1150 ppm used in the material investigated here, the dye is barely detectable by

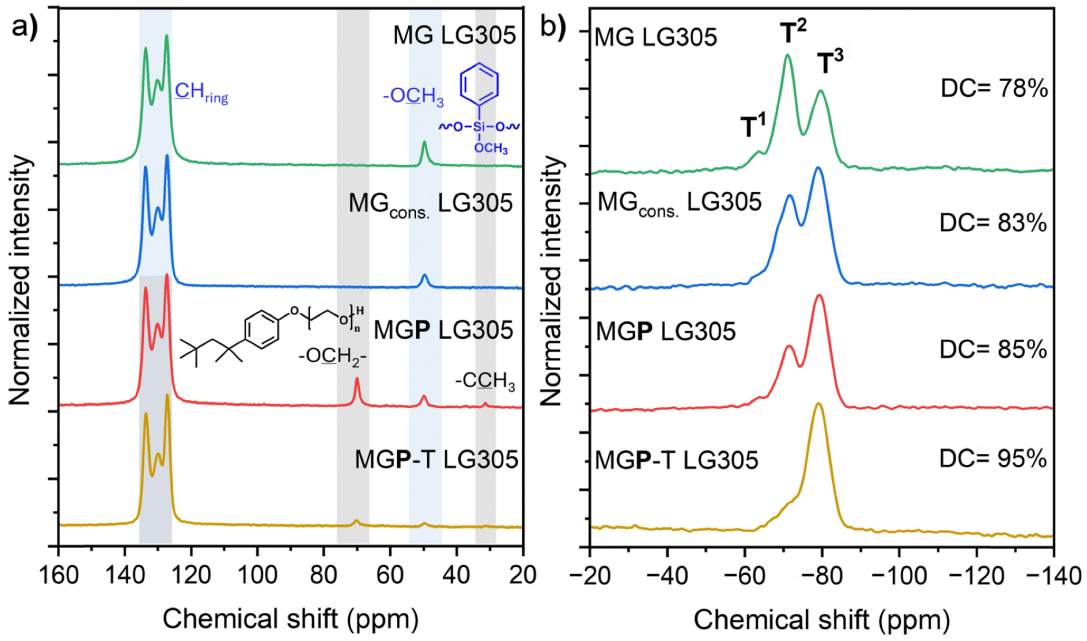

Fig. 3 (a) ^{13}C SP-MAS NMR spectra of MG LG305, $MG_{cons.}$ LG305, MGP LG305 and MGP-T LG305, illustrating the removal of the surfactant and further condensation of the microsphere structure, (b) ^{29}Si SP-MAS NMR spectra of MG LG305, $MG_{cons.}$ LG305, MGP LG305 and MGP-T LG305, showing the changes in T units and the degree of condensation (DC), calculated from deconvoluted ^{29}Si SP-MAS NMR spectra according to the formula: DC (%) = (T^3 (%)·3 + T^2 (%)·2 + T^1 (%))/3.

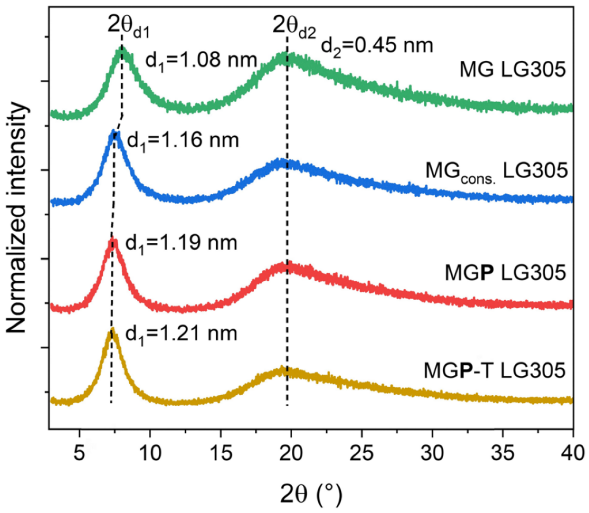

Fig. 4 Powder XRD patterns of MG LG305, $MG_{cons.}$ LG305, MGP LG305 and MGP-T LG305 with marked positions of $2\theta_{d_1}$ and $2\theta_{d_2}$ and corresponding d_1 and d_2 values.

NMR and IR spectroscopy. Only at an increased concentration of over 2000 ppm do peaks appear in the NMR spectra that can be attributed to LG305 (Fig. S9).

Formation of microspheres *via* melt emulsion

For the subsequent formation of microspheres, MG LG305 was added to a boiling aqueous solution of the nonionic surfactant Triton™ X-405 (Fig. 5). Upon heating, the material softened, and continuous stirring led to the formation of a hot emulsion in which the surfactant stabilized the molten droplets, preserving their spherical morphology and controlling particle size. In the absence of surfactant, particle formation is not driven by controlled dispersion but rather by mechanical fragmentation, resulting in angular, irregularly shaped particles (Fig. S12).

The hydrophobic perylene-based dye LG305 remained confined within the organic phase, preventing leaching into the aqueous medium. Subsequent addition of NaOH initiated base-catalyzed hydrolysis and condensation of residual hydroxy and methoxy groups at the droplet surface, chemically consolidating the microspheres and preserving their shape. The resulting particles (MGP LG305) were isolated by centrifugation.

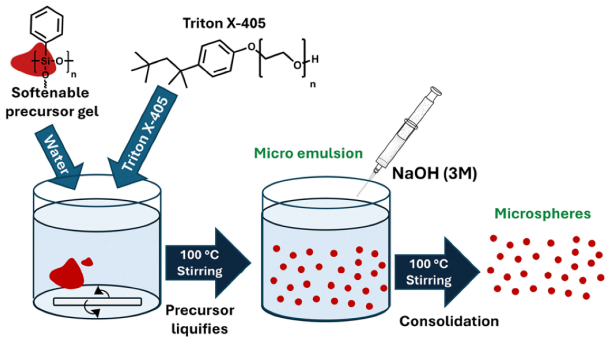

Fig. 5 Schematic workflow for the preparation of PPSQ microspheres.

Due to light scattering effects, the color of the material changed from red to pinkish (Fig. 6(a)).

Microscopic analysis reveals spherical particles within the micrometer range (Fig. 6(b)). SEM measurements confirm the spherical morphology of the particles, but also show the presence of cavities within the spheres that are larger than ≈5 μm in diameter (Fig. 6(c)). These holes can be explained by the formation of water and methanol as by-products of the base-catalyzed polycondensation reaction. As these volatile compounds evaporate, gas bubbles become trapped within the partially solidified microspheres. Since the material can no longer soften at this stage, the cavities remain open and persist within the particle structure. Consistently, similar voids are also observed in control samples prepared without surfactant (Fig. S12b), indicating that outgassing of condensation by-products is the main origin of this morphology, while the surfactant appears to have little or no direct influence on cavity formation.

Notably, such hollow features are absent in smaller microspheres <5 μm (Fig. 6(d)).

The obtained microspheres are completely insoluble in water or ethanol but exhibit swelling and partial solubility in acetone or chloroform, leading to the degradation of the particulate structure and leaching of the dye (Fig. S13 and S14). In hydrophilic

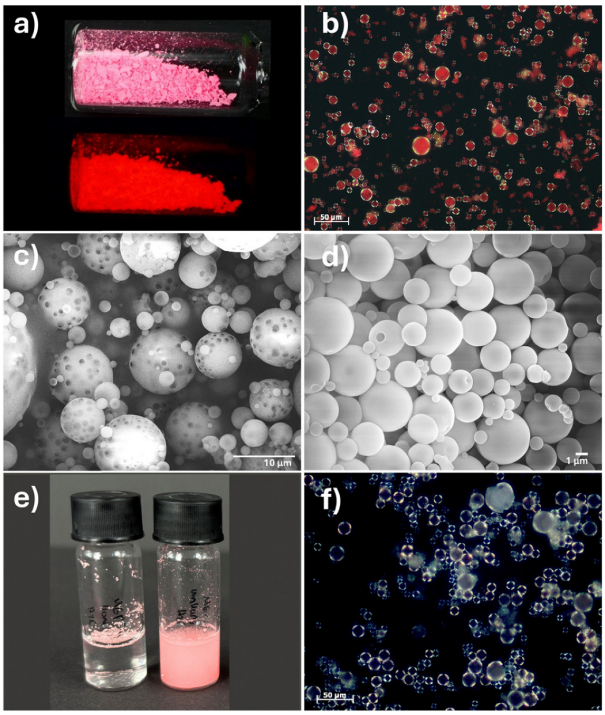

Fig. 6 (a) Image of MGP LG305 under natural light and showing red fluorescence under LED light (λ = 450 nm), (b) microscopy image of MGP LG305, dispersed in EtOH, (c) SEM image of MGP LG305 at 2500× magnification, (d) SEM image of MGP LG305 at 10 000× magnification, showing a region with sub-5 μm particle sizes, (e) image of isolated microspheres, dispersed in water, left MGP-T LG305 and right MGP LG305, (f) microscopy image of MGP-T LG305 after dispersion in acetone for 30 minutes.

solvents, the particles remain dispersible due to the residual surfactant coating from the synthesis, which imparts a hydrophilic surface to the spheres (Fig. 6(e)).

For a more comprehensive characterization of the materials structure, ^{29}Si and ^{13}C SP-MAS NMR, PXRD, FTIR spectroscopy, and thermal analysis were performed in comparison with both the precursor MG LG305 and the consolidated precursor material $MG_{cons.}$ LG305.

FTIR spectroscopy confirmed the presence of Triton™ X-405 in MGP LG305 *via* the C–H vibration at 2873 cm^{-1} in the FTIR spectrum (Fig. 2). The ^{13}C MAS-NMR spectrum (Fig. 3(a)) showed characteristic signals of both the surfactant and the PPSQ matrix. The aromatic carbons appear at 133, 130, 127 ppm (C–H (phenoxy/phenyl)) and additional signals at 70 (O–$\underline{C}H_2$) and 31 ppm (C–$\underline{C}H_3$) can be attributed to Triton™ X-405. A peak at 50 ppm indicated residual methoxy groups of the T^2 units, suggesting that the base-induced condensation also results in a partially crosslinked structure, similar to that of the $MG_{cons.}$ LG305. This result is further supported by ^{29}Si SP-MAS NMR data. In the NMR spectrum of MGP LG305, T^2 and T^3 units are observed at −71 and −79 ppm (Fig. 3(b)). The calculated percentage of T^3 units is 55%, and the DC is 85%.

Although the crosslinking of the MGP LG305 is not significantly different from that of the $MG_{cons.}$ LG305, changes in microstructure are evident in the Si–O–Si vibrational range of the FTIR spectra. The relative intensity of $\nu(\text{Si–O–Si})_{\text{ring-asym}}$ absorption band at 1106 cm^{-1} increases markedly compared to $\nu(\text{Si–O–Si})_{\text{ring-sym}}$ upon base treatment (Fig. 2). This shift indicates the formation of highly symmetrical $(SiO)_4$ subunits, suggesting a pronounced increase in ladder-type segments.[55] PXRD measurements confirm this observation, showing a further increase in the d_1 value (Fig. 4) and a narrowing of the $2\theta_{d_1}$ reflection, both of which support the higher degree of ordering within the PPSQ network.[52,53] These findings imply that NaOH-induced consolidation in an excess of water promotes rearrangement within the precursor material, yielding a more ordered architecture than thermal curing alone. It is expected that the presence of water as the reaction medium increases the number of hydrolyzed groups, facilitating hydrogen bonding and alignment of polymer chains.[58] At the same time, the basic catalyst accelerates the condensation within the preorganized regions formed by hydrogen bonding, thereby enhancing the degree of condensation within the network.[59]

The solubility and softenability of MGP LG305 are comparable to those of the consolidated precursor material. The increase in crosslinking due to the addition of basic catalyst results in a rigid structure, preventing softening and ensuring that the spherical morphology remains stable even at high temperatures. However, the incomplete crosslinking (DC = 85%) allows the particles to swell in moderately polar solvents (*e.g.* acetone, dichloromethane (DCM), toluene, dimethyl sulfoxide (DMSO)), resulting in the loss of their spherical structure and leaching of the dye (Fig. S13 and S14).

In conclusion, the thermoplastic properties of the MG LG305 facilitate the preparation of micrometer-sized spheres *via* melt emulsion, which are coated with the surfactant Triton™ X-405. When NaOH is used as a catalyst, the particles become non-softenable and maintain their spherical shape even at elevated temperatures. The particle morphology is size-dependent: larger microspheres exhibit internal cavities, while smaller ones appear uniform and compact. The treatment conditions of the precursor gel (NaOH and water) promote the formation of a more ordered PPSQ architecture with a ladder-like structure.

Thermal crosslinking of microspheres

In a subsequent thermal treatment step, the particles were heated to 200 °C for 24 hours. During this process, no softening of the particles was observed, allowing the spherical morphology to be preserved (Fig. S16). However, increasing the temperature to 200 °C leads to the removal of the surfactant from the surface, as confirmed by the TGA of MGP LG305 (Fig. 7(a)). A mass loss of 8% was detected, beginning at 230 °C. This mass loss can be assigned to the removal of Triton™ X-405 by TG-FTIR spectroscopy, including an oxidation in the hydrophilic chain and a decomposition of the surfactant under air (Fig. 7(a) and (b)).[60] In the TGA of the tempered particles, the surfactant is no longer detectable (Fig. 7(a) and (c)).

The release of Triton™ X-405 is also evident in the ^{13}C MAS NMR spectrum, where a significant decrease in the signal at 70 ppm (Fig. 3(a)) is observed. Additionally, FTIR spectroscopy confirms this removal through the disappearance of C–H vibrations between 2800 and 2900 cm^{-1} (Fig. 2). The decomposition of the surfactant on the surface of the microspheres results in a more hydrophobic surface, whereby a dispersion of the particles in hydrophilic solvents was no longer possible (Fig. 6(e)). Simultaneously, the microsphere structure undergoes further crosslinking. In the ^{13}C SP-MAS NMR spectrum, the chemical shift of the methoxy groups nearly disappears, and the ^{29}Si SP-MAS NMR spectrum shows a predominant T^3 signal at −79 ppm, with a degree of condensation of 95%, indicating the formation of a highly crosslinked $PhSiO_{1.5}$ network (Fig. 3). The significant increase in crosslinking upon NaOH treatment at elevated temperatures has also been reported by other groups.[61,62] It reveals that the thermal consolidation process of the microspheres differs from that of the precursor, where a significant amount of T^2 units remains afterwards. The increased DC and the reduction of defects in the form of OH and OCH_3 groups are also reflected in the XRD analysis by a further shift of the d_1 value to larger interplanar distances and a narrowing of the $2\theta_{d_1}$ diffraction peak (Fig. 4 and Table S2).

The results indicate a direct influence of sodium hydroxide pretreatment on the subsequent structure formation, as discussed earlier in the structural characterization of untempered MGP LG305. In the postulated ladder-like arrangement, the phenyl groups exert less steric hindrance on the nucleophilic attack of Si–OR groups, enabling almost complete condensation, as is typical for silsesquioxanes with a ladder architecture.[50,57,63]

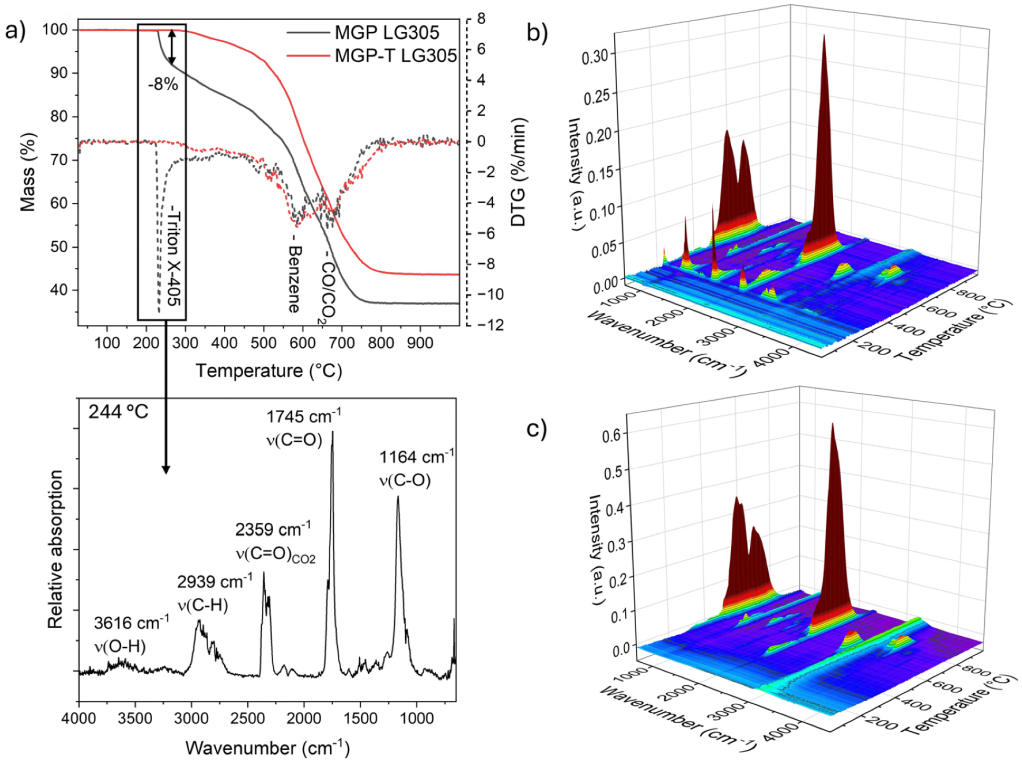

Fig. 7 (a) TGA of MGP LG305 and MGP-T LG305, along with FTIR spectrum of the gases released at the first degradation step at 244 °C for MGP LG305, (b) 3D TGA-FTIR spectrum of gas-phase thermal degradation products of MGP LG305, (c) 3D TGA-FTIR spectrum of gas-phase thermal degradation products of MGP-T LG305.

The increased crosslinking significantly enhances the stability of the particles against swelling in organic solvents, ensuring that their spherical morphology is retained even after treatment with acetone (Fig. 6(f)). However, the dye tends to diffuse out of the particles when exposed to moderately polar solvents (Fig. S15) similar to the untempered particles. Under conditions relevant for optoelectronic or bio-related applications, where the microspheres are typically embedded in polymer matrices or dispersed in aqueous media, the dye remains stably incorporated in the particle structure.

For applications where the particles are exposed to solvents such as acetone or DCM, strategies to suppress dye diffusion could be considered. These include covalent attachment of the dye to the silsesquioxane framework, for example by using perylene-functionalized trialkoxysilane during the melting-gel synthesis,[64] or post-synthetic surface sealing through the

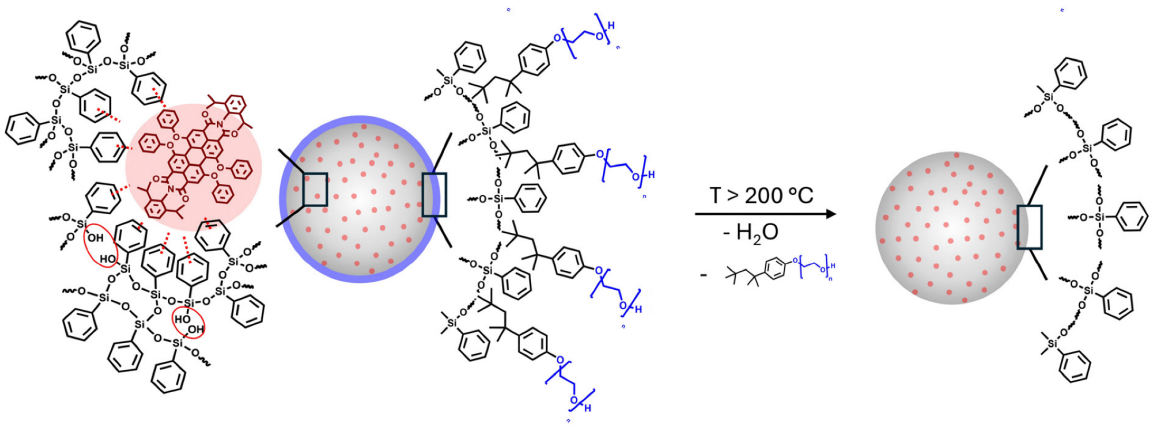

Fig. 8 Schematic representation of the influence of thermal treatment on MGP LG305. Perylene dye molecules are dispersed within the PPSQ matrix, while the surfactant resides on the particle surface. Upon heating to 200 °C, the degree of condensation increases and the surfactant is removed, changing the surface character from hydrophilic (surfactant-covered) to hydrophobic (phenyl-dominated).

addition of a dense silica shell or the application of thin polymeric coatings.[21,65]

The results indicate that additional thermal treatment effectively removes the surfactant from the particle surface (Fig. 8) and increases the degree of condensation, which enhances hydrophobicity and prevents dispersion in water.

Influence of stirring on particle size distribution

During microsphere synthesis, an emulsion is formed, and adjusting the stirring velocity with a standard laboratory stirring bar allows for controlled variations in microsphere size and size distribution. To optimize these parameters, five additional experiments were conducted, varying the stirring rate, duration, and method.

The stirring rate with a standard bar was adjusted from 500 (MGP-1) to 800 rpm (MGP-3), and the stirring time was increased from 1 h (MGP-1) to 2 h (MGP-2) at 500 rpm. To investigate the impact of high-energy processes on particle morphology, an ultrasonic finger (150 W, MGP-US) or an Ultra-Turrax™ disperser (10 000 rpm, MGP-UT) was applied after stirring at 500 rpm for 10 minutes. All experiments were performed using the hot emulsion of the precursor material MG LG305 before the addition of sodium hydroxide, which initiated consolidation and suspension formation, respectively.

The particle size and distribution were determined by measuring and counting particles from microscopy images (Fig. S17–S21). All measured particles fall within a small micrometer range, regardless of the procedure used. Stirring the emulsion at 500 rpm for 1 or 2 h (MGP-1/2) does not significantly alter the particle size distribution (Fig. 9). Increasing the stirring speed to 800 rpm (MGP-3) results in a narrower size distribution and smaller particle sizes. Additional ultrasonic treatment (MGP-US) leads to a broader distribution and larger particle sizes (MGP-US). The narrowest size distribution and the smallest particles were obtained using the Ultra-Turrax™ dispenser (MGP-UT).

Overall, when using a standard stirring bar, an increase of stirring velocity leads to a decrease in both particle size and size distribution. Increasing the stirring time at the same velocity does not lead to any significant change. In contrast to reports in the literature on sol–gel synthesis procedures,[66,67] the use of ultrasound does not reduce particle size but instead results in the broadest size distribution observed in this study. In general, the final droplet size is equal to the distribution immediately after droplet disruption by mechanical energy and is influenced by the dispersed phase viscosity.[68] The high viscosity prevents the destructions of the droplets by ultrasonic energy. Using the disperser results in smaller particles with a narrow distribution. This effect is attributed to the high rotational speed of the rotor, which generates intense shear and thrust forces, effectively breaking up the droplets. Consequently, mechanical energy is essential for producing smaller particles through droplet disruption, whereas the energy introduced by ultrasonic waves does not facilitate size reduction.

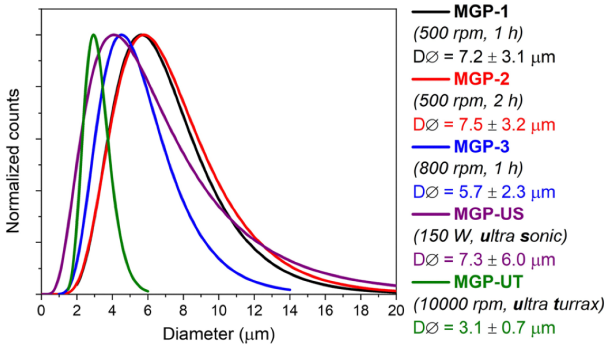

Fig. 9 Particle size distribution of the different experiments MGP-1, MGP-2, MGP-3 MGP-US and MGP-UT, determined by measuring and counting particles from microscopy images.

Photophysical properties of the dye microspheres

The perylene dye LG305 was incorporated into the precursor melting gel during gelation. Its high solubility in phenyl-containing matrices ensures homogeneous distribution.[36] Once embedded in the PPSQ network, dye aggregation is markedly reduced, as evidenced by the pronounced increase in the average fluorescence lifetime from 0.8 ns in the neat dye to 12.4 ns in MG LG305 (1150 ppm) (Fig. S22 and Table S3). This effect is attributed to the reduced chromophore mobility in the rigid matrix and may be further supported by weak π–π interactions between the perylene cores and the phenyl groups of the silsesquioxane, which can spatially separate chromophores and thereby suppress aggregation.[4,36]

The isolated and heat-treated microspheres exhibit red fluorescence, with two emission maxima at 622 nm and 647 nm (Fig. 10(a)). The excitation spectrum displays three bands at 578 nm, 530 nm and 440 nm. Compared to the fluorescence spectra of LG305 in toluene, a slight bathochromic shift in emission is observed (the Stokes shift, which was determined to be 29 nm in toluene, increases to 44 nm in the microspheres).[36] The absolute quantum yield of the microspheres was 64%, while in the precursor material MG LG305 the quantum yield is higher with 83%. A morphology and size-dependent decrease in quantum yield in silica and polymeric particles has already been reported.[69] The observed shift in emission and reduction in quantum yield are attributed to reabsorption processes within the sample, induced by spectral distortions caused by scattering and reabsorption effects. These effects arise due to the transition from transparent hybrid to a microparticle powder, altering the solid-phase morphology.[70,71]

Since the dye can be incorporated into the precursor gel in any quantity, the content of the hydrophobic component in the particles can be adjusted as needed. To demonstrate this, melting gels with varying dye concentrations (220 to 26 000 ppm, Fig. 10(b)) were prepared and used to synthesize microspheres. Particles with a dye concentration of 4350 ppm exhibited the highest quantum yield of 75%. At lower concentrations, the number of emitting centers is reduced, while at higher concentrations π–π stacking between perylene chromophores causes aggregation and fluorescence quenching, leading to a significant reduction in quantum yield.[72] The optimum at intermediate loading therefore reflects the balance between efficient excitation and the onset of concentration quenching, with the PPSQ matrix playing a decisive role in defining this

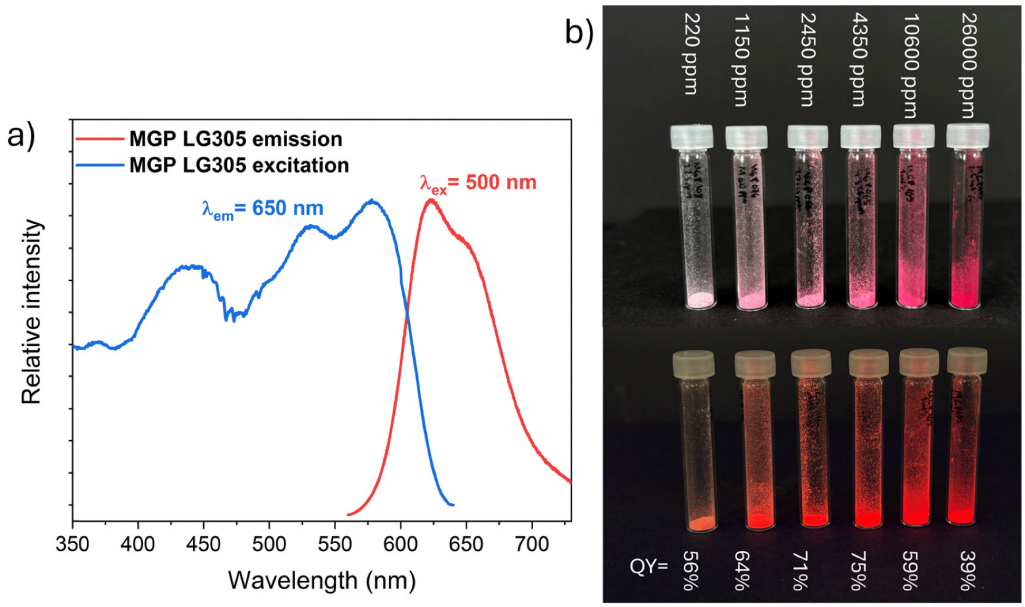

Fig. 10 (a) Emission and excitation spectra of MGP LG305 (1150 ppm LG305) at an excitation wavelength of 500 nm and an emission wavelength of 650 nm, (b) image of MGP LG305 with varying dye concentrations (220–26 000 ppm) under natural light (top) and 450 nm light (bottom), along with their respective quantum yields (QY).

regime by stabilizing isolated chromophores and delaying aggregation.[4,36,73]

Although aggregation-induced quenching cannot be fully avoided at high dye loadings, the integration of a hydrophobic perylene dye into PSSQ microspheres could be realized in a wide concentration range, yielding a fluorescent microsphere powder.

Physical incorporation of alternative dyes and encapsulation in a secondary encapsulation material

Due to the straightforward integration of dyes into the precursor gel, not only LG305 but also other dyes can be incorporated into the particles. It is essential that these molecules are stable under acidic and basic conditions and sufficiently hydrophobic to remain within the emulsion during synthesis without leaching. As an example, additional perylene-based dyes such as Oracet® FL Pink 285 and Oracet® FL Orange 240 were embedded in silica particles using the melt emulsion strategy (Fig. 11, further pictures and fluorescence spectra can be found in Fig. S23 and S24). All particles exhibited the characteristic excitation and emission of the incorporated molecules, confirming successful integration.

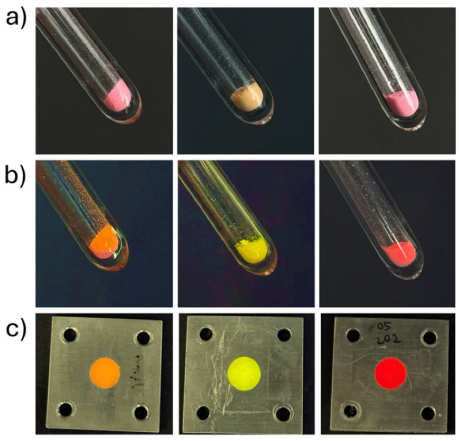

Fig. 11 Microspheres with encapsulated Oracet® FL Pink 285, Oracet® FL Orange 240, and Lumogen® F Red 305 (from left to right): (a) under natural light, (b) under 450 nm light, (c) integrated into polymethylphenylsiloxane resin cured in aluminum frames, under 450 nm light.

For applications such as organic hybrid LEDs or luminescent solar concentrators, the microspheres must be homogeneously encapsulated within a polymer matrix. Therefore, the temperature treated particles were integrated into an elastomeric two-component polyphenylmethylsiloxane resin (Dow Corning OE6630) which cures *via* a hydrosilylation reaction. The resulting composite materials exhibited a homogenous distribution of microspheres and characteristic fluorescence under UV light exposure (Fig. 11(c) and Fig. S25).

This experiment demonstrates that the microsphere synthesis *via* melt emulsion is not limited to LG305, but can also be extended to other hydrophobic dyes. It is conceivable that, beyond dyes, other hydrophobic molecules could be incorporated by the same approach. Owing to the good biocompatibility of the silsesquioxane matrix, this may also open opportunities for the encapsulation of drugs or fragrances, which is of interest in cosmetic and pharmaceutical formulations.[74,75]

Furthermore, this part highlights the potential use of the dye-loaded microspheres as bulk components in optical materials, for example in light-conversion applications.[4]

Conclusion

Acid-catalyzed hydrolysis and condensation of phenyltrimethoxysilane yielded a partially crosslinked PPSQ, known as melting gel, which softens above 70 °C and consolidates above 130 °C. Incorporation of the hydrophobic perylene dye Lumogen® F Red 305 during gelation resulted in a red-colored fluorescent precursor material.

For the first time, a hot emulsification approach of a thermoplastic PPSQ was used to produce spherical ORMOSIL particles. The softening of the precursor enabled emulsification in hot surfactant–water mixtures, followed by NaOH-catalyzed curing to rigid microspheres. Depending on the mechanical energy input during emulsion formation, different particle sizes and size distributions were achieved, with an optimized mean diameter of 3.1 ± 0.7 μm using an Ultra-Turrax disperser.

Spectroscopic analyses and PXRD measurements revealed that the PPSQ network consisted of partially crosslinked structures with predominantly ladder-like motifs. A surfactant layer of Triton™ X was detected on the particle surface. Additional heat treatment led to nearly complete crosslinking of the microsphere framework and the simultaneous surfactant removal, as confirmed by TGA, thereby converting the particle surface from hydrophilic (surfactant-covered) to hydrophobic (phenyl dominated).

Fluorescence lifetime measurements on the precursor gel showed a pronounced increase in lifetime upon dye encapsulation, while concentration-dependent quantum yield studies indicated enhanced emission within a defined concentration range. Microspheres with dye loadings between 220 and 26 000 ppm LG305 were prepared, with the maximum quantum yield of 75% observed at ∼4350 ppm. The photophysical results suggest that the dye distributes homogeneously during synthesis due to its good solubility in the phenyl-rich hydrophobic matrix, while the aromatic groups of the host contribute to the effective separation of chromophores and reduced aggregation.

In aqueous solvents (water, ethanol), the dye remained stably encapsulated, whereas exposure to moderately polar organic solvents such as acetone or chloroform led to leaching.

Finally, other hydrophobic dyes such as Oracet® FL Pink 285 or Oracet® FL Orange 240, were successfully incorporated into microspheres *via* the melt-emulsion strategy. The fluorescent particles can then be incorporated into a secondary encapsulation material, with the siloxane-based particle matrix acting as a protective barrier against external influences, like moisture, oxygen or high temperatures.

Beyond optoelectronic and light-harvesting applications, this new approach also opens opportunities in cosmetics, for instance for the encapsulation of hydrophobic drugs or fragrances.

Declaration of AI and AI-assisted technologies in the writing process

During the preparation of this work, the authors utilized AI tools, including Deepl.com and ChatGPT to enhance the clarity of the language and to correct spelling, punctuation, and grammatical errors. After using these tools, the authors carefully reviewed and edited the content as necessary and take full responsibility for the accuracy and integrity of the publication.

Author contributions

Svenja Pohl: formal analysis, investigation, methodology, validation, visualization, writing – original draft. Nils Steinbrück: conceptualization, formal analysis, investigation, methodology, visualization, writing – original draft. Michał P. Pachnicz: investigation, writing – review & editing. Guido Kickelbick: conceptualization, funding acquisition, project administration, supervision, writing – review & editing.

Conflicts of interest

There are no conflicts to declare.

Data availability

The data supporting the findings of this study are available within the article and its supplementary information (SI). Supplementary information: NMR spectra, viscosity measurement, PXRD, TGA, leaching tests, SEM, microscopic images, fluorescence measurements, TCSPC analysis and additional photos. See DOI: **https://doi.org/10.1039/d5ma00849b**.

Acknowledgements

This research has been funded by the Federal Ministry of Education and Research (BMBF, Germany) in the project ORCA – Organic and rare earth reduced conversion materials for LED-based lightning (project number 03XP0050). Instrumentation and technical assistance for this work were provided by the Service Center X-ray Diffraction, with financial support from Saarland University and the German Science Foundation (project number INST 256/349-1). We would like to thank Elias Gießelmann for SP-MAS NMR support, Viktoria Kiefer for assistance with quantum yield and TCSPC experiments and BASF and Sunchemical for providing us with various fluorescent dyes.

References

1 W.-H. Zhang, X.-X. Hu and X.-B. Zhang, Dye-Doped Fluorescent Silica Nanoparticles for Live Cell and *In Vivo* Bioimaging, *Nanomaterials*, 2016, **6**, 81.

2 F. Gao, L. Tang, L. Dai and L. Wang, A fluorescence ratiometric nano-pH sensor based on dual-fluorophore-doped silica nanoparticles, *Spectrochim. Acta, Part A*, 2007, **67**, 517–521.

3 X. Huang, Z. P. Aguilar, H. Li, W. Lai, H. Wei, H. Xu and Y. Xiong, Fluorescent $Ru(phen)_3^{2+}$-Doped Silica Nanoparticles-Based ICTS Sensor for Quantitative Detection of Enrofloxacin Residues in Chicken Meat, *Anal. Chem.*, 2013, **85**, 5120–5128.

4 F. Corsini, E. Tatsi, A. Colombo, C. Dragonetti, C. Botta, S. Turri and G. Griffini, Highly emissive fluorescent silica-based core/shell nanoparticles for efficient and stable luminescent solar concentrators, *Nano Energy*, 2021, **80**, 105551.

5 S. Saita, K. Niwa, Y. B. Pottathara and H. Kawasaki, Highly bright full-color emission from dye-doped silica nanoparticles with prevention of dye self-quenching, *Opt. Mater.*, 2023, **139**, 113803.

6 X. Ning, J. Chittigori, Y. Li, G. Horner, Z. Zhou, C. K. Ullal and L. Schadler, Dye doped concentric shell nanoparticles for enhanced photophysical performance of downconverting light emitting diodes, *J. Colloid Interface Sci.*, 2019, **556**, 753–760.

7 S. Kwon, R. K. Singh, R. A. Perez, E. A. Abou Neel, H.-W. Kim and W. Chrzanowski, Silica-based mesoporous nanoparticles for controlled drug delivery, *J. Tissue Eng.*, 2013, **4**, 2041731413503357.

8 H. Li, X. Chen, D. Shen, F. Wu, R. Pleixats and J. Pan, Functionalized silica nanoparticles: classification, synthetic approaches and recent advances in adsorption applications, *Nanoscale*, 2021, **13**, 15998–16016.

9 Y. Choi, J. Kim, S. Yu and S. Hong, pH- and temperature-responsive radially porous silica nanoparticles with high-capacity drug loading for controlled drug delivery, *Nanotechnology*, 2020, **31**, 335103.

10 H.-S. Jung, Y.-J. Kim, S.-W. Ha and J.-K. Lee, White light-emitting diodes using thermally and photochemically stable fluorescent silica nanoparticles as color-converters, *J. Mater. Chem. C*, 2013, **1**, 5879–5884.

11 V. Gubala, G. Giovannini, F. Kunc, M. P. Monopoli and C. J. Moore, Dye-doped silica nanoparticles: synthesis, surface chemistry and bioapplications, *Cancer Nanotechnol.*, 2020, **11**, 1.

12 I. A. Rahman, P. Vejayakumaran, C. S. Sipaut, J. Ismail and C. K. Chee, Size-dependent physicochemical and optical properties of silica nanoparticles, *Mater. Chem. Phys.*, 2009, **114**, 328–332.

13 W. Stöber, A. Fink and E. Bohn, Controlled growth of monodisperse silica spheres in the micron size range, *J. Colloid Interface Sci.*, 1968, **26**, 62–69.

14 F. J. Arriagada and K. Osseo-Asare, Synthesis of Nanosize Silica in Aerosol OT Reverse Microemulsions, *J. Colloid Interface Sci.*, 1995, **170**, 8–17.

15 C. Odenwald and G. Kickelbick, Additive-free continuous synthesis of silica and ORMOSIL micro- and nanoparticles applying a microjet reactor, *J. Sol-Gel Sci. Technol.*, 2019, **89**, 343–353.

16 J. G. Croissant, X. Cattoën, J.-O. Durand, M. Wong Chi Man and N. M. Khashab, Organosilica hybrid nanomaterials with a high organic content: syntheses and applications of silsesquioxanes, *Nanoscale*, 2016, **8**, 19945–19972.

17 A. L. Mohamed, T. A. Khattab and A. G. Hassabo, Color-tunable encapsulated perylene-labeled silica fluorescent hybrid nanoparticles, *Results Chem.*, 2023, **5**, 100769.

18 X. Ren, B. Sun, C.-C. Tsai, Y. Tu, S. Leng, K. Li, Z. Kang, R. M. V. Horn, X. Li, M. Zhu, C. Wesdemiotis, W.-B. Zhang and S. Z. D. Cheng, Synthesis, Self-assembly, and Crystal Structure of a Shape-Persistent Polyhedral-Oligosilsesquioxane-Nanoparticle-Tethered Perylene Diimide, *J. Phys. Chem. B*, 2010, **114**, 4802–4810.

19 H.-J. Ben, Y. Fan, Y.-J. Shi, R. Liu, Y. Chen, X.-K. Ren and S. Jiang, Polyhedral-oligosilsesquioxane containing poly(methyl methacrylate) perylenebisimide microspheres with high solid state emission, *Dyes Pigm.*, 2017, **137**, 584–592.

20 J. Chen, S. Jia, X. Ji, M. Nourrein, H. Xiang, Z. Zhou, C.-L. Wang, B. Sun and M. Zhu, The morphologies and fluorescence quantum yields of perylene diimide dye-doped PS and PHVB microspheres, *RSC Adv.*, 2018, **8**, 35534–35538.

21 N. Klippel, G. Jung and G. Kickelbick, Hybrid inorganic-organic fluorescent silica nanoparticles - influence of dye binding modes on dye leaching, *J. Sol-Gel Sci. Technol.*, 2023, **107**, 2–19.

22 X. Lu, Y. Hou, J. Zha and Z. Xin, Facile Synthesis of Rhodamine B-Doped Poly(3-mercaptopropylsilsesquioxane) Fluorescent Microspheres with Controllable Size, *Ind. Eng. Chem. Res.*, 2013, **52**, 5880–5886.

23 C. L. Nistor, D. Donescu, R. Ianchis, C. Spataru, V. Raditoiu, C. Petcu, M. Ghiurea and C. Deleanu, Encapsulation of three different hydrophobic dyes in functionalized silica particles, *J. Sol-Gel Sci. Technol.*, 2011, **59**, 48–56.

24 R. Tapec, X. J. Zhao and W. Tan, Development of organic dye-doped silica nanoparticles for bioanalysis and biosensors, *Int. J. Nanosci.*, 2002, **2**, 405–409.

25 K. Köhler, A. Hensel, M. Kraut and H. P. Schuchmann, Melt emulsification—Is there a chance to produce particles without additives?, *Particuology*, 2011, **9**, 506–509.

26 W. Mehnert and K. Mäder, Solid lipid nanoparticles: Production, characterization and applications, *Adv. Drug Delivery Rev.*, 2012, **64**, 83–101.

27 S. Fanselow, S. E. Emamjomeh, K.-E. Wirth, J. Schmidt and W. Peukert, Production of spherical wax and polyolefin microparticles by melt emulsification for additive manufacturing, *Chem. Eng. Sci.*, 2016, **141**, 282–292.

28 L. C. Klein, S. Kallontzi, L. Fabris, A. Jitianu, C. Ryan, M. Aparicio, L. Lei and J. P. Singer, Applications of melting gels, *J. Sol-Gel Sci. Technol.*, 2019, **89**, 66–77.

29 L. C. Klein and A. Jitianu, Hybrid organic-inorganic gels that are melting gels, *J. Sol-Gel Sci. Technol.*, 2025, **113**, 30–38.

30 D. Yu, M. Kleemeier, G. M. Wu, B. Schartel, W. Q. Liu and A. Hartwig, A low melting organic-inorganic glass and its effect on flame retardancy of clay/epoxy composites, *Polymer*, 2011, **52**, 2120–2131.

31 A. Jitianu, J. Doyle, G. Amatucci and L. C. Klein, presented in part at the Proceeding at Material Science & Technology Pittsburgh, PA, 2008.

32 K. Kajihara, R. Suzuki, R. Seto, H. Itakura and M. Ishijima, Poly(cyclohexylsilsesquioxane)-Based Hydrophilic Thermoset-Resistant Deep-Ultraviolet-Transparent Glasses with Low Melting Temperatures, *ACS Appl. Mater. Interfaces*, 2023, **15**, 31880–31887.

33 B. Menaa, M. Takahashi, Y. Tokuda and T. Yoko, Preparation and properties of polyphenylsiloxane-based hybrid

glass films obtained from a non-aqueous coating sol via a single-step dip-coating, *Opt. Mater.*, 2007, **29**, 806–813.
34 S. Castelletto and A. Boretti, Luminescence solar concentrators: A technology update, *Nano Energy*, 2023, **109**, 108269.
35 N. Steinbrück and G. Kickelbick, Perylene polyphenylmethylsiloxanes for optoelectronic applications, *J. Polym. Sci., Part B: Polym. Phys.*, 2019, **57**, 1062–1073.
36 N. Steinbrück, M. Könemann and G. Kickelbick, Effect of polysiloxane encapsulation material compositions on emission behaviour and stabilities of perylene dyes, *RSC Adv.*, 2018, **8**, 18128–18138.
37 MestReNova, v14.2.0-26256, Mestrelab Research, S.L., Santiago de Compostela, Spain.
38 C. A. Schneider, W. S. Rasband and K. W. Eliceiri, NIH Image to ImageJ: 25 years of image analysis, *Nat. Methods*, 2012, **9**, 671–675.
39 *SymPhoTime, version 2.1.3764*, Pico-Quant, Berlin, Germany.
40 Topas 5, Bruker AXS, Karlsruhe, Germany.
41 S. Pohl, O. Janka, E. Füglein and G. Kickelbick, Thermoplastic Silsesquioxane Hybrid Polymers with a Local Ladder-Type Structure, *Macromolecules*, 2021, **54**, 3873–3885.
42 A. Jitianu, G. Amatucci and L. C. Klein, Phenyl-Substituted Siloxane Hybrid Gels that Soften Below 140 °C, *J. Am. Ceram. Soc.*, 2009, **92**, 36–40.
43 Y.-S. Li, Y. Wang and S. Ceesay, Vibrational spectra of phenyltriethoxysilane, phenyltrimethoxysilane and their sol–gels, *Spectrochim. Acta, Part A*, 2009, **71**, 1819–1824.
44 A. Jitianu, G. Gonzalez and L. C. Klein, Hybrid Sol–Gel Glasses with Glass-Transition Temperatures Below Room Temperature, *J. Am. Ceram. Soc.*, 2015, **98**, 3673–3679.
45 N. Hu, Y. Rao, S. Sun, L. Hou, P. Wu, S. Fan and B. Ye, Structural Evolution of Silica Gel and Silsesquioxane Using Thermal Curing, *Appl. Spectrosc.*, 2016, **70**, 1328–1338.
46 Z. Li, S. Tolbert and D. A. Loy, Hybrid Organic-Inorganic Membranes on Porous Supports by Size Exclusion and Thermal Sintering of Fluorescent Polyphenylsilsesquioxane Nanoparticles, *Macromol. Mater. Eng.*, 2013, **298** 715–721.
47 K. Katagiri, K. Hasegawa, A. Matsuda, M. Tatsumisago and T. Minami, Preparation of Transparent Thick Films by Electrophoretic Sol–Gel Deposition Using Phenyltriethoxysilane-Derived Particles, *J. Am. Ceram. Soc.*, 1998, **81**, 2501–2503.
48 R. H. Baney, M. Itoh, A. Sakakibara and T. Suzuki, Silsesquioxanes, *Chem. Rev.*, 1995, **95**, 1409–1430.
49 S. L. B. Lana and A. B. Seddon, X-Ray Diffraction Studies of Sol–Gel Derived ORMOSILs Based on Combinations of Tetramethoxysilane and Trimethoxysilane, *J. Sol-Gel Sci. Technol.*, 1998, **13**, 461–466.
50 S.-S. Choi, A. S. Lee, S. S. Hwang and K.-Y. Baek, Structural Control of Fully Condensed Polysilsesquioxanes: Ladderlike vs Cage Structured Polyphenylsilsesquioxanes, *Macromolecules*, 2015, **48**, 6063–6070.
51 K. A. Andrianov, A. A. Zhdanov and V. Y. Levin, Some Physical Properties of Organosilicon Ladder Polymers, *Annu. Rev. Mater. Res.*, 1978, **8**, 313–326.
52 Z. Xinsheng, S. Lianghe and H. Chaoran, More on the Structures of Polyphenylsilsesquioxanes, *Chin. J. Polym. Sci.*, 1987, **5**, 353–358.
53 L. A. S. D. A. Prado, E. Radovanovic, H. O. Pastore, I. V. P. Yoshida and I. L. Torriani, Poly(phenylsilsesquioxane)s: Structural and morphological characterization, *J. Polym. Sci., Part A: Polym. Chem.*, 2000, **38**, 1580–1589.
54 I. M. Petrova, A. K. Buryak, A. S. Peregudov, T. V. Strelkova, E. G. Kononova, I. S. Bushmarinov and N. N. Makarova, Effect of stereoisomerism of (tetrahydroxy)(tetraphenyl)cyclotetrasiloxanes on the siloxane framework in polyphenylsilsesquioxanes obtained by polycondensation in the presence of layered-architecture compounds, *Mendeleev Commun.*, 2015, **25**, 229–231.
55 E. S. Park, H. W. Ro, C. V. Nguyen, R. L. Jaffe and D. Y. Yoon, Infrared Spectroscopy Study of Microstructures of Poly(silsesquioxane)s, *Chem. Mater.*, 2008, **20**, 1548–1554.
56 A. A. Anisimov, N. V. Polshchikova, Y. S. Vysochinskaya, P. A. Zader, G. G. Nikiforova, A. S. Peregudov, M. I. Buzin, O. I. Shchegolikhina and A. M. Muzafarov, Condensation of all-*cis*-tetraphenylcyclotetrasiloxanetetraol in ammonia: new method for preparation of ladder-like polyphenylsilsesquioxanes, *Mendeleev Commun.*, 2019, **29**, 421–423.
57 W. Zhang, X. Wang, Y. Wu, Z. Qi and R. Yang, Preparation and Characterization of Organic-Inorganic Hybrid Macrocyclic Compounds: Cyclic Ladder-like Polyphenylsilsesquioxanes, *Inorg. Chem.*, 2018, **57**, 3883–3892.
58 J.-F. Kannengießer, B. Morgenstern, O. Janka and G. Kickelbick, Oligo-Condensation Reactions of Silanediols with Conservation of Solid-State-Structural Features, *Chem. – Eur. J.*, 2024, **30**, e202303343.
59 C. J. Brinker, Hydrolysis and condensation of silicates: Effects on structure, *J. Non-Cryst. Solids*, 1988, **100**, 31–50.
60 K. Mitsuda, H. Kimura and T. Murahashi, Evaporation and decomposition of Triton X-100 under various gases and temperatures, *J. Mater. Sci.*, 1989, **24**, 413–419.
61 H. Masai, M. Takahashi, Y. Tokuda and T. Yoko, Enhancement of Polycondensation Reaction by Diethyl Ether-Aqueous NaOH Immiscible Two Phase Liquid Treatment of Phenyl-Modified Polysiloxane Glass, *J. Ceram. Soc. Jpn.*, 2005, **113**, 259–262.
62 D. Schneider, D. Loy, B. Baugher, D. Wheeler, R. Assink, T. Alam and R. Saunders, Preparation and characterization of phenyl-, benzyl-, and phenethyl-substituted polysilsesquioxanes, *Polym. Prepr.*, 1998, **39**, 513–514.
63 M. Nowacka, A. Kowalewska and T. Makowski, Structural studies on ladder phenylsilsesquioxane oligomers formed by polycondensation of cyclotetrasiloxanetetraols, *Polymer*, 2016, **87**, 81–89.
64 D. Sriramulu, S. P. Turaga, A. A. Bettiol and S. Valiyaveettil, Molecular Organization Induced Anisotropic Properties of Perylene – Silica Hybrid Nanoparticles, *Sci. Rep.*, 2017, **7**, 7842.
65 H. Ow, D. R. Larson, M. Srivastava, B. A. Baird, W. W. Webb and U. Wiesner, Bright and Stable Core−Shell Fluorescent Silica Nanoparticles, *Nano Lett.*, 2005, **5**, 113–117.

66 K. A. Mani, N. Yaakov, Y. Itzhaik Alkotzer, E. Zelikman and G. Mechrez, A Robust Fabrication Method for Amphiphilic Janus Particles via Immobilization on Polycarbonate Microspheres, *Polymers*, 2018, **10**, 900.

67 H. E. Romeo, M. A. Fanovich, R. J. J. Williams, L. Matějka, J. Pleštil and J. Brus, Fast Synthesis of Nanostructured Microspheres of a Bridged Silsesquioxane via Ultrasound-Assisted Sol–Gel Processing, *Macromol. Chem. Phys.*, 2008, **210**, 172–178.

68 O. Behrend, K. Ax and H. Schubert, Influence of continuous phase viscosity on emulsification by ultrasound, *Ultrason. Sonochem.*, 2000, **7**, 77–85.

69 K. Trofymchuk, A. Reisch, I. Shulov, Y. Mély and A. S. Klymchenko, Tuning the color and photostability of perylene diimides inside polymer nanoparticles: towards biodegradable substitutes of quantum dots, *Nanoscale*, 2014, **6**, 12934–12942.

70 L. R. Wilson and B. S. Richards, Measurement method for photoluminescent quantum yields of fluorescent organic dyes in polymethyl methacrylate for luminescent solar concentrators, *Appl. Opt.*, 2009, **48**, 212–220.

71 M. G. Lagorio and E. San Román, How Does Light Scattering Affect Luminescence? Fluorescence Spectra and Quantum Yields in the Solid Phase, *J. Chem. Educ.*, 2002, **79**, 1362–1367.

72 E. Lucenti, C. Botta, E. Cariati, S. Righetto, M. Scarpellini, E. Tordin and R. Ugo, New organic–inorganic hybrid materials based on perylene diimide–polyhedral oligomeric silsesquioxane dyes with reduced quenching of the emission in the solid state, *Dyes Pigm.*, 2013, **96**, 748–755.

73 M. Buffa, S. Carturan, M. G. Debije, A. Quaranta and G. Maggioni, Dye-doped polysiloxane rubbers for luminescent solar concentrator systems, *Sol. Energy Mater. Sol. Cells*, 2012, **103**, 114–118.

74 L. J. Green, N. D. Bhatia, O. Toledano, M. Erlich, A. Spizuoco, B. C. Goodyear, J. P. York and J. Jakus, Silica-based microencapsulation used in topical dermatologic applications, *Arch. Dermatol. Res.*, 2023, **315**, 2787–2793.

75 J. Yeom, W. S. Shim and N. G. Kang, Eco-Friendly Silica Microcapsules with Improved Fragrance Retention, *Appl. Sci.*, 2022, **12**, 6759.

5 Concluding Remarks

The presented studies systematically define the structural requirements that govern the formation of melting gel-type polysilsesquioxanes. These hybrid materials are characterized by thermoplastic softening at moderate temperatures and irreversible curing at elevated temperatures. Their behavior originates from a delicate balance between molecular structure, network architecture, defect density, and non-covalent interactions.

The structural model of melting gel formation was derived from detailed investigations of a phenyl-substituted system, which served as a reference for understanding the molecular origin of this behavior. The essential feature of such systems is a low but coherent degree of crosslinking that maintains sufficient chain mobility within the Si–O–Si backbone. The material consists of local ladder-like and network segments alternating with less crosslinked, flexible domains. These dynamic regions are stabilized by hydrogen bonds between silanol and alkoxy groups as well as π–π interactions of the aromatic substituents. Upon heating, these interactions are gradually weakened, allowing deformation, whereas further temperature increase induces condensation of residual silanols and densification of ladder motifs, leading to irreversible hardening.

The substituent attached to the silicon atom has a decisive influence on this structural equilibrium. Increasing the aromatic size from phenyl to naphthyl enables thermoplastic behavior, though distinct differences arise from isomerism within the naphthyl series. Networks bearing 2-naphthyl groups exhibit behavior comparable to classical phenyl-based systems, including softening and curing. In contrast, 1-naphthyl substitution results in permanently softenable materials that do not undergo irreversible hardening. The higher steric demand of the 1-naphthyl group stabilizes residual hydroxyl and methoxy groups, hindering further condensation and preventing the formation of an extended network structure.

Further enlargement of the aromatic system to 9-phenanthrenyl substituents suppresses melting gel formation altogether. Pronounced steric hindrance and the rigidity of the large π-system restrict segmental mobility and favor intramolecular condensation, yielding isolated POSS-like structures, resulting in brittle solids. Thus, the size and geometry of the aromatic substituent govern the balance between intra- and intermolecular condensation, and together with the intrinsic rigidity of the aromatic system, they determine the final material properties.

When aromatic groups are replaced by aliphatic *n*-alkyl substituents, melting gel-like structures are no longer obtained. Short-chain n-alkyl groups (C_1–C_3) lead to highly crosslinked, brittle

non-softenable solids, while medium-chain derivatives (C_6, C_8) form viscous oligomeric systems with local crosslinking that do not harden upon heating. Long-chain derivatives (C_{12}–C_{18}) self-organize into lamellar, semicrystalline phases exhibiting true melting points rather than melting gel softening. These results demonstrate that melting gel formation requires an amorphous, defect-rich network in which excessive self-organization of the organic groups that lead to crystallization must be avoided. Defects, particularly silanol and alkoxy groups stabilized by the organic substituent, play a key role in this context. They contribute to network reinforcement while enabling thermally induced post-condensation.

Based on these insights, the structural prerequisites for melting gel formation can be defined as: an intermediate crosslinking density, the predominance of amorphous ladder-like network motifs and a controlled number of defect sites in form of OH and OR groups. Aromatic groups, like naphthyl fulfill these conditions particularly well, enabling the design of new melting gel systems that combine high refractive indices, fluorescence, and excellent thermal stability.

Finally, the aromatic substituent environment also proved suitable for incorporating hydrophobic functional molecules. Perylene-based dyes were successfully encapsulated within melting gels and processed into fluorescent microparticles via a melt-emulsion approach, demonstrating the versatility of these hybrid systems for optical applications.

Based on these findings, numerous opportunities for further development arise. A targeted variation in the type and number of alkoxy groups, for example by using ethoxy or isopropoxy groups, could be used to control hydrolysis and condensation kinetics, thereby tailoring the processing temperature and the final network structure.[150, 197] Further functionalization of the aromatic substituents, for instance through the introduction of vinyl or ionic groups, also opens new possibilities. Additional UV-induced crosslinking could be achieved via vinyl functionalities,[412] while ionic substituents might contribute to network cohesion through electrostatic interactions, provided they are dimensioned to maintain sufficient mobility and enable effective network formation.[55]

A promising next step lies in the co-condensation with functional siloxanes in order to exploit the so-called melting gel window, the temperature range between thermoplastic deformability and irreversible curing, for applications such as the fabrication of textured surfaces, thin films, or imprint lithography.[388]

In addition, the synthetic approach used in this work also holds promise from the perspective of sustainable material development. The reactions employed proceed under mild conditions and are often solvent-free, which aligns with the principles of green chemistry and ongoing

efforts to establish eco-friendly synthetic routes for hybrid materials, a research direction of growing importance in today's scientific landscape.[106, 413, 414]

This study provides a fundamental contribution to understanding the structure–property relationships of melting gels and a precise definition of the structural parameters necessary for their formation. This has not only significantly deepened the understanding of the underlying condensation processes and molecular interactions, but has also created a basis for the targeted development of novel functional inorganic-organic hybrid materials. In view of the increasing demand for processable, functionalizable, and thermally stable materials for applications in microelectronics, optoelectronics, or encapsulation technologies, melting gels represent a highly promising new class of materials.

6 References

(1) Maeder, T. Review of Bi_2O_3 based glasses for electronics and related applications. *Int. Mater. Rev.* **2013**, *58*, 3-40. DOI: https://doi.org/10.1179/1743280412y.0000000010.
(2) Lu, Q.; Yang, Z.; Meng, X.; Yue, Y.; Ahmad, M. A.; Zhang, W.; Zhang, S.; Zhang, Y.; Liu, Z.; Chen, W. A Review on Encapsulation Technology from Organic Light Emitting Diodes to Organic and Perovskite Solar Cells. *Adv. Funct. Mater.* **2021**, *31*, 2100151. DOI: https://doi.org/10.1002/adfm.202100151.
(3) Gomez-Romero, P.; Pokhriyal, A.; Rueda-García, D.; Bengoa, L. N.; González-Gil, R. M. Hybrid Materials: A Metareview. *Chem. Mater.* **2024**, *36*, 8-27. DOI: https://doi.org/10.1021/acs.chemmater.3c01878.
(4) Klein, L. C.; Jitianu, A. Hybrid organic-inorganic gels that are melting gels. *J. Sol-Gel Sci. Technol.* **2025**, *113*, 30-38. DOI: https://doi.org/10.1007/s10971-024-06524-4.
(5) Masai, H.; Takahashi, M.; Tokuda, Y.; Yoko, T. Gel-melting method for preparation of organically modified siloxane low-melting glasses. *J. Mater. Res.* **2005**, *20*, 1234-1241. DOI: https://doi.org/10.1557/JMR.2005.0151.
(6) Issa, A. A.; Luyt, A. S. Kinetics of Alkoxysilanes and Organoalkoxysilanes Polymerization: A Review. *Polymers* **2019**, *11*, 537. DOI: https://doi.org/10.3390/polym11030537.
(7) Judeinstein, P.; Sanchez, C. Hybrid organic–inorganic materials: a land of multidisciplinarity. *J. Mater. Chem.* **1996**, *6*, 511-525. DOI: https://doi.org/10.1039/JM9960600511.
(8) Kickelbick, G. Ed. *Hybrid Materials - Synthesis, Characterization and Applications*; Wiley-VCH Weinheim, Germany, 2007.
(9) Sanchez, C.; Belleville, P.; Popall, M.; Nicole, L. Applications of advanced hybrid organic–inorganic nanomaterials: from laboratory to market. *Chem. Soc. Rev.* **2011**, *40*, 696-753. DOI: https://doi.org/10.1039/C0CS00136H.
(10) Kickelbick, G. Hybrid Materials – Past, Present and Future. *Hybrid Mater.* **2014**, *1*, 39-51. DOI: https://doi.org/10.2478/hyma-2014-0001.
(11) Faustini, M.; Nicole, L.; Ruiz-Hitzky, E.; Sanchez, C. History of Organic–Inorganic Hybrid Materials: Prehistory, Art, Science, and Advanced Applications. *Adv. Funct. Mater.* **2018**, *28*, 1704158. DOI: https://doi.org/10.1002/adfm.201704158.
(12) Mir, S. H.; Nagahara, L. A.; Thundat, T.; Mokarian-Tabari, P.; Furukawa, H.; Khosla, A. Review - Organic-Inorganic Hybrid Functional Materials: An Integrated Platform for Applied Technologies. *J. Electrochem. Soc.* **2018**, *165*, B3137-B3156. DOI: https://doi.org/10.1149/2.0191808jes.
(13) Rejab, M. R. B. M.; Hamdan, M. H. B. M.; Quanjin, M.; Siregar, J. P.; Bachtiar, D.; Muchlis, Y. Historical Development of Hybrid Materials. In *Encyclopedia of Renewable and Sustainable Materials*, Hashmi, S., Choudhury, I. A. Eds.; Elsevier: Oxford, UK, 2020; pp 445-455. DOI: https://doi.org/10.1016/B978-0-12-803581-8.10546-6.
(14) Das, P. P.; Chaudhary, V.; Kumar Singh, R.; Singh, D.; Aditya Bachchan, A. Advancement in hybrid materials, its applications and future challenges: A review. *Mater. Today Proc.* **2021**, *47*, 3794-3801. DOI: https://doi.org/10.1016/j.matpr.2021.03.009.
(15) Gomez-Romero, P. Hybrid organic–inorganic materials - in search of synergic activity. *Adv. Mater.* **2001**, *13*, 163-174. DOI: https://doi.org/10.1002/1521-4095(200102)13:3<163::AID-ADMA163>3.0.CO;2-U.
(16) Nassif, N.; Livage, J. From diatoms to silica-based biohybrids. *Chem. Soc. Rev.* **2011**, *40*, 849-859. DOI: https://doi.org/10.1039/C0CS00122H.

(17) Faivre, D.; Godec, T. U. From Bacteria to Mollusks: The Principles Underlying the Biomineralization of Iron Oxide Materials. *Angew. Chem. Int. Ed.* **2015**, *54*, 4728-4747. DOI: https://doi.org/10.1002/anie.201408900.
(18) Weiner, S.; Wagner, H. D. THE MATERIAL BONE: Structure-Mechanical Function Relations. *Annu. Rev. Mater. Res.* **1998**, *28*, 271-298. DOI: https://doi.org/10.1146/annurev.matsci.28.1.271.
(19) Sanchez, C.; Arribart, H.; Giraud Guille, M. M. Biomimetism and bioinspiration as tools for the design of innovative materials and systems. *Nat. Mater.* **2005**, *4*, 277-288. DOI: https://doi.org/10.1038/nmat1339.
(20) Nudelman, F.; Sommerdijk, N. A. J. M. Biomineralization as an Inspiration for Materials Chemistry. *Angew. Chem. Int. Ed.* **2012**, *51*, 6582-6596. DOI: https://doi.org/10.1002/anie.201106715.
(21) Menu, M. L'analyse de l'art préhistorique. *L'Anthropologie* **2009**, *113*, 547-558. DOI: https://doi.org/10.1016/j.anthro.2009.09.011.
(22) Carretero, M. I. Clay minerals and their beneficial effects upon human health. A review. *Appl. Clay Sci.* **2002**, *21*, 155-163. DOI: https://doi.org/10.1016/S0169-1317(01)00085-0.
(23) Van Olphen, H. Maya Blue: A Clay-Organic Pigment? *Science* **1966**, *154*, 645-646. DOI: https://doi.org/10.1126/science.154.3749.645.
(24) Yang, F.; Zhang, B.; Ma, Q. Study of Sticky Rice−Lime Mortar Technology for the Restoration of Historical Masonry Construction. *Acc. Chem. Res.* **2010**, *43*, 936-944. DOI: https://doi.org/10.1021/ar9001944.
(25) Ebelmann, J.-J. *Annales de Chimie et de Physique*; 1846.
(26) Sanchez, C.; Rozes, L.; Ribot, F.; Laberty-Robert, C.; Grosso, D.; Sassoye, C.; Boissiere, C.; Nicole, L. "Chimie douce": A land of opportunities for the designed construction of functional inorganic and hybrid organic-inorganic nanomaterials. *C. R. Chim.* **2010**, *13*, 3-39. DOI: https://doi.org/10.1016/j.crci.2009.06.001.
(27) Schleich, D. M. Chimie douce: Low temperature techniques for synthesizing useful compounds. *Solid State Ion.* **1994**, *70-71*, 407-411. DOI: https://doi.org/10.1016/0167-2738(94)90345-X.
(28) Schubert, U. Sol-Gel-Chemie: Einfach und doch kompliziert. *Chem. Unserer Zeit* **2018**, *52*, 18-25. DOI: https://doi.org/10.1002/ciuz.201700792.
(29) Huang, H.-H.; Orler, B.; Wilkes, G. L. Ceramers: Hybrid materials incorporating polymeric/oligomeric species with inorganic glasses by a sol-gel process. *Polym. Bull.* **1985**, *14*, 557-564. DOI: https://doi.org/10.1007/BF00271615.
(30) Livage, J.; Henry, M.; Sanchez, C. Sol-gel chemistry of transition metal oxides. *Prog. Solid State Chem.* **1988**, *18*, 259-341. DOI: https://doi.org/10.1016/0079-6786(88)90005-2.
(31) Bokov, D.; Turki Jalil, A.; Chupradit, S.; Suksatan, W.; Javed Ansari, M.; Shewael, I. H.; Valiev, G. H.; Kianfar, E. Nanomaterial by Sol-Gel Method: Synthesis and Application. *Adv. Mater. Sci. Eng.* **2021**, *2021*, 5102014. DOI: https://doi.org/10.1155/2021/5102014.
(32) Dehghanghadikolaei, A.; Ansary, J.; Ghoreishi, R. Sol-gel process applications: A mini-review. *Proc. Nat. Res. Soc.* **2018**, *2*, 02008-02029. DOI: https://doi.org/10.11605/j.pnrs.201802008.
(33) Amiri, S.; Rahimi, A. Hybrid nanocomposite coating by sol–gel method: a review. *Iran. Polym. J.* **2016**, *25*, 559-577. DOI: https://doi.org/10.1007/s13726-016-0440-x.
(34) Hench, L. L.; West, J. K. The sol-gel process. *Chem. Rev.* **1990**, *90*, 33-72. DOI: https://doi.org/10.1021/cr00099a003.
(35) Mehrotra, R. C.; Singh, A. Recent Trends in Metal Alkoxide Chemistry. In *Progress in Inorganic Chemistry*, Karlin, K. D. Ed.; John Wiley & Sons, Inc.: Hoboken, NJ, USA, 1997; pp 239-454. DOI: https://doi.org/10.1002/9780470166475.ch4.

(36) Aboualigaledari, N.; Rahmani, M. A review on the synthesis of the TiO_2-based photocatalyst for the environmental purification. *J. Compos. Compd.* **2021**, *3*, 25-42. DOI: https://doi.org/10.52547/jcc.3.1.4.
(37) Mackenzie, J. D. Glasses from melts and glasses from gels, a comparison. *J. Non-Cryst. Solids* **1982**, *48*, 1-10. DOI: https://doi.org/10.1016/0022-3093(82)90241-1.
(38) Aelion, R.; Loebel, A.; Eirich, F. Hydrolysis of Ethyl Silicate. *J. Am. Chem. Soc.* **1950**, *72*, 5705-5712. DOI: https://doi.org/10.1021/ja01168a090.
(39) Brinker, C. J. Hydrolysis and condensation of silicates: Effects on structure. *J. Non-Cryst. Solids* **1988**, *100*, 31-50. DOI: https://doi.org/10.1016/0022-3093(88)90005-1.
(40) Knight, C. T. G.; Balec, R. J.; Kinrade, S. D. The Structure of Silicate Anions in Aqueous Alkaline Solutions. *Angew. Chem. Int. Ed.* **2007**, *46*, 8148-8152. DOI: https://doi.org/10.1002/anie.200702986.
(41) Schmidt, H. K.; Seiferling, B.; Philipp, G.; Deichmann, K. Development of organic-inorganic hard coatings by the sol-gel process. In *Ultrastructure processing of advanced veramics*, Mackenzie, J. D., Ulrich, D. R. Eds.; John Wiley & Sons: New York, NY, USA, 1988; pp 651-660.
(42) Avnir, D.; Levy, D.; Reisfeld, R. The nature of the silica cage as reflected by spectral changes and enhanced photostability of trapped Rhodamine 6G. *J. Phys. Chem.* **1984**, *88*, 5956-5959. DOI: https://doi.org/10.1021/j150668a042.
(43) Tranquillo, E.; Barrino, F.; Dal Poggetto, G.; Blanco, I. Sol–Gel Synthesis of Silica-Based Materials with Different Percentages of PEG or PCL and High Chlorogenic Acid Content. *Materials* **2019**, *12*, 155. DOI: https://doi.org/10.3390/ma12010155.
(44) Grandi, S.; Tomasi, C.; Mustarelli, P.; Clemente, F.; Carbonaro, C. M. Characterisation of a new sol-gel precursor for a SiO_2-rhodamine 6G hybrid class II material. *J. Sol-Gel Sci. Technol.* **2007**, *41*, 57-63. DOI: https://doi.org/10.1007/s10971-006-0119-4.
(45) Hüsing, N.; Schubert, U. Organofunctional silica aerogels. *J. Sol-Gel Sci. Technol.* **1997**, *8*, 807-812. DOI: https://doi.org/10.1007/BF02436942.
(46) Kramer, S. J.; Rubio-Alonso, F.; Mackenzie, J. D. Organically Modified Silicate Aerogels, "Aeromosils". *MRS Proc.* **1996**, *435*, 295. DOI: https://doi.org/10.1557/PROC-435-295.
(47) Baney, R. H.; Itoh, M.; Sakakibara, A.; Suzuki, T. Silsesquioxanes. *Chem. Rev.* **1995**, *95*, 1409-1430. DOI: https://doi.org/10.1021/cr00037a012.
(48) Bautista, Y.; Gozalbo, A.; Mestre, S.; Sanz, V. Improvement in Char Strength with an Open Cage Silsesquioxane Flame Retardant. *Materials* **2017**, *10*, 567. DOI: https://doi.org/10.3390/ma10060567.
(49) Latthe, S. S.; Imai, H.; Ganesan, V.; Venkateswara Rao, A. Porous superhydrophobic silica films by sol–gel process. *Microporous Mesoporous Mater.* **2010**, *130*, 115-121. DOI: https://doi.org/10.1016/j.micromeso.2009.10.020.
(50) Feinle, A.; Leichtfried, F.; Straßer, S.; Hüsing, N. Carboxylic acid-functionalized porous silica particles by a co-condensation approach. *J. Sol-Gel Sci. Technol.* **2017**, *81*, 138-146. DOI: https://doi.org/10.1007/s10971-016-4090-4.
(51) Ye, Q.; Zhou, H.; Xu, J. Cubic Polyhedral Oligomeric Silsesquioxane Based Functional Materials: Synthesis, Assembly, and Applications. *Chem.: Asian J.* **2016**, *11*, 1322-1337. DOI: https://doi.org/10.1002/asia.201501445.
(52) Ahmed, N.; Fan, H.; Dubois, P.; Zhang, X.; Fahad, S.; Aziz, T.; Wan, J. Nano-engineering and micromolecular science of polysilsesquioxane materials and their emerging applications. *J. Mater. Chem. A* **2019**, *7*, 21577-21604. DOI: https://doi.org/10.1039/c9ta04575a.
(53) Thomas, N. R. Frederic Stanley Kipping—Pioneer in Silicon Chemistry: His Life & Legacy. *Silicon* **2010**, *2*, 187-193. DOI: https://doi.org/10.1007/s12633-010-9051-x.

(54) Itoh, M. Polyhedral Oligomeric Silsesquioxanes (POSS). In *Encyclopedia of Polymeric Nanomaterials*, Kobayashi, S., Müllen, K. Ed.; Springer: Berlin, Heidelberg, Germany, 2014; pp 1-8. DOI: https://doi.org/10.1007/978-3-642-36199-9_220-1.
(55) Kaneko, Y. Ionic silsesquioxanes: Preparation, structure control, characterization, and applications. *Polymer* **2018**, *144*, 205-224. DOI: https://doi.org/10.1016/j.polymer.2018.03.059.
(56) Scott, D. W. Thermal Rearrangement of Branched-Chain Methylpolysiloxanes. *J. Am. Chem. Soc.* **1946**, *68*, 356-358. DOI: https://doi.org/10.1021/ja01207a003.
(57) Brown, J. F.; Vogt, L. H. The Polycondensation of Cyclohexylsilanetriol. *J. Am. Chem. Soc.* **1965**, *87*, 4313-4317. DOI: https://doi.org/10.1021/ja00947a016.
(58) Morimoto, Y.; Watanabe, K.; Ootake, N.; Inagaki, J.; Yoshida, K.; Ohguma, K. Silsesquioxane Derivatives and Process for Production Thereof. US 2004/0249103 A1 2004.
(59) Ullah, A.; Ullah, S.; Khan, G. S.; Shah, S. M.; Hussain, Z.; Muhammad, S.; Siddiq, M.; Hussain, H. Water soluble polyhedral oligomeric silsesquioxane based amphiphilic hybrid polymers: Synthesis, self-assembly, and applications. *Eur. Polym. J.* **2016**, *75*, 67-92. DOI: https://doi.org/10.1016/j.eurpolymj.2015.11.023.
(60) Cordes, D. B.; Lickiss, P. D.; Rataboul, F. Recent developments in the chemistry of cubic polyhedral oligosilsesquioxanes. *Chem. Rev.* **2010**, *110*, 2081-2173. DOI: https://doi.org/10.1021/cr900201r.
(61) Behbehani, H.; Brisdon, B. J.; Mahon, M. F.; Molloy, K. C. The structure of hexa(cyclohexylsesquisiloxane), $(C_6H_{11})_6Si_6O_9$. *J. Organomet. Chem.* **1994**, *469*, 19-23. DOI: https://doi.org/10.1016/0022-328X(94)80073-1.
(62) Laird, M.; Van der Lee, A.; Dumitrescu, D. G.; Carcel, C.; Ouali, A.; Bartlett, J. R.; Unno, M.; Wong Chi Man, M. Styryl-Functionalized Cage Silsesquioxanes as Nanoblocks for 3-D Assembly. *Organometallics* **2020**, *39*, 1896-1906. DOI: https://doi.org/10.1021/acs.organomet.0c00119.
(63) Hunsicker, M.; Ankur; Morgenstern, B.; Zimmer, M.; Scheschkewitz, D. Polyhedral Oligomeric Silsesquioxane D_{3h}-$(RSiO_{1.5})_{14}$. *Chem. Eur. J.* **2024**, *30*, e202303640. DOI: https://doi.org/10.1002/chem.202303640.
(64) Laird, M.; Herrmann, N.; Ramsahye, N.; Totée, C.; Carcel, C.; Unno, M.; Bartlett, J. R.; Wong Chi Man, M. Large Polyhedral Oligomeric Silsesquioxane Cages: The Isolation of Functionalized POSS with an Unprecedented $Si_{18}O_{27}$ Core. *Angew. Chem. Int. Ed.* **2021**, *60*, 3022-3027. DOI: https://doi.org/10.1002/anie.202010458.
(65) Agaskar, P. A.; Klemperer, W. G. The higher hydridospherosiloxanes: synthesis and structures of $H_nSi_nO_{1.5n}$ (n=12, 14, 16, 18). *Inorg. Chim. Acta* **1995**, *229*, 355-364. DOI: https://doi.org/10.1016/0020-1693(94)04266-X.
(66) Yuan, H.; Li, Q.; Zuo, Y.; Zhang, H.; Zhang, J.; Liu, H.; Xie, J. New insight into the structural stability of large POSS by quantum chemistry calculation. *Inorg. Chem. Commun.* **2025**, *172*, 113761. DOI: https://doi.org/10.1016/j.inoche.2024.113761.
(67) Nusser, K.; Schneider, G. J.; Pyckhout-Hintzen, W.; Richter, D. Viscosity Decrease and Reinforcement in Polymer–Silsesquioxane Composites. *Macromolecules* **2011**, *44*, 7820-7830. DOI: https://doi.org/10.1021/ma201585v.
(68) Tanaka, K.; Adachi, S.; Chujo, Y. Structure–property relationship of octa-substituted POSS in thermal and mechanical reinforcements of conventional polymers. *J. Polym. Sci., Part A: Polym. Chem.* **2009**, *47*, 5690-5697. DOI: https://doi.org/10.1002/pola.23612.
(69) Hamada, T.; Nakanishi, Y.; Okada, K.; Tsukada, S.; Uedono, A.; Ohshita, J. Thermal Insulating Property of Silsesquioxane Hybrid Film Induced by Intramolecular Void Spaces. *ACS Appl. Polym. Mater.* **2021**, *3*, 3383-3391. DOI: https://doi.org/10.1021/acsapm.1c00344.

(70) Ervithayasuporn, V.; Wang, X.; Kawakami, Y. Synthesis and characterization of highly pure azido-functionalized polyhedral oligomeric silsesquioxanes (POSS). *Chem. Commun.* **2009**, 5130-5132. DOI: https://doi.org/10.1039/B909802J.
(71) Olivero, F.; Renò, F.; Carniato, F.; Rizzi, M.; Cannas, M.; Marchese, L. A novel luminescent bifunctional POSS as a molecular platform for biomedical applications. *Dalton Trans.* **2012**, *41*, 7467-7473. DOI: https://doi.org/10.1039/C2DT30218G.
(72) Abad, M. J.; Barral, L.; Fasce, D. P.; Williams, R. J. J. Epoxy Networks Containing Large Mass Fractions of a Monofunctional Polyhedral Oligomeric Silsesquioxane (POSS). *Macromolecules* **2003**, *36*, 3128-3135. DOI: https://doi.org/10.1021/ma021539f.
(73) Chi, H.; Lim, S. L.; Wang, F.; Wang, X.; He, C.; Chin, W. S. Pure blue-light emissive poly(oligofluorenes) with bifunctional POSS in the main chain. *Macromol. Rapid Commun.* **2014**, *35*, 801−806. DOI: https://doi.org/10.1002/marc.201400006.
(74) Wen, Z.; Xu, L.; Liu, X.; Fang, L.; Wu, L. Crosslinked silsesquioxane with high thermal stability and low dielectric constant by the autopolymerization of Q-type H-POSS. *Polymer* **2025**, *316*, 127843. DOI: https://doi.org/10.1016/j.polymer.2024.127843.
(75) Lichtenhan, J. D. Polyhedral Oligomeric Silsesquioxanes: Building Blocks for Silsesquioxane-Based Polymers and Hybrid Materials. *Comments Inorg. Chem.* **1995**, *17*, 115-130. DOI: https://doi.org/10.1080/02603599508035785.
(76) Zhou, H.; Ye, Q.; Xu, J. Polyhedral oligomeric silsesquioxane-based hybrid materials and their applications. *Mater. Chem. Front.* **2017**, *1*, 212-230. DOI: https://doi.org/10.1039/C6QM00062B.
(77) Zhang, C.; Zhang, J.; Xu, T.; Sima, H.; Hou, J. Effects of Polyhedral Oligomeric Silsesquioxane (POSS) on Thermal and Mechanical Properties of Polysiloxane Foam. *Materials* **2020**, *13*, 4570. DOI: https://doi.org/10.3390/ma13204570.
(78) Fernández, M. J.; Fernández, M. D.; Cobos, M. Synthesis, characterization and properties of telechelic hybrid biodegradable polymers containing polyhedral oligomeric silsesquioxane (POSS). *RSC Adv.* **2014**, *4*, 21435-21449. DOI: https://doi.org/10.1039/C4RA02172J.
(79) Dintcheva, N.; Morici, E.; Arrigo, R.; La mantia, F. p.; Malatesta, V.; Schwab, J. Structure-properties relationships of polyhedral oligomeric silsesquioxane (POSS) filled PS nanocomposites. *Express Polym. Lett.* **2012**, *6*, 561–571. DOI: https://doi.org/10.3144/expresspolymlett.2012.59.
(80) Piorecka, K.; Janaszewska, A.; Majkowska, M.; Marcinkowska, M.; Kurjata, J.; Kazmierski, S.; Radzikowska-Cieciura, E.; Kost, B.; Sowinski, P.; Klajnert-Maculewicz, B.; Stanczyk, W. A. Hydrophilic Polyhedral Oligomeric Silsesquioxane, $POSS(OH)_{32}$, as a Complexing Nanocarrier for Doxorubicin and Daunorubicin. *Materials* **2020**, *13*, 5512. DOI: https://doi.org/10.3390/ma13235512.
(81) Gunawidjaja, R.; Huang, F.; Gumenna, M.; Klimenko, N.; Nunnery, G. A.; Shevchenko, V.; Tannenbaum, R.; Tsukruk, V. V. Bulk and Surface Assembly of Branched Amphiphilic Polyhedral Oligomer Silsesquioxane Compounds. *Langmuir* **2009**, *25*, 1196-1209. DOI: https://doi.org/10.1021/la803182n.
(82) Wu, G.; Chen, L.; Liu, L. Direct grafting of octamaleamic acid-polyhedral oligomeric silsesquioxanes onto the surface of carbon fibers and the effects on the interfacial properties and anti-hydrothermal aging behaviors of silicone resin composites. *J. Mater. Sci.* **2017**, *52*, 1057-1070. DOI: https://doi.org/10.1007/s10853-016-0401-y.
(83) Wu, Y.-C.; Kuo, S.-W. Self-assembly supramolecular structure through complementary multiple hydrogen bonding of heteronucleobase-multifunctionalized polyhedral oligomeric silsesquioxane (POSS) complexes. *J. Mater. Chem.* **2012**, *22*, 2982-2991. DOI: https://doi.org/10.1039/C1JM14699H.

(84) Wu, J.; Haddad, T. S.; Mather, P. T. Vertex Group Effects in Entangled Polystyrene−Polyhedral Oligosilsesquioxane (POSS) Copolymers. *Macromolecules* **2009**, *42*, 1142-1152. DOI: https://doi.org/10.1021/ma8024267.
(85) Ayandele, E.; Sarkar, B.; Alexandridis, P. Polyhedral Oligomeric Silsesquioxane (POSS)-Containing Polymer Nanocomposites. *Nanomaterials* **2012**, *2*, 445-475. DOI: https://doi.org/10.3390/nano2040445.
(86) Kannan, A.; Muthuraj, C.; Mayavan, A.; Gandhi, S. Multifaceted applications of polyhedral oligomeric silsesquioxane and their composites. *Mater. Today Chem.* **2023**, *30*, 101568. DOI: https://doi.org/10.1016/j.mtchem.2023.101568.
(87) Li, L.; Lu, B.; Fan, Q.; Wu, J.; Wei, L.; Hou, J.; Guo, X.; Liu, Z. Synthesis and self-assembly behavior of pH-responsive star-shaped POSS-(PCL-P(DMAEMA-co-PEGMA))$_{16}$ inorganic/organic hybrid block copolymer for the controlled intracellular delivery of doxorubicin. *RSC Adv.* **2016**, *6*, 61630-61640. DOI: https://doi.org/10.1039/C6RA09803G.
(88) Knight, P. T.; Kirk, J. T.; Anderson, J. M.; Mather, P. T. In vivo kinetic degradation analysis and biocompatibility of aliphatic polyester polyurethanes. *J. Biomed. Mater. Res. A* **2010**, *94A*, 333-343. DOI: https://doi.org/10.1002/jbm.a.32806.
(89) Sachan, A.; Castro, M.; Choudhary, V.; Feller, J.-F. vQRS Based on Hybrids of CNT with PMMA-POSS and PS-POSS Copolymers to Reach the Sub-PPM Detection of Ammonia and Formaldehyde at Room Temperature Despite Moisture. *Chemosensors* **2017**, *5*, 22. DOI: https://doi.org/10.3390/chemosensors5030022.
(90) Gao, T.; Zhou, W.-F.; Zhao, Y.; Shen, L.; Chang, W.-Y.; Musendo, R.-K.; Chen, E.-Q.; Song, Y.-L.; Ren, X.-K. Polyhedral oligosilsesquioxane tethered perylene diimide for application in optical limiting and rapid detection of fluoride ions. *Chem. Commun.* **2019**, *55*, 3012-3014. DOI: https://doi.org/10.1039/C8CC09725A.
(91) Bai, W.; Sheng, Q.; Zheng, J. Hydrophobic interface controlled electrochemical sensing of nitrite based on one step synthesis of polyhedral oligomeric silsesquioxane/reduced graphene oxide nanocomposite. *Talanta* **2016**, *150*, 302-309. DOI: https://doi.org/10.1016/j.talanta.2015.12.030.
(92) Soares, I. V.; Vieira, E. G.; Filho, N. L. D.; Bastos, A. C.; da Silva, N. C.; Garcia, E. F.; Lima, L. J. A. Adsorption of heavy metal ions and epoxidation catalysis using a new polyhedral oligomeric silsesquioxane. *Chem. Eng. J.* **2013**, *218*, 405-414. DOI: https://doi.org/10.1016/j.cej.2012.11.126.
(93) Yin, Y.; Liu, M.; Wei, W.; Zhang, Y.; Gutowski, V.; Zhang, W.; Deng, P. "Open-Mouth" Mesoporous Hollow Micro/Nano Coatings Based on POSS/PDMS: Fabrication, Mechanisms, and Anti-Icing Performance. *Part. Part. Syst. Charact.* **2018**, *35*, 1800323. DOI: https://doi.org/10.1002/ppsc.201800323.
(94) Atar, N.; Grossman, E.; Gouzman, I.; Bolker, A.; Murray, V. J.; Marshall, B. C.; Qian, M.; Minton, T. K.; Hanein, Y. Atomic-Oxygen-Durable and Electrically-Conductive CNT-POSS-Polyimide Flexible Films for Space Applications. *ACS Appl. Mater. Interfaces.* **2015**, *7*, 12047-12056. DOI: https://doi.org/10.1021/acsami.5b02200.
(95) Brown, J. F. The Polycondensation of Phenylsilanetriol. *J. Am. Chem. Soc.* **1965**, *87*, 4317-4324. DOI: https://doi.org/10.1021/ja00947a017.
(96) Brown Jr., J. F. Double chain polymers and nonrandom crosslinking. *J. Polym. Sci. Part C* **1963**, *1*, 83-97. DOI: https://doi.org/10.1002/polc.5070010106.
(97) Brown, J. F.; Vogt, L. H.; Prescott, P. I. Preparation and characterization of the lower equilibrated phenylsilsesquioxanes. *J. Am. Chem. Soc.* **1964**, *86*, 1120-1125. DOI: https://doi.org/10.1021/ja01060a033.
(98) Frye, C. L.; Klosowski, J. M. Concerning the So-Called "Ladder Structure" of Equilibrated Phenylsilsesquioxane. *J. Am. Chem. Soc.* **1971**, *93*, 4599-4601. DOI: https://doi.org/10.1021/ja00747a047.

(99) Shklover, V. E.; Yuri, T. S. The Structure of Organocyclosiloxanes. *Russ. Chem. Rev.* **1980**, *49*, 518-556. DOI: https://doi.org/10.1070/RC1980v049n03ABEH002459.
(100) Brown, J. F.; Vogt, L. H.; Katchman, A.; Eustance, J. W.; Kiser, K. M. Double chain polymers of phenylsilsesquioxane. *J. Am. Chem. Soc.* **1960**, *82*, 6194-6195. DOI: https://doi.org/10.1021/ja01508a054.
(101) Unno, M.; Suto, A.; Matsumoto, T. Laddersiloxanes - silsesquioxanes with defined ladder structure. *Russ. Chem. Rev.* **2013**, *82*, 289-302. DOI: https://doi.org/10.1070/RC2013v082n04ABEH004360.
(102) Liu, Y.; Chaiprasert, T.; Ouali, A.; Unno, M. Well-defined cyclic silanol derivatives. *Dalton Trans.* **2022**, *51*, 4227-4245. DOI: https://doi.org/10.1039/D1DT04270J.
(103) Seki, H.; Kajiwara, T.; Abe, Y.; Gunji, T. Synthesis and structure of ladder polymethylsilsesquioxanes from sila-functionalized cyclotetrasiloxanes. *J. Organomet. Chem.* **2010**, *695*, 1363-1369. DOI: https://doi.org/10.1016/j.jorganchem.2010.02.008.
(104) Handke, M.; Kowalewska, A.; Mozgawa, W. Spectroscopic study of ceramic precursors obtained by hydrolytic condensation of ethoxycyclotetrasiloxane. *J. Mol. Struct.* **2008**, *887*, 152-158. DOI: https://doi.org/10.1016/j.molstruc.2007.12.037.
(105) Lee, H. S.; Choi, S.-S.; Baek, K.-Y.; Hong, S. M.; Lee, E. C.; Lee, J.-C.; Hwang, S. S. Synthesis and structure characterization of ladder-like polymethylsilsesquioxane (PMSQ) by isolation of stereoisomer. *Eur. Polym. J.* **2012**, *48*, 1073-1081. DOI: https://doi.org/10.1016/j.eurpolymj.2012.03.008.
(106) Anisimov, A. A.; Polshchikova, N. V.; Vysochinskaya, Y. S.; Zader, P. A.; Nikiforova, G. G.; Peregudov, A. S.; Buzin, M. I.; Shchegolikhina, O. I.; Muzafarov, A. M. Condensation of all-cis-tetraphenylcyclotetrasiloxanetetraol in ammonia: new method for preparation of ladder-like polyphenylsilsesquioxanes. *Mendeleev Commun.* **2019**, *29*, 421-423. DOI: https://doi.org/10.1016/j.mencom.2019.07.022.
(107) Chen, Z.; Ren, Z.; Zhang, J.; Fu, W.; Li, Z.; Zhang, R. Reactive ladder-like poly(p-decyl anilino)silsesquioxane for functional material's precursor: Synthesis, characterization and functionalization. *React. Funct. Polym.* **2012**, *72*, 503-508. DOI: https://doi.org/10.1016/j.reactfunctpolym.2012.05.003.
(108) Zhang, X.; Xie, P.; Shen, Z.; Jiang, J.; Zhu, C.; Li, H.; Zhang, T.; Han, C. C.; Wan, L.; Yan, S.; Zhang, R. Confined Synthesis of a cis-Isotactic Ladder Polysilsesquioxane by Using a π-Stacking and H-bonding Superstructure. *Angew. Chem. Int. Ed.* **2006**, *45*, 3112-3116. DOI: https://doi.org/10.1002/anie.200504474.
(109) Zhang, Z.-X.; Hao, J.; Xie, P.; Zhang, X.; Han, C. C.; Zhang, R. A Well-Defined Ladder Polyphenylsilsesquioxane (Ph-LPSQ) Synthesized via a New Three-Step Approach: Monomer Self-Organization-Lyophilization - Surface-Confined Polycondensation. *Chem. Mater.* **2008**, *20*, 1322-1330. DOI: https://doi.org/10.1021/cm071602l.
(110) Kaneko, Y.; Toyodome, H.; Shoiriki, M.; Iyi, N. Preparation of ionic silsesquioxanes with regular structures and their hybridization. *Int. J. Polym. Sci.* **2012**, *2012*, 684278. DOI: https://doi.org/10.1155/2012/684278.
(111) Choi, S.-S.; Lee, A. S.; Hwang, S. S.; Baek, K.-Y. Structural Control of Fully Condensed Polysilsesquioxanes: Ladderlike vs Cage Structured Polyphenylsilsesquioxanes. *Macromolecules* **2015**, *48*, 6063-6070. DOI: https://doi.org/10.1021/acs.macromol.5b01539.
(112) Lee, A. S.; Choi, S.-S.; Baek, K.-Y.; Hwang, S. S. Hydrolysis kinetics of a sol-gel equilibrium yielding ladder-like polysilsesquioxanes. *Inorg. Chem. Commun.* **2016**, *73*, 7-11. DOI: https://doi.org/10.1016/j.inoche.2016.09.004.
(113) Kaneko, Y.; Iyi, N.; Kurashima, K.; Matsumoto, T.; Fujita, T.; Kitamura, K. Hexagonal-Structured Polysiloxane Material Prepared by Sol−Gel Reaction of Aminoalkyltrialkoxysilane without Using Surfactants. *Chem. Mater.* **2004**, *16*, 3417-3423. DOI: https://doi.org/10.1021/cm0495212.

(114) Kaneko, Y.; Imamura, H.; Sugioka, T.; Sumida, Y. Preparation and thermal properties of soluble polysilsesquioxanes containing hydrophobic side-chain groups and their hybridization with organic polymers. *Polymer* **2016**, *92*, 250-255. DOI: https://doi.org/10.1016/j.polymer.2016.04.007.
(115) Andropova, U. S.; Aysin, R. R.; Serenko, O. A.; Ershova, T. O.; Anisimov, A. A.; Chernik, V. N. Ladder Polyphenylsilsesquioxanes and Their Niobium–Siloxane Composite as Coating Materials: Spectroscopy and Atomic Oxygen Resistance Study. *Polymers* **2023**, *15*, 3299. DOI: https://doi.org/10.3390/polym15153299.
(116) Hwang, S. O.; Lee, A. S.; Lee, J. Y.; Park, S.-H.; Jung, K. I.; Jung, H. W.; Lee, J.-H. Mechanical properties of ladder-like polysilsesquioxane-based hard coating films containing different organic functional groups. *Prog. Org. Coat.* **2018**, *121*, 105-111. DOI: https://doi.org/10.1016/j.porgcoat.2018.04.022.
(117) Kim, Y. H.; Choi, G.-M.; Bae, J. G.; Kim, Y. H.; Bae, B.-S. High-Performance and Simply-Synthesized Ladder-Like Structured Methacrylate Siloxane Hybrid Material for Flexible Hard Coating. *Polymers* **2018**, *10*, 449. DOI: https://doi.org/10.3390/polym10040449.
(118) Miyauchi, S.; Sugioka, T.; Sumida, Y.; Kaneko, Y. Preparation of soluble polysilsesquioxane containing phthalimido side-chain groups and its optical and thermal properties. *Polymer* **2015**, *66*, 122-126. DOI: https://doi.org/10.1016/j.polymer.2015.04.035.
(119) Herc, A. S.; Lewiński, P.; Kaźmierski, S.; Bojda, J.; Kowalewska, A. Hybrid SC-polylactide/poly(silsesquioxane) blends of improved thermal stability. *Thermochim. Acta* **2020**, *687*, 178592. DOI: https://doi.org/10.1016/j.tca.2020.178592.
(120) Harada, A.; Shikinaka, K.; Ohshita, J.; Kaneko, Y. Preparation of a one-dimensional soluble polysilsesquioxane containing phosphonic acid side-chain groups and its thermal and proton-conduction properties. *Polymer* **2017**, *121*, 228-233. DOI: https://doi.org/10.1016/j.polymer.2017.06.025.
(121) Jo, Y. Y.; Lee, A. S.; Baek, K. Y.; Lee, H.; Hwang, S. S. Thermally reversible self-healing polysilsesquioxane structure-property relationships based on Diels-Alder chemistry. *Polymer* **2017**, *108*, 58-65. DOI: https://doi.org/10.1016/j.polymer.2016.11.040.
(122) Park, S.; Lee, A. S.; Do, Y. S.; Kim, J. F.; Hwang, S. S.; Lee, Y. M.; Lee, J.-H.; Lee, J. S. Side-chain engineering of ladder-structured polysilsesquioxane membranes for gas separations. *J. Membr. Sci.* **2016**, *516*, 202-214. DOI: https://doi.org/10.1016/j.memsci.2016.06.016.
(123) Choi, M. H.; Seo, J. Y.; Ahn, J.; Woo, H. Y.; Cho, S.; Hwang, S. S.; Lee, A. S.; Baek, K.-Y. Flowable polysilsesquioxanes as robust solvent-free optical hard coatings. *React. Funct. Polym.* **2021**, *167*, 105030. DOI: https://doi.org/10.1016/j.reactfunctpolym.2021.105030.
(124) Kessler, D.; Theato, P. Reactive Surface Coatings Based on Polysilsesquioxanes: Defined Adjustment of Surface Wettability. *Langmuir* **2009**, *25*, 14200-14206. DOI: https://doi.org/10.1021/la9005949.
(125) Lee, A. S.; Lee, J. H.; Choi, S.-S.; Cho, K. Y.; Yu, S.; Koo, C. M.; Baek, K.-Y.; Hwang, S. S. UV-curable antibacterial ionic polysilsesquioxanes: Structure-property relationships investigating the effect of various cations and anions. *Eur. Polym. J.* **2017**, *95*, 323-334. DOI: https://doi.org/10.1016/j.eurpolymj.2017.08.005.
(126) Kim, D.; Kim, C. A Ladder-Type Organosilicate Copolymer Gate Dielectric Materials for Organic Thin-Film Transistors. *Coatings* **2018**, *8*, 236. DOI: https://doi.org/10.3390/coatings8070236.
(127) Shin, S. C.; Kim, J.; Modigunta, J. K. R.; Murali, G.; Park, S.; Lee, S.; Lee, H.; Park, S. Y.; In, I. Bio-mimicking organic-inorganic hybrid ladder-like polysilsesquioxanes as a surface modifier for polyethylene separator in lithium-ion batteries. *J. Membr. Sci.* **2021**, *620*, 118886. DOI: https://doi.org/10.1016/j.memsci.2020.118886.

(128) Park, S.; Lee, A. S.; Do, Y. S.; Hwang, S. S.; Lee, Y. M.; Lee, J.-H.; Lee, J. S. Rational molecular design of PEOlated ladder-structured polysilsesquioxane membranes for high performance CO_2 removal. *Chem. Commun.* **2015**, *51*, 15308-15311. DOI: https://doi.org/10.1039/C5CC06269A.
(129) Shang, X. X.; Duan, S.; Zhang, M.; Cao, X. Y.; Zheng, K.; Zhang, J. N.; Ma, Y. M.; Zhang, R. B. UV-curable ladder-like diphenylsiloxane-bridged methacryl-phenyl-siloxane for high power LED encapsulation. *RSC Adv.* **2018**, *8*, 9049-9056. DOI: https://doi.org/10.1039/c8ra00063h.
(130) Loy, D. A.; Carpenter, J. P.; Alam, T. M.; Shaltout, R.; Dorhout, P. K.; Greaves, J.; Small, J. H.; Shea, K. J. Cyclization Phenomena in the Sol−Gel Polymerization of α,ω-Bis(triethoxysilyl)alkanes and Incorporation of the Cyclic Structures into Network Silsesquioxane Polymers. *J. Am. Chem. Soc.* **1999**, *121*, 5413-5425. DOI: https://doi.org/10.1021/ja982751v.
(131) Jeong, S.; Kim, D.; Lee, S.; Park, B.-K.; Moon, J. Organic-inorganic hybrid dielectrics with low leakage current for organic thin-film transistors. *Appl. Phys. Lett.* **2006**, *89*, 092101. DOI: https://doi.org/10.1063/1.2338753.
(132) Prado, L. A. S. D. A.; Radovanovic, E.; Pastore, H. O.; Yoshida, I. V. P.; Torriani, I. L. Poly(phenylsilsesquioxane)s: Structural and morphological characterization. *J. Polym. Sci., Part A: Polym. Chem.* **2000**, *38*, 1580-1589. DOI: https://doi.org/10.1002/(SICI)1099-0518(20000501)38:9<1580::AID-POLA22>3.0.CO;2-7.
(133) Hwang, S. O.; Lee, J. Y.; Lee, J.-H. Effect of the silsesquioxane structure on the mechanical properties of the silsesquioxane-reinforced polymer composite films. *Prog. Org. Coat.* **2019**, *137*, 105316. DOI: https://doi.org/10.1016/j.porgcoat.2019.105316.
(134) Loy, D. A.; Baugher, B. M.; Baugher, C. R.; Schneider, D. A.; Rahimian, K. Substituent effects on the sol-gel chemistry of organotrialkoxysilanes. *Chem. Mater.* **2000**, *12*, 3624-3632. DOI: https://doi.org/10.1021/cm000451i.
(135) Kuniyoshi, M.; Takahashi, M.; Tokuda, Y.; Yoko, T. OH-Free Phenyl Modified Siloxane Low-Melting Glasses with Ultra Low Saturated Water -Absorption. *J. Ceram. Soc. Jpn.* **2006**, *114*, 660-664. DOI: https://doi.org/10.2109/jcersj.114.660.
(136) Kurumada, K.-i.; Ashraf, K. M.; Matsumoto, S. Effects of heat treatment on various properties of organic–inorganic hybrid silica derived from phenyltriethoxysilane. *Mater. Chem. Phys.* **2014**, *144*, 132-138. DOI: https://doi.org/10.1016/j.matchemphys.2013.12.031.
(137) Liu, F.; Zeng, X.; Lai, X.; Li, H. Synthesis and characterization of polyphenylsilsesquioxane terminated with methyl and vinyl groups low-melting glass. *J. Adhes. Sci. Technol.* **2017**, *31*, 2399-2409. DOI: https://doi.org/10.1080/01694243.2017.1302699.
(138) Kino, D.; Okada, K.; Tokudome, Y.; Takahashi, M.; Malfatti, L.; Innocenzi, P. Reactivity of silanol group on siloxane oligomers for designing molecular structure and surface wettability. *J. Sol-Gel Sci. Technol.* **2021**, *97*, 734-742. DOI: https://doi.org/10.1007/s10971-020-05448-z.
(139) Zhang, W.; Wang, X.; Wu, Y.; Qi, Z.; Yang, R. Preparation and Characterization of Organic-Inorganic Hybrid Macrocyclic Compounds: Cyclic Ladder-like Polyphenylsilsesquioxanes. *Inorg. Chem.* **2018**, *57*, 3883-3892. DOI: https://doi.org/10.1021/acs.inorgchem.7b03264.
(140) Curto, Y.; Koch, M.; Kickelbick, G. Chemical and Structural Comparison of Different Commercial Food Supplements for Silicon Uptake. *Solids* **2023**, *4*, 1-21. DOI: https://doi.org/10.3390/solids4010001.
(141) Nowacka, M.; Kowalewska, A.; Makowski, T. Structural studies on ladder phenylsilsesquioxane oligomers formed by polycondensation of cyclotetrasiloxanetetraols. *Polymer* **2016**, *87*, 81-89. DOI: https://doi.org/10.1016/j.polymer.2016.01.058.

(142) Jitianu, A.; Cadars, S.; Zhang, F.; Rodriguez, G.; Picard, Q.; Aparicio, M.; Mosa, J.; Klein, L. C. ^{29}Si NMR and SAXS investigation of the hybrid organic-inorganic glasses obtained by consolidation of the melting gels. *Dalton Trans.* **2017**, *46*, 3729-3741. DOI: https://doi.org/10.1039/c6dt04394a.
(143) Temnikov, M. N.; Vasil'ev, V. G.; Buzin, M. I.; Muzafarov, A. M. Synthesis and comparison of the rheological and thermal properties of acyclic and polycyclic forms of polyphenylsilsesquioxane. *Eur. Polym. J.* **2020**, *130*, 109676. DOI: https://doi.org/10.1016/j.eurpolymj.2020.109676.
(144) Sakuragi, A.; Igarashi, Y.; Kajihara, K.; Kanamura, K. Synthesis of silanol-rich long-life polysilsesquioxane liquids by cosolvent-free hydrolytic polycondensation of organotrimethoxysilanes followed by aging. *Dalton Trans.* **2016**, *45*, 3151-3157. DOI: https://doi.org/10.1039/c5dt04611d.
(145) Kim, J. H.; Han, J. S.; Lee, M. E.; Moon, D. H.; Lah, M. S.; Yoo, B. R. Solid-state structure and condensation reaction of (triphenylmethyl)silanetriol. *J. Organomet. Chem.* **2005**, *690*, 1372-1378. DOI: https://doi.org/10.1016/j.jorganchem.2004.12.012.
(146) Suzuki, J.; Shimojima, A.; Fujimoto, Y.; Kuroda, K. Stable Silanetriols That Contain tert-Alkoxy Groups: Versatile Precursors of Siloxane-Based Nanomaterials. *Chem. Eur. J.* **2008**, *14*, 973-980. DOI: https://doi.org/10.1002/chem.200700914.
(147) Korkin, S. D.; Buzin, M. I.; Matukhina, E. V.; Zherlitsyna, L. N.; Auner, N.; Shchegolikhina, O. I. Phenylsilanetriol—synthesis, stability, and reactivity. *J. Organomet. Chem.* **2003**, *686*, 313-320. DOI: https://doi.org/10.1016/S0022-328X(03)00721-6.
(148) Shimojima, A.; Sugahara, Y.; Kuroda, K. Inorganic–Organic Layered Materials Derived via the Hydrolysis and Polycondensation of Trialkoxy(alkyl)silanes. *Bull. Chem. Soc. Jpn.* **2006**, *70*, 2847-2853. DOI: https://doi.org/10.1246/bcsj.70.2847.
(149) Fujimoto, Y.; Shimojima, A.; Kuroda, K. Formation of Layered Silica−Alcohol Nanostructured Materials from Alkoxytrichlorosilanes. *Chem. Mater.* **2003**, *15*, 4768-4774. DOI: https://doi.org/10.1021/cm030432j.
(150) Jitianu, A.; Amatucci, G.; Klein, L. C. Phenyl-Substituted Siloxane Hybrid Gels that Soften Below 140°C. *J. Am. Ceram. Soc.* **2009**, *92*, 36-40. DOI: https://doi.org/10.1111/j.1551-2916.2008.02841.x.
(151) Fardad, M. A. Catalysts and the structure of SiO_2 sol-gel films. *J. Mater. Sci.* **2000**, *35*, 1835-1841. DOI: https://doi.org/10.1023/A:1004749107134.
(152) Pope, E. J. A.; Mackenzie, J. D. Sol-gel processing of silica: II. The role of the catalyst. *J. Non-Cryst. Solids* **1986**, *87*, 185-198. DOI: https://doi.org/10.1016/S0022-3093(86)80078-3.
(153) Fricke, J.; Emmerling, A. Aerogels—Preparation, properties, applications. In *Chemistry, Spectroscopy and Applications of Sol-Gel Glasses*, Reisfeld, R., Jjørgensen, C. K. Eds.; Springer Berlin, Heidelberg, Germany, 1992; pp 37-87. DOI: https://doi.org/10.1007/BFb0036965.
(154) Linhares, T.; de Amorim, M. T. P.; Durães, L. Silica aerogel composites with embedded fibres: a review on their preparation, properties and applications. *J. Mater. Chem. A* **2019**, *7*, 22768-22802. DOI: https://doi.org/10.1039/C9TA04811A.
(155) Schubert, U. Chemistry and Fundamentals of the Sol–Gel Process. In *The Sol-Gel Handbook*, Levy, D., Zayat, M. Eds.; Wiley-VCH: Weinheim, Germany, 2015; pp 1-28.
(156) Collina, D.; Fornasari, G.; Rinaldo, A.; Trifirò, F.; Leofanti, G.; Paparatto, G.; Petrini, G. Silica preparation via sol-gel method: a comparison with ammoximation activity. *Stud. Surf. Sci. Catal.* **1995**, *91*, 401-410. DOI: https://doi.org/10.1016/S0167-2991(06)81776-3.
(157) Stöber, W.; Fink, A.; Bohn, E. Controlled growth of monodisperse silica spheres in the micron size range. *J. Colloid Interface Sci.* **1968**, *26*, 62-69. DOI: https://doi.org/10.1016/0021-9797(68)90272-5.

(158) Altmann, S.; Pfeiffer, J. The Hydrolysis/Condensation Behaviour of Methacryloyloxyalkylfunctional Alkoxysilanes: Structure-Reactivity Relations. *Monatsh. Chem.* **2003**, *134*, 1081-1092. DOI: https://doi.org/10.1007/s00706-003-0615-y.
(159) Takamura, N.; Gunji, T.; Hatano, H.; Abe, Y. Preparation and properties of polysilsesquioxanes: Polysilsesquioxanes and flexible thin films by acid-catalyzed controlled hydrolytic polycondensation of methyl- and vinyltrimethoxysilane. *J. Polym. Sci., Part A: Polym. Chem.* **1999**, *37*, 1017-1026. DOI: https://doi.org/10.1002/(SICI)1099-0518(19990401)37:7<1017::AID-POLA16>3.0.CO;2-F.
(160) Hamada, T.; Sugimoto, T.; Maeda, T.; Katsura, D.; Mineoi, S.; Ohshita, J. Robust and Transparent Antifogging Polysilsesquioxane Film Containing a Hydroxy Group. *Langmuir* **2022**, *38*, 5829-5837. DOI: https://doi.org/10.1021/acs.langmuir.2c00438.
(161) Kajihara, K.; Sakuragi, A.; Igarashi, Y.; Kanamura, K. Synthesis of monolithic deep-ultraviolet-transparent polysilsesquioxane glasses from organotrimethoxysilane–water binary system. *RSC Adv.* **2012**, *2*, 8946-8948. DOI: https://doi.org/10.1039/C2RA21377J.
(162) Li, Y.-S.; Ba, A. Spectroscopic studies of triethoxysilane sol–gel and coating process. *Spectrochim. Acta A Mol. Biomol. Spectrosc.* **2008**, *70*, 1013-1019. DOI: https://doi.org/10.1016/j.saa.2007.09.050.
(163) Kajihara, K.; Suzuki, R.; Seto, R.; Itakura, H.; Ishijima, M. Poly(cyclohexylsilsesquioxane)-Based Hydrophilic Thermoset-Resistant Deep-Ultraviolet-Transparent Glasses with Low Melting Temperatures. *ACS Appl. Mater. Interfaces.* **2023**, *15*, 31880-31887. DOI: https://doi.org/10.1021/acsami.3c05758.
(164) Sturm, M. T.; Herbort, A. F.; Horn, H.; Schuhen, K. Comparative study of the influence of linear and branched alkyltrichlorosilanes on the removal efficiency of polyethylene and polypropylene-based microplastic particles from water. *Environ. Sci. Pollut. Res.* **2020**, *27*, 10888-10898. DOI: https://doi.org/10.1007/s11356-020-07712-9.
(165) Yevchuk, I.; Demchyna, O.; Kopylets, V.; Koval, Z.; Romaniuk, H. Kinetic regularities of the early stages of sol-gel process in tetraethoxysilane-based systems. *Chem. Chem. Technol.* **2014**, *8*, 147-155. DOI: https://doi.org/10.23939/chcht08.02.147.
(166) Mori, H.; Miyamura, Y.; Endo, T. Synthesis and Characterization of Water-Soluble Silsesquioxane-Based Nanoparticles by Hydrolytic Condensation of Triethoxysilane Derived from 2-Hydroxyethyl Acrylate. *Langmuir* **2007**, *23*, 9014-9023. DOI: https://doi.org/10.1021/la700706a.
(167) Ageenkov, A. D.; Bredov, N. S.; Shcherbina, A. A.; Khasbiullin, R. R.; Tupikov, A. S.; Soldatov, M. A. The Influence of Conditions of Polycondensation in Acid Medium on the Structure of Oligosilsesquioxanes with a Novel Eugenol-Containing Substituent. *Polymers* **2024**, *16*, 2951. DOI: https://doi.org/10.3390/polym16202951.
(168) Matějka, L.; Dukh, O.; Brus, J.; Simonsick Jr, W. J.; Meissner, B. Cage-like structure formation during sol–gel polymerization of glycidyloxypropyltrimethoxysilane. *J. Non-Cryst. Solids* **2000**, *270*, 34-47. DOI: https://doi.org/10.1016/S0022-3093(00)00074-0.
(169) Yagihashi, F.; Igarashi, M.; Nakajima, Y.; Ando, W.; Sato, K.; Yumoto, Y.; Matsui, C.; Shimada, S. Acid-Catalyzed Condensation Reaction of Phenylsilanetriol: Unexpected Formation of cis,trans-1,3,5-Trihydroxy-1,3,5-triphenylcyclotrisiloxane as the Main Product and Its Isolation. *Organometallics* **2014**, *33*, 6278-6281. DOI: https://doi.org/10.1021/om500691c.
(170) Dixit, C. K.; Bhakta, S.; Kumar, A.; Suib, S. L.; Rusling, J. F. Fast nucleation for silica nanoparticle synthesis using a sol–gel method. *Nanoscale* **2016**, *8*, 19662-19667. DOI: https://doi.org/10.1039/C6NR07568A.
(171) Brochier Salon, M.-C.; Bayle, P.-A.; Abdelmouleh, M.; Boufi, S.; Belgacem, M. N. Kinetics of hydrolysis and self condensation reactions of silanes by NMR spectroscopy.

Colloids Surf. A: Physicochem. Eng. Asp. **2008**, *312*, 83-91. DOI: https://doi.org/10.1016/j.colsurfa.2007.06.028.
(172) Kaneko, Y.; Shoiriki, M.; Mizumo, T. Preparation of cage-like octa(3-aminopropyl)silsesquioxane trifluoromethanesulfonate in higher yield with a shorter reaction time. *J. Mater. Chem.* **2012**, *22*, 14475-14478. DOI: https://doi.org/10.1039/C2JM32355A.
(173) Bassindale, A. R.; Liu, Z.; MacKinnon, I. A.; Taylor, P. G.; Yang, Y.; Light, M. E.; Horton, P. N.; Hursthouse, M. B. A higher yielding route for T_8 silsesquioxane cages and X-ray crystal structures of some novel spherosilicates. *Dalton Trans.* **2003**, 2945-2949. DOI: https://doi.org/10.1039/B302950F.
(174) Foorginezhad, S.; Zerafat, M. Effect of Solvent properties on Crystallinity and Morphology of Octavinyl-POSS: A Comparative Study. *J. Nanostructures* **2020**, *10*, 375-391. DOI: https://doi.org/10.22052/jns.2020.02.016.
(175) Kudo, T.; Gordon, M. S. Theoretical studies of the mechanism for the synthesis of silsesquioxanes. 1. Hydrolysis and initial condensation. *J. Am. Chem. Soc.* **1998**, *120*, 11432-11438. DOI: https://doi.org/10.1021/ja980943k.
(176) Kudo, T.; Gordon, M. S. Theoretical Studies of the Mechanism for the Synthesis of Silsesquioxanes. 2. Cyclosiloxanes (D_3 and D_4). *J. Phys. Chem. A* **2000**, *104*, 4058-4063. DOI: https://doi.org/10.1021/jp993643d.
(177) Kudo, T.; Gordon, M. S. Exploring the mechanism for the synthesis of silsesquioxanes. 3. The effect of substituents and water. *J. Phys. Chem. A* **2002**, *106*, 11347-11353. DOI: https://doi.org/10.1021/jp0214108.
(178) Brinker, C. J.; Scherer, G. W. CHAPTER 3 - Hydrolysis and Condensation II: Silicates. In *Sol-Gel Science*, Brinker, C. J., Scherer, G. W. Eds.; Academic Press: San Diego, CA, USA, 1990; pp 96-233. DOI: https://doi.org/10.1016/B978-0-08-057103-4.50008-8.
(179) Bari, A. H.; Jundale, R. B.; Kulkarni, A. A. Understanding the role of solvent properties on reaction kinetics for synthesis of silica nanoparticles. *Chem. Eng. J.* **2020**, *398*, 125427. DOI: https://doi.org/10.1016/j.cej.2020.125427.
(180) Artaki, I.; Bradley, M.; Zerda, T. W.; Jonas, J. NMR and Raman study of the hydrolysis reaction in sol-gel processes. *J. Phys. Chem.* **1985**, *89*, 4399-4404. DOI: https://doi.org/10.1021/j100266a050.
(181) Władyczyn, A.; John, Ł. Silsesquioxane Cages under Solvent Regimen: The Influence of the Solvent on the Hydrolysis and Condensation of Alkoxysilane. *Inorg. Chem.* **2024**, *63*, 9145-9155. DOI: https://doi.org/10.1021/acs.inorgchem.4c00460.
(182) Sadasivan, S.; Dubey, A. K.; Li, Y.; Rasmussen, D. H. Alcoholic Solvent Effect on Silica Synthesis—NMR and DLS Investigation. *J. Sol-Gel Sci. Technol.* **1998**, *12*, 5-14. DOI: https://doi.org/10.1023/A:1008659708390.
(183) Peace, B. W.; Mayhan, K. G.; Montle, J. F. Polymers from the hydrolysis of tetraethoxysilane. *Polymer* **1973**, *14*, 420-422. DOI: https://doi.org/10.1016/0032-3861(73)90006-2.
(184) Hollstein, S.; Erdmann, P.; Ulmer, A.; Löw, H.; Greb, L.; von Delius, M. Trialkoxysilane Exchange: Scope, Mechanism, Cryptates and pH-Response. *Angew. Chem. Int. Ed.* **2023**, *62*, e202304083. DOI: https://doi.org/10.1002/anie.202304083.
(185) Avnir, D.; Kaufman, V. R. Alcohol is an unnecessary additive in the silicon alkoxide sol-gel process. *J. Non-Cryst. Solids* **1987**, *92*, 180-182. DOI: https://doi.org/10.1016/S0022-3093(87)80368-X.
(186) Giasuddin, A. B. M.; Britt, D. W. Monitoring Silane Sol-Gel Kinetics with In-Situ Optical Turbidity Scanning and Dynamic Light Scattering. *Molecules* **2019**, *24*, 2931. DOI: https://doi.org/10.3390/molecules24162931.

(187) Jiang, H.; Zheng, Z.; Li, Z.; Wang, X. Effects of Temperature and Solvent on the Hydrolysis of Alkoxysilane under Alkaline Conditions. *Ind. Eng. Chem. Res.* **2006**, *45*, 8617-8622. DOI: https://doi.org/10.1021/ie0607550.
(188) Zhai, Q.; Zhou, C.; Zhao, S.; Peng, C.; Han, Y. Kinetic Study of Alkoxysilane Hydrolysis under Acidic Conditions by Fourier Transform Near Infrared Spectroscopy Combined with Partial Least-Squares Model. *Ind. Eng. Chem. Res.* **2014**, *53*, 13598-13609. DOI: https://doi.org/10.1021/ie5012195.
(189) Kannengießer, J.-F.; Morgenstern, B.; Janka, O.; Kickelbick, G. Oligo-Condensation Reactions of Silanediols with Conservation of Solid-State-Structural Features. *Chem. Eur. J.* **2024**, *30*, e202303343. DOI: https://doi.org/10.1002/chem.202303343.
(190) Tyler, L. J. Phenylsilanetriol. *J. Am. Chem. Soc.* **1955**, *77*, 770-771. DOI: https://doi.org/10.1021/ja01608a078.
(191) Criado, M.; Sobrados, I.; Sanz, J. Polysiloxane Hybrids via Sol-Gel Process: Effect of Temperature on Network Formation. *Coatings* **2020**, *10*, 677. DOI: https://doi.org/10.3390/coatings10070677.
(192) Zhang, X.-Q.; Trinh, T. T.; van Santen, R. A.; Jansen, A. P. J. Mechanism of the Initial Stage of Silicate Oligomerization. *J. Am. Chem. Soc.* **2011**, *133*, 6613-6625. DOI: https://doi.org/10.1021/ja110357k.
(193) Jiang, Y.; Wan, Q.-H. Separation and identification of oligomeric phenylethoxysiloxanols by liquid chromatography-electrospray ionization mass spectrometry. *J. Chromatogr. A* **2015**, *1394*, 95-102. DOI: https://doi.org/10.1016/j.chroma.2015.03.043.
(194) Jia, G.; Wan, Q.-H. Separation and identification of oligomeric vinylmethoxysiloxanes by gradient elution chromatography coupled with electrospray ionization mass spectrometry. *J. Chromatogr. A* **2015**, *1395*, 129-135. DOI: https://doi.org/10.1016/j.chroma.2015.03.079.
(195) Brochier Salon, M. C.; Belgacem, M. N. Competition between hydrolysis and condensation reactions of trialkoxysilanes, as a function of the amount of water and the nature of the organic group. *Colloids Surf. A* **2010**, *366*, 147-154. DOI: https://doi.org/10.1016/j.colsurfa.2010.06.002.
(196) Issa, A. A.; El-Azazy, M. S. Polymerization of 3-cyanopropyl (triethoxy) silane : A kinetic study using gas chromatography. *Int. J. Chem. Kinet.* **2018**, *50*, 846-855. DOI: https://doi.org/10.1002/kin.21219.
(197) Hamada, T.; Goto, T.; Takase, S.; Okada, K.; Uedono, A.; Ohshita, J. Structure–Thermal Property Relationships of Polysilsesquioxanes for Thermal Insulation Materials. *ACS Appl. Polym. Mater.* **2022**, *4*, 2851-2859. DOI: https://doi.org/10.1021/acsapm.1c01812.
(198) Pescarmona, P. P.; Maschmeyer, T. Oligomeric Silsesquioxanes: Synthesis, Characterization and Selected Applications. *Aust. J. Chem.* **2002**, *54*, 583-596. DOI: https://doi.org/10.1071/CH02003.
(199) Schmidt, H.; Scholze, H.; Kaiser, A. Principles of hydrolysis and condensation reaction of alkoxysilanes. *J. Non-Cryst. Solids* **1984**, *63*, 1-11. DOI: https://doi.org/10.1016/0022-3093(84)90381-8.
(200) Arkles, B.; Steinmetz, J. R.; Zazyczny, J.; Mehta, P. Factors contributing to the stability of alkoxysilanes in aqueous solution. *J. Adhes. Sci. Technol.* **1992**, *6*, 193-206. DOI: https://doi.org/10.1163/156856192X00133.
(201) Jitianu, A.; Doyle, J.; Amatucci, G.; Klein, L. C. Methyl modified siloxane melting gels for hydrophobic films. *J. Sol-Gel Sci. Technol.* **2010**, *53*, 272-279. DOI: https://doi.org/10.1007/s10971-009-2087-y.
(202) Gunji, T.; Iizuka, Y.; Arimitsu, K.; Abe, Y. Preparation and properties of alkoxy(methyl)silsesquioxanes as coating agents. *J. Polym. Sci., Part A: Polym. Chem.* **2004**, *42*, 3676-3684. DOI: https://doi.org/10.1002/pola.20233.

(203) Naik, V. V.; Städler, R.; Spencer, N. D. Effect of Leaving Group on the Structures of Alkylsilane SAMs. *Langmuir* **2014**, *30*, 14824-14831. DOI: https://doi.org/10.1021/la503739j.
(204) Jitianu, A.; Britchi, A.; Deleanu, C.; Badescu, V.; Zaharescu, M. Comparative study of the sol-gel processes starting with different substituted Si-alkoxides. *J. Non-Cryst. Solids* **2003**, *319*, 263-279. DOI: https://doi.org/10.1016/S0022-3093(03)00007-3.
(205) Issa, A. A.; El-Azazy, M.; Luyt, A. S. Kinetics of alkoxysilanes hydrolysis: An empirical approach. *Sci. Rep.* **2019**, *9*, 1-15. DOI: https://doi.org/10.1038/s41598-019-54095-0.
(206) Dirè, S.; Borovin, E.; Ribot, F. Architecture of Silsesquioxanes. In *Handbook of Sol-Gel Science and Technology*, Klein, L., Aparicio, M., Jitianu, A. Eds.; Springer International Publishing: Cham, Switzerland, 2018; pp 3119-3151. DOI: https://doi.org/10.1007/978-3-319-32101-1_119.
(207) Sprung, M. M.; Guenther, F. O. The hydrolysis of n-amyltriethoxysilane and phenyltriethoxysilane. *J. Polym. Sci.* **1958**, *28*, 17-34. DOI: https://doi.org/10.1002/pol.1958.1202811603.
(208) Murugavel, R.; Voigt, A.; Walawalkar, M. G.; Roesky, H. W. Hetero- and Metallasiloxanes Derived from Silanediols, Disilanols, Silanetriols, and Trisilanols. *Chem. Rev.* **1996**, *96*, 2205-2236. DOI: https://doi.org/10.1021/cr9500747.
(209) Pietschnig, R.; Spirk, S. The chemistry of organo silanetriols. *Coord. Chem. Rev.* **2016**, *323*, 87-106. DOI: https://doi.org/10.1016/j.ccr.2016.03.010.
(210) Ishida, H.; Koenig, J. L.; Gardner, K. C. Structure of cyclohexylsilanetriol: The first x-ray crystal structure of a silanetriol. *J. Chem. Phys.* **1982**, *77*, 5748-5751. DOI: https://doi.org/10.1063/1.443730.
(211) Pietschnig, R.; Belaj, F. Synthesis and structure of a silanetriol via hydroxodearylation involving C–Si bond cleavage. *Inorg. Chim. Acta* **2005**, *358*, 444-448. DOI: https://doi.org/10.1016/j.ica.2004.09.018.
(212) Kim, H. J.; Lee, J. K.; Kim, J. B.; Park, E. S.; Park, S. J.; Yoo, D. Y.; Yoon, D. Y. Substituent effects on microstructure and polymerization of polyalkylsilsesquioxanes. *J. Am. Chem. Soc.* **2001**, *123*, 12121-12122. DOI: https://doi.org/10.1021/ja0168099.
(213) Lee, L.-H.; Chen, W.-C.; Liu, W.-C. Structural control of oligomeric methyl silsesquioxane precursors and their thin-film properties. *J. Polym. Sci., Part A: Polym. Chem.* **2002**, *40*, 1560-1571. DOI: https://doi.org/10.1002/pola.10246.
(214) Meng, G.; Li, Y.; Wang, Z.; Pan, C.; Gao, W.; Cheng, Y. Preparation and Characterization of Narrow Size Distribution PMSQ Microspheres for High-Frequency Electronic Packaging. *Materials* **2021**, *14*, 4233. DOI: https://doi.org/10.3390/ma14154233.
(215) Park, E. S.; Ro, H. W.; Nguyen, C. V.; Jaffe, R. L.; Yoon, D. Y. Infrared Spectroscopy Study of Microstructures of Poly(silsesquioxane)s. *Chem. Mater.* **2008**, *20*, 1548-1554. DOI: https://doi.org/10.1021/cm071575z.
(216) Parikh, A. N.; Schivley, M. A.; Koo, E.; Seshadri, K.; Aurentz, D.; Mueller, K.; Allara, D. L. n-Alkylsiloxanes: From Single Monolayers to Layered Crystals. The Formation of Crystalline Polymers from the Hydrolysis of n-Octadecyltrichlorosilane. *J. Am. Chem. Soc.* **1997**, *119*, 3135-3143. DOI: https://doi.org/10.1021/ja963284p.
(217) Huber, M. P.; Kelch, S.; Berke, H. FTIR investigations on hydrolysis and condensation reactions of alkoxysilane terminated polymers for use in adhesives and sealants. *Int. J. Adhes. Adhes.* **2016**, *64*, 153-162. DOI: https://doi.org/10.1016/j.ijadhadh.2015.10.014.
(218) Torry, S. A.; Campbell, A.; Cunliffe, A. V.; Tod, D. A. Kinetic analysis of organosilane hydrolysis and condensation. *Int. J. Adhes. Adhes.* **2006**, *26*, 40-49. DOI: https://doi.org/10.1016/j.ijadhadh.2005.03.008.
(219) Savard, S.; Blanchard, L.-P.; Léonard, J.; Prud'homme, R. E. Hydrolysis and condensation of silanes in aqueous solutions. *Polym. Compos.* **1984**, *5*, 242-249. DOI: https://doi.org/10.1002/pc.750050403.

(220) Wu, X.; Qin, Z.; Zhang, W.; Yang, R. Influence of monomer concentration on structures of fully condensed polyphenylsilsesquioxanes. *High Perform. Polym.* **2024**, *36*, 82-93. DOI: https://doi.org/10.1177/09540083231222593.
(221) Dasgupta, D.; Srividhya, M.; Sarkar, A.; Dubey, M.; Wrobel, D.; Saxena, A. Rubber nanocomposites with polyhedral oligomeric silsesquioxanes (POSS) as the nanofiller. In *Progress in Rubber Nanocomposites*, Thomas, S., Maria, H. J. Eds.; Woodhead Publishing: Sawston, Cambridge, UK, 2017; pp 231-247. DOI: https://doi.org/10.1016/B978-0-08-100409-8.00007-3.
(222) Urano, S.; Tomita, R.; Tadanaga, K. Synthetic control of cage/network ratio of poly(methylsilsesquioxane)s for storage stability, hardness, and weather resistance of coating films. *J. Polym. Sci., Part A: Polym. Chem.* **2013**, *51*, 653-663. DOI: https://doi.org/10.1002/pola.26415.
(223) Sato, Y.; Hayami, R.; Gunji, T. Characterization of NMR, IR, and Raman spectra for siloxanes and silsesquioxanes: a mini review. *J. Sol-Gel Sci. Technol.* **2022**, *104*, 36-52. DOI: https://doi.org/10.1007/s10971-022-05920-y.
(224) Voronkov, M. G.; Lavrent'yev, V. I. Polyhedral Oligosilsesquioxanes and Their Homo Derivatives. *Top. Curr. Chem.* **1982**, *102*, 199-236. DOI: https://doi.org/10.1007/3-540-11345-2_12.
(225) Engelhardt, G.; Jancke, H. Über die ^{1}H-, ^{13}C- und ^{29}Si-NMR chemischen Verschiebungen einiger linearer, verzweigter und cyclischer Methylsiloxan-Verbindungen. *J. Organomet. Chem.* **1971**, *28*, 293-300. DOI: https://doi.org/10.1016/S0022-328X(00)88009-2.
(226) Postma, A.; Davis, T. P.; Donovan, A. R.; Li, G.; Moad, G.; Mulder, R.; O'Shea, M. S. A simple method for determining protic end-groups of synthetic polymers by ^{1}H NMR spectroscopy. *Polymer* **2006**, *47*, 1899-1911. DOI: https://doi.org/10.1016/j.polymer.2006.01.050.
(227) Kolahdouzan, K.; Ogba, O. M.; O'Leary, D. J. ^{1}H NMR Studies of Intramolecular OH/OH Hydrogen Bonds via Titratable Isotope Shifts. *J. Org. Chem.* **2022**, *87*, 1732-1744. DOI: https://doi.org/10.1021/acs.joc.1c01910.
(228) Borovin, E.; Callone, E.; Ribot, F.; Diré, S. Mechanism and Kinetics of Oligosilsesquioxane Growth in the In Situ Water Production Sol–Gel Route: Dependence on Water Availability. *Eur. J. Inorg. Chem.* **2016**, *2016*, 2166-2174. DOI: https://doi.org/10.1002/ejic.201501220.
(229) Kuniyoshi, M.; Takahashi, M.; Tokuda, Y.; Yoko, T. Hydrolysis and polycondensation of acid-catalyzed Phenyltriethoxysilane (PhTES). *J. Sol-Gel Sci. Technol.* **2006**, *39*, 175-183. DOI: https://doi.org/10.1007/s10971-006-7465-0.
(230) Chen, X.; Eldred, D.; Liu, J.; Chiang, H.; Wang, X.; Rickard, M. A.; Tu, S.; Cui, L.; LaBeaume, P.; Skinner, K. Simultaneous In Situ Monitoring of Trimethoxysilane Hydrolysis Reactions Using Raman, Infrared, and Nuclear Magnetic Resonance (NMR) Spectroscopy Aided by Chemometrics and Ab Initio Calculations. *Appl. Spectrosc.* **2018**, *72*, 1404-1415. DOI: https://doi.org/10.1177/0003702818774570.
(231) Steinbrück, N.; Pohl, S.; Kickelbick, G. Platinum free thermally curable siloxanes for optoelectronic application – synthesis and properties. *RSC Adv.* **2019**, *9*, 2205-2216. DOI: https://doi.org/10.1039/C8RA09801H.
(232) Briesenick, M.; Gallei, M.; Kickelbick, G. High-Refractive-Index Polysiloxanes Containing Naphthyl and Phenanthrenyl Groups and Their Thermally Cross-Linked Resins. *Macromolecules* **2022**, *55*, 4675-4691. DOI: https://doi.org/10.1021/acs.macromol.2c00265.
(233) Nam, K.-H.; Lee, T.-H.; Bae, B.-S.; Popall, M. Condensation reaction of 3-(methacryloxypropyl)-trimethoxysilane and diisobutylsilanediol in non-hydrolytic sol-gel process. *J. Sol-Gel Sci. Technol.* **2006**, *39*, 255-260. DOI: https://doi.org/10.1007/s10971-006-7884-y.

(234) Delak, K. M.; Farrar, T. C.; Sahai, N. ^{29}Si NMR sensitivity enhancement methods for the quantitative study of organosilicate hydrolysis and condensation. *J. Non-Cryst. Solids* **2005**, *351*, 2244-2250. DOI: https://doi.org/10.1016/j.jnoncrysol.2005.05.013.
(235) Echeverría, J. C.; Moriones, P.; Arzamendi, G.; Garrido, J. J.; Gil, M. J.; Cornejo, A.; Martínez-Merino, V. Kinetics of the acid-catalyzed hydrolysis of tetraethoxysilane (TEOS) by ^{29}Si NMR spectroscopy and mathematical modeling. *J. Sol-Gel Sci. Technol.* **2018**, *86*, 316-328. DOI: https://doi.org/10.1007/s10971-018-4637-7.
(236) Xu, X.; Wu, C.; Zhang, B.; Dong, H. Preparation, structure characterization, and thermal performance of phenyl-modified MQ silicone resins. *J. Appl. Polym. Sci.* **2013**, *128*, 4189-4200. DOI: https://doi.org/10.1002/app.38638.
(237) Sen, T.; Bruce, I. J. Surface engineering of nanoparticles in suspension for particle based bio-sensing. *Sci. Rep.* **2012**, *2*, 564. DOI: https://doi.org/10.1038/srep00564.
(238) Cabañas, M. V.; Lozano, D.; Torres-Pardo, A.; Sobrino, C.; González-Calbet, J.; Arcos, D.; Vallet-Regí, M. Features of aminopropyl modified mesoporous silica nanoparticles. Implications on the active targeting capability. *Mater. Chem. Phys.* **2018**, *220*, 260-269. DOI: https://doi.org/10.1016/j.matchemphys.2018.09.005.
(239) Shea, K. J.; Loy, D. A.; Webster, O. Arylsilsesquioxane gels and related materials. New hybrids of organic and inorganic networks. *J. Am. Chem. Soc.* **1992**, *114*, 6700-6710. DOI: https://doi.org/10.1021/ja00043a014.
(240) Ren, Z.; Xie, P.; Jiang, S.; Yan, S.; Zhang, R. Study of the supramolecular Architecture-Directed synthesis of a Well-Defined Triple-Chain ladder polyphenylsiloxane. *Macromolecules* **2010**, *43*, 2130-2136. DOI: https://doi.org/10.1021/ma100145j.
(241) Wang, X.; Li, J.; Wu, L. Preparation of poly(phenylsilsesquioxane) (PPSQ) particles with ladder structure and the thermal stability of PP/PPSQ composites. *Polym. Adv. Technol.* **2011**, *22*, 2151-2156. DOI: https://doi.org/10.1002/pat.1737.
(242) Fina, A.; Tabuani, D.; Carniato, F.; Frache, A.; Boccaleri, E.; Camino, G. Polyhedral oligomeric silsesquioxanes (POSS) thermal degradation. *Thermochim. Acta* **2006**, *440*, 36-42. DOI: https://doi.org/10.1016/j.tca.2005.10.006.
(243) Qi, Z.; Zhang, W.; He, X.; Yang, R. High-efficiency flame retardency of epoxy resin composites with perfect T_8 caged phosphorus containing polyhedral oligomeric silsesquioxanes (P-POSSs). *Compos. Sci. Technol.* **2016**, *127*, 8-19. DOI: https://doi.org/10.1016/j.compscitech.2016.02.026.
(244) Majeed, S.; Filiz, V.; Shishatskiy, S.; Wind, J.; Abetz, C.; Abetz, V. Pyrene-POSS nanohybrid as a dispersant for carbon nanotubes in solvents of various polarities: Its synthesis and application in the preparation of a composite membrane. *Nanoscale Res. Lett.* **2012**, *7*, 1-11. DOI: https://doi.org/10.1186/1556-276X-7-296.
(245) Petrova, I. M.; Buryak, A. K.; Peregudov, A. S.; Strelkova, T. V.; Kononova, E. G.; Bushmarinov, I. S.; Makarova, N. N. Effect of stereoisomerism of (tetrahydroxy)(tetraphenyl)cyclotetrasiloxanes on the siloxane framework in polyphenylsilsesquioxanes obtained by polycondensation in the presence of layered-architecture compounds. *Mendeleev Commun.* **2015**, *25*, 229-231. DOI: https://doi.org/10.1016/j.mencom.2015.05.025.
(246) Abe, Y.; Gunji, T. Oligo- and polysiloxanes. *Prog. Polym. Sci.* **2004**, *29*, 149-182. DOI: https://doi.org/10.1016/j.progpolymsci.2003.08.003.
(247) Grill, A.; Neumayer, D. A. Structure of low dielectric constant to extreme low dielectric constant SiCOH films: Fourier transform infrared spectroscopy characterization. *J. Appl. Phys.* **2003**, *94*, 6697-6707. DOI: https://doi.org/10.1063/1.1618358.
(248) Unno, M.; Alias, S. B.; Saito, H.; Matsumoto, H. Synthesis of Hexasilsesquioxanes Bearing Bulky Substituents: Hexakis((1,1,2-trimethylpropyl)silsesquioxane) and Hexakis(tert-

butylsilsesquioxane). *Organometallics* **1996**, *15*, 2413-2414. DOI: https://doi.org/10.1021/om950737a.
(249) Weinhold, F.; West, R. Hyperconjugative Interactions in Permethylated Siloxanes and Ethers: The Nature of the SiO Bond. *J. Am. Chem. Soc.* **2013**, *135*, 5762-5767. DOI: https://doi.org/10.1021/ja312222k.
(250) Lin-Vien, D.; Colthup, N. B.; Fateley, W. G.; Grasselli, J. G. CHAPTER 15 - Organosilicon Compounds. In *The handbook of infrared and Raman characteristic frequencies of organic molecules*, Elsevier Inc.: San Diego, CA, USA, 1991; pp 251-261. DOI: https://doi.org/10.1016/B978-0-08-057116-4.50021-3.
(251) Launer, P.; Arkles, B. Infrared Analysis of Organosilicon Compounds. In *Silicon Compounds: Silanes & Silicones*, 3rd ed.; Launer, P., Arkles, B. Eds.; Gelest Inc.: Morrisville, PA, USA 2013; pp 175-178.
(252) Jiang, H.; Zheng, Z.; Wang, X. Kinetic study of methyltriethoxysilane (MTES) hydrolysis by FTIR spectroscopy under different temperatures and solvents. *Vib. Spectrosc.* **2008**, *46*, 1-7. DOI: https://doi.org/10.1016/j.vibspec.2007.07.002.
(253) Hu, N.; Rao, Y.; Sun, S.; Hou, L.; Wu, P.; Fan, S.; Ye, B. Structural Evolution of Silica Gel and Silsesquioxane Using Thermal Curing. *Appl. Spectrosc.* **2016**, *70*, 1328-1338. DOI: https://doi.org/10.1177/0003702816654063.
(254) Nowacka, M.; Fischer, C.; Kowalewska, A.; Hebda, M.; Hodor, K. Thermally induced phenomena leading to degradation of poly(silsesquioxane) materials. *Eur. Polym. J.* **2017**, *86*, 17-28. DOI: https://doi.org/10.1016/j.eurpolymj.2016.11.015.
(255) Zhou, W.; Yang, H.; Guo, X.; Lu, J. Thermal degradation behaviors of some branched and linear polysiloxanes. *Polym. Degrad. Stab.* **2006**, *91*, 1471-1475. DOI: https://doi.org/10.1016/j.polymdegradstab.2005.10.005.
(256) Snyder, R. G.; Hsu, S. L.; Krimm, S. Vibrational spectra in the C-H stretching region and the structure of the polymethylene chain. *Spectrochim. Acta A Mol. Biomol. Spectrosc.* **1978**, *34*, 395-406. DOI: https://doi.org/10.1016/0584-8539(78)80167-6.
(257) Chemtob, A.; Ni, L.; Croutxé-Barghorn, C.; Demarest, A.; Brendlé, J.; Vidal, L.; Rigolet, S. Self-Organized Poly(n-octadecylsilsesquioxane) Films via Sol–Gel Photopolymerization. *Langmuir* **2011**, *27*, 12621-12629. DOI: https://doi.org/10.1021/la202253v.
(258) Smith, E.; Dent, G. *Modern Raman spectroscopy: a practical approach*; John Wiley & Sons Ltd: Chichester, UK, 2005.
(259) Pakjamsai, C.; Kobayashi, N.; Koyano, M.; Sasaki, S.; Kawakami, Y. Characterization of the Benzene-Insoluble Fraction of the Hydrolyzate of Phenyltrimethoxysilanes in the Presence of Benzyltrimethylammonium Hydroxide. *J. Polym. Sci., Part A: Polym. Chem.* **2004**, *42*, 4587-4597. DOI: https://doi.org/10.1002/pola.20381.
(260) Marcolli, C.; Calzaferri, G. Monosubstituted Octasilsesquioxanes. *Appl. Organometal. Chem.* **1999**, *13*, 213-226. DOI: https://doi.org/10.1002/(SICI)1099-0739(199904)13:4<213::AID-AOC841>3.0.CO;2-G.
(261) Tomioka, Y.; Yasui, T.; Naka, K.; Imoto, H. Polymethylene with cage silsesquioxane: densely grafted structure prevents side-chain crystallization. *Polym. Chem.* **2025**, *16*, 1155-1161. DOI: https://doi.org/10.1039/D4PY01222D.
(262) Lana, S. L. B.; Seddon, A. B. X-Ray Diffraction Studies of Sol-Gel Derived ORMOSILs Based on Combinations of Tetramethoxysilane and Trimethoxysilane. *J. Sol-Gel Sci. Technol.* **1998**, *13*, 461-466. DOI: https://doi.org/10.1023/A:1008685614559.
(263) Biswas, R. K.; Khan, P.; Mukherjee, S.; Mukhopadhyay, A. K.; Ghosh, J.; Muraleedharan, K. Study of short range structure of amorphous Silica from PDF using Ag radiation in laboratory XRD system, RAMAN and NEXAFS. *J. Non-Cryst. Solids* **2018**, *488*, 1-9. DOI: https://doi.org/10.1016/j.jnoncrysol.2018.02.037.

(264) Chodkowska, E. M.; Rayss, J. X-ray diffraction as a tool of ORMOSIL gels' structure's investigation. In Photonics Applications in Astronomy, Communications, Industry, and High-Energy Physics Experiments 2007; Proc. SPIE 6937; SPIE: Bellingham, WA, 2007; 69371P. DOI: https://doi.org/10.1117/12.784699.
(265) Rios, X.; Moriones, P.; Echeverría, J. C.; Luquin, A.; Laguna, M.; Garrido, J. J. Ethyl group as matrix modifier and inducer of ordered domains in hybrid xerogels synthesised in acidic media using ethyltriethoxysilane (ETEOS) and tetraethoxysilane (TEOS) as precursors. *Mater. Chem. Phys.* **2013**, *141*, 166-174. DOI: https://doi.org/10.1016/j.matchemphys.2013.04.042.
(266) Andrianov, K. A.; Zhdanov, A. A.; Levin, V. Y. Some Physical Properties of Organosilicon Ladder Polymers. *Annu. Rev. Mater. Res.* **1978**, *8*, 313-326. DOI: https://doi.org/10.1146/annurev.ms.08.080178.001525.
(267) Takahashi, T.; Kaschta, J.; Münstedt, H. Melt rheology and structure of silicone resins. *Rheol. Acta* **2001**, *40*, 490-498. DOI: https://doi.org/10.1007/s003970100173.
(268) Xinsheng, Z.; Lianghe, S.; Chaoran, H. More on the Structures of Polyphenylsilsesquioxanes. *Chin. J. Polym. Sci.* **1987**, *5*, 353-358.
(269) Xavier Perrin, F.; Viet Nguyen, T. B.; Margaillan, A. Linear and branched alkyl substituted octakis(dimethylsiloxy)octasilsesquioxanes: WAXS and thermal properties. *Eur. Polym. J.* **2011**, *47*, 1370-1382. DOI: https://doi.org/10.1016/j.eurpolymj.2011.04.004.
(270) Shimojima, A. Design of nanohybrid and nanoporous materials through self-assembly of organosilane molecules. *J. Ceram. Soc. Jpn.* **2008**, *116*, 278-283. DOI: https://doi.org/10.2109/jcersj2.116.278.
(271) Waddon, A. J.; Coughlin, E. B. Crystal Structure of Polyhedral Oligomeric Silsequioxane (POSS) Nano-materials: A Study by X-ray Diffraction and Electron Microscopy. *Chem. Mater.* **2003**, *15*, 4555-4561. DOI: https://doi.org/10.1021/cm034308b.
(272) Mya, K. Y.; He, C.; Huang, J.; Xiao, Y.; Dai, J.; Siow, Y.-P. Preparation and thermomechanical properties of epoxy resins modified by octafunctional cubic silsesquioxane epoxides. *J. Polym. Sci., Part A: Polym. Chem.* **2004**, *42*, 3490-3503. DOI: https://doi.org/10.1002/pola.20168.
(273) Sheen, Y. C.; Lu, C. H.; Huang, C. F.; Kuo, S. W.; Chang, F. C. Synthesis and characterization of amorphous octakis-functionalized polyhedral oligomeric silsesquioxanes for polymer nanocomposites. *Polymer* **2008**, *49*, 4017-4024. DOI: https://doi.org/10.1016/j.polymer.2008.06.055.
(274) Hongo, Y.; Kaneko, Y. Thermally stable soluble polymers prepared via the tris(pentafluorophenyl)borane-catalyzed polymerization of hydrosilyl-functionalized cage octasiloxane. *Polym. J.* **2025**, *57*, 975–984. DOI: https://doi.org/10.1038/s41428-025-01059-z.
(275) Gao, X.; Liu, H.; Wei, H.; Zheng, J.; Huang, G. Effect of incompletely condensed tri-silanol-phenyl-POSS on the thermal stability of silicone rubber. *Polym. Bull.* **2019**, *76*, 2835-2850. DOI: https://doi.org/10.1007/s00289-018-2499-3.
(276) Shi, Y.; Gao, X.; Zhang, D.; Liu, Y.; Huang, G. Synthesis and thermal properties of modified room temperature vulcanized (RTV) silicone rubber using polyhedral oligomeric silsesquioxane (POSS) as a cross linking agent. *RSC Adv.* **2014**, *4*, 41453-41460. DOI: https://doi.org/10.1039/C4RA06706A.
(277) Ramli, M. R.; Othman, M. B. H.; Arifin, A.; Ahmad, Z. Cross-link network of polydimethylsiloxane via addition and condensation (RTV) mechanisms. Part I: Synthesis and thermal properties. *Polym. Degrad. Stab.* **2011**, *96*, 2064-2070. DOI: https://doi.org/10.1016/j.polymdegradstab.2011.10.001.
(278) Shimojima, A.; Sugahara, Y.; Kuroda, K. Inorganic-Organic Layered Materials Derived via the Hydrolysis and Polycondensation of Trialkoxy(alkyl)silanes. *Bull. Chem. Soc. Jpn.* **1997**, *70*, 2847-2853. DOI: https://doi.org/10.1246/bcsj.70.2847.

(279) Ni, L.; Chemtob, A.; Croutxé-Barghorn, C.; Brendlé, J.; Vidal, L.; Rigolet, S. Photoinduced synthesis and ordering of lamellar n-alkylsiloxane films. *J. Mater. Chem.* **2012**, *22*, 643-652. DOI: https://doi.org/10.1039/C1JM13053F.
(280) Matějka, L.; Dukh, O.; Hlavatá, D.; Meissner, B.; Brus, J. Cyclization and Self-Organization in Polymerization of Trialkoxysilanes. *Macromolecules* **2001**, *34*, 6904-6914. DOI: https://doi.org/10.1021/ma010136x.
(281) Turetskii, A.; Out, G. J. J.; Klok, H.-A.; Möller, M. Structural transformations in poly(di-n-alkylsiloxane)s with alkyl side groups containing 7 to 10 carbon atoms. *Polymer* **1995**, *36*, 1303-1308. DOI: https://doi.org/10.1016/0032-3861(95)93934-E.
(282) Jitianu, A.; Britchi, A.; Badescu, V.; Deleanu, C.; Zaharescu, M. Influence of the alkoxy group of the Si-alkoxides on the sol-gel process and on the structure of the obtained gels. *Rev. Roum. Chim.* **2007**, *52*, 93-99.
(283) Trathnigg, B. Size-Exclusion Chromatography of Polymers. In *Encyclopedia of Analytical Chemistry*, Meyers, R. A., Provder, T. Eds.; John Wiley & Sons Ldt.: Chichester, UK, 2006; pp 1-26. DOI: https://doi.org/10.1002/9780470027318.a2032.
(284) Bassindale, A. R.; Gentle, T. E. Siloxane and hydrocarbon octopus molecules with silsesquioxane cores. *J. Mater. Chem.* **1993**, *3*, 1319-1325. DOI: https://doi.org/10.1039/JM9930301319.
(285) Falkenhagen, J.; Jancke, H.; Krüger, R.-P.; Rikowski, E.; Schulz, G. Characterization of silsesquioxanes by size-exclusion chromatography and matrix-assisted laser desorption/ionization time-of-flight mass spectrometry. *Rapid Commun. Mass Spectrom.* **2003**, *17*, 285-290. DOI: https://doi.org/10.1002/rcm.911.
(286) Bürgy, H.; Calzaferri, G. Separation of the oligomeric silsesquioxanes $(HSiO_{3/2})_{8–18}$ by size-exclusion chromatography. *J. Chromatogr. A* **1990**, *507*, 481-486. DOI: https://doi.org/10.1016/S0021-9673(01)84227-8.
(287) Anokhina, T. S.; Ershova, T. O.; Anisimov, A. A.; Temnikov, M. N.; Grushevenko, E. A.; Borisov, I. L.; Volkov, A. V.; Muzafarov, A. M. Pervaporation and Gas Separation Properties of High-Molecular Ladder-like Polyphenylsilsesquioxanes. *Polymers* **2023**, *15*, 3277. DOI: https://doi.org/10.3390/polym15153277.
(288) Kessler, D.; Löwe, H.; Theato, P. Synthesis of Defined Poly(silsesquioxane)s: Fast Polycondensation of Trialkoxysilanes in a Continuous-Flow Microreactor. *Macromol. Chem. Phys.* **2009**, *210*, 807-813. DOI: https://doi.org/10.1002/macp.200800611.
(289) Sun, A. B.; Li, S.; Kou, X. Applications of MALDI-TOF-MS in structural characterization of synthetic polymers. *Anal. Methods* **2023**, *15*, 868-883. DOI: https://doi.org/10.1039/D2AY01583H.
(290) Wallace, W. E.; Guttman, C. M.; Antonucci, J. M. Polymeric silsesquioxanes: degree-of-intramolecular-condensation measured by mass spectrometry. *Polymer* **2000**, *41*, 2219-2226. DOI: https://doi.org/10.1016/S0032-3861(99)00386-9.
(291) Li, L.; Whittal, R. M. TIME-OF-FLIGHT MASS SPECTROMETRY FOR POLYMER CHARACTERIZATION. In *MALDI Mass Spectrometry for Synthetic Polymer Analysis*, Li, L. Ed.; John Wiley & Sons, Inc.: Hoboken, NJ, USA, 2010; pp 27-52.
(292) Jaumann, M.; Rebrov, E. A.; Kazakova, V. V.; Muzafarov, A. M.; Goedel, W. A.; Möller, M. Hyperbranched Polyalkoxysiloxanes via AB3-Type Monomers. *Macromol. Chem. Phys.* **2003**, *204*, 1014-1026. DOI: https://doi.org/10.1002/macp.200390067.
(293) Fasce, D. P.; Williams, R. J. J.; Erra-Balsells, R.; Ishikawa, Y.; Nonami, H. One-Step Synthesis of Polyhedral Silsesquioxanes Bearing Bulky Substituents: UV-MALDI-TOF and ESI-TOF Mass Spectrometry Characterization of Reaction Products. *Macromolecules* **2001**, *34*, 3534-3539. DOI: https://doi.org/10.1021/ma001711k.
(294) Eisenberg, P.; Erra-Balsells, R.; Ishikawa, Y.; Lucas, J. C.; Mauri, A. N.; Nonami, H.; Riccardi, C. C.; Williams, R. J. J. Cagelike Precursors of High-Molar-Mass Silsesquioxanes

Formed by the Hydrolytic Condensation of Trialkoxysilanes. *Macromolecules* **2000**, *33*, 1940-1947. DOI: https://doi.org/10.1021/ma9912507.
(295) Wallace, W. E.; Guttman, C. M.; Antonucci, J. M. Molecular structure of silsesquioxanes determined by matrix-assisted laser desorption/ionization time-of-flight mass spectrometry. *J. Am. Soc. Mass Spectrom.* **1999**, *10*, 224-230. DOI: https://doi.org/10.1016/S1044-0305(98)00147-0.
(296) Lee, A. S.; Choi, S.-S.; Lee, H. S.; Baek, K.-Y.; Hwang, S. S. A new, higher yielding synthetic route towards dodecaphenyl cage silsesquioxanes: synthesis and mechanistic insights. *Dalton Trans.* **2012**, *41*, 10585-10588. DOI: https://doi.org/10.1039/C2DT30659J.
(297) Matsumoto, T.; Kaneko, Y. Correlation between molecular structures and reaction conditions (temperature–pressure–time) in the preparation of secondary, tertiary, and quaternary ammonium-functionalized polyhedral oligomeric silsesquioxanes. *J. Sol-Gel Sci. Technol.* **2020**, *95*, 670-681. DOI: https://doi.org/10.1007/s10971-020-05343-7.
(298) Tokunaga, T.; Shoiriki, M.; Mizumo, T.; Kaneko, Y. Preparation of low-crystalline POSS containing two types of alkylammonium groups and its optically transparent film. *J. Mater. Chem. C* **2014**, *2*, 2496-2501. DOI: https://doi.org/10.1039/C3TC32292K.
(299) Zhou, D.-L.; Li, J.-H.; Guo, Q.-Y.; Lin, X.; Zhang, Q.; Chen, F.; Han, D.; Fu, Q. Polyhedral Oligomeric Silsesquioxanes Based Ultralow-k Materials: The Effect of Cage Size. *Adv. Funct. Mater.* **2021**, *31*, 2102074. DOI: https://doi.org/10.1002/adfm.202102074.
(300) Stutz, H.; Illers, K.-H.; Mertes, J. A generalized theory for the glass transition temperature of crosslinked and uncrosslinked polymers. *J. Polym. Sci., Part B: Polym. Phys.* **1990**, *28*, 1483-1498. DOI: https://doi.org/10.1002/polb.1990.090280906.
(301) Takahashi, K.; Tadanaga, K.; Matsuda, A.; Hayashi, A.; Tatsumisago, M. Effects of Phenyltriethoxysilane Concentration in Starting Solutions on Thermal Properties of Polyphenylsilsesquioxane Particles Prepared by a Two-Step Acid-Base Catalyzed Sol-Gel Process. *J. Ceram. Soc. Jpn.* **2007**, *115*, 131-135. DOI: https://doi.org/10.2109/jcersj.115.131.
(302) Borova, S.; Tokarev, V.; Stahlhut, P.; Luxenhofer, R. Crosslinking of hydrophilic polymers using polyperoxides. *Colloid. Polym. Sci.* **2020**, *298*, 1699-1713. DOI: https://doi.org/10.1007/s00396-020-04738-w.
(303) Deng, K.; Zhang, T.; Zhang, X.; Zhang, A.; Xie, P.; Zhang, R. A Concerted H-Bonding Self-Assembly-Based Approach to Ladder Poly(silsesquioxane). *Macromol. Chem. Phys.* **2006**, *207*, 404-411. DOI: https://doi.org/10.1002/macp.200500446.
(304) Yu-zhong, F.; Sheng-li, Q.; Jing-jing, L.; Zhan-peng, W.; Xiao-ping, Y.; Ri-guang, J.; De-zhen, W. Preparation and Characterization of Ordered Ladder Like Polyphenylsilsesquioxane via Two-step Sol-gel Method. *Chem. Res. Chin. Univ.* **2011**, *27*, 516-519.
(305) van der Sman, R. G. M. Predictions of Glass Transition Temperature for Hydrogen Bonding Biomaterials. *J. Phys. Chem. B* **2013**, *117*, 16303-16313. DOI: https://doi.org/10.1021/jp408184u.
(306) Allcock, H. R.; Connolly, M. S.; Sisko, J. T.; Al-Shali, S. Effects of organic side group structures on the properties of poly(organophosphazenes). *Macromolecules* **1988**, *21*, 323-334. DOI: https://doi.org/10.1021/ma00180a008.
(307) Takahashi, K.; Tadanaga, K.; Hayashi, A.; Tatsumisago, M. Substituent effects on the glass transition phenomena of polyorganosilsesquioxane particles prepared by two-step acid–base catalyzed sol–gel process. *J. Ceram. Soc. Jpn.* **2011**, *119*, 173-179. DOI: https://doi.org/10.2109/jcersj2.119.173.
(308) Fujii, K.; Fujita, T.; Iyi, N.; Kodama, H.; Kitamura, K.; Yamagishi, A. Synthesis of 2-dimensional inorganic/organic hybrid polymers: Novel meltable layered alkylsiloxanes. *J. Mater. Sci. Lett.* **2003**, *22*, 1459-1461. DOI: https://doi.org/10.1023/A:1025779918534.

(309) Poliskie, G. M.; Haddad, T. S.; Blanski, R. L.; Gleason, K. K. Characterization of the phase transitions of ethyl substituted polyhedral oligomeric silsesquioxane. *Thermochim. Acta* **2005**, *438*, 116-125. DOI: https://doi.org/10.1016/j.tca.2005.08.028.
(310) Kopesky, E. T.; Haddad, T. S.; Cohen, R. E.; McKinley, G. H. Thermomechanical Properties of Poly(methyl methacrylate)s Containing Tethered and Untethered Polyhedral Oligomeric Silsesquioxanes. *Macromolecules* **2004**, *37*, 8992-9004. DOI: https://doi.org/10.1021/ma048934l.
(311) Heeley, E. L.; Hughes, D. J.; El Aziz, Y.; Taylor, P. G.; Bassindale, A. R. Linear Long Alkyl Chain Substituted POSS Cages: The Effect of Alkyl Chain Length on the Self-Assembled Packing Morphology. *Macromolecules* **2013**, *46*, 4944-4954. DOI: https://doi.org/10.1021/ma400635e.
(312) Chimjarn, S.; Kunthom, R.; Chancharone, P.; Sodkhomkhum, R.; Sangtrirutnugul, P.; Ervithayasuporn, V. Synthesis of aromatic functionalized cage-rearranged silsesquioxanes (T_8, T_{10}, and T_{12}) via nucleophilic substitution reactions. *Dalton Trans.* **2015**, *44*, 916-919. DOI: https://doi.org/10.1039/C4DT02941K.
(313) Gültek, A.; Seckin, T.; ADIGÜZEL, H. İ. Design and characterization of amino and chloro functionalized rhombohedral silsesquioxanes. *Turk. J. Chem.* **2005**, *29*, 391-399.
(314) Jovanovic, J. D.; Govedarica, M. N.; Dvornic, P. R.; Popovic, I. G. The thermogravimetric analysis of some polysiloxanes. *Polym. Degrad. Stab.* **1998**, *61*, 87-93. DOI: https://doi.org/10.1016/S0141-3910(97)00135-3.
(315) Zielecka, M.; Rabajczyk, A.; Pastuszka, Ł.; Jurecki, L. Flame Resistant Silicone-Containing Coating Materials. *Coatings* **2020**, *10*, 479. DOI: https://doi.org/10.3390/coatings10050479.
(316) Camino, G.; Lomakin, S. M.; Lageard, M. Thermal polydimethylsiloxane degradation. Part 2. The degradation mechanisms. *Polymer* **2002**, *43*, 2011-2015. DOI: https://doi.org/10.1016/S0032-3861(01)00785-6.
(317) Bolln, C.; Tsuchida, A.; Frey, H.; Mülhaupt, R. Thermal Properties of the Homologous Series of 8-fold Alkyl-Substituted Octasilsesquioxanes. *Chem. Mater.* **1997**, *9*, 1475-1479. DOI: https://doi.org/10.1021/cm970090f.
(318) Mantz, R. A.; Jones, P. F.; Chaffee, K. P.; Lichtenhan, J. D.; Gilman, J. W.; Ismail, I. M. K.; Burmeister, M. J. Thermolysis of Polyhedral Oligomeric Silsesquioxane (POSS) Macromers and POSS−Siloxane Copolymers. *Chem. Mater.* **1996**, *8*, 1250-1259. DOI: https://doi.org/10.1021/cm950536x.
(319) Mutin, P. H. Role of redistribution reactions in the polymer route to silicon–carbon–oxygen ceramics. *J. Am. Ceram. Soc.* **2002**, *85*, 1185-1189. DOI: https://doi.org/10.1111/j.1151-2916.2002.tb00243.x.
(320) Xiao, S.; Cui, X.; Iroh, J. O. A Study of the Degradation Mechanism of Ladder-like Polyhedral Oligomeric Silsesquioxane via Fourier Transform Infrared Spectroscopy. *Fire* **2023**, *6*, 429. DOI: https://doi.org/10.3390/fire6110429.
(321) Endo, H.; Takeda, N.; Unno, M. Synthesis and Properties of Phenylsilsesquioxanes with Ladder and Double-Decker Structures. *Organometallics* **2014**, *33*, 4148-4151. DOI: https://doi.org/10.1021/om500010y.
(322) Kowalewska, A.; Nowacka, M.; Makowski, T. Macroporous materials by self-assembly of linear oligo(phenylsilsesquioxanes). *Express Polym. Lett.* **2015**, *9*, 984-1000. DOI: https://doi.org/10.3144/expresspolymlett.2015.89.
(323) Zhang, D.; Yang, R.; Qin, Z.; Zhang, W. Study on the thermal behaviors of polyhedral oligomeric octaphenylsilsesquioxane (OPS). *J. Therm. Anal. Calorim.* **2023**, *148*, 2345-2355. DOI: https://doi.org/10.1007/s10973-022-11887-3.

(324) Liu, T.; Sun, C.; Ma, F. Study on the synthesis and thermal degradation of vinylphenylpolysilsesquioxane. *J. Anal. Appl. Pyrolysis* **2018**, *130*, 249-255. DOI: https://doi.org/10.1016/j.jaap.2017.12.024.
(325) Förster, T. Formation and dissociation of excited dimers. *Pure Appl. Chem.* **1963**, *7*, 73-78. DOI: https://doi.org/10.1351/pac196307010073.
(326) Förster, T.; Kasper, K. Ein Konzentrationsumschlag der Fluoreszenz des Pyrens. *Z. Elektrochem. Ber. Bunsenges. Phys. Chem.* **1955**, *59*, 976-980. DOI: https://doi.org/10.1002/bbpc.19550591018.
(327) Stevens, B.; Hutton, E. Radiative Life-time of the Pyrene Dimer and the Possible Role of Excited Dimers in Energy Transfer Processes. *Nature* **1960**, *186*, 1045-1046. DOI: https://doi.org/10.1038/1861045b0.
(328) Birks, J. B.; Christophorou, L. G.; Flowers, B. H. 'Excime' fluorescence. IV. Solution spectra of polycyclic hydrocarbons. *Proc. R. Soc. London, Ser. A* **1964**, *277*, 571-582. DOI: https://doi.org/10.1098/rspa.1964.0041.
(329) Jr., M. T. V.; Haebig, J.; Rice, S. A. Experimental Study of Luminescence and Excitation Trapping in Vinyl Polymers, Paracyclophanes, and Related Compounds. *J. Chem. Phys.* **1965**, *43*, 886-897. DOI: https://doi.org/10.1063/1.1696866.
(330) Salom, C.; Horta, A.; Hernandez-Fuentes, I.; Pierola, I. F. Poly(phenylsiloxanes) electronic spectra. *Macromolecules* **1987**, *20*, 696-698. DOI: https://doi.org/10.1021/ma00169a041.
(331) Liu, C.; Liu, Y.; Shen, Z.; Xie, P.; Zhang, R.; Yang, J.; Bai, F. Study of the Steric Tacticity of Novel Soluble Ladderlike Poly(phenylsilsesquioxane) Prepared by Stepwise Coupling Polymerization. *Macromol. Chem. Phys.* **2001**, *202*, 1581-1585. DOI: https://doi.org/10.1002/1521-3935(20010601)202:9<1581::AID-MACP1581>3.0.CO;2-5.
(332) Yanari, S. S.; Bovey, F. A.; Lumry, R. Fluorescence of Styrene Homopolymers and Copolymers. *Nature* **2000**, *200*, 242-244. DOI: https://doi.org/10.1038/200242a0.
(333) Kuo, A. Fluorescence Resulting from π-stacking in Polystyrene Solutions. *CheM* **2011**, *1*, 80-86. DOI: https://doi.org/10.5618/chem.2011.v1.n1.9.
(334) Nishihara, T.; Kaneko, M. The dependence of excimer formation of polystyrene solutions on solvent and concentration. *Makromol. Chem.* **1969**, *124*, 84-90. DOI: https://doi.org/10.1002/macp.1969.021240109.
(335) Hirayama, F. Intramolecular excimer formation. I. Diphenyl and triphenyl alkanes. *J. Chem. Phys.* **1965**, *42*, 3163-3171. DOI: https://doi.org/10.1063/1.1696395.
(336) Torkelson, J. M.; Tirrell, M.; Lipsky, S.; Tirrell, D. A. Fluorescence and Absorbance of Polystyrene in Dilute and Semidilute Solutions. *Macromolecules* **1983**, *16*, 326-330. DOI: https://doi.org/10.1021/ma00236a031.
(337) Nowacka, M.; Kowalewska, A.; Plażuk, D.; Makowski, T. Hybrid polysilsesquioxanes for fluorescence resonance energy transfer. *Dyes Pigm.* **2019**, *170*. DOI: https://doi.org/10.1016/j.dyepig.2019.107622.
(338) Chaoran, H.; Guangzhi, X.; Xinsheng, Z.; Lianghe, S. Studies on the Excimer Fluorescence and the Steric Tacticity of Polyphenylsilsesquioxanes. *Chin. J. Polym. Sci.* **1987**, *5*, 347-352.
(339) Okumoto, S.; Fujita, N.; Yamabe, S. Theoretical Study of Hydrolysis and Condensation of Silicon Alkoxides. *J. Phys. Chem. A* **1998**, *102*, 3991-3998. DOI: https://doi.org/10.1021/jp980705b.
(340) Kakiuchida, H.; Takahashi, M.; Tokuda, Y.; Masai, H.; Kuniyoshi, M.; Yoko, T. Viscoelastic and structural properties of a phenyl-modified polysiloxane system with a three-dimensional structure. *J. Phys. Chem. B* **2006**, *110*, 7321-7327. DOI: https://doi.org/10.1021/jp0573543.

(341) Abel, M.-L.; Joannic, R.; Fayos, M.; Lafontaine, E.; Shaw, S. J.; Watts, J. F. Effect of solvent nature on the interaction of γ-glycidoxy propyl trimethoxy silane on oxidised aluminium surface: A study by solution chemistry and surface analysis. *Int. J. Adhes. Adhes.* **2006**, *26*, 16-27. DOI: https://doi.org/10.1016/j.ijadhadh.2002.10.001.
(342) Moreau, J. J. E.; Vellutini, L.; Chi, W.; Bied, C. Lamellar Bridged Silsesquioxanes : Self-Assembly through a Combination of Hydrogen Bonding and Hydrophobic Interactions. *Chem. Eur. J.* **2005**, *11*, 1527-1537. DOI: https://doi.org/10.1002/chem.200401012.
(343) Bogush, G. H.; Zukoski, C. F. Studies of the kinetics of the precipitation of uniform silica particles through the hydrolysis and condensation of silicon alkoxides. *J. Colloid Interface Sci.* **1991**, *142*, 1-18. DOI: https://doi.org/10.1016/0021-9797(91)90029-8.
(344) Takeda, Y.; Komori, Y.; Yoshitake, H. Direct stöber synthesis of monodisperse silica particles functionalized with mercapto-, vinyl- and aminopropylsilanes in alcohol–water mixed solvents. *Colloids Surf. A: Physicochem. Eng. Asp.* **2013**, *422*, 68-74. DOI: https://doi.org/10.1016/j.colsurfa.2013.01.024.
(345) Rahman, I. A.; Padavettan, V. Synthesis of Silica Nanoparticles by Sol-Gel: Size-Dependent Properties, Surface Modification, and Applications in Silica-Polymer Nanocomposites—A Review. *J. Nanomater.* **2012**, *2012*, 132424. DOI: https://doi.org/10.1155/2012/132424.
(346) Bikiaris, D. N.; Papageorgiou, G. Z.; Pavlidou, E.; Vouroutzis, N.; Palatzoglou, P.; Karayannidis, G. P. Preparation by melt mixing and characterization of isotactic polypropylene/SiO_2 nanocomposites containing untreated and surface-treated nanoparticles. *J. Appl. Polym. Sci.* **2006**, *100*, 2684-2696. DOI: https://doi.org/10.1002/app.22849.
(347) Tadano, T.; Zhu, R.; Suzuki, S.; Hoshi, T.; Sasaki, D.; Hagiwara, T.; Sawaguchi, T. Thermal degradation of transparent poly(methyl methacrylate)/silica nanoparticle hybrid films. *Polym. Degrad. Stab.* **2014**, *109*, 7-12. DOI: https://doi.org/10.1016/j.polymdegradstab.2014.06.009.
(348) Kang, S.; Hong, S. I.; Choe, C. R.; Park, M.; Rim, S.; Kim, J. Preparation and characterization of epoxy composites filled with functionalized nanosilica particles obtained via sol–gel process. *Polymer* **2001**, *42*, 879-887. DOI: https://doi.org/10.1016/S0032-3861(00)00392-X.
(349) Shin, Y.; Lee, D.; Lee, K.; Ahn, K. H.; Kim, B. Surface properties of silica nanoparticles modified with polymers for polymer nanocomposite applications. *J. Ind. Eng. Chem.* **2008**, *14*, 515-519. DOI: https://doi.org/10.1016/j.jiec.2008.02.002.
(350) Mahtabani, A.; Rytöluoto, I.; Anyszka, R.; He, X.; Saarimäki, E.; Lahti, K.; Paajanen, M.; Dierkes, W.; Blume, A. On the Silica Surface Modification and Its Effect on Charge Trapping and Transport in PP-Based Dielectric Nanocomposites. *ACS Appl. Polym. Mater.* **2020**, *2*, 3148-3160. DOI: https://doi.org/10.1021/acsapm.0c00349.
(351) van Blaaderen, A.; Vrij, A. Synthesis and Characterization of Monodisperse Colloidal Organo-silica Spheres. *J. Colloid Interface Sci.* **1993**, *156*, 1-18. DOI: https://doi.org/10.1006/jcis.1993.1073.
(352) Dirè, S.; Tagliazucca, V.; Callone, E.; Quaranta, A. Effect of functional groups on condensation and properties of sol-gel silica nanoparticles prepared by direct synthesis from organoalkoxysilanes. *Mater. Chem. Phys.* **2011**, *126*, 909-917. DOI: https://doi.org/10.1016/j.matchemphys.2010.12.015.
(353) Arkhireeva, A.; Hay, J. N.; Oware, W. A versatile route to silsesquioxane nanoparticles from organically modified silane precursors. *J. Non-Cryst. Solids* **2005**, *351*, 1688-1695. DOI: https://doi.org/10.1016/j.jnoncrysol.2005.04.063.
(354) Sankaraiah, S.; Lee, J. M.; Kim, J. H.; Choi, S. W. Preparation and Characterization of Surface-Functionalized Polysilsesquioxane Hard Spheres in Aqueous Medium. *Macromolecules* **2008**, *41*, 6195-6204. DOI: https://doi.org/10.1021/ma8003345.

(355) Choi, J. Y.; Kim, C. H.; Kim, D. K. Formation and Characterization of Monodisperse, Spherical Organo-Silica Powders from Organo-Alkoxysilane-Water System. *J. Am. Ceram. Soc.* **1998**, *81*, 1184-1188. DOI: https://doi.org/10.1111/j.1151-2916.1998.tb02466.x.
(356) Miller, C. R.; Vogel, R.; Surawski, P. P. T.; Jack, K. S.; Corrie, S. R.; Trau, M. Functionalized Organosilica Microspheres via a Novel Emulsion-Based Route. *Langmuir* **2005**, *21*, 9733-9740. DOI: https://doi.org/10.1021/la0514112.
(357) Odenwald, C.; Kickelbick, G. Additive-free continuous synthesis of silica and ORMOSIL micro- and nanoparticles applying a microjet reactor. *J. Sol-Gel Sci. Technol.* **2019**, *89*, 343-353. DOI: https://doi.org/10.1007/s10971-018-4626-x.
(358) Matsuda, A.; Sasaki, T.; Hasegawa, K.; Tatsumisago, M.; Minami, T. Thermal Softening Behavior of Poly(phenylsilsesquioxane) and Poly (benzylsilsesquioxane) Particles. *J. Ceram. Soc. Jpn.* **2000**, *108*, 830-835. DOI: https://doi.org/10.2109/jcersj.108.1261_830.
(359) Takahashi, K.; Tadanaga, K.; Matsuda, A.; Hayashi, A.; Tatsumisago, M. Thermoplastic and thermosetting properties of polyphenylsilsesquioxane particles prepared by two-step acid-base catalyzed sol-gel process. *J. Sol-Gel Sci. Technol.* **2007**, *41*, 217-222. DOI: https://doi.org/10.1007/s10971-006-1501-y.
(360) Dong, F.; Guo, W.; Park, S.-S.; Ha, C.-S. Uniform and monodisperse polysilsesquioxane hollow spheres: synthesis from aqueous solution and use in pollutant removal. *J. Mater. Chem.* **2011**, *21*, 10744-10749. DOI: https://doi.org/10.1039/C1JM11337B.
(361) Gubala, V.; Giovannini, G.; Kunc, F.; Monopoli, M. P.; Moore, C. J. Dye-doped silica nanoparticles: synthesis, surface chemistry and bioapplications. *Cancer Nanotechnol.* **2020**, *11*, 1. DOI: https://doi.org/10.1186/s12645-019-0056-x.
(362) Khoz, R.; Yazdian, F.; Pourmadadi, M.; Rahdar, A.; Fathi-karkan, S.; Pandey, S. Current trends in silica based drug delivery systems. *Eur. J. Med. Chem. Rep.* **2024**, *12*, 100206. DOI: https://doi.org/10.1016/j.ejmcr.2024.100206.
(363) Roy, I.; Kumar, P.; Kumar, R.; Ohulchanskyy, T. Y.; Yong, K.-T.; Prasad, P. N. Ormosil nanoparticles as a sustained-release drug delivery vehicle. *RSC Adv.* **2014**, *4*, 53498-53504. DOI: https://doi.org/10.1039/C4RA10293B.
(364) Kim, S.; Ohulchanskyy, T. Y.; Pudavar, H. E.; Pandey, R. K.; Prasad, P. N. Organically modified silica nanoparticles co-encapsulating photosensitizing drug and aggregation-enhanced two-photon absorbing fluorescent dye aggregates for two-photon photodynamic therapy. *J. Am. Chem. Soc.* **2007**, *129*, 2669-2675. DOI: https://doi.org/10.1021/ja0680257.
(365) Corsini, F.; Tatsi, E.; Colombo, A.; Dragonetti, C.; Botta, C.; Turri, S.; Griffini, G. Highly emissive fluorescent silica-based core/shell nanoparticles for efficient and stable luminescent solar concentrators. *Nano Energy* **2021**, *80*, 105551. DOI: https://doi.org/10.1016/j.nanoen.2020.105551.
(366) Ashraf, M. A.; Khan, A. M.; Ahmad, M.; Sarfraz, M. Effectiveness of silica based sol-gel microencapsulation method for odorants and flavors leading to sustainable environment. *Front. Chem.* **2015**, *3*, 42. DOI: https://doi.org/10.3389/fchem.2015.00042.
(367) Mohamed, A. L.; Khattab, T. A.; Hassabo, A. G. Color-tunable encapsulated perylene-labeled silica fluorescent hybrid nanoparticles. *Results Chem.* **2023**, *5*, 100769. DOI: https://doi.org/10.1016/j.rechem.2023.100769.
(368) Klippel, N.; Jung, G.; Kickelbick, G. Hybrid inorganic-organic fluorescent silica nanoparticles - influence of dye binding modes on dye leaching. *J. Sol-Gel Sci. Technol.* **2023**, *107*, 2-19. DOI: https://doi.org/10.1007/s10971-021-05578-y.
(369) Chen, F.; Zhao, E.; Kim, T.; Wang, J.; Hableel, G.; Reardon, P. J. T.; Ananthakrishna, S. J.; Wang, T.; Arconada-Alvarez, S.; Knowles, J. C.; Jokerst, J. V. Organosilica Nanoparticles with an Intrinsic Secondary Amine: An Efficient and Reusable Adsorbent for Dyes. *ACS Appl. Mater. Interfaces* **2017**, *9*, 15566-15576. DOI: https://doi.org/10.1021/acsami.7b04181.

(370) Lu, X.; Hou, Y.; Zha, J.; Xin, Z. Facile Synthesis of Rhodamine B-Doped Poly(3-mercaptopropylsilsesquioxane) Fluorescent Microspheres with Controllable Size. *Ind. Eng. Chem. Res.* **2013**, *52*, 5880-5886. DOI: https://doi.org/10.1021/ie302556t.
(371) Tapec, R.; Zhao, X. J.; Tan, W. Development of organic dye-doped silica nanoparticles for bioanalysis and biosensors. *Int. J. Nanosci.* **2002**, *2*, 405-409. DOI: https://doi.org/10.1166/jnn.2002.114.
(372) Sriramulu, D.; Turaga, S. P.; Bettiol, A. A.; Valiyaveettil, S. Molecular Organization Induced Anisotropic Properties of Perylene – Silica Hybrid Nanoparticles. *Sci. Rep.* **2017**, *7*, 7842. DOI: https://doi.org/10.1038/s41598-017-07892-4.
(373) Klein, L. C.; Jitianu, A. Organic-Inorganic hybrid melting gels. *J. Sol-Gel Sci. Technol.* **2010**, *55*, 86-93. DOI: https://doi.org/10.1007/s10971-010-2219-4.
(374) Hurwitz, F. I.; Hyatt, L.; Gorecki, J.; D'Amore, L. Silsesquioxanes as Precursors to Ceramic Composites. In *11th Annual Conference on Composites and Advanced Ceramic Materials: Ceramic Engineering and Science Proceedings*, Smothers, W. Ed.; The American Ceramic Society: Westerville, OH, USA, 1987; pp 732-743. DOI: https://doi.org/10.1002/9780470320402.ch29.
(375) Ishida, H.; Shick, R.; Hurwitz, F. Rheology of phenylpropylsilsesquioxane in the fiber-spinning regime. *Macromolecules* **1990**, *23*, 5279-5285. DOI: https://doi.org/10.1021/ma00227a017.
(376) Leśniak, E.; Michalska, Z. M.; Chojnowski, J. One-Step Synthesis of Thermoplastic Phenylsilsesquioxane Polymer and Its Copolymers with Diphenylsiloxanes. *J. Inorg. Organomet. Polym.* **1998**, *8*, 1-21. DOI: https://doi.org/10.1023/A:1021617902162.
(377) Schneider, D.; Loy, D.; Baugher, B.; Wheeler, D.; Assink, R.; Alam, T.; Saunders, R. Preparation and characterization of phenyl-, benzyl-, and phenethyl-substituted polysilsesquioxanes. *Polym. Prepr.* **1998**, *39*, 513-514. DOI: https://doi.org/10.2172/658253.
(378) Matsuda, A.; Sasaki, T.; Hasegawa, K.; Tatsumisago, M.; Minami, T. Thermal Softening Behavior and Application to Transparent Thick Films of Poly(benzylsilsesquioxane) Particles Prepared by the Sol–Gel Process. *J. Am. Ceram. Soc.* **2001**, *84*, 775-780. DOI: https://doi.org/10.1111/j.1151-2916.2001.tb00740.x.
(379) Masai, H.; Takahashi, M.; Tokuda, Y.; Yoko, T. Enhancement of Polycondensation Reaction by Diethyl Ether-Aqueous NaOH Immiscible Two Phase Liquid Treatment of Phenyl-Modified Polysiloxane Glass. *J. Ceram. Soc. Jpn.* **2005**, *113*, 259-262. DOI: https://doi.org/10.2109/jcersj.113.259.
(380) Kakiuchida, H.; Takahashi, M.; Tokuda, Y.; Masai, H.; Yoko, T. Effects of Organic Groups on Structure and Viscoelastic Properties of Organic - Inorganic Polysiloxane Hybrid System. *J. Phys. Chem.* **2007**, *111*, 982-988. DOI: https://doi.org/10.1021/jp064252j.
(381) Kamimura, Y.; Kurumada, K.-i.; Asaba, K.; Ban-no, H.; Kambara, H.; Hiro, M. Evaluation of activation energy of viscous flow of sol–gel derived phenyl-modified silica glass. *J. Non-Cryst. Solids* **2006**, *352*, 3175-3178. DOI: https://doi.org/10.1016/j.jnoncrysol.2006.05.020.
(382) Kuniyoshi, M.; Takahashi, M.; Tokuda, Y.; Yoko, T. Thermosoftening phenyl siloxane glasses prepared via sol concentration. *J. Non-Cryst. Solids* **2007**, *353*, 4162-4169. DOI: https://doi.org/10.1016/j.jnoncrysol.2007.06.044.
(383) Kuniyoshi, M.; Takahashi, M.; Tokuda, Y.; Yoko, T. Preparation of Phenyl-modified Siloxane Glasses with Softening Temperature Controlled by Rapid Heat Treatment (RHT). *Chem. Lett.* **2006**, *35*, 1384-1385. DOI: https://doi.org/10.1246/cl.2006.1384.
(384) Klein, L. C.; Al-Marzoki, K.; Jitianu, A.; Rodriguez, G. Effect of tetraethoxysilane (TEOS) on melting gel behavior. *J. Am. Ceram. Soc.* **2020**, *103*, 4140-4149. DOI: https://doi.org/10.1111/jace.17106.

(385) Klein, L. C.; Al-Marzoki, K.; Jitianu, A. Phase separation in melting gels. *Phys. Chem. Glasses: Eur. J. Glass Sci. Technol. B* **2017**, *58*, 142–149. DOI: https://doi.org/10.13036/17533562.58.4.142.
(386) Gambino, L.; Jitianu, A.; Klein, L. C. Dielectric behavior of organically modified siloxane melting gels. *J. Non-Cryst. Solids* **2012**, *358*, 3501-3504. DOI: https://doi.org/10.1016/j.jnoncrysol.2012.01.002.
(387) Jitianu, A.; Gonzalez, G.; Klein, L. C. Hybrid Sol-Gel Glasses with Glass-Transition Temperatures Below Room Temperature. *J. Am. Ceram. Soc.* **2015**, *98*, 3673-3679. DOI: https://doi.org/10.1111/jace.13798.
(388) Klein, L. C.; Kallontzi, S.; Fabris, L.; Jitianu, A.; Ryan, C.; Aparicio, M.; Lei, L.; Singer, J. P. Applications of melting gels. *J. Sol-Gel Sci. Technol.* **2019**, *89*, 66-77. DOI: https://doi.org/10.1007/s10971-018-4599-9.
(389) Macan, J.; Tadanaga, K.; Tatsumisago, M. Influence of copolymerization with alkyltrialkoxysilanes on condensation and thermal behaviour of poly(phenylsilsesquioxane) particles. *J. Sol-Gel Sci. Technol.* **2010**, *53*, 31-37. DOI: https://doi.org/10.1007/s10971-009-2051-x.
(390) Macan, J.; Tadanaga, K.; Tatsumisago, M. Softening of Octyl-modified Phenylsilsesquioxanes. *Polimeri* **2011**, *32*, 112-118.
(391) Seto, R.; Kanamura, K.; Yoshida, S.; Kajihara, K. Cosolvent-free synthesis and characterisation of poly(phenyl-co-n-alkylsilsesquioxane) and poly(phenyl-co-vinylsilsesquioxane) glasses with low melting temperatures. *Dalton Trans.* **2020**, *49*, 2487-2495. DOI: https://doi.org/10.1039/C9DT04579A.
(392) Yu, D.; Kleemeier, M.; Wu, G. M.; Schartel, B.; Liu, W. Q.; Hartwig, A. A low melting organic-inorganic glass and its effect on flame retardancy of clay/epoxy composites. *Polymer* **2011**, *52*, 2120-2131. DOI: https://doi.org/10.1016/j.polymer.2011.03.033.
(393) Pohl, S.; Janka, O.; Füglein, E.; Kickelbick, G. Thermoplastic Silsesquioxane Hybrid Polymers with a Local Ladder-Type Structure. *Macromolecules* **2021**, *54*, 3873-3885. DOI: https://doi.org/10.1021/acs.macromol.1c00310.
(394) Pohl, S.; Steinbrück, N.; Pachnicz, M. P.; Kickelbick, G. Melt, mix, and glow: emulsion-based fabrication of polyphenylsilsesquioxane microspheres with embedded hydrophobic fluorophores. *Mater. Adv.* **2025**. DOI: https://doi.org/10.1039/D5MA00849B.
(395) Takahashi, K.; Tadanaga, K.; Matsuda, A.; Hayashi, A.; Tatsumisago, M. Formation of convex shaped poly(phenylsilsesquioxane) micropatterns on indium tin oxide substrates with hydrophobic-hydrophilic patterns using the electrophoretic sol-gel deposition method. *J. Mater. Res.* **2006**, *21*, 1255-1260. DOI: https://doi.org/10.1557/jmr.2006.0150.
(396) Pohl, S.; Gallei, M.; Kickelbick, G. Impact of Size and Substitution Isomerism in Polycyclic Aromatic-Substituted Trialkoxysilanes on the Formation of Softenable Polysilsesquioxanes. *Macromolecules* **2025**, *58*, 1298-1313. DOI: https://doi.org/10.1021/acs.macromol.4c02737.
(397) Gießelmann, E. C. J.; Engel, S.; Pohl, S.; Briesenick, M.; Rüthing, L. P.; Kloos, C.; Koldemir, A.; Schumacher, L.; Wiethölter, J.; Schmedt auf der Günne, J.; Kickelbick, G.; Janka, O. Rapid Synthesis of a Green Emitting Phosphor by Sulfidation of Intermetallic EuAl2 and its Use in a Hybrid Material. *Chem. Mater.* **2024**, *37*, 97-108. DOI: https://doi.org/10.1021/acs.chemmater.4c02093.
(398) Jitianu, A.; Doyle, J.; Amatucci, G.; Klein, L. C. Methyl-modified Melting Gels for Hermetic Barrier Coatings. In Proceeding at Material Science & Technology Pittsburgh, PA; 2008.
(399) Jitianu, M.; Jitianu, A.; Stamper, M.; Aboagye, D.; Klein, L. C. Melting Gel Films for Low Temperature Seals. *Mater. Res. Soc. Symp. Proc.* **2013**, *1547*, 81-86. DOI: https://doi.org/10.1557/opl.2013.506.

(400) Aparicio, M.; Jitianu, A.; Rodriguez, G.; Degnah, A.; Al-Marzoki, K.; Mosa, J.; Klein, L. C. Corrosion Protection of AISI 304 Stainless Steel with Melting Gel Coatings. *Electrochim. Acta* **2016**, *202*, 325-332. DOI: https://doi.org/10.1016/j.electacta.2015.12.142.
(401) Huang, S.-Y.; Wang, J.-S. Thermally stable conformal encapsulation material for high-power ultraviolet light-emitting diodes. *Opt. Eng.* **2017**, *56*, 077105. DOI: https://doi.org/10.1117/1.OE.56.7.077105.
(402) Aparicio, M.; Mosa, J.; Rodriguez, G.; Guzman, J.; Picard, Q.; Klein, L. C.; Jitianu, A. Consolidated Melting Gel Coatings on AZ31 Magnesium Alloy with Excellent Corrosion Resistance in NaCl Solutions: An Interface Study. *ACS Appl. Mater. Interfaces.* **2019**, *11*, 3493-3505. DOI: https://doi.org/10.1021/acsami.8b20199.
(403) Kallontzi, S.; Fabris, L.; Jitianu, M.; Hernandez, A.; Jitianu, A.; Klein, L. C. Gold nanoparticles in melting gels. *J. Sol-Gel Sci. Technol.* **2019**, *91*, 189-197. DOI: https://doi.org/10.1007/s10971-019-04997-2.
(404) Picarda, Q.; Akalonua, G.; Mercadoa, J.; Mosa, J.; Aparicio, M.; Kleinc, L. C.; Jitianua, A. Electrodeposition of Hybrid Sol-Gel Glass Coatings on 304 Stainless Steel for Corrosion Protection. In *Advances in Ceramics for Environmental, Functional, Structural, and Energy Applications*, Sridharan, K., Bhalla, A., Manjooran, N. J., Mahmoud, M., Jitianu, A., Singh, J., Colorado, H., Gupta, S., Langhorn, J. Eds.; John Wiley & Sons, Inc.: Hoboken, NJ, USA, 2018; pp 205-217. DOI: https://doi.org/10.1002/9781119543299.ch19.
(405) Jenkins, S.; Sciarrone, E.; Klein, L. C. Texturing melting gels for water harvesting. *J. Sol-Gel Sci. Technol.* **2022**, *101*, 37-45. DOI: https://doi.org/10.1007/s10971-021-05654-3.
(406) Kuo, C.-F. J.; Chen, J.-B. Study on the synthesis and application of silicone resin containing phenyl group. *J. Sol-Gel Sci. Technol.* **2015**, *76*, 66-73. DOI: https://doi.org/10.1007/s10971-015-3752-y.
(407) Jitianu, A.; Lammers, K.; Arbuckle-Kiel, G. A.; Klein, L. C. Thermal analysis of organically modified siloxane melting gels. *J. Therm. Anal. Calorim.* **2012**, *107*, 1039-1045. DOI: https://doi.org/10.1007/s10973-011-2024-5.
(408) Katagiri, K.; Hasegawa, K.; Matsuda, A.; Tatsumisago, M.; Minami, T. Preparation of Transparent Thick Films by Electrophoretic Sol – Gel Deposition Using Phenyltriethoxysilane-Derived Particles. *J. Am. Ceram. Soc.* **1998**, *81*, 2501-2503. DOI: https://doi.org/10.1111/j.1151-2916.1998.tb02653.x.
(409) Menaa, B.; Takahashi, M.; Tokuda, Y.; Yoko, T. Preparation and properties of polyphenylsiloxane-based hybrid glass films obtained from a non-aqueous coating sol via a single-step dip-coating. *Opt. Mater.* **2007**, *29*, 806-813. DOI: https://doi.org/10.1016/j.optmat.2005.12.009.
(410) Pohl, S. Synthese und Charakterisierung polymerer aromatischer Silsesquioxan-Hybrid-Systeme. Saarland University Saarbrücken, Master Thesis, **2020**.
(411) Steinbrück, N. Polysiloxane and polysilsesquioxane based materials for optoelectronic applications and organic dye integration. Saarland University, **2020**.
(412) Yaacoub, S.; Calas-Etienne, S.; Jabbour, J.; Courson, R.; Tauk, R.; Khoury, A.; Mehdi, A.; Etienne, P. Synthesis of new vinyl ether functionalized silica for UV-patterning. *J. Sol-Gel Sci. Technol.* **2013**, *67*, 384-393. DOI: https://doi.org/10.1007/s10971-013-3092-8.
(413) Emel'yanov, A. I.; Bolgova, Y. I.; Trofimova, O. M.; Pozdnyakov, A. S. Green Synthesis of Soluble Polysilsesquioxane with Phthalimide Groups. *Int. J. Mol. Sci.* **2024**, *25*, 57. DOI: https://doi.org/10.3390/ijms25010057.
(414) Kalinina, A. A.; Gorbatsevich, O. B.; Yakhontov, N. G.; Demchenko, N. V.; Vasilenko, N. G.; Kazakova, V. V.; Muzafarov, A. M. Synthesis of Multifunctional Oligomethylsilsesquioxanes by Catalyst-Free Hydrolytic Polycondensation of Methyltrimethoxysilane under Microwave Radiation. *Polymers* **2023**, *15*, 291. DOI: https://doi.org/10.3390/polym15020291.

7 Supplementary Information

Supporting Information

Thermoplastic Silsesquioxane Hybrid Polymers with a Local Ladder-Type Structure

Svenja Pohl[a], Oliver Janka[a], Ekkehard Füglein[b] and Guido Kickelbick[a]*

[a] Saarland University, Inorganic Solid-State Chemistry, Campus, Building C4 1, 66123 Saarbrücken, Germany

[b] NETZSCH-Gerätebau GmbH, Wittelsbacherstraße 42, 95100 Selb, Germany

Content

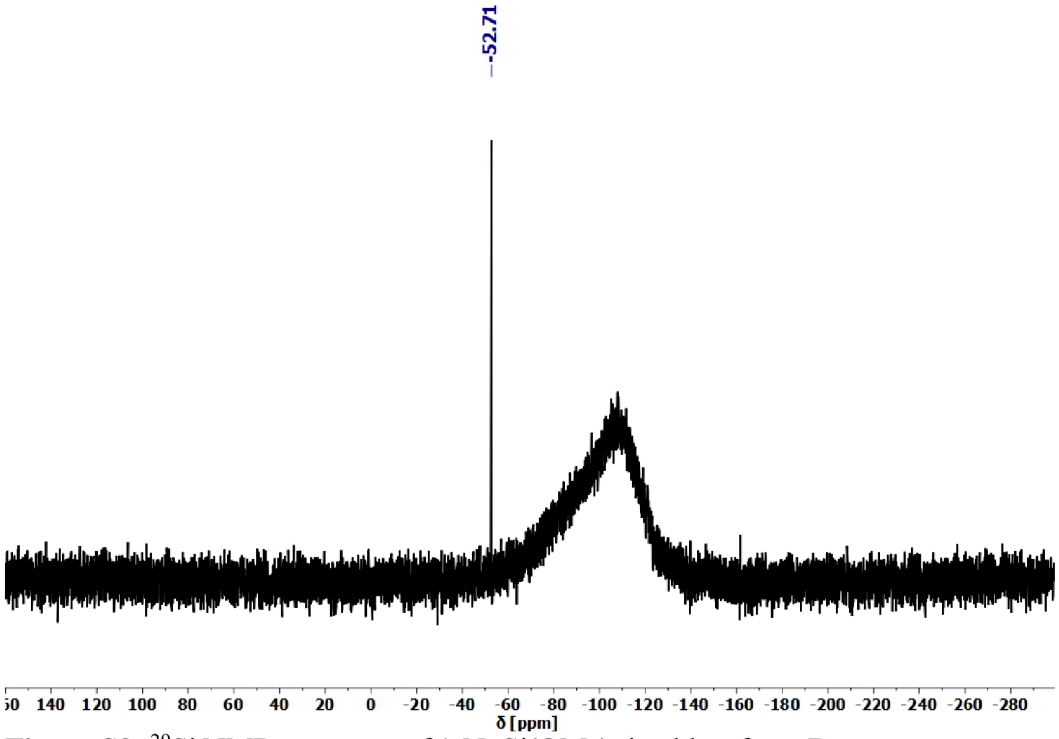

Figure S3: ^{29}Si NMR spectrum of 1-NpSi(OMe)$_3$ in chloroform-D.

FT-IR spectrum

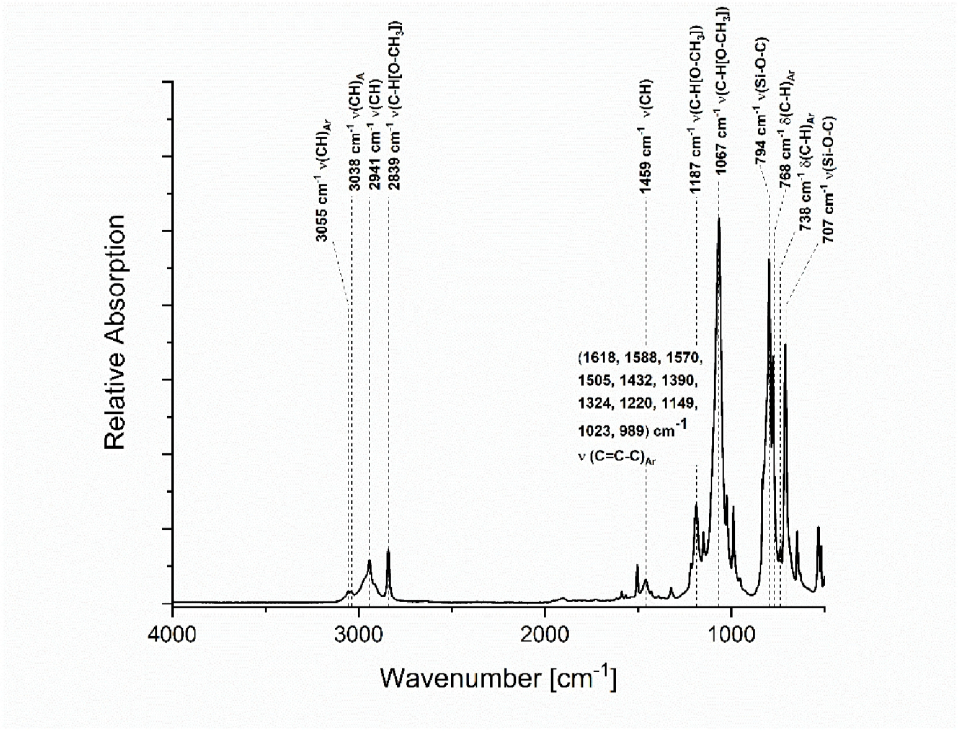

Figure S4. FT-IR spectrum of 1-NpSi(OMe)$_3$.

Characterization 1-NpSi(OMe)$_3$

NMR spectra

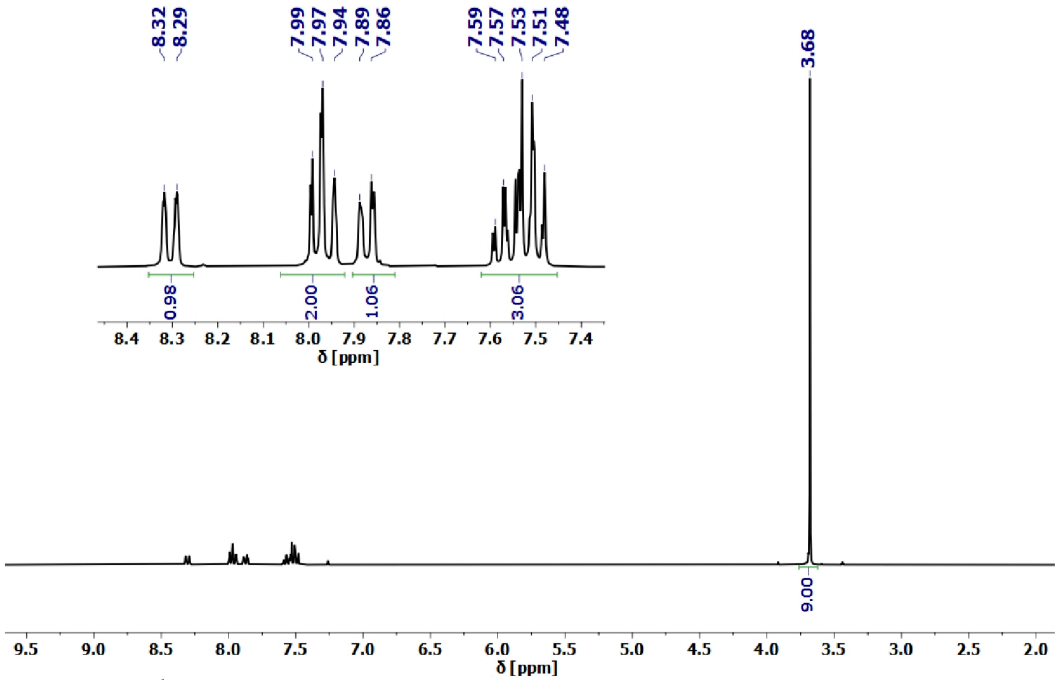

Figure S1.: ^{1}H NMR spectrum of 1-NpSi(OMe)$_3$ in chloroform-D.

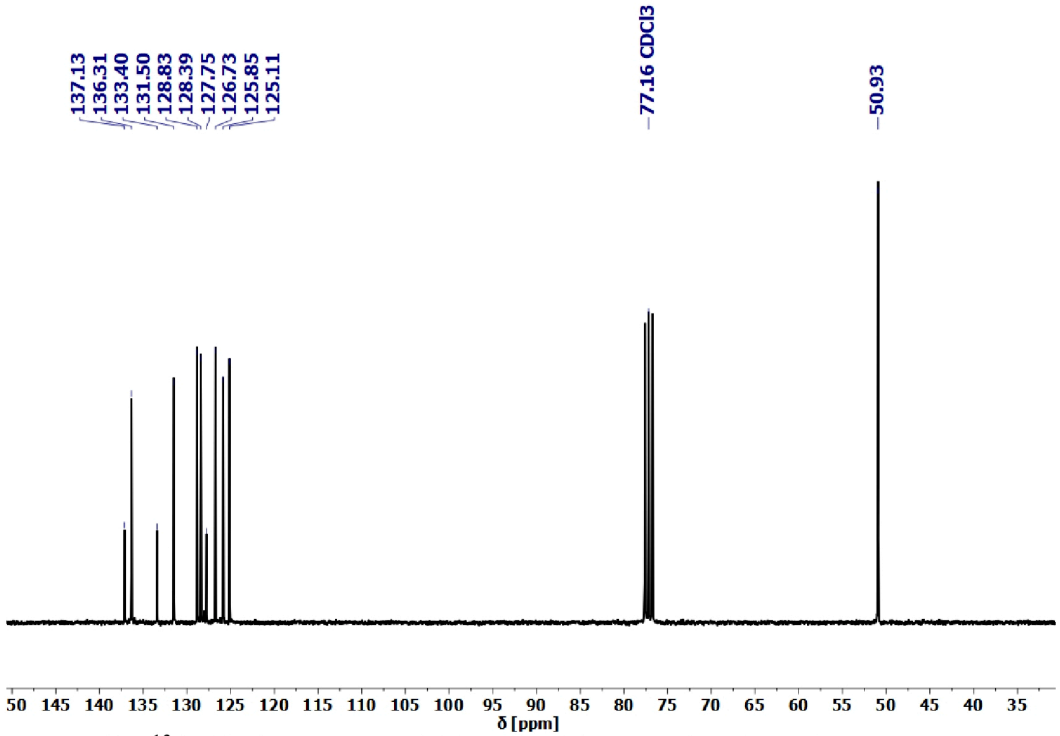

Figure S2.: ^{13}C NMR spectrum of 1-NpSi(OMe)$_3$ in chloroform-D.

Characterization $PhMG_{prec}$ and $PhMG_{cons}$

NMR spectra

$PhMG_{prec}$

^{1}H NMR (400 MHz, $CDCl_3$): δ = 7.90-6.78 (m, Ph), 3.72-2.80 (m, OMe)
^{13}C NMR (100 MHz, $CDCl_3$): δ= 134.17, 130.38, 127.77 (Ph), 50.73 (OMe) ppm
^{29}Si NMR (80 MHz, $CDCl_3$): δ= -61.26 (T^1), -70.04 (T^2), -79.58 (T^3) ppm
^{13}C CP-MAS (100 MHz, $CDCl_3$): δ= 134.34, 130.65, 127.95 (Ph), 50.51 (OMe) ppm
^{29}Si CP-MAS (80 MHz, $CDCl_3$): δ= -69.89 (T^2), -77.83 (T^3) ppm

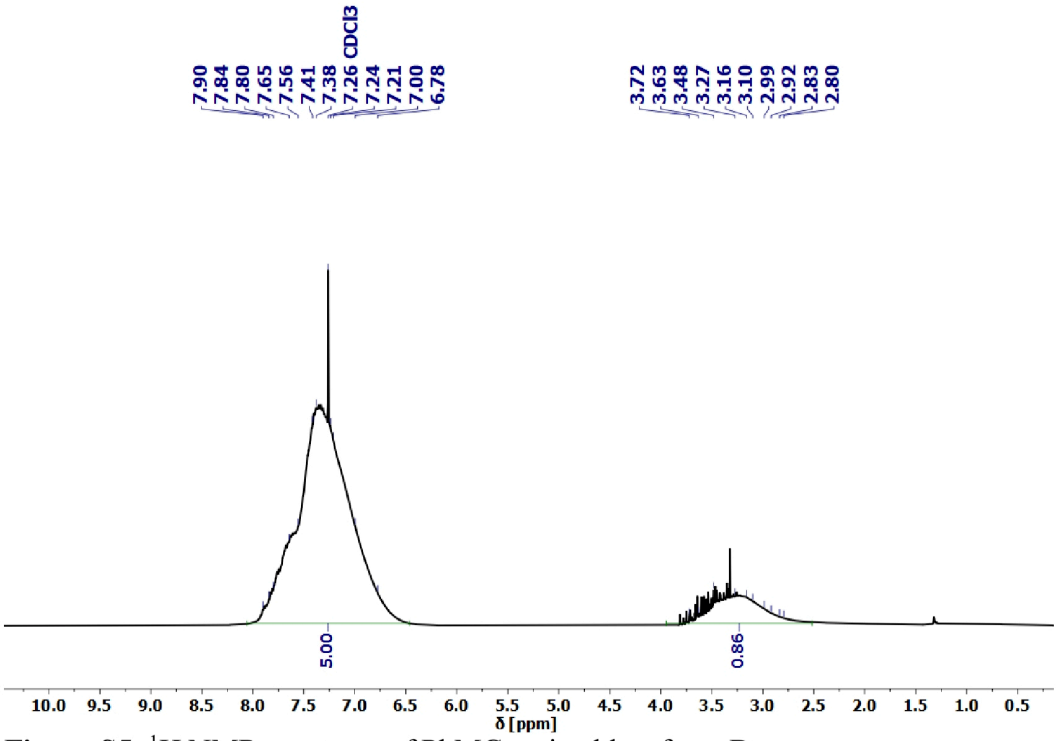

Figure S5. ^{1}H NMR spectrum of $PhMG_{prec}$ in chloroform-D.

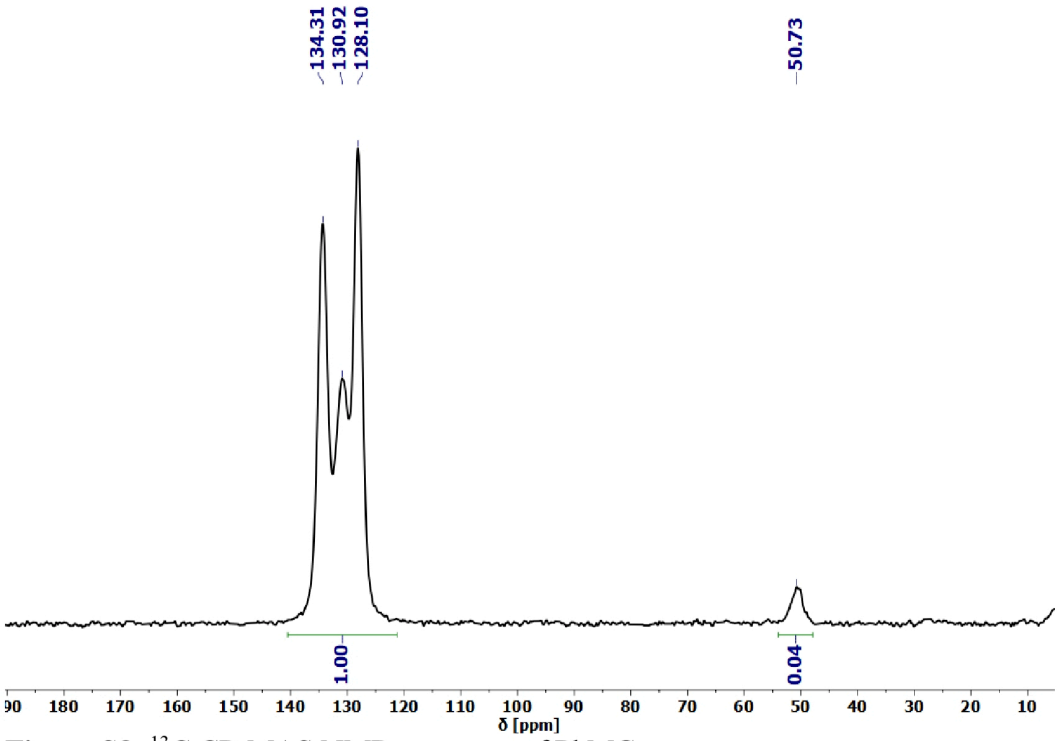

Figure S8. ^{13}C CP-MAS NMR spectrum of $PhMG_{prec}$.

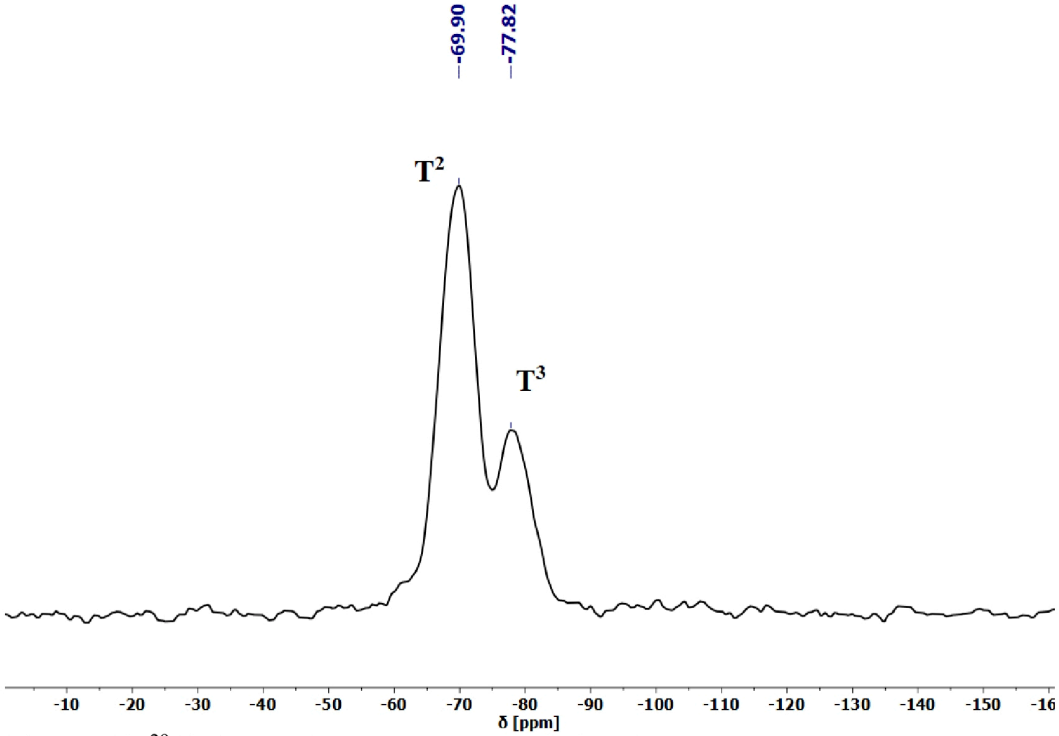

Figure S9. ^{29}Si CP-MAS NMR spectrum of $PhMG_{prec}$.

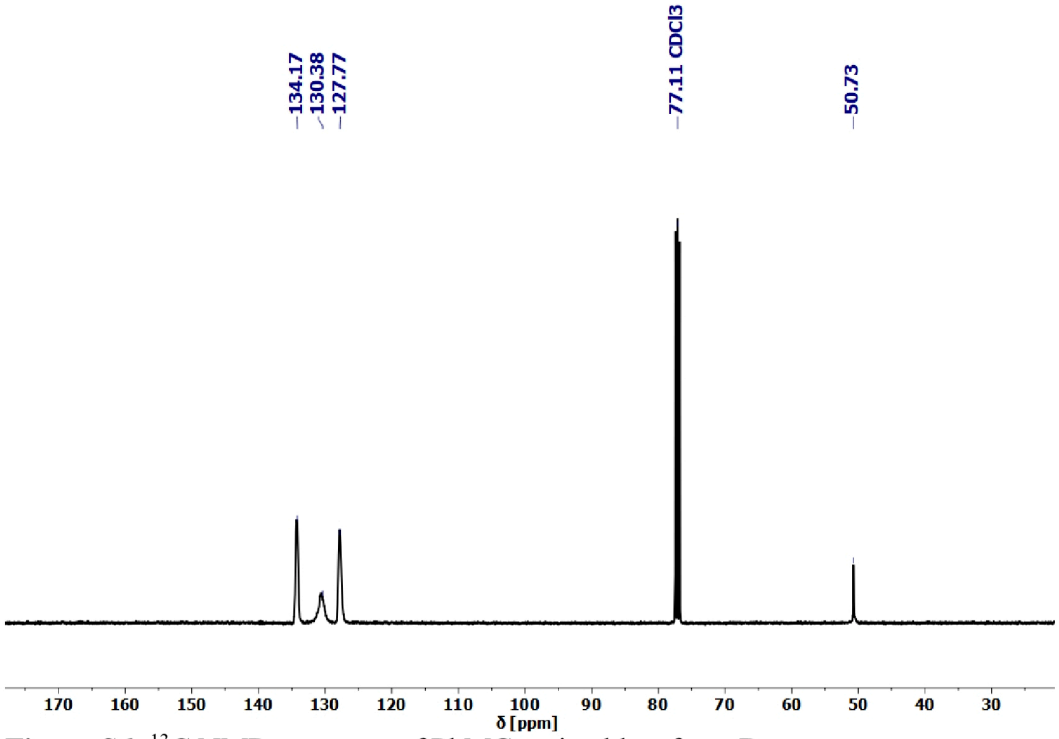

Figure S6. ^{13}C NMR spectrum of $PhMG_{prec}$ in chloroform-D.

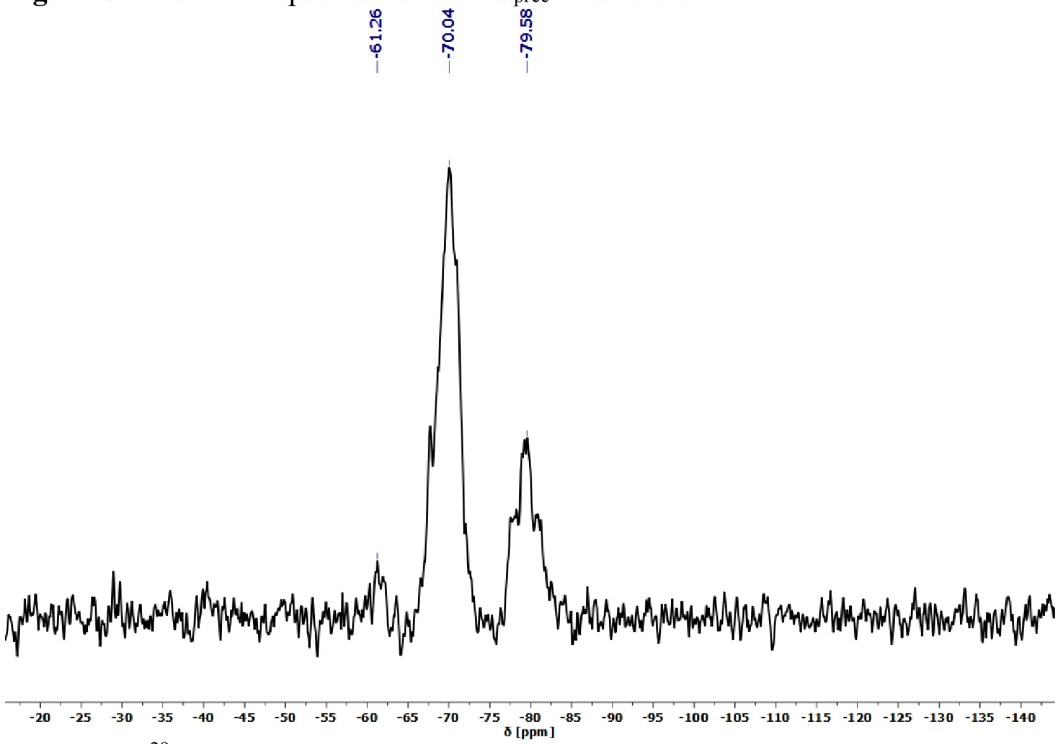

Figure S7. ^{29}Si NMR spectrum of $PhMG_{prec}$ in chloroform-D.

PhMG$_{cons}$

^{13}C CP-MAS (100 MHz, $CDCl_3$): δ= 134.32, 130.92, 128.10 (Ph), 50.80 (OMe) ppm

^{29}Si CP-MAS (80 MHz, $CDCl_3$): δ= -70.81 (T^2), -78.06 (T^3) ppm

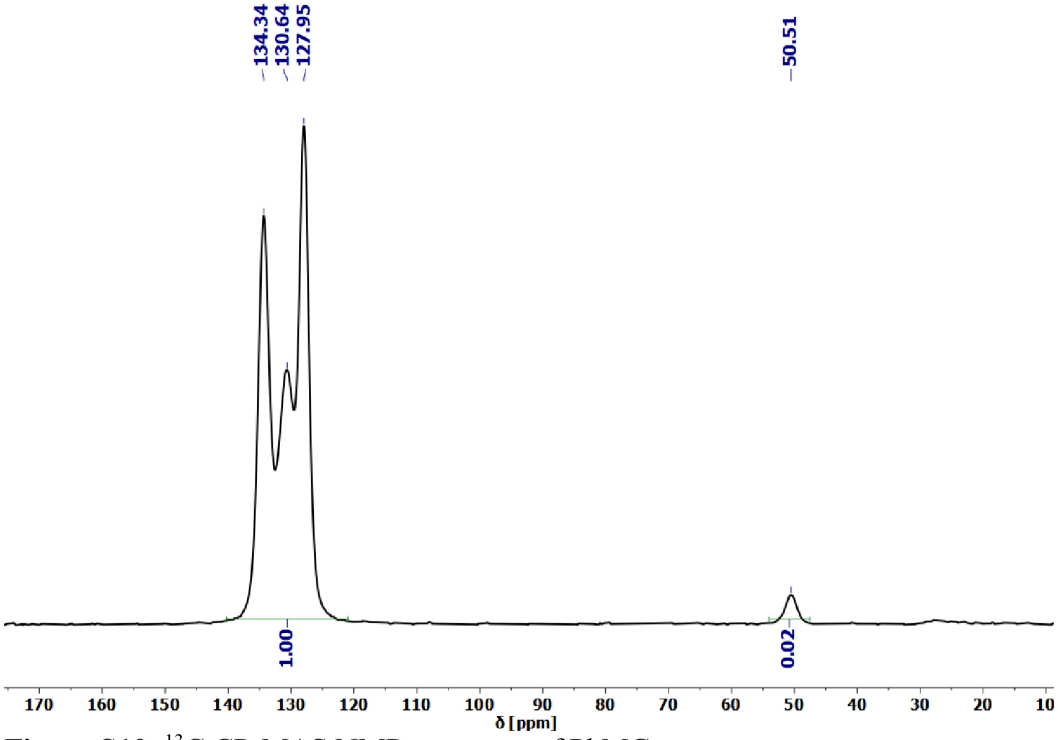

Figure S10. ^{13}C CP-MAS NMR spectrum of PhMG$_{cons}$.

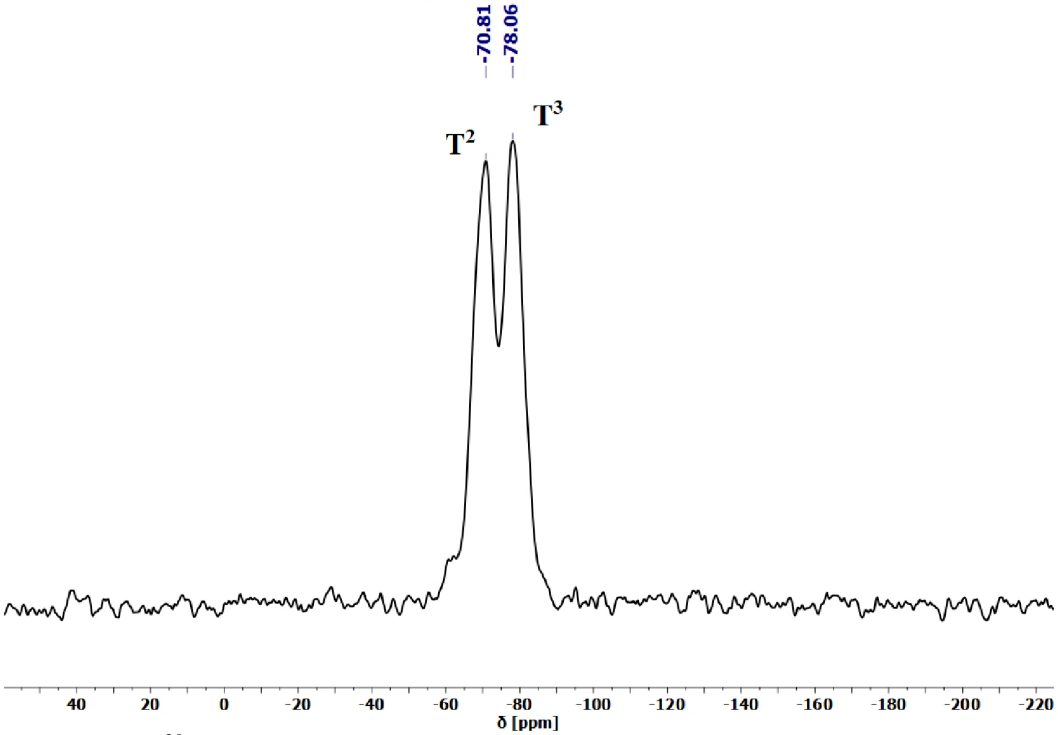

Figure S11. ^{29}Si CP-MAS NMR spectrum of PhMG$_{cons}$.

Time dependent IR spectra

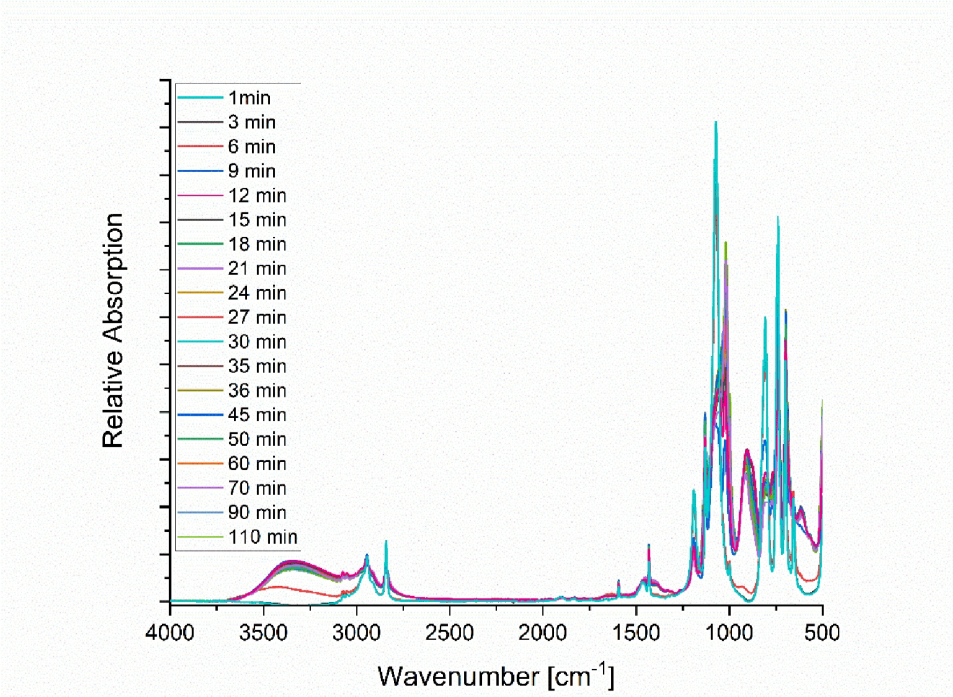

Figure S12. Time-dependent FT-IR spectra from the hydrolysis and condensation of phenyltrimethoxysilane.

Raman spectra

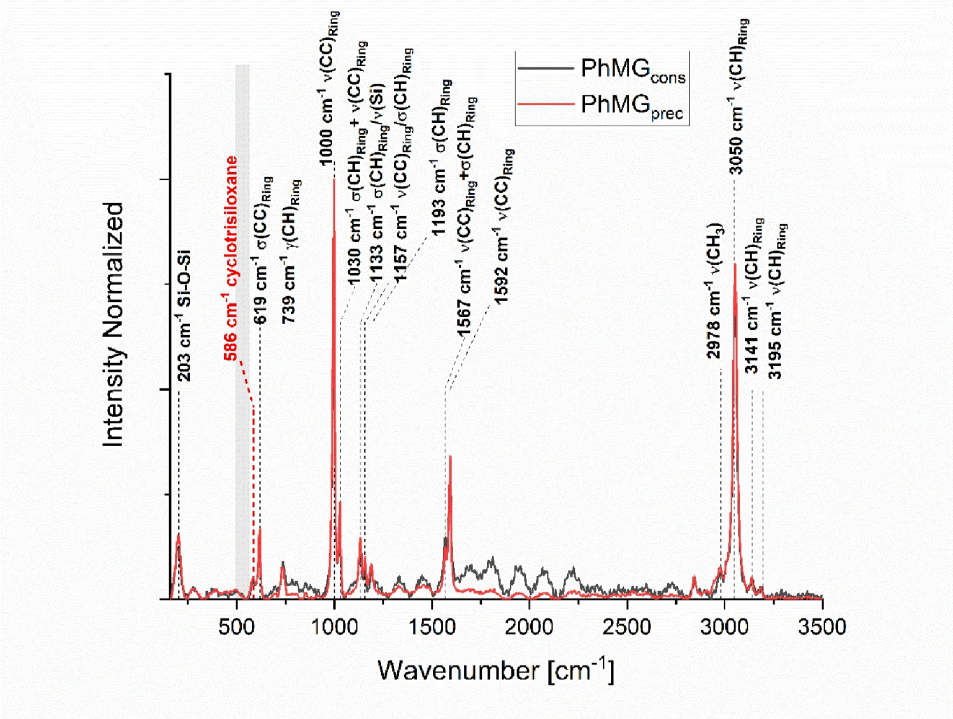

Figure S13. Raman spectra of $PhMG_{prec}$ and $PhMG_{cons}$.

XRD reference sample

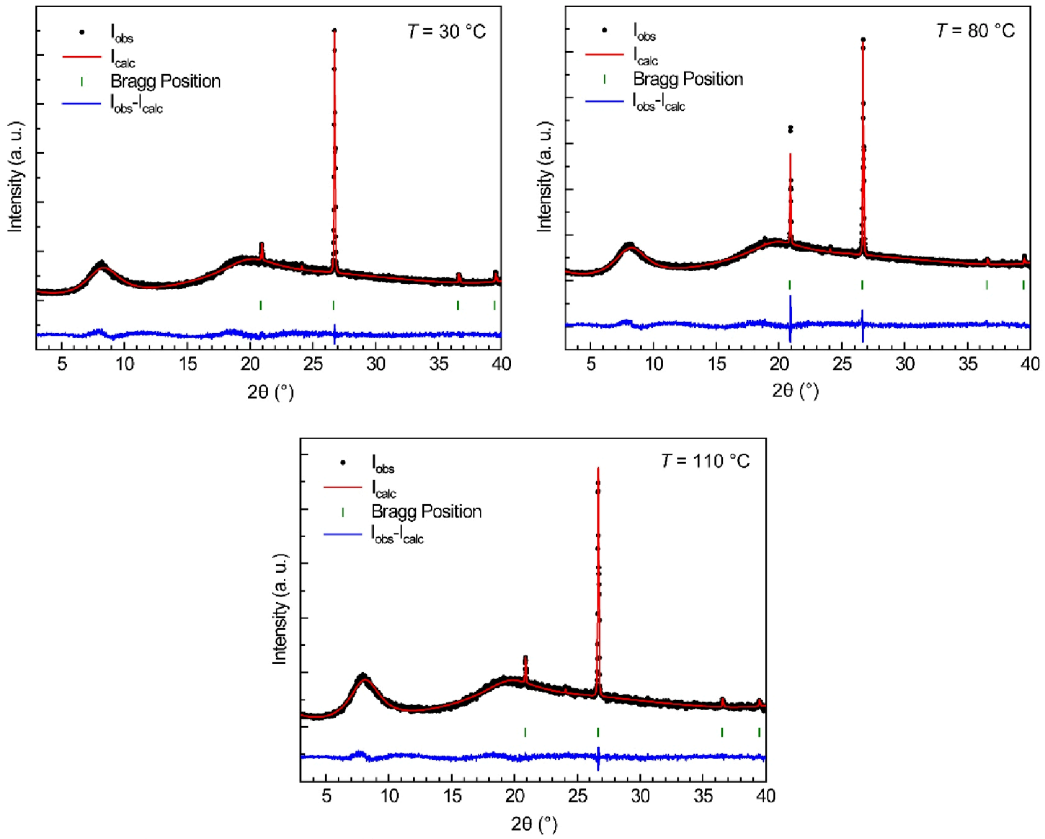

Figure S14. Powder X-ray diffraction pattern of the $PhMG_{prec}$, mixed with SiO_2 at 30, 80 and 110 °C.

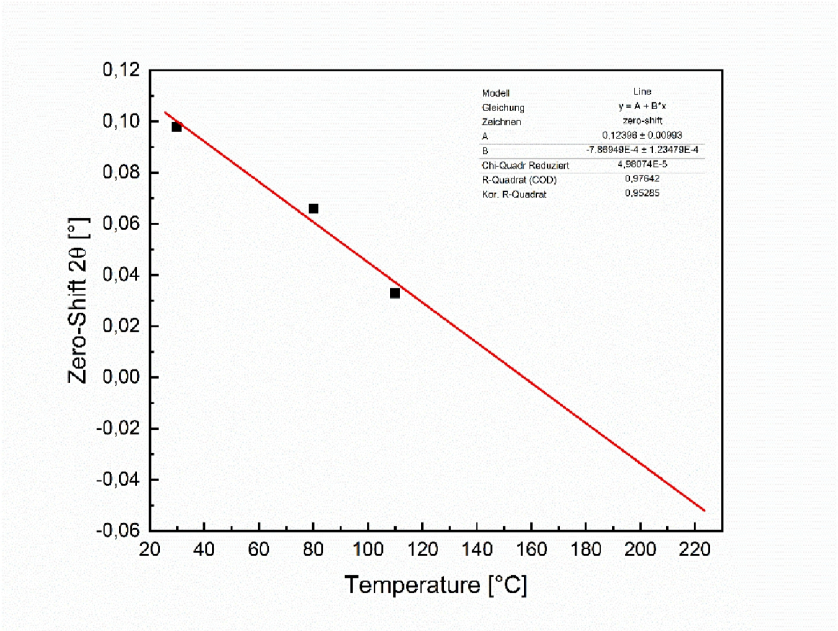

Figure S15. Determination of the zero-shift by linear regression.

Size exclusion chromatography

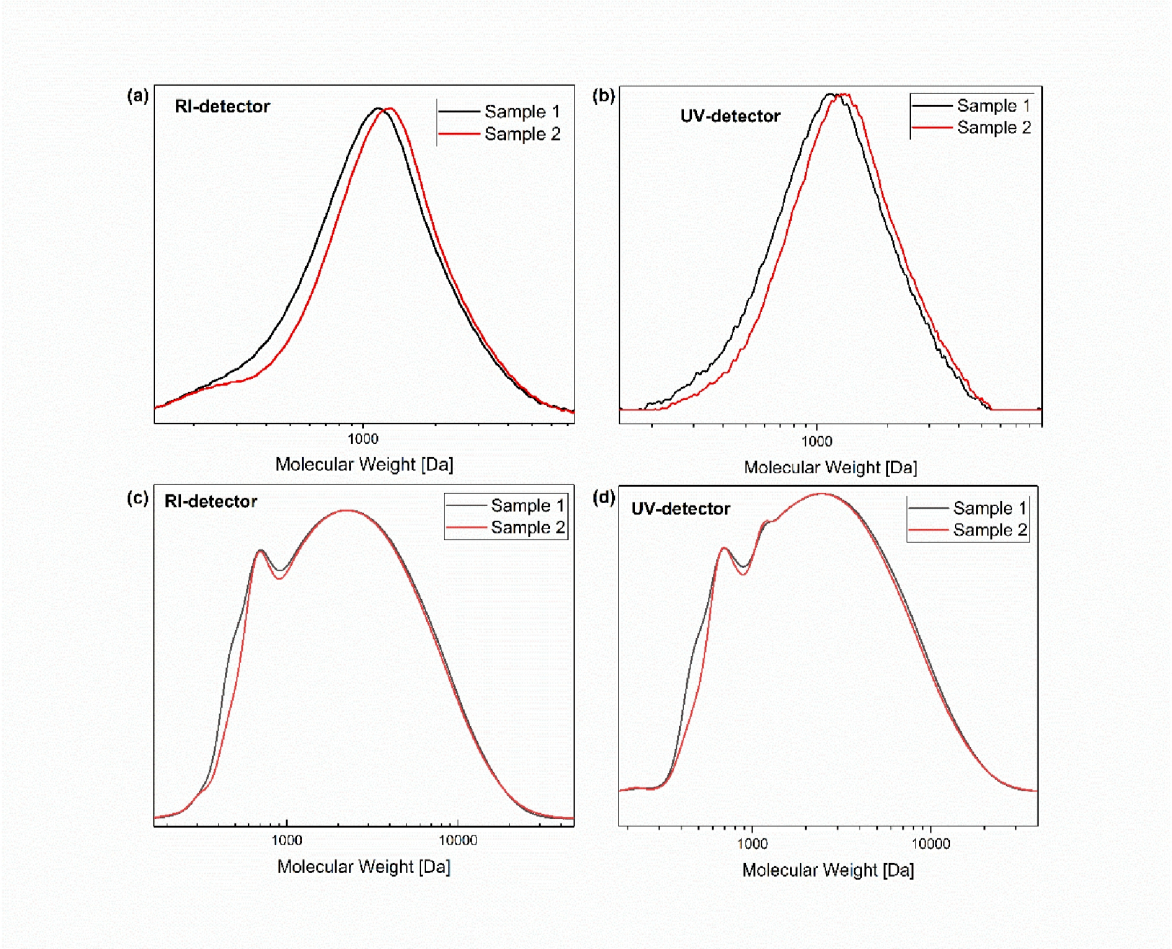

Figure S16. SEC profiles for $PhMG_{prec}$, a) in DMF, RI-detector, b) in DMF, UV-detector, c) in THF, RI-detector, d) in THF, UV-detector.

Table S1. SEC results of $PhMG_{prec}$, in THF and DMF, detected via IR and UV.

	DMF				THF			
	Sample 1		Sample 2		Sample 1		Sample 2	
	RI	UV	RI	UV	RI	UV	RI	UV
M_n	846	951	922	1086	1397	1501	1466	1576
M_w	1317	1328	1416	1462	3367	3540	3451	3578
M_z	1950	1790	2010	1920	7195	7442	7487	7501
PDI	1.557	1.396	1.534	1.346	2.411	2.358	2.354	2.271

Characterization of 1-NpMG$_{prec}$ and 1-NpMG$_T$

NMR spectra

1-NpMG$_{prec}$
^{1}H NMR (400 MHz, $CDCl_3$): δ = 8.48-7.04 (m, Np), 4.03-2.97 (m, OMe) ppm
^{29}Si NMR (80 MHz, $CDCl_3$): δ= -59.80 (T^1), -68.32 (T^2), -78.47 (T^3) ppm
^{13}C CP-MAS (100 MHz, $CDCl_3$): δ= 136.17, 133.05, 127.82 (Np), 50.40 (OMe) ppm
^{29}Si CP-MAS (80 MHz, $CDCl_3$): δ= -60.57 (T^1), -68.69 (T^2), -77.44 (T^3) ppm

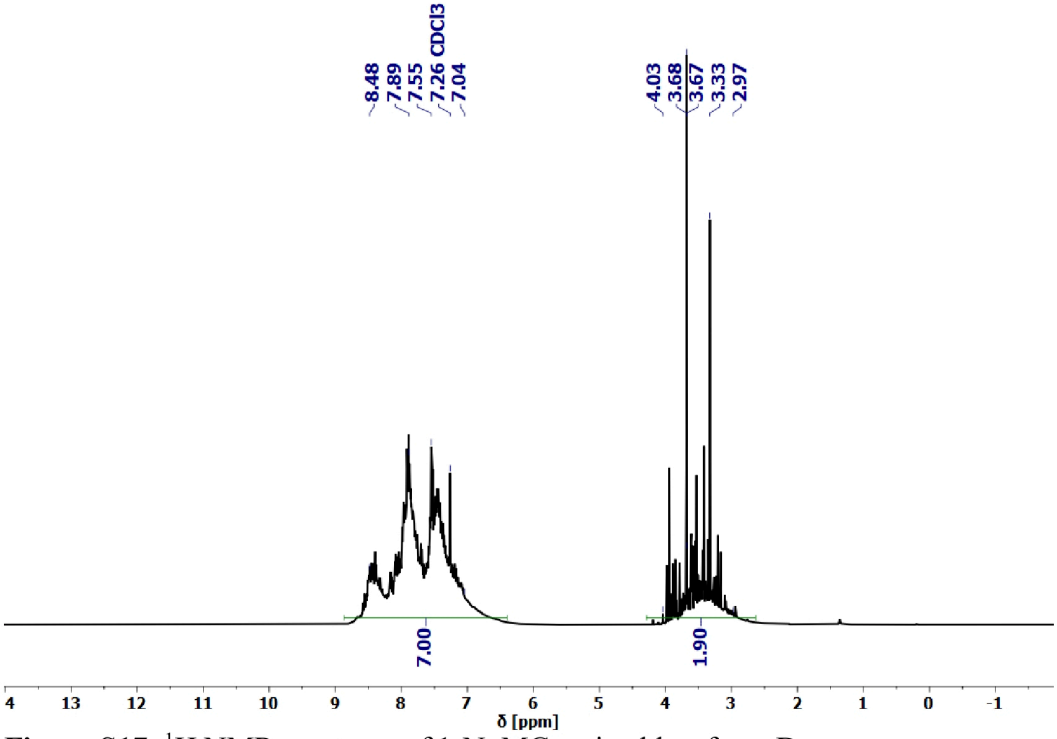

Figure S17. ^{1}H NMR spectrum of 1-NpMG$_{prec}$ in chloroform-D.

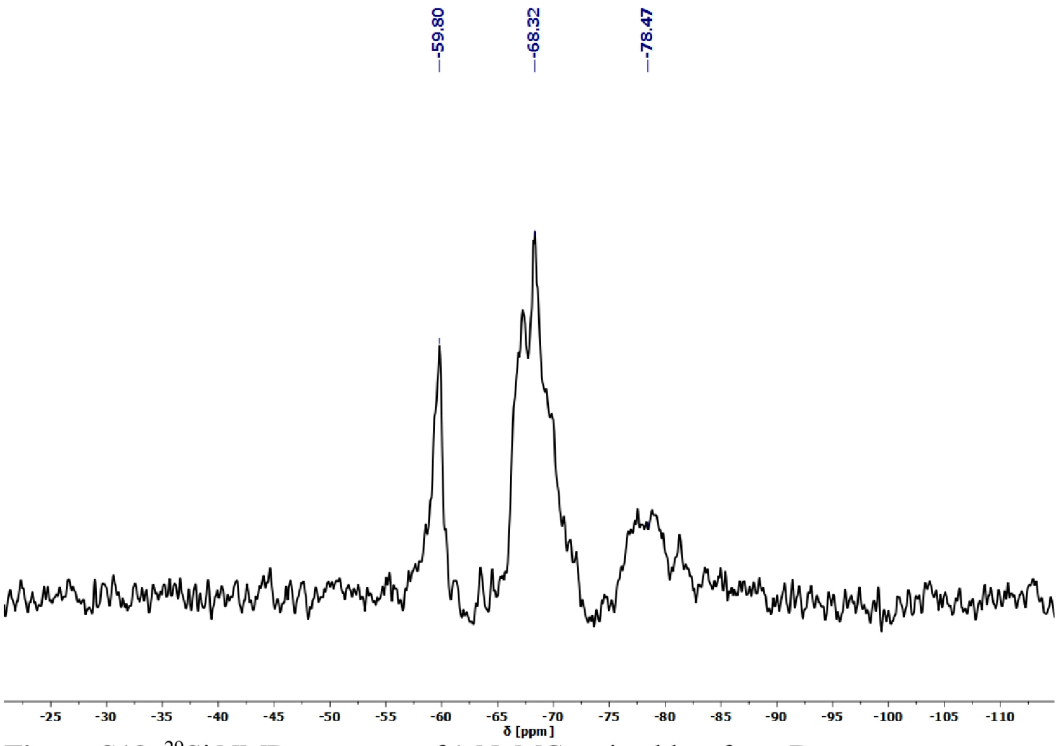

Figure S18. ^{29}Si NMR spectrum of 1-NpMG$_{prec}$ in chloroform-D.

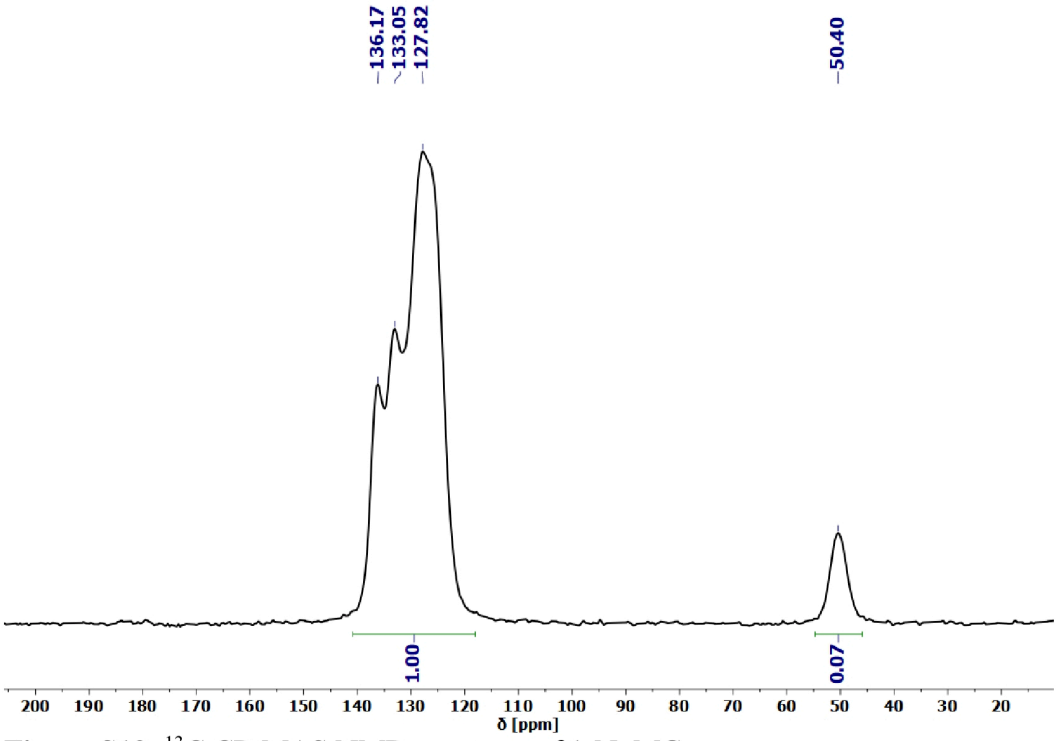

Figure S19. ^{13}C CP-MAS NMR spectrum of 1-NpMG$_{prec}$.

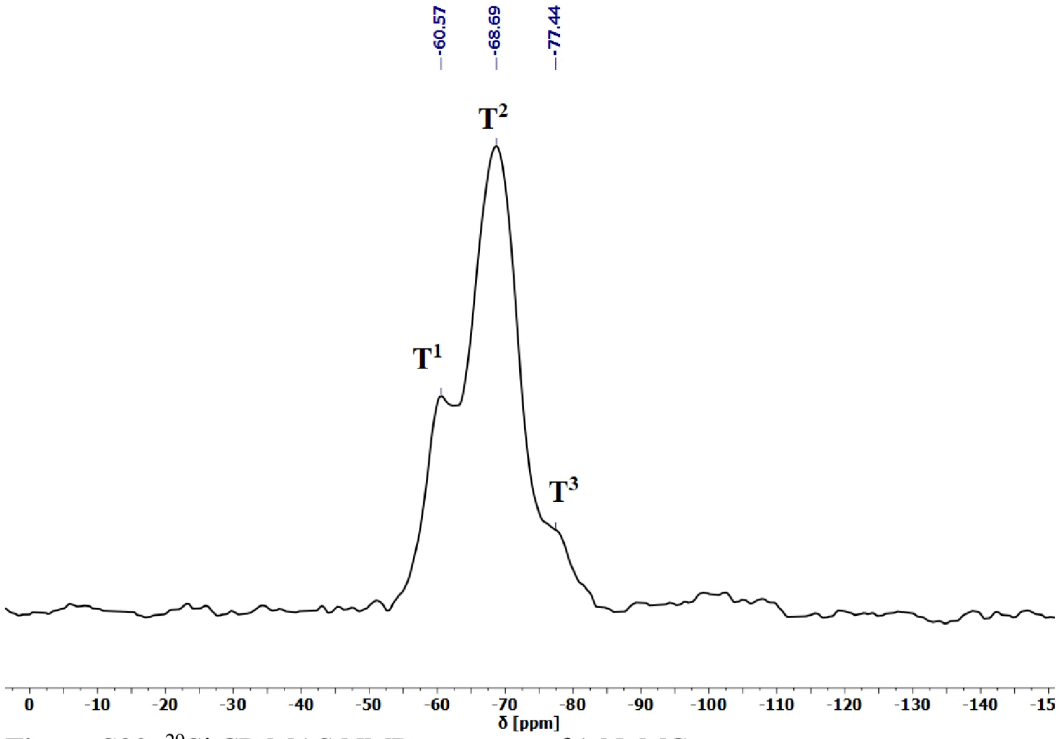

Figure S20. ^{29}Si CP-MAS NMR spectrum of 1-NpMG$_{prec.}$

1-NpMG$_T$

^{1}H NMR (400 MHz, CDCl3): δ = 8.29-6.16 (m, Np), 3.80-2.40 (m, OMe)

^{29}Si NMR (80 MHz, CDCl3): δ= -61.49 (T^1), -68.92 (T^2), -78.94 (T^3) ppm

^{13}C CP-MAS (100 MHz, CDCl3): δ= 136.14, 133.05, 128.04, 126.02 (Np), 50.13 (-OMe) ppm

^{29}Si CP-MAS (80 MHz, CDCl3): δ= -61.16 (T^1), -70.03 (T^2), -77.13 (T^3) ppm

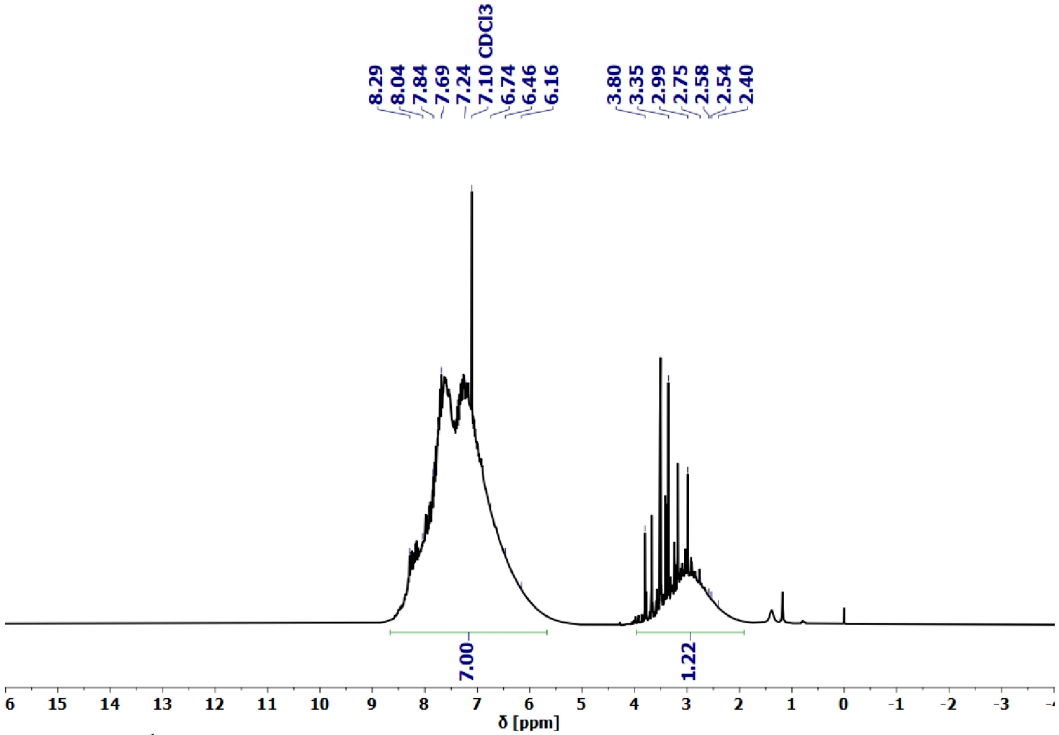

Figure 21. ^{1}H NMR spectrum of 1-NpMG$_T$ in chloroform-D.

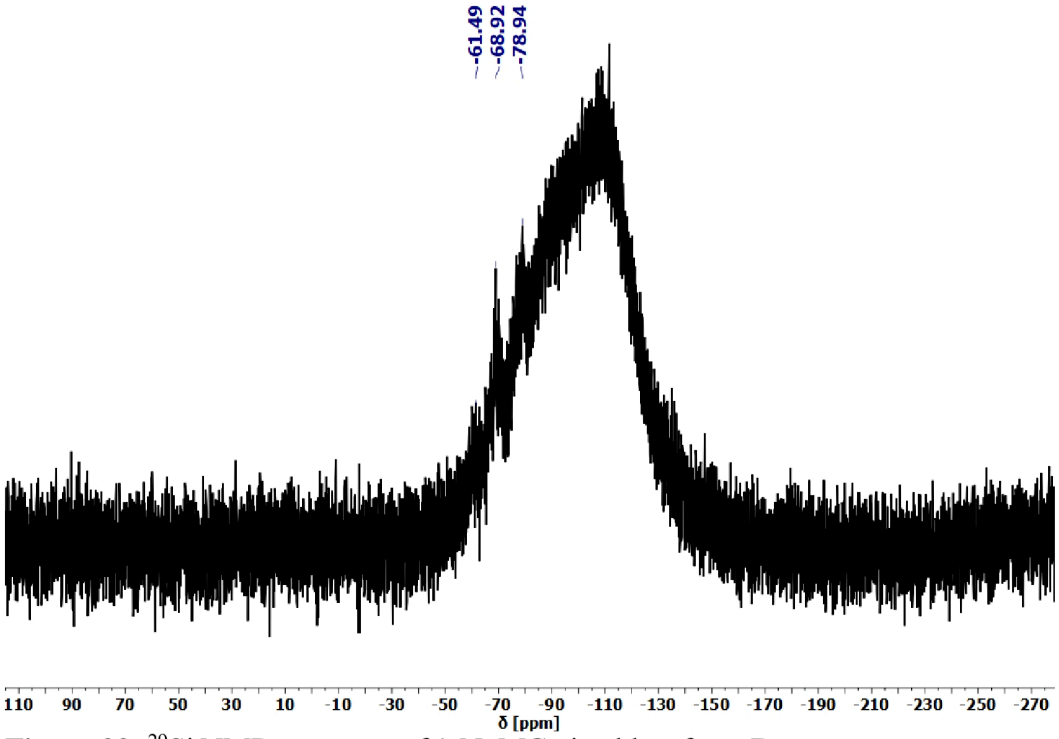

Figure 22. ^{29}Si NMR spectrum of 1-NpMG$_T$ in chloroform-D.

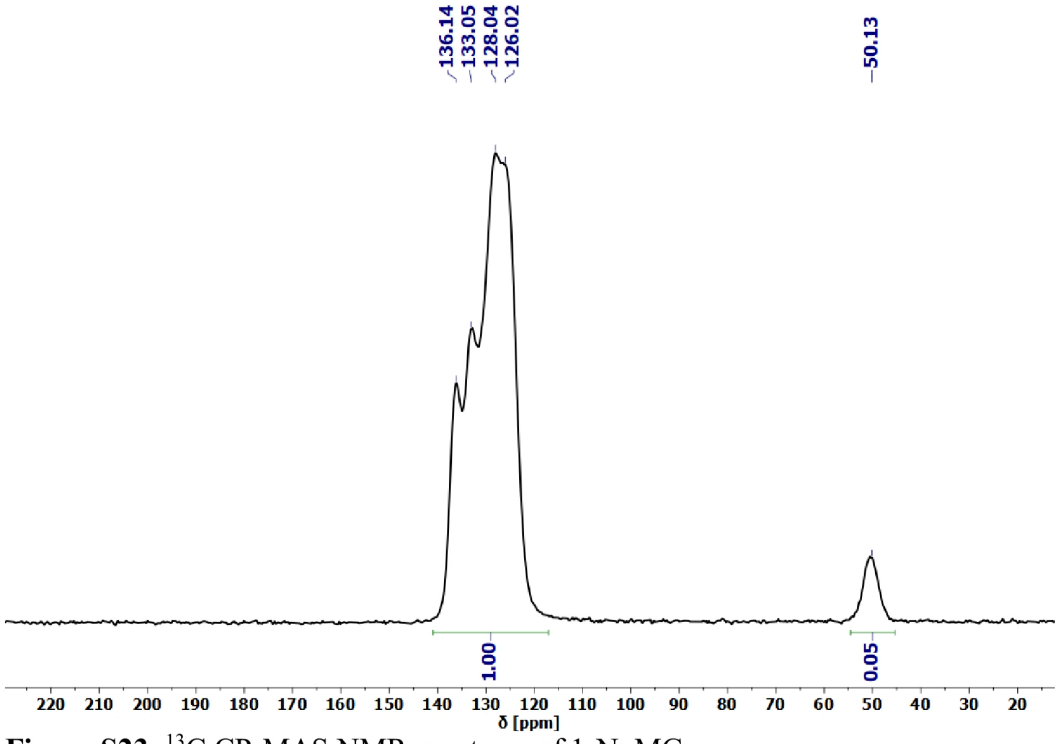

Figure S23. ^{13}C CP-MAS NMR spectrum of 1-NpMG$_T$.

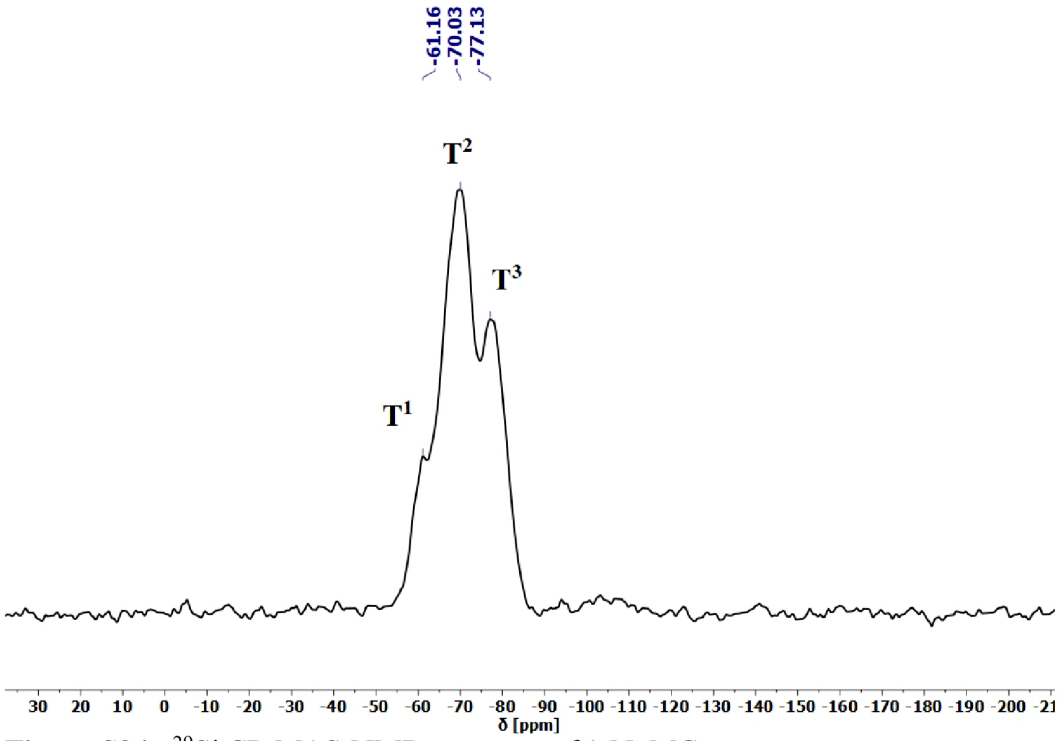

Figure S24. ^{29}Si CP-MAS-NMR spectrum of 1-NpMG$_T$.

Table S2. Ratio of condensation products T^2 and T^3, degree of condensation and ratio of OMe-, OH-groups of 1-NpMG$_{prec}$ and 1-NpMG$_T$

	T^1 [%]	T^2 [%]	T^3 [%]	DC [%]	OMe [%]	OH [%]
1-NpMG$_{prec}$	22	70	8	55	21	24
1-NpMG$_T$	15	54	31	67	14	19

FT-IR spectra

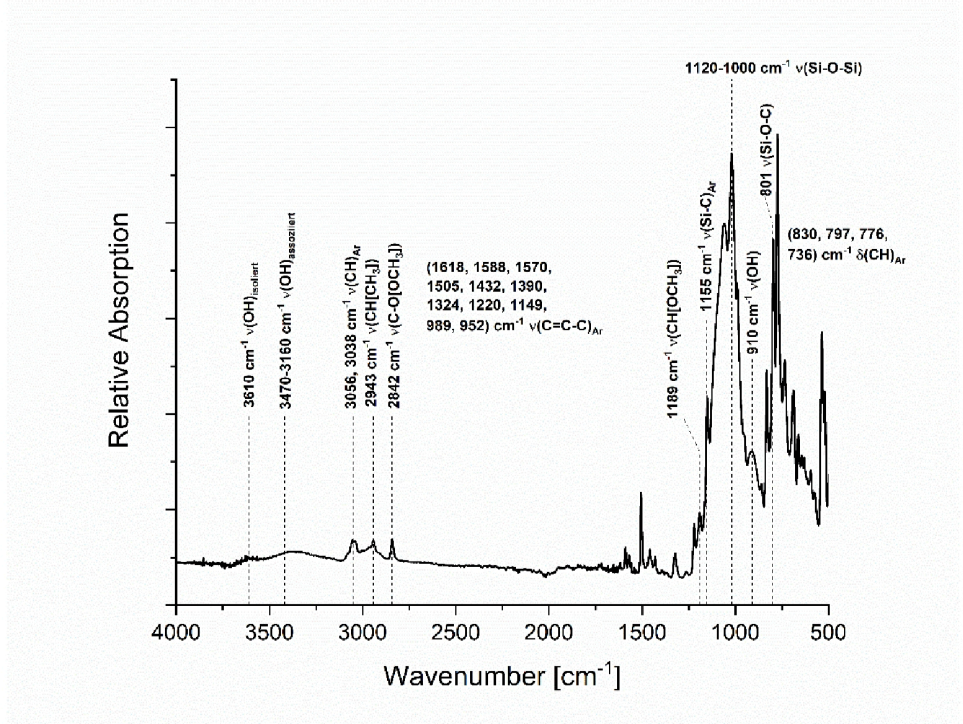

Figure S25. FT-IR spectrum of 1-NpMG$_{prec}$.

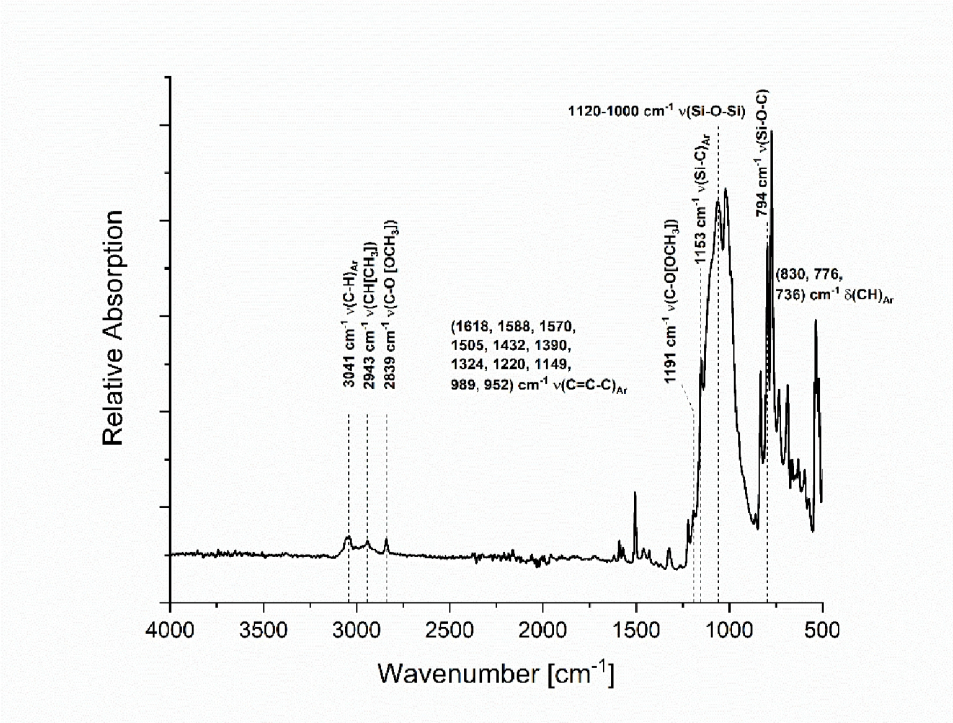

Figure S26. FT-IR spectrum of 1-NpMG$_T$.

XRD measurements

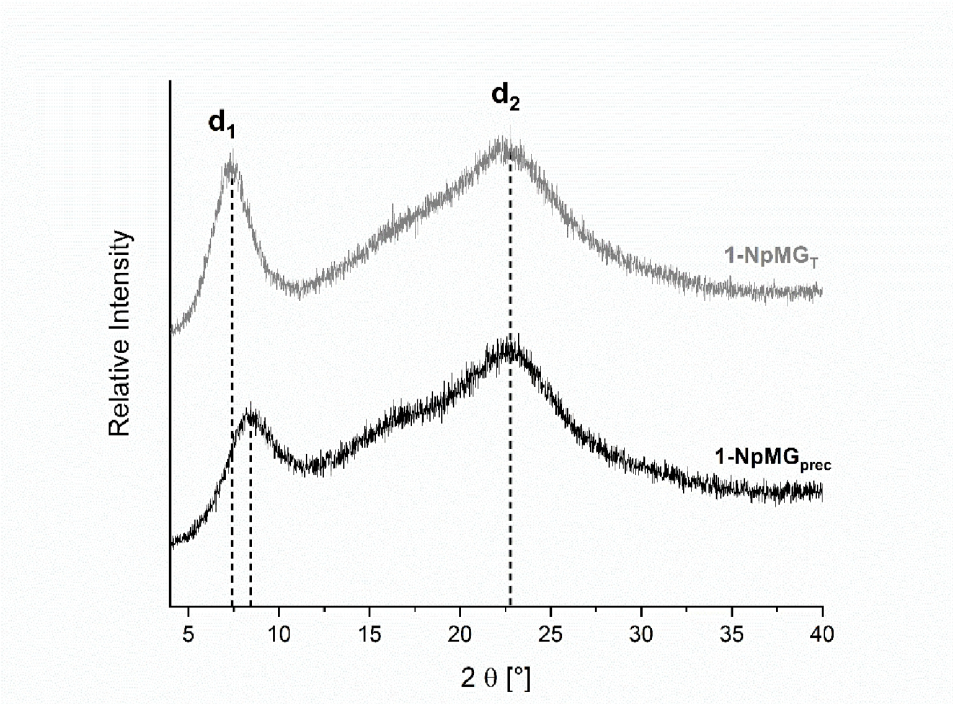

Figure S27. Powder X-ray diffraction pattern of 1-NpMG$_{prec}$ and 1-NpMG$_T$.

Table S3. XRD values and determined R values of 1-NpMG$_{prec}$ and 1-NpMG$_T$.

	1-NpMG$_{prec}$	1-NpMG$_T$
d_1 [nm]	1.07	1.20
d_2 [nm]	0.39	0.39
R	0.89	0.93

TG measurements

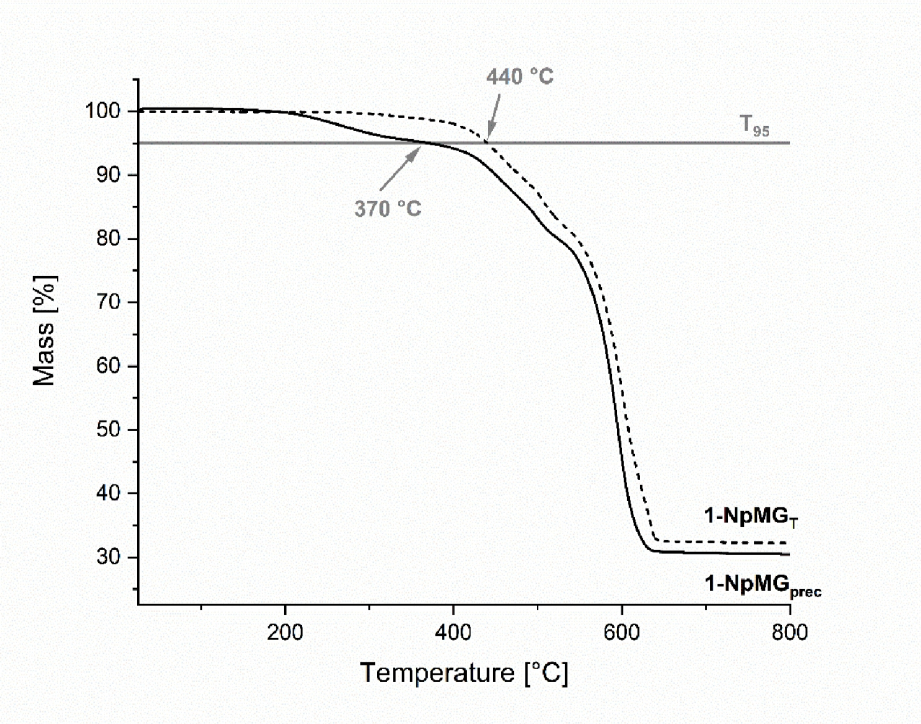

Figure S28. Thermogravimetric analysis of 1-NpMG$_{prec}$ and 1-NpMG$_T$.

DSC measurements

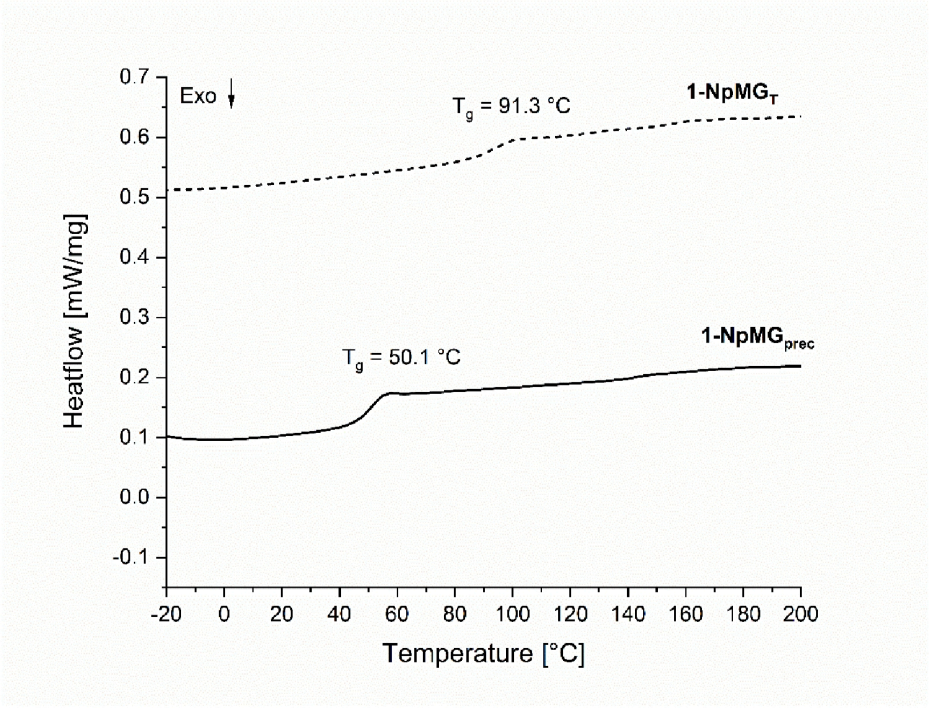

Figure S29. DSC measurements of 1-NpMG$_{prec}$ and 1-NpMG$_T$.

Supporting Information

Influence of alkyl groups on the formation of softenable polysilsesquioxanes

Svenja Pohl and Guido Kickelbick*

Saarland University, Inorganic Solid-State Chemistry, Campus, Building C4.1, 66123 Saarbrücken, Germany

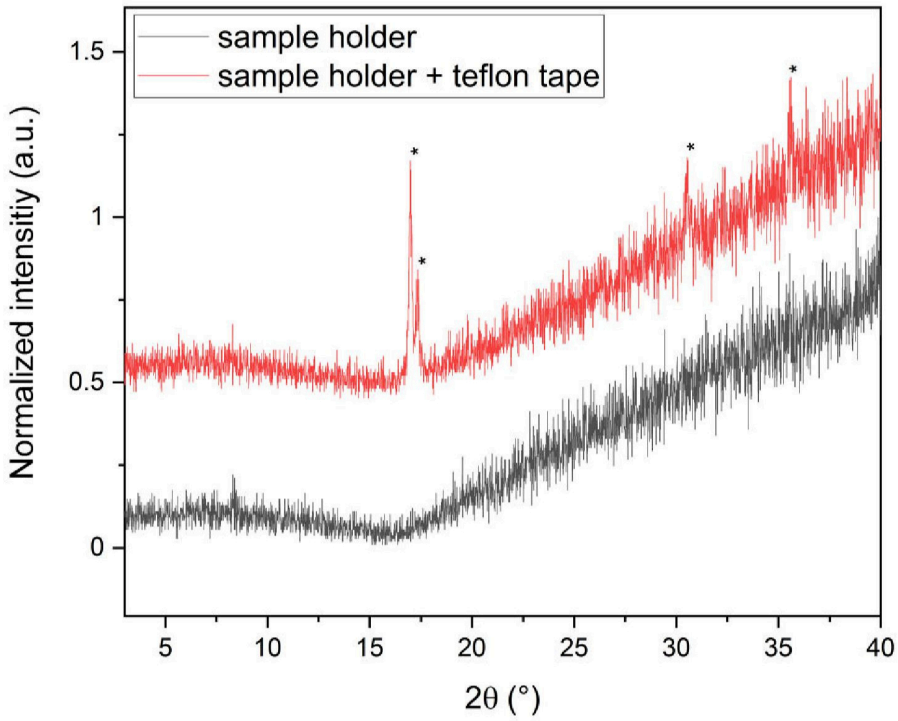

Figure S1. XRD measurement of the sample holder and the sample holder with teflon tape.

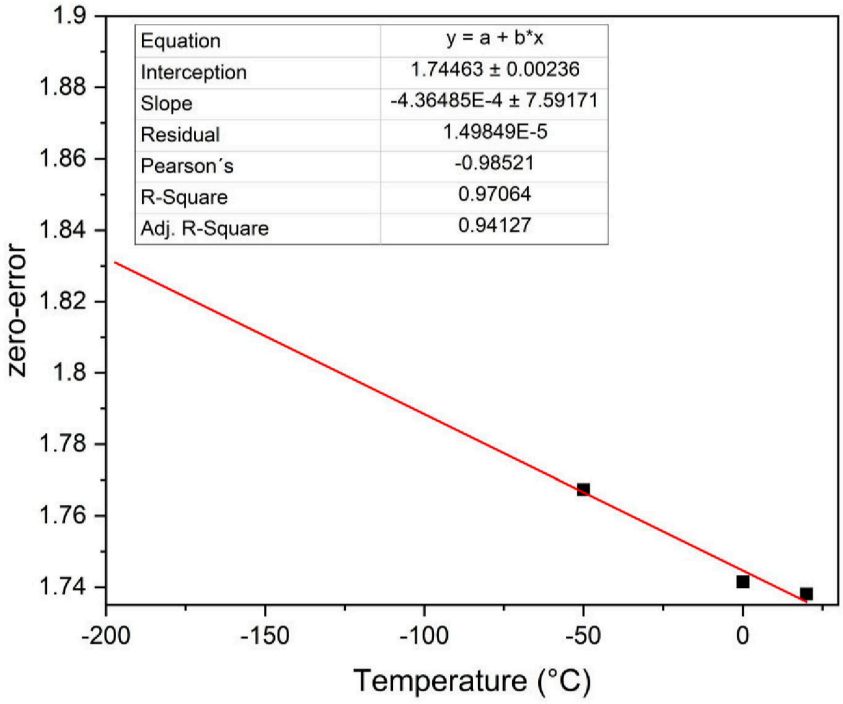

Figure S2. Determination of the zero-error by linear regression.

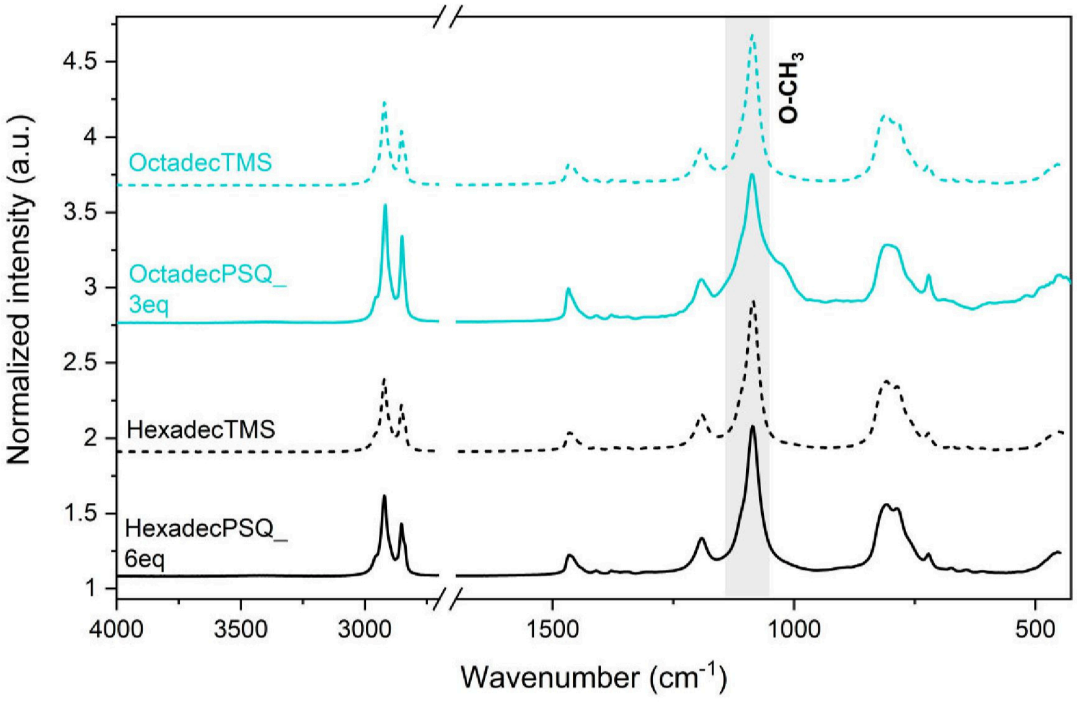

Figure S3. FTIR spectra of Octadec- and HexadecPSQ

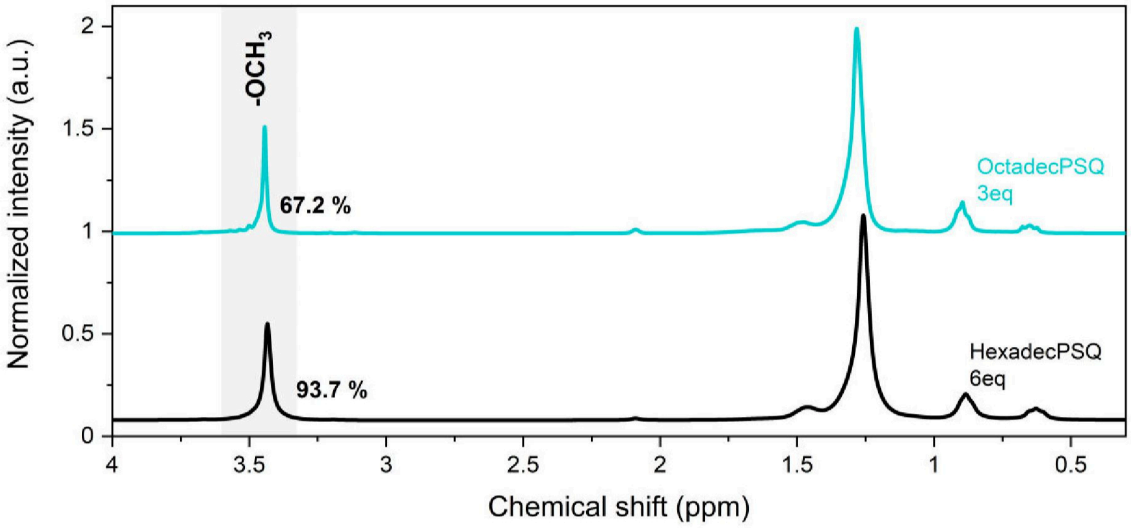

Figure S4. ^{1}H NMR of Octadec- and HexadecPSQ

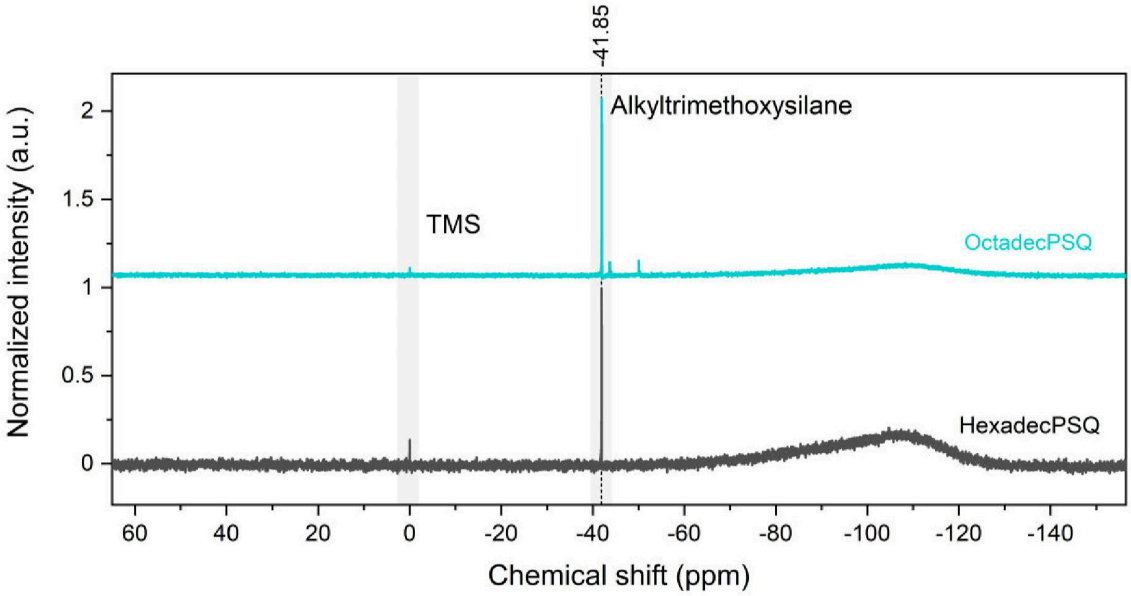

Figure S5. ^{29}Si NMR of Octadec- and HexadecPSQ

Table S1. Residual masses and T_{95} values of AlkylPSQ and AlkylPSQ$_T$ under N_2 and O_2 atmosphere, determined via TG measurements

Sample	$Mass_{min}$ [%]			T_{95} [°C]		
	AlkylPSQ N_2	AlkylPSQ$_T$ N_2	AlkylPSQ O_2	AlkylPSQ N_2	AlkylPSQ$_T$ N_2	AlkylPSQ O_2
MePSQ	87.9	90.8	86.4	604.8	721.7	451.0
EtPSQ	17.2	61.8	70.7	440.0	476.1	275.7
PrPSQ	28.8	38.1	60.7	356.2	424.6	255.9
HexPSQ	27.2	36.2	41.7	326.2	421.3	248.4
OctPSQ	28.0	28.8	36.1	448.6	445.7	299.4
DecPSQ	25.3	27.8	31.0	444.5	453.2	311.6
DodecPSQ	16.2	23.0	22.6	262.6	447.3	230.1

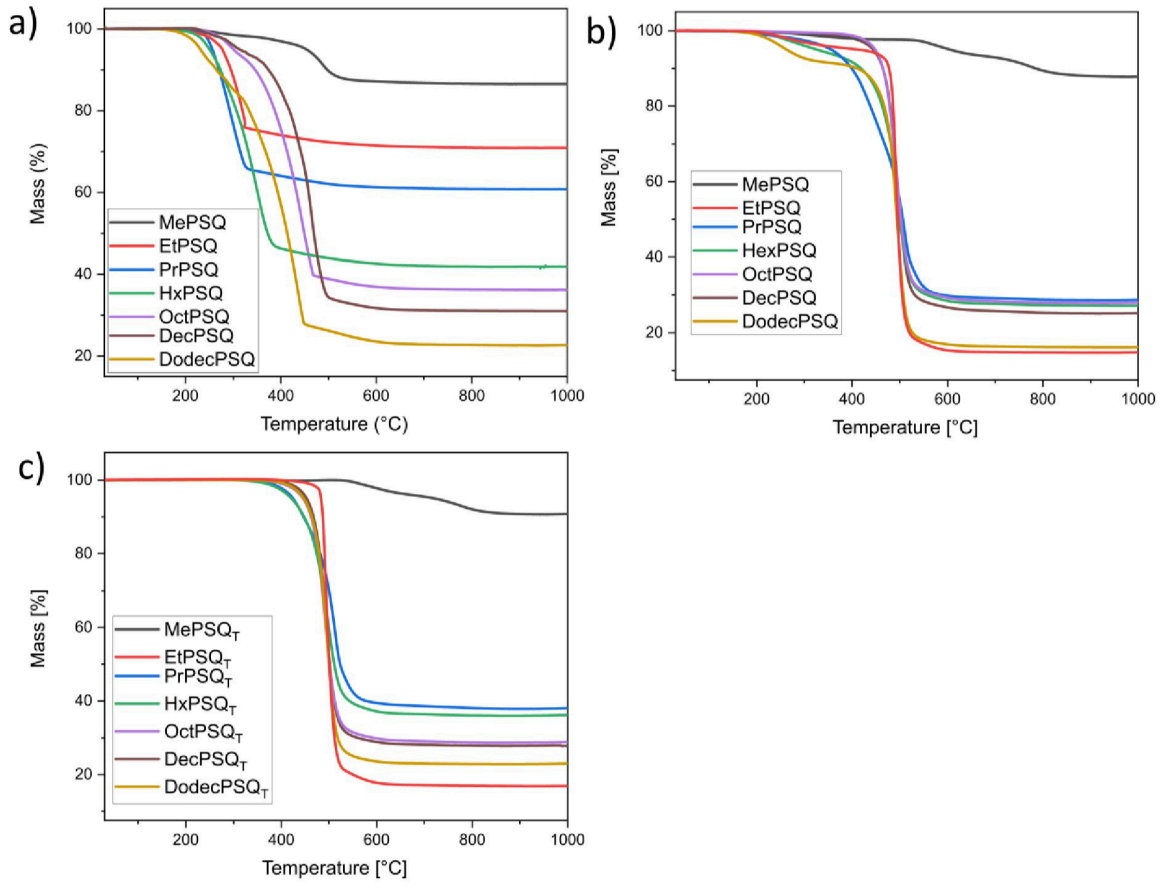

Figure S6. a) TGA of AlkylPSQ in O_2 atmosphere, b) TGA of AlkylPSQ in N_2 atmosphere, c) TGA of AlkylPSQ$_T$ in N_2 atmosphere

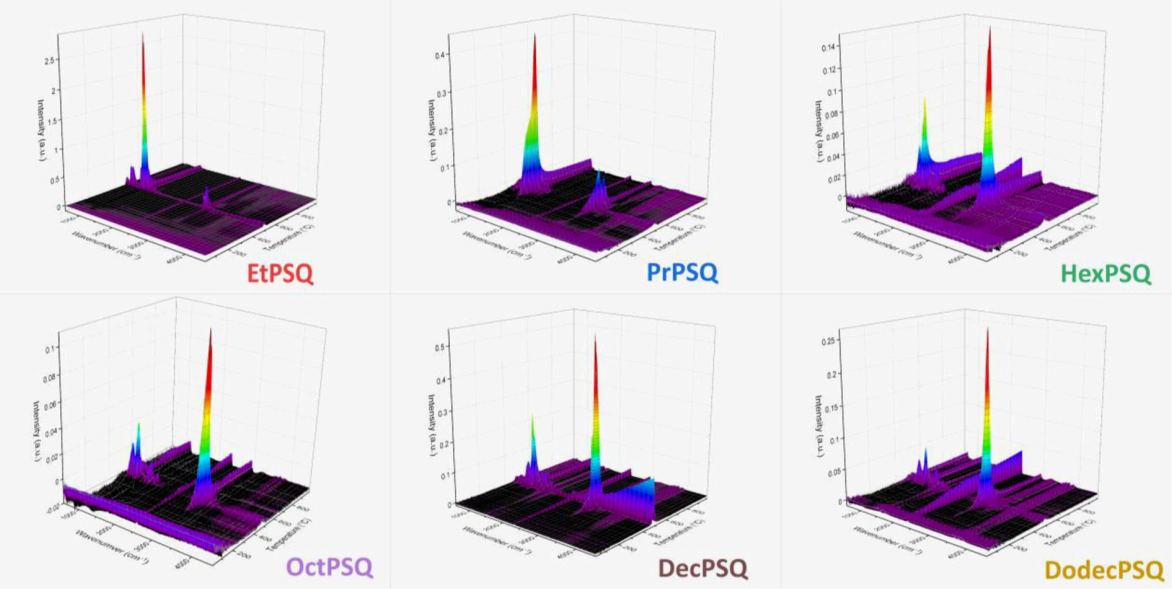

Figure S7.TG-FTIR 3D spectra of the AlkylPSQ.

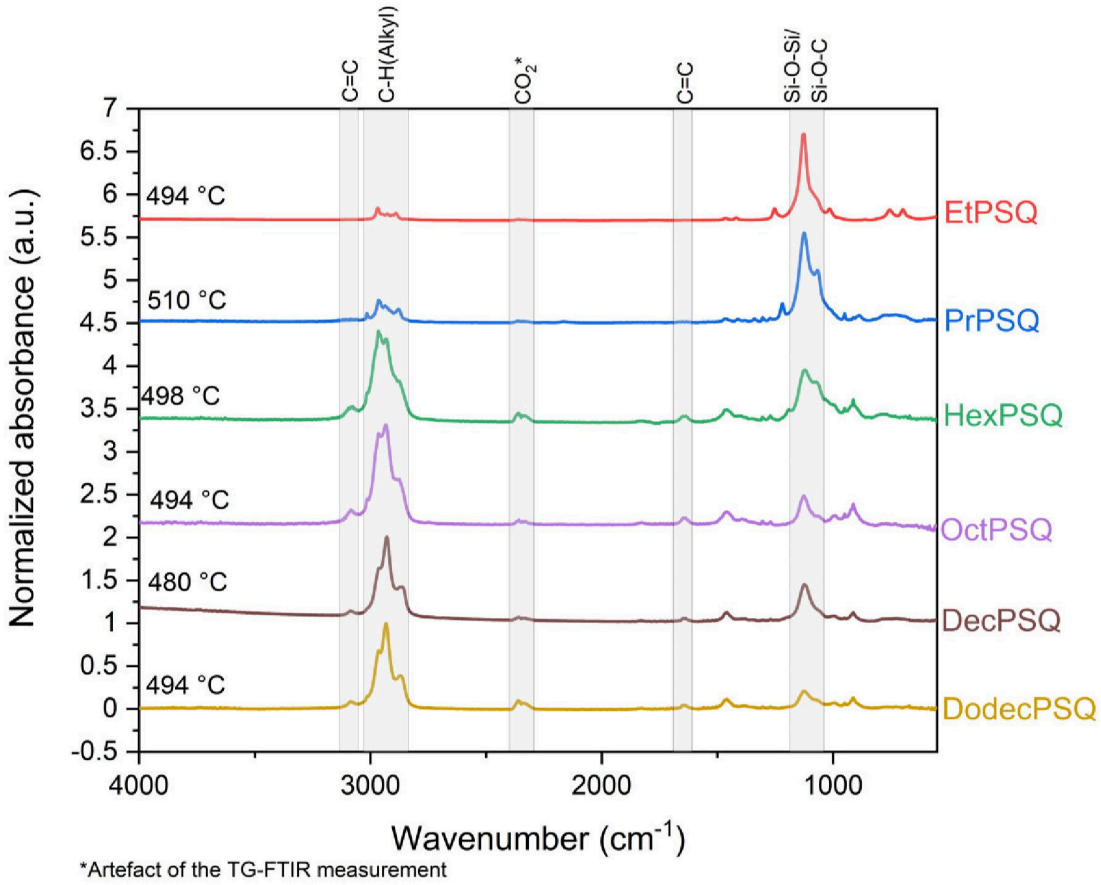

Figure S8. FTIR spectra of the degradation gases of AlkylPSQ at the temperature where the DTG of the TG has its minimum.

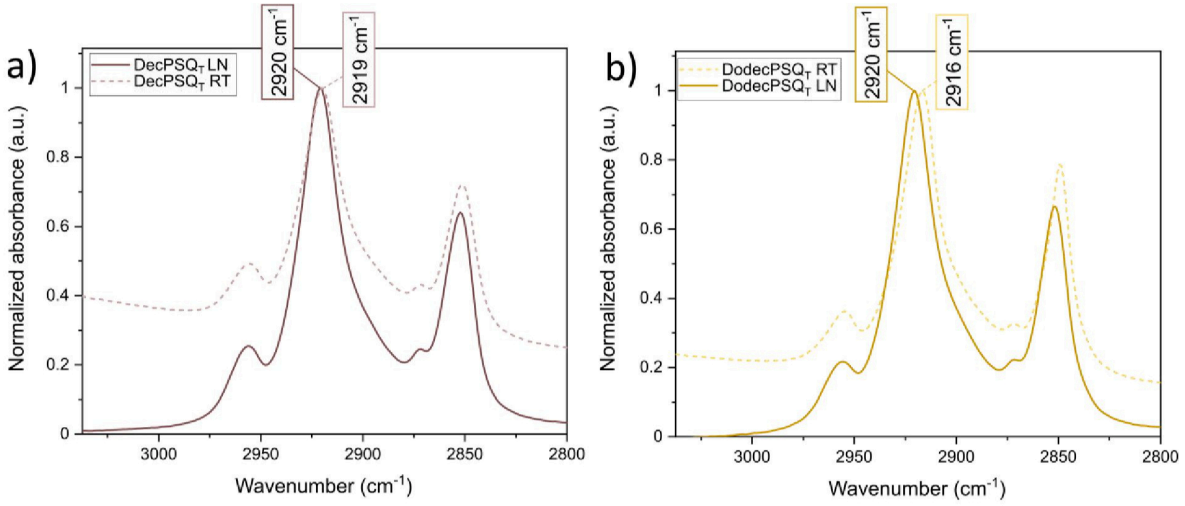

Figure S9. FTIR-spectra of the CH-region between 2800 und 3040 cm^{-1} of AlkylPSQ$_T$ and liquid N_2 cooled AlkylPSQ$_T$ with a) Decyl and b) Dodecyl as alkyl group.

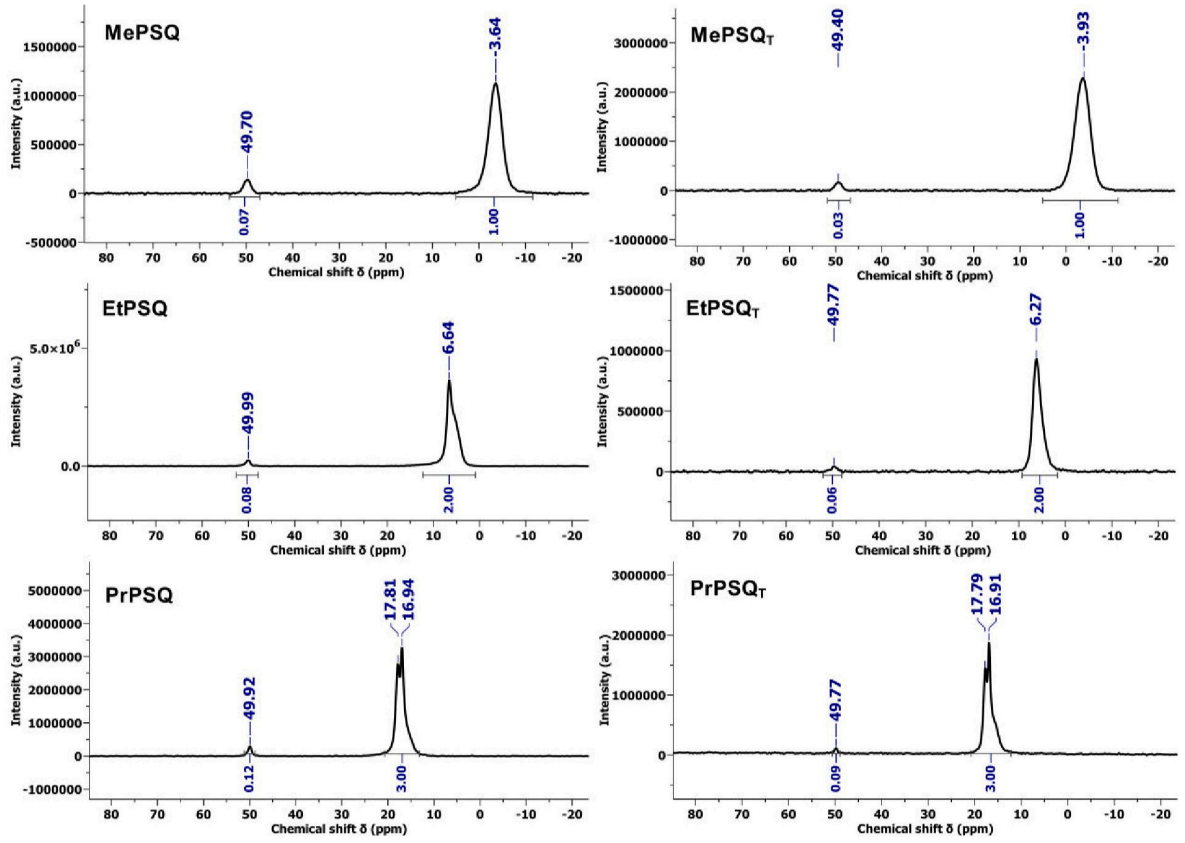

Figure S10. ^{13}C MAS NMR of AlkylPSQ and AlkylPSQ$_T$.

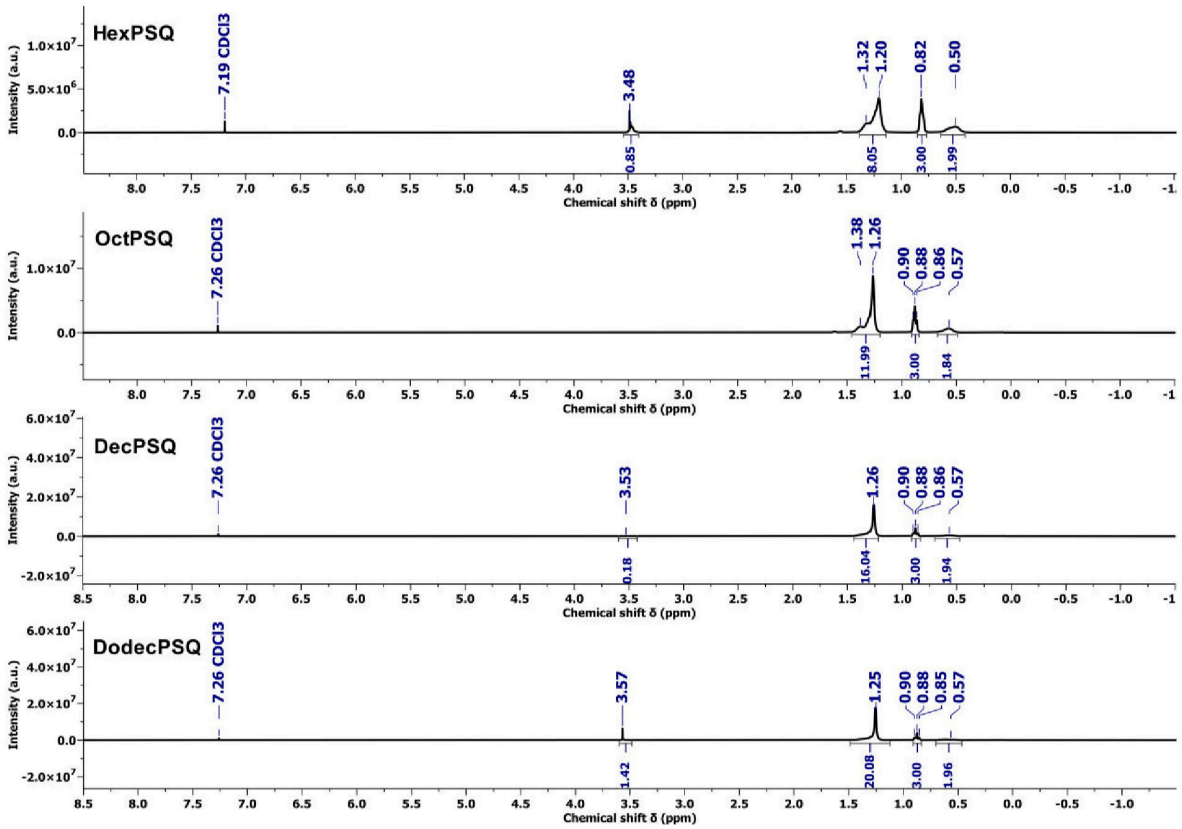

Figure S11. ^{1}H NMR of AlkylPSQ.

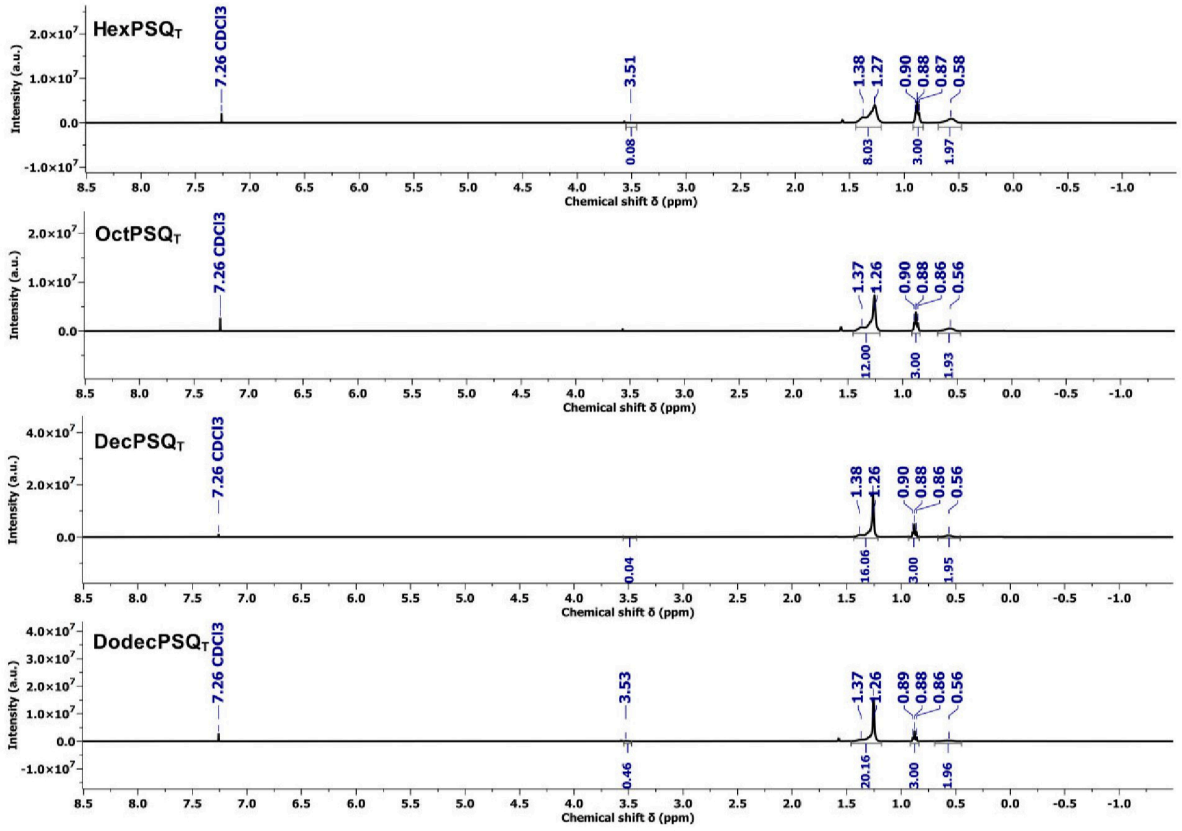

Figure S12. ^{1}H NMR of AlkylPSQ$_{T}$.

Table S2. M_w, M_n, M_z, and $Đ$ of AlkylPSQs, measured by SEC

Sample	M_w [g/mol]	M_n [g/mol]	M_z [g/mol]	Đ
HexPSQ	3172.9	1887.6	5075.1	1.68
$HexPSQ_T$	4425.1	2448.9	7149.2	1.81
OctPSQ	8153.7	4523.3	1322.6	1.8
$OctPSQ_T$	5905.2	3393.5	8684.1	1.74
DecPSQ	11849	7629.6	18658	1.55
$DecPSQ_T$	6867.6	4283.3	9629.6	1.6
DodecPSQ	10592	6959.2	24789	1.52
$DodecPSQ_T$	6366.3	5049.6	7952.5	1.26

Supporting Information

Impact of Size and Substitution Isomerism in Polycyclic Aromatic-Substituted Trialkoxysilanes on the Formation of Softenable Polysilsesquioxanes

Svenja Pohl[a], Markus Gallei[b], [c] and Guido Kickelbick[a], [c]*

[a] Inorganic Solid-State Chemistry, Saarland University, Campus, Building C4 1, 66123 Saarbrücken, Germany

[b] Polymer Chemistry, Saarland University, Campus, Building C4 2, 66123 Saarbrücken, Germany

[c] Saarene, Saarland Center for Energy Materials and Sustainability, Saarbrücken 66123, Germany

Table of Contents

1. Experimental section

1.1 Materials

2-Bromnaphthalene (Chempur, 98%), 9-bromphenanthrene (Chempur, 97%), 1-bromnaphthalene (abcr GmbH, 97%), tetramethoxysilane (abcr GmbH, 98%), magnesium chips (99.9%, Acros Organics), *n*-hexane (BCD Chemie GmbH, for synthesis), acetone (BCD Chemie GmbH, 97 %), dichloromethane (DCM) (Fisher Scientific GmbH, 99 %), tetrahydrofuran (THF) (Fisher Scientific GmbH, 99.5 %), dimethyl sulfoxide (DMSO) (Fisher Scientific GmbH, 99.5 %), chloroform-*d* + Ag (Deutero GmbH, 99.8%), DMSO-d_6 (Deutero GmbH, 99.8%) were used as received. THF for synthesis (Fisher Chemical, 99.8% HPLC grade) was purified in an SPS-5 solvent purification system (MBraun, Garching, Germany). Hydrochloric acid (HCl) (Fisher Scientific GmbH, 37%) was diluted to pH = 2.5 with demineralized water.

1.2 Instrumentation

Differential scanning calorimetry (DSC) was performed with a DSC 204 F1 Phoenix calorimeter (NETZSCH-Gerätebau GmbH, Selb, Germany) using aluminum crucibles with pierced lids under nitrogen (100 mL/min) applying a heating rate of 10 K/min and a cooling rate of 15 K/min in the temperature range between 0 and 250 °C. The value of the T_g was taken by determining the inflection point of the glass event.

Solution nuclear magnetic resonance (NMR) spectra were recorded on an Avance III HD 400 MHz spectrometer (Bruker, Billerica, USA) with 400.13 MHz for ^{1}H NMR spectra, 100.61 MHz for ^{13}C NMR spectra and 79.49 MHz for ^{29}Si NMR spectra. NMR samples were prepared in $CDCl_3$ and DMSO-d_6. Spectra were analyzed using MestReNova.[1]

Single-pulse (SP) magic angle spinning (MAS) and cross-polarization (CP) MAS NMR spectra were recorded on an Avance III HD – Ascend 400WB spectrometer (Bruker, Billerica, USA) using 4 mm inner diameter ZrO_2 rotors with 13 kHz rotation frequency. The resonance frequencies were 79.53 MHz for ^{29}Si NMR spectra and 100.65 MHz for ^{13}C NMR spectra. The measurements were performed with a relaxation of 20 s for SP-MAS spectra and 4 s and 3 s für ^{29}Si and ^{13}C CP-MAS spectra. Adamantane was used for ^{13}C NMR and octakis(trimethylsiloxy)silsesquioxane for ^{29}Si NMR as external standard. Peaks of ^{29}Si CP-MAS spectra were deconvoluted and integrated with OriginPro.[2]

Size exclusions chromatography (SEC) measurements were performed with a PSS SECcurity2 system composed of a 1260 IsoPump-G7110B (Agilent Technologies, Santa Clara,

CA), a 1260 VW-detector G7162A at 290 nm (Agilent Technologies, Santa Clara, CA), and a 1260 RI detector G7114A at 30 °C (Agilent Technologies, Santa Clara, CA), with THF as the mobile phase (flow rate 1 mL/min) on an SDV column set (SDV 10^3, SDV 10^5, SDV 10^6) from PSS (Polymer Standard Service, Mainz, Germany). Calibration was carried out using polystyrene (PS) standards (from PSS). For data acquisition and evaluation of the measurements, PSS WinGPC® UniChrom was used.[3]

For **Matrix-assisted laser desorption/ionization time-of-flight mass spectrometry (MALDI-ToF MS)** measurements, MALDI targets were prepared in the dried-droplet method. 1 mL of GC-grade THF (from Sigma-Aldrich) were added to 10 mg of each sample, resulting in the sample solution. A mixture of PMMA standards (Agilent Technologies) was used for the calibration spots, namely 1260 Da, 3040 Da and 5440 Da (each 10 mg in THF). Na salt solution was prepared by adding 13.6 mg NaTFA to 1 mL of HPLC-MS-grade water (Merck). An Ag salt solution was prepared by adding 22 mg NaTFA to 1 mL of GC-grade THF (from Sigma-Aldrich).

20 µL of the MALDI matrix solution containing DCTB (Sigma-Aldrich) at a concentration of 20 mg mL^{-1} in GC-grade THF (Sigma Aldrich) was added to 3 µL of sample solution and 1 µL of the salt solution and mixed with an Eppendorf pipette. PMMA standards were prepared with NaTFA, the samples with AgTFA (and without any salt). 1 µL of the mixed matrix/sample solution was spotted over three MALDI spots of a Polished Steel 384 MALDI MTP target. The drops were then dried at room temperature, and the MALDI target was inserted in the source chamber of an Autoflex Speed II (Bruker Daltonics, Bremen, Germany). All MALDI-ToF analyses were performed in both linear positive (LP) mode and reflectron positive (RP) modes. For RP, the equipment parameters were as follows: voltage values of ion sources #1 and #2 set as 19.00 and 16.60 keV, respectively; voltage values of reflectron #1 and #2 set as 21.00 and 9.60 keV, respectively; lens tension 8.15 keV; pulsed extraction 130 ns. For LP, the equipment parameters were as follows: voltage values of ion sources #1 and #2 set as 19.00 and 18.25 keV, respectively; lens tension 7.15 keV; pulsed extraction 350 ns. Mass spectra of the sample were first visualized using FlexAnalysis software (version 3.4; Bruker Daltonics, Billerica, MA, USA).[4]

Attenuated total reflectance Fourier transform infrared (ATR-FTIR) spectra were recorded on a Vertex 70 spectrometer (Bruker Optics, Billerica, USA) in total reflectance mode from 400 - 4500 cm^{-1} with a resolution of 4 cm^{-1} and 16 scans.

UV-VIS measurements were performed on a Lambda 750 instrument (Perkin Elmer Inc., Shelton, USA) equipped with a 100 mm integration sphere with a 2 nm increment and 0.2 s

integration time. Absorbance of monomers and polymers was measured in a quartz glass cuvette with 1 cm thickness, diluted in DCM from 250 to 400 nm. Transmission spectra of free-standing polymer lenses with 1.6 mm thickness were recorded from 250 to 800 nm. The lenses were produced by molding the non-consolidated gels into round silicone molds with a diameter of 1.9 cm and thickness of 1.6 mm. Trapped bubbles were removed in a vacuum at 110 °C. For consolidation, the lenses were treated in their molds at 200 °C for 24 hours.

Refractive indices (RI) were measured as a dilution series in THF on an Abbemat 350 (Anton-Paar OptoTec GmbH, Seelze-Letter, Germany) at a wavelength of 589 nm and 20 °C.

Thermogravimetric analysis (TGA) was carried out using a TG F1 Iris (NETZSCH-Gerätebau GmbH, Selb, Germany), applying a heating rate of 10 K/min between 30 and 1000 °C under synthetic air flow (40 mL/min, N_2/O_2 75%:25%).

TG-FTIR measurements were performed using Vertex 70 spectrometer (Bruker Optics, Ettlingen, Germany) coupled to a TG F1 Iris (NETZSCH-Gerätebau GmbH, Selb, Germany). Each FTIR spectrum was performed in the wavenumber range 550–4500 cm^{-1} and by averaging 16 scans with a spectral resolution of 4 cm^{-1}. The measurements were carried out at 10 K/min heating rate in the temperature range between 30 and 1000 °C under synthetic air flow (40 mL/min, N_2/O_2 75%:25%).

Fluorescence spectroscopy was performed applying a FluoroMax 4 Spectrofluorometer (Horiba Scientific, Kyoto, Japan) with an excitation wavelength of 285 nm as solid in a glass tube with a diameter of 2 mm or as solution in DCM in a quartz glass cuvette with 1 cm thickness from 295 to 550 nm. A Peltier-based temperature-controlled cuvette holder QNW Luma 40 (Quantum Northwest, Inc., WA, USA) was used for temperature-dependent fluorescence measurements. The fluorescence spectrum was measured with the settings described above from 25 to 105 °C, in 10 °C steps with DMSO as solvent.

Powder X-ray diffraction (PXRD) patterns of the pulverized samples were recorded at room temperature on a D8-A25-Advance diffractometer (Bruker AXS, Karlsruhe, Germany) in Bragg-Brentano θ-θ-geometry (goniometer radius 280 mm) with non-monochromatic Cu K_α radiation (λ = 154.0596 pm). A 12 µm Ni foil working as K_β filter and a variable divergence slit were mounted at the primary beam side. A Lynxeye detector with 192 channels and a variable anti-scatter slit in front of it was used at the secondary beam side. Experiments were carried out in a 2θ range of 3 to 40° with a step size of 0.013° and a total scan time of 1 h. The recorded data was evaluated using the TOPAS 5.0 software.[5] The observed reflections were fitted as independent single peaks. For the evaluation, the relation $R(I)$ of the intensities of the maxima of the two reflections d_1 and d_2 were compared as described by Liu et al.[6]

1.3 Monomer synthesis

The aryltrimethoxysilanes were synthesized according to a modified literature procedure (NMR spectra can be found in Figure S1–S3).[7]

1-Naphthyltrimethoxysilane (1-NpSi(OMe)$_3$). Magnesium chips (3.70 g, 0.152 mol, 1.5 eq.), tetramethoxysilane (46.35 g, 0.304 mol, 3 eq.) and absolute THF (160 mL) were stirred in a three-neck round bottom flask at 30 °C under an argon atmosphere. 1-Bromnaphthalene (20.72 g, 0.100 mol, 1 eq.) was added dropwise over a period of 20 minutes at 30 °C with a dropping funnel. The reaction mixture was heated to 50 °C for 1 h, then the temperature was raised further to 75 °C for 1 h, and finally allowed to cool to room temperature overnight. Magnesium and THF were removed from the reaction mixture by filtration and concentration. Afterwards, 250 mL *n*-hexane were added to the residue, boiled 10 minutes under reflux conditions, and filtered after cooling to room temperature. The procedure was repeated a second time using 125 mL *n*-hexane. The solvent of the combined filtrates was removed, and the product was distilled ($2 \cdot 10^{-2}$ mbar, 140 °C) resulting in a transparent liquid (yield: 19.32 g, 78 %).

2-Naphthyltrimethoxysilane (2-NpSi(OMe)$_3$). 2-NpSi(OMe)$_3$ was synthesized in the same synthesis procedure as 1-NpSi(OMe)$_3$, yielded 63 % of a transparent liquid.

9-Phenanthrenyltrimethoxysilane (9-PhenSi(OMe)$_3$). 9-PhenSi(OMe)$_3$ was synthesized in the same synthesis procedure as 1-NpSi(OMe)$_3$. Distillation (6×10^{-3} mbar, 200 °C) yielded 35.2 % of a white solid.

2. Monomer NMR spectra

2.1 1-Naphthyltrimethoxysilane

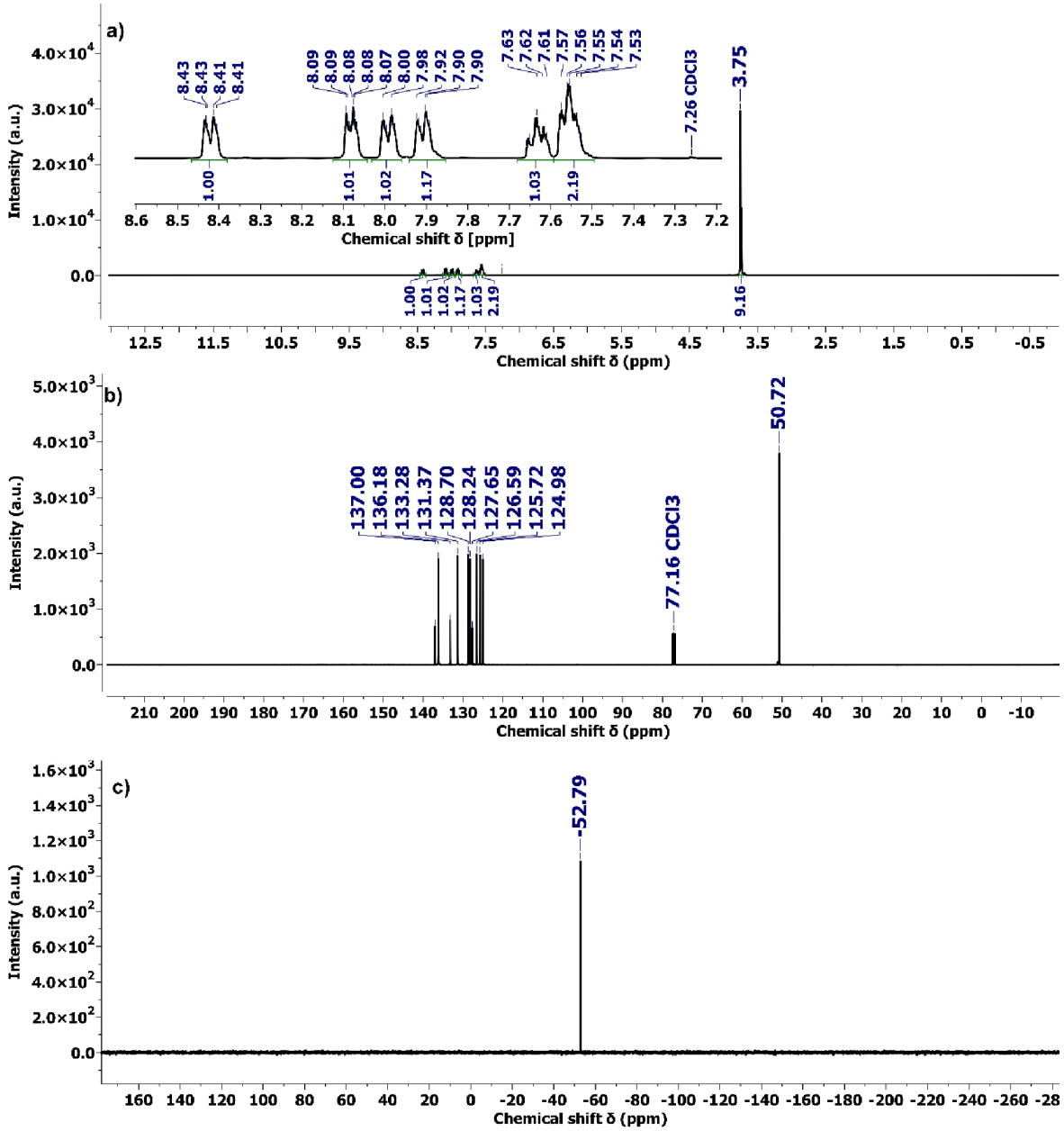

Figure S1: *NMR spectra of 1-NpSi(OCH$_3$)$_3$ in CDCl$_3$, a) ^{1}H NMR, b) ^{13}C NMR and c) ^{29}Si NMR.*

^{1}H NMR (300 MHz, $CDCl_3$): δ = 8.43–8.29 (m, 1H, 1-Np), 7.99–7.94 (m, 2H, 1-Np), 7.89 - 7.86 (m, 1H, 1-Np), 7.59–7.48 (m, 3H, 1-Np), 3.68 (s, 9H, O-CH_3) ppm.

^{13}C NMR (75 MHz, $CDCl_3$): δ = 50.72 (O-CH_3), 124.98, 125.72, 126.59, 127.65, 128.24, 128.70, 131.37, 133.28, 136.18, 137.00 (1-Np) ppm.

^{29}Si NMR (60 MHz, CDCl3): δ = -52.79 ppm.

2.2 2-Naphthyltrimethoxysilane

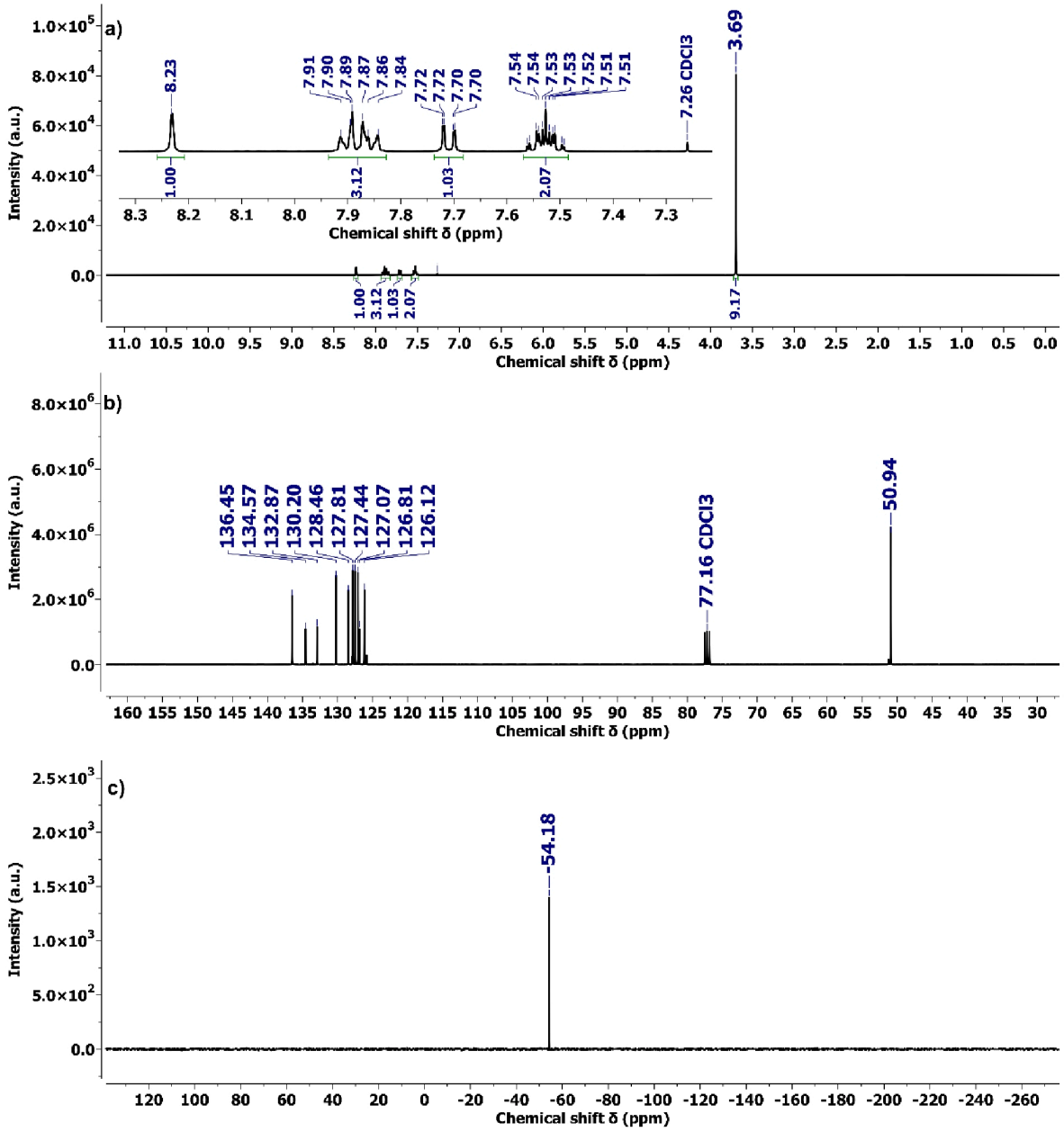

Figure S2: *NMR spectra of 2-NpSi(OCH₃)₃ in CDCl₃, a) ^{1}H NMR, b) ^{13}C NMR and c) ^{29}Si NMR.*

^{1}H NMR (400 MHz, CDCl₃): δ = 8.23 (s, 1H, Np), 7.92–7.84 (m, 3H, 2-Np), 7.72–7.70 (m, 1H, Np), 7.56–7.49 (m, 2H, Np), 3.69 (s, 9H, O-CH₃) ppm.

^{13}C NMR (100 MHz, CDCl₃): δ = 50.94 (O-CH₃), 126.12, 126.81, 127.07, 127.44, 127.81, 128.46, 130.20, 132.87, 134.57, 136.45 (1-Np) ppm

^{29}Si NMR (80 MHz, CDCl₃): δ = -54.18 ppm

2.3 9-Phenanthrenyltrimethoxysilane

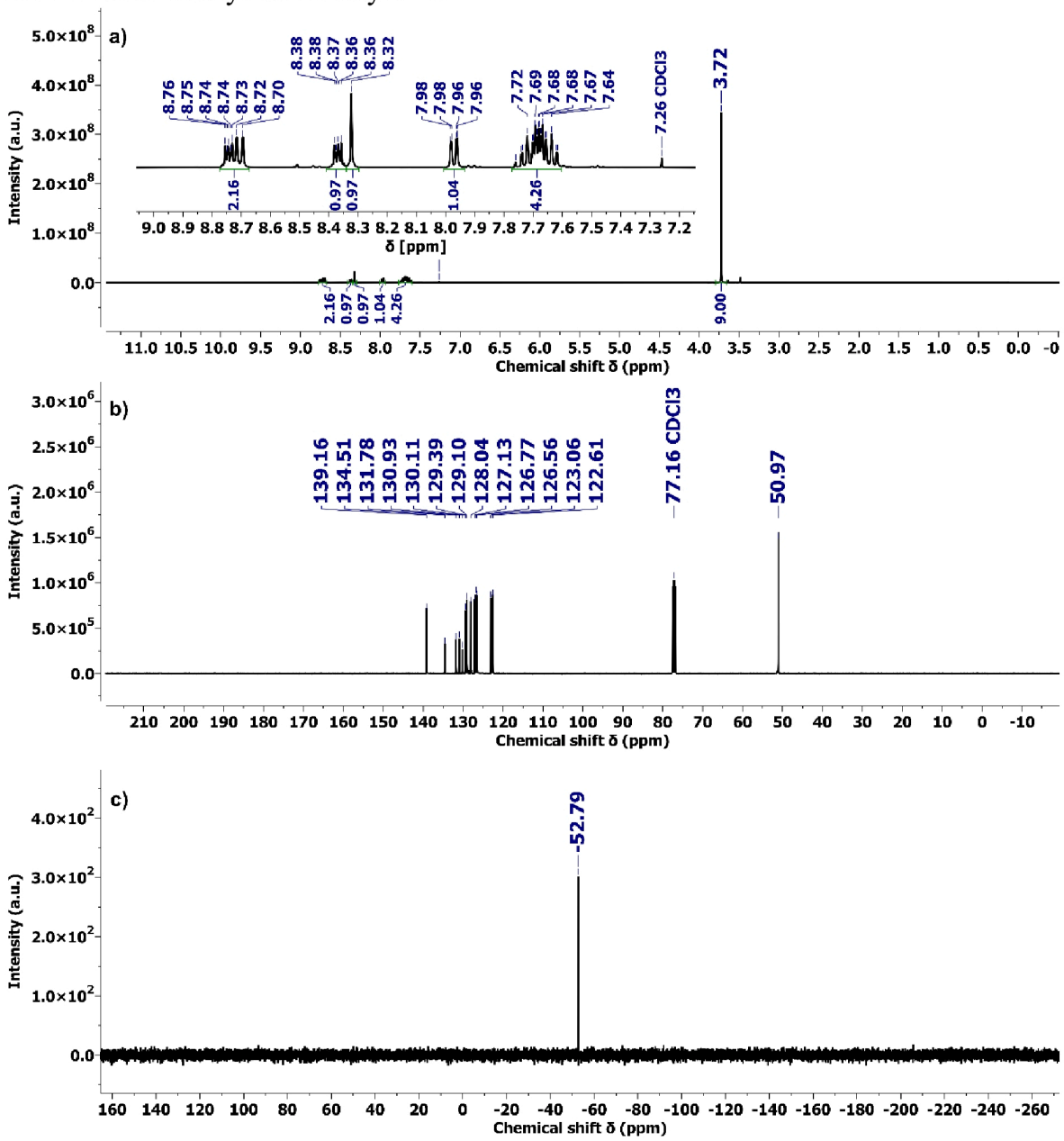

Figure S3: *NMR spectra of 9-PhenSi(OCH$_3$)$_3$ in CDCl$_3$, a) ^{1}H NMR, b) ^{13}C NMR and c) ^{29}Si NMR.*

^{1}H NMR (400 MHz, CDCl$_3$): δ = 8.76–8.70 (m, 2H, Phen), 8.38–8.36 (m, 1H, Phen), 8.32 (s, 1H, Phen), 7.98–7.96 (m, 1H, Phen), 7.76 - 7.62 (m, 4H, Phen), 3.72 (s, 9H, O-CH$_3$) ppm.

^{13}C NMR (100 MHz, CDCl$_3$): δ = 50.97 (O-CH$_3$), 122.61, 123.06, 126.56, 126.77, 127.13, 128,04, 129.10, 129.39, 130.11, 130.93, 131.78, 134.51, 139.16 (Phen)

^{29}Si NMR (80 MHz, CDCl$_3$): δ = -52.79

3. Intermediates during melting gel synthesis

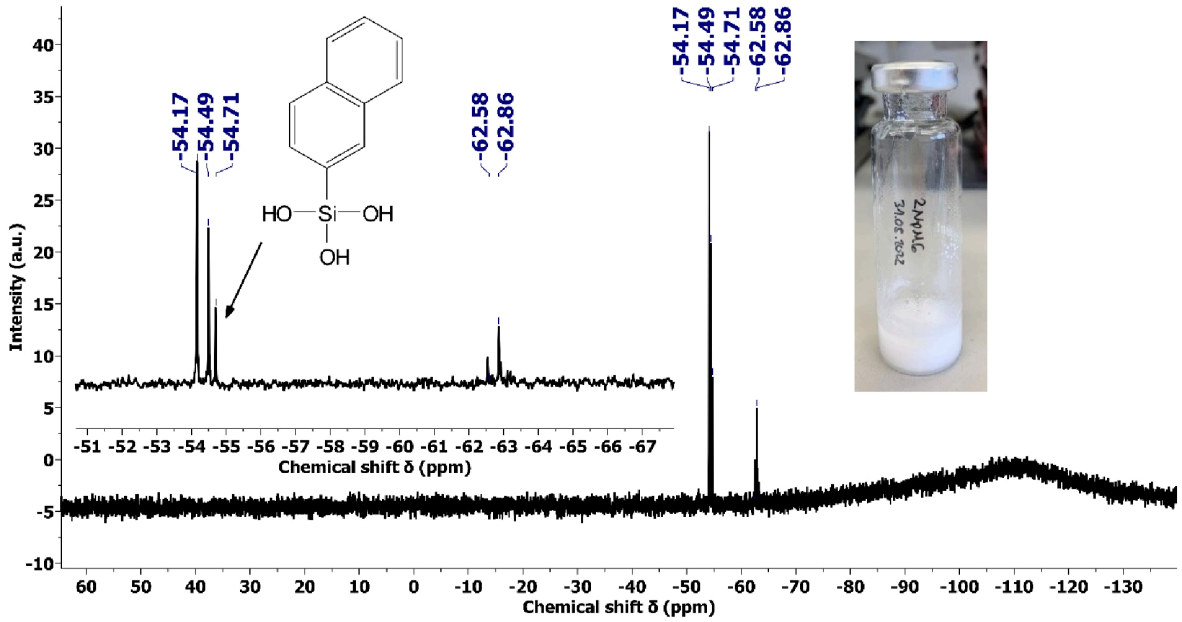

Figure S4: *^{29}Si NMR spectrum of the reaction solution during the reaction of 2-NpSi(OCH$_3$)$_3$ with aqueous acid after 2 h, showing the formation of a white solid (reaction solution shown in the added picture) in DMSO-d$_6$.*

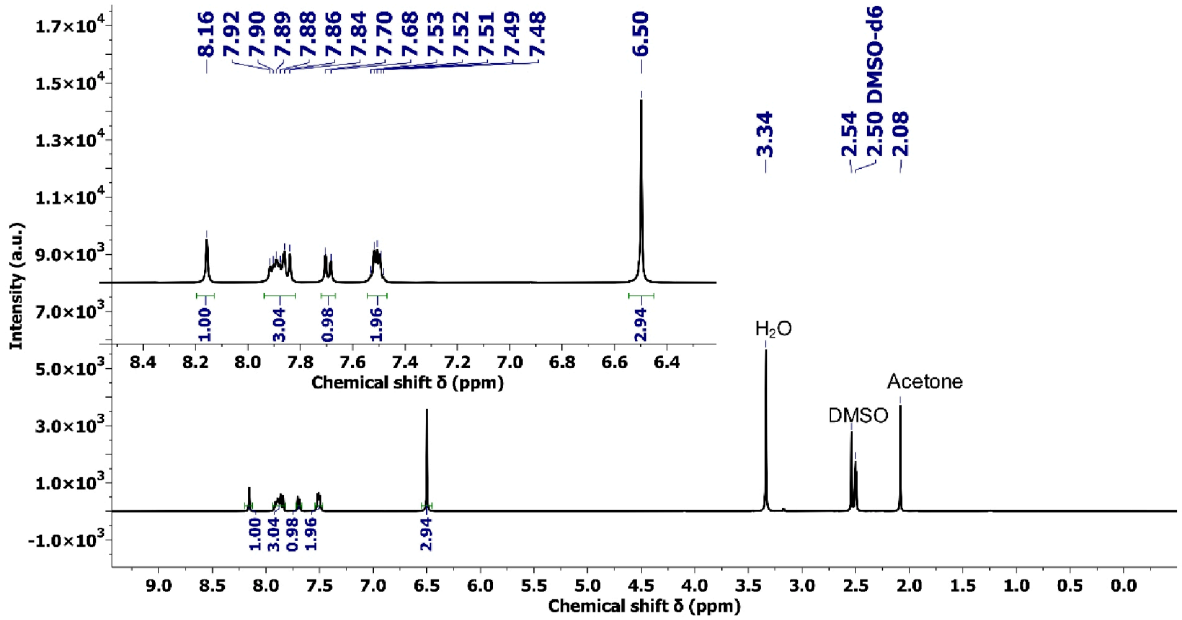

Figure S5: *^{1}H NMR spectrum of the isolated white solid from the reaction solution, washed with acetone, in DMSO-d$_6$.*

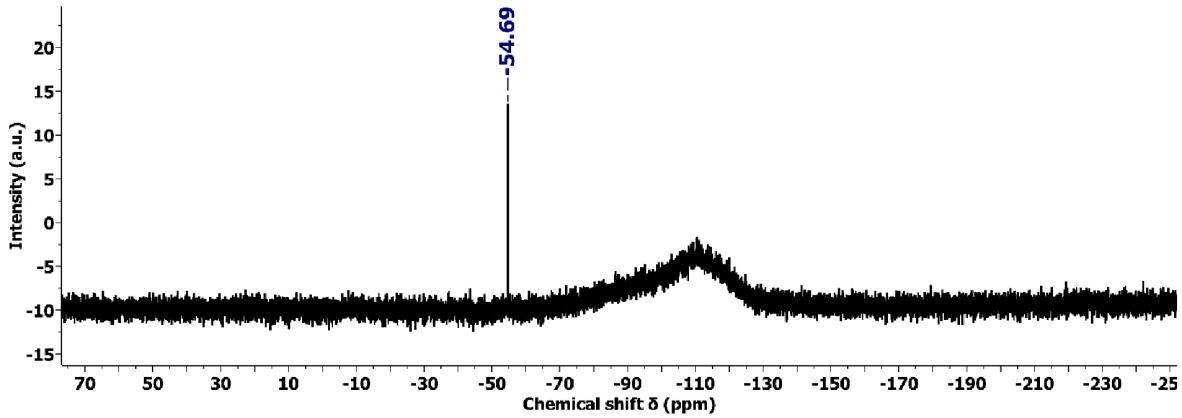

Figure S6: *^{29}Si NMR spectrum of the isolated white solid from the reaction solution, washed with acetone, in DMSO-d_6.*

2-NpSi(OH)$_3$

^{1}H NMR (400 MHz, DMSO-d_6): δ = 8.16 (s, 1H, 2-Np), 7.92–7.84 (m, 3H, 2-Np), 7.69 (dd, J = 8.1, 1.1 Hz, 1H, 2-Np), 7.52–7.48 (m, 2H, 2-Np), 6.50 (s, 3H, OH) ppm.

^{29}Si NMR (79,5 MHz, DMSO-d_6): δ = -54.69 ppm.

4. Melting gel characterization

4.1 UV-VIS spectroscopy

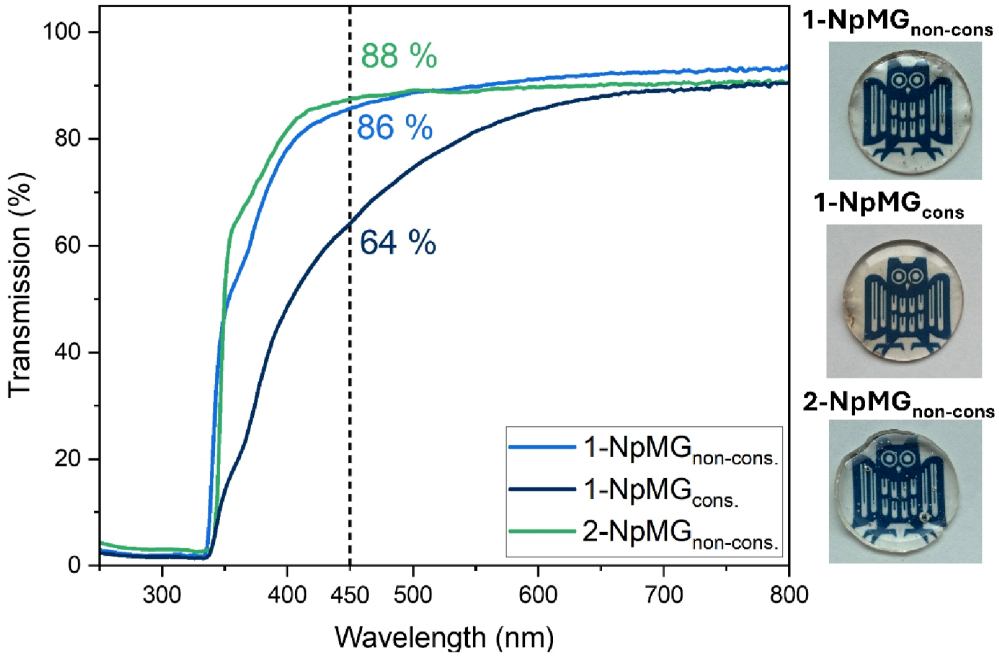

Figure S7: *UV-VIS spectra of lenses with a thickness of 1.6 mm, made from 1-NpMG$_{non\text{-}cons.}$, 1-NpMG$_{cons.}$, and 2-NpMG$_{non\text{-}cons.}$, shown on the right side, with the transmission at 450 nm highlighted.*

4.2 Refractive index

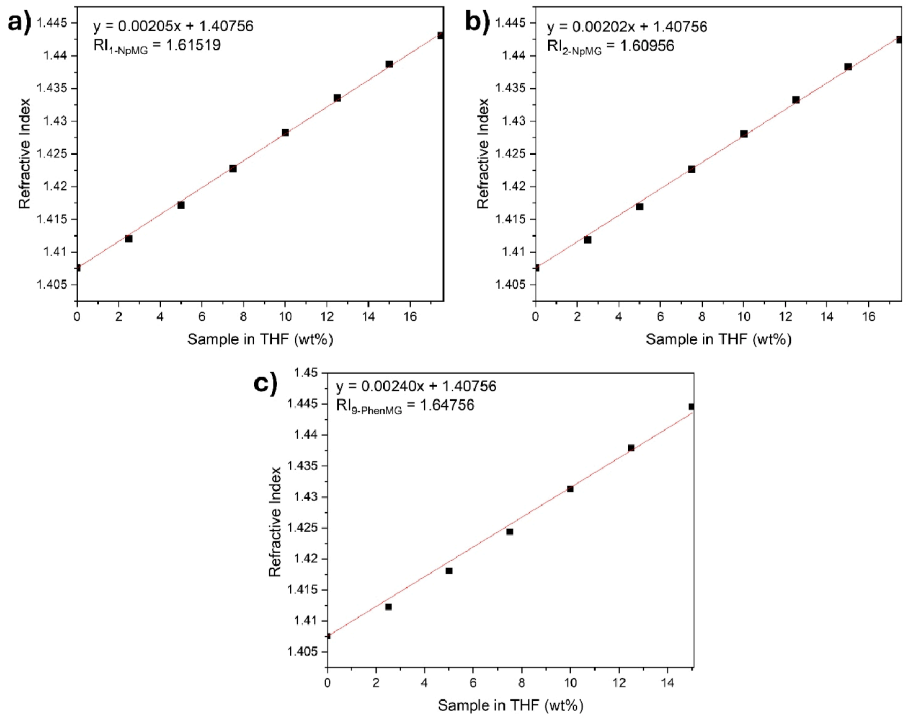

Figure S8: *Calibration curve of a) 1-NpMG$_{non\text{-}cons.}$, b) 2-NaphMG$_{non\text{-}cons.}$, c) 9-PhenMG$_{non\text{-}cons.}$, diluted in different amounts of THF. Linear regression was used to determine the refractive index at 100 wt%.*

4.3 NMR spectroscopy

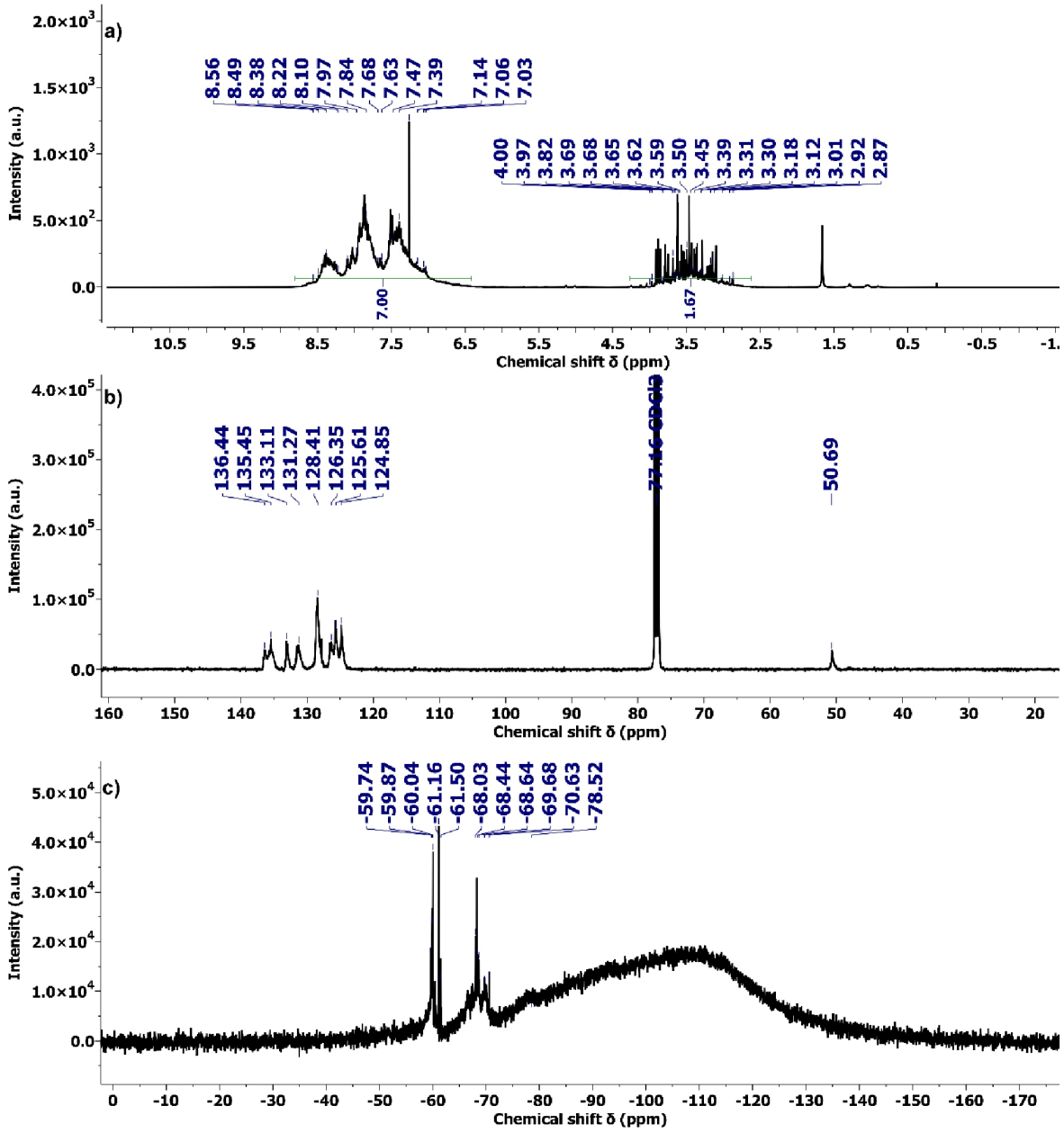

Figure S9: a) *^{1}H NMR, b) ^{13}C NMR and c) ^{29}Si NMR spectrum of 1-NpMG$_{non\text{-}cons.}$ in $CDCl_3$.*

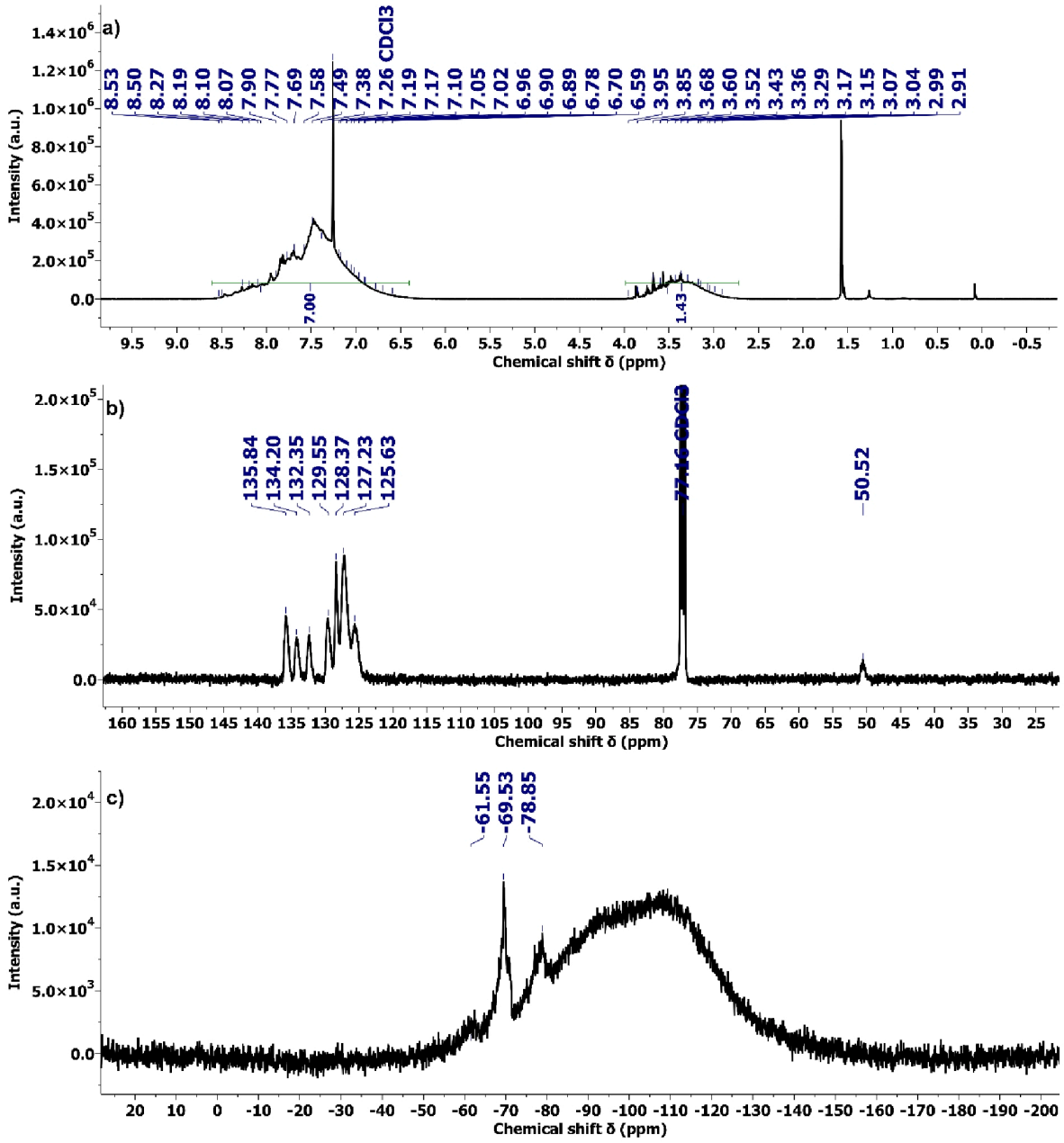

Figure S10: a) *^{1}H NMR, b) ^{13}C NMR and c) ^{29}Si NMR spectrum of the 2-NpMG$_{non\text{-}cons.}$ in $CDCl_3$.*

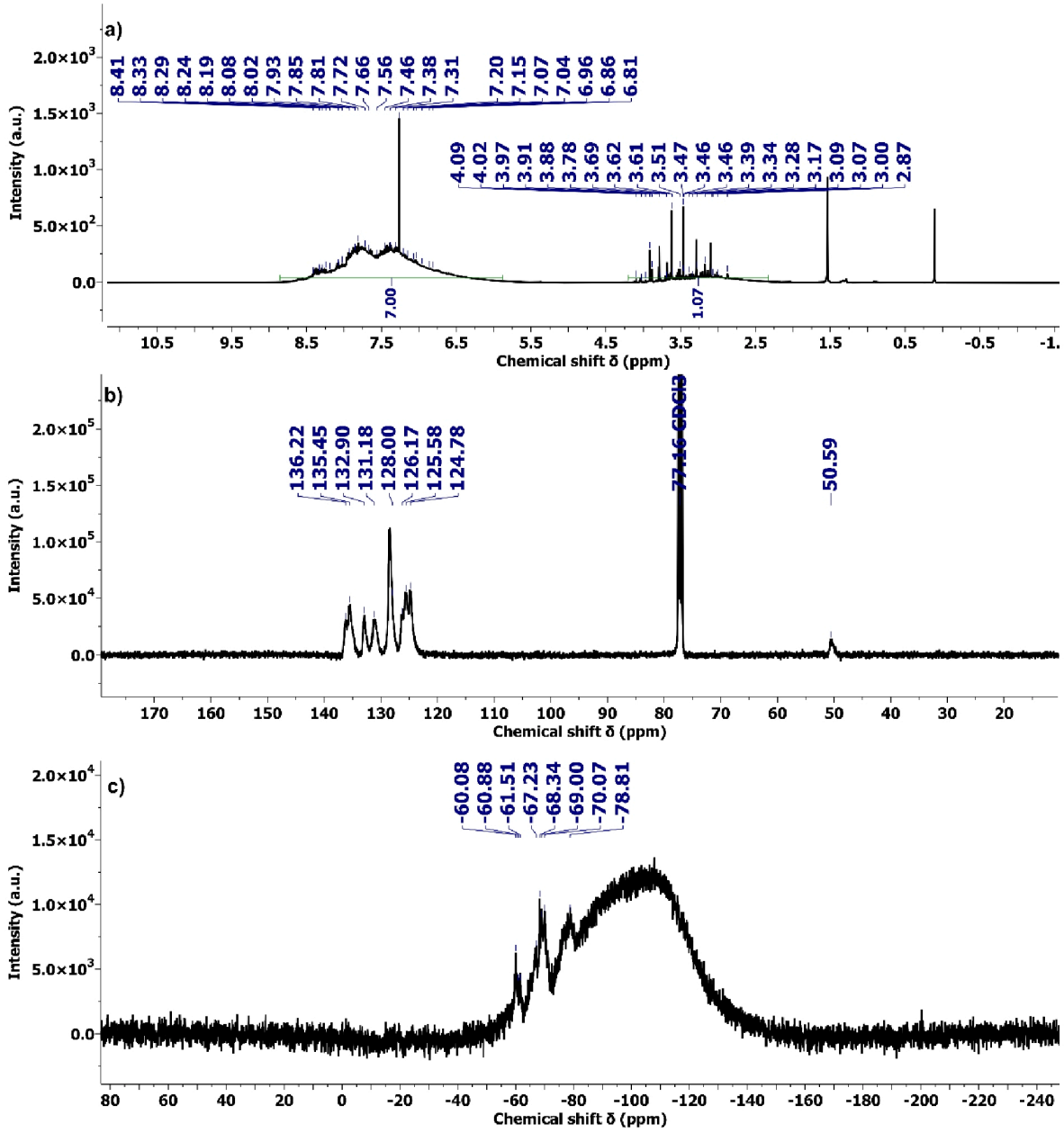

Figure S11: a) *^{1}H NMR, b) ^{13}C NMR and c) ^{29}Si NMR spectrum of 1-NpMG$_{cons.}$ in $CDCl_3$.*

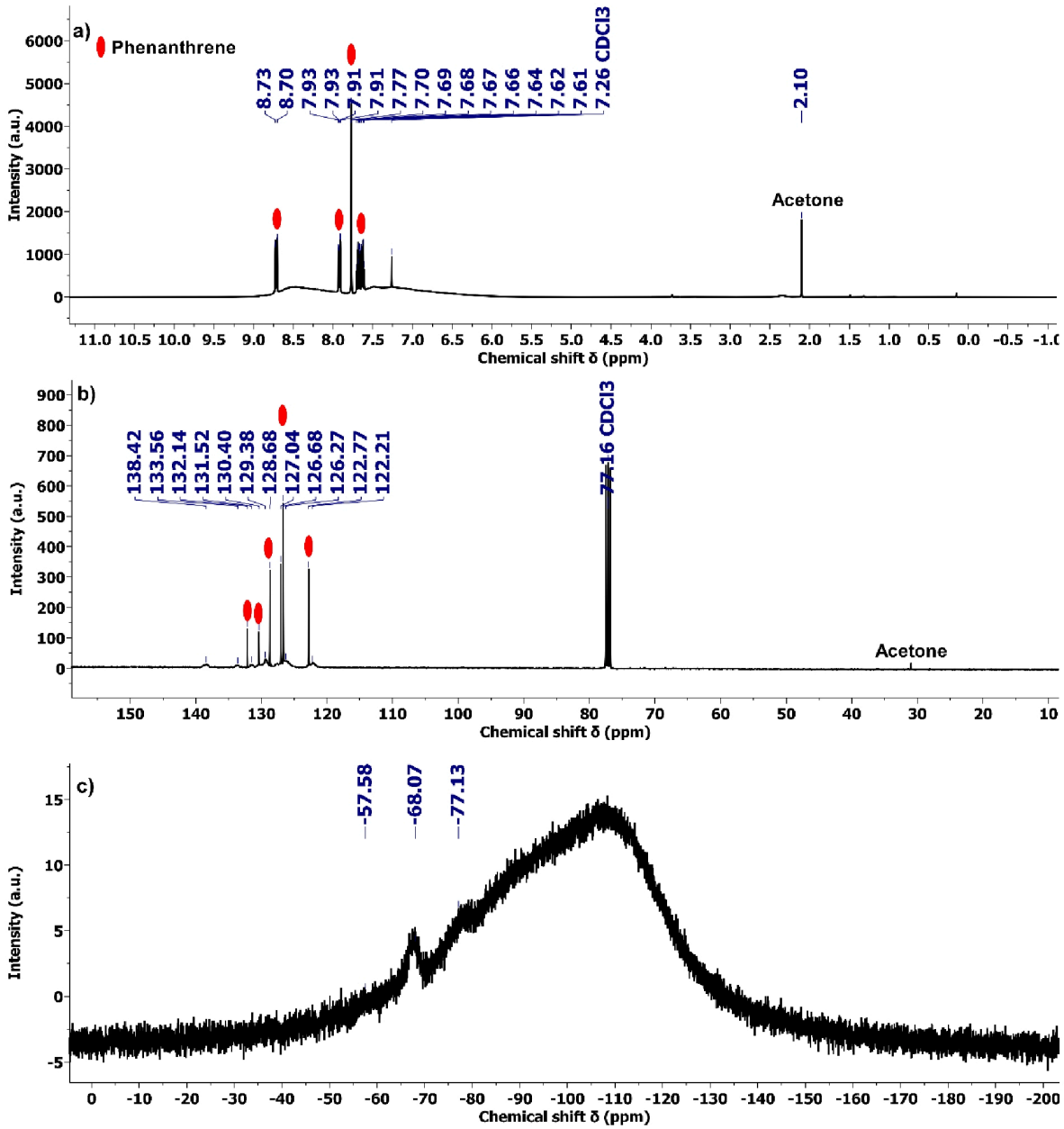

Figure S12: a) *^{1}H NMR and b) ^{13}C NMR with labeling of the signals of phenanthrene and acetone (see Figure S13 for exact assignment), c) ^{29}Si NMR spectrum of 9-PhenMG$_{non\text{-}cons.}$ in $CDCl_3$.*

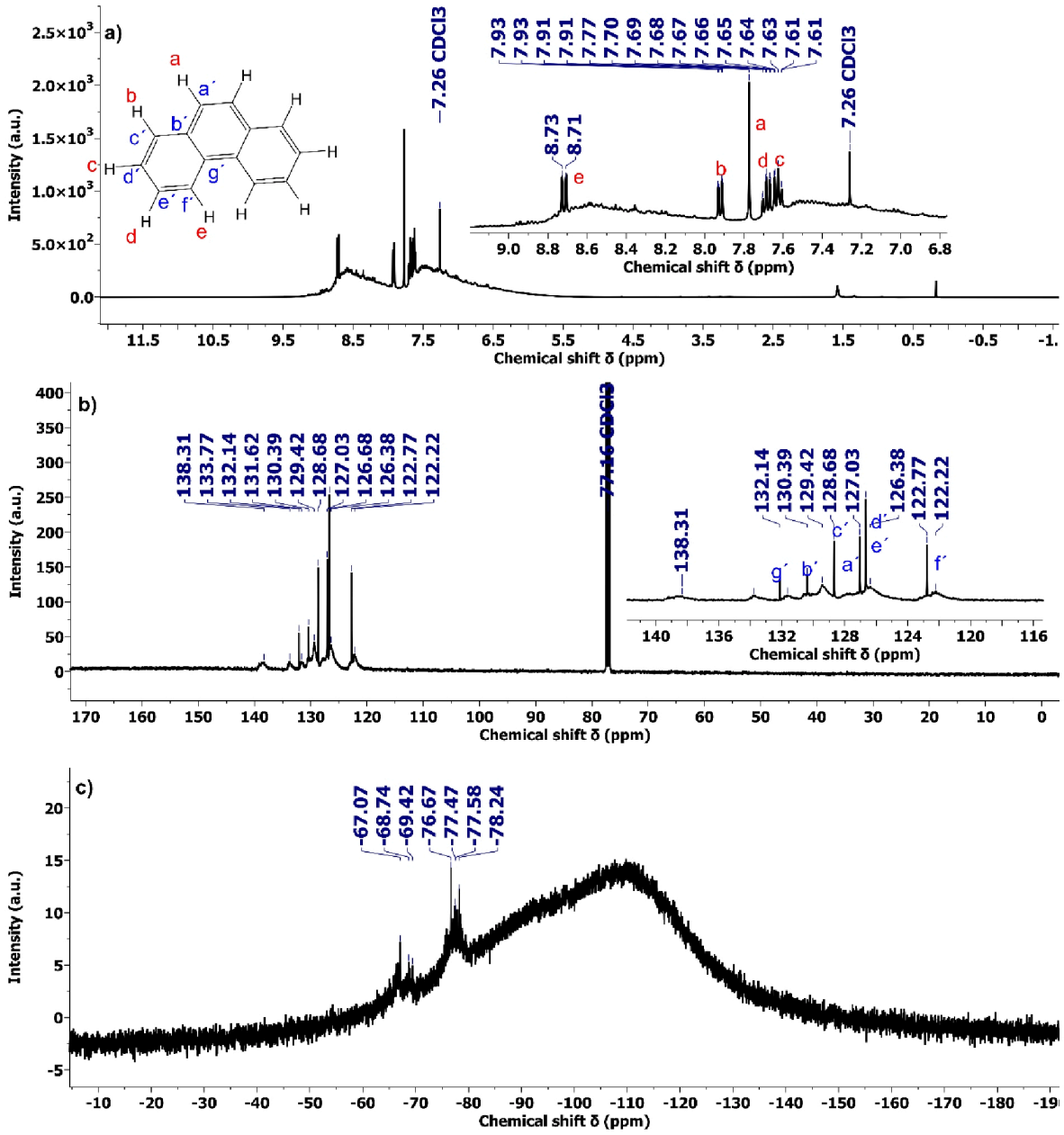

Figure S13: a) *^{1}H NMR and b) ^{13}C NMR with labeling of the signals of phenanthrene, c) ^{29}Si NMR of 9-PhenMG$_{cons.}$ in $CDCl_3$.*

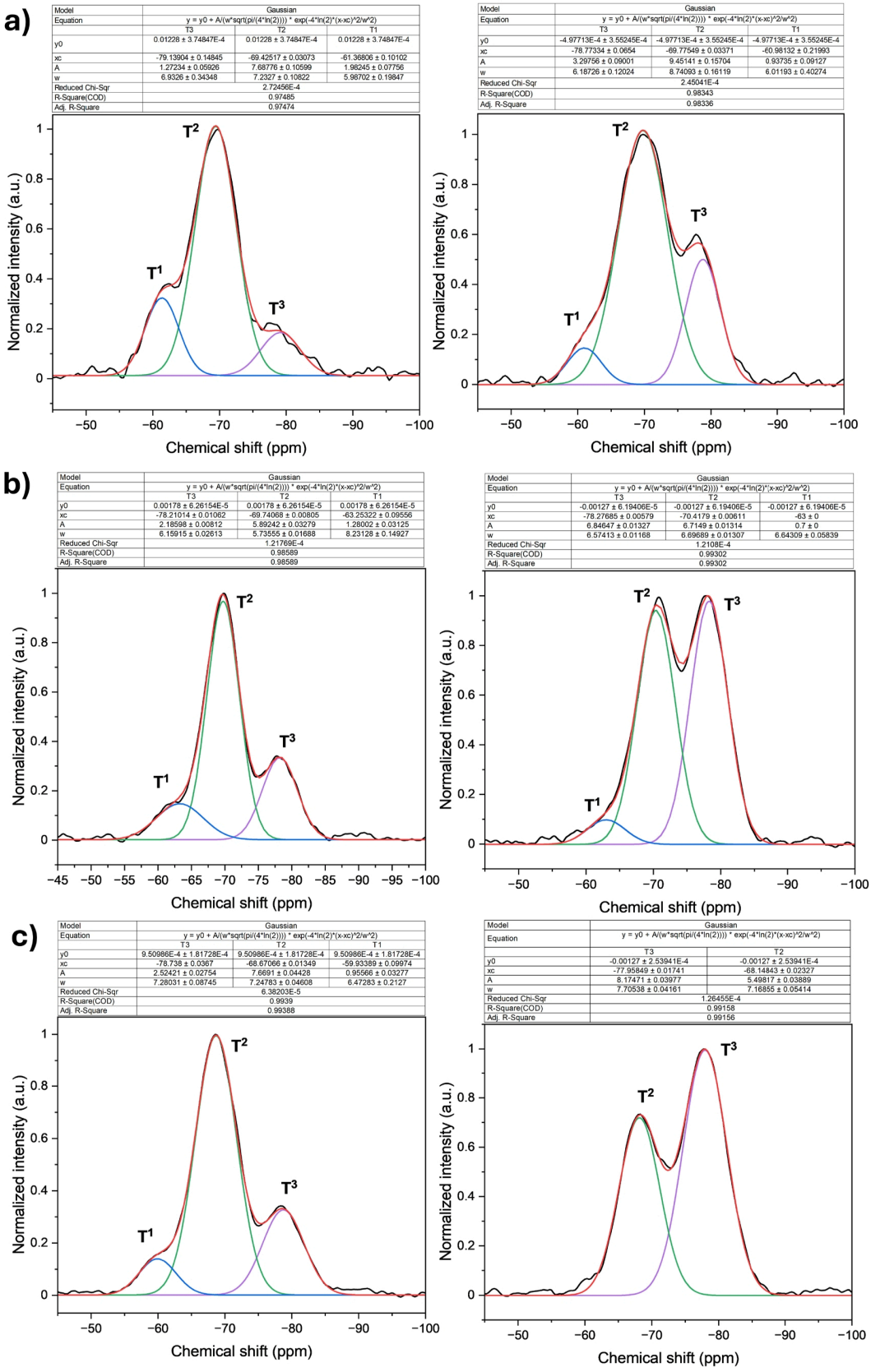

Figure S14: *Deconvoluted ^{29}Si CP-MAS NMR spectra with marked T-species, a) 1-NpMG, b) 2-NpMG, c) 9-PhenMG, left: non-consolidated, right: consolidated sample.*

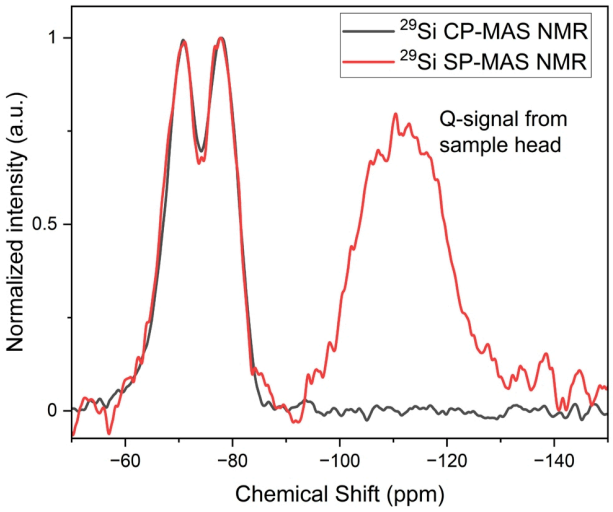

Figure S15: *Comparison of ^{29}Si CP-MAS and ^{29}Si SP-MAS NMR of 2-NpMG$_{cons.}$.*

4.4 TG-FTIR

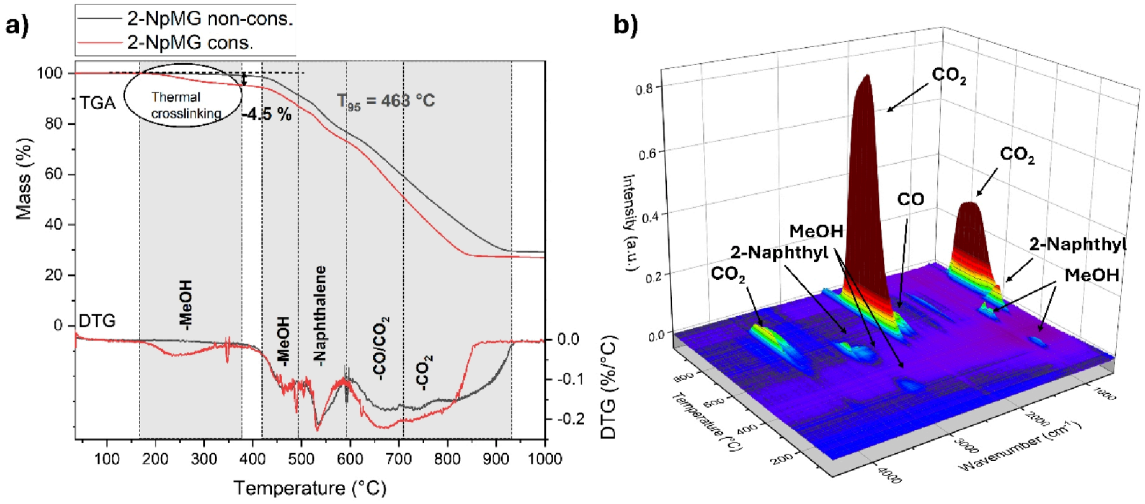

Figure S16: *a) TGA under air and DTG curve of the non-consolidated and consolidated 2-NpMGs, with assignment of the gases released during the individual decomposition steps, b) 3D graphic of the FTIR spectra of the degradation products as a function of temperature for 2-NpMG$_{non-cons.}$.*

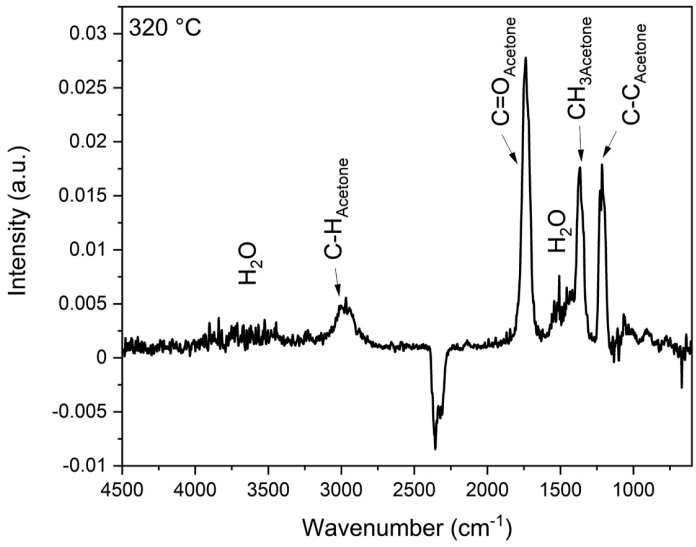

Figure S17: *FTIR spectra of the degradation gases from 9-PhenMG$_{non\text{-}cons.}$ at 320 °C. Acetone and water were detected during the first degradation step.*[8]

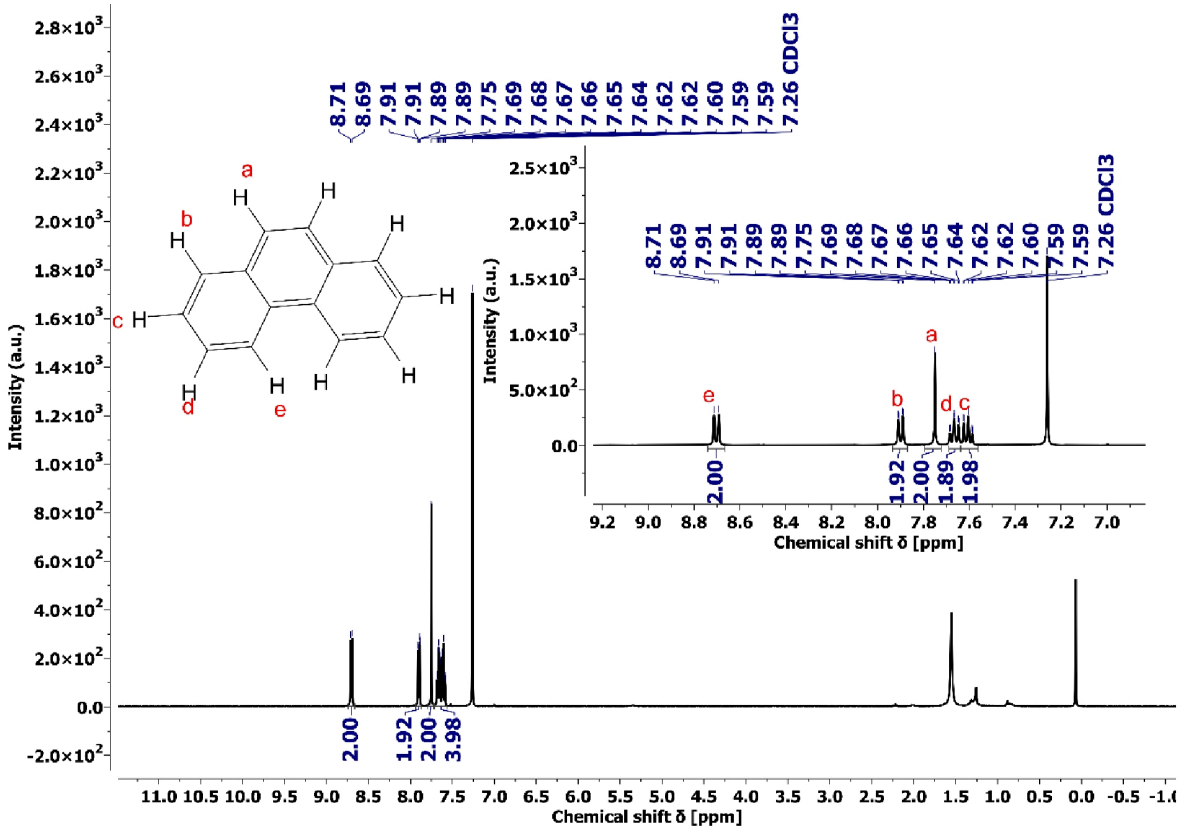

Figure S18: *^{1}H NMR spectrum of crystalline products found in the furnace after a TG-FTIR measurement of 9-PhenMG$_{non\text{-}cons.}$. Peak assignment confirms the presence of phenanthrene.*

4.5 Fluorescence spectroscopy

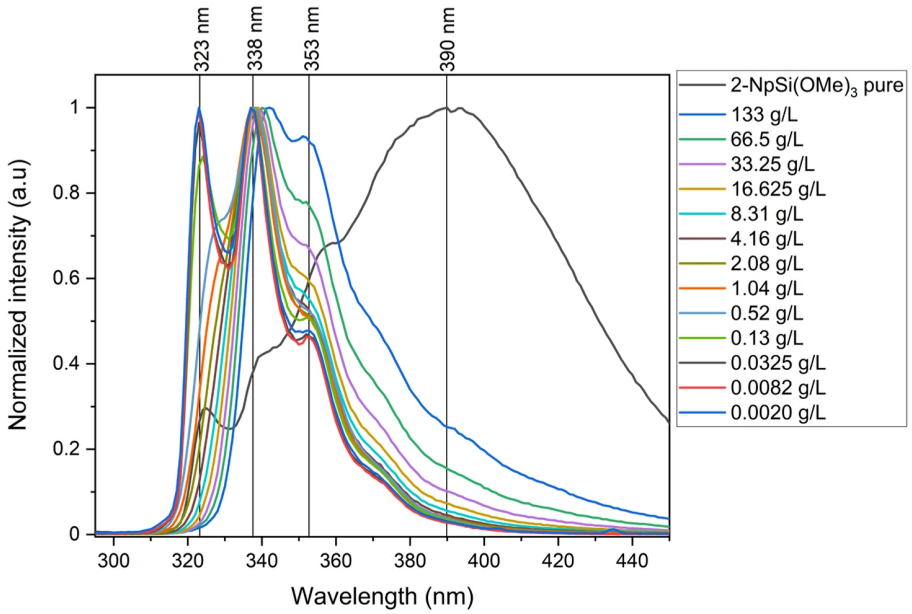

Figure S19: *Concentration-dependent fluorescence spectra of 2-NpSi(OMe)$_3$, in DCM, λ_{ex}=285 nm.*

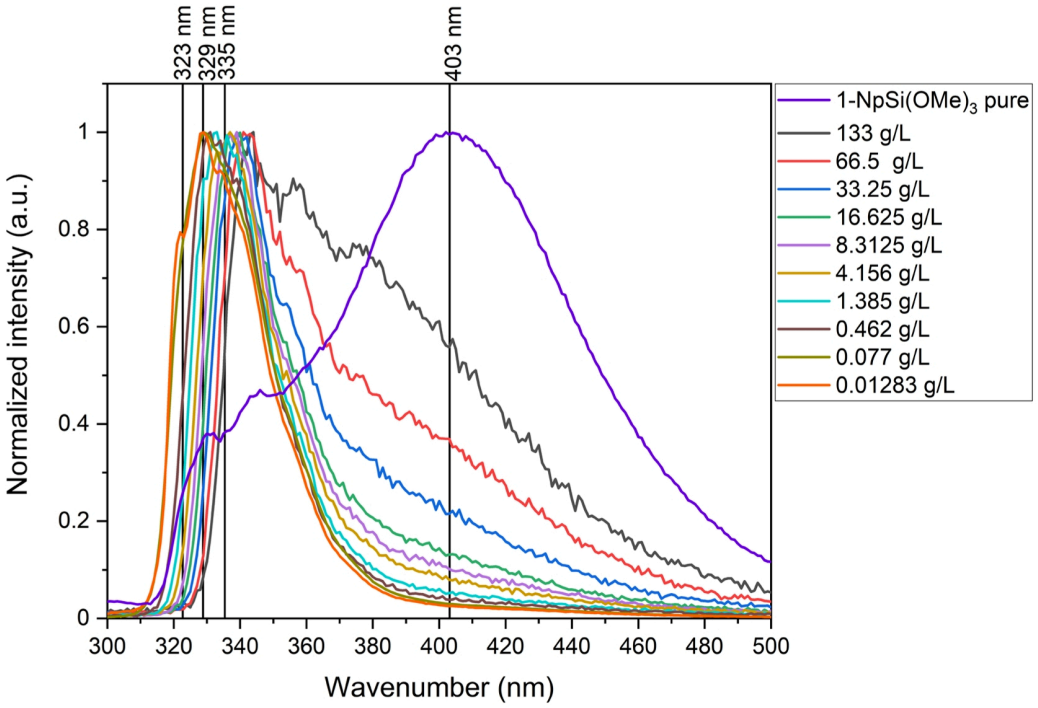

Figure S20: *Concentration-dependent fluorescence spectra of 1-NpSi(OMe)$_3$, in DCM, λ_{ex}=285 nm.*

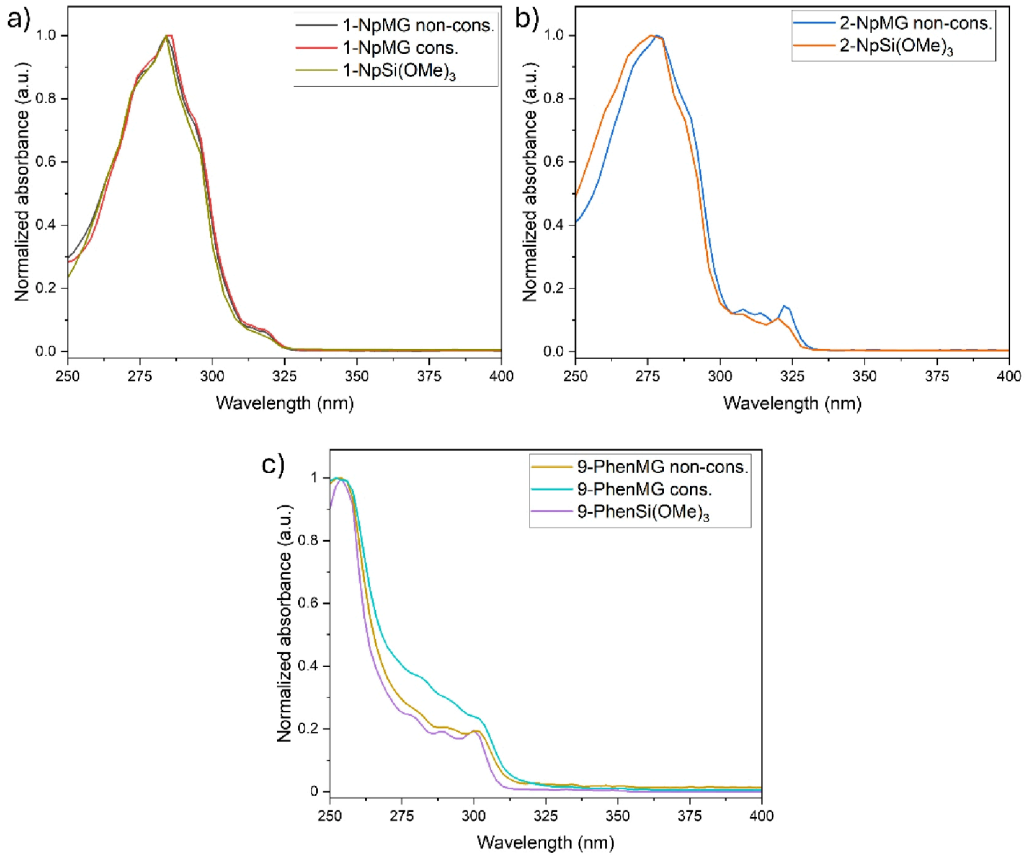

Figure S21: *UV-VIS spectra of the soluble aryl melting gels and aryltrimethoxysilane monomers in DCM, with a) 1-naphthyl, b) 2-naphthyl, and c) 9-phenanthrenyl as organic group.*

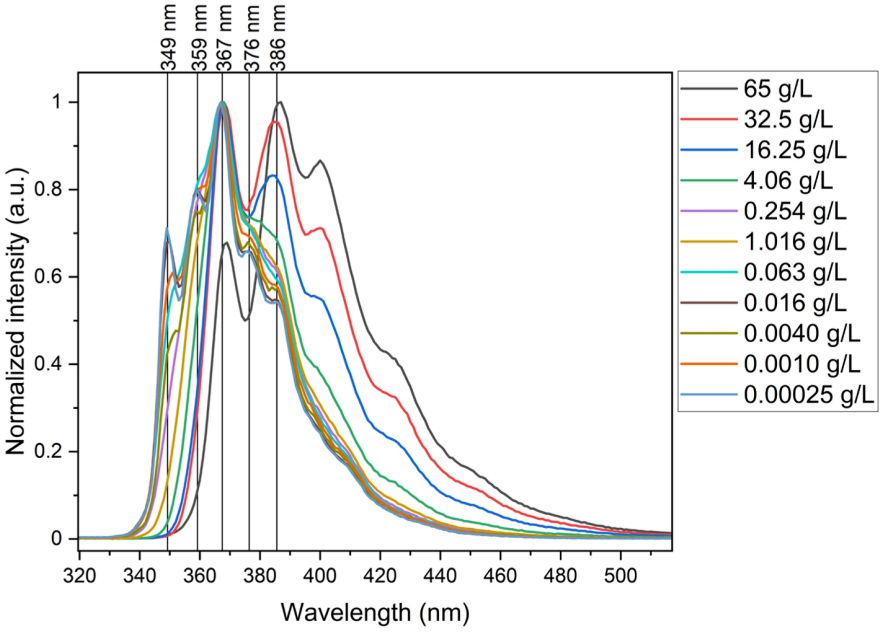

Figure S22: *Concentration-dependent fluorescence spectra of 9-PhenSi(OMe)$_3$, in DCM, λ_{ex}=300 nm.*

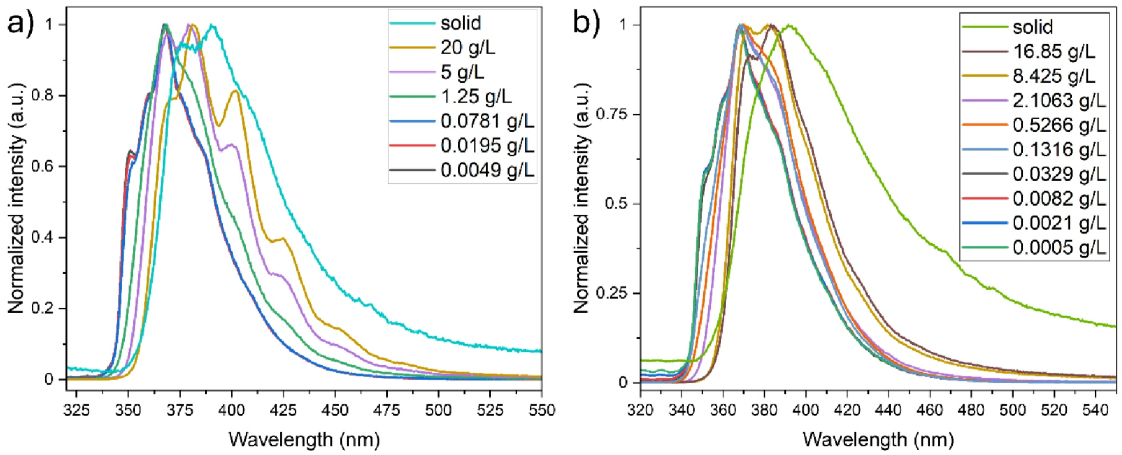

Figure S23: *Concentration-dependent fluorescence spectra of a)9-PhenMG$_{non\text{-}cons.}$ and b) 9-PhenMG$_{cons.}$ in DCM, λ_{ex}=300 nm.*

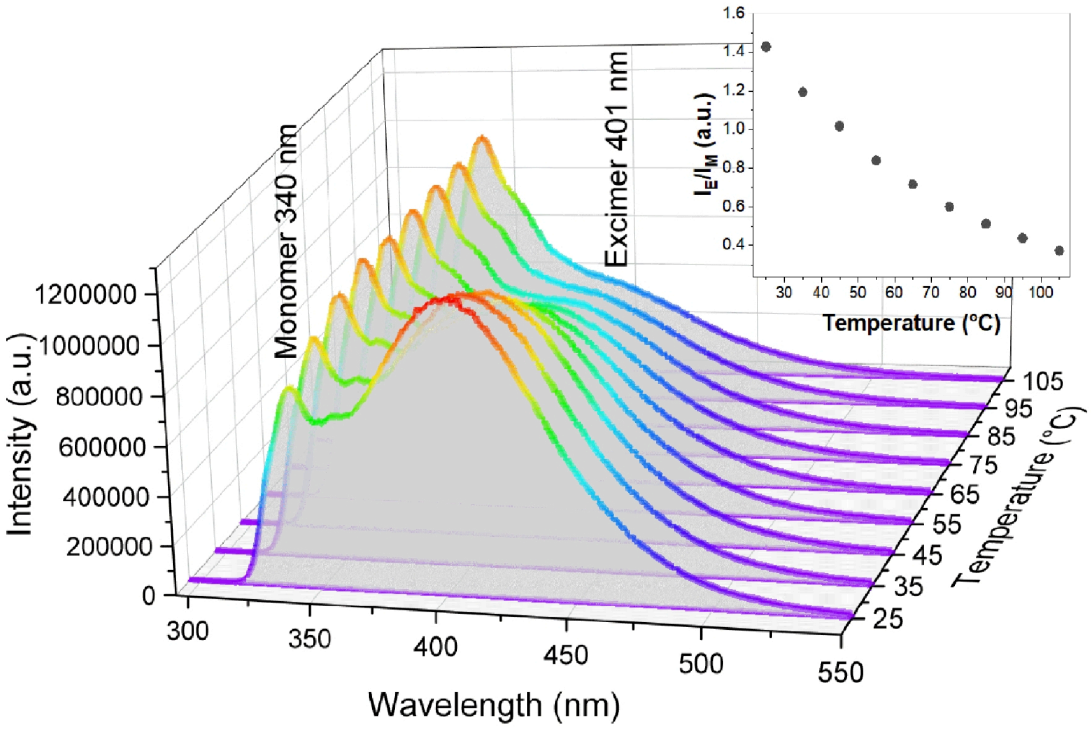

Figure S24: *Temperature-dependent measurements of 2-NpMG$_{non\text{-}cons.}$ in DMSO between 25 and 105 °C, λ_{ex}=285 nm, c= 0.6 g/L, with labeling of monomer fluorescence and excimer fluorescence. The inset shows the dependence of the excimer-to-monomer fluorescence ratio on temperature.*

5. References

(1) MestReNova, v14.2.0-26256, Mestrelab Research, S.L., Santiago de Compostela, Spain.
(2) Origin(Pro), 2023b, OriginLab Corporation, Northampton, MA, USA.

(3) PSS WinGPC® UniChrom 8.2, PSS-Polymer Standards Service - USA Inc Amherst, MA, USA
(4) FlexAnalysis 3.4, Bruker Daltonics, Billerica, MA, USA.
(5) Topas 5, Bruker AXS, Karlsruhe, Germany.
(6) Liu, F.; Zeng, X.; Lai, X.; Li, H. Synthesis and characterization of polyphenylsilsesquioxane terminated with methyl and vinyl groups low-melting glass. *J. Adhes. Sci. Technol.* **2017**, *31*, 2399-2409. DOI: https://doi.org/10.1016/10.1080/01694243.2017.1302699.
(7) Wei, H.; Bichen, P.; Xin, Y.; Youxue, Y.; Ying, Z.; Xiaojuan, Z. Preparation Method of Naphthyl Alkoxysilane. CN104788488A, 2015.
(8) Zhang, X. K.; Lewars, E. G.; March, R. E.; Parnis, J. M. Vibrational spectrum of the acetone-water complex: a matrix isolation FTIR and theoretical study. *J. Phys. Chem.* **1993**, *97* (17), 4320-4325. DOI: https://doi.org/10.1021/j100119a012.

Supporting Information

Melt, Mix, and Glow: Emulsion-Based Fabrication of Polyphenylsilsesquioxane Microspheres with Embedded Hydrophobic Fluorophores

Svenja Pohl,[a] Nils Steinbrück,[a] Michał P. Pachnicz,[a] and Guido Kickelbick*[a,b]

[a] Inorganic Solid-State Chemistry, Saarland University, Campus, Building C4.1, 66123 Saarbrücken, Germany

[b] Saarene – Saarland Center for Energy Materials and Sustainability, Campus C4.2, 66123 Saarbrücken, Germany.

*Corresponding author, e-mail: guido.kickelbick@uni-saarland.de

Content

1. Characterization Educts

Phenyltrimethoxysilane
^{1}H NMR (400 MHz, $CDCl_3$): δ=7.69-7.66 (2 H, m, Ph), 7.49-7.37 (3 H, m, Ph), 3.64 (9 H, s, O-CH_3)
^{13}C NMR (80 MHz, $CDCl_3$): δ=134.65, 130.52, 129.45, 127.89 (Ph), 50.59 (O-CH_3)
^{29}Si NMR (100 MHz, $CDCl_3$): δ=-54.54

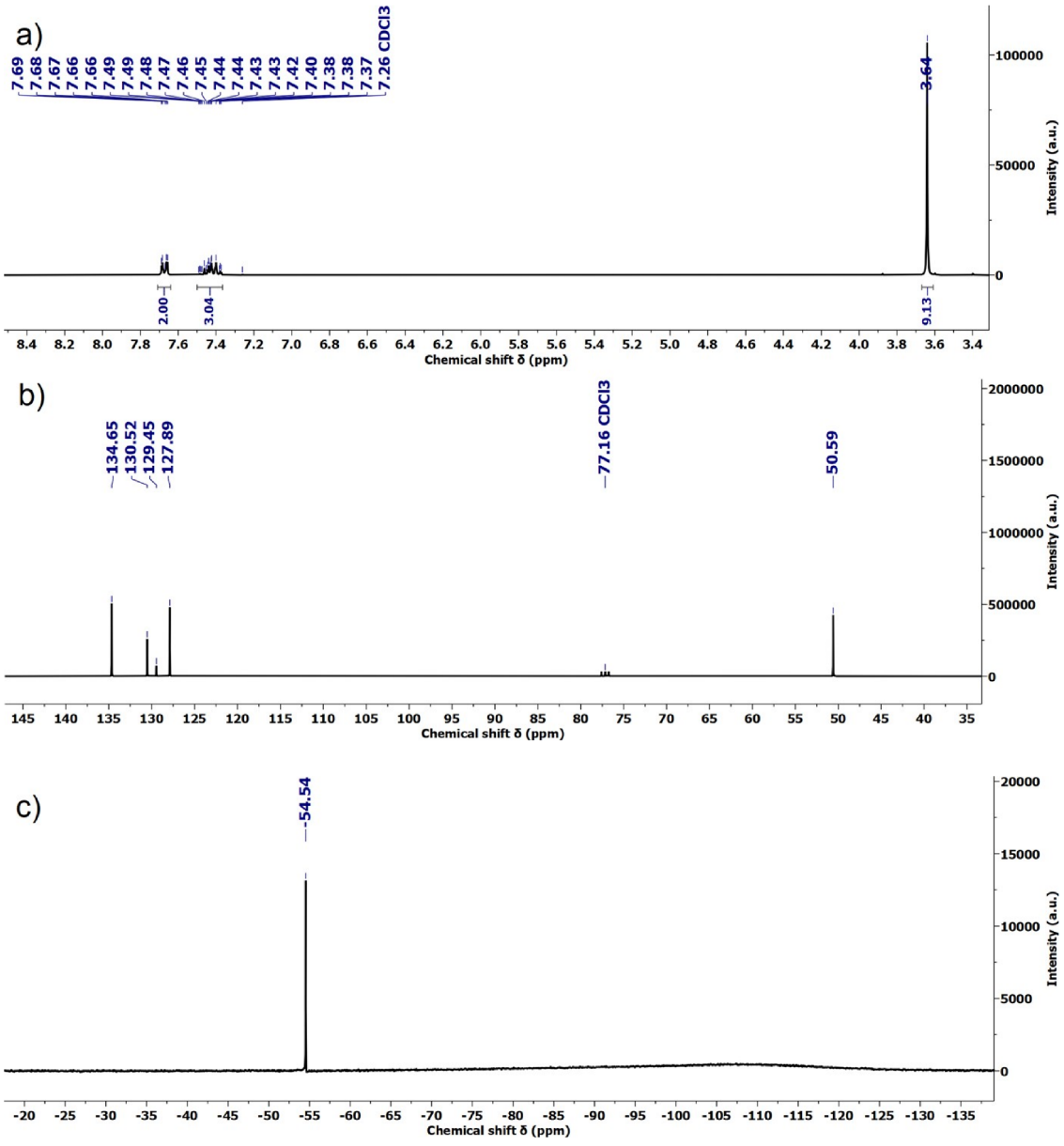

Fig. S1. a) ^{1}H NMR spectrum, b) ^{13}C NMR spectrum, c) ^{29}Si NMR spectrum of phenyltrimethoxysilane.

Lumogen® F Red 305

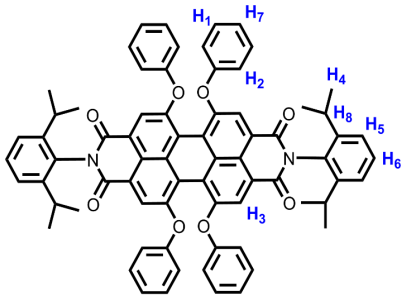

^{1}H NMR (300 MHz, $CDCl_3$): δ=8.27 (4 H, s, H_3), 7.47 – 7.39 (2 H, m, H_6), 7.31 – 7.23 (12 H, m, H_2, H_5), 7.14 – 7.07 (4 H, m, H_7), 7.02 – 6.95 (8 H, m, H_1), 2.71 (4 H, sept, J 6.7, H_8), 1.12 (24 H, d, J 6.8, H_4).

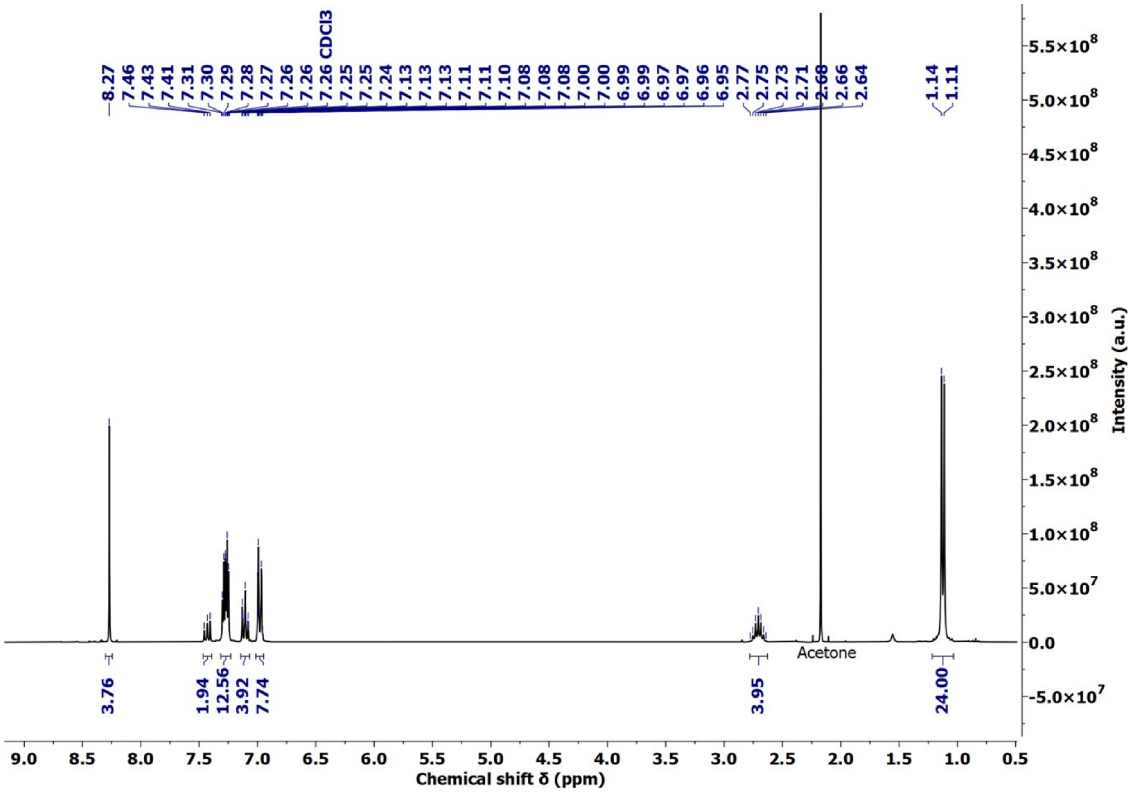

Fig. S2. ^{1}H NMR spectrum of Lumogen® F 305 Red.

Triton™ X-405

^{1}H NMR (300 MHz, D_2O): δ=7.1 (2 H_g, d, J=9,0 Hz), 6.83 (2 H_h, d, J=9.0 Hz), 4.03 (2 H, s), 3.87 – 3.51 (161 $H_{j,k}$, m), 1.66 (2 H_c, s), 1.28 (6 H_e, s), 0.70 (9 H_a, s).
^{13}C NMR (80 MHz, D_2O): δ=165.22 (C_i), 141.81 (C_f), 126.87 (C_g), 113.89 (C_h), 71.69, 69.55, 68.13, 60.30 ($C_{n,o}$), 56.80 (C_b), 37.68 (C_d), 32.11, 31.84, 31.72 ($C_{a,e}$)

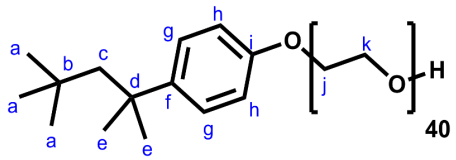

M_w = 1968,45 g mol^{-1}

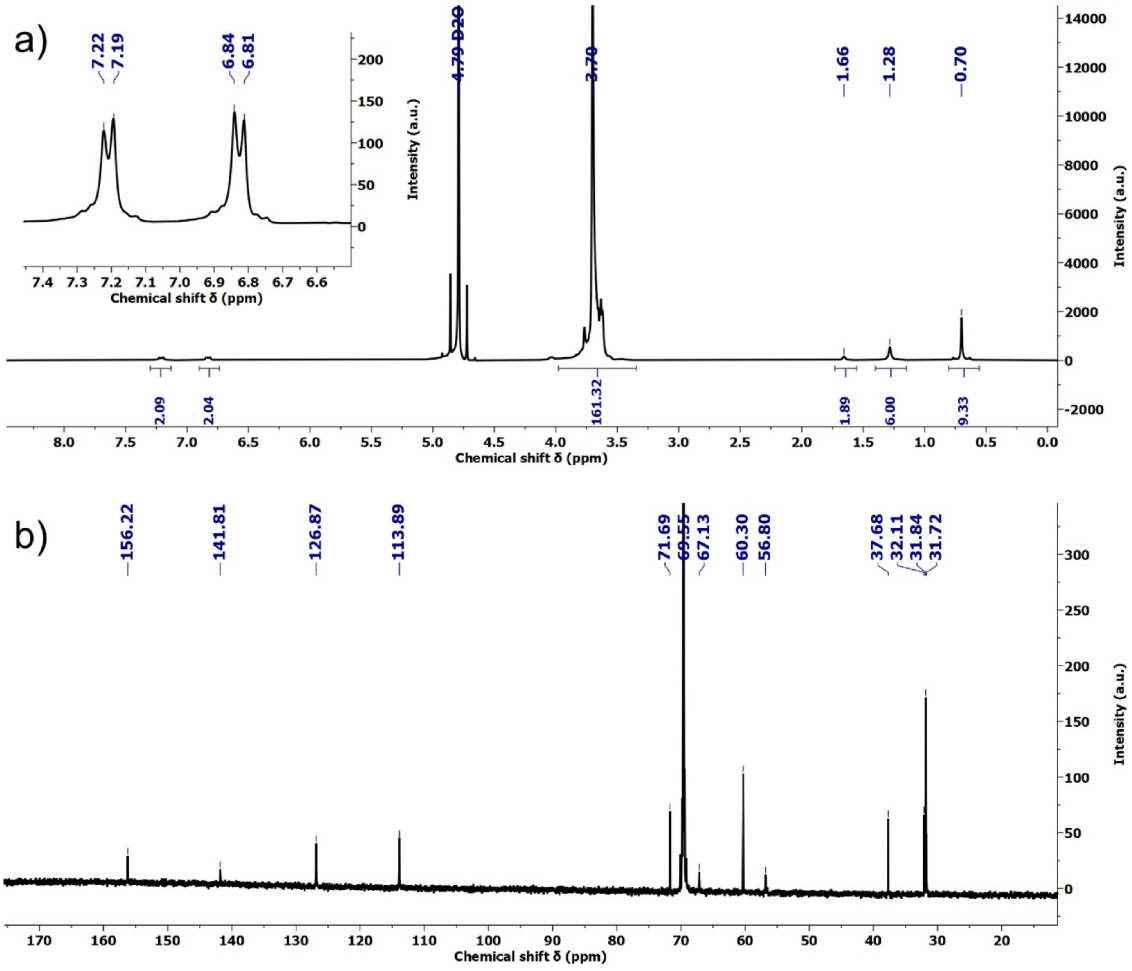

Fig. S3. a) ^{1}H NMR spectrum, b) ^{13}C NMR spectrum of Triton™ X-405.

2. Characterization Products

2.1 Dye concentration

Table S1: Sample weights and exact dye concentration in MG precursors with *Lumogen® F Red 305 (LG305),* Oracet® FL Pink 285 (FL Pink), and Oracet® FL Orange 240 (FL Orange). All samples were prepared with 7 g PhTMS and 1.5 eq H_2O (aqueous HCl, pH 2.5, 0.95 g). The dye concentration was determined using the mass of the integrated dye and the MG precursors.

Sample	Dye	Mass dye [mg]	Mass MG precursor [g]	Dye conc. [ppm]
MG_LG305_220 ppm	LG305	1.03	4.637	222
MG_LG305_1150 ppm	LG305	5.15	4.478	1146
MG_LG305_2450 ppm	LG305	10.80	4.404	2452
MG_LG305_4350 ppm	LG305	20.10	4.626	4345
MG_LG305_10600 ppm	LG305	50.90	4.805	10593
MG_LG305_26000 ppm	LG305	125.70	4.833	26008
MG_FL Pink_1150 ppm	FL Pink	5.50	4.783	1150
MG_FL Orange_1120 ppm	FL Orange	5.09	4.563	1115

Since no significant loss of dye into the reaction medium is expected during synthesis, the concentrations shown here were also assumed for the particles. However, further condensation reactions involving the elimination of methanol and water lead to a reduction of the total particle mass. Therefore, the reported concentrations for the final consolidated particles should be regarded as approximate values rather than exact figures.

2.2 NMR spectroscopy

MG precursor (MG LG305)
^{1}H NMR (400 MHz, $CDCl_3$): δ=7.84 – 6.65 (m, Ph), 3.76 – 2.86 (m, O-CH_3)
^{13}C NMR (80 MHz, $CDCl_3$): δ=134.35, 134.20, 130.63, 127.80 (Ph), 50.65 (O-CH_3)
^{29}Si NMR (100 MHz, $CDCl_3$): δ=-62.00 (T^1), -69.64 (T^2), -79.67 (T^3)

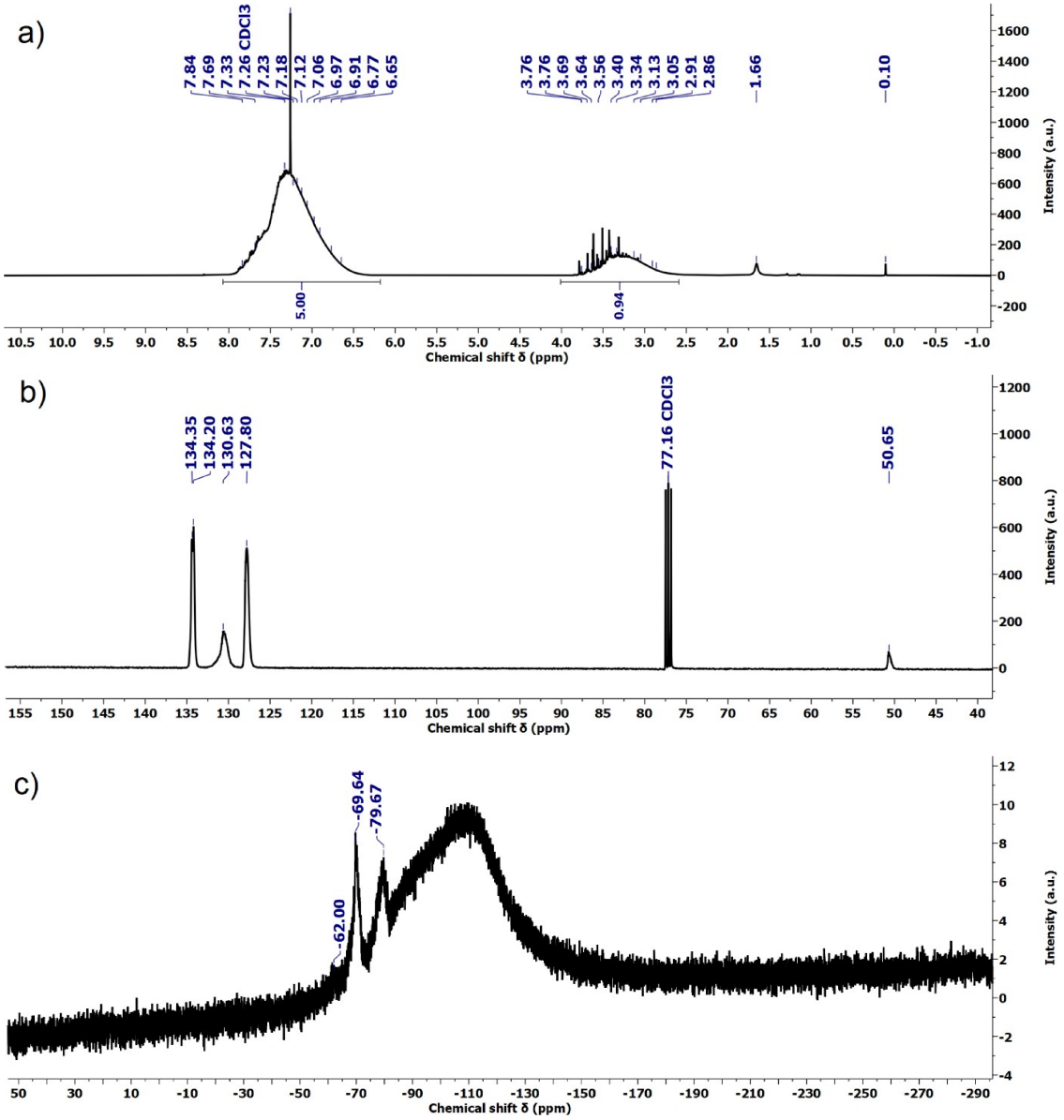

Fig. S4. a) ^{1}H NMR spectrum, b) ^{13}C NMR spectrum, c) ^{29}Si NMR spectrum of MG LG305 precursor.

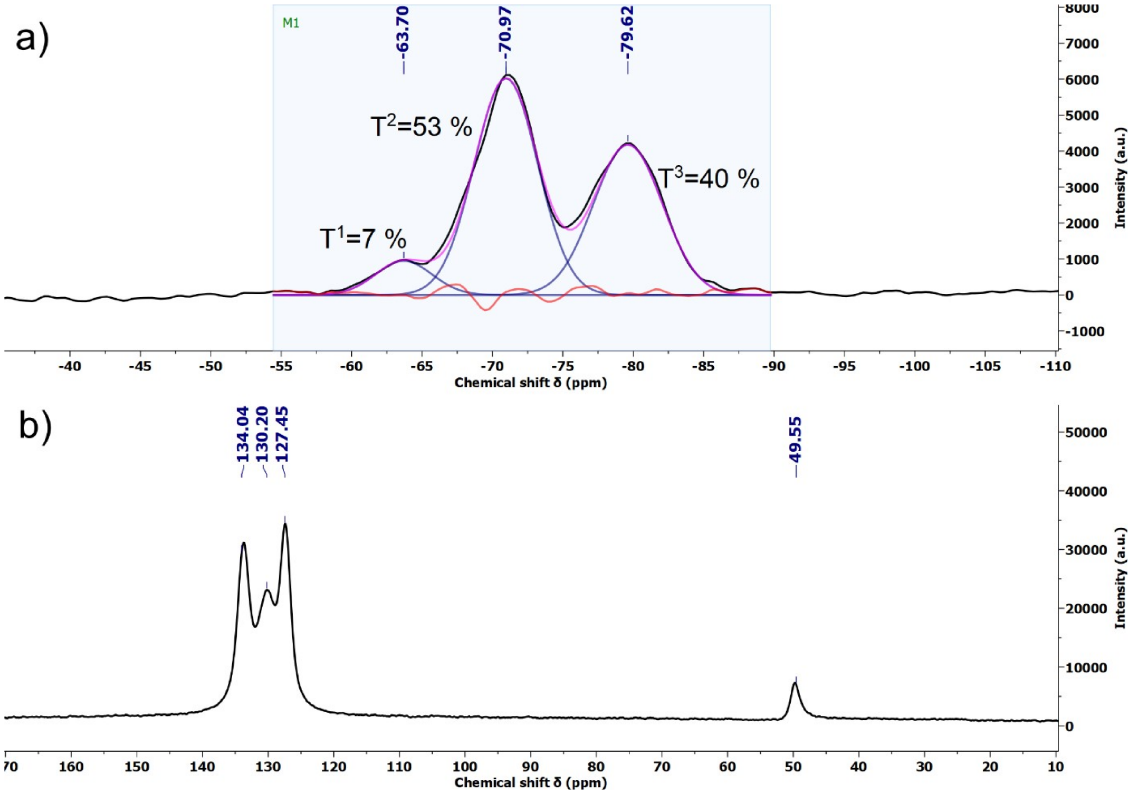

Fig. S5. a) ^{29}Si SP-MAS NMR spectra with Lorentz-Gaussian fit of the peaks and percentage ratios of T^1, T^2 and T^3, b) ^{13}C SP-MAS NMR of MG LG305 precursor.

MG consolidated ($MG_{cons.}$ LG305)
^{29}Si SP-MAS NMR (100 MHz, $CDCl_3$): δ=-72.37 (T^2), -79.17 (T^3)
^{13}C SP-MAS NMR (80 MHz, $CDCl_3$): δ=133.83, 130.16, 127.23 (Ph), 49.77 ($-OCH_3$)

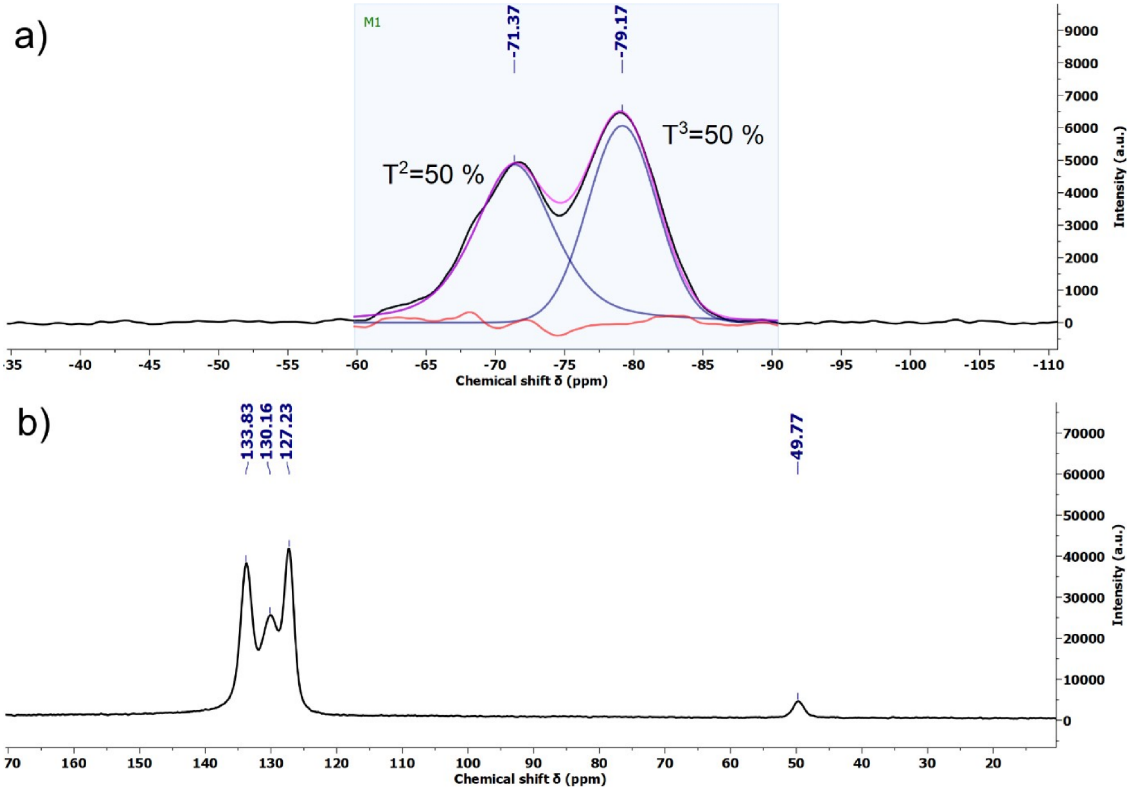

Fig. S6. a) ^{29}Si SP-MAS NMR spectra with Lorentz-Gaussian fit of the peaks and percentage ratios of T^1, T^2 and T^3, b) ^{13}C SP-MAS NMR of $MG_{cons.}$ LG305.

Untempered microspheres (MGP LG305)
^{29}Si SP-MAS NMR (100 MHz, $CDCl_3$): δ=-71.42 (T^2), -79.44 (T^3) **^{13}C SP-MAS NMR (80 MHz, $CDCl_3$):** δ=133.83, 130.16, 127.38 (Phenyl [Polyphenylsilsesquioxane], Phenoxy [Triton™ X-405]), 70.01 (-OCH_2 [Triton™ X-405]), 49.77 (-OCH_3 [Polyphenylsilsesquioxane]), 31.43 (-$C\underline{C}H_3$ [Triton™ X-405])

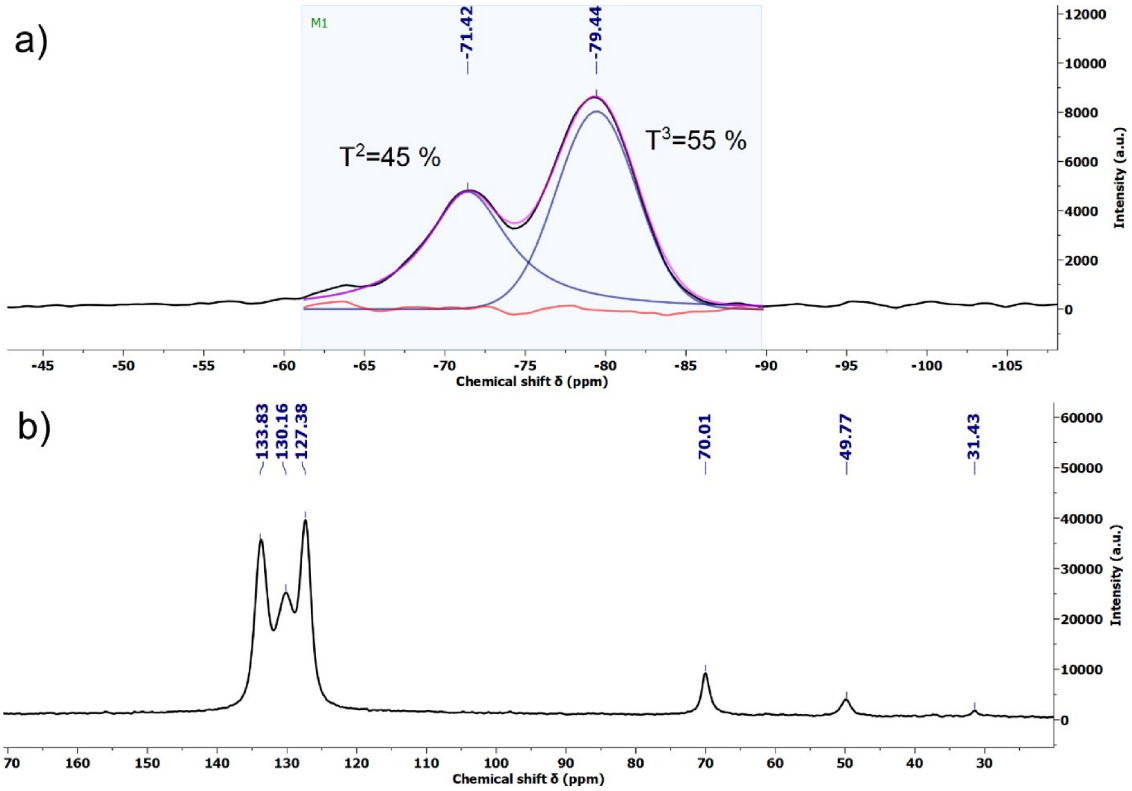

Fig. S7. a) ^{29}Si SP-MAS NMR spectra with Lorentz-Gaussian fit of the peaks and percentage ratios of T^1, T^2 and T^3, b) ^{13}C SP-MAS NMR of MGP LG305.

Tempered microspheres, 200°C, 24h (MGP-T LG305)
^{29}Si SP-MAS NMR (100 MHz, $CDCl_3$): δ=-71.50 (T^2), -79.09 (T^3) **^{13}C SP-MAS NMR (80 MHz, $CDCl_3$):** δ=133.68, 130.02, 127.08 (Phenyl [Polyphenylsilsesquioxane], Phenoxy [Triton™ X-405]), 70.31 (-OCH_2 [Triton™ X-405]), 49.77 (-OCH_3 [Polyphenylsilsesquioxane])

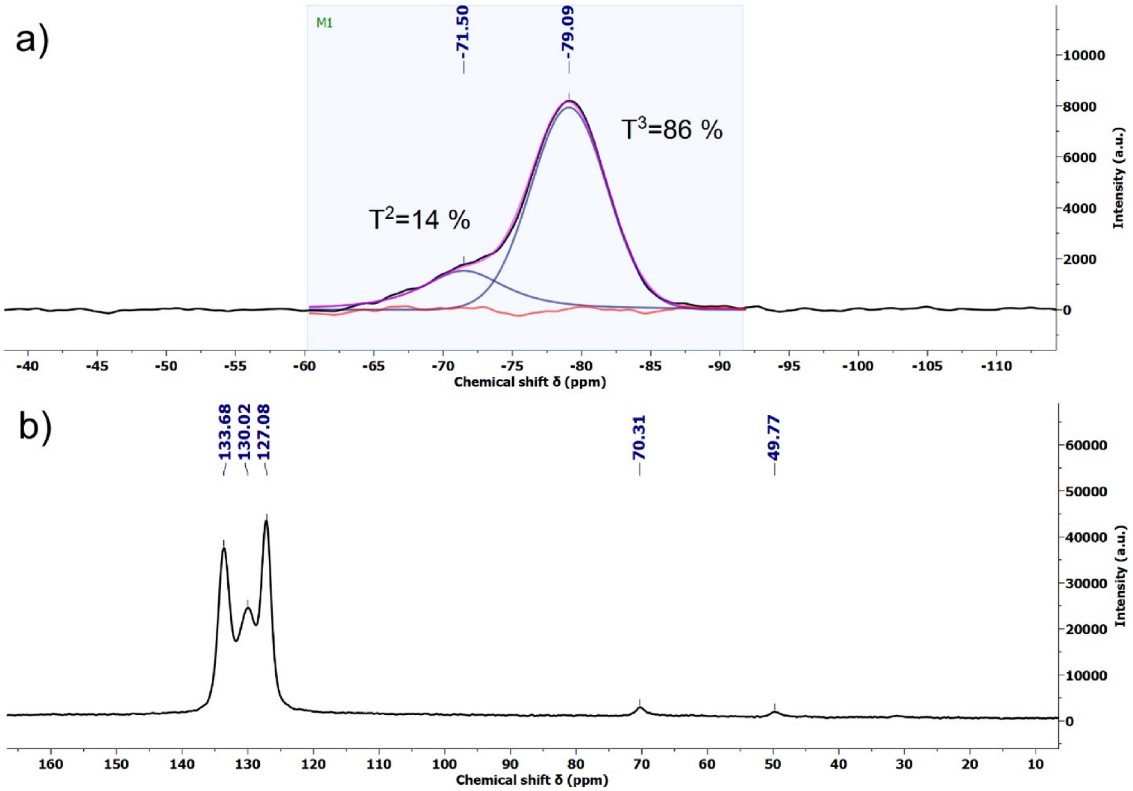

Fig. S8. ^{29}Si SP-MAS NMR spectra with Lorentz-Gaussian fit of the peaks and percentage ratios of T^1, T^2 and T^3, b) ^{13}C SP-MAS NMR of MGP-T_LG305.

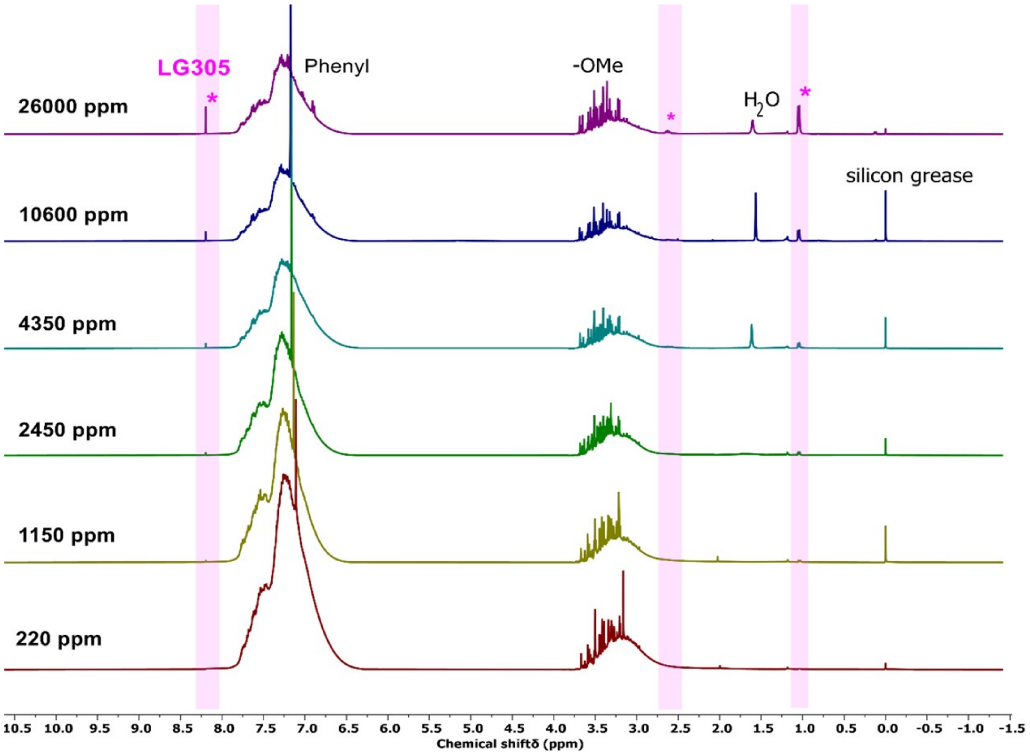

Fig. S9. ^{1}H NMR spectra (in $CDCl_3$) of MG prepared with different concentrations of LG305. Peaks originating from the dye are highlighted in pink.

2.3 Viscosity measurement

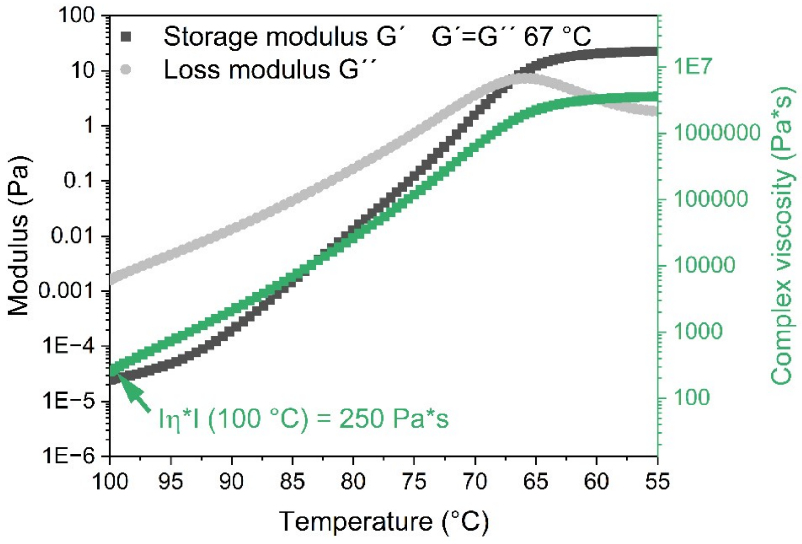

Fig. S10. Rheological characterization of MG LG305. Storage modulus, loss modulus, and complex viscosity measured between 100 °C and 55 °C. The crossover point of storage and loss modulus is highlighted, along with the complex viscosity at the temperature used for microsphere synthesis (100 °C). When G" > G' (T > 67 °C), the material exhibits more liquid-like behavior.

2.4 Powder XRD

Table S2. d_1 values, half-width of $2\theta_{d1}$ and relative intensities of $2\theta_{d1}$ and $2\theta_{d2}$

Sample	d_1 [nm]	Full width at half maximum of $2\theta_{d1}$ [°]	$I_{2\theta d1}/I_{2\theta d2}$
MG LG305	1.08	2.5	1.09
$MG_{cons.}$ LG305	1.16	2.2	1.52
MGP LG305	1.19	2.0	1.39
MGP-T LG305	1.21	1.9	1.84

2.5 TGA/TG-FTIR

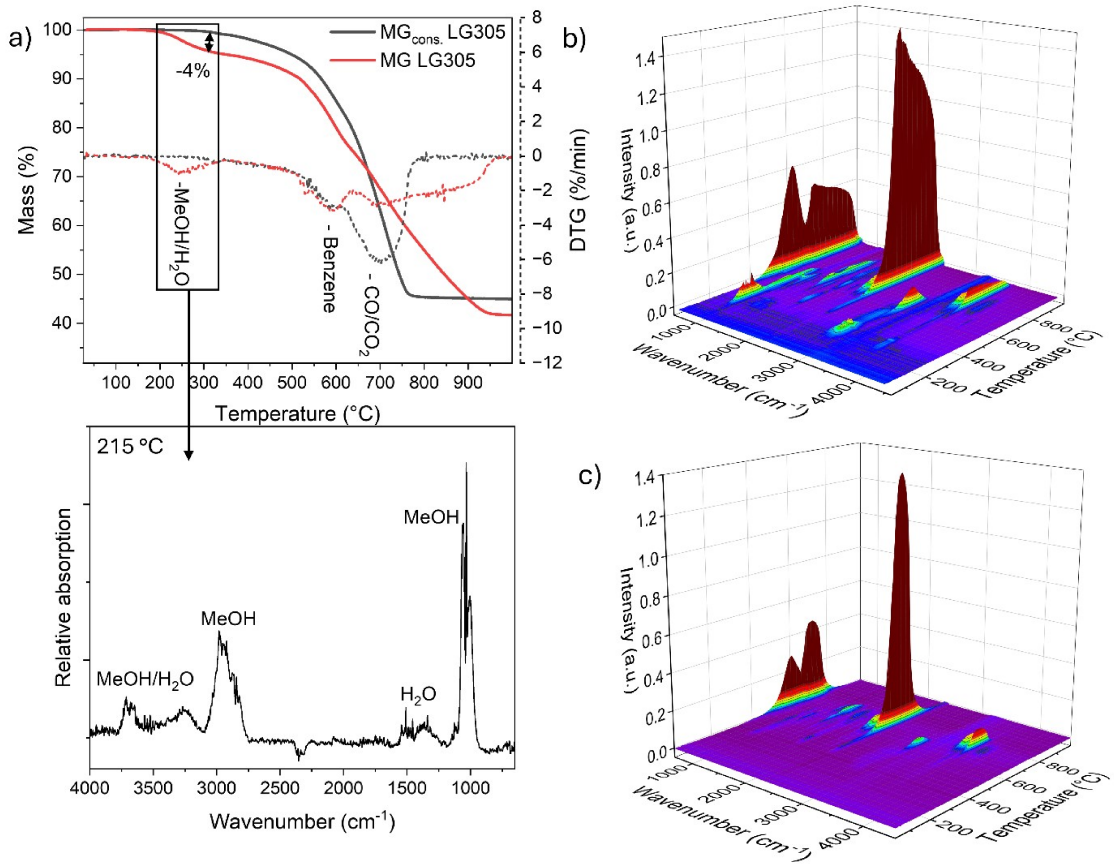

Fig. S11. a) TGA of MG LG305 and $MG_{cons.}$LG305, along with FTIR spectrum of the gases released at the first degradation step at 215 °C, b) 3D TGA-FTIR spectrum of gas-phase thermal degradation products of MG LG305, c) 3D TGA-FTIR spectrum of gas-phase thermal degradation products of $MG_{cons.}$LG305.

2.6 Changing synthesis conditions

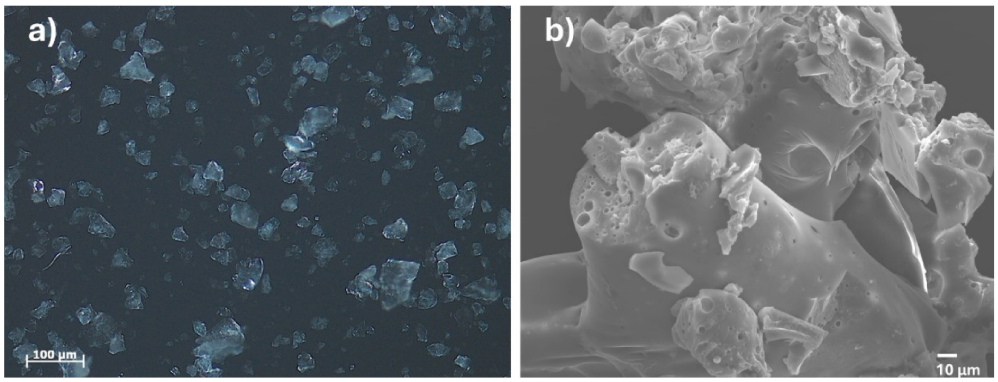

Fig. S12. The particle synthesis was prepared according to the standard procedure, but no surfactant was added. The microscopic picture shows the resulting particles after centrifugation and drying at 80 °C in a vacuum drying oven. A precursor gel without dye was used, a) microscopy image, b) SEM image at 500× magnification.

2.7 Leaching tests

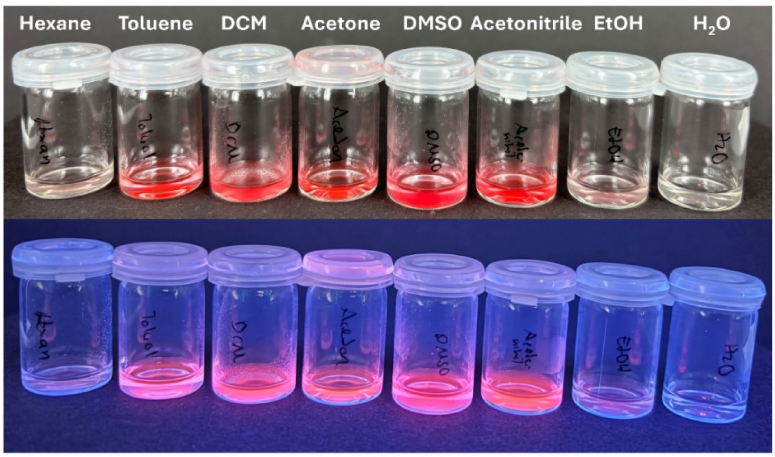

Fig. S13. MGP LG305 was dispersed in solvents of different polarity for 30 minutes. After centrifugation, the supernatant showed dye leaching in toluene, DCM, acetone, DMSO, and acetonitrile, while the dye remained encapsulated in hexane, ethanol, and water. The pictures show the supernatant after the particles have been removed, above under visible light and below under UV light.

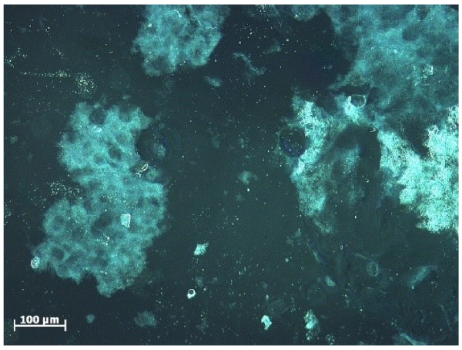

Fig. S14. Microscopy image of MGP LG305 after treatment with acetone for 30 minutes. The acetone causes swelling and partial dissolution of the particles, resulting in the loss of their spherical morphology.

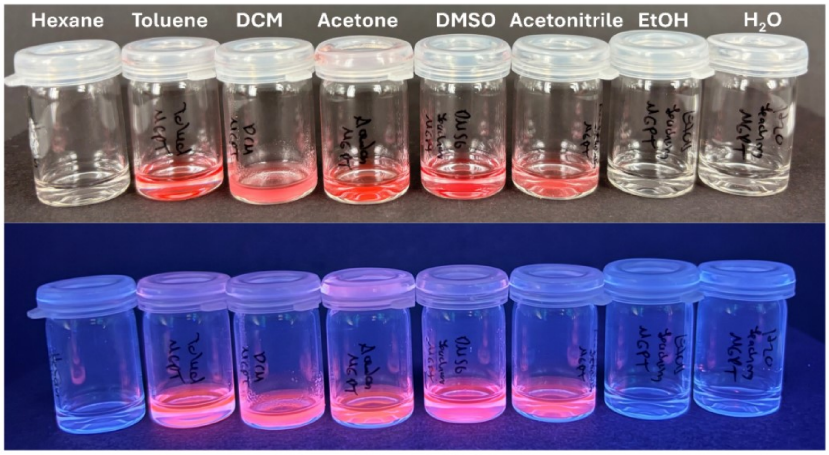

Fig. S15. MGP-T LG305 was dispersed in solvents of different polarity for 30 minutes. After centrifugation, the supernatant showed dye leaching in toluene, DCM, acetone, DMSO, and acetonitrile, while the dye remained encapsulated in hexane, ethanol, and water. The pictures show the supernatant after the particles have been removed, above under visible light and below under UV light.

2.8 SEM

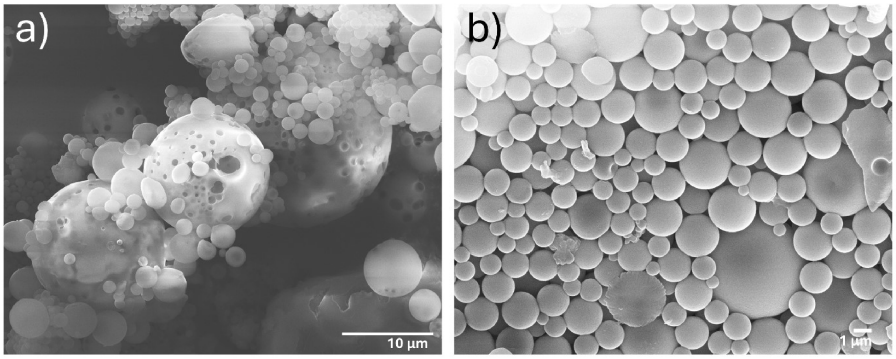

Fig. S16. SEM image of MGP-T LG305 a) at 2500× magnification, b) at 10,000× magnification, showing a region with sub-5 µm particle sizes.

2.9 Influence stirring on particle size

MGP-1

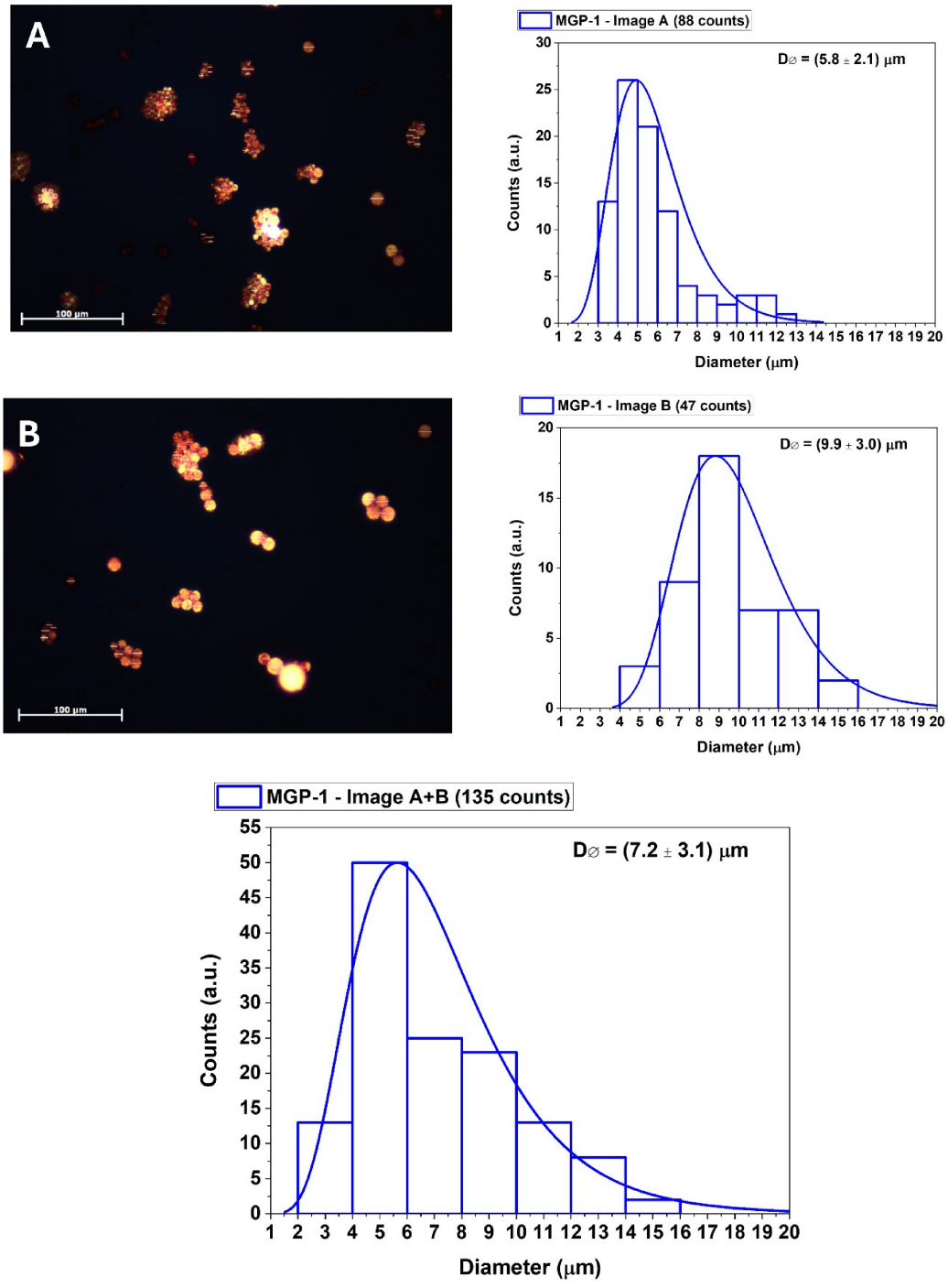

Fig. S17. Microscopic images and size determination of the MGP-1 particles made with 500 rpm stirring for 1h.

MGP-2

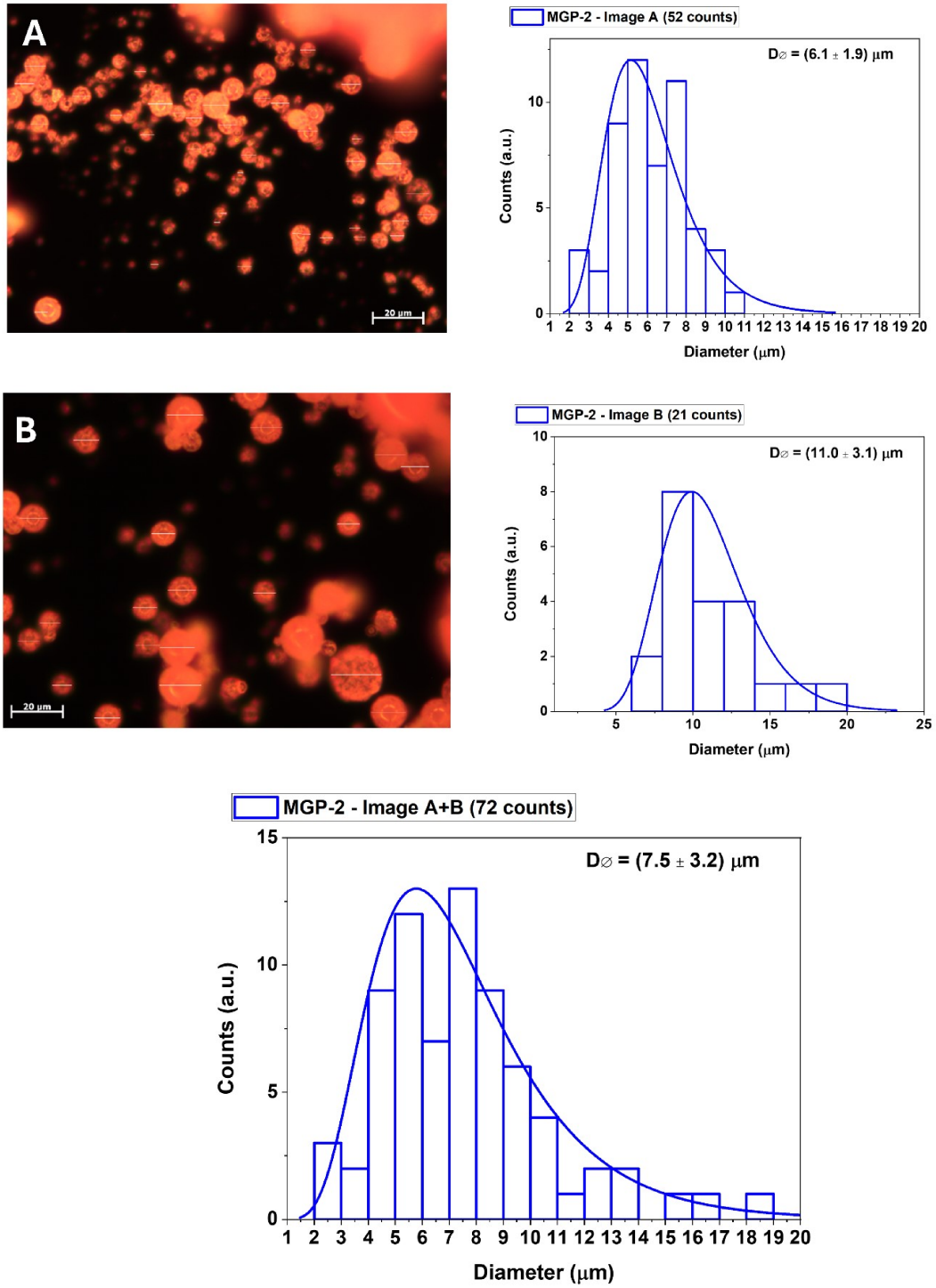

Fig. S18. Microscopic images and size determination of the MGP-2 particles made with 500 rpm stirring for 2h.

MGP-3

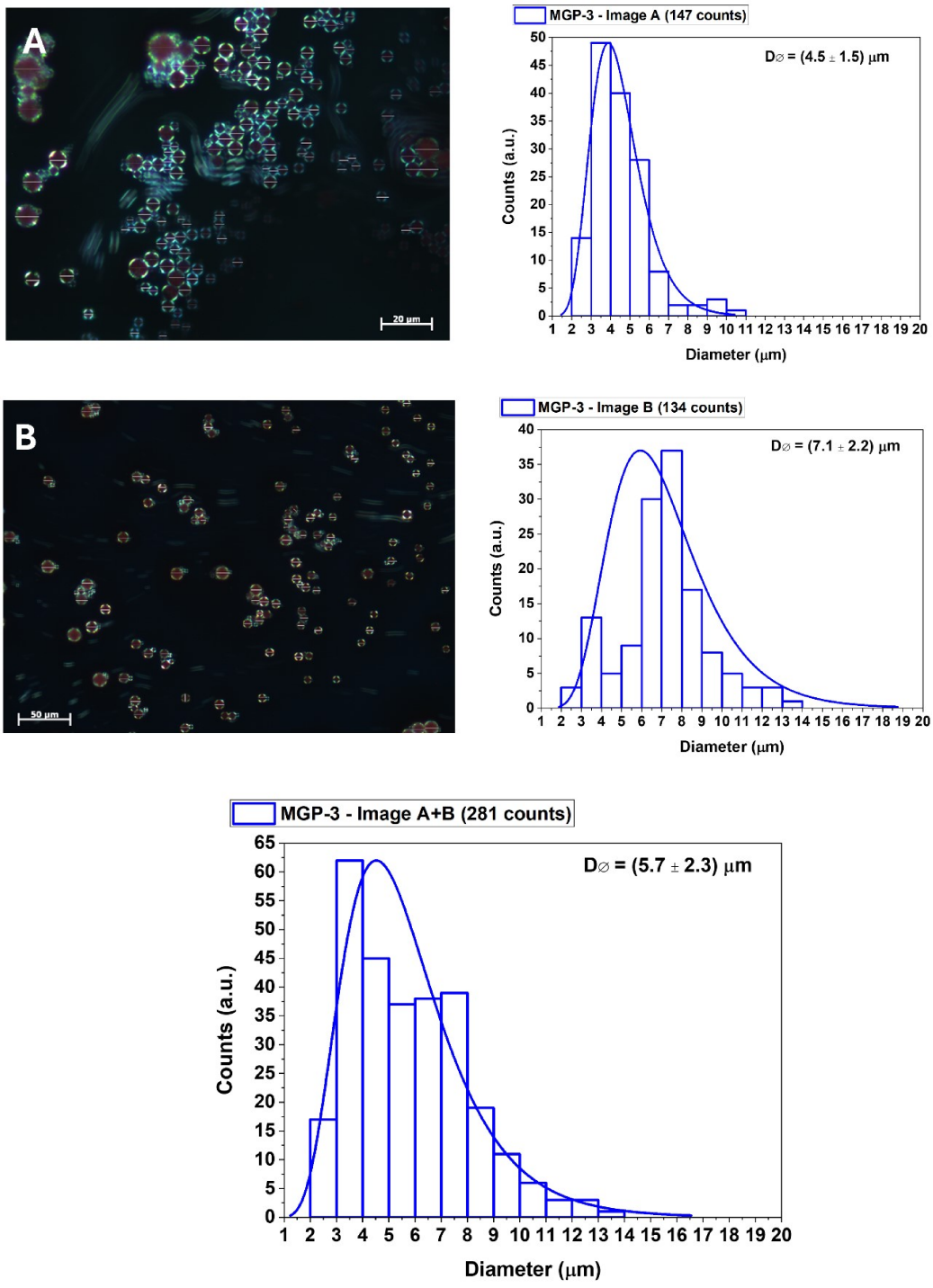

Fig. S19. Microscopic images and size determination of the MGP-3 particles made with 800 rpm stirring for 1h.

MGP-UT

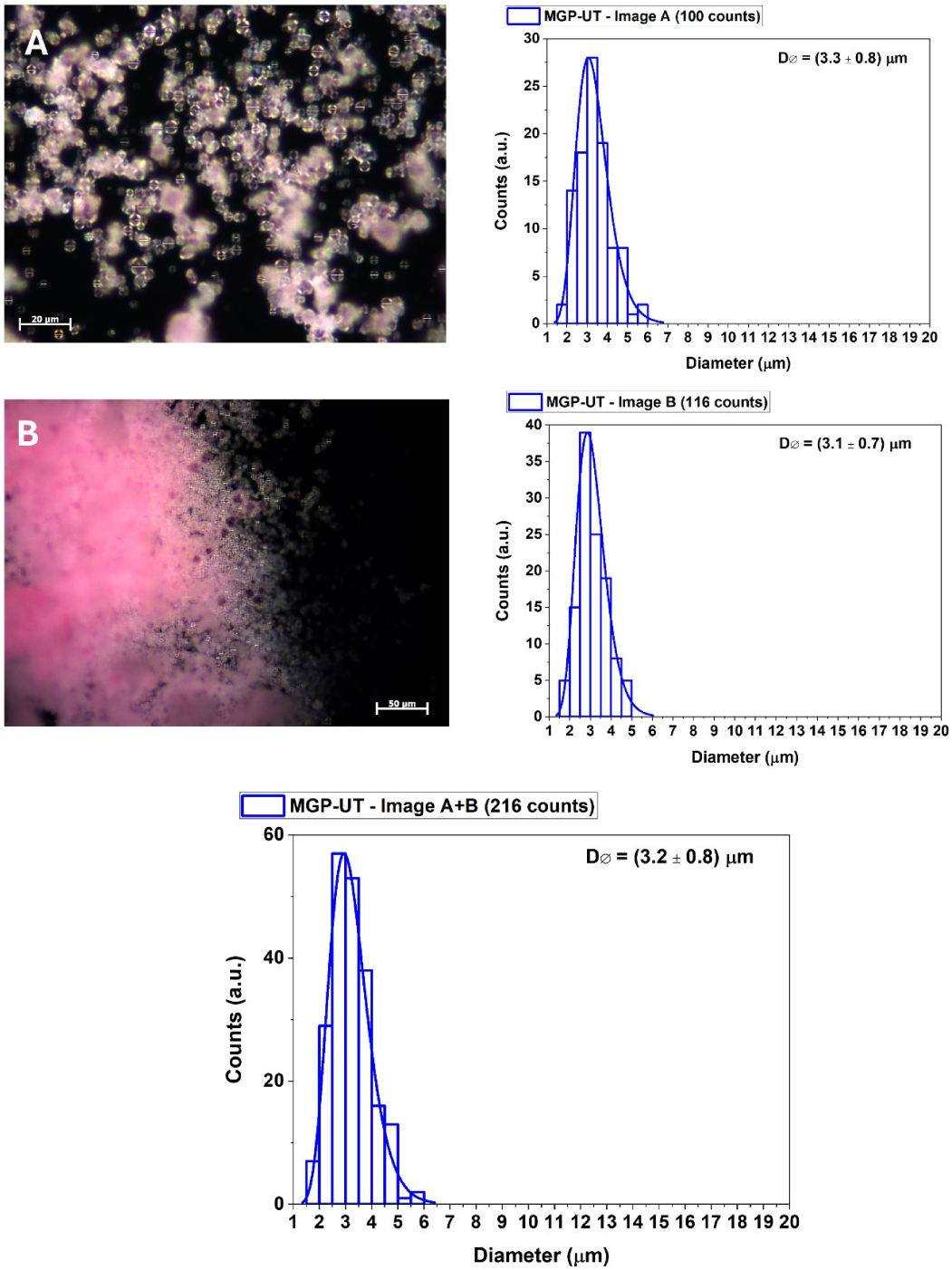

Fig. S20. Microscopic images and size determination of the MGP-UT particles made with 500 rpm stirring followed by 10000 rpm with an Ultra-Turrax™ dispenser.

MGP-US

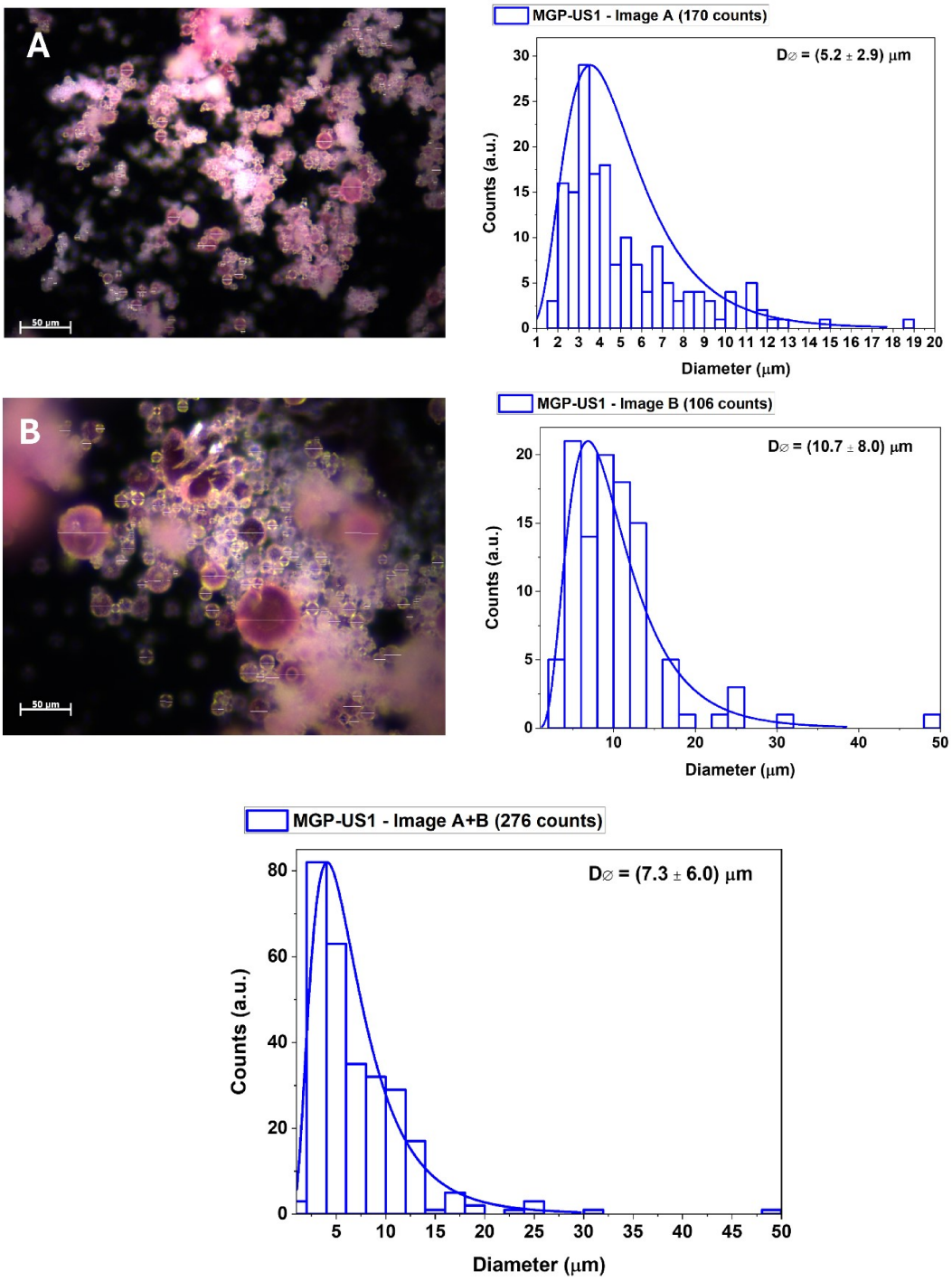

Fig. S21. Microscopic images and size determination of the MGP-US particles made with 500 rpm stirring followed by 150 W ultra-sonic treatment.

2.10 Time-resolved fluorescence measurements

Table S3. Fluorescence lifetime parameters of neat LG305 and MG LG305 (1150 ppm). λ_{exc} = 490 nm, λ_{det} = 650-720 nm. All decay curves were analyzed using a bi-exponential reconvolution fit.

Sample	Lifetime τ [ns]	±Err	Amplitude	±Err	Average lifetime τ_{av} [ns]	±Err
LG305	1.27	0.04	0.29	0.02	0.83	0.01
	0.39	0.01	0.95	0.02		
MG LG305	12.2	1.6	0.10	0.02	12.4	1.5
	1.42	0.31	-0.14	0.06		

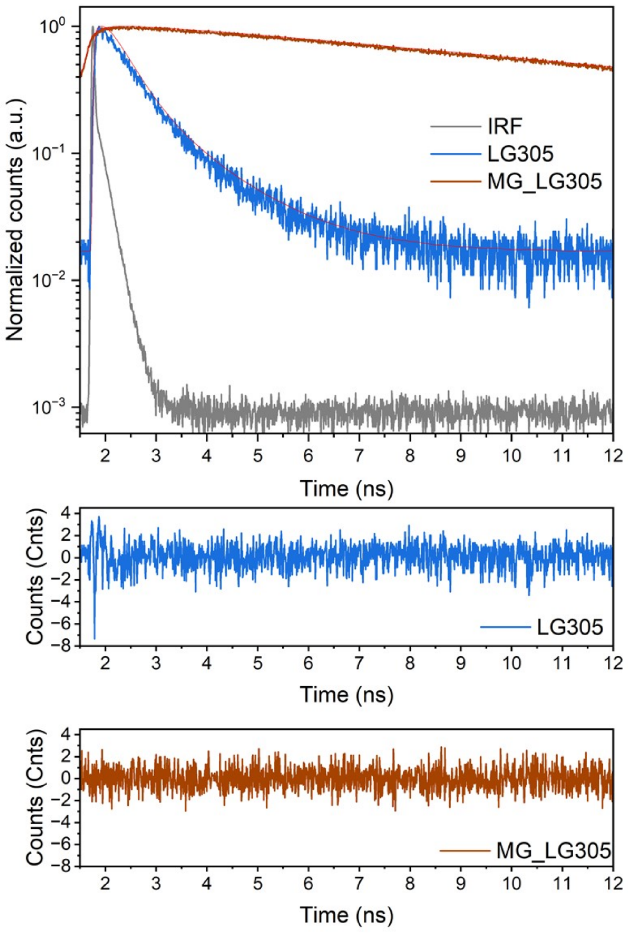

Figure S22. TSCPS histogram of LG305 and MG LG305 (1150 ppm) in solid state at λ_{exc} = 490 nm and λ_{det} = 650-720 nm with the fit residuals for both traces.

2.11 Variation of dye in microsphere synthesis

Fig. S23. Precursor gels prepared with 1150 ppm of Oracet® FL Pink 285, Lumogen® F Red 305 and Oracet® FL Orange 240 (from left to right).

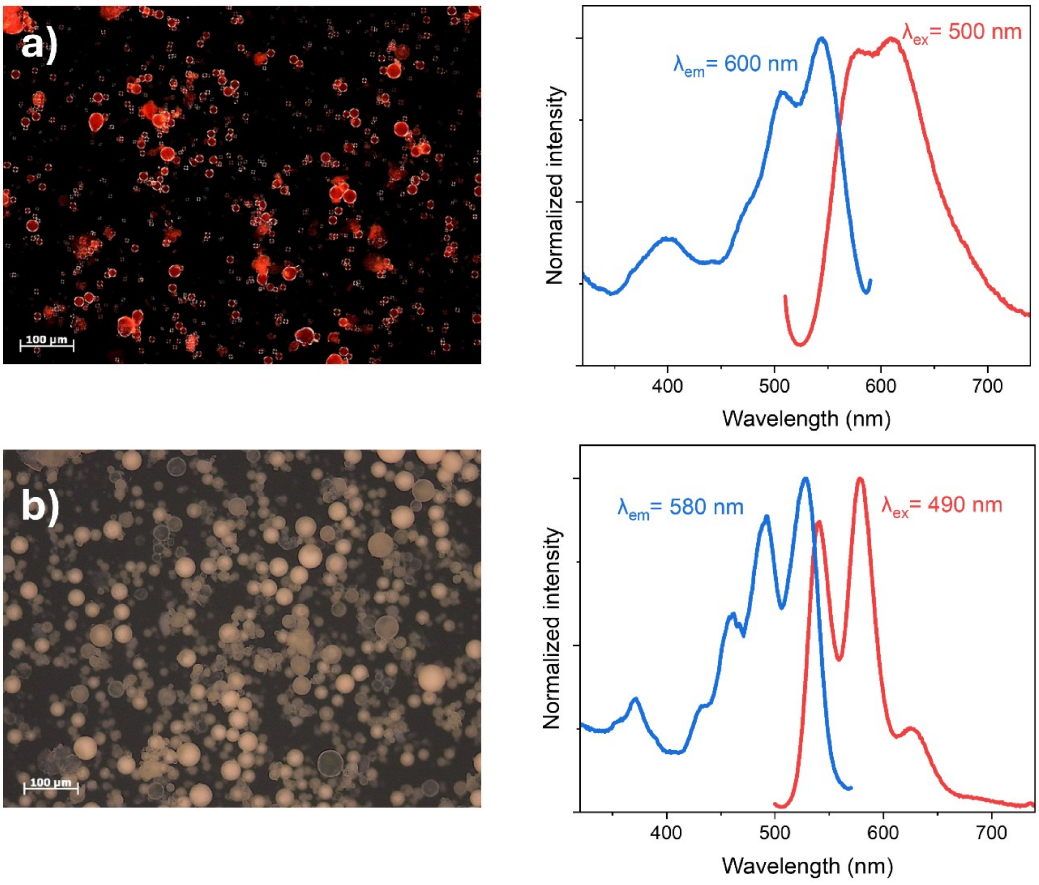

Fig. S24. Left: microscopy images of the microspheres; right: emission and extinction spectra of the microspheres containing (a) Oracet® FL Pink 285, (b) Oracet® FL Orange 240.

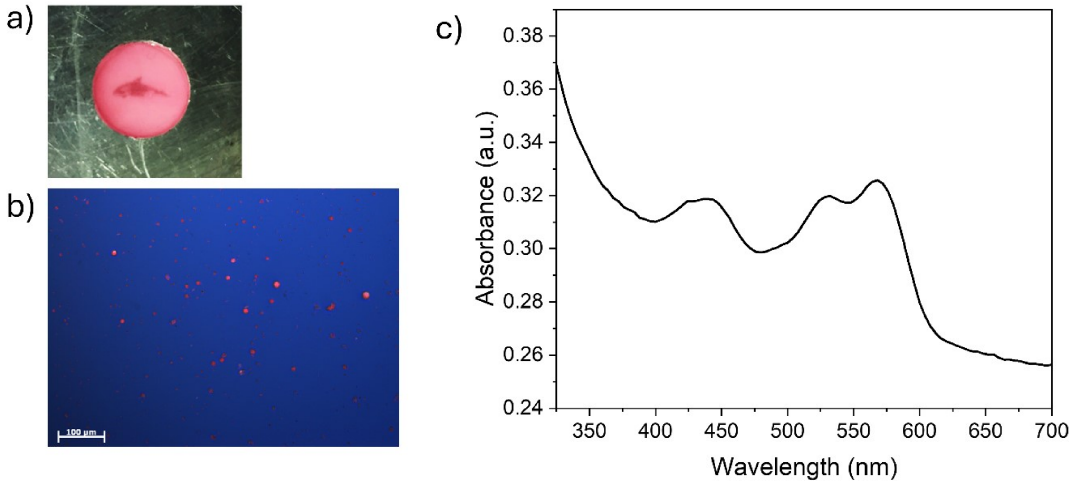

Fig. S25. a) Cured, MGPT containing, Dow Corning OE660 resin, b) microscope image of the sample under 450 nm light, and c) UV-Vis spectrum of the sample showing the characteristic absorption bands of LG305.